



# **The Isolation and Characterisation of Bioactive Metabolites from *Ficus carica* and their Effects on Acrolein- induced Oxidative Stress and NQO1 Expression in Neuronal Differentiated SH-SY5Y Cell Line**

A Thesis Submitted in Fulfilment of the Requirements  
for Degree of Doctor of Philosophy  
Institute of Pharmacy and Biomedical Sciences at the  
University of Strathclyde

By

HANAN KHOJAH

BSc., MSc. (Honours)

2018

## **Declaration**

---

I declare, except where it is specifically indicated, that this thesis is the result of my own research. It has been composed by myself and has not been previously submitted for examination which has led to the award of a degree.

“The copyright of this thesis belongs to the author under the terms of the United Kingdom Copyright Acts as qualified by University of Strathclyde Regulation 3.50. Due acknowledgement must always be made of the use of any material contained in, or derived from, this thesis”.

Signed: Hanan B. Khojah

Date: 16/5/2018

## **Acknowledgment**

---

First and foremost, thank you **Allah Almighty** for your grace and for your blessing to have the opportunity to complete my studies and ignite the light to have a better career in the future.

I would like to express my gratitude to my very special lead supervisor **Dr. RuAngelie Edrada-Ebel** I owe very much of my understanding of this research to her dedicated supervising and guidance. I am fully grateful to have a supervisor like her. My appreciation and thanks also goes to my second supervisor Dr David Watson for his supervising and guidance, as well.

I would also like to express my gratitude to Dr. Darren Edwards, to Dr. Benjamin Pickard, to Dr. Katherine Lawrence to Dr. Roth Tate, to Dr. Louise Young, to Grainne Abbott and to Professor Robert Plevin for the wonderful support team and for facilitating their bioassay equipment's during the entire or part of my project.

I would additionally like to express my gratitude with unlimited naming to the entire research group in Dr. RuAn's lab whom are currently with the group or have recently left the group for gaining more career experience. It was such a rewarding experience working with such a delightful group of intelligent people. My appreciation and thanks goes to my friends, as well. My special thanks go to Aisha Ezmirly who has taken care of my daughter during my difficult labour.

My unconditional thanks dedicated to my beloved husband **Dr. Nasser Mohammed Aldekhail** and my beloved daughter **Nourah** for their faith, sacrifices, support, and endless love during the study. My unconditional thanks dedicated to Allah omce again for having my baby born girl **Rayhan** (22th Jan 2018) into our life.

Finally, this project was sponsored by United Kingdom Saudi Cultural Bureau (UKSCB) along with the Ministry of Education in Saudi Arabia. Therefore, sincere appreciation and thanks goes to my government and to be accepted among the Custodian of the Two Holy Mosques program applicant's students for undertaking this research.

## **Dedication**

---

This work is dedicated, first and foremost, to my beloved husband **Nasser Mohammed Aldekhail**. Who has supported me during my Master and later my PhD and mostly during the tough time when Dr. Elizabeth Ellis has passed away with cancer, and was my supervisor in the 1st year of my PhD project.

There was a crucial chapter of my life when I couldn't ever find any supervisor to undertake my project. Then, all of my positive emotion and motivation have been going down and was the most difficult part of my life. Until one day, the brightest day of my life has begun when Dr. RuAngelie Edrada-ebel has accepted to lead my PhD project with all of her kindness and nobility. This was my new chapter of my happy and successful part of my PhD journey. My notice of her presence gave me anticipation, and the mere thought of finishing up my thesis under her professional supervision was my expectation of encouragement.

Finally, for all my husband's love, my daughter's patience, and my lead supervisor's unlimited support during my PhD journey, I will forever beholden to my husband **Nasser**, warmhearted to my both daughters **Nourah** and **Rayhan** as well as unforgetten Dr. RuAn's supervision. Hence, this achievement is for my husband and my daughters as well as to inspire my current and future children to always aim for more and never to give-up and once again I dedicate this work to my admirer and beloved **Nasser** who has been awarded a PhD on 18<sup>th</sup> December 2017.

Hanan Khojah

University of Strathclyde

<b>Declaration .....</b>	<b>I</b>
<b>Acknowledgment.....</b>	<b>II</b>
<b>Dedication.....</b>	<b>III</b>
<b>List of Figures.....</b>	<b>IX</b>
<b>List of Tables .....</b>	<b>XX</b>
<b>List of Abbreviations .....</b>	<b>XXII</b>
<b>List of Symbols And Synonyms .....</b>	<b>XXV</b>
<b>Published work.....</b>	<b>XXVII</b>
<b>Abstract.....</b>	<b>XXVIII</b>
<b>CHAPTER ONE INTRODUCTION .....</b>	<b>0</b>
<b>1. INTRODUCTION .....</b>	<b>1</b>
<b>1.1. Natural product and drug discovery.....</b>	<b>1</b>
<b>1.2. History of natural product .....</b>	<b>2</b>
<b>1.3. Characterisation of Ficus carica L.....</b>	<b>5</b>
1 .....	6
1.1 .....	6
1.2 .....	6
1.3 .....	6
1.3.1 Overview of the biomedical uses of F. carica.....	6
1.3.2 Phytochemistry of F. carica .....	12
1.3.3 F. carica in Alzheimer disease prevention .....	20
<b>1.4. Alzheimer's disease.....</b>	<b>21</b>
1.4 .....	22
1.4.1 The significance of Alzheimer's disease .....	22
1.4.2 Pathophysiological theory of Alzheimer's disease .....	22
1.4.3 Oxidative stress.....	24
1.4.4 Anti-oxidative stress enzyme.....	30
1.4.5 NAD(P)H:quinine oxidoreductase (NQO1) .....	33

<b>1.5. Drugs approved by the FDA for the treatment of Alzheimer’s disease.....</b>	<b>34</b>
1.5 .....	34
1.5.1 Cholinesterase inhibition (AChE).....	34
1.5.2 N-methyl-D-aspartate (NMDA) receptor antagonist.....	39
1.5.3 Monoclonal Antibodies (mABs).....	39
1.5.4 Gamma Secretase Inhibitors .....	42
1.5.5 Other target drugs in clinical trials for AD .....	43
<b>1.6. Role of medicinal plants in Alzhiemer’s disease .....</b>	<b>47</b>
<b>1.7. Metabolomic approaches in NP chemistry .....</b>	<b>50</b>
<b>1.8. Hypothesis, aims and outcomes of this study .....</b>	<b>51</b>
1.6 .....	51
1.7 .....	51
1.8 .....	51
1.8.1 Hypothesis .....	51
1.8.2 Aims.....	52
1.8.3 Present and future outcomes .....	53
<b>CHAPTER TWO METHODOLOGY .....</b>	<b>55</b>
<b>2. METHODOLOGY .....</b>	<b>56</b>
<b>2 .....</b>	<b>56</b>
<b>2.1. Health and safety .....</b>	<b>56</b>
<b>2.2. General equipment .....</b>	<b>56</b>
<b>2.3. Plant Materials .....</b>	<b>56</b>
2.1 .....	56
2.2 .....	56
2.3 .....	56
2.3.1 Plant collection .....	56
2.3.2 Plant extraction and partitioning.....	57
<b>2.4. Phytochemical methods.....</b>	<b>58</b>
2.4 .....	58
2.4.1 Chromatographic techniques .....	58
2.4.2 Structure identification technique.....	63
2.4.3 Structure elucidation techniques .....	64
<b>2.5. Metabolomic methods.....</b>	<b>66</b>
2.5 .....	66
2.5.1 Metabolomics workflow .....	66
2.5.2 Data analysis using MZmine 2.10 .....	67
2.5.3 Data analysis using dereplication via DNP-Macrodrive 2015 database.....	68

2.5.4	Multivariate analysis using SIMCA-P as High-throughput screening .....	68
<b>2.6.</b>	<b>Biological methods .....</b>	<b>70</b>
2.6	.....	70
2.6.1	Biological equipment's and reagents .....	70
2.6.2	Cell culture.....	70
2.6.3	Haemocytometer .....	71
2.6.4	Cell viability test via AlamarBlue® assay.....	71
2.6.5	Cytotoxicity test.....	73
2.6.6	MTT assay .....	74
2.6.7	Western blotting test (WB).....	74
2.6.8	Statistical Analysis.....	79
<b>CHAPTER THREE</b>	<b>MESOCARP RESULTS.....</b>	<b>80</b>
<b>3.</b>	<b>ISOLATION AND IDENTIFICATION OF BIOACTIVE METABOLITES FROM THE MESOCARP OF FICUS CARICA AND BIOACTIVITY ON DIFFERENTIATED SH-SY5Y NEURONAL CELL LINE .....</b>	<b>81</b>
<b>3.1</b>	<b>First fractionation .....</b>	<b>81</b>
<b>3.2</b>	<b>Second fractionation .....</b>	<b>86</b>
<b>3.3</b>	<b>Third fractionation .....</b>	<b>90</b>
<b>3.4</b>	<b>NMR.....</b>	<b>91</b>
3.4.1	<sup>1</sup> H-NMR data obtained from 1 <sup>st</sup> fractionation of crude organic mesocarp extract	91
3.4.2	<sup>1</sup> H-NMR data obtained from fractionation of bioactive eluates F4,5,6 and F12,14	92
3.4.3	<sup>1</sup> H-NMR of fractions obtained from preparative TLC of F4,5,6/F1 .....	95
<b>3.5</b>	<b>Cell viability test.....</b>	<b>95</b>
3.5.1	Bioscreening of fractions from the crude organic mesocarp extract .....	95
3.5.2	Bioscreening of fractions from bioactive eluates F4,5,6 and F12,14 .....	97
3.5.3	Bioscreening of fractions obtained from preparative TLC of F4,5,6/F1 .....	99
<b>3.6</b>	<b>Cell cytotoxicity test.....</b>	<b>99</b>
<b>3.7</b>	<b>Western blotting test.....</b>	<b>102</b>
<b>3.8</b>	<b>Metabolomic-guided screening of F. carica mesocarp .....</b>	<b>103</b>
3.8.1	Metabolomic profiling of fractions from the crude organic mesocarp extract	103
3.8.2	Metabolomic profiling of fractions from bioactive eluates F4,5,6 and F12,14	110
<b>3.9</b>	<b>Identification and elucidation of the mesocarp pure fractions.....</b>	<b>114</b>

3.9.1	$\gamma$ -Sitosterol 1.1 .....	114
3.9.2	Oleoyl- $\beta$ -D-arabinoside 1.2 .....	122
3.9.3	Lupeol acetate 1.3 .....	133
<b>CHAPTER FOUR ENDOCARP RESULTS.....</b>		<b>139</b>
<b>4. ISOLATION AND IDENTIFICATION OF BIOACTIVE METABOLITES FROM THE ENDOCARP OF FICUS CARICA AND BIOACTIVITY ON DIFFERENTIATED SH-SY5Y NEURONAL CELL LINE .....</b>		<b>140</b>
<b>4.1. The isolation of F. carica endocarp .....</b>		<b>140</b>
4.1.1.	Normal phase REVELERIS <sup>®</sup> flash chromatography from the crude extract	142
4.1.2.	Thin-layer chromatography (TLC (Crude extract) .....	143
<b>4.2. Proton NMR (<sup>1</sup>H-NMR) analysis.....</b>		<b>145</b>
<b>4.3. Cell viability test.....</b>		<b>146</b>
<b>4.4. Cell cytotoxicity test.....</b>		<b>147</b>
<b>4.5. Western blotting test.....</b>		<b>148</b>
<b>4.6. Metabolomic-guided screening of F. carica endocarp.....</b>		<b>149</b>
<b>4.7. Identification and elucidation of bioactive compounds from F. carica endocarp .....</b>		<b>155</b>
4.7.1.	Lawsaritol 2.1 .....	155
4.7.2.	P-hydroxybenzoic acid 2.6 and vanillic acid 2.7 .....	166
<b>CHAPTER FIVE EXOCARP RESULTS .....</b>		<b>176</b>
<b>5 ISOLATION AND IDENTIFICATION OF BIOACTIVE METABOLITES FROM THE EXOCARP OF FICUS CARICA AND THEIR BIOACTIVITY ON DIFFERENTIATED SH-SY5Y NEURONAL CELL LINE .....</b>		<b>177</b>
<b>5.1 The isolation of F. carica exocarp.....</b>		<b>177</b>
5.1.1	Normal phase REVELERIS <sup>®</sup> flash chromatography from crude extract .....	180
5.1.2	Normal phase REVELERIS <sup>®</sup> flash chromatography for purification .....	181
5.1.3	TLC screening.....	185
5.1.4	<sup>1</sup> H-NMR spectra of exocarp fractions .....	186
<b>5.2 Biological assay .....</b>		<b>188</b>
5.2.1	Cell viability test .....	188
5.2.2	Cell cytotoxicity test .....	189
5.2.3	Western blotting test .....	191
<b>5.3 Metabolomic-guided screening of F. carica exocarp .....</b>		<b>192</b>
5.3.1	First fractionation of F. carica exocarp.....	192

5.3.2	Sub-fractions of <i>F. carica</i> exocarp .....	197
<b>5.4</b>	<b>Identification and elucidation and of <i>F. carica</i> exocarp.....</b>	<b>202</b>
5.4.1	$\beta$ -amyrin acetate 3.1 and lupeol acetate 3.2.....	202
5.4.2	Campesterol 3.3 .....	213
<b>CHAPTER SIX DISCUSSION AND CONCLUSION OF <i>F. CARICA</i> .....</b>		<b>221</b>
<b>6.</b>	<b>GENERAL DISCUSSION AND CONCLUSION .....</b>	<b>222</b>
<b>6.1.</b>	<b>The discovery and the chemistry study.....</b>	<b>222</b>
<b>6.2.</b>	<b>Metabolomics .....</b>	<b>226</b>
<b>6.3.</b>	<b>The biological study .....</b>	<b>227</b>
6.1.	.....	230
6.2.	.....	230
6.3.	.....	230
6.3.1.	The study of prevention of oxidative stress .....	230
6.3.2.	Passing the blood brain barrier .....	236
<b>6.4.</b>	<b>Biosynthesis of the secondary metabolites.....</b>	<b>237</b>
<b>6.5.</b>	<b>Significances and limitations.....</b>	<b>240</b>
<b>6.6.</b>	<b>Future work and recommendation .....</b>	<b>241</b>
<b>6.7.</b>	<b>Conclusion .....</b>	<b>242</b>
<b>REFERENCES.....</b>		<b>243</b>
<b>SUPPLEMENTARY INFORMATION.....</b>		<b>282</b>

## List of Figures

---

- Figure 1.1:** A detailed analysis of the 112 FDA-approved drugs between 1999 and 2013 reveals that 28% of those (31 drugs) were derived from NPs and their derivatives, in comparison to 42% (47 drugs) that were synthetic small molecules, and 30% (34 drugs) that were biological agents. Figure adapted from Ding *et al.* (2016). ..... 4
- Figure 1.2:** Pie chart analysis of ethnomedicinal studies of different parts of *F. carica* and the number of articles published from 2013 to 2017 for their effects in percentages..... 11
- Figure 1.3:** Classification of polyphenols (Essa *et al.*, 2016). ..... 13
- Figure 1.4:** Identified compounds from fruits of *F. carica* (Barolo, Mostacero Silvia and López, 2014; Loizzo *et al.*, 2014). ..... 14
- Figure 1.5:** Other organic acids reported in aqueous lyophilised pulp extracts of *F. carica*, peel, and traces in leaves (Oliveira *et al.*, 2010; Ribechini, Pérez-Arategui and Colombini, 2011). ..... 16
- Figure 1.6:** Identified compounds of *F. carica* in leaves and root (Barolo *et al.*, 2014).17
- Figure 1.7:** Identified compounds of *F. carica* in latex (Barolo *et al.*, 2014). ..... 19
- Figure 1.8:** Identified steroid compounds of *F. carica* in latex (Ribechini, Pérez-Arategui and Colombini, 2011; Soltana *et al.*, 2016). ..... 20
- Figure 1.9:** The proteolytic cleavage of the amyloid precursor protein (APP) produces A $\beta$  as a consequence of the secretase action. Following its production, A $\beta$  is subjected to aggregations, after which its deposition takes place in an extracellular way in the form of senile plaques. Oligomeric A $\beta$  has the capacity to facilitate its own insertion into the lipid bilayer, as a consequence of which the lipid peroxidation process is initiated. This gives rise to highly reactive products, including MDA, HNE, and acrolein, where the latter two have the capacity to react with proteins. In turn, acrolein-protein adducts or HNE-protein adducts change the functional and structural characteristics of the proteins, thereby leading to impairment. This result is linked to the following: (i) lowered autophagy; (ii) a reduced rate of unfolded response ubiquitin-proteasome system (UPS); (iii) reduced glucose metabolism; (iv) lowered antioxidant defence; (v) defective neuronal axons; and (vi) lowered adenosine triphosphate (ATP) production (and, consequently, neuronal trafficking). Over the course of AD's onset, cellular impairment gives rise to AD pathogenesis (Barone *et al.*, 2016; Sultana, Perluigi and Butterfield, 2013). ..... 27
- Figure 1.10:** Chemical structures of natural and synthetic low molecule compounds based on the activation of Nrf2 pathway and NQO1. L-3-n-butylphthalide, 3H-1, 2-dithiole-3-thione, epigallocatechin 3- gallate, 2-cyano-3,12-dioxooleana-1,9-dien-28-oic acid and 2-cyano-3,12-dioxooleana-1,9-dien-28-oic acid methyl amine labelled as L-NBP, D3T, EGCG, CDDO and CDDO-MA, respectively. .... 32
- Figure 1.11:** The mechanism of action of the regulation of Nrf2. Under basal conditions, Nrf2 is polyubiquitylated by the KEAP1–Cul3 E3 ligase and subsequently degraded by the proteasome. Under conditions of oxidative stress including ROS and cytotoxic electrophiles (acrolein), the KEAP1–Nrf2 interaction is destabilised, causing Nrf2 to dimerise with Maf protein within the nucleus. Nrf2 bind to ARE, promoting transcription of cellular defence genes of phase II enzymes such as NQO1. .... 33
- Figure 1.12:** Structure of memantine [189] an NMDA receptor antagonist with a Mwt 179.31 ..... 39

<b>Figure 2.1:</b> The successful splitting of the exocarp (A) shows the primary components of REVELERIS® flash. (B) Depicts a schematic diagram showing the solvent flow via the primary system components .....	59
<b>Figure 2.2:</b> (A) shows the primary components of REVELERIS® flash. (B) Depicts a schematic diagram showing the solvent flow via the primary system components. ....	60
<b>Figure 2.3:</b> The mechanism by which the coloured fractions can be observed when <i>P</i> -anisaldehyde/sulfuric acid reagent is sprayed on TLC plates.....	63
<b>Figure 2.4:</b> Metabolomics flowchart cascade tools for mining active metabolites of <i>F. carica</i> endocarp, exocarp and mesocarp against acrolein induced oxidative stress in AD.....	68
<b>Figure 2.5:</b> Flowchart of the multivariant analysis strategy applied using SIMCA-P for <i>F. carica</i> exocarp, endocarp, and mesocarp against oxidative stress related AD.....	70
<b>Figure 2.6:</b> Haemocytometer plate illustrated the four corner squares margin of the counted cells in the chambers of the bright line haemocytometer and the cells in each primary square. ....	72
<b>Figure 2.7:</b> The oxidation-reduction reaction of the non-fluorescent resazurin blue dye turning to highly fluorescent resorufin pink dye due to the transformation of NADH to NAD <sup>+</sup> . ....	73
<b>Figure 2.8:</b> The preparation of the serial concentrations of the treatments for the cytotoxicity test. A multiple-channel pipette (Eppendorf®) was used to measure and transfer the concentrations to their appropriate wells.....	74
<b>Figure 2.9:</b> Shows the sequences for assembling WB sandwich and the directions of (+ve) at the red top and (-ve) at the black top voltages. ....	79
<b>Figure 3.1:</b> Fractionation scheme for crude <i>F. carica</i> mesocarp extract (1.3 g) affording 17 fractions shown in green. Further fractionation of the bioactive pooled fractions F4,5,6 and F12,14 yielded an additional 47 sub-fractions. Boxes in red colour were excluded from further bioassay and elucidation work due to their low yield, while fractions in blue boxes were subjected for further work. Purification of F4,5,6 gave six fractions denoted in brown boxes.....	83
<b>Figure 3.2:</b> Normal phase chromatogram for the fractionation of the dry crude <i>F. carica</i> mesocarp extract. Solvents used were hexane (A) and ethyl acetate (B) with 0% B at 0-5 min, 10% B at 5-10 min, 20% B at 10-20 min, 30% B at 20-30 min, 40% B at 30-40 min, 50% B at 40-50 min, 60% B at 50-60 min, 70% B at 60-70 min, 80% B at 70-80 min, 90% B at 80-90 min, and 100% B at 90-115 min. Subsequently, solvents were switched to methanol (C) and dichloromethane (D) with gradient elution from 90% to 70% D. The ELSD was denoted by the green line, UV1 and UV2 denoted by the blue and violet lines, respectively. Collection volume was set at a maximum of 20 ml and mode of collection was by peak detection as denoted by the coloured bars on the X-axis. The highlighted peaks in orange and grey represented the pooled fractions F4,5,6 and F12,14, respectively. DCM and MeOH respectively stand for dichloromethane and methanol. The % in black colour.....	84
<b>Figure 3.3:</b> TLC summary plate of the 1st fractionation of mesocarp crude extract on Si60. Hexane (Hex) with ethyl acetate (EtOAc) and dichloromethane with methanol constituted the mobile phase solvents. Hex and EtOAc were employed at ratios of 90:10, 70:30, 50:50, 30:70 and 10:90 and subsequently with dichloromethane and	

- methanol at 90:10 and 80:20. Fractions 4, 5, 6 were pooled, as well as fractions 12 and 14 and were coded F4,5,6 and F12,14, respectively. Eluates observed under long UV were represented by coloured circles and those with pencil markings were detected under short UV, whilst yellow to brown spots of colour were visualised with *P*-anisaldehyde/sulfuric acid spray reagent. .... 86
- Figure 3.4:** Normal phase chromatogram for the further fractionation of the pooled fraction F4,5,6. The solvents used were hexane (A) and ethyl acetate (B) with 0% B at 0-5 min, 10% B at 5-10 min, 20% B at 10-20 min, 30% B at 20-30 min, 40% B at 30-40 min, 50% B at 40-50 min, 60% B at 50-60 min, 70% B at 60-70 min, 80% B at 70-80 min, 90% B at 80-90 min, and 100% B at 90-115 min. High, medium and low ELSD peaks. No peaks were detected for both UV1 and UV2 wavelengths. Peak highlighted in grey F4,5,6/F1..... 88
- Figure 3.5:** Normal phase chromatogram for the further fractionation of the pooled fraction F12,14. The solvents used were methanol (C) and dichloromethane (D) commencing with 90% D for 10 min, followed by 85% D for the next 10 min, then with 80% D for another 10 min and increased to 70% D in 30 min. The bioactive sub-fractions F12,14/F8 and F12,14/F9 were highlighted in grey and subjected for further analysis. DCM and MeOH stand for dichloromethane and methanol, respectively. .... 89
- Figure 3.6:** TLC of fractions obtained from F4,5,6 on silica gel 60 F254 using hexane and ethyl acetate as mobile phase. The soft black circles denote the spots observed under short UV of 250nm, whereas the circles of varying colours, depending on how the colour was visualised under long UV of 280nm. Spraying with *P*-anisaldehyde/sulfuric acid reagent allowed further differentiation between the observed spots. The R<sub>f</sub> value of the fractions of interest was the same F4,5,6/F9 = 0.4, and is indicated in the figure by the black dotted line. .... 90
- Figure 3.7:** TLC of fractions obtained from F12,14 on silica gel 60 F254 using dichloromethane and methanol as mobile phase. The soft black circles denoted the compounds observed under short UV at 250nm, whereas the circles of varying colours, depending on their colour of visualisation under long UV of 280nm. Spraying with *P*-anisaldehyde/sulfuric acid spray reagent allowed differentiation to be made between the observed spots. The R<sub>f</sub> value of the fractions of interest, F8 and F9, was the same at 0.4, and is indicated in the figure by the black dotted line. An additional weak spot with a R<sub>f</sub> value of 0.3 is denoted by the blue dotted line.....90
- Figure 3.8:** Preparative TLC of F4,5,6/F1/F5. R<sub>f</sub> value for was calculated as  $\{[(a+b)/2]/c\} = [(12+8.9)/2]/17\} = 0.6$ . ....92
- Figure 3.9:** Stacked 1H-NMR spectra (400 MHz, CDCl<sub>3</sub>) of fractions obtained from flash chromatography of crude ethyl acetate mesocarp extract. The CDCl<sub>3</sub> solvent peak was referenced at 7.25 ppm..... 93
- Figure 3.10:** Stacked 1H-NMR spectra (400 and 500 MHz, CDCl<sub>3</sub>) of fractions obtained from F4,5,6 by flash chromatography. CDCl<sub>3</sub> solvent peak referenced at 7.25 ppm.....95
- Figure 3.11:** Stacked 1H-NMR spectra (400MHz, CDCl<sub>3</sub>) of F12,14 after they were subjected to flash chromatography. CDCl<sub>3</sub> solvent peaks were resonate at 7.25ppm.....95
- Figure 3.12:** Stacked 1H-NMR spectra (400MHz, CDCl<sub>3</sub>) of fractions obtained from preparative TLC of F4,5,6/F1.....96

- Figure 3.13:** Photomicrograph of undifferentiated and differentiated SH-SY5Y cell line at 20X Magnification. A) Undifferentiated SH-SY5Y cell line shows a loosely supported cell body and a prominent nucleolus, in which neurite length is unchanged without the addition of 10  $\mu$ M RA for 2 days incubation. B) Differentiated SH-SY5Y cell line shows an extensively branching and outgrowth of neurites and ganglions following treatment with 10  $\mu$ M RA for 2 days; yellow arrows indicated the neurites connection. .... 97
- Figure 3.14:** Preliminary cell viability screening of chromatographic fractions of *F. carica* mesocarp on differentiated SH-SY5Y cells. Viability was displayed by fractions with values higher than 100% (red), while fractions lacked viability, with values of equally or less than 100% (blue); the control (100%) is shown in black. Every group constituted a mean of three SDs, and ANOVA was significant ( $P < 0.001$ ) when to the control. ....98
- Figure 3.15:** Preliminary cell viability screening of chromatographic fractions of (A) F4,5,6 and (B) F12,14 on differentiated SH-SY5Y cells. Viability was displayed by fractions with values higher than 100% (red), while fractions lacked viability, with values of equally or less than 100% (blue); the control (100%) is shown in black. Every group constituted a mean of three SDs, and ANOVA was significant ( $P < 0.001$ ) when to the control. ....99
- Figure 3.16:** Preliminary cell viability screening of fractions obtained from preparative TLC of F4,5,6/F1 on differentiated SH-SY5Y cells. Viability was displayed by fractions with values higher than 100% (red), while fractions lacked viability, with values of equally or less than 100% (blue); the control (100%) is shown in black. Every group constituted a mean of three SDs, and ANOVA was significant ( $P < 0.001$ ) when to the control. .... 100
- Figure 3.17:** Dose-dependent toxic effects of acrolein on differentiated SH-SY5Y cell viability. .... 101
- Figure 3.18:** A) Results of the alamar Blue test upon treatment of acrolein-induced oxidative stress associated SH-SY5Y neuroblastoma cells (red) with fractions F12,14/F8 [1] (green), F12,14/F9 [2] (grey), F4,5,6/F9 [3] (orange) and F4,5,6/F1/F5 [4] (blue). (B) The antioxidant effect of the tested fractions against acrolein on differentiated SH-SY5Y cell line. One-way ANOVA indicated significance compared to control at  $p < 0.05$ . Experiments were performed thrice and data expressed in mean  $\pm$  SD. .... 102
- Figure 3.19:** The effect of F12,14/F9, F4,5,6/F9, and F4,5,6/F1/F5 on the level of protein expressions of NQO1 and  $\beta$ -actin measured by Western blotting using lysates from differentiated SH-SY5Y cell line. All data were significant ( $P < 0.05$ ) and were represented as a mean  $\pm$  SD of three independent experiments. ....104
- Figure 3.20:** PCA-HCA dendrogram and heat map of chromatographic fractions of the crude ethyl acetate extract of *F. carica* mesocarp. ....106
- Figure 3.21:** A) PCA scores scatter plot of mass spectral data showed mesocarp fractions groupings based on their similarities in discriminatory metabolites. B) PCA loadings scatter plot disclosed the m/z values of the grouped metabolites. .... 107
- Figure 3.22:** A) Scores scatter plot for the OPLS-DA model of 17 sub-fractions of bioactive eluates from the mesocarp. Green represents the active fractions and blue represent the inactive fractions. B) Loadings scatter plot for OPLS-DA model. Target molecules in m/z encircled in red and blue as distributed in the two active

- quadrants respectively. Colours represent molecular ion peak ranges in m/z. C) S-plot indicating target molecules in m/z. ....108
- Figure 3.23:** A) Expansion of S-plot indicating the six discriminatory molecules from the mesocarp fractions at m/z 583.455; 566.428, 469.206, 307.102, 415.211, 661.446, 1347.88 and 397.383. B) Expansion of S-plot indicating the position of the isolated compounds from the mesocarp fractions at m/z 468.332, 414.321 and 414.394, which are on the bioactive side of the S-plot.....109
- Figure 3.24:** A) PCA-HCA of fractions of bioactive eluate F4,5,6 via ward linkage. B) PCA-scores scatter plot of fractions of bioactive eluate F4,5,6. C) OPLS-DA scores scatter plot of active and inactive fractions. D) OPLS-DA loadings scatter plot showed ion peaks of target metabolites from active fractions. E) S-plot generated from the OPLS-DA model to predict the bioactive metabolites. F) Expansion of the active end of the S-plot where the interested metabolite ion was detected as m/z 414.381. .... 112
- Figure 3.25:** A) PCA-HCA analysis of chromatographic fractions of bioactive eluate F12,14. B) PCA scores plot of chromatographic fractions of bioactive eluate F12,14. C) OPLS-DA scores plots between active and inactive fractions. D) OPLS-DA loadings scatter plot was detected to show metabolites ion peaks of active metabolites. R<sup>2</sup>Y(sum) =0.984, Q<sup>2</sup>X =0.498. E) and F) S-plot analysis was performed and m/z 414.298 was indicated as the target metabolite. .... 113
- Figure 3.26:** (A) <sup>1</sup>H-NMR spectrum of  $\gamma$ -sitosterol 1.1 dissolved in CDCl<sub>3</sub> at 400 MHz. (B) Expansion of <sup>1</sup>H NMR spectrum between 0.6 and 6.5 ppm.....117
- Figure 3.27:** <sup>13</sup>C & Dept NMR spectrum of  $\gamma$ -sitosterol 1.1 (500 MHz, CDCl<sub>3</sub>). ....118
- Figure 3.28:** HSQC spectra of semi-pure  $\gamma$ -sitosterol in CDCl<sub>3</sub> at 500MHz; X-axis represents H-NMR and y-axis represents C<sup>13</sup> and Dept; blue colour of signals represents either CH or CH<sub>3</sub> while the red colour represents CH<sub>2</sub>; horizontal lines represents the carbon and vertical lines represent the number of proton..... 119
- Figure 3.29:** The overlay of HMBC (500 MHz, CDCl<sub>3</sub>) between the correlation of H-NMR vs Dept; horizontal lines are related to the number of carbon, while vertical lines represent the number of proton. .... 121
- Figure 3.30:** HMBC correlation of  $\gamma$ -sitosterol structure 1.1..... 121
- Figure 3.31:** Over view of <sup>1</sup>H-NMR spectrum of oleoyl  $\beta$ -D-arabinoside 1.2 dissolved in acetone-d<sub>6</sub> and run at 500 MHz; with an expansion of <sup>1</sup>H NMR spectrum between 3.5 and 5.4 ppm.....126
- Figure 3.32:** Jmod-NMR (125 MHz, acetone-d<sub>6</sub>) of compound 1.2; A) Stacked <sup>13</sup>C NMR of both fractions F8 and F9 of F12,14 showed their similarity. B) <sup>13</sup>C NMR with carbon assignments. Acetone-d<sub>6</sub> was observed at 26 ppm. The most crowded signals were observed in the upfield region, while fewer signals were observed in downfield region; zoom in of some signals were included at the top; the positive signals correspond to CH<sub>2</sub>, while the negative signals correspond to either CH<sub>3</sub>, CH or quaternary-C.....127
- Figure 3.33:** <sup>1</sup>H-<sup>1</sup>H COSY correlations of oleoyl  $\beta$ -D-arabinoside 1.2. A) Correlation between protons within arabinoside structure. B) two spin system were detected, as correlations were observed in the oleic side connected in an orange lines while monosaccharide of arabinoside were shown correlation presented in blue lines; other black spots were confirmed as artefacts. .... 1129

- Figure 3.34:** HSQC spectra of oleoyl  $\beta$ -D-arabinoside 1.2 in acetone-d<sub>6</sub> at 500MHz; X-axis represents <sup>1</sup>H-NMR and y-axis represents Jmod-NMR; blue colour of signals represent either CH, CH<sub>3</sub> while the red colour represents CH<sub>2</sub>; Cross link of protons represented as vertical line in green colour with carbon assignments presented horizontally in green colours. Detailed assignments of signals were fully presented in Table 3.10. ....130
- Figure 3.35:** HMBC of compound 1.2 (500 MHz, acetone-d<sub>6</sub>).....132
- Figure 3.36:** <sup>1</sup>H-<sup>1</sup>H COSY correlations of oleoyl  $\beta$ -D-arabinoside compound 1.2 were depicted in red lines and the <sup>1</sup>H-<sup>13</sup>C HMBC correlations are indicated by each carbon with arrows. The carbons were numbered according to IUPAC-IUB. (Detailed assignment of HMBC correlation is described in Table 3.9).IUPAC-IUB. (Detailed assignment of HMBC correlation is described in Table 3.9).....132
- Figure 3.37:** Overview of a selected <sup>1</sup>H-NMR spectrum of lupeol acetate 1.3 dissolved in CDCl<sub>3</sub> and run at 400 MHz.....136
- Figure 3.38:** Jmod NMR spectrum of lupeol 1.3 (125 MHz, CDCl<sub>3</sub>) of 3.3. The signals at 77 ppm were allocated to the CDCl<sub>3</sub> solvent. CH<sub>3</sub> and CH are indicated the positive signals, while quaternary carbon and CH<sub>2</sub> are indicated the negative signals.....137
- Figure 4.1:** Fractionation scheme for crude ethyl acetate *F. carica* endocarp extract (2 g). Boxes highlighted in yellow were neglected for further analysis due to their low yield.....141
- Figure 4.2:** Chromatogram obtained in the normal phase separation of the dried crude *F. carica* endocarp extract using the REVELERIS® system. Solvent systems: AB = hexane and ethyl acetate, CD = methanol and dichloromethane. UV1 wavelength is at 254 nm represented in blue coloured line, UV2 wavelength is at 280 nm represented in bright purple coloured line and the green coloured line represented the evaporative light scattering detection (ELSD). The X-axis represents the collected fractions across the area of the respective peaks. The highlighted orange and grey represents F14 and F20, respectively..... 142
- Figure 4.3:** TLC on silica gel 60 F254 employing different mixtures of hexane and ethyl acetate or dichloromethane and methanol as mobile phase. Detection was achieved under short UV-250 nm spots drawn in a soft black circle, while under long UV365 nm, spots were drawn in the same colour as the spots were observed. Spots visualised by spraying with anisaldehyde-sulfuric acid were indicated by charred colours. Blue arrows indicated the two target compounds from the bioactive fractions F14 and F20.....144
- Figure 4.4:** Stacked <sup>1</sup>H-NMR spectra of bioactive fractions from *F. carica* endocarp. Shown from the bottom to the top are F1, F2, F5, F13, F14, F15, F16, F20, F30 and F32. Highlighted with the orange grid indicated the resonances for an aliphatic structure found between  $\geq 1.0$  and 2.5 ppm. The aromatic region is highlighted in grey found between 6.75 and 7.75 ppm, while olefinic peaks resonated between 3 and 5.5 ppm. CDCl<sub>3</sub> appeared at 7.25 ppm, which is highlighted in green. .... 145
- Figure 4.5:** Cell viability test using differentiated SH-SY5Y cells incubated for 72 hours after 24 hours of RA incubation followed by 24 hours treatment with different *F. carica* endocarp fractions at 30  $\mu$ g/mL. Y-axis represents percentage cell viability and X-axis represents the respective fraction number. Results are shown as fluorescence counts using a microplate absorbance/fluorometer plate reader with 1420 Multilabel counter. Twelve fractions afforded cell viability at above 100% in

- red bars. Whereas, seventeen fractions in blue bars have shown viability below 100% of the control that is in black bar. Each group was done in triplicate in a mean 3 SD; ANOVA  $P < 0.05$  compared with control.....146
- Figure 4.6:** F14 and F20 protected differentiated SH-SY5Y cells against the toxicity of acrolein. A) AlamarBlue® assay following exposure to 20  $\mu\text{M}$  acrolein and treatment of differentiated SH-SY5Y cells with F14 and F20. B) Dose-response curves for F14 (blue) and F20 (red) suppressing acrolein-induced oxidative stress related AD; which were detected by alamarBlue® fluorescence and plotted in percentage viability after 24 hours treatment; (each group represents mean 3 SD; ANOVA  $P < 0.001$  compared with control)..... 148
- Figure 4.7:** Quantification of the western blot by densitometry. The bars represent the standard deviation and  $p < 0.01$ . Western blotting image of the total NQO1 protein level (30 kDa) in the presence of acrolein..... 149
- Figure 4.8:** PCA-HCA dendrogram and heat map of chromatographic fractions of the crude ethyl acetate extract of *F. carica* endocarp..... 150
- Figure 4.9:** (A) Unsupervised PCA scores scatter plot for *F. carica* endocarp with 29 fractions; orange irregular circle indicates sugar metabolites, irregular green circles indicate sterol derivatives, violet circle indicates phenol and flavonoid metabolites and black arrows indicate the metabolite of interest. (B) PCA loadings scatter plot indicated the corresponding  $m/z$  features related to the regular and irregular circles. (C) OPLS-DA scores scatter plot resulting from the preliminary bioassay screening with active metabolites labelled in green spots and inactive in blue; green circle is most likely to represent fatty acids and phenols; orange circle is most likely to represent sterols and sugars, while, black spots represent the fractions of interest. (D) OPLS-DA loadings scatter plot indicated the corresponding  $m/z$  features with the isolated metabolites at  $m/z$  168.03 and 414.381..... 152
- Figure 4.10:** Putative discriminatory metabolites were selected using an S-plot..... 153
- Figure 4.11:** A) Structures of non-polar constituents identified from *F. carica* endocarp by GCMS analysis. B) Characteristic fragmentation of a cholesta-3,5-dien-7-one skeleton. Groups I and II was fragmented through ring C to observe  $\text{C}_{12}\text{H}_{14}\text{O}_2^\bullet$  at  $m/z$  174.10, and  $\text{C}_{13}\text{H}_{16}\text{O}_2^\bullet$  at  $m/z$  187. Group III was fragmented at aliphatic chain to yield  $\text{C}_{19}\text{H}_{25}\text{O}^\bullet$  at  $m/z$  269.19. The fragmentation pattern is similar to that earlier described in the literature (Sarwar Alam *et al.*, 1992).....156
- Figure 4.12:** Dereplication of major GCMS. peaks from the NIST library with similarity scores of 27.7% for cholesta-4,6-dien-3-ol 2.3 and 84.5% for stigmasta-3,5-dien-7-one..... 157
- Figure 4.13:** Jmod-NMR spectrum (125 MHz,  $\text{CDCl}_3$ ) of compound 2.1. Positive signals correspond to  $\text{CH}_2$ s, while negative signals correspond to either  $\text{CH}_3$ s, CHs or quaternary-Cs.....158
- Figure 4.14:**  $^1\text{H}$ -NMR spectrum of F20 elucidated as lawsaritol 2.1 in  $\text{CDCl}_3$  and run at 400 MHz.....159
- Figure 4.15:** 2D  $^1\text{H}$ - $^1\text{H}$  COSY correlations of F20 elucidate as lawsaritol 2.1. .... 160
- Figure 4.16:** HSQC spectrum of F20 elucidated as lawsaritol 2.1 in  $\text{CDCl}_3$  at 500MHz. Blue colour of signals represent either CH,  $\text{CH}_3$  or quaternary-C while the red colour represents  $\text{CH}_2$ ..... 161
- Figure 4.17:** A)  $^1\text{H}$ - $^{13}\text{C}$ -HMBC spectrum of F20 elucidated as lawsaritol 2.1 in  $\text{CDCl}_3$  at 500MHz; X-axis represents  $^1\text{H}$ -NMR and y-axis represents Jmod-NMR; horizontal

lines correspond to the carbon number in the structural drawing. B) Expansion of 1H-13C-HMBC spectrum of F20 in the upfield region.....	163
<b>Figure 4.18:</b> The 1H-1H COSY correlations of F20 elucidated as lawsaritol 2.1 were depicted in bold lines and the 1H-13C HMBC correlations are indicated by each carbon with arrows. The carbons were numbered according to IUPAC-IUB. (Detailed assignment of HMBC correlation is presented in Table 4.6).....	164
<b>Figure 4.19:</b> 1H-NMR spectrum of F14 consisting of both <i>P</i> -hydroxy benzoic acid 2.6 and vanillic acid 2.7 dissolved in CDCl <sub>3</sub> and run at 500 MHz.....	169
<b>Figure 4.20:</b> Cosy spectrum for F14 revealing two spin systems; blue line for vanillic acid; and yellow line for <i>P</i> -hydroxybenzoic acid.....	170
<b>Figure 4.21:</b> HSQC spectrum of F14 for <i>P</i> -hydroxybenzoic acid 2.6 and vanillic acid compound 2.7 in CDCl <sub>3</sub> at 500MHz.....	172
<b>Figure 4.22:</b> -HMBC spectrum of F14 for <i>P</i> -hydroxybenzoic acid 2.6 and vanillic acid compound 2.7 in CDCl <sub>3</sub> at 500MHz.....	172
<b>Figure 4.23:</b> The 1H-1H COSY correlations of <i>P</i> -hydroxybenzoic acid 2.6 and vanillic acid compound 2.7 depicted in vibrant blue lines and the 1H-13C HMBC correlations are indicated to their correlation of carbon as each in arrows. ....	172
<b>Figure 5.1:</b> The fractionation scheme for the crude <i>F. carica</i> exocarp (1.74 g) extract affording 21 fractions (green box) .., Further fractionation of the bioactive fractions F2, F3, F4, F15, F18 and F19 yielded an additional of 51 sub-fractions. Fractions in blue coloured boxes were excluded from further work due to their low yield, while the rest of the fractions in red boxes were subjected for further bioassays and elucidation work.....	178
<b>Figure 5.2:</b> Normal phase REVELERIS® flash chromatogram of the crude exocarp extract. The pink, blue, and green lines represented the chromatogram detected by UV1 at 254nm, UV2 at 280nm, and ELSD, respectively. AB indicated the hexane and ethyl acetate mobile phase solvent ratio and CD indicated the dichloromethane and methanol used for gradient elution. The fractions of interest, F2, F3, F4, and F18, which were subjected for further purification work, were highlighted in orange, purple, light blue and red bars, respectively. ....	180
<b>Figure 5.3:</b> Normal phase REVELERIS® flash chromatograms of fractions F2 (A) F3 (B) and F4 (C) employing the ELSD detector as shown by the green peaks. AB indicated gradient elution with hexane and ethyl acetate ratio. The semi-purified sub-fractions of interest, F2.6, F3.8 and F4.9 were highlighted with light blue, purple and orange bars, respectively.....	182
<b>Figure 5.4:</b> Normal phase REVELERIS® flash chromatograms of fractions F15 (A) F18 (B) and F19 (C) employing the ELSD detector as shown by the green peaks. AB indicated the step gradient elution with hexane and ethyl acetate and CD indicated isocratic elution by dichloromethane and methanol. The semi-purified sub-fractions of interest, F15.4, F18.6 and F19.3 were highlighted with red, yellow and brown bars, respectively. ....	183
<b>Figure 5.5:</b> TLC screening of 21 fractions obtained from the crude exocarp extract. Coloured circles, squares and rectangles were allocated to those spots visualised under UV at 365nm. Colours used represent the same colour visualised by 365 nm. Spots detected under 254nm were drawn with a black contour line. <i>P</i> -anisaldehyde/sulfuric acid spray reagent was also used to visualise other secondary metabolites. ....	184

- Figure 5.6:** TLC plates showing the elution of A) F2.6, B) F3.8, and D) F15.4 in 90:10 v/v of ethyl acetate and hexane, represented as semi-brown to brown spots, with the elution of C) F4.9 in a 70:20 v/v ratio of hexane and ethyl acetate, represented as reddish-brown spot, together with E) F18.6 and F) F19.3 in a 70:20 v/v ratio and in a 90:10 v/v ratio of dichloromethane and methanol, respectively after spraying with anisaldehyde-H<sub>2</sub>SO<sub>4</sub> reagent, respectively. .... 185
- Figure 5.7:** Stacked 1H-NMR (400 MHz, CDCl<sub>3</sub>) spectra of bioactive sub-fractions. F2.6, F3.8 and F4.9 presented features of phytosterol derivatives whereas F18.6 displayed features of fatty acid derivatives extracted from *F. carica* exocarp. ....186
- Figure 5.8:** Preliminary cell viability screening of the fractions of *F. carica* exocarp in differentiated SH-SY5Y cells. Viability was displayed by 10 fractions with values higher than 100% (red), while 10 fractions lacked viability, with values of equally or less than 100% (blue); the control (100%) is shown in black. Every group constituted a mean of 3 SDs, and ANOVA was significant ( $P < 0.001$ ) by comparison to the control. ....187
- Figure 5.9:** Preliminary cell viability screening of the sub-fractions of *F. carica* exocarp in differentiated SH-SY5Y cells. Viability was displayed by 19 fractions with values greater than 100% (red), while seven fractions lacked viability, with values of less than 100% (blue); the control (100%) is shown in black. Every group constituted a mean of 3 SDs, and ANOVA was significant at  $P < 0.001$  by comparison to the control. Highlighted in yellow are the most bioactive fractions.....188
- Figure 5.10:** The cytotoxicity of bioactive fractions. (A) Acrolein cytotoxicity on cell viability; (B) EC<sub>50</sub> calculation for F2.6, F3.8, F4.9 and F18.6, based on the dose-response curve. The AlamarBlue® assay was used to analyse the cell viability, with the significance of confidence intervals at 95%, and values representing the means of  $n = 3 \pm \text{SEM}$ .....189
- Figure 5.11:** Effect of F2.6 F3.8 and F4.9 on differentiated SH-SY5Y cell line in the level of NQO1 protein in the presence of acrolein after 24 hours prior to 6 hours incubation with 20  $\mu\text{M}$  acrolein. The control was an untreated differentiated SH-SY5Y cell. Cell lysates were then carried out to western blot analysis with antibody against NQO1. Protein levels were normalised to total protein level of B-actin and expressed relative to the corresponding value of the control. Results were plotted as mean $\pm$ SD from three experiments and P value showed significance as  $P < 0.05$  vs control in one-way ANOVA test..... 192
- Figure 5.12:** HCA dendrogram determined by Ward's linkage technique, showing the suggested four group of clusters, based on their metabolite similarities. HCA dendrogram were correlated through the linkage of a statistical heatmap..... 193
- Figure 5.13:** A) PCA scores scatter plot of mass spectral data shows the exocarp fractions grouped based on similarity of their metabolites. B) PCA loadings scatter plot of shows the m/z values of the grouped metabolites encircled in blue, red, yellow, and green. C) OPLS-DA scores scatter plot shows the active fractions denoted in green versus inactive fractions denoted in blue against oxidative stress related AD prevention. D) OPLS-DA loadings scatter plot shows the distribution of metabolites in m/z between active versus inactive groups.....195

<b>Figure 5.14:</b> S-plot generated from the OPLS-DA model shows the end point compounds of <i>F. carica</i> exocarp fractions that are the predicted metabolites responsible for the bioactivity encircled in red. Identity of the metabolites listed in Table 5.3. ....	196
<b>Figure 5.15:</b> HCA dendrogram determined by Ward's linkage, showing the suggested five clusters, based on metabolite similarities. ....	198
<b>Figure 5.16:</b> A) PCA scores plot of mass spectral data indicating three chemical groups; B) PCA loadings plot via m/z values; C) OPLS-DA scores plot to discriminate the active versus the inactive metabolites against oxidative stress in AD prevention; D) OPLS-DA loadings plot via m/z values determining the bioactive target metabolites at m/z 401[M+H] and 469 [M+H]. ....	199
<b>Figure 5.17:</b> A) OPLS-DA S-plot analysis of the putative bioactive metabolites in <i>F. carica</i> exocarp fractions corresponding to the analysis of, values of m/z 401.341 and m/z 469.331 were determined as the putative molecular biomarkers against oxidative stress related AD prevention. B) Expansion of S-Plot quadrant showing the predicted bioactive metabolites in <i>F. carica</i> exocarp fractions, values of m/z 469.404. ....	200
<b>Figure 5.18:</b> Stacked <sup>13</sup> C-Dept and Jmod NMR spectra (125 MHz, CDCl <sub>3</sub> ) illustrated the similarities between fractions of F2.6 exocarp and F3/5 mesocarp. F3.8 exocarp presented similar signals to F3/5 mesocarp as well, indicating the presence of lupeol acetate. The numbers in green correspond to the carbon signals of the lupeol acetate. ....	204
<b>Figure 5.19:</b> <sup>1</sup> H-NMR spectrum of β-amyrin acetate 3.1 in CDCl <sub>3</sub> at 400 MHz. ....	205
<b>Figure 5.20:</b> Expansion of the upfield region <sup>1</sup> H-NMR spectrum of β-amyrin acetate 3.1 in CDCl <sub>3</sub> at 400 MHz. ....	206
<b>Figure 5.21:</b> 2D-COSY of compound 3.1 exhibited proton correlations between H-3 and H-2 (blue line); between H-9, H-11, and H-12 (orange line); and between H-18 and H-19 (violet line). Cross peak lines shown in green were allocated to their corresponding proton signals. ....	207
<b>Figure 5.22:</b> A) <sup>13</sup> C-NMR of 3.1 and B) Jmod-NMR spectrum (125 MHz, CDCl <sub>3</sub> ) of 3.1. ....	208
<b>Figure 5.23:</b> A) <sup>1</sup> H- <sup>13</sup> C HSQC NMR spectrum of [3.1] highlighting the cross peaks positions 3 and C-12. B) The expansion of the <sup>1</sup> H- <sup>13</sup> C HSQC NMR spectrum showing the allocation of methyl group signals. ....	210
<b>Figure 5.24:</b> The <sup>1</sup> H- <sup>13</sup> C-HMBC spectrum in CDCl <sub>3</sub> at 500MHz of β-amyrin acetate 3.1 are indicated by the horizontal green lines; The presence of lupeol acetate 3.2 are indicated by the yellow lines. ....	211
<b>Figure 5.25:</b> Representative <sup>1</sup> H- <sup>1</sup> H-COSY and <sup>1</sup> H- <sup>13</sup> C-HMBC correlations of 3.1; the <sup>1</sup> H- <sup>1</sup> H-COSY correlation and the <sup>1</sup> H- <sup>13</sup> C-HMBC correlation are respectively indicated by the red lines, and multi-coloured arrows, respectively. ....	211
<b>Figure 5.26:</b> <sup>1</sup> H-NMR spectrum of campesterol 3.3 (500 MHz, CDCl <sub>3</sub> ), with an expansion of the <sup>1</sup> H-NMR spectrum between 0.66 to 1.06 ppm. ....	216
<b>Figure 5.27:</b> Jmod-NMR spectrum (125 MHz, CDCl <sub>3</sub> ) of 3.3. The signals at 77 ppm were allocated to the CDCl <sub>3</sub> solvent. CH <sub>3</sub> and CH constituted the negative signals, whereas quaternary carbon and CH <sub>2</sub> are indicated by the positive signals. ....	217
<b>Figure 5.28:</b> <sup>1</sup> H- <sup>1</sup> H-COSY spectrum of 3.3. Their chemical shift within the campesterol structure is denoted by the green lines. ....	218
<b>Figure 5.29:</b> <sup>1</sup> H- <sup>13</sup> C-HMBC spectrum of 3.3 in CDCl <sub>3</sub> at 500MHz. ....	219

<b>Figure 5.30:</b> Characteristic <sup>1</sup> H- <sup>1</sup> H-COSY and <sup>1</sup> H- <sup>13</sup> C-HMBC correlations of compound 3.3.....	219
<b>Figure 6.1:</b> Possible resonance structures of 2.7 phenoxy radical. Free radical initiation occurs at the 4-hydroxyl group by abstraction of hydroxyl H-atom; possible free radical initiation at carboxylic group is conceivable. ....	231
<b>Figure 6.2:</b> Chemical structure of ferulic acid and vanillic acid; both possess the same functionality with the additional of double bond in the aliphatic chain of ferulic acid (red colour). ....	232
<b>Figure 6.3:</b> The effect of lipophilicity on penetrating BBB (Di and Kerns, 2016).....	237
<b>Figure 6.4:</b> Biosynthesis pathway of vanillic acid and parahydroxybenzoic acid via the shikimate pathway (Ni <i>et al.</i> , 2015).....	238
<b>Figure 6.5:</b> Biosynthesis of phytosterols via the MVA pathway (Hartmann, 1998; Springob and Kutchan, 2009).....	239
<b>Figure 6.6:</b> Fatty acid biosynthesis. ACC: Acetyl-CoA carboxylase (Chow, 2008)..	239
<b>Figure 6.7:</b> A general scheme protocol for drug discovery and development from NP (F. carica) using HTS.....	241

## List of Tables

---

<b>Table 1.1:</b> Chemical compositions that have been isolated from <i>F. carica</i> .....	8
<b>Table 1.2:</b> AChE drugs in clinical development for AD, including European registration (Francis <i>et al.</i> , 1999; Jann, 2000; Mohan and Gupta, 2016; Mount and Downton, 2006; Nordberg and Svensson, 1998).....	35
<b>Table 1.3:</b> mABs drugs from Immunoglobulin G (IgG) isotope in clinical development for AD.....	40
<b>Table 1.4:</b> Gamma secretase inhibitors - clinical trial drugs that target A $\beta$ clearance. .	42
<b>Table 1.5:</b> Short summary of clinical trial compounds, listing the pharmaceutical company, the chemical structure, and their current progress status. ....	45
<b>Table 1.6:</b> Natural Compounds with protective effect against A $\beta$ .....	48
<b>Table 2.1:</b> The measurements for preparing transfer buffer.....	76
<b>Table 2.2:</b> The measurements for the resolving gel chemicals and buffers.....	78
<b>Table 2.3:</b> The measurements for the stacking gel chemicals and buffers.....	78
<b>Table 3.1:</b> Chromatographic conditions employed for the purification of the crude <i>F. carica</i> mesocarp via flash chromatography by gradient elution 147.66 min and isocratic elution 68.30 min. EtOAc, MeOH and DCM represent ethyl acetate, methanol and dichloromethane, respectively.....	84
<b>Table 3.2:</b> REVELERIS <sup>®</sup> flash chromatography system conditions for pooled fractions F4,5,6 and F12,14. ....	87
<b>Table 3.3:</b> Antioxidant activities vs differentiated SH-SY5Y cell line of the identified fractions of the mesocarp <i>F. carica</i> ; values were expressed in triplicate. ....	103
<b>Table 3.4:</b> Dereplication of the discriminatory metabolites from DNP 2015 database from the active fractions against oxidative stress related AD prevention obtained from the S-plot in Figure 3.22 and 3.23.....	110
<b>Table 3.5:</b> Dereplication of F4,5,6/F9 and F12,14/F9 from DNP 2015 database.....	114
<b>Table 3.6:</b> Physical properties of F4,5,6/F9 of <i>F. carica</i> mesocarp.....	115
<b>Table 3.7:</b> Carbon and proton assignments for $\gamma$ -sitosterol 1.1 <sup>13</sup> C- <sup>1</sup> H cross-signals in the HMBC spectra. <sup>13</sup> C-NMR (100 MHz, CDCl <sub>3</sub> ) and <sup>1</sup> H-NMR (400 MHz) are compared with the corresponding articles in CDCl <sub>3</sub> . ....	122
<b>Table 3.8:</b> Physical properties of F12,14/F8 and F12,14/F9 of <i>F. carica</i> mesocarp.....	123
<b>Table 3.9:</b> Carbon and proton assignments for oleoyl $\beta$ -D-arabinoside 1.2 <sup>13</sup> C- <sup>1</sup> H cross-signals in the HMBC spectra. <sup>13</sup> C-NMR (125 MHz, aceton-d <sub>6</sub> ) and <sup>1</sup> H-NMR (400 MHz) are compared with the corresponding articles in CDCl <sub>3</sub> .....	133
<b>Table 3.10:</b> Physical properties of F4,5,6/F1/F5 of <i>F. carica</i> mesocarp. ....	133
<b>Table 3.11:</b> <sup>1</sup> H-NMR (500 MHz), Jmod-NMR (125 MHz) data of lupeol acetate 1.3 in CDCl <sub>3</sub> correlated with the literature in CDCl <sub>3</sub> .....	138
<b>Table 4.1:</b> Step gradient protocol for normal phase chromatography of the <i>F. carica</i> endocarp crude extract. Mobile phase A:B=Hexane:Ethyl acetate, C:D= Methanol:Dichloromethane. ....	140
<b>Table 4.2:</b> The chromatographic conditions for crude ethyl acetate endocarp extract was fractionated via REVELERIS <sup>®</sup> flash chromatography system (Grace Davison Discovery Sciences, USA).....	140
<b>Table 4.3:</b> Antioxidant activities of the F14 and F20 from <i>F. carica</i> endocarp vs acrolein induced oxidative stress in differentiated SH-SY5Y cell line; values were indicated	

in triplicate. F20 represents compound and F14 represents a mixture of two compounds.....	148
<b>Table 4.4:</b> Discriminatory metabolites deduced from the active fractions obtained from the S-plot “end point” data shown in Figure 4.12. Dereplication was accomplished from the DNP 2015 database. (P indicated positive mode, N indicated negative mode). Highlighted row represent isolated compounds in this study.....	153
<b>Table 4.5:</b> F20 of <i>F. carica</i> endocarp. Description of lawsaritol 2.1; chemical structure; LC-MS analysis, and the identification of GCMS.....	155
<b>Table 4.6:</b> Compound 2.1; <sup>1</sup> H-NMR (500 MHz) including integral, coupling constant and multiplicity, Jmod-NMR (125 MHz), HSQC data and HMBC correlation of lawsaritol and correlated literature at <sup>1</sup> H-NMR, 400MHz in CDCl <sub>3</sub> and <sup>13</sup> C-NMR (100 MHz).....	165
<b>Table 4.7:</b> Semi-pure F14 fraction of <i>F. carica</i> endocarp; <i>P</i> -hydroxybenzoic acid 2.6 and vanillic acid 2.7; chemical configurations; LCMS detection of 2.7 at Rt run 7.29 min. ....	166
<b>Table 4.8:</b> Compounds 2.6; <sup>1</sup> H-NMR (500 MHz), including integral, coupling constant and multiplicity, HSQC and HMBC correlation of 2.6 and 2.7 exhibited consistency with previous studies. <sup>1</sup> H-NMR was recorded at 400MHz in CDCl <sub>3</sub> and HSQC and HMBC at 500 MHz.....	173
<b>Table 4.9:</b> Compounds 2.7; <sup>1</sup> H-NMR (500 MHz), including integral, coupling constant and multiplicity, HSQC and HMBC correlation of 2.7 exhibited consistency with previous studies.....	174
<b>Table 5.1:</b> Chromatographic conditions employed for the purification of the crude and sub-fractions of the exocarp, via the REVELERIS <sup>®</sup> flash chromatography system (Grace Davison Discovery Sciences, USA). EtOAc, MeOH and DCM represent ethyl acetate, methanol and dichloromethane, respectively. ....	177
<b>Table 5.2:</b> The capability of <i>F. carica</i> exocarp metabolites to protect against oxidative stress caused by acrolein in a differentiated SH-SY5Y cell line. The values were verified thrice.....	190
<b>Table 5.3:</b> The dereplication list of unique metabolites using macro DNP 2015 database from the active fractions against oxidative stress related AD prevention obtained from the S-plot “end point” data shown in Figure 5.17. (P indicated positive mode). Highlighted rows represented the isolated compounds.....	196
<b>Table 5.4:</b> Semi-pure F2.6 fraction of <i>F. carica</i> exocarp; characterisation of β-amyryn acetate 3.1 and lupeol acetate 3.2; chemical configurations; LCMS detection of 3.1; and GCMS of 3.1 at Rt run 20.55 min.....	201
<b>Table 5.5:</b> Full carbon and proton assignments for β-amyryn acetate 3.1 <sup>13</sup> C- <sup>1</sup> H cross-signals in the HSQC and HMBC spectra. <sup>13</sup> C-NMR (125 MHz, CDCl <sub>3</sub> ) and <sup>1</sup> H-NMR (400 MHz, CDCl <sub>3</sub> ) are compared with the corresponding articles in CDCl <sub>3</sub> . ....	212
<b>Table 5.6:</b> F4.9 of <i>F. carica</i> exocarp. Description of campesterol 3.3; chemical structure; LC-MS analysis, and the identification of GCMS.....	213
<b>Table 5.7:</b> Compound 3.3; <sup>1</sup> H-NMR (500 MHz), including integral, coupling constant and multiplicity, Jmod-NMR (125 MHz) and HMBC correlation of 3.3 exhibited consistency with previous studies. <sup>1</sup> H-NMR was recorded at 600MHz in CDCl <sub>3</sub> and <sup>13</sup> C-NMR at 150 MHz). ....	220

## List of abbreviations

Ab	Anti-body/ Anti-bodies
AChE	Acetylcholinesterase
Acr	Acrolein
ACSL	acyl-CoA synthetase
AD	Alzheimer disease
ADAS-Cog	Alzheimer's Disease Assessment Scale-cognitive subscale
ALA	$\alpha$ -Linolenic acid
ALT	Alanine Aminotransferase
APH-1	Anterior pharynx-defective 1
API	Alzheimer's Prevention Initiative
APS	amonium persulphate
AREDS	Age-related eye disease study
ATP	Adenosine Triphosphate
<i>B. cereus</i>	<i>Bacillus cereus</i>
<i>B. subtilis</i>	<i>Bacillus subtilis</i>
BACE-1	Beta-site APP cleaving enzyme-1 Beta-secretase 1
BBB	Blood brain barrier
BDNF	Brain-derived neurotrophic factor
BuChE	Butyrylcholinesterase
<i>C. Albicans</i>	<i>Candida Albicans</i>
<i>C. violaceum</i>	<i>Chromobacterium violaceum</i>
CAT	Catalase
CDDO	2-cyano-3,12-dioxooleana-1,9-dien-28-oic acid
CDDO-MA	2-cyano-3,12-dioxooleana-1,9-dien-28-oic acid methyl amine
CHF	Congestive heart failures
CNS	Central nervous system
Cosy	correlation spectroscopy
CpHV-1	Caprine Herpesvirus 1
CREB	cAMP-response element binding protein
D3T	3H-1, 2-dithiole-3-thione
DHA	Docosahexaenoic acid
DMSO	Dimethyl sulfoxide
DNP	Dictionary of Natural Products
DOU	Degree of unsaturation
DPPH	1,1-Diphenyl-2-picrylhydrazyl radical, 2,2-Diphenyl-1-(2,4,6-trinitrophenyl) hydrazyl
<i>E. coli</i>	<i>Escherichia coli</i>
ECL	Enhanced Chemiluminescence Luminol
EEG	Electroencephalogram
EGCG	epigallocatechin 3- gallate
ELSD	evaporative light scattering detection
EPA	Eicosapentaenoic acid
ESI	Electrospray ionisation
<i>F. carica</i>	<i>Ficus carica L.</i>

<i>F. columnare</i>	<i>Flavobacterium columnare</i>
<i>F. oxysporum</i>	<i>Fusarium oxysporum</i>
FA	Fatty acid
FABPs	Fatty acid-binding proteins
FCV	Feline calicivirus
FDA	Food and Drug Administration
GC	Gas chromatography
GCL	Glutamine cysteine ligase
GCS	Glutamine cysteine synthase
GPx	Glutathione peroxidase
GR	Glutathione reductase
GR	Glutathione reductase
GSH	Glutathione
GSK-3 $\beta$	Glycogen synthase kinase 3 $\beta$
GST	Glutathione S-transferase
HCA	Hierarchical clustering analysis
HDL-SR-B1	High-density lipoprotein-SR-B1
HMBC	Heteronuclear Multiple Bond Correlation
HNE	4-hydroxy-2-nonenal
Hsp	Heat shock protein
HSQC	heteronuclear single quantum correlation
HTS	High-Throughput Screening
IgG	Immunoglobulin G
Keap1	Kelch-like ECH associated protein 1
<i>L. monocytogenes</i>	<i>Listeria monocytogenes</i>
LC-MS	Liquid chromatography-Mass spectroscopy
LDL	low-density lipoprotein
LNA	Linoleic acid
L-NBP	L-3-n-butylphthalide
<i>M. tuberculosis</i>	<i>Mycobacterium tuberculosis</i>
mABs	Monoclonal Antibodies
MAPK	Mitogen-activated protein kinase
mCI	mean Cultural Importance
MDA	Malondialdehyde
MMSE	MiniMental Status Examination
MNV	Murine norovirus
MPTP	1-methyl-4-phenyl-1,2,3,6-tetrahydropyridine
MW	Molecular weight
NCSTN	Nicastrin
NF- $\kappa$ B	Nuclear factor- $\kappa$ B
NGF	Nerve growth factor
NICE	National Institute for Health and Care Excellence
NMDA	Nmethyl-D-aspartate
NMR	Nuclear magnetic resonance spectroscopy
NO	Nitric oxide
NPs	Natural products

NQO1	NAD(P)H dehydrogenase(quinone 1)
Nrf2	Nuclear factor erythroid 2–related factor 2
Nrf2/ARE	The transcription factor (Nrf2) / antioxidant responsive element (ARE)
OH-1	Heme oxygenase-1
OPLS-DA	Orthogonal Partial Least Square-Discriminant Analysis
OS	Oxidative stress
<i>P. aeruginosa</i>	<i>Pseudomonas aeruginosa</i>
PCA	Principal Component Analysis
PC-Acr	protein-conjugated acrolein
PD	Parkinson's disease
PD	Parkinson's disease
PEN-1	Presenilin
PEN-2	Presenilin enhancer 2
PLS-DA	Partial Least Square-Discriminant Analysis
Prdx	Peroxiredoxin
PUFAs	Polyunsaturated fatty acids
RA	Retenoic acid
R <sub>f</sub>	Retardation factor
rt	Retention time
<i>S. aureus</i>	<i>Staphylococcus aureus</i>
<i>S. cerevisiae</i>	<i>Staphylococcus cerevisiae</i>
SE	Standard Error
SIMCA	Soft Independent Modeling of Class Analogies
SOD	Superoxide dismutase
spp	Species
Srx	Sulfaredoxin
SUVR	standardized uptake value ratio
TBS	Tris-buffered saline
TCM	Traditional Chinese Medicine
TEMED	N'-N' tetramethylethylene-diamine
TLC	Thin layer chromatography
Trx	Thioredoxin
UPS	Ubiquitin-proteasome system
UV	Ultra violet
VA	Vanillic acid
WB	Western blotting
WHO	World Health Organization

## List of symbols and synonyms

&	And
$\cong$	Approximately or around
$\geq$	Equal or larger than
$\mu\text{g}$	Microgram
$\mu\text{M}$	Micromolar
1D	One dimension
$^1\text{H}$ - $^{13}\text{C}$	Proton- carbon
$^1\text{H}$ - $^1\text{H}$	Proton-proton
$^1\text{H}$ -NMR	Proton- Nuclear magnetic resonance spectroscopy
2D	Two dimension
A.D.	Anno Domini
B.C.	Before Christ
br	Broad
br s	Broad singlet
C	Carbon
C=C	Double bond
C=O	Carbonyl group
C32	Human amelanotic melanoma cell line
Ca	Calcium
$\text{CD}_3\text{OD}$	Methanol- $\text{d}^4$
$\text{CDCl}_3$	Chloroform- $\text{d}$
$\text{CH}_3\text{=O}$	Methoxy group
d	Doublet
D	Dextro
DCM	Dichloromethane
dd	Doublet of doublet
Di	Two
SH-SY5Y	Human neuroblastoma cell line
dq	Doublet of quartet
dt	Doublet of triplet
EtOAc	Ethyl acetate
h	Hours
H	Hydrogen
$\text{H}_2\text{O}_2$	Hydrogen peroxidase
HepG-2	Human hepatocellular carcinoma cell line
Hex	Hexane
HT22	Immortalized mouse hippocampal neuronal cell line
MHz	Hertz
$\text{IC}_{50}$	Growth Inhibition
J	Coupling constant
K	Potassium
L	Litre
L(-)	Levo
m	Meter

m	Multiplet
$m/z$	Mass/charge number of ion
MCF-7	Human breast adenocarcinoma cell line
Me	Methyl
MeOH	Methanol
MHz	Megahertz
mL	Millilitre
Mono	Single
Mwt	Molecular Weight
n	Replicate of number
Neuro-2A	Human neuroblastoma cell line
nm	Nanometer
NO·	Nitric monoxide
O	Oxygen
O <sup>-2</sup>	Superoxide
OH	Hydroxyl group
OH·	Hydroxyl radical
ONOO <sup>-</sup>	peroxynitrite
<i>p</i>	Pentet
<i>P</i> -	Para
q	Quartet
s	Singlet
t	Triplet
T98G	Human Glioblastoma multiforme cell line
U-138 MG	Human Glioblastoma multiforme cell line
U2OS	Human osteosarcoma cell line
U-87 MG	Human Glioblastoma multiforme cell line
v/v	Volume per volume
WEHI-164	Mouse fibro sarcoma
Wnt	One of the signalling transduct pathways
$\alpha$	Alfa
$\beta$	Betta
$\gamma$	Gamma

## Published work

---

Khojah, H & Edrada-Ebel, R. (2017), 'P43 The isolation and purification of bioactive metabolites from *Ficus carica* and their neuroprotective effects in Alzheimer's disease' *Biochemical Pharmacology*, vol 139, no. Supplement C, pp. 140. DOI: [10.1016/j.bcp.2017.06.044](https://doi.org/10.1016/j.bcp.2017.06.044)

Khojah, H & Edrada-Ebel, R. (2016), 'Identification of Bioactive Metabolites from *Ficus carica* and Their Neuroprotective Effects of Alzheimer's Disease', *World Academy of Science, Engineering and Technology, International Science Index, Medical and Health Sciences*, 3(2), 2158.

## Abstract

---

Alzheimer's disease (AD) is a progressive neurodegenerative disorder. Evidence has shown that a key feature of AD is increased brain oxidative stress. This oxidative damage causes the formation of reactive oxygen species (ROS), leading to the expression of endogenous anti-oxidant proteins such as NAD(P)H dehydrogenase (quinone 1) (NQO1) and to the production of A $\beta$  peptides and thereafter to neuronal death. The current drug treatments available for the treatment of AD cause various severe side effects. Therefore, herbal therapies should be considered as alternative/complementary medicines to existing therapeutic approaches due to its traditional used and its richness of anti-oxidant constituents (Wightman, 2017).

The fig (*Ficus carica* L., or *F. carica*) is a classic fruit tree associated with the beginning of horticulture in the Mediterranean region. Middle Eastern countries in particular have been an important centre of fig growth for centuries (Khedr *et al.*, 2016). Few studies have focused on *F. carica* in the treatment of AD; however, this edible fruit has been shown to be effective in managing the disease (Ango *et al.*, 2016; Bhangale and Acharya, 2016; Essa *et al.*, 2015).

In this study, metabolite profiling was performed on the exocarp, endocarp, and mesocarp of *F. carica*'s fruit via high throughput screening (HTS) (namely metabolomics). The secondary metabolites of these parts were extracted using TLC and Flash<sup>®</sup> chromatography. The secondary metabolites were then screened and their putative biomarkers targeted through a multivariate analysis conducted using SIMCA-P, including dereplication, HCA, PCA, OPLS-DA, and S-plot analysis. No higher molecular ion peaks ( $m/z$ ) were detected. Moreover, the isolation and structural identification of phytosterols (namely  $\gamma$ -Sitosterol, lupeol acetate) and unsaturated fatty acid (Oleioyl- $\beta$ -D-arabinoside) from the mesocarp, and polyphenols (namely *P*-hydroxybenzoic acid and vanillic acid) and triterpene (namely lawsaritol) from the endocarp of *F. carica* were carried out. As well as the isolation and structural elucidation of  $\beta$ -amyryn acetate and campesterol from the fruit's exocarp. The structures of these compounds were verified using various spectroscopic methods, including HRESIMS, GC-MS, and NMR spectroscopy.

The cell viability test, cytotoxic activities as well as the qualitative western blotting test with the anti-oxidant NQO1 anti-body of the isolated compounds were evaluated, and

exhibited activity that mitigated the oxidative stress of acrolein-related AD in *in-vitro* differentiated SH-SY5Y neuro-cell line. These findings introduced the potential of using phytosterol as a therapeutic intervention in AD in addition to other protective agents. This is the first study to implement metabolomics on the chemical composition and biological potential of *F. carica* parts.

## **CHAPTER ONE INTRODUCTION**

---

## 1. Introduction

---

### 1.1. Natural product and drug discovery

Natural products (NPs) are bioactive chemical compounds that are found in nature, produced by a living organism, and consist of small molecules also known as secondary metabolites<sup>1</sup> (Krause and Tobi, 2013). NPs play a central role in the pharmaceutical, nutraceutical, and cosmeceutical industries (Eugster *et al.*, 2014; Krause and Tobi, 2013; Lahlou, 2013). As NPs have been closely linked to the use of traditional medicine (Butler, 2004), they have received a great deal of attention from both health professionals and the public in terms of their ability to improve overall well-being. NPs are also known for their significant contribution as a sole means to treat injuries in their biological source, as well as their use in the prevention of diseases, such as cardiovascular disease, diabetes, cancer and neurodegenerative disease (Mata *et al.*, 2016).

NPs, including fruits and vegetables, have been recognised as valuable sources of bioactive polyphenolic compounds that must be consumed on a daily basis throughout one's lifetime, and they are expected to contribute to the discovery of new therapeutic agents, as they have guided the development of many of the world's most commonly used drugs (Gosslau *et al.*, 2010). The investigation of NPs as source of novel human therapeutics reached its peak in the western pharmaceutical industry in the 1970s and 1980s, which led to a pharmaceutical landscape influenced by non-synthetic molecules (Koehn and Carter, 2005). The Nobel Prize in Physiology or Medicine that was presented in 2015 highlighted the importance of NPs such as artemisinin<sup>2</sup>, which is now part of standard anti-malarial drugs (Katz and Baltz, 2016).

Additionally, NPs provide important clues to guide the identification and development of synergistic drugs that, so far, research has largely neglected. Most of these drugs are predominantly derived from plants and were medicinally used as therapeutic agents such as salicin from *Salix alba* (white willow); emetine from *Cephaelis ipecacuanha*

---

<sup>1</sup> Secondary metabolites are organic compounds in the correct chiral configuration to exhibit biological activity, but have no 'primary' function that is directly involved in the development of normal growth or reproduction of an organism (Krause and Tobi, 2013).

<sup>2</sup> Artemisinin is structurally isolated from the leaves of the *cinchona* tree native to China, and is a sesquiterpene lactone that bears a peroxide grouping, which its therapeutic actions likely arise from (Klayman, 1985).

(ipecacuanha); strychnine and brucine from *Strychnos nux-vomica* (strychnos); quinine from *Cinchona ledgeriana* (cinchona bark); colchicine from *Colchicum autumnale* (colchicum); caffeine from *Coffea arabica*; nicotine from *Nicotiana tabacum*; atropine from *Atropa belladonna*; and cocaine from *Erythroxylum coca* (Butler, 2004; Ji, Li and Zhang, 2009). Subsequently, NPs have been a constant and rich source of inspiration for analytical and structural chemists to provide the tools for purification and identification of various compounds in their structures, which, in turn, has provided insights into their mechanisms of drug action (Ji, Li and Zhang, 2009).

## 1.2. History of natural product

NPs precede recorded human history, by millennia (Katz and Baltz, 2016). Historically, they have been the most productive source of bioactive compounds and chemical lead structures for the discovery and development of new therapeutic agents (Krause and Tobi, 2013). In ancient times, before the Food and Drug Administration (FDA) existed, civilisations relied on plants and plant extracts to ameliorate illnesses and promote healing (Rahman *et al.*, 2016). Among such treatments clay tablets in cuneiform from *Mesopotamia* (2600 B.C.) reveal the use of oils from *Cupressus sempervirens* (Cypress) and *Commiphora* species (myrrh), which are today still used to treat coughs and colds, and reduce inflammation (Dias *et al.*, 2012).

The *Ebers Papyrus* (2900 B.C.) is an Egyptian pharmaceutical record that contains reports of the usage of over 700 plant-based drugs, including gargles, pills, infusions, and ointments. In addition, the Chinese Materia Medica (1100 B.C.) and the Tang Herbal (659 A.D.) are ancient records of the uses of NPs (Dias *et al.*, 2012). Later, in 1560, cane sugar, starch, camphor, and benzoic acid were structurally isolated (Abbasi *et al.*, 2015). K. W. Scheele (1742–1786) successfully isolated citric, gallic, malic, oxalic, lactic, tartaric and prussic acids, and glycerol from various NPs (Smeaton, 1986). In 1870, Schiff, established the first alkaloid structure derived from *Coniine*<sup>3</sup> (Abbasi *et al.*, 2015).

Another plant with a historical medical use is *Digitalis lanata L.*, which is derived from *foxglove*; in the early years of the 16th century it was used to treat congestive heart failure

---

<sup>3</sup> Coniine is piperidine alkaloids which bears a saturated heterocyclic ring and is known as piperidine in their structure (Diaz, 2015). It is derived from the seed of *Conium maculatum L* (Diaz, 2015).

(CHF) (Krause and Tobi, 2013). On the other hand, bioactive metabolites, such as digitoxin and digoxin, were not utilised until the 1700s and the 1930s, respectively, when they were found to lead to improvement of CHF (Dias *et al.*, 2012; Lahlou, 2013; Patridge *et al.*, 2016; Ward and Pasinetti, 2016).

In 1804, *opium poppy* plants were discovered to manifest anti-analgesic properties when German pharmacist Friedrich Serturmer isolated the active ingredient (morphine) derived from *Papaver somniferum L* (Krause and Tobi, 2013; Patridge *et al.*, 2016). In 1827, morphine was commercialised by Heinrich Merck of the plant alkaloid (Ji, Li and Zhang, 2009; Patridge *et al.*, 2016). However, it wasn't until the 1870s that crude morphine was boiled with acetic anhydride to yield diacetyl-morphine (heroin), which it was discovered could be easily converted to codeine to be used as a narcotic painkiller (Dias *et al.*, 2012; Ward and Pasinetti, 2016).

In 1829, salicin was extracted from white willow (*Salix alba L.*) bark and used as an analgesic (Krause and Tobi, 2013; Shara and Stohs, 2015). The archetypal anti-inflammatory agent currently would likely be acetylsalicylic acid, commonly known as aspirin, which is derived from salicin extract, which was first reported as being used in this way between 1803 and 1838 (Dias *et al.*, 2012; Ward and Pasinetti, 2016). The study of the history of NP continuously expanded throughout the 20<sup>th</sup> century, eventually reaching the study of anti-bacterials, which resulted in the discovery of penicillin, cephalosporins, tetracyclines, aminoglycosides, rifamycin, chloramphenicol, and lipopeptides (Krause and Tobi, 2013).

In the 1950s, scientists further expanded their research to study Caribbean marine sponges, which led to the synthesis of vidarabine as well as cytarabine, and clinical approval was eventually received for their therapeutic use in treating viral diseases and cancer, respectively (Krause and Tobi, 2013). In the 1970s, paclitaxel, isolated from Yew tree, and commercially known as Taxol, was the most commonly used anti-cancer drug, but due to commercial barriers to producing sufficient quantities of Taxol, it was only distributed until late 1992 (Krause and Tobi, 2013).

Between 1981s and 2010s, 34% of the drugs approved by the FDA were based on small-molecule NPs and their derivatives (Harvey *et al.*, 2015; Han *et al.*, 2016). Between the

1999s and 2013, the FDA approved 28% of 31 drugs among those 112 of the FDA-approved drugs, as illustrated in the pie chart below in Figure 1.1, although the proportions of the three different FDA-approved drug categories varied (Ding *et al.*, 2016). 547 of NPs and their derivatives were FDA-approved drugs by the end of 2013, representing more than a third (38%) of all FDA-approved drugs (Patridge *et al.*, 2016).

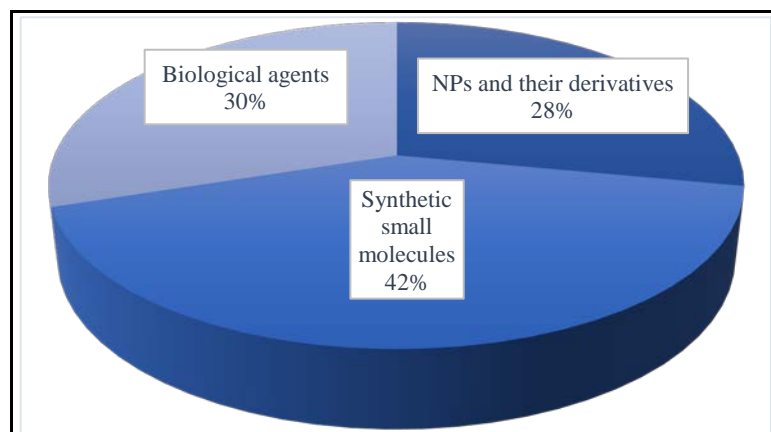


**Figure 1.3.11:** A detailed analysis of the 112 FDA-approved drugs between 1999 and 2013 reveals that 28% of those (31 drugs) were derived from NPs and their derivatives, in comparison to 42% (47 drugs) that were synthetic small molecules, and 30% (34 drugs) that were biological agents. Figure adapted from Ding *et al.* (2016).

It is clear that, throughout the 20<sup>th</sup> century, FDA approval was recognised, as NPs are better in terms of characterisation, although some remain as complex mixtures, including *Veratrum viride* root, *ergoloid mesylates* and *sinecatechins* plants (Patridge *et al.*, 2016). In spite of the complexity of some plant types, the World Health Organisation (WHO) documented that between 70-80% of the population in developing countries still relies on herbal medicines, including plants and plant extracts, as their primary healthcare in order to ameliorate illnesses and promote healing (Rahman *et al.*, 2016; Panday and Rauniar, 2016).

In the new, modern era, the attention of NP researchers has turned to a variety of lead micro-molecule<sup>4</sup> structures and their interaction within biological macro-molecule<sup>5</sup>

---

<sup>4</sup> Micromolecules are structures that possess small molecular weight (MW), such as sugars, phenols, cinnamic, hydroxytyrosol, gallic, and caffeic acid, cinnamic acid derivatives, flavonoids, and anthocyanins (Galanakis, 2015).

<sup>5</sup> A macromolecule has been defined by Dias (2013) as “a very large molecule, such as a polymer or protein, consisting of many smaller structural units linked together.”

activities (Lahlou, 2013; Abbasi et al., 2015). Therefore, there is no doubt that NPs, particularly those from plants have historically been, and will continue to be, vital sources of new pharmaceutical compounds.

### 1.3. Characterisation of *Ficus carica* L.

*Ficus carica* L. (*F. carica*), also known as the common fig, cultivated fig, edible fig, and wild fig, is considered to belong to one of the largest genera of flowering plants (Lim, 2012; Umerie, 2004). They normally occur as swollen, young twigs that are glabrous or softly hairy with urn-shaped receptacles or pyriform-obovoid, which simultaneously present an enclosed inflorescence and *syconia*<sup>6</sup> or edible fruit (Abbasi et al., 2015; Galil and Meiri, 2006). In general, the *Ficus* species were associated as hemi-epiphytes, which is a group of strangling or hispid and large woody climbers or trees that can be found axially or on a trunk, (Dominy et al., 2016). In particular, *F. carica* is a deciduous shrub or tree reaching between 4-6 metres in height, with silvery-grey and smooth bark (Crivellaro and Schweingruber, 2013; El-Sakhawy et al., 2016; Nautiyal, Bhaskar and Khan, 2015).

Moreover, *F. carica* is considered amongst the 37 genera under the Moraceae family, a taxon that can withstand any tropical or semi-tropical lowland rainforest climate, including moist, dry, cold cave or rocky sites, or even close to streams (Chen et al., 2015). *F. carica* releases a rich, sticky white latex when cut, and induces a complex and volatile olfactory response; it includes a combination of external plant pigments, graded from yellowish to brownish violet, by which it relies on the composition of anthocyanin synthesis along with the potential integration of tannins (Bhatt et al., 2016; Cao et al., 2016; Giblin-Davis et al., 1995; Ramawat et al., 2014).

The genus *Ficus* comprises of approximately 800 fig species, which are scattered throughout the world, including in Europe, India, Afghanistan, Russia, Iran, the Far East and Africa. Although *F. carica* is most commonly found in the Middle East, where it was described to be the first plant to be cultivated by humans, for over 11,000 years (Barolo, et al., 2014; Chen et al., 2016).

---

<sup>6</sup> *Syconia* is a modern Latin word from Greek, and has been defined by Gray (1880) as resulting “from a multitude of flowers concealed in a hollow flower-stalk, which becomes pulpy and edible when ripe.”

The use of *F. carica* dates back to ancient times, where its importance have been mentioned in the Bible, the Gospels, and named in the Holy Qura'an as "Teen" (Ali *et al.*, 2015). There is also evidence of the use of *F. carica* in Ayurvedic<sup>7</sup> and Traditional Chinese Medicine (TCM) (Uddin, 2013).

A study using a statistical method, graded from 0.0 to 3.0 by mean cultural importance (mCI), has been reported that *F. carica* was the most cited species of above 2.5 mCI. *F. carica* is among the top ten species of wild edible fruits across five localities in the Lesser Himalayas, namely the Margalla Hills, Haripur, Abbottabad and Murree (Abbasi *et al.*, 2015). These included *Ficus palmata*, *Bauhinia variegata*, *Solanum nigrum*, *Amaranthus viridis*, *Medicago polymorpha*, *Chenopodium album*, *Cichorium intybus*, *Amaranthus hybridus*, and *Vicia faba*, .

Nevertheless, this statistical review was considered reliable as *F. carica* is traditionally known as source of food, medicine, fodder, and wood for fuel, construction, sheltering, and fencing (Abbasi *et al.*, 2015; El-Sakhawy *et al.*, 2016). In addition, it is also an excellent source of vitamin A and B complex, as well as a significant source of iron, magnesium (Mg), calcium (Ca), potassium (K), protein, fat, and fibre (Kristbergsson and Ötles, 2016; Weli, Al-Blushi and Hossain, 2015). *F. carica* is nutritionally awarded by its potentially high Ca concentration at 235 mg/100 g fruit, (Kristbergsson and Ötles, 2016). It has been reported to contain 67.6% protein and 30% iron estimated in 100g of fruit (Weli *et al.* 2015 and Khan *et al.* 2014).

### **1.3.1 Overview of the biomedical uses of *F. carica***

There have been many studies examining the contemporary ethno-biomedical uses of *F. carica* against different diseases. The first scientific investigation of figs involved its latex and was conducted by Ullman *et al.* between 1945 and 1952. Table 1.1 provides some examples of the ethnomedical uses of fig to combat various diseases, and mainly focuses on the isolation of secondary metabolites from *F. carica*. Other medicinal uses, such as in the treatment of pain in general, and various other ailments and diseases are included. Overall, a review of various studies (Figure 1.2) revealed the most common treatment of

---

<sup>7</sup> Ayurvedic refers to the ancient Indian medicinal system and methods of disease prevention (Gajalakshmi, Vijayalakshmi and Deni-Rajeswari, 2012).

*F. carica* included anti-viral, anti-pyretic, antimutagenic, and anti-depressant properties (Badgujar *et al.*, 2017; Bhanushali *et al.*, 2014). A formulation of *F. carica* paste to be used to relieve constipation *in vivo* has also been investigated for future clinical trials (Baek *et al.*, 2016; Lee *et al.*, 2012; Oh *et al.*, 2011).

Different parts of *F. carica*, including the stem, fruit, latex and leaves have also been found to have immunostimulant, hypolipidemic, cytotoxic, anti-bacterial and hepatoprotective effects (Aghel *et al.*, 2011; Ali *et al.*, 2011; Gond and Khadabadi, 2008; Irudayaraj *et al.*, 2016; Jing *et al.*, 2015; Joerin *et al.*, 2013; Khodarahmi *et al.*, 2011; Ma *et al.*, 2016; Mujeeb *et al.*, 2011; Saoudi and El Feki, 2017; Singab *et al.*, 2010; Stephen Irudayaraj *et al.*, 2017; Turan and Celik, 2016; Yang *et al.*, 2015). Antihelmintic, anticancer and antiangiogenesis studies have also been conducted on *F. carica* latex and leaves (Badgujar *et al.*, 2017; Conforti *et al.*, 2012; De-Amorin *et al.*, 1999; Eteraf-Oskouei *et al.*, 2015; Hashemi *et al.*, 2011; Menichini *et al.*, 2012; Tezcan *et al.*, 2014). Previous studies have disclosed further medicinal benefits of *F. carica* fruit, including anti-wrinkle, anti-pigmentation, and antioxidant, H<sub>2</sub>O<sub>2</sub>, 1,1-diphenyl-2-picrylhydrazyl radical, and 2,2-diphenyl-1-(2,4,6-trinitrophenyl) hydrazyl (DPPH) scavenging properties. Leaf parts have been reported to exhibit anti-inflammatory, hypoglycemic, and hypocholesterolemia activities. The latex has been shown to demonstrate anti-wart, anti-fungal activity and haemostatic effects (Badgujar *et al.*, 2017; Canal *et al.*, 2000; Ghimeray *et al.*, 2015; Irudayaraj *et al.*, 2016; Pérez *et al.*, 1999; Pérez *et al.*, 2000; Pèrez *et al.*, 2003; Raskovic *et al.*, 2015; Serraclara *et al.*, 1998; Yang *et al.*, 2009). However, the use of *F. carica* against neurodegenerative diseases has barely been studied.

**Table 1.1:** Chemical compositions that have been isolated from *F. carica*.

Extract/ secondary metabolite	Area of collection	Part	Treatment	Biological subject	References
Lipophilic extracts	Korea	Not defined	Anti-viral	Murine norovirus (MNV) Feline calicivirus (FCV)	(Seo and Choi, 2016)
Lipophilic extracts	North Western Himalaya	Root, leaf, flower	Anti-microbial	<i>Staphylococcus aureus</i> ( <i>S. aureus</i> )	(Sharma <i>et al.</i> , 2016)
Lipophilic extracts	USA	Fruit	Anti- bacterial	<i>Mycobacterium tuberculosis</i> ( <i>M. tuberculosis</i> )	(Coronado-Aceves <i>et al.</i> , 2016)
Lipophilic extracts	China	Not defined	Anti-bacterial	<i>Chromobacterium violaceum</i> ( <i>C. violaceum</i> ) and <i>Pseudomonas aeruginosa</i> ( <i>P. aeruginosa</i> )	(Sun <i>et al.</i> , 2015)
Lipophilic extracts	Not defined	Latex	Anti-viral	Caprine Herpesvirus 1 (CpHV-1)	(Camero <i>et al.</i> , 2014; Camero <i>et al.</i> , 2015)
Helvolic acid methyl ester	China	Leaf	Anti-bacterial	<i>Bacillus subtilis</i> ( <i>B. subtilis</i> ) and <i>S. aureus</i>	(Liang <i>et al.</i> , 2016)
Cis-1,4-polyisoprene	Montenegro	Latex	Anti-fungal	<i>Staphylococcus aureus</i> ( <i>S. cerevisiae</i> )	(Raskovic, <i>et al.</i> , 2015)
Lipophilic extracts	Turkey	Leaf	Anti-bacterial	<i>S. aureus</i> , <i>Listeria monocytogenes</i> ( <i>L.monocytogenes</i> ), <i>Escherichia coli</i> ( <i>E. coli</i> ) and <i>P. aeruginosa</i>	(Nostro <i>et al.</i> , 2016)
Lipophilic extracts	Oman	Leaf	Anti-bacterial	<i>S. aureus</i> , <i>E. coli</i> and <i>P. aeruginosa</i>	(Weli <i>et al.</i> , 2015)

Bergapten, furocoumarin and psoralen Lipophilic extracts	Not defined	Leaf	Nematicidal activity	Bursaphelenchus xylophilus <sup>8</sup>	(Guo <i>et al.</i> , 2015)
Linolenic acid methyl ester bergapten and psoralen Fruit paste	Iran	Root, stem and leaf	Anti-cytotoxic	HeLa cell line	(Ghafari <i>et al.</i> , 2015)
Fruit paste	Italy	Leaf and bark	Anti-phototoxicity	Human amelanotic melanoma (C32) cell line	(Conforti <i>et al.</i> , 2012)
Fruit paste	Korea	Fruit	Anti-constipation	Sprague–Dawley rats	(Lee <i>et al.</i> , 2012)
Furanocoumarin	Not defined	Fruit	Anti-constipation	Patient clinical trial	(Sardari <i>et al.</i> , 2015)
Fruit, powdered	Italy	Fruit	Anti-melanocarcinoma	Human melanoma cell line	(Marrelli <i>et al.</i> , 2012)
Ficusin	Turkey	Dried fruit	Anti-hepatotoxicity	Wistar albino rats	(Turan and Celik, 2016)
Lipophilic extracts	India	Leaf	Anti-diabetic and anti-lipidemic	Wistar rats	(Irudayaraj <i>et al.</i> , 2016)
Ficutirucin as tirucallane-type triterpenoids	Iran	Leaf	Fertility	NMRI male mice	(Naghdi <i>et al.</i> , 2016)
	China	Fruit	Anti-cancer	Human osteosarcoma U2OS, HepG2 (human hepatocellular liver carcinoma) and MCF-7 (human breast adenocarcinoma) cell lines	(Jing <i>et al.</i> , 2015)

<sup>8</sup> Guo *et al.* (2015) state that, “Bursaphelenchus xylophilus is one of the pine wood nematodes and is normally the pathogen of pine wilt disease, which has greatly damaged some pine species and become a severe worldwide threat to forest resources.”

Lipophilic extracts	Turkey	Latex	Anti-cancer		Human glioblastoma multiforme (U-138 MG, T98G, and U-87 MG) cell lines	(Tezcan <i>et al.</i> , 2014)
Lipophilic extracts	Iran	Leaf	Anti-angiogenesis and anti-inflammation	Wistar rats		(Eteraf-Oskouei <i>et al.</i> , 2015)
Formulated fruit extract	China	Fruit	Anti-wrinkles		Clinical study in women	(Ghimeray <i>et al.</i> , 2015)
Lipophilic extracts	Iran	Leaf	Anti-obesity		Lipase assay kit	(Gholamhose <i>et al.</i> , 2010; Seyedan <i>et al.</i> , 2015)
Polysaccharide	China	Fruit	Anti-bacterial, anti-inflammation and immunostimulants	anti- <i>Flavobacterium columnare</i> (F. <i>columnare</i> ), grass carp fish		(Yang <i>et al.</i> , 2015)
Lipophilic extracts	Turkey	Leaf	Anti-bacterial		<i>Candida Albicans</i> (C. <i>Albicans</i> )	(Okmen <i>et al.</i> , 2014)
Lipophilic extracts	India	Fruit	Anti-diabetic and anti-lipidemic	Swiss Albino mice		(Kannur and Khandelwal, 2012)
Lipophilic extracts	Iran	Leaf	Anti-cardiac arrhythmia	Wistar rats		(Allahyari <i>et al.</i> , 2014)
Lipophilic extracts	Iran	Leaf	Anti-angiogenic		HUVECs endothelial cell line	(Ghambarali <i>et al.</i> , 2014)
Lipophilic extracts	Pakistan	Fruit	Anti-bacterial		Salmonella typhi ( <i>S. typhi</i> ) P. <i>aeruginosa</i> and <i>E. coli</i>	(Shad <i>et al.</i> , 2014)
Hydrophilic extract, polysaccharides	China	Fruit	Anti-cancer		C57BL/6 mice	(Tian <i>et al.</i> , 2014)

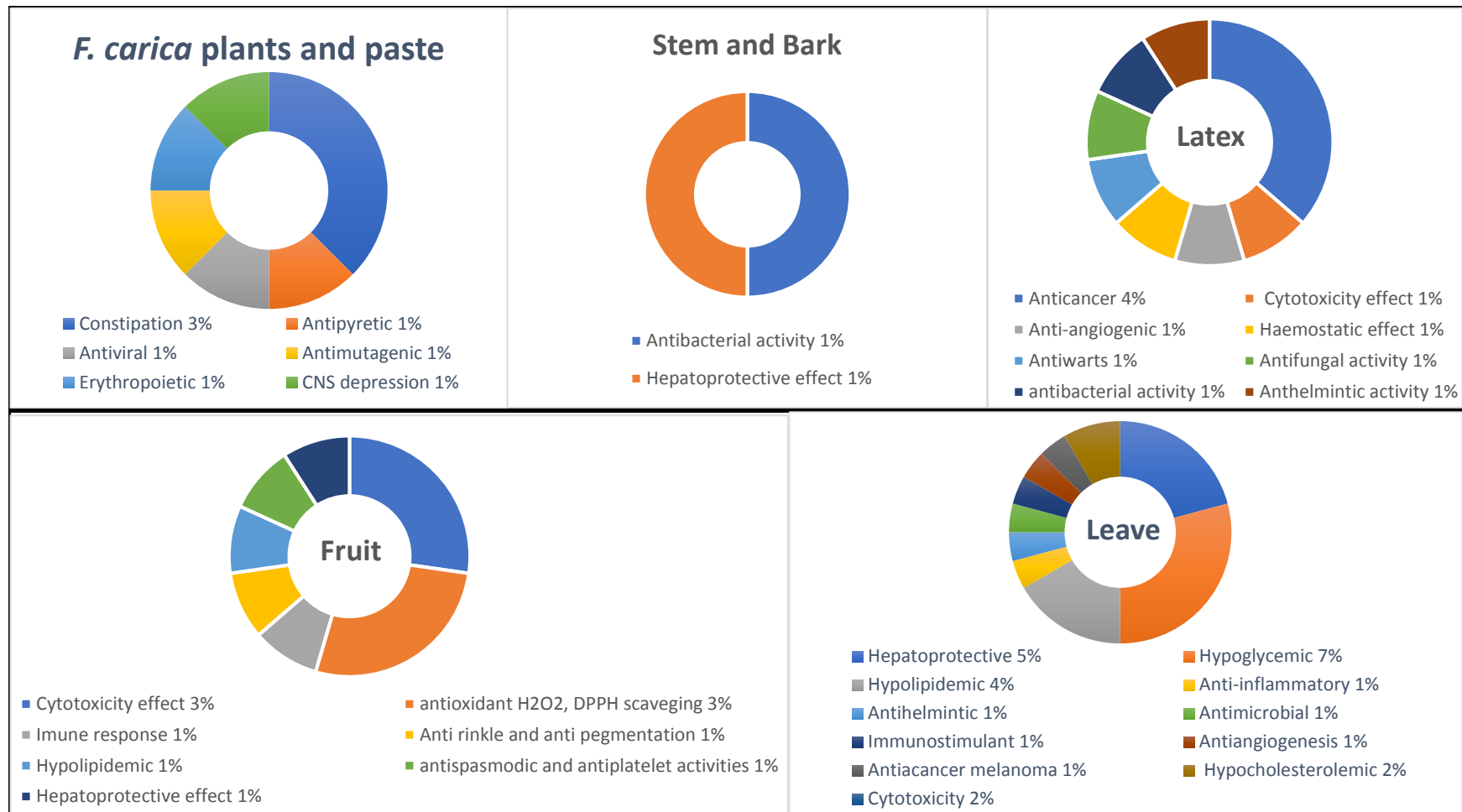


**Figure 1.2:** Pie chart analysis of ethnomedicinal studies of different parts of *F. carica* and the number of articles published from 2013 to 2017 for their effects in percentages.

### 1.3.2 Phytochemistry of *F. carica*

According to Chawla *et al.* (2012), phytochemicals are compounds or secondary metabolites produced by plants for a variety of protective reasons. A series of bioactive compounds have been documented for *F. carica* in a literature review conducted by Badgujar *et al.* (2014). The schematic list in Figure 1.3 includes amino acids, organic acids, fatty acids, triterpenoids, and phytosterols, as well as flavonoids (e.g., hydrocarbons, aliphatic alcohols, and polyphenolic compounds) and non-flavonoids (e.g., curcuminoids). Elements of the overall set of bioactive compounds include different classes of secondary metabolites. In two notable studies (Solomon *et al.*, 2006; Barolo *et al.*, 2014), evidence was found to suggest that the isolation of a range of coumarins, along with esters of phenylpropanoic acids, occurred in the leaves and roots of various *Ficus* species (spp.), including *F. carica*, *F. hispida*, and *F. septica*. In addition, two of the studies found that polyphenols occurred in fruits.

Triterpenoids are also found in plants in a free form, but also as esters and glycosidic conjugates called saponins (Ruamrungsri *et al.*, 2016). These forms differ in their polarity and water-solubility, and, consequently, they are accumulated in different plant organs and cellular compartments (Ruamrungsri *et al.*, 2016). Low-polarity compounds located in free and esterified forms have been identified in significant quantities within stem bark and surface cuticles, especially in the leaves and edible fruits, including *Ficus spp.* (Ruamrungsri *et al.*, 2016). Nevertheless, it is important to note that the triterpenoids produced in fruits are regularly lost when fruits are peeled or processed into certain products (e.g., juices). In general, phytochemicals of this kind can be identified in latex, leaves, fruits, and roots (Badgujar *et al.*, 2014; Mawa *et al.*, 2013).

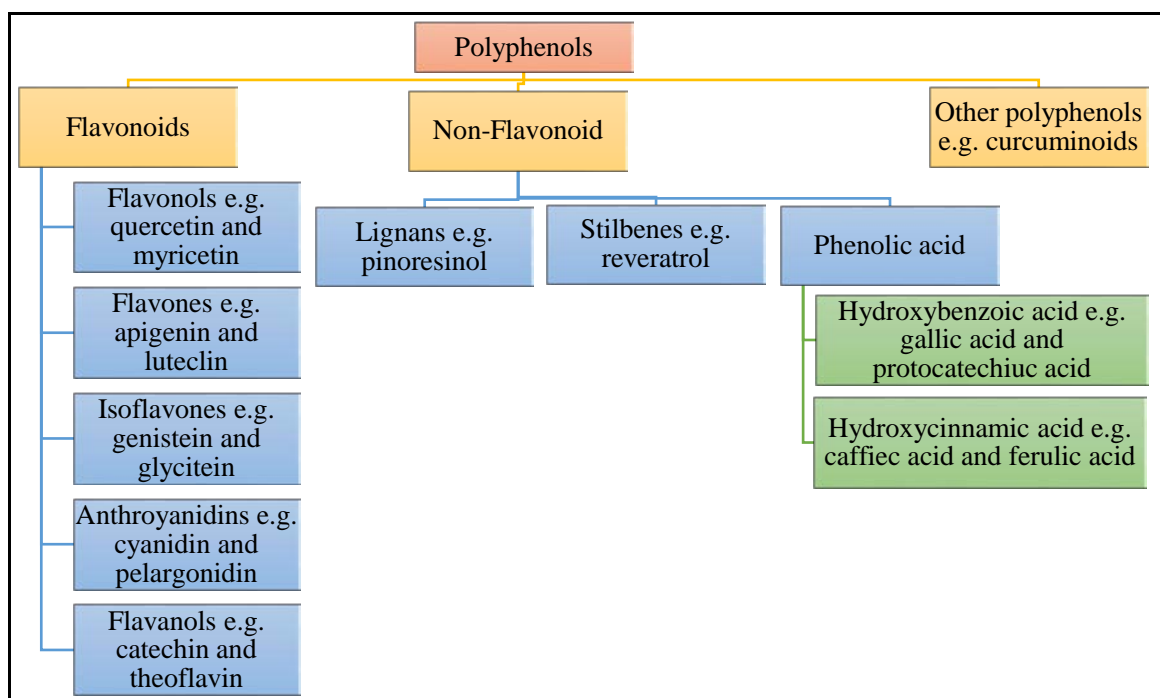


**Figure 1.3:** Classification of polyphenols (Essa *et al.*, 2016).

### 1.3.2.1 Phytochemicals previously isolated from *F. carica* fruit

A literature review of the identified secondary metabolites from fruits of *F. carica* was carried out by Barolo *et al.* (2014), which highlighted ten different classes of compounds including: 1) anthocyanin (cyanidine-3-*O*-glucoside [1], cyanidine-3-*O*-rhamnoglucoside [2], rutinoside [3], (epi)catechin-(4–8)-cyanidine-3-glucoside [6], glucoside, cyanidine-3,5-diglucoside [7], cyanidine -3-*O*-glucoside [8], pelargonidin -3-*O*-glucoside [9], malonyl, cyanidine-3-malonylglucoside [10]); 2) alcohol (benzyl alcohol [11], phenylethyl alcohol [12], 4-methyl-butanol [13], methyl alcohol [14], ethyl alcohol [15] and 1-Penten-3-ol [16]); 3) ketones (6-Methyl-5-hepten-2-one [17]); 4) norisoprenoids ( $\beta$ -cyclocitral [18]); 5) esters (methyl hexanoate [19], methyl salicylate [20] and ethyl salicylate [21]); 6) aldehydes (2-methylbutanal [22], (E)-2-pentanal [23], (Z)-2-heptanal [24], (E)-2-hexanal [25], (E)-2-nonanal [26], hexanal [27], heptanal [28], octanal [29], nonanal [30], benzaldehyde [31], 2-Methyl-2-butanal [32] and 3-Methyl-butanal [33]); 7) flavonol (kaempferol 3-*O*-utinoside [34], quercetin acetyl glucoside [35], quercetin 3-*O*-nrutinoside [36], and quercetin 3-*O*-glucoside [37]); 8) flavones (luteolin-(6-hexose-8-pentose) [38] and apigenin-6-rutinoside [39]); 9) phenolic acids (chlorogenic acid [40]); and 10) miscellaneous compounds (eugenol [41]), as illustrated in Figure 1.4.

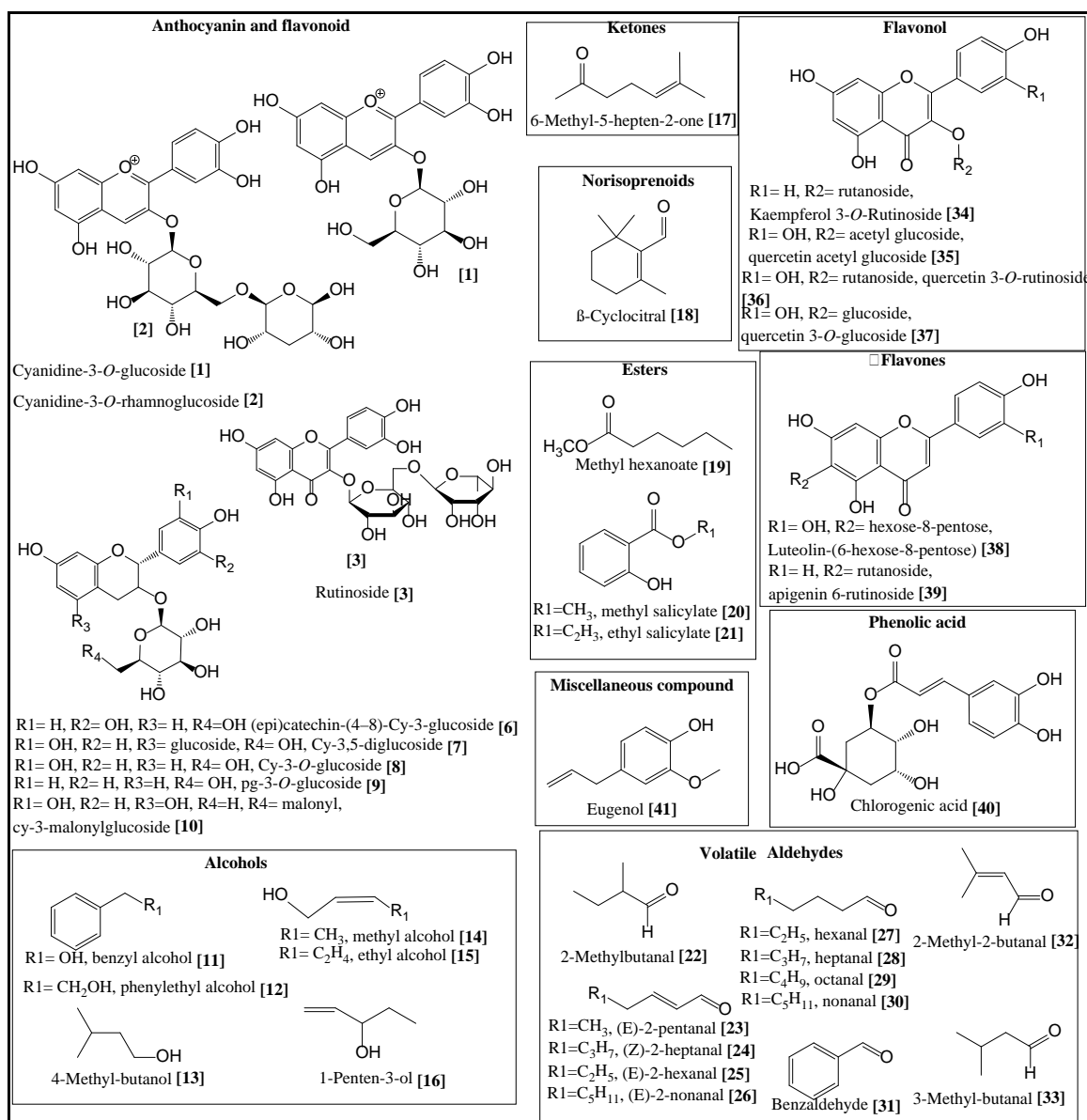


**Figure 1.4:** Identified compounds from fruits of *F. carica* (Barolo *et al.*, 2014; Loizzo *et al.*, 2014).

The occurrence of 40 compounds (Figure 1.5) included: pinene [70], eucalyptol [71], arsenous acid [72], quinoline [73], terpinolene [74], linalool oxide [75], levoglucosan [76], ferulic acid [77], isoeugenol [78], isoferulic acid [79], resorcinol [80], guaiacol [81], pyrocatechol [82], vanillic acid [83], vanillin [84], pyrogallol [85], *P*-cresol [86], *O*-cresol [87], oxalic acid [88], hexadecane [89], glycerol [90], isovaleric acid [91], ethyleneglycol [92], citric acid [93], linalool [94], lactic acid [95], octanedioic acid [96], nonanedioic acid [97], decanedioic acid [98], eicosanol [99], eicosenoic acid [100], valeric acid [101], caproic acid [102], heptanoic acid [103], nonanoic acid [104], dodecanoic acid [105],

tridecanoic acid [106], tetradecanoic acid [107], pentadecanoic acid [108] and pentacosanoic acid [109] have been reported in the pulp (endocarp) and peel (exocarp) of *F. carica*, and traces of these compounds have also been found to occur in the leaves of *F. carica* (Oliveira *et al.*, 2010).

These compounds have been found to possess antioxidant and antimicrobial properties (Silva *et al.*, 2004; Oliveira *et al.*, 2009; Valentão *et al.*, 2005). Naidu (2003) and Sousa *et al.*, (2009) have reported that ascorbic acids and citric acid [93] are likely the most widely distributed water-soluble antioxidant in vegetables. On the other hand, Oliveira *et al.* (2008) found that citric [93] and mallic acid [153] are commonly found in fruits, while oxalic acid [88] is present in higher amounts in green leaves. The authors also found that the rutinoid content in peel was significantly higher than that found in pulp and leaves, while [43] occurred in pulp at significantly higher levels when compared with peel. Oliveira *et al.* (2010) also indicated that the most abundant chemical compositions in the pulp and peel of *F. carica* are triterpenoids, and others such as compounds [20], [43], [55], [63], [68], [71], [73], [74] and [75].

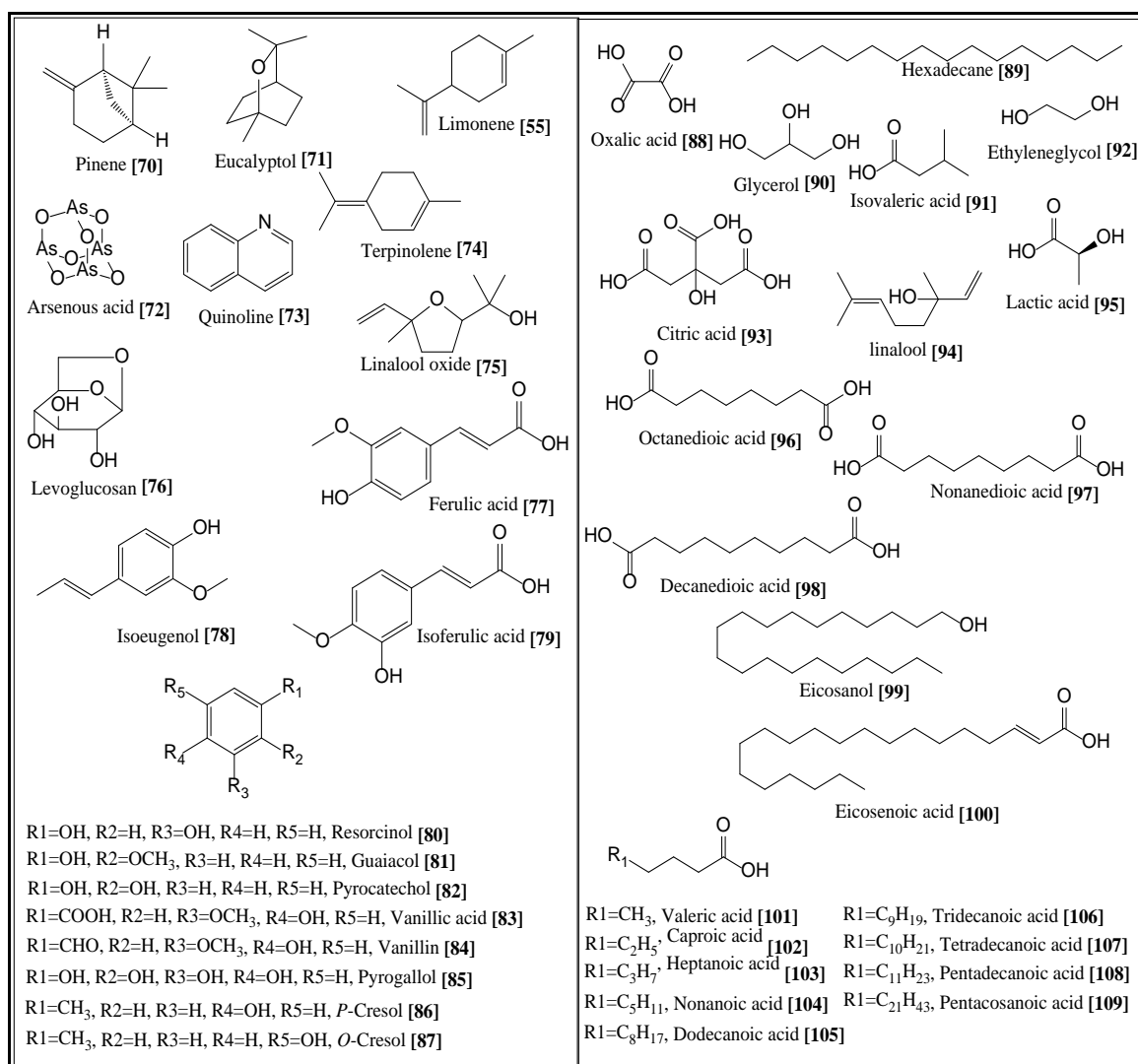


**Figure 1.5:** Other compounds reported in aqueous lyophilised pulp extracts of *F. carica*, peel, and traces in leaves (Oliveira *et al.*, 2010; Ribechini *et al.*, 2011).

### 1.3.2.2 Phytochemicals previously isolated from *F. carica* leaves and roots

In general, triterpenoids and sterols have been identified in the roots and leaves of different *Ficus spp.* (Lansky *et al.*, 2008). In particular, sterols (baurenol [49], 24-methylenecycloartanol [50],  $\psi$ -taraxasterol [51] and lupeol [52]) have been identified in the roots and leaves of *F. carica* (Figure 1.6), as well as terpenes, including monoterpenes (Limonene [55] and Menthol [56]) and sesquiterpenes (guaiene [57],  $\beta$ -gurjunene [58], caryophyllene [59],  $\alpha$ -murolene [60],  $\alpha$ -cubebene [61], copaene [62], t-muurolene [63],  $\alpha$ -ylangene [64],  $\beta$ -bourbonene [65],  $\beta$ -elemene [66], alloaromadendrene [67] and germacrene D [68]). Other phytochemical compounds, including aldehydes ([23], [25], [27] and [33]); alcohols ([11], [12], [13], [15] and [16]); esters ([19], [20], [21], methyl

butanoate [53], Hexyl acetate [54]); ketone (pentanone [48]); norisoprenoid [18]; coumarins (bergapten [42], psoralen [43], marmesin [44], umbelliferone [45] and coumaric acid [46]); flavonoid (rutinoside [3]); and miscellaneous compounds (nonalactone [69]) were identified in *F. carica* leaves and roots, as well (Barolo *et al.*, 2014).

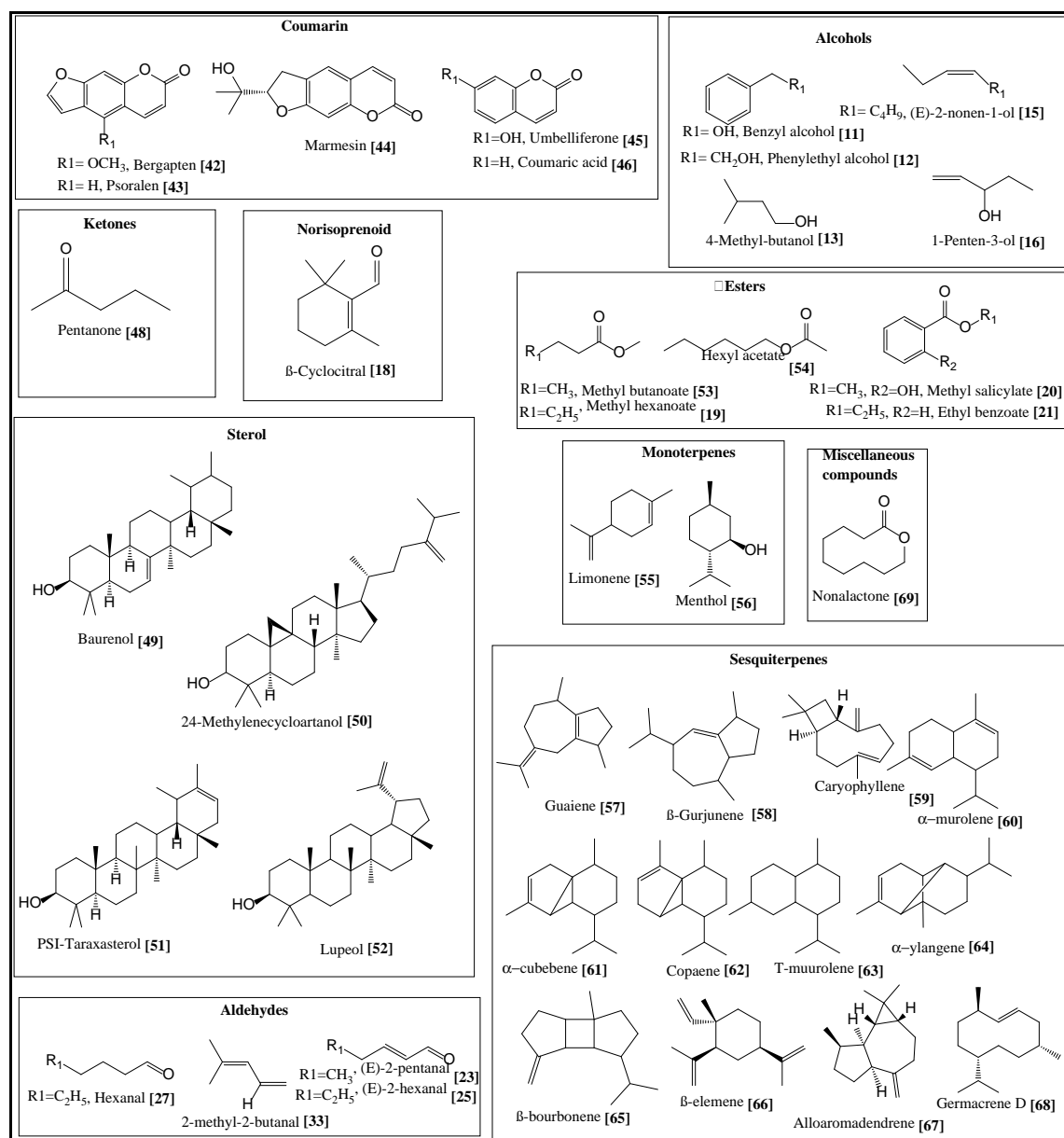


**Figure 1.6:** Identified compounds of *F. carica* in leaves and root (Barolo *et al.*, 2014).

### 1.3.2.3 Phytochemicals previously isolated from *F. carica*'s latex

As documented by Lansky *et al.* (2008), *Ficus spp* are characterised by the presence of latex-like material within their vasculatures. As a consequence of the presence of this

material, members of the species possess defensive and self-healing properties. Kim *et al.* (2008) noted how latex is constituted of the cytoplasmatic fluid of laticiferous tissues, which include the typical organelles of plant cells (including nuclei, mitochondria, ribosomes, and vacuoles). To be more specific, latex has been classified as an aqueous suspension of a complex molecular mixture, where the molecules are located in dedicated secretory cells of the plants (namely, laticifers). These laticifers facilitate the synthesis and storage of a range of secondary metabolites in considerable quantities, which Agrawal and Konno (2009) state include terpenoids, alkaloids, sterols, proteins, and tannins. Figure 1.7 presents the organic compounds of *F. carica* latex identified in the literature.

According to Oliveira *et al.* (2010), the organic acids profile of *F. carica* latex is composed of six organic acids ([88], [93], shikimic acid [151], quinic acid [152], malic acid [153] and fumaric acid [154]). These compounds have previously been reported to exist in *F. carica* pulp, peel, and traces in leaves (Oliveira *et al.* 2010). Additionally, Barolo, Mostacero *et al.* (2014) reported the presence of 13 fatty acids (myristic acid [110], pentadecanoic acid [111], palmitic acid [112], heptadecanoic [113], stearic acid [114], arachidic acid [115], heneicosanoic acid [116], behenic acid [117], tricosanoic acid [118], lignoceric acid [119], oleic acid [120], elaidic acid [121] and linoleic acid [122]); six steroids (betulol [123], lanosterol [124], 6-*O*-linoleyl- $\beta$ -D-glucosyl- $\beta$ -sitosterol [125], 6-*O*-palmitoyl- $\beta$ -D-glucosyl- $\beta$ -sitosterol [126], 6-*O*-oleyl- $\beta$ -D-glucosyl- $\beta$ -sitosterol [127] and 6-*O*-stearyl- $\beta$ -D-glucosyl- $\beta$ -sitosterol [128]); and 14 amino acids in latex (histidine [132], tryptophan [133], asparagines [134], glutamine [135], phenylalanine [136], tyrosine [137], phenylalanine [138], serine [139], glycine [140], alanine [141], leucine [142], cysteine [143], ornithine [144] and lysine [145]).

Nevertheless, the presence of monoterpenes, including [55], [71], [74], [75], pinene [149] and  $\alpha$ -thujene [150]; sesquiterpenes, including [57], [59], [63], [65], [68], trans- $\alpha$ -bergamotene [129], cadinene [130] and  $\alpha$ -calacorene [131]; alcohols, including [12], [13], [16], hexanol [146], heptanol [147] and phenylpropyl [148]; aldehydes, including [27], [28] and [31]; ketone, including [17]; and other compounds, such as [20], [43] and [73], were also reported by Barolo *et al.* (2014) to characterise *F. carica* latex. Some of these compounds have been identified in *F. carica* fruit, pulp and peel.

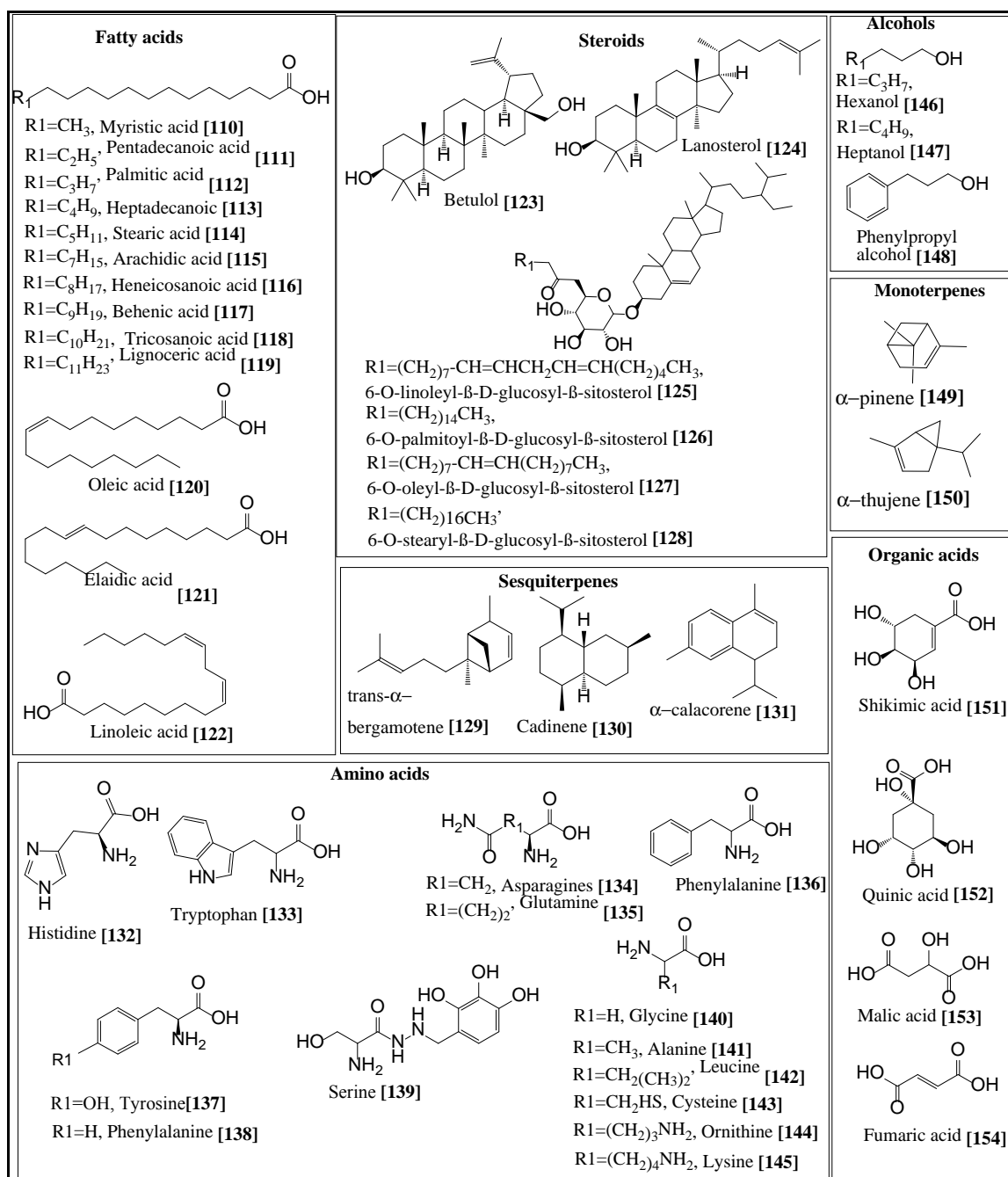


**Figure 1.7:** Identified compounds of *F. carica* in latex (Barolo *et al.*, 2014).

In addition to what Barolo, Mostacero Silvia and López (2014) reported in steroids, recent studies, such as those by Ribechini and colleagues (2011), and Soltana and colleagues (2016), have identified a number of phytosterols in *F. carica* latex, including Lupeol acetate [156], Lupeol [157], Cholesterol [158], Ergosterol [159], Taraxasterol [160], Campesterol [161], Coprostanol [162], Coprostanol [163], Cholestanol [164], Clerosterol [165], Campestanol [166], Brassicasterol [167], β-Amyrin [168], β-Sitosterol [169],

Sitostanol [170], Stigmasterol [171] and Stigmastanol [172], as shown in Figure 1.8 below.

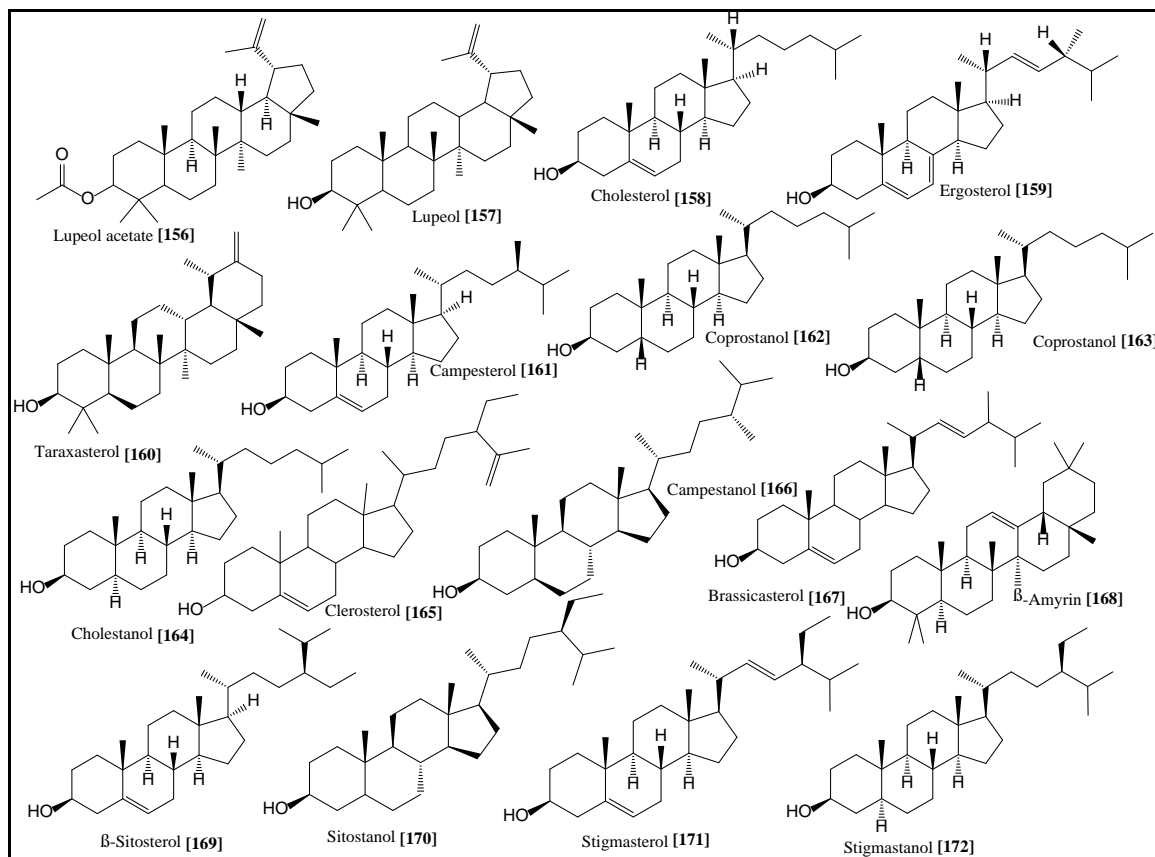


**Figure 1.8:** Identified steroid compounds of *F. carica* in latex (Ribechini, *et al.*, 2011; Soltana *et al.*, 2016).

Some of the phytoconstituents of *F. carica* are produced in the preparation of sunscreen and colouring agents, such as [43]. In addition to this, several studies, including those by Badgujar *et al.* (2014), Chawla *et al.* (2012), and Mawa, *et al.* (2013) have identified notable biological characteristics, including antioxidant activity, anti-cancer properties, anti-inflammatory, and hypolipidemic effects. Nevertheless, it is important to recognise that the extant literature pertaining to the issue of the biological properties for anti-Alzheimer's compounds is not extensive.

### 1.3.3 *F. carica* in Alzheimer disease prevention

One notable recent study was conducted by Subash *et al.* (2017), which examined the effects of supplementing diets of Alzheimer disease transgenic mice with figs. This resulted in an anti-anxiolytic impact along with memory enhancement, which was

accounted for by the high levels of antioxidant active components in figs (for example, flavonoids and, more specifically, quercetin). Other notable results included decreased impact in the plasma A $\beta$ <sub>1-40</sub> and A $\beta$ <sub>1-42</sub> levels, as well as decreased impact in AChE activity; enhanced depletion of GSH levels and Na<sup>+</sup> K<sup>+</sup> ATPase; and a significant inhibitory impact on the accumulation of MDA observed in oxidative stress, glutathione peroxidase (GPx), glutathione reductase (GR), and the protein carbonyl levels in the cerebral cortex and hippocampus of AD Tg mice.

Another study of the use of figs was conducted by Essa *et al.* (2015), a research team based in Oman. Notably, the researchers reported that the inhibitory impact of AD-like A $\beta$ , inflammatory cytokines, and ATP inhibitions in aged APPsw/Tg2576 mice was significant. In light of the AD prevention via *Ficus spp.* extracts, Oliveira *et al.* (2010) carried out a study and found that crude *F. carica* latex exhibited a prominent inhibitory impact on AChE activity with IC<sub>50</sub> of 5 mg/mL; this result was noteworthy, compared to leaves, pulp, and peel, which showed no impact with respect to the enzyme. Contrastingly, Ariffin and Hasham (2016) found that *Ficus deltoidea* extracts from leaves exhibited potent antioxidant activity against 1,1-Diphenyl-2-picrylhydrazyl radical, DPPH free radicals with IC<sub>50</sub> of 3.5 mg/mL. The same found to be true of the n-hexane, chloroform, acetone, methanol, n-butanol, and water extracts of the leaves of *F. carica* from Turkey, which were screened for AChE and BChE inhibitory activity (Loizzo *et al.*, 2014). The researchers found that n-hexane and acetone extracts have a significant inhibitory impact with respect to both AChE (62.9% and 50.8%, respectively) and BChE (76.9% and 45.6%, respectively).

#### **1.4. Alzheimer's disease**

As the most prevalent neurodegenerative condition, Alzheimer's disease (henceforth AD) is the common type of dementia (Ahmad, 2012). Here, it should be noted that, according to the definition given by Raskind *et al.* (1995), dementia should be regarded as a condition in which the complications include the gradual degradation of a sufferer's cognitive faculties (including memory, reason, judgement, and language), thereby decreasing quality of life due to the individual's inability to complete previously accomplishable tasks. Regarding the aetiological underpinnings of progressive memory

impairment, cognitive deficits, and functional alterations, AD constitutes the primary contributing factor, as well as Tönnies and Trushina (2017) provided evidence to suggest a link between AD and neuropsychiatric conditions among older people (e.g., hallucinations, delusions, aggressiveness, and irritability).

#### **1.4.1 The significance of Alzheimer's disease**

At present, over 5 million individuals in the United Kingdom have been diagnosed with AD; approximately 47.5 million sufferers have been diagnosed worldwide, and an estimated 7.7 million new diagnoses occur annually (Tönnies and Trushina, 2017; Islam *et al.*, 2017). Furthermore, given that dementia is expected to have an impact on approximately 5% to 8% of all individuals older than 60, the number of AD diagnoses in the coming years is expected to increase with the growth of the elderly population (Islam *et al.*, 2017). AD prevalence worldwide for individuals aged over 65 years is approximately 5%, and for individuals aged over 85 years, prevalence has been estimated at around 30% (Ahmad, 2013; Huang *et al.*, 2013).

Epidemiological research indicates that AD prevalence varies based on an individual's age: for individuals aged between 65 and 69, prevalence amounts to 1%; for individuals aged 70 to 74, prevalence has been estimated at 3%; and for those aged 80-84, and 85 and above, prevalence has been estimated at 12% and 25%, respectively (Maczurek *et al.*, 2008). Another notable statistic that further highlights the significance of AD is that while global prevalence amounted to 26.6 million diagnoses in 2006, this figure is expected to reach 106.4 million by 2050 (Athari *et al.*, 2017; Habtemariam, 2018b). Notably, Islam *et al.*'s (2017) forecast for 2050 with respect to dementia is even more severe, stating a figure of 135.5 sufferers. However, since AD is a fundamental aetiological underpinning of dementia (associated with 60-70% of new diagnoses), this has critical implications for AD prevalence in the coming years (Islam *et al.*, 2017).

#### **1.4.2 Pathophysiological theory of Alzheimer's disease**

In the majority of cases, AD arises sporadically, and the aetiological underpinnings of the condition are not well understood. However, it has been hypothesised that AD occurs as a consequence of environmental factors, genetic risk factors, gender, age group, and mitochondrial haplotypes. According to Maczurek *et al.* (2008), sufferers of AD are

essentially uniform in the way they present with gradual neuronal cell loss, and this is linked to region-specific brain atrophy. Some scholars, including Athari Nik Azm *et al.* (2017) have provided strong support for the idea that the occurrence of AD is linked to intricate mechanisms within the brain over a considerable timespan.

In a review of the literature, Jomova *et al.* (2010) concluded that the primary explanation for AD onset that the last twenty years was the over-accumulation of A $\beta$ -amyloid (A $\beta$ )<sup>9</sup>. The primary hypothesis associated with A $\beta$  cascade connected it with the basal forebrain (collection of cholinergic neurons), including the basal nucleus of meynert, followed by deposition as oligomers or neurofibrillary tangles characterised by toxicity (Jomova *et al.* 2010). These toxic oligomers or neurofibrillary tangles have been identified as mainly constituted of an irregular type of tau protein, which is a microtubule-associated protein typified by significant water solubility. It is closely linked to the cytoplasm of pyramidal neurons, and research has suggested that it facilitates the disruption of synaptic function within the neurotransmitters (Bernhardi and Inestrosa, 2008; Jomova *et al.*, 2010). Consequently, a reduction in the efficacy of information transmission was hypothesised to take place among neuronal cells, thereby resulting in neuronal degeneration and, ultimately, dementia (Bernhardi and Inestrosa, 2008; Jomova *et al.*, 2010).

The pathological mechanism by which the over-accumulation of A $\beta$  takes place is not known to contemporary medical researchers. Notably, and as highlighted by Jomova *et al.* (2010), in the last 20 years the A $\beta$  cascade theory has become a ‘null hypothesis’. Scientists have since begun to support the ‘alternative hypothesis’, which suggests that the pathogenesis of A $\beta$  cascade is not an initiating event but is rather a secondary event of the disease (Jomova *et al.*, 2010). Irrespective of this dichotomy and, furthermore, uncertainty regarding the issue, studies such as those by Athari Nik Azm *et al.* (2017), Jomova *et al.* (2010), and Tönnies and Trushina (2017) have argued that the A $\beta$  cascade has the capacity to produce free radicals as a consequence of the oxidative stress action mechanism. When taken together, then, a majority proportion of the literature addressing the issue of the pathology of AD and, to a lesser extent, Parkinson’s disease (PD),

---

<sup>9</sup> A $\beta$ -amyloid is a peptide of 39–43 amino acids, and appears to be the main constituent of amyloid plaques in the brains of AD sufferers (Jomova *et al.*, 2010).

associate the causes of the two conditions with empirical evidence connected to oxidative stress within the brain (Jomova *et al.*, 2010).

### 1.4.3 Oxidative stress

It is unsurprising that the idea of oxidative stress (OS) involves the significant generation of free radicals<sup>10</sup> and reactive oxygen species (ROS), which are produced as a consequence of mitochondrial aberrances. This takes place as a result of a functional disequilibrium with respect to ROS, including NADPH oxidase activation, and reactive nitrogen species, including nitric oxide synthase (NOS) activation (Athari *et al.*, 2017; Rahman, 2016). As outlined by Sultana *et al.* (2013), the role played by radical-mediated oxidative damage in the context of neurodegenerative disorder pathogenesis is firmly established. A report by Jones (2016) confirms these findings, where the role of OS in aging is described as having the potential to arise as a consequence of disequilibrium between pro-oxidants and antioxidants, characterised by extensive and destructive free radical chemistry. This can take place as a result of the inhalation of toxic gas (e.g., cigarette smoke), as well as age-related conditions, the chief implication being that older individuals and smokers ought to elevate their consumption of antioxidants with radical-scavenging abilities (Sultana *et al.*, 2013).

In another noteworthy study conducted by Butterfield *et al.* (2010) and Sultana *et al.* (2013), the primary characteristics of enhanced OS in a human brain suffering from AD include free radical attacks on polyunsaturated fatty acids (PUFAs). Ultimately, this results in the establishment of highly reactive electrophilic aldehydes, which include malondialdehyde (MDA) and 4-hydroxy-2-nonenal (HNE) as the primary products, along with acrolein (Acr, the biomolecule typified by the greatest level of reactivity). Significantly, each of these biomolecules is neurotoxic, and so preventive measures should be taken to safeguard against their negative impacts.

Owing to the fact that the brain is highly sensitive to oxidative stress - this 1300 g organ is consuming 20–30% of the oxygen inhaled by the average person - its elevated level of

---

<sup>10</sup> The most common of free radicals reported are hydroxyl (OH<sup>•</sup>), superoxide (O<sub>2</sub><sup>•-</sup>) and nitric monoxide (NO<sup>•</sup>). However, H<sub>2</sub>O<sub>2</sub> and peroxynitrite (ONOO<sup>-</sup>) are not free radicals, but are reported to produce free radicals through various chemical reactions (Uttara *et al.*, 2009).

sensitivity with respect to OS is self-evident due to the expression of endogenous enzymes (Sultana *et al.*, 2013). In terms of redox transition metals, these perform a critical function in initiating and propagating the torrent of reactions beginning with electron abstraction from the conjugate double-bond system of fatty acid acyl chain. It is important to recognise, as shown in Figure 1.9, that the abovementioned process results in the targeting of the generation of lipid peroxidation process. At the same time, the issue is implicated in protein glycoxidation production and a series of reactive aldehydic intermediates, referred to as ‘free carbonyls’, in the central nervous system (CNS). As documented in the work of Sultana *et al.*, (2013) and Rahman (2016), these free carbonyls include MDA, 4-hydroxy-2-nonenal (4-HNE), and acrolein.

Furthermore, it is noteworthy that the aldehydes rapidly attack, modify, and deactivate proteins, thereby producing hydrophilic protein-bound carbonyls. In turn, this facilitates the alteration of cellular metabolism, as well as the down-regulation of the endogenous antioxidants, including reduced glutathione antioxidant enzymes, and glutathione peroxidase (Athari *et al.*, 2017; Kawaguchi-Niida *et al.*, 2006). At the same time, the redox pathway and the issue of cellular stress centres around one particular idea within free radical theory, highlighted in the literature, that a fundamental underpinning of OS is the disturbance of connective circuits owing to the following reasons: (i) the inhibition of electron transfer and the obstruction of functional redox pathways; (ii) the short-circuiting of typically insulated electron transfer pathways; and (iii) interference with the gating mechanisms that are responsible for regulating redox pathways (Rahman, 2016). From the perspective of the redox system, OS can be regarded as a type of perturbation with respect to the overall non-equilibrium redox system. As such, the perturbation could denote an overly-high ROS concentration (Rahman, 2016).

When taken together, ROS are characterised by elevated instability and a high capacity to react with proteins, nucleic acids, lipids, and every other macromolecule (Sultana *et al.*, 2013). In the context of the brain, the aggravation of events of this kind takes place to an even greater extent owing to the way in which neuronal cells are generally incapable of neutralising free radicals. As noted by Essa *et al.* (2015) and Sultana *et al.* (2013), this inability stems from the general scarcity of internal enzymatic and external non-antioxidants. Therefore, it has been hypothesised that the perturbation of all the above-

noted functions displayed by acrolein to address brain dysfunction, leading to AD. Taking this into account, the purpose of the present literature review is to outline the way in which acrolein production in the brain can be mitigated with reference to an *in vitro* human neuronal model.

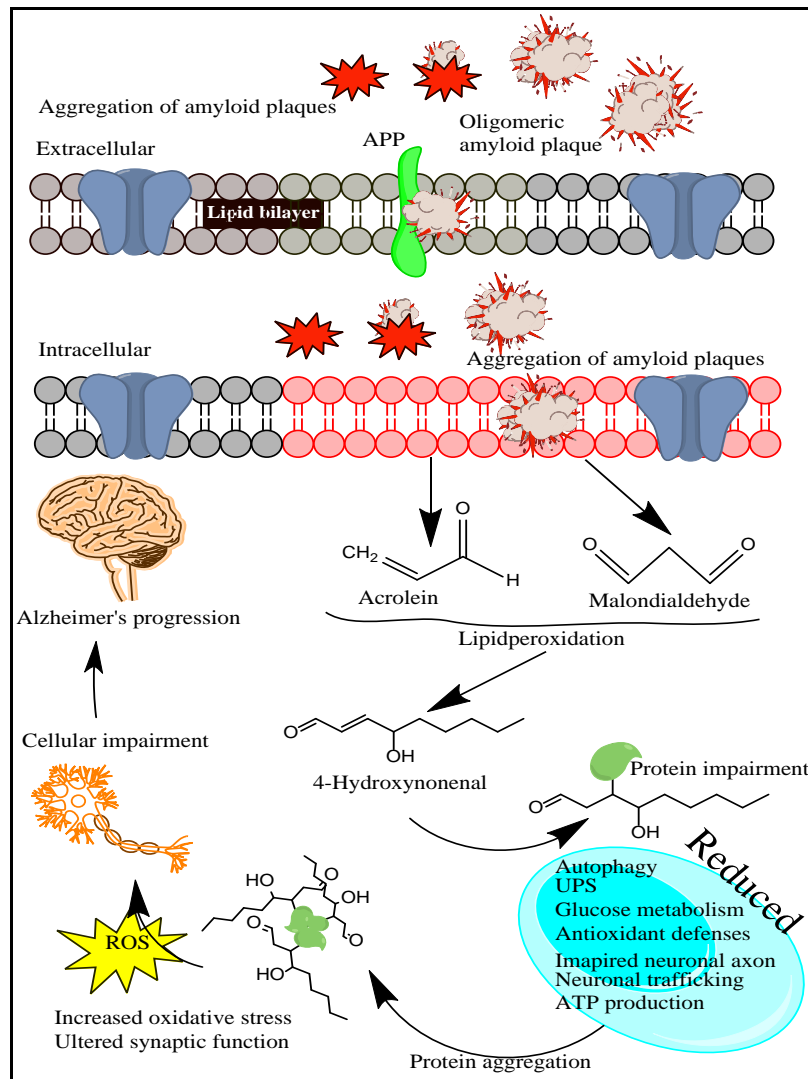


**Figure 1.9:** The proteolytic cleavage of the amyloid precursor protein (APP) produces A $\beta$  as a consequence of the secretase action. Following its production, A $\beta$  is subjected to aggregations, after which its deposition takes place in an extracellular way in the form of senile plaques. Oligomeric A $\beta$  has the capacity to facilitate its own insertion into the lipid bilayer, as a consequence of which the lipid peroxidation process is initiated. This gives rise to highly reactive products, including MDA, HNE, and acrolein, where the latter two have the capacity to react with proteins. In turn, acrolein-protein adducts or HNE-protein adducts change the functional and structural characteristics of the proteins, thereby leading to impairment. This result is linked to the following: (i) lowered autophagy; (ii) a reduced rate of unfolded response ubiquitin-proteasome system (UPS); (iii) reduced glucose metabolism; (iv) lowered antioxidant defence; (v) defective neuronal axons; and (vi) lowered adenosine triphosphate (ATP) production (and, consequently, neuronal trafficking). Over the course of AD's onset, cellular impairment gives rise to AD pathogenesis (Barone *et al.*, 2016; Sultana, Perluigi and Butterfield, 2013).

Acrolein (Acr), is (2-propen-1-al) the strongest electrophilic  $\alpha,\beta$ -unsaturated aldehyde among the unsaturated aldehydes, and is a ubiquitous byproduct of lipid peroxidation

(Moghe *et al.*, 2015; Tsou *et al.*, 2016). One of the most notable findings reported by Moghe *et al.* (2015) with respect to Acr is the identification of unsaturated aldehyde as a significant danger to public health, and one, which is abundant in almost all domestic and educational environments. In addition, Acr is a diverse chemical family, and the commonly found water-soluble type 2 alkenes have been identified in alcoholic beverages, water, and food products, ranging from donuts to coffee. Acr has also been identified as arising when organic materials are burnt, for example, timber, tobacco, and cooking oils, as well as beer, wine and rum (Carini *et al.*, 2003; Huang *et al.*, 2013a; LoPachin *et al.*, 2008; Moghe *et al.*, 2015; Tsou *et al.*, 2016).

Chemicals in this family, which includes other well-known neurotoxicants, for example, acrylamide and acrylonitrile, are characterised by a conjugated structure formed when an electrophilic group (e.g., carbonyl) is linked to an alkene carbon (LoPachin *et al.*, 2008). Owing to the fact that the pi electrons of a conjugated system are characterised by a significant capacity to be polarised, the  $\alpha$ ,  $\beta$ -unsaturated carbonyl structure of Acr, along with different type 2 alkenes, is a soft electrophile (LoPachin *et al.*, 2008). Michael-type adducts are typically established as a result of soft electrophiles, and these create soft nucleophiles, which have toxicological significance as evidenced by the way in which numerous neuronal processes, including the emission neurotransmitter incorporate proteins, are governed by the redox state of specific cysteine sulfhydryl groups (LoPachin *et al.*, 2008).

In clinical terms, the most effective estimate at present for the tolerable daily intake of Acr is 7.5  $\mu\text{g}/\text{kg}$ , which is based on body weight (Moghe *et al.*, 2015). With respect to Acr levels that result from metabolic processes, quantifying this is not straightforward, but it is known that they can be with a critical effect under particular cellular microenvironmental conditions. In individuals suffering from AD, Acr has been identified as existing in significant quantities in the hippocampus and the temporal cortex, with the particularly notable finding being that levels were almost five times greater when compared to HNE in the same group of patients (Bradley *et al.*, 2010; Huang *et al.*, 2013a; Huang *et al.*, 2013b; Huang *et al.*, 2014). At the same time, these studies have drawn attention to the way in which Acr facilitates the hyperphosphorylation of microtubule-

associated protein tau, while elevating A $\beta$  aggregation in senile plaques (see Figure 1.8) (Bradley *et al.*, 2010; Huang *et al.*, 2013; Huang *et al.*, 2014).

One of the most notable findings of a study by Uchida *et al.* (1998) was the initial confirmatory report that an acrolein-lysine adduct is associated with the oxidation of human low-density lipoprotein (LDL). Notably, the researchers indicated that certain antibodies are present against the adduct *in vivo* (Uchida *et al.*, 1998). In a study by Tsou *et al.* (2016), the researchers found that the quick incorporation of Acr can take place with respect to proteins, thereby producing what is referred to as a protein-conjugated acrolein (PC-Acr). The study demonstrated that in the brains of AD sufferers, when compared with control groups, either PC-Acr or free-form Acr is present at a higher level (Tsou *et al.*, 2016). Notably, studies conducted by Huang *et al.* (2013) and Huang *et al.* (2014) reported that lithium plays a role in significantly mitigating Acr-induced oxidative damage in HT22 neuronal cells. The two studies taken together confirm that the mechanism of action in this context was the inactivation of glycogen synthase kinase-3 $\beta$  (GSK-3 $\beta$ ), which resulted in the uP-regulation of the anti-oxidative capacity of HT22 cells (Huang *et al.*, 2013; Huang *et al.*, 2014).

Previous studies have identified anti-oxidant epigallocatechin gallate polyphenols and pycnogenol, a patented combination of bioflavonoids and polyphenols extracted from the bark of French maritime pine (*Pinus maritima*), and primarily characterised by high levels of catechin, epicatechin, and taxifolin, and which have been found to protect human neuroblastoma SH-SY5Y cells from acrolein-induced damage through the attenuation of ROS, an uP-regulation glutathione system, and the prevention of lipid peroxidation (Ansari *et al.*, 2008; Huang *et al.*, 2010). Two recent studies, by Nama *et al.* (2010) and Belkacemi and Ramassamy (2016), reported that anthocyanins (a certain group of polyphenols) administered at the level of 5  $\mu$ M play a protective role for SK-N-SH neuronal cells with respect to Acr-induced oxidative damage. The two studies confirmed that this takes place via the up-regulation of glutathione within the transcription of nuclear factor erythroid 2-related factor 2 (Nrf2). In addition, Huang *et al.* (2013a) identified that caffeic acid (25  $\mu$ M) and caffeic acid phenanthryl ester (30  $\mu$ M) play a critical role in up-regulating heme oxygenase-1 (HO-1) antioxidant enzyme with respect to Acr-induced cell damage. In addition, the acid and ester were found to limit the damage caused by

AD-like pathologies in the context of immortalised mouse hippocampal neurons, HT22 cells (Huang *et al.*, 2013a).

Although the above studies have shown promise regarding the variety of protective roles of various chemical compounds that have been identified, it is important to note that the significant generation of endogenous antioxidants cannot be uniformly effective in establishing equilibrium regarding the over-accumulation of Acr-induced oxidative stress. Taking this into consideration, in addition to the fact that relatively few studies have been published with respect to this issue, it is important to highlight the greater number of naturally-occurring metabolites with protective functions regarding Acr-induced oxidative damage.

#### **1.4.4 Anti-oxidative stress enzyme**

A growing body of research suggests that the main pathological changes of AD are all related to oxidative stress, and oxidative stress could integrate, at least in part, other hypotheses for pathogenesis of AD. Thus, attenuating oxidative stress is a potential therapeutic strategy for AD (Wang *et al.*, 2017). But as a matter of fact, some exogenous antioxidants are insufficient to resist the overload of oxidative stress, which results in eventual mortality. Nrf2 is an important regulator of antioxidant response element (ARE)-activated gene expression (Wang *et al.*, 2017). It has been reported that there is a reduced level of Nrf2 in post-mortem brain tissue from AD patients (Wang *et al.*, 2017). Previous *in vivo* studies also found that the Nrf2–ARE pathway was suppressed in APP/PS1 transgenic mouse brain (Wang *et al.*, 2017). Further, intrahippocampal injection of a lentiviral vector expressing Nrf2 improves spatial learning in a mouse model of AD (Wang *et al.*, 2017).

Nevertheless, there are numbers of natural and synthetic small molecules that can activate Nrf2/ARE pathway. Growing studies over the past several years have demonstrated that 2-dithiole-3-thione (D3T) (Figure 1.10) is a protect inducer of endogenous antioxidants. D3T can protect against acrolein-induced neurocytotoxicity and 1-methyl-4-phenyl-1,2,3,6-tetrahydropyridine (MPTP)-induced neurotoxicity in SH-SY5Y cells and in wild-type mice, respectively, through *uP*-regulation of cellular antioxidant genes and knockout mice (Wang *et al.*, 2017). Polyphenols, although not electrophilic, can cross the

hydrophobic lipid membrane and get oxidised intracellularly to form quinonelike electrophiles (Joshi and Johnson, 2012). Hence, these catechol-like molecules can function as pro-drugs. Carnosic acid (Figure 1.10), a catechol-like electrophile has been shown to protect neurons against glutamate-mediated toxicity *in vitro* and brain against ischemia reperfusion injury *in vivo* via activation of Nrf2-ARE pathway (Joshi and Johnson, 2012). Among other non-flavanoid polyphenols, curcumin and resveratrol have shown to activate Nrf2 leading to subsequent protection of neural cells from oxidative insult and toxins in *in vitro* and *in vivo* models of AD (Joshi and Johnson, 2012). Flavonoid polyphenols such as epigallocatechin-3-gallate (EGCG) and quercetine, and organo-sulphur based compounds such as sulforaphane (Figure 1.10) are potent activator of Nrf2 that have been shown to be neuroprotective against oxidative stress *in vitro* (Joshi and Johnson, 2012).

Another class of Nrf2 activators is triterpenoid-based compounds. Synthetic triterpenoids are derived from 2-cyano-3,12-dioxooleana-1,9-dien-28-oic acid (CDDO). CDDO and its derivatives have been tested for their antioxidant and anti-inflammatory properties and are known to activate the Nrf2-ARE pathway in *in vitro* and *in vivo* in animal models of various disorders. As mentioned earlier, in the neurodegenerative disorder paradigm, CDDO-methyl amine (CDDO-MA), an analogue of CDDO (Figure 1.10), showed improved memory and reduced A $\beta$  plaques and oxidised proteins in AD transgenic mouse model (Joshi and Johnson, 2012). Accordingly, previous animal and clinical studies have demonstrated that Nrf2-ARE pathway is of great significance in the neuroprotection (Cao *et al.*, 2016; Wang *et al.*, 2017). However, the underlying mechanisms of low expression of Nrf2 in AD patients remain largely unknown and need to be further investigated (Cao *et al.*, 2016).

Despite that, Nrf2 is mainly sequestered in the cytoplasm by Kelch-like ECH associated protein 1 (Keap1) (Figure 1.11). In response to ROS, Nrf2 could be translocated from the cytoplasm to the nucleus and subsequently binds with ARE. This process can promote expression of a variety of antioxidant genes, such as redox regulation, including SOD, CAT, sulfaredoxin (Srx), thioredoxin (Trx), peroxiredoxin (Prdx) system; glutathione synthesis and metabolism, including Gpx, glutathione reductase (GR), -glutamine cysteine ligase (GCL) and synthase (GCS); quinone recycling, including NAD(P)H

quinone oxidoreductase (NQO1); and iron homeostasis including heme oxygenase 1 (HO-1) and Ferritin, which exert cytoprotective effects against oxidative stress (Cao *et al.*, 2016; Joshi and Johnson, 2012).

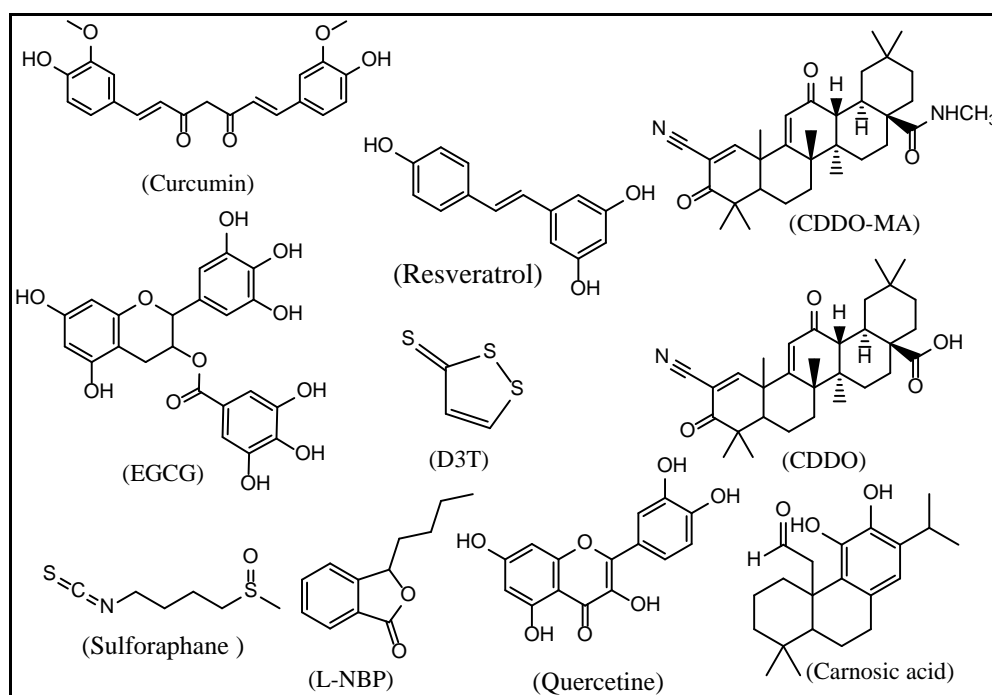


**Figure 1.10:** Chemical structures of natural and synthetic low molecule compounds based on the activation of Nrf2 pathway and NQO1. L-3-n-butylphthalide, 3H-1, 2-dithiole-3-thione, epigallocatechin 3- gallate, 2-cyano-3,12-dioxooleana-1,9-dien-28-oic acid and 2-cyano-3,12-dioxooleana-1,9-dien-28-oic acid methyl amine labelled as L-NBP, D3T, EGCG, CDDO and CDDO-MA, respectively.

Keap1 functions as adaptor for the culin 3-based E3 ligase (Figure 1.11). Under normal unstressed condition, Nrf2 is ubiquitinated and rapidly degraded (half life ~ 20 min) by ubiquitin-proteasome system (Joshi and Johnson, 2012). Under conditions of oxidative stress by either reactive electrophiles such as acrolein, toxins or ARE inducers, the interaction between Nrf2 and Keap1 is disrupted and Nrf2 translocates to the nucleus. In the nucleus, it binds to small Maf proteins that increase the transcription rate of ARE-driven genes such as NQO1 (Joshi and Johnson, 2012).

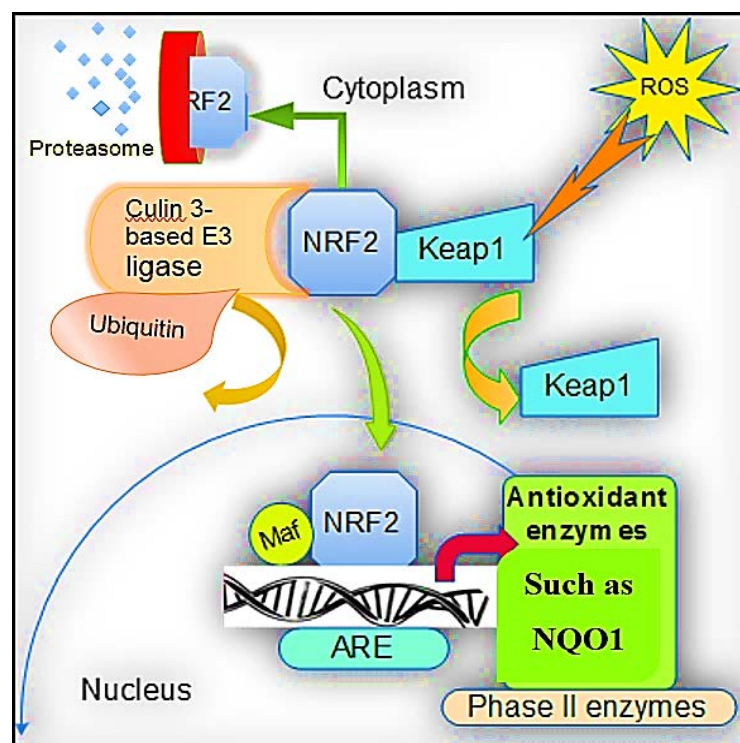


**Figure 1.11:** The mechanism of action of the regulation of Nrf2. Under basal conditions, Nrf2 is polyubiquitylated by the KEAP1–Cul3 E3 ligase and subsequently degraded by the proteasome. Under conditions of oxidative stress including ROS and cytotoxic electrophiles (acrolein), the KEAP1–Nrf2 interaction is destabilised, causing Nrf2 to dimerise with Maf protein within the nucleus. Nrf2 bind to ARE, promoting transcription of cellular defence genes of phase II enzymes such as NQO1.

#### 1.4.5 NAD(P)H:quinine oxidoreductase (NQO1)

NAD(P)H:quinine oxidoreductase 1 (NQO1) is an antioxidant enzyme a member of the NAD(P)H dehydrogenase(quinone) family and involved in an obligate two-electron reductase characterised by its capacity for using NADH or NADPH as a reducing cofactor (Joshi and Johnson, 2012; SantaCruz *et al.*, 2004; Wang *et al.*, 2017). NQO1 is generally expressed in various tissues and cells and highly expressed in the CNS (Joshi and Johnson, 2012; Luo *et al.*, 2015). NQO1 is expressed under transcriptional regulation by Keap1/Nrf2 pathway or uP-regulation of NQO1 which has been extensively used as a biomarker. It has been hypothesised that regulation of NQO1 may protect the cell from oxidative damage due to the ability of NQO1 to reduce acrolein, H<sub>2</sub>O<sub>2</sub> and ROS free radical that have been produced from unstable formation of hydroquinone (Siegel *et al.*, 2012).

In response to oxidative stress, cytoprotection is afforded by the upregulation of multiple antioxidant enzyme systems (Raina *et al.*, 1999). This co-ordinately transcriptionally regulated phase II enzyme functions in quinone detoxification (via a two-electron transfer), redox-sensitive chemoprotection in certain neoplastic models, activation of prodrugs (Raina *et al.*, 1999). Therefore, NQO1 acts as a sensitive indicator of the redox state of cells (Raina *et al.*, 1999). Preliminary evidence suggests that increased NQO1 activity has been found in hippocampal pyramidal neurons of AD patients, suggesting that the variants of the NQO1 gene might confer susceptibility for AD progression by affecting NQO1 activity (Luo *et al.*, 2015). One of these studies has been published by Peng *et al.*, (2010) that an extract from Chinese celery called L-3-n-butylphthalide (L-NBP) (Figure 1.10) has found to produce neuro-protections in AD where NQO1 was significantly up-regulated via L-NBP. The importance of NQO1 as a monitor of redox balance together with the proposed importance of oxidative stress in AD provided the impetus to explore the status of NQO1 in AD.

### **1.5. Drugs approved by the FDA for the treatment of Alzheimer's disease**

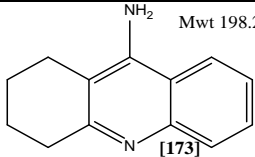
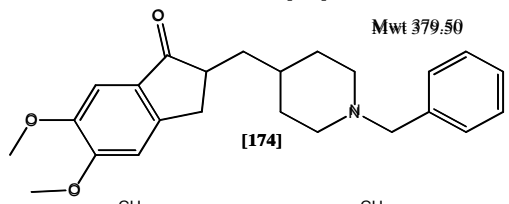
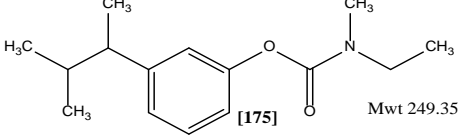
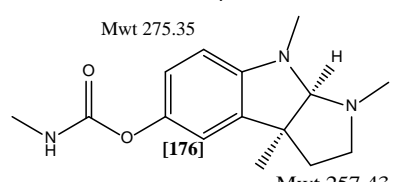
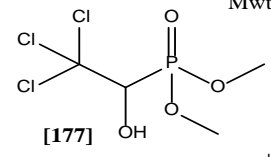
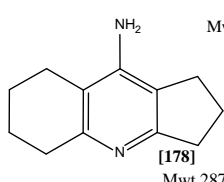
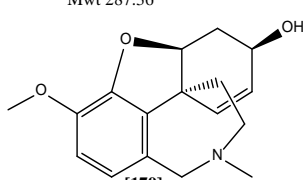
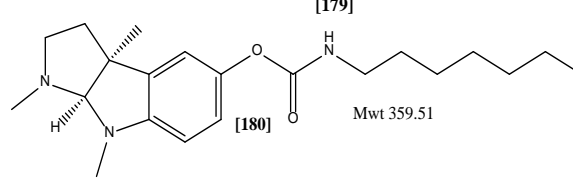
According to Islam *et al.* (2017), and Brahmachari (2012), the discovery of a link between AD and the inhibition of cholinergic neuron activity signified that the 1970s bore witness to the development of a range of naturally-occurring compounds (mainly derived from plants) capable of elevating cholinergic neurotransmission. For the most part, these natural substances act as direct stimulants of agonist receptors, or alternatively inhibit the breakdown of AChE inhibitors at the neuromuscular junction. At present, however, it is important not to overlook the fact that no curative or preventive therapeutic interventions exist that can be applied to AD. In certain cases, FDA-approved drugs are administered to manage AD, and each is associated with a range of symptomatic advantages as described in subheadings as below.

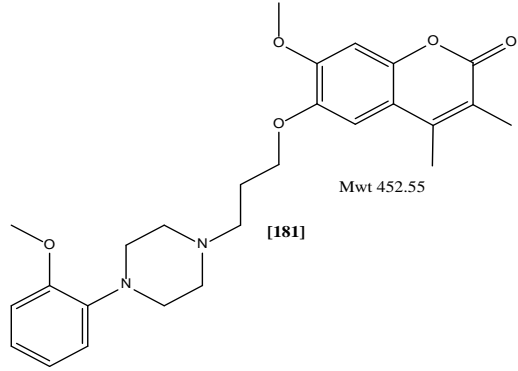
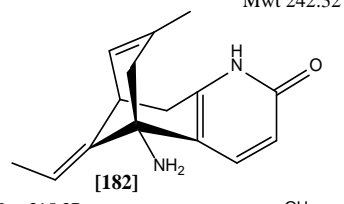
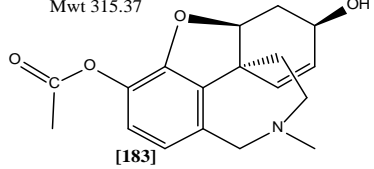
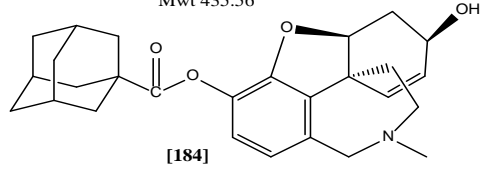
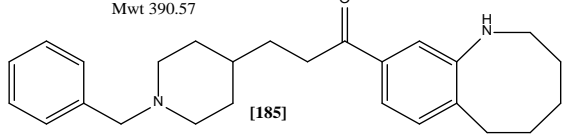
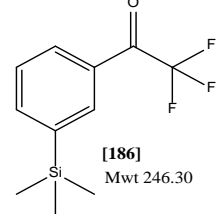
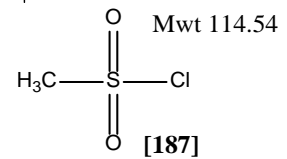
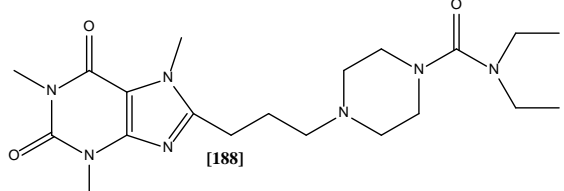
#### **1.5.1 Cholinesterase inhibition (AChE)**

The mechanisms by which AChE inhibitors act are associated with the prolongation of the action of synaptic acetylcholine by preventing its breakdown (Mount and Downton, 2006). Certain drugs have already received FDA approval, and others have yet to be tested and approved by the organisation (a full list is given in Table 1.2). It is worth noting that

almost all drugs submitted for investigation as potential candidates for AD treatment or prevention have been rejected, primarily as a consequence of the unfavourable – and often dangerous – secondary effects they give rise to. These will be outlined in the following sections.

**Table 1.2:** AChE drugs in clinical development for AD, including European registration (Francis *et al.*, 1999; Jann, 2000; Mohan and Gupta, 2016; Mount and Downton, 2006; Nordberg and Svensson, 1998).

Phase	Drug name	Company	Chemical structure
Registered	Tacrine (Cognex <sup>®</sup> )	Parke-Davis	 Mwt 198.27 [173]
Registered	Donepezil (Aricept <sup>®</sup> )	Eisai /Pfizer	 Mwt 379.50 [174]
Registered	Revastigmine (Exelon <sup>®</sup> )	Novartis	 Mwt 249.35 [175]
Registered	Physostigmine (Synapton <sup>®</sup> )	Forset laboratories	 Mwt 275.35 [176]
Waiting approval	Metrifonate	Bayer	 Mwt 257.43 [177]
III	Amiridin	Nikken chemicals Co Inc	 Mwt 224.73 [178]
III	Galantamine	Razadyne, Johnson & Johnson	 Mwt 287.36 [179]
III	Eptastigmine	Mediolanum Farmaceutical SpA	 Mwt 359.51 [180]

II	Ensaculin hydrochloride	Dr Wilmar Schawbe GmbH and Co	 <p>Mwt 452.55</p> <p>[181]</p>
II	Huperazine A	Mayo foundation	 <p>Mwt 242.32</p> <p>[182]</p>
II	P-11012 <sup>11</sup>	Hoechst AG	 <p>Mwt 315.37</p> <p>[183]</p>
II	P-11149 <sup>12</sup>	Hoechst AG	 <p>Mwt 435.56</p> <p>[184]</p>
II	TAK-147	Takeda Chemical Industries Ltd	 <p>Mwt 390.57</p> <p>[185]</p>
II	Zifrosilone	Hoechst Marion Roussel Inc	 <p>Mwt 246.30</p> <p>[186]</p>
II	Methanesulfonyl chloride	University of texas system	 <p>Mwt 114.54</p> <p>[187]</p>
II	S-9977	Servier	 <p>[188]</p>

<sup>11</sup> P-11012 is one of the derivatives of the galantamine structure (Mohan and Gupta, 2016).

<sup>12</sup> P-11149 is also one of the derivatives of the chemical structure of galantamine (Mohan and Gupta, 2016).

### 1.5.1.1 Tacrine (Cognex®)

Tetrahydroaminoacridine (also referred to as Tacrine (Cognex®) [173] is a potent, centrally active and first generation of AChE inhibitor, which was at one point routinely applied in the treatment of AD. It was the first cholinesterase inhibitor, and received approval from the FDA at the beginning of the 1990s (Benjamin and Burns, 2007; Farlow, 1992; Knopman, 1995; Eagger, *et al.*, 1991; Mount and Downton, 2006). Despite the fact that small-scale clinical trials have underlined the cognitive improvements AD sufferers have displayed when subjected to tacrine treatment, Farlow (1992) indicated that no statistically significant evidence for any beneficial impact. In light of these findings, tacrine treatment has been discontinued, due to its low selectivity for AChE in the CNS, undesirable systemic side effects, including hepatotoxic effects due to elevated Alanine Aminotransferase (ALT) levels, approximately 49% higher than normal, and the need to be taken four times daily due to its phenolic derivative, which is excreted rapidly from the body and associated with a short half-life (Benjamin and Burns, 2007; Farlow, 1992; Jann, 2000; Knopman, 1995; Eagger, Levy and Sahakian, 1991; Mount and Downton, 2006).

### 1.5.1.2 Donepezil (Aricept®)

As a synthetic, non-covalent reversible that is a member of the second generation of AChE inhibitors, donepezil hydrochloride (also referred to as Aricept®) [174] can be legally prescribed in the United States and the United Kingdom for the treatment of AD cases that are not severe (Benjamin and Burns, 2007; Burns *et al.*, 1999). One of the most notable features of donepezil is that it was the second drug to reach the commercial market; it received approval from the US FDA in 2006 for the treatment of severe AD, and later in the same year from the UK National Institute for Health and Care Excellence (NICE) for the treatment of moderate AD (Benjamin and Burns, 2007; Desai and Grossberg, 2005). Nevertheless, preclinical, and clinical studies conducted relatively recently in Japan and the United States have demonstrated that donepezil is associated with hepatotoxicity, as well as other unfavourable secondary effects including anorexia, muscle cramps, cardiovascular disorders, abnormalities in electroencephalogram EEG tests, and, most frequently, gastrointestinal side effect including nausea, vomiting and

diarrhoea (Burns *et al.*, 1999; Kogan *et al.*, 2001; Tan *et al.*, 2014; Nordberg and Svensson, 1998).

#### **1.5.1.3 Rivastagmine (Exelon®/ Reminyl®)**

As a sustained inhibitor of AChE and Butyrylcholinesterase (BuChE<sup>13</sup>), rivastigmine [175] is a drug often prescribed for cases of non-severe AD (Sadeghi *et al.*, 2016; Nordberg and Svensson, 1998). The drug first received approval in Europe, and was the third generation of AChE inhibitor to be commercially released (Desai and Grossberg, 2005). Nevertheless, a crucial feature that is absent in almost all studies pertaining to the drug is quantifications of the plasma concentration of rivastigmine in AD patients. For the most part, the literature utilises the Mini-Mental Status Examination (MMSE) and the AD Assessment Scale-Cognitive Subscale (ADAS-Cog) to measure the cognitive results of cholinesterase inhibitors (ChEI) therapy, as noted by Chen *et al.* (2017). However, routine gastrointestinal secondary impacts of the drug have been identified, and have been ranked as even more severe as those of donepezil (Tan *et al.*, 2014; Nordberg and Svensson, 1998).

#### **1.5.1.4 Galantamine (Razadyne®)**

Galantamine [179] is a phenanthrene alkaloid similar to codeine which was isolated from the European daffodil or common snowdrop, *Galanthus nivalis* and process a reversible inhibitor of AChE (Desai and Grossberg, 2005; Nordberg and Svensson, 1998). Although it has been approved in the United States for treatment interventions with patients with non-severe cases of AD (Ohta *et al.*, 2017), the unfavourable secondary effects of the drug are well-documented, with 63% of patients reporting nausea symptoms and a further 4% presenting with abdominal pains, anorexia, and diarrhoea in a study conducted by Nordberg and Svensson (1998).

#### **1.5.1.5 Physostigmine (Synapton®)**

This drug [176] is classified as a tertiary amine, and it is characterised by lipophilic properties. In addition, according to the research conducted by Nordberg and Svensson

---

<sup>13</sup> BuChE is a carboxylic ester hydrolysis originated from the glial cell of the brain (Desai and Grossberg, 2005).

(1998), it serves as a reversible inhibitor of AChE and BuChE. However, due to its unfavourable oral bioavailability, very short half-life (16 minutes) resulting in a dosing frequency of every 2 to 4 hours, it is relatively restricted in terms of its clinical utility (Desai and Grossberg, 2005; Nordberg and Svensson, 1998; Polinsky, 1998). In addition, it was associated with dizziness (10.9%), diarrhoea (12.6%), and anorexia (10.9%) in the sample group of a study by Nordberg and Svensson (1998). Furthermore, a study by Mount and Downton (2006) found that 30-40% of the AD patients treated with the drug failed to provide positive indications after treatment with AChE inhibitors, while 29% withdrew from clinical trials owing to the side effects (in comparison to 18% of patients from the placebo group).

### 1.5.2 N-methyl-D-aspartate (NMDA) receptor antagonist

Memantine [189], as illustrated in Figure 1.12, constitutes a low-to-moderate affinity NMDA receptor (NMDAR) antagonist, and is understood to operate by facilitating the regulation of glutamate. It received FDA approval towards the end of 2003 for the treatment of AD patients (based in the United Kingdom and United States) exhibiting moderate-to-severe symptoms (Ansari and Khodagholi, 2013; Chen *et al.*, 2017; Tan *et al.*, 2014). Nevertheless, based on the low cost-effectiveness of the drug, NICE has argued that the drug should be discontinued in clinical contexts (Benjamin and Burns, 2007; Hansen *et al.*, 2008; Marum, 2009).

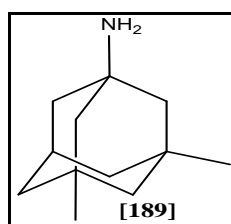


**Figure 1.12:** Structure of memantine [189] an NMDA receptor antagonist with a Mwt 179.31

### 1.5.3 Monoclonal Antibodies (mABs)

The following subsections will examine a series of mABs that have been studied with respect to their potential as anti-A $\beta$  treatment options (see Table 1.3).

**Table 1.3:** mABs drugs from Immunoglobulin G (IgG) isotope in clinical development for AD.

Phase	Drug name	Company	Reference
<u>III</u> *	Solanezumab (LY2062430)	Eli Lilly	(Hung and Fu, 2017)
<u>II</u> *	Ponezumab (PF-04360365)	Pfizer	(Imbimbo <i>et al.</i> , 2012)
<u>II</u>	Bapineuzumab (AAB-001)	Pfizer/Elan	(Cummings <i>et al.</i> , 2017; Khorassani and Hilar, 2013)
<u>III</u>	Crenezumab (MABT5102A)	Roche/Genentech	(Hung and Fu, 2017)
<u>II</u>	Gantenerumab (RO4909832)	Roche	(Hung and Fu, 2017)

\* Indicated that the drug has been failed for further examination and discontinued.

### 1.5.3.1 Solanezumab (LY2062430)

As a humanised monoclonal antibody (mABs) characterised by the binding with respect to the A $\beta$  central region in AD patients, solanezumab is a peptide that research suggests performs a critical function in AD pathogenesis (Imbimbo *et al.*, 2017). Nevertheless, owing to the way in which the mAB failed to satisfy the primary and secondary endpoints in two phases of IIB-III A research projects, the use of the drug is no longer a clinical possibility (Imbimbo *et al.*, 2012; Mehta *et al.*, 2017).

### 1.5.3.2 Ponezumab (PF-04360365)

The defining characteristic of this mAB relates to the way in which it engages in the targeting of the free C-terminus of A $\beta$ <sub>1-40</sub>. Although it made its way to Phase I and Phase II of clinical development, Pfizer facilitated its discontinuation in the summer of 2011 owing to the way in which its Phase II development failed to provide a comprehensive account of the Phase III design (Mehta *et al.*, 2017; Imbimbo *et al.*, 2017).

### 1.5.3.3 Bapineuzumab (AAB-001)

According to Mehta *et al.* (2017), bapineuzumab is virtually unique owing to the way in which it constitutes an mAB that reached clinical Phase III trials. The researchers further described that it operates by targeting A $\beta$  oligomers and plaque (Mehta *et al.*, 2017). During the Phase III trials, it was noted that administration of the drug facilitated a reduction in the cerebrospinal fluid (CSF) tau protein, but considerable clinical

advantages were not observed with respect to the investigated cognitive or functional goals (Mehta *et al.*, 2017). Limitations of this drug emerged when ApoE4 carriers were found to be more likely to develop a higher propensity with this drug (Mehta *et al.*, 2017).

#### **1.5.3.4 Crenezumab (MABT5102A)**

Crenezumab has recently become relevant and was safe owing to its allocation as the central point of the Alzheimer's Prevention Initiative (API) trial, which was initiated in 2012, and is planned to complete in 2017 (Mehta *et al.*, 2017). During Phase II trials, the drug was identified as being associated with a positive level of penetration with respect to the blood-brain barrier (BBB), along with a favourable affinity for A $\beta$  monomers, oligomers, and fibrils (Mehta *et al.*, 2017). Furthermore, one of its key strengths was found to be that it is not associated with the negative impact of vasogenic oedema, as observed with solanezumab and bapineuzumab (Mehta *et al.*, 2017). Although the outcomes from Phase II did not show a significant benefit in treatment of AD compared to the placebo, the next phase of the trials is now being conducted (Mehta *et al.*, 2017).

#### **1.5.3.5 Gantenerumab (RO4909832)**

During Phase III trials, this drug was ineffective in demonstrating its clinical utility, but it is important to note that it was shown to inhibit A $\beta$ , owing to a standardised uptake value ratio (SUVR), in a dose-dependent way, along with CSF tau<sup>14</sup> (Mehta *et al.*, 2017). This is indicative of brain amyloid clearance, as well as an impact on the downstream indicators of neurodegeneration (Mehta *et al.*, 2017). Accordingly, the use of mABs as a target for clearing amyloid has become prominent in recent trials. The prospect of using amyloid as a target is an attractive one because of its extra-neuronal nature, as well as its toxicity in the milieu. Nevertheless, as highlighted by Mehta *et al.* (2017), it is important to recognise that one of the fundamental determinants of mABs' lack of concrete achievement in recent years is the fact that amyloid is uncorrelated with cognitive decline in the symptomatic phase of dementia (Mehta *et al.*, 2017).

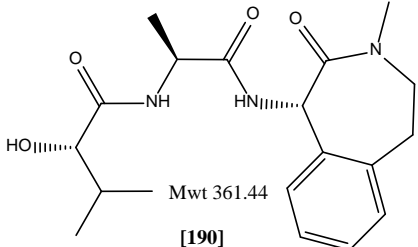
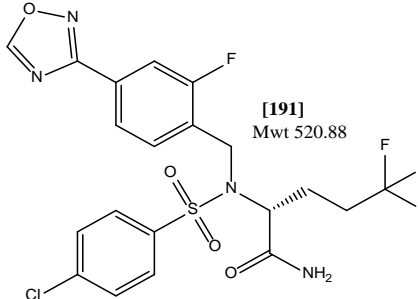
---

<sup>14</sup> Tau protein is the major component of the intracellular filamentous deposits that define a number of neurodegenerative diseases (Goedert, 2004).

### 1.5.4 Gamma Secretase Inhibitors

The inhibition of  $\gamma$ -secretase, a protease complex constituted of various subunits (namely, nicastrin (NCSTN), presenilin (PEN-1), anterior pharynx-defective 1 (APH-1), and presenilin enhancer 2 (PEN-2)), has been identified as a potential means of lowering amyloid production, primarily because the aforementioned subunits are seen as viable therapeutic targets for the modulation of A $\beta$  production (or, alternatively, an increase in A $\beta$  clearance) (Hung and Fu, 2017). Given that the inhibition of  $\gamma$ -secretase could facilitate a decrease in the production of A $\beta_{42}$ , certain clinical trial drugs are given in Table 1.4 (Mehta *et al.*, 2017).

**Table 1.4:** Gamma secretase inhibitors - clinical trial drugs that target A $\beta$  clearance.

Phase	Drug name	Company	Structure	Reference
II*	Semagacestat LY451039	Elli Lilly	 Mwt 361.44 [190]	(Hung and Fu, 2017)
II*	Avagacestat BMS-708163	Bristol-Myers Squibb	 Mwt 520.88 [191]	(Hung and Fu, 2017; Tong <i>et al.</i> , 2012)

\* Indicated that the drug is discontinued

#### 1.5.4.1 Semagacestat (LY451039)

Owing to the way that this  $\gamma$ -secretase inhibitor [190] provided an indication of dose-dependent changes to CSF biomarkers in its Phase I trial, Phase II trials were initiated (Mehta *et al.*, 2017). However, it should be noted that its Phase III trials yielded dissatisfactory results, as the inhibitor could not satisfy its main endpoints; symptoms for certain AD patients became more severe, and infections, cancers, and other permanent secondary effects were identified (Hung and Fu, 2017; Mehta *et al.*, 2017).

#### 1.5.4.2 Avagacestat (BMS-708163)

One of the notable features of this  $\gamma$ -secretase inhibitor [191] is that it facilitates a dose-dependent reduction in A $\beta$  isoforms. Nevertheless, despite clinical advancement in the conditions of certain patients after treatment, a 12-week washout follow-up offered no clear indication that status changes had taken place. In prodromal situations, the drug heightened the likelihood of skin cancers, diarrhoea, nausea, glycosuria, rashes, and cerebral microbleeds (Hung and Fu, 2017; Mehta *et al.*, 2017). As a consequence of these considerations, along with the inhibitor's relatively limited therapeutic window with respect to effectiveness and severe secondary effects, trials were stopped in 2012 after the second phase (Hung and Fu, 2017; Mehta *et al.*, 2017).

#### 1.5.5 Other target drugs in clinical trials for AD

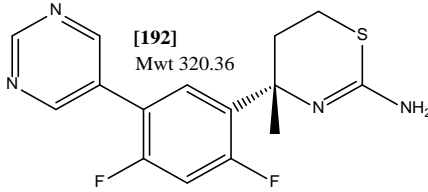
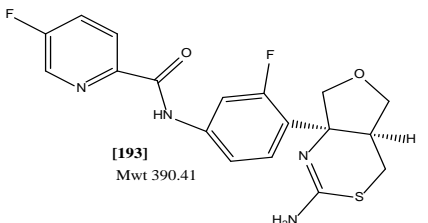
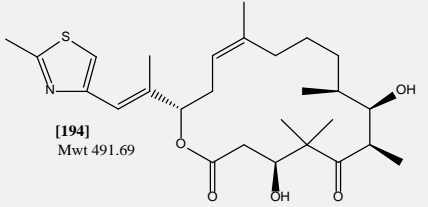
Various approaches have been taken to AD clinical trials, including the use of Beta-secretase 1 (BACE) inhibitors, the targeting of neurofibrillary tangles (NFTs<sup>15</sup>), and microglial activation. At the same time, numerous synthetic compounds have been sought for the treatment of AD via different target pathways (listed in Table 1.5); however, all have been linked to unfavourable secondary effects (Islam *et al.*, 2017). Perhaps most importantly, no drug has yet emerged that can consistently facilitate the effective prevention or treatment of AD (Islam *et al.*, 2017).

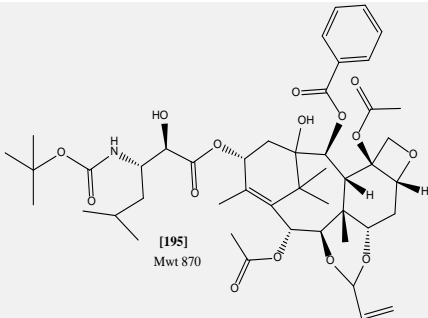
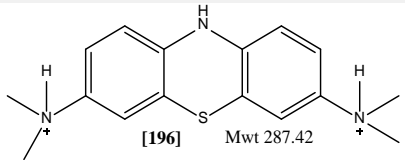
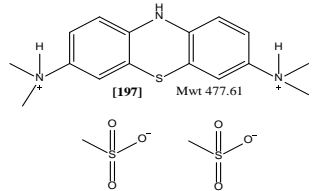
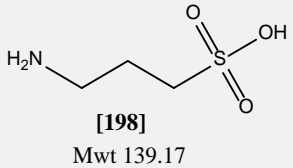
According to Essa *et al.* (2016), synthetic inhibitors can be categorised into the following groups: (i) carbonyl-capturing agents, the purpose of which is to mitigate carbonyl stress; (ii) cross-link breakers; and (iii) metal ion chelators. Ultimately, owing to their ineffective pharmacokinetic properties, their poor efficacy, and absent safety standards, all clinical trials involving these treatment interventions have been discontinued (Essa *et al.*, 2016). However, evidence has been found to suggest that NP are non-hazardous when consumed (Essa *et al.*, 2016). Therefore, researchers are currently searching for new AD treatments in natural product, as safer and more effective therapies that can more precisely target the pathophysiology of AD (Islam *et al.*, 2017).

---

<sup>15</sup> NFTs it is one of the pathogenetic factor of AD that consist of aggregates of paired of helically twisted filaments of hyperphosphorylated tau (Godyń *et al.*, 2016).

**Table 1.5:** Short summary of clinical trial compounds, listing the pharmaceutical company, the chemical structure, and their current progress status.

Target	Phase	Drug name	Cause for Discontinuation	Company	Structure	Reference
BACE inhibitor	I* in 2015	BI 1181181	Low oral bioavailability and low blood-brain barrier penetration	Boehringer Ingelheim, Vitae Pharmaceuticals	Not disclosed	(Chackalamanil <i>et al.</i> , 2017)
	I* in 2013	RG7129	Liver toxicity	Roche	Not disclosed	(Erlanson <i>et al.</i> , 2016)
	I* in 2008	LY2811376	Liver toxicity	Eli Lilly	 <p>[192] Mwt 320.36</p>	(Hung and Fu, 2017; Holenz <i>et al.</i> , 2016)
	II* in 2013	LY2886721	Liver toxicity	Eli Lilly	 <p>[193] Mwt 390.41</p>	(Chackalamanil <i>et al.</i> , 2017)
Tau	I* in 2013	Epothilone D	Not applicable	Bristol-Myers Squibb	 <p>[194] Mwt 491.69</p>	(Hung and Fu, 2017; Neidle, 2014)

	II	TPI 287	Not applicable	Cortice Biosciences	 <p>[195] Mwt 870</p>	(Hung and Fu, 2017; Ballatore <i>et al.</i> , 2016)
Tau inhibitor	I* in 2007	Rember™ (MTC)	diarrhea, urinary urgency, painful urination, etc	TauRx Therapeutics Ltd	 <p>[196] Mwt 287.42</p>	(Hung and Fu, 2017; Sabnis, 2010)
	III	TRx0237 (LMTX)	Not applicable	TauRx Therapeutics Ltd	 <p>[197] Mwt 477.61</p>	(Hung and Fu, 2017; Seneci, 2015)
Microglial	III* in 2007	Alzhemed™ (tramiprosate)	No clinical efficacy	Neurochem, Inc	 <p>[198] Mwt 139.17</p>	(Hung and Fu, 2017; Adejare, 2016)

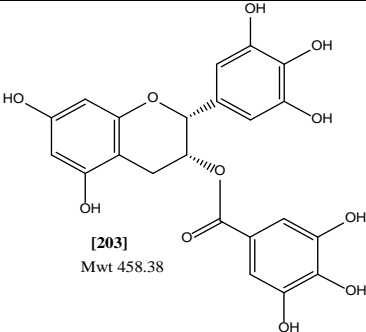
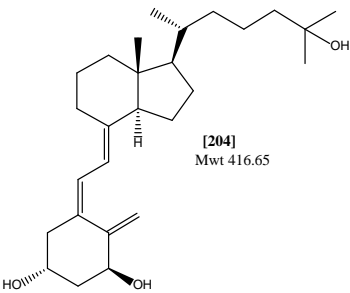
III	Azeliragon	Not applicable	Pfizer, TransTech Pharma, Inc., Therapeutics LLC	<p>[199] Mwt 532.13</p>	(Hung and Fu, 2017; Godyń <i>et al.</i> , 2016)
IV* in 2005	Ibuprofen	No clinical efficacy	Not available	<p>[200] Mwt 206.29</p>	(Hung and Fu, 2017)
III* in 2008	Flurizan™	No clinical efficacy	Myriad Genetics & Laboratories	<p>[201] Mwt 244.27</p>	(Hung and Fu, 2017)
II	CHF 5074	Not applicable	CereSpir™ Incorporated, Chiesi Pharmaceuticals Inc.	<p>[202] Mwt 325.16</p>	(Hung and Fu, 2017)

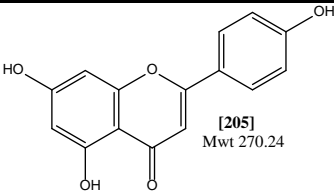
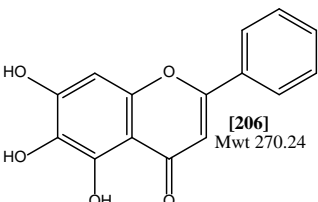
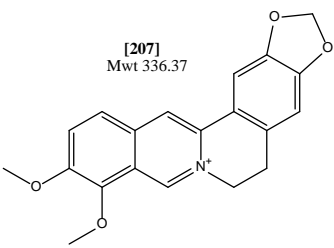
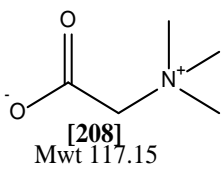
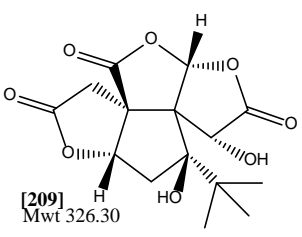
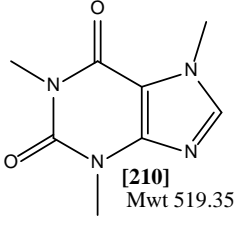
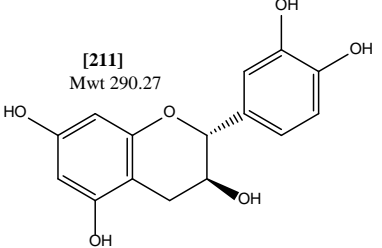
\*Compounds were discontinued

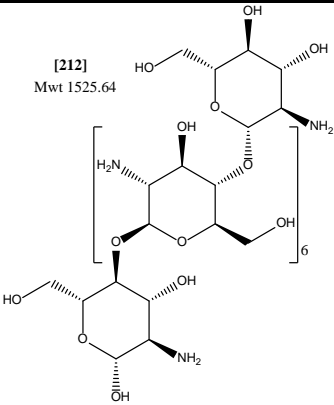
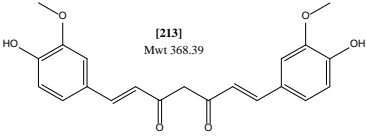
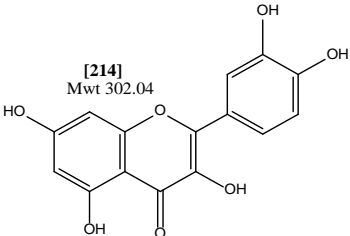
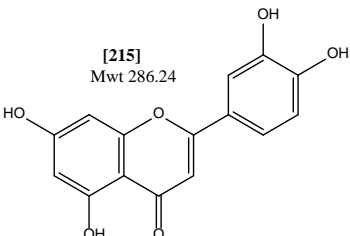
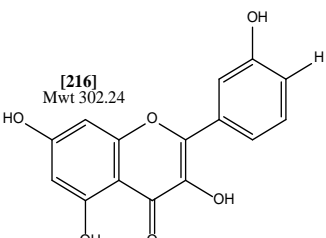
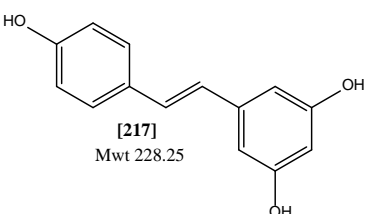
## 1.6. Role of medicinal plants in Alzheimer's disease

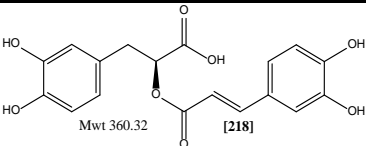
Medicinal plants are a major source from which modern medicine is deriving protective compounds for the treatment and prevention of AD, are crucial to the present clinical context worldwide (Brahmachari, 2012). Arguably, the key advantages of naturally-occurring medicinal plants are their cost-effectiveness, as well as their less severe secondary effects such as gallantamine and physostigmine. In recent years, certain studies have sought to gain insight into the impact that crude plant extract has on AD patients, and researchers have attempted to isolate the active substance that brings about protective impacts (such as the lowering of OS, A $\beta$  accumulation, toxicity, tau phosphorylation, and neuroinflammation) (Ansari and Khodagholi, 2013; Brantley *et al.*, 2012; Islam *et al.*, 2017). The following subsections will therefore outline the key studies in this area, and present the main findings of those studies regarding the existence of neuroprotective natural compounds, along with their chemical structure, source, and mechanisms of action (see Table 1.6).

**Table 1.6:** Natural Compounds with protective effect against A $\beta$ .

Compound	Chemical structure	Source of NP	MOA* against A $\beta$	Reference
(-)-Epigallocatechin-3-gallate	 <p>[203] Mwt 458.38</p>	<i>Camellia sinensis</i> L. Kuntze (Theaceae) leave	$\uparrow\alpha$ -secretase, $\downarrow\gamma$ -secretase, $\downarrow$ BACE, $\downarrow$ AChE, $\downarrow$ NO**, $\downarrow$ ROS, $\downarrow$ Iron chelating, $\downarrow$ Inflammatory factors, $\downarrow$ MAPK**, $\downarrow$ Mitochondrial dysfunction	(Ansari and Khodagholi, 2013; Williams <i>et al.</i> , 2011)
Dihydroxyvitamin-D3	 <p>[204] Mwt 416.65</p>	<i>Agaricus bisporus</i>	$\uparrow$ macrophage-mediated $\downarrow$ A $\beta$ phagocytosis apoptosis	(Ansari and Khodagholi, 2013; Jasinghe and Perera, 2005)

Apigenin		<i>Apium graveolens</i>	↓Aβ burden, ↓oxidative stress, ↑ERK**, ↑BDNF**, ↓caspase-12 ↓UPR**, ↓MAPK	(Ansari and Khodagholi, 2013; Gao <i>et al.</i> , 2013)
Baicalein		<i>Scutellaria baicalensis</i> (Root)	↓Aβ production	(Ansari and Khodagholi, 2013; Gao, Huang and Xu, 2001).
Berberine		<i>Berberis</i> and <i>Vitis vinifera</i>	↓tau hyperphosphorylation, ↓Aβ, ↓Inflammatory factors, ↓NF-κB, ↓PI3K/PKB, ↓MAPK	(Ansari and Khodagholi, 2013; Reddy <i>et al.</i> , 2007; Cromwell, 1933).
Betaine		Most fruits and vegetable except <i>Spinacia oleracea</i>	↓tau hyperphosphorylation	(Konstantinova <i>et al.</i> , 2008).
Bilobalide		<i>Ginkgo biloba</i> tree	↓ROS, ↓apoptosis, ↓BACE, ↓GSK-3β, ↑cAMP** -response element binding protein (CREB), ↑BDNF	(Ansari and Khodagholi, 2013).
Caffeine		<i>Coffea arabica</i> L.	Restores memory and ↓Aβ levels	(Ansari and Khodagholi, 2013; Ky <i>et al.</i> , 2001).
Catechin		<i>Camellia sinensis</i> L. <i>Kuntze</i> (Theaceae) leaves	↓Aβ-induced apoptosis	(Williams, Sorribas and Howes, 2011).

Chitosan		<i>Camellia sinensis</i> leave	<p>↓apoptosis, ↓BACE-1, ↓ROS, ↓Ca<sup>2+</sup>, ↑Nrf2, ↑Hsp32, ↑γ-GCS, ↓Hsp90, ↑Hsp70, ↓MAPK, ↓Inflammatory factors</p>	(Ansari and Khodagholi, 2013; Tsuchiya <i>et al.</i> , 1996).
Curcumin		<i>Curcuma longa</i> L.	<p>↓AChE, ↓B-secretase activity, ↑P-GSK-3β, apoptosis, ↑NGF<sup>**</sup>, ↓oxidative stress, ↓Mitochondrial dysfunction</p>	(Ansari and Khodagholi, 2013; Williams <i>et al.</i> , 2011).
Ginkgo		<i>Ginkgo biloba</i> L.	<p>↓OS</p>	(Gao <i>et al.</i> , 2013).
Luteolin		<i>Dahlia variabilis</i>	<p>↓ROS, ↓tau hyperphosphorylation, ↓Aβ, SOD, ↑Nrf2, ↑P-CREB, ↓OS</p>	(Ansari and Khodagholi, 2013; Harborne, 1967).
Quercetin		<i>Agrimonia pilosa</i>	<p>↓Aβ formation, ↓lipid peroxide, ↓apoptosis, ↑pCREB, ↑BDNF, ↓OS, ↓glutathion</p>	(Ansari and Khodagholi, 2013; Williams <i>et al.</i> , 2011).
Resveratrol		<i>Vitis vinifera</i> L.	<p>↓ROS, ↑GSH, ↓AChE, ↓Aβ, ↓Inflammatory factors, ↓NF-κB<sup>**</sup>, ↑Hsp32<sup>**</sup>, ↓OS</p>	(Ansari and Khodagholi, 2013; Williams <i>et al.</i> , 2011).

Rosmarinic acid		<i>Perilla frutescens</i>	↓apoptosis, ↓NF-κB, ↓tau hyperphosphorylation, ↓ROS, ↓DNA fragmentation	(Ansari and Khodagholi, 2013; Takano <i>et al.</i> , 2004).
-----------------	---	---------------------------	---	---

MOA\* = Mechanism of action. MAPK\*\* = mitogen-activated protein kinase. NO\*\* = nitric oxide. UPR\*\* = unfolded protein response. ERK\*\* = Extracellular Signal-regulated Kinase. cAMP\*\* = cyclic adenosine monophosphate. BDNF\*\* = brain-derived neurotrophic factor. NGF\*\* = nerve growth factor. Hsp\*\* = heat shock protein. NF-κB\*\* = nuclear factor-κB.

### 1.7. Metabolomic approaches in NP chemistry

One of the key features of metabolomics is the ability to produce impartial data in a way that can be easily replicated and, ultimately, generate statistically significant results (Dias *et al.*, 2012). A range of separation chemistries should be applied to achieve the highest level of rigour in the analysis of any collected information (Dias *et al.*, 2012). Owing to the technological improvement in sensitivity and resolution, the analysis of multiple compounds can be achieved in a rapid way via data extraction, filtration algorithms, the removal of background noise, detection of peaks throughout large data sets, and transformation of resulting data matrices prior to any statistical analysis (Dias *et al.*, 2012). However, it is important to recognise that the primary intention of metabolomics is to identify the chemical nature of detected signals (Dias *et al.*, 2012). Relatively limited scholarly attention has been directed towards the compatibility of classical NP chemistry approaches with metabolomics, could lead to the identification of bioactive natural products (Dias *et al.*, 2012).

Given that plants are characterised by significant variegation in terms of their chemical nature, identifying bioactive NP in plant extracts is not a straightforward or singular task (Dias *et al.*, 2012). As such, metabolomic profiling various plant extracts or fractions by employing notable analytical platforms (including mass spectrometry with gas chromatography (GC), or liquid chromatography (LC) and nuclear magnetic resonance (NMR) spectroscopy) have been correlated with the plant's biological activity and the use of databases (including the Dictionary of Natural Products (DNP)) as well (Dias *et al.*, 2012; Harvey *et al.*, 2015; Wishart *et al.*, 2007).

Utilising a liquid chromatography mass spectrometry (LCMS) platform in metabolomics profiling has employed high-resolution methods, as opposed to gas chromatography mass

spectrum (GCMS) (Schripsema, 2010). This is primarily due to the limitation of GCMS with respect to its analytical capabilities regarding non-volatile compounds (namely, sugars and amino acids). LCMS is highly sensitive and conducive to the investigation of numerous and more diverse classes of chemical structures for both volatile and non-volatile compounds (Schripsema, 2010).

Analysts would benefit enormously from NMR-based metabolomics, primarily because it could be utilised in identifying chemical composition for the differentiation of plants from other species, and also following various treatment (Dias *et al.*, 2012). In a study conducted by Kim *et al.* (2010), the researchers stated that it would be useful to have an NMR-based metabolomic analysis, with the detection of metabolites via comparative examinations of NMR data against references, or alternatively via structural examinations with 2D-NMR. Similarly, Deyrupa *et al.* (2011) utilised 2D-NMR spectroscopy for the purpose of screening a collection of bioactive metabolite samples of substructures. As a result, new or lead derivative compounds could be examined in intricate metabolite mixtures without the need to fractionate and isolate.

## **1.8. Hypothesis, aims and outcomes of this study**

### **1.8.1 Hypothesis**

The literature addressed the occurrence of phenolic compounds in *F. carica* figs. Earlier studies have accounted for the variability in total anthocyanins and overall phenolic content of the whole fresh fruit, pulp, and the skin of commercial fig cultivars (Solomon *et al.* 2006). It has been described in the literature how phenolic contents can be affected by different approaches in cultivar drying, extraction, pollinisation, and maturation (Anmar *et al.*, 2015; Ango *et al.*, 2016; Ruamrungsri *et al.*, 2016). A study by Oliveira *et al.* (2010) reported quantitative variability in the skin, pulp, and leaves of Portuguese fig cultivars; however, the study neglected to address the occurrence of triterpenes and phytosterol compounds. As such, its focus was limited to volatile and partially volatile compounds, including phenols, aldehydes, ketones, and amino acids. In view of these limited earlier studies on chemical composition, triterpenoid and phytosterol contents of *F. carica* fruit parts have yet to be examined.

Although the anti-platelet, anti-spasmodic, anti-bacterial, anti-inflammatory, and anti-fungal properties of *F. carica* have been extensively documented, relatively little has been said about the impact on anti-oxidative stress associated with AD on the organic soluble compounds obtained from the exocarp, endocarp, and mesocarp of the edible fruit. Traditionally, colourimetric approaches have been employed to examine the chemical compositions of plants (Schofield *et al.*, 2001). However, selective analytical methodologies and High Throughput Screening (HTS) must be used to supplement the existing information found in the literature in order to gain a comprehensive understanding of the connection between secondary metabolites composition and their potential health benefits. In addition to further studies that suggested increased NQO1 activity may be neuroprotective (Bian *et al.*, 2008), it should be emphasised that the impact of the isolated secondary metabolites on acrolein-induced oxidative stress-related AD has yet to be documented.

### 1.8.2 Aims

Therefore, the aim of this study was to:

- (i) Achieve the extraction and isolation of the bioactive metabolites from the exocarp, endocarp and mesocarp parts of the fruit of *F. carica* using high-throughput chromatographic methods such as normal phase Flash<sup>®</sup> chromatography.
- (ii) Integrate the dereplication results to HTS.
- (iii) Explore new insights into the contribution of metabolomic profiling and multivariate analyses that includes Hierarchical Clustering Analysis (HCA), heat mapping, Principal Component Analysis (PCA), and Orthogonal Partial Least Square-Discriminant Analysis (OPLS-DA) as complementary methods to HTS and targeted isolation work.
- (iv) Instead of employing Neuro-2A and rat PC12 cells, bioassay-guided cell viability of the fractions obtained from three fruit parts of *F. carica* were tested using alamarBlue<sup>®</sup> assay on human *in vitro* differentiated SH-SY5Y cell line, to elongate its neurites to create a homogenous and viable human-like neuronal cultures and (Shipley *et al.*, 2016).

- (v) Investigate the effect of mesocarp, endocarp, and exocarp ethyl acetate crude extracts of *F. carica* on acrolein-induced anti-oxidative stress against human *in vitro* differentiated SH-SY5Y cell line.
- (vi) Examine the regulation of the anti-oxidative NQO1 protein by the mesocarp, endocarp, and exocarp ethyl acetate crude extracts by using the qualitative western blotting test against the human *in vitro* differentiated SH-SY5Y cell line.
- (vii) Isolate and identify the active 'lead' compounds from the endocarp, exocarp and mesocarp of *F. carica* via liquid chromatography-mass spectrum (LCMS) in a negative or positive ionisation mode, gas chromatography-mass spectrum (GCMS), and NMR spectroscopy depending on the nature of the target secondary metabolites.

### **1.8.3 Present and future outcomes**

The present outcomes of this study could first provide useful information on the chemical composition of *F. carica* (endocarp, exocarp and mesocarp) extracts in association to the anti-oxidative effect on AD by employing assays on human *in vitro* differentiated SH-SY5Y cells. This would offer possible avenues in the up-regulation of NQO1 activity for future treatment of the prevention of AD. Employing a combination of analytical techniques and HTS will be useful in identifying new sources of secondary metabolites that can be used against AD.

The future outcomes of this study are as follows:

- (i) to fully document the less understood aspects of otherwise well-known medicinal plants, thereby facilitating the upkeep, preservation, and development of these resources, and ideally promoting an elevation in frequency of use that will give rise to employment opportunities and profit;
- (ii) to foster an understanding of the benefits associated with certain medicinal plants, thereby encouraging manufacturers to produce with a view to the economic scale of production and ultimately lowering the price for consumers over synthetic compounds; and

(iii) to contribute to the development of baseline data regarding the nutraceutical potential of *Ficus spp*, thereby facilitating the utilisation of preparations of herbal supplements or selected isolated chemical supplements in the management and prevention of neurodegenerative conditions, including AD.

## **CHAPTER TWO METHODOLOGY**

---

## **2. Methodology**

---

### **2.1. Health and safety**

All of the procedures and experiments in this study were performed in accordance with the laboratory health and safety risk assessments of the University of Strathclyde, Institute of Pharmacy and Biomedical Sciences. A risk assessment was conducted, for which Control of Substances Hazardous to Health Regulation (CoSHH) forms were completed; the outcome was favourable, allowing to work in reasonably practicable and safe working environment conditions.

### **2.2. General equipment**

An IKAA11Basic model analytic miller was purchased from IKA (Breisgau, German). In addition, model R-110 and model R-3 rotary evaporators were purchased from BÜCHI (Flawil, Switzerland). An ultrawave sonicator was purchased from Scientific Laboratories Ltd, and a handheld UV-light (UVGL-55 model) was purchased from UVP (Cambridge, UK). Steinel<sup>®</sup>, an HL heat gun, E-type 3482 (Teningen, German) was used for TLC analysis undertaken in this research. Bibby Scientific Ltd., (Stafford, UK), supplied a Stuart block heater (model SBH 130D/3). Martin Christ Gefriertrocknungsanlagen GmbH, (Osterode am Harz, German), supplied a Christ Alpha 2-4 model freeze dryer.

### **2.3. Plant Materials**

#### **2.3.1 Plant collection**

The native edible fruits were collected in Saudi Arabia during the month of May, 2014, which is the fruiting season for the *Ficus carica*. The fruits were then imported to the UK. The fruit part of *F. carica* was separated into three parts, exocarp, mesocarp and endocarp. Each part was freeze dried separately at -80°C and then left in the desiccator under vacuum for two weeks until required for extractions. The *Ficus spp* was identified by Professor/Curator Jacob Thomas Pandalayil, a taxonomist at the Department of Botany and Microbiology, College of Science, King Saud University. Voucher specimens were deposited at the herbarium of King Saud University (KSU), under KSU number 10561.

### 2.3.2 Plant extraction and partitioning

Plant constituents were extracted via cold and continual maceration, with the use of an overhead and/or magnetic stirrer. This approach has been described to be efficacious due to its comprehensiveness, particularly when organic solvents are used (Harbone, 1998; Heinrich *et al.*, 2004; Waksmundzka-Hajnos *et al.*, 2008). Methanol, acetone and ethyl acetate are the most common solvents used and are good all-purpose solvent for preliminary extractions.

In the present study, dried plant parts from the mesocarp 1.3 g, endocarp 2 g and exocarp 1.74 g (Figure 2.1) were employed. These materials were subsequently ground down to make a fine powder so that the extraction time could be expedited because of the increased surface area. For each different part of the crude material, a different maceration solvent of the aforementioned organic solvents was used. The freeze-dried mesocarp and endocarp granules were first reconstituted with water then the resulting viscous solution was partitioned with equal volumes of ethyl acetate. On the other hand, the exocarp was macerated in HPLC-grade aqueous methanol under continuous stirring with an overhead stirrer at 70 rpm (IKA, RW 16 basic, Germany) for three hours at room temperature; the procedure was carried out thrice. The extract was filtered at the end of every maceration step while the residue was subjected to further maceration. The procedure was repeated until the yellow colour of the organic extract had finally diminished or become transparent. After the extraction was exhausted with methanol, the extraction solvent was changed to acetone and the extraction step was again repeated thrice.

The crude organic extracts for each respective plant part were pooled together and concentrated under vacuum with a rotary evaporator. The dried crude extract was reconstituted with 250 water and solvent partitioned with an equal volume of ethyl acetate by using a separatory funnel. The mixture was shaken in an eight-motion rotation, with air being released following every rotation. Solvent partitioning was carried out thrice, the organic layer was pooled together and the solvent was evaporated under vacuum.



**Figure 2.1:** The successful splitting of the exocarp (A) and endocarp (B) of *F. carica* from the other edible fruit parts, before it was freeze-dried and ground.

## 2.4. Phytochemical methods

For the extraction and chromatographic purification procedures, various solvent systems were used on the three fruit extracts. Chemical profiling was accomplished using LC-MS, TLC and  $^1\text{H-NMR}$ . A phytochemistry profile of the fruit *F. carica* was the outcome of the chemical profiling and biological assay.

### 2.4.1 Chromatographic techniques

Bioactive compounds can be separated and purified by using the chromatographic technique. Chromatography is efficacious because of the various affinities that many constituents of a mixture have toward their mobile and stationary phases. As a result, these different constituent substances move along the stationary phase at various rates, causing the stationary phases and the mobile phases to separate chemical compositions according to differential partitioning. In trying to purify or isolate the chemical components or constituents from a crude extract, several chromatographic techniques can be employed. Generally, based on their polarity to the stationary phase, compounds are then purified and isolated. The present study employed several techniques as part of normal phase chromatography; two of these techniques were thin-layer chromatography (TLC) and flash<sup>®</sup> chromatography.

#### 2.4.1.1 Flash Chromatography

The Flash chromatography method utilises air pumps and compressed air; the mobile phase of the chromatography is pushed through the column by the pressure of the

compressed air, and thus a higher flow-rate in the mobile phase is achieved by a vacuum line. Another term for this technique is medium pressure liquid chromatography (MPLC). The REVELERIS<sup>®</sup> flash chromatography system is among the most contemporaneous and most reliable automated systems, the details of which are shown in Figure 2.2. So that the non-chromophoric and chromophoric constituents of a sample can be detected simultaneously, the instrument is comprised of an integrated UV/UV-Vis/ELSD detection system. Pure components of a given sample may be obtained, though this is reliant on the type of column utilised, and the methodological approach to the experiment has been optimised so that proper resolution can be ensured between the individuated peaks. Dry-loaded samples within a cartridge are chromatographically washed as part of a dry-run on the REVELERIS<sup>®</sup>; within this column, the separation takes place according to the solvents used and the column itself. Consequently, it is possible to ensure both gradient and isocratic elutions.

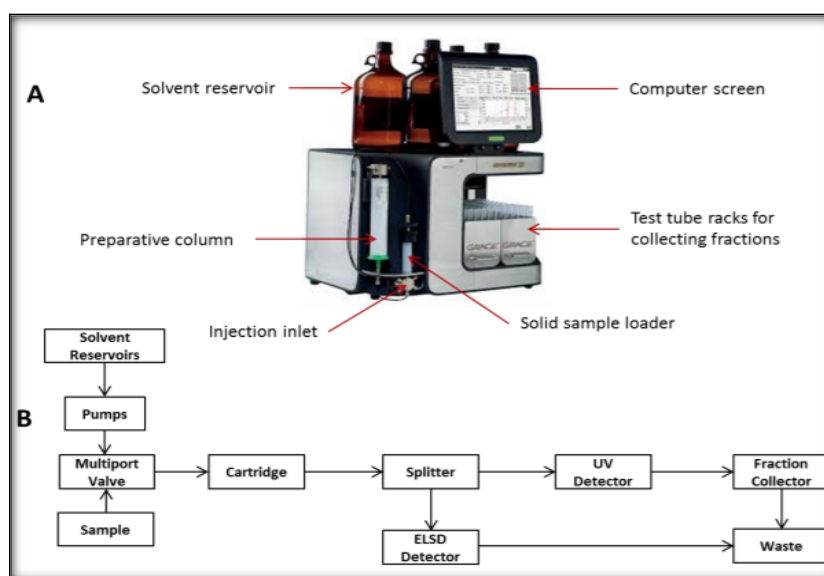


**Figure 2.2:** (A) shows the primary components of REVELERIS<sup>®</sup> flash. (B) Depicts a schematic diagram showing the solvent flow via the primary system components.

The respective crude *F. carica* extracts were loaded and absorbed on inert Celite<sup>®</sup> (Sigma-Aldrich, USA). A gradient of 100% pure-grade hexane to 100% ethyl acetate (HPLC grade) in 5% increments was used for the elution of the compounds. The column was then washed with 200 ml of 100% HPLC grade dichloromethane that was progressively reduced to 70% with 30% methanol.

Those parts of the eluate containing signals that have intensities above the UV detector threshold are collated automatically by the system depending on the capacity of the compounds to absorb UV. Compounds such as these need to have chromophores; these are conjugated double-bond structures, examples of which are those contained within benzenoids. Nevertheless, there are compounds that fail to absorb UV/Vis and therefore they cannot be detected. ELSD (evaporative light scattering detection) was also used on the Grace<sup>®</sup> flash system. Since its response is autonomous from the spectral properties of the compound, ELSD is a universal detector in comparison to the UV (Mefoulas and Kouppris, 2005).

Analyte detection using the ELSD method is completed in three steps: nebulisation, mobile-stage evaporation, and detection. By mixing with an appropriate, nebulising gas (for instance air, or nitrogen), the chromatographic column effluent is nebulised. During post-nebulisation, the liquid then enters the region of the heated drift tube, and herein the mobile stage is evaporated. Only the solid particles of the analyte remain for analysis. Light is scattered by the analyte particles, and detection takes place as incoming radiation hits the analyte entering into the light-scattering cell situated in the drift tube itself (Megoulas and Koupparis 2005).

#### **2.4.1.2 Thin Layer Chromatography (TLC)**

One technique that may be employed to separate and analyse plant extracts in a qualitative manner is thin-layer chromatography (TLC). This is generally utilised to identify the initial characteristic and idiosyncratic fingerprint of an extract and thus demonstrates the various and varied crude mixture constituents, as well as the purity of the isolated compound, (Waksmundzka-Hajnos *et al.* 2008; Rabel and Sherma, 2016a). This process is undertaken according to the differences in migration properties of compounds within various and varied solvent systems. It can also be described as substance partitioning between two immiscible phases (Touchstone 2011).

In this study, a thin layer of adsorbent material was employed as a stationary phase. Silica gel with 60 Å pores immobilised on an aluminium plate and coated with a fluorescent layer (F254) (gel 60 F254; obtained from Merck 105554.0001, Germany) was used. With the F254 layer, UV active compounds could be visualised under short and long-wave

frequencies of UV light, specifically with wavelengths of 254 nm and 365 nm. *P*-anisaldehyde/sulfuric acid spraying reagent was used to visualise UV inactive compounds. The spraying reagent was freshly prepared by dissolving 0.5 mL *P*-anisaldehyde into a solution of 1 mL of concentrated sulphuric acid (Sigma-Aldrich 32,050-1, UK) in 50 mL of glacial acid. The mobile phase is a mixture of organic solvents into which the plate is allowed to develop by capillary diffusion. The solvent mixture migrates to the top of the plate and due to the elution strength of the solvent mixture; compounds will migrate to the top of the plate at different rates. Solvent mixture must have polar properties if the mixture is dominated by polar compounds, and the inverse is true for non-polar components. The  $R_f$  values can be used to describe the migration of the mixture compounds, using the following equation (Cheng *et al.*, 2011):

$$R_f \text{ value} = \frac{\text{distance of analyte migration}}{\text{distance of mobile phase migration}}$$

TLC was performed on the crude fractions by dissolving 1 mg of the dried fractions in 50  $\mu$ L of appropriate solvent. Roughly 2  $\mu$ L  $\cong$  5 spots were used to draw up the solvent with a capillary tube, after which one end of the capillary was then placed in contact with the TLC surface, roughly 1 cm over the bottom plate of the TLC, a rounded spot was created. After the previous spot application had evaporated, the next spot was applied, in order to safeguard against possible distortion of the zone locations/spots. TLC tank was saturated and equilibrated with the relevant mobile phase prior to developing the plates. The various spotted fractions were allowed to migrate on the TLC plates to a distance of half a centimetre from the top of the plate to separate the various components from one another.

A hair dryer was used to dry the plates with an air stream. Subsequently, the plates were viewed under short-wavelength UV<sub>254</sub> nm and long wavelength UV<sub>365</sub> nm (UVP from Cambridge in the UK). Under short wavelength UV<sub>254</sub> nm, light dark spots indicated substances that quenched fluorescence, while observed spots were drawn over with a soft pencil upon the surface of the TLC plate. Bright spots may also be observed under long wavelength UV<sub>366</sub> nm for those substances that fluoresce at 365 nm. A spraying reagent of *P*-anisaldehyde/sulfuric acid was used to spray the plates to ensuring visualisation of UV inactive compounds, after which a heating gun was used to heat the plates at a temperature of 210°C for a total of roughly two minutes. Despite the fact that the

mechanism by which the visible colour of the stain remained is not known, according to Sherma and Freid (1996), the likely detection is explained as shown in Figure 2.3.

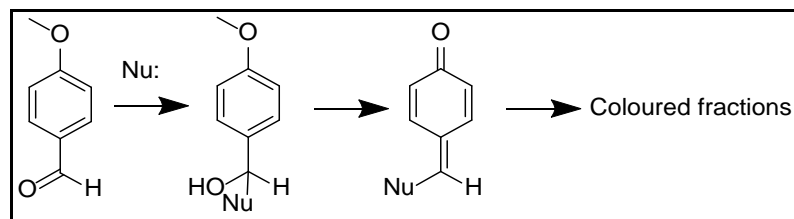


**Figure 2.3:** The mechanism by which the coloured fractions can be observed when *P*-anisaldehyde/sulfuric acid reagent is sprayed on TLC plates.

### 2.4.1.3 Preparative TLC for 3<sup>rd</sup> fractionation of mesocarp

Another technique that can be used to qualitatively assess and separate the various plant extracts is preparative TLC (Berezkin and Chausov, 2012). In the present study, semi-pure fractions of *F. carica* mesocarp coded as (F4,5,6/ F1) were purified with the use of a larger (20 x 20 cm) TLC plate of silica gel 60 F254. The low yield fraction of interest (section 3.3) was dissolved in a 10 mL solvent and dispensed through a 10  $\mu$ l micropipette to be loaded on the surface of the TLC plate, producing a band of a total of 10 mL in each TLC plate. Subsequently, to facilitate tank equilibration, the inner walls were lined with either thick chromatography paper (from VWR in the UK; Whatman 1 grade), or blotting paper. The appropriate mobile phase (i.e hexane:ethyl acetate 90:10) were then mixed, after which they were poured over the lining paper and into the TLC chamber itself. In order that complete equilibration of the chamber could be achieved, a sufficiently long time-frame was permitted. The plate is developed in a saturated equilibrated chamber tank, as described above in section 2.4.1.2.

A certain and fixed distance of 5 cm was marked at the top of the TLC plate prior to it being vertically placed in the chamber; this meant that the plate could be taken out from the chamber expediently as soon as the marked line was reached by the mobile phase. After the intended distance of the mobile phase had been reached, the TLC plate was then removed from the chamber and left to dry. Visualised bands (section 3.3) were cut and placed into a flask after being cut with care, and were subsequently immersed in sufficient acetone solvent. For two hours, the silica plates were macerated with acetone with continuous stirring. Whatman filter paper was then used to filter the acetone extract.

Extraction with acetone was repeated three times. The solvent was then evaporated with the use of a rotavapor (sourced from Buchi in the UK) or dried under nitrogen with a heating block (sourced from Stuart in the UK). The dried preparative TLC fractions were weighed and analysed.

## **2.4.2 Structure identification technique**

### **2.4.2.1 HPLC-ESI-MS**

Once the samples had dried, they were then dissolved in hexane: ethyl acetate (50:50) mixture making a concentration of 1 mg/mL. A millilitre sample was transferred to the HPLC-MS vials (sourced from ThermoScientific, C4015-88) and the solvent subsequently evaporated under nitrogen. The dried samples were reconstituted with 1000  $\mu$ l dichloromethane: methanol (20:80 v/v) for HPLC-MS analysis. Using the sample solvent mixture, blank was also made. Herein, the automatic pipette (Eppendorf PhysioCare) was used for all measurements.

The molecular weight of a compound can be determined with mass spectroscopy (MS). In this study, both negative and positive modes of ionisation were employed, using the Exactive Orbitrap instrument (from the ThermoFischer Corporation, based in Hemel Hempstead, UK). HPLC was coupled and interfaced with Electron spray ionisation (ESI) mass spectrometer. With ESI less fragmentation data was produced for structure elucidation; the acquisition of the data was achieved through the use of the Xcalibur 2.1.1 software programme. The analytical HPLC column ACE 5 C18 (sourced from Hichrom Ltd. V11-6348) with 5  $\mu$ m sized particles, and a pore size of 100  $\text{\AA}$  (dimensions measuring 75x3.0 m) was used. Temperature was kept constant at 22  $^{\circ}$ C, while the pressure was roughly at 37 bars. Purified water (A) and acetonitrile (B) comprised the mobile phase, with a total of 0.1% v formic acid in each solvent. A linear gradient of 90% A and 10-100% B was used for the sample elution, for a total of 30 minutes. Then, the mode was switched to isocratic for five minutes, and was reduced to 10% for a total of one minute. Subsequently the column was re-equilibrated using 10% of solvent B for a total of nine minutes prior to the next sample injection. A flow rate of 300  $\mu$ L/min was utilised within this method, with a capillary temperature of 275 $^{\circ}$ C, a voltage of 32.5V, and a 10  $\mu$ l injection volume. The ESI spray voltage used was at 4.Kv.

#### **2.4.2.2 GC-MS**

GC-MS identification was used with a GC-DSQ II Mass Spectral system (Thermo Scientific, Bremen, Germany) and coupled to the NIST Library (Hewlett Packard, Palo Alto, CA, USA). The InertCap 1 MS capillary column (GL Sciences Inc, Japan) was used by 30 m long, 0.25 mm i.d, and 0.25  $\mu\text{m}$  film thickness. The sample was injected, in splitless mode, into an inlet maintained at 250 °C and with a split flow of 11 mL/min (splitless time one minute). The carrier nitrogen gas flow was maintained at a constant 1.5 mL/min. The oven temperature was increased from 80 °C to 320 °C at a rate of 10 °C/min after an initial hold of one minute. The MS transfer line was maintained at a temperature of 320 °C, and the mass range used was 50.0-800.0. Therefore, the subsequent sample preparation procedure involved the dissolution of 1 mg of the selected fractions including (mesocarp coded F/4,5,6 F9, F12,14/F9 and F4,5,6/F1/F5) (exocarp coded F2.6, F3.8 and F4.9) and (endocarp coded F14 and F20) in 1000  $\mu\text{L}$  of chloroform (Sigma-Aldrich, USA) in GC-MS vials, which were then sealed shut. The samples underwent GC-MS analysis, which was carried out by Ms Patricia Keating at the Department of Pure and Applied Chemistry at the University of Strathclyde.

#### **2.4.3 Structure elucidation techniques**

##### **2.4.3.1 Nuclear Magnetic Resonance (NMR) Spectroscopy**

###### **2.4.3.1.1 Proton Nuclear Magnetic Resonance ( $^1\text{H}$ -NMR)**

One spectroscopic technique used to identify the hydrogen frameworks of organic compounds in naturally occurring crude extracts is  $^1\text{H}$ -NMR Proton Nuclear Magnetic Resonance technique. Particular chemical functional groupings and clades, such as aldehydes, aromatics, carboxylic acids, sugars, fatty acids, and steroids can be partially identified using this technique. However, other spectroscopic techniques are also applied to distinguish between chemical classes that are closely related and that appear in the same region on the spectra.

Nuclei that have an overall hydrogen ( $^1\text{H}$ ) net spin can be detected by NMR spectroscopy. This involves two distinct stages; lower energy levels, and higher energy levels. Referred to as nuclear magnetic resonance, lower-energy-state nuclei are able, with electromagnetic radiation, to be brought to a higher energy state. The energy absorption

is then detected and captured as signals and plotted against the chemical shift ( $\delta$ ). The amount of energy that is required is dependent on the chemical binding properties of the atom.

$^1\text{H-NMR}$  was used to get an overview of the chemical profile of the extracts of each part of *F. carica*. Thus, 5 mg or 2 mg of the dry plant extracts or fractions were dissolved in 600  $\mu\text{L}$  or 200  $\mu\text{L}$ , respectively, of appropriate solvent ( $\text{CDCl}_3$  or acetone- $\text{d}_6$ ) depending on the polarity and solubility of the samples. The samples were transferred into NMR tubes and run on a Brüker 400 MHz equipment or on a JNM-LA400 instrument (JEOL, Japan).

#### **2.4.3.1.2 Carbon Magnetic Resonance ( $^{13}\text{C-NMR}$ )**

$^1\text{H-NMR}$  is sometimes complemented by utilisation of carbon magnetic resonance techniques ( $^{13}\text{C-NMR}$ ), which provide additional information concerning enumeration of the carbon atoms present in the sample, the means by which the aforementioned atoms correlate to hydrogens, as well as the environment of the various functional groupings.  $^{13}\text{C-NMR}$  can provide a considerable, powerful and efficacious tool for structural elucidation. The distortionless enhancements achieved via polarisation transfer (Dept-135), and, alternatively, *J*-mod or *J*-modulation, represent a further one-dimensional, complementary technique assisting the confirmation of the type carbons according to the number of attached proton, i.e.,  $\text{CH}_3$ ,  $\text{CH}_2$  or  $\text{CH}$  as well as carbons that have no attached hydrogens, known as quaternary carbons. Samples of *F. carica* mesocarp, endocarp and exocarp fractions and sub-fractions were subjected to either *J*-mod,  $^{13}\text{C-NMR}$ , or Dept-135 analysis using Brüker-400 MHz or 400 MHz-500 MHz equipment. The Dept-135 parameters of number of scan was either 2048, 3072 or 4096; receiver gain 198.2 or 2050, relaxation delay 2 ms, and pulse width 10 Hz.

#### **2.4.3.1.3 Two-dimensional NMR experiments**

Two-dimensional NMR experiments include Correlation spectroscopy (COSY); Heteronuclear Single Quantum Correlation (HSQC) spectroscopy; and Heteronuclear Multiple Bond Correlation (HMBC) spectroscopy. The spin couplings between proximate protons can be detected by COSY; one bond coupling between a proton and a carbon can be identified using HSQC (referred to as a 1-bond H-C); any correlations

between the carbon atoms and protons that goes through either four, three or two bonds away from one another are highlighted by HMBC. The HSQC parameters of number of scan was between 8 to 16; receiver gain was between 16 to 198, relaxation delay was between 1.5, and pulse width was between 10 to 12. Moreover, HMBC parameter of number of scan was 32, receiver gain was 198, relaxation delay was 2 ms, and pulse delay width was 12 Hz. These spectra are thus very useful, yielding considerable and useful information, and permit the construction of partial structure fragments so that the complete structure of the compounds can be revealed.

Fractions and sub-fractions of *F. carica* mesocarp, endocarp and exocarp were analysed using either 600, 400 or 500 MHz spectrometers (the AVANCE-III, sourced from Brüker). The samples, measuring 2 mg or 5 mg were subsequently dissolved into 200 µL or 600 µL of acetone-d<sub>6</sub> (Aldrich, 151793-10X0.75mL) or, alternatively, chloroform-d (CDCl<sub>3</sub>) (Aldrich, 151823-100G), before being transferred to a 5 mm or 2 mm diameter NMR tube (Z118257-1EA Aldrich).

## **2.5. Metabolomic methods**

### **2.5.1 Metabolomics workflow**

A pre-defined metabolomics workflow was designed to fit the aim of the study. Several steps were involved; these are illustrated in Figure 2.4 below.

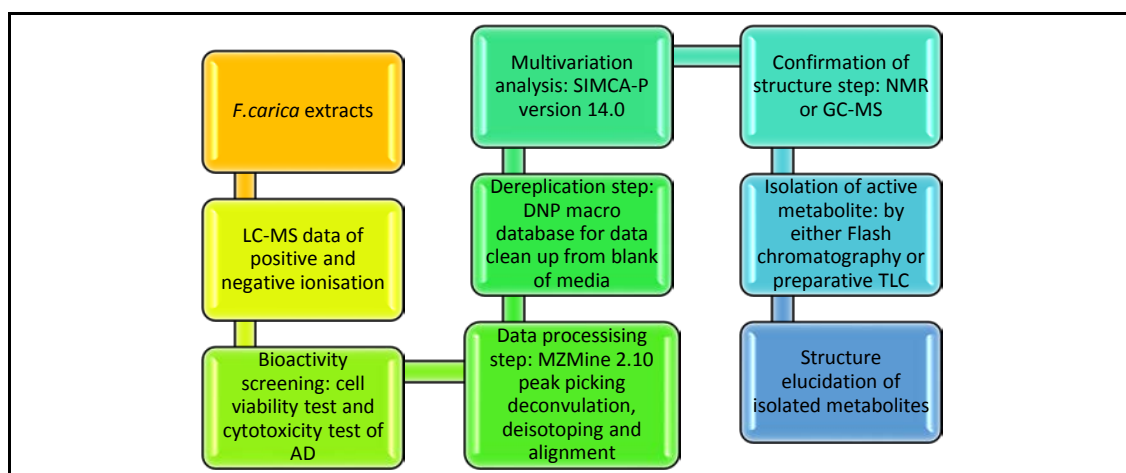


**Figure 2.4:** Metabolomics flowchart cascade tools for mining active metabolites of *F. carica* endocarp, exocarp and mesocarp against acrolein induced oxidative stress in AD.

### 2.5.2 Data analysis using MZmine 2.10

A key feature of the MZmine software design is the inclusion of data processing modules as well as strict separation of core functionality (Pluskal *et al.* 2010). Embedded visualisation tools are used by data processing modules, allowing for an instant preview of parameter settings. Furthermore, peak identification using online databases is a functionality that has been recently introduced. By using the algorithm for random-sample consensus, features were established that include isotopic pattern recognition, scatter plot visualisation, and peak list alignment. Mass spectral raw data were then subsequently subjected to further processing through the utilisation of other programmes, such as Macrodrive.

The LC-MS raw data were sliced into positive and negative ionisation modes using the MassConvert tool file slicer from the data-to-split wizard. The MZmine 2.10 programme was then used to import the sliced MS data. The peak-detection and centroid-mass detector was chosen following cropping of the chromatograms (0.0 to 28.0 min). The noise and the MS levels were set to 1.0. Chromatogram builder, deconvolution and threshold levels were set automatically. Normalisation, as well as isotopic peaks grouping, was undertaken according to an  $m/z$  tolerance (values: at 0.001  $m/z$  or 5.0 ppm); the minimum standard intensity was set at 5%, and the RT tolerance was also set to 5%. A join-aligner was used to align all peaks: weight for  $m/z$ : 20,  $m/z$  tolerance: 0.001  $m/z$  (or, alternatively, 5.0 ppm). The aligned peak list was gap-filled with the use of a peak-

finder function (intensity tolerance: 1%,  $m/z$  tolerance: 0.001  $m/z$  or 5.0 ppm, RT tolerance: 0.5 min). The following criteria were used for an adduct search: maximum relative adduct peak height at 30%;  $m/z$  tolerance at 0.001  $m/z$  or, alternatively, 5.0 ppm; RT tolerance set at 0.2 absolute (min). [M-H] was used for the negative ionisation mode, and [M+H] was used for positive ionisation mode and performed for searched adducts, including Na, K, NH and ACN+H. For an additional clean-up (as detailed below), all the information and data was saved and stored in a DNP Macrodrive 2015 database in the form of a CSV file.

### **2.5.3 Data analysis using dereplication via DNP-Macrodrive 2015 database**

Macrodrive 2015 database is a systematic dereplication method for crude extract samples that can be combined with HTS for screening of NP mixtures using LC-MS (Ito and Masubuchi 2014). In this study, the MZmine-processed data was exported into the relevant sections of the Macrodrive 2015 database. The MACROS remove ion peaks found from the blanks and clean up background noise. Additional analysis was completed by selecting the 'dereplication' function. For further analysis, a SIMCA-P generation file (see below) was collated to a CSV file format.

### **2.5.4 Multivariate analysis using SIMCA-P as High-throughput screening**

Advanced statistical chemometric techniques were used in combinatorial and HTS so that visualisation, lead identification, and pattern recognition can be successfully achieved (Ward, 1963). In this study, SIMCA 14 (Umetrics, Sweden) software was employed to generate the metabolomics principles. Figure 2.5 depicts a flowchart of the multivariate analysis process used.

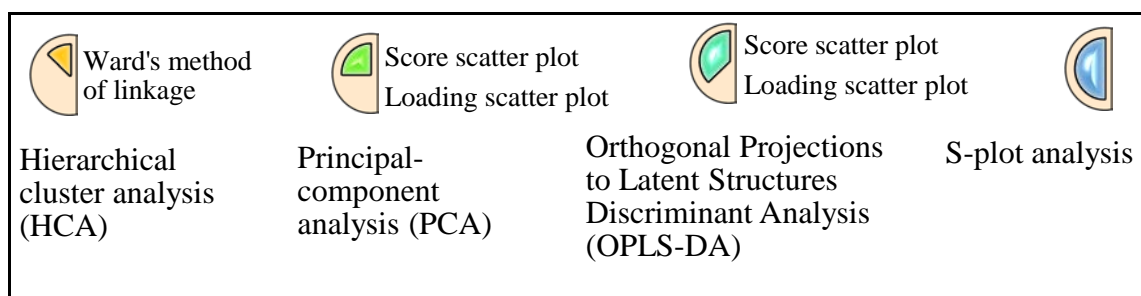


**Figure 2.5:** Flowchart of the multivariate analysis strategy applied using SIMCA-P for *F. carica* exocarp, endocarp, and mesocarp against oxidative stress related AD.

#### 2.5.4.1 Principal-component analysis (PCA)

Within the discipline of chemometrics, PCA is a notable basic workhorse that aims to summarise the variation per few scatter and informative scores of groups (Eriksson *et al.* 2004). In the present study, all *F. carica* fractions were subjected to PCA to indicate similarity through clustering.

#### 2.5.4.2 Hierarchical cluster analysis (HCA)

HCA was used to identify comparatively similar fractions to a set of characteristics used for measuring qualities such as chemical composition. The method begins with each of the metabolites, subsequently proceeding to assimilate these clusters in a sequence, and finally reducing the number of clusters. In this study, HCA was performed using Ward's method of linkage. Ward's (1963) method of analysis employs a variance approach to determine the distance between clusters. This method is considered a particularly efficient HCA, since it aims to separate the various groups in a way that minimises the potential loss of information. In this study, Ward's method was used to cluster the fractions from different fruit parts of *F. carica* that included the mesocarp, endocarp, and exocarp based on their LC-MS data. The aim was to verify the similar chemical composition of these fractions and extracts.

#### 2.5.4.3 Orthogonal Projections to Latent Structures Discriminant (OPLS-DA)

Active metabolites can be distinguished from inactive ones by OPLS-DA, by setting against their biological activities per scattered cluster or a grouped cluster (Bylesjö *et al.* 2006). In this study, OPLS-DA was utilised for the fractions of each fruit part of *F. carica* by sorting the active from the inactive fractions.

#### **2.5.4.4 S-plot analysis**

S-plot analysis is a statistical tool that facilitates the visualisation of discriminating variables so that the putative biomarkers can be targeted (Tugizimana *et al.* 2016). S-plot analysis is implemented under the OPLS-DA model. In the present study, each part of *F. carica* was subjected to S-plot analysis and the putative targets were finally elucidated using NMR, as described in Section 2.4.3.

### **2.6. Biological methods**

#### **2.6.1 Biological equipment's and reagents**

For the experiments in this study, 75 cm<sup>2</sup> sterilised tissue culture flasks were obtained from Flasks Corning<sup>®</sup> (NY), and 96 well plates were purchased from Bio-one<sup>®</sup> (UK). Penicillin/streptomycin was obtained from GipcoBRL<sup>®</sup> (UK), and tryptan blue from (SigmaAldrich, T8154-20mL). Dimethyl sulfoxide (DMSO) was obtained from Fisher Scientific<sup>®</sup> (bp231-100, UK). Cell culture DMEM/F-12 (1:1) and Glutamax<sup>™</sup> was purchased from Gipco<sup>®</sup> (31331-028, UK), and foetal bovine serum (FBS) from Gipco<sup>®</sup> (UK). AlamarBlue<sup>®</sup> was obtained from Biorad<sup>®</sup> (BUF012B, USA). Trypsin tetra methylethylenediamine (TEMED), Hank's balanced salt solution, and acrolein were all obtained from SigmaAldrich<sup>®</sup> (UK).

#### **2.6.2 Cell culture**

The neuroblastoma SH-SY5Y cell line was generously provided by Dr. Ben Pickard at the University of Strathclyde (Glasgow, UK), and the cell line that mostly employed was in the 20<sup>th</sup> to 30<sup>th</sup> passages (Zadina *et al.*, 1993). In this study, the neuroblastoma SH-SY5Y cell line was re-suspended and cultured in an equal volume (1:1). DMEM and Ham F12 media to which 50 mL foetal bovine serum (10% FBS), 5 ml non-essential amino acid, and 5 mL penicillin-streptomycin antibiotic (10,000 unit) was added. The cells were contained in 75cm<sup>2</sup> flask with 10 mL of the media mixture incubated in a humidified incubator at 37°C, 5% CO<sup>2</sup> and 95% air. The media within the culture flask was regularly changed every 3-4 days to ensure healthy cells while floating cells were discarded. Additionally, differentiated SH-SY5Y cell lines were achieved via the addition of 10 µM

retinoic acid when the cells were transferred to 96-wells on two-day of cell culture. Retinoic acid (RA) was generously provided by Dr. Ben Pickard.

### 2.6.3 Haemocytometer

The cell suspension was diluted up to 10 mL media in a falcon tube after splitting the cell suspension to prevent cell clumping and clustering. A bright-line haemocytometer (Sigma-Aldrich, Germany) was used to count the cells. The device was properly washed and cleaned with both distilled water and 70% alcohol. Then, a 20  $\mu$ L drop of the diluted cell suspension in trypan blue was placed on one of the sides of the haemocytometer grid. The lid was then gently placed on top of the drop, to prevent the appearance of any bubbles. Cells were then counted in each 1 mm corner squares of the chamber (Figure 2.6) under the Olympus CK40 microscope (Japan). The total number of cells counted in the four corner squares were calculated accordingly:

Total number of cell =  $[(\sum \text{counted cell}) / 4] \times 10^4 = (\text{cell/mL})$ . Where,  $C \times V = C' \times V'$

$\therefore$  Total number of cell =  $[(\text{cell/mL}) \times V (\mu\text{L}) = 3.33 \times 10^4 \text{ cell/ml} \times 10000 \mu\text{L}]$ .

$V = (3.33 \times 10^4 \times 10000) / \text{total number of the cell} = \text{the total final volume in } \mu\text{L}$ .

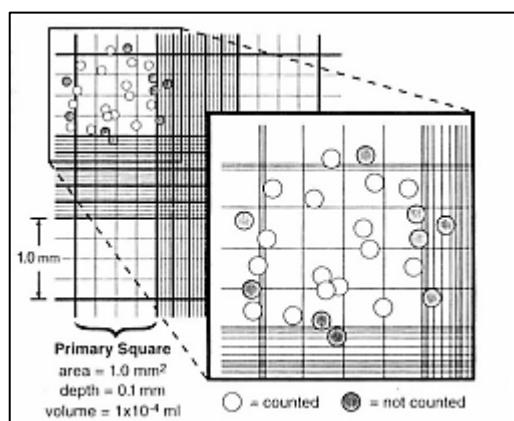


**Figure 2.6:** Haemocytometer plate illustrated the four corner squares margin of the counted cells in the chambers of the bright line haemocytometer and the cells in each primary square.

### 2.6.4 Cell viability test via AlamarBlue® assay

The AlamarBlue® assay was used to measure cell viability. The assay is a fluorometric measurement of metabolic activity used to detect the effect of potentially active compounds on cell viability. In metabolically active cells, the active ingredient of AlamarBlue® is resazurin (IUPAC name: 7-hydroxy-10-oxidophenoxazin-10-ium-3-

one), which is water-soluble but is capable of permeating cell membranes and non-toxic. Resazurin is reduced to resorufin and the dye changes from non-fluorescent blue to highly fluorescent pink. The dye acts as an intermediate electron acceptor in the electron transport chain, as shown in Figure 2.7. The change from the oxidised to the reduced form can be quantitatively measured as a colourimetric or fluorometric reading at a wavelength of 560 nm and 590 nm (Rampersad, 2012).

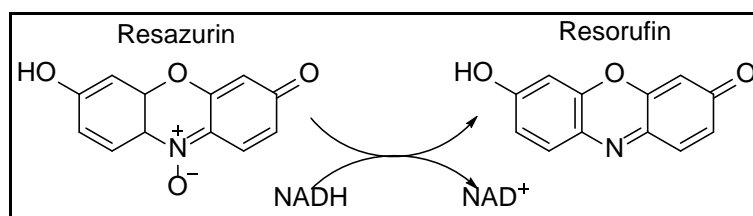


**Figure 2.7:** The oxidation-reduction reaction of the non-fluorescent resazurin blue dye turning to highly fluorescent resorufin pink dye due to the transformation of NADH to NAD<sup>+</sup>.

Initial cell viability screening was undertaken to the net of the fractions in each part of *F. carica* at a concentration of 30 µg/mL against *in vitro* differentiated SH-SY5Y cell lines. All of the samples were dissolved in 1000 µL of hexane: ethyl acetate (1:1 v/v) solvent to reach a concentration of 30 µg/mL. Then, a single mg of each of these samples was calculated before being transferred into a clean vial. The samples were dried under nitrogen, after which, each sample was reconstituted with 100 µL DMSO as a stock solution to be used later for serial dilution. In the second step of the procedure, 99 µL was taken from each of the reconstituted samples and transferred to 96-well plate where they were diluted in 1.2 µL of the stock media. In the final step of the procedure, 25 µL of the second diluted solvent was re-transferred to another 96-well plate and re-diluted in 75 µL of cell media. Cells that went untreated were reserved as positive controls with 100% viability. The results were also validated using a negative control and maintained by diluting 25 µL of triton x (that is, 8 µL of triton x in addition to a total of 2 mL of fresh media). A concentration of 10 µL of AlamarBlue<sup>®</sup> was added to the 96-well plate 24 hours after the treated cells were incubated, and re-incubation occurred for another 4-6 hours at 37°C, 5% (v/v) CO<sub>2</sub> and 100% humidity. The aforementioned procedure was undertaken three times, and the relative cell viability was calculated using the formula below:

$$\text{Relative cell viability} = \text{mean} (\text{Absorbance}_{\text{sample}} / \text{Absorbance}_{\text{control}}) \times 100$$

### 2.6.5 Cytotoxicity test

The principle of a cytotoxicity test is the adverse effects resulting from the interference by molecular structures and/or processes essential for cell survival, proliferation and/or function (Ekwall, 1983). Mesocarp fractions that included F4,5,6/F9; F12,14/F9; and F4,5,6/F1/F5; endocarp fractions F14 and F20; and exocarp fractions including F2.6, F3.8, and F4.9 were subjected to cytotoxicity test by which SH-SY5Y cells were seeded in 96-well plastic plates for 48 hours, then 10  $\mu\text{M}$  (RA) was added to the 96-well plastic plates to cease proliferation and induce differentiation. Serial concentrations of 30  $\mu\text{g}/100 \mu\text{L}$ , 10  $\mu\text{g}/100 \mu\text{L}$ , 3  $\mu\text{g}/100 \mu\text{L}$ , 1  $\mu\text{g}/100 \mu\text{L}$ , 300 ng/100  $\mu\text{L}$ , 100 ng/100  $\mu\text{L}$ , 30 ng/100  $\mu\text{L}$  and 10 ng/100  $\mu\text{L}$  were measured from a stock treatment solution (1000  $\mu\text{g}/100 \mu\text{L}$ ) and were diluted as shown in Figure 2.8.

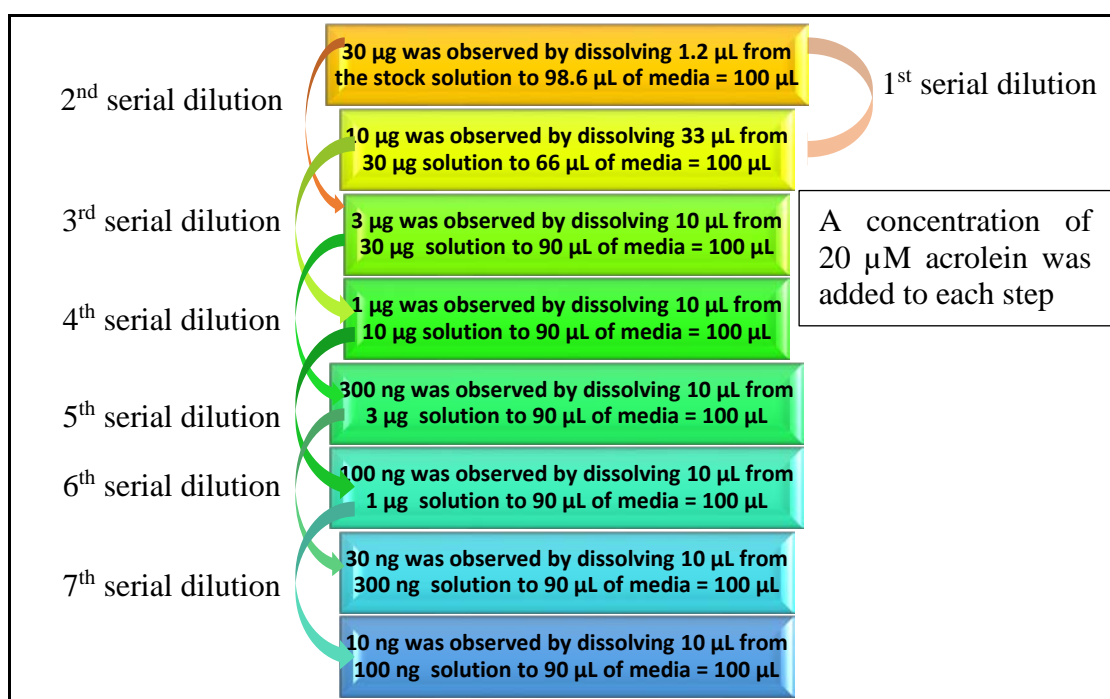


**Figure 2.8:** The preparation of the serial concentrations of the treatments for the cytotoxicity test. A multiple-channel pipette (Eppendorf<sup>®</sup>) was used to measure and transfer the concentrations to their appropriate wells. 30  $\mu\text{g}$  was diluted as 1<sup>st</sup> serial dilution denoted in yellow box then was diluted as 2<sup>nd</sup> serial dilution denoted in light green box.

Next, the 96-well plates were cultured for 24 hours prior to the addition of 20  $\mu$ M acrolein and treatment. Cell viability was evaluated using AlamarBlue<sup>®</sup>. Spectrophotometric measurements were taken at 560 nm and 590 nm wavelengths. Both positive (non-treated cells) and negative controls (triton-x) were maintained in order to validate the test; in addition, the viability of each test culture was calculated prior to the addition of AlamarBlue<sup>®</sup>, as described above in section 2.6.4. The statistical analysis was performed as described below.

### **2.6.6 MTT assay**

Briefly, 3-(4,5-Dimethylthiazol-2-yl)-2,5-diphenyltetrazolium bromide for (MTT) was dissolved in Phosphate-buffered saline (PBS) solution at a concentration of 5 mg/ml, and then cells ( $5 \times 10^3$  cells/well) were seeded in 96-well plates. After exposure to different concentration of acrolein (0.01, 0.1, 1, 10 and 100  $\mu$ M) for 24 hours, then 10  $\mu$ l MTT solution was added to each well and the plates were incubated for additional 4 hours at 37 °C. Then, the medium containing MTT was aspirated off. To achieve solubilisation of the formazan crystal formed in viable cells, 200  $\mu$ l of DMSO was added to each well. The absorbance was read at 570 nm with Dimethyl sulfoxide (DMSO).

### **2.6.7 Western blotting test (WB)**

The principle of western blotting is to identify specific proteins from a complex mixture of proteins extracted from cells (Yang and Mahmood, 2012). In this study, the mesocarp fractions including F4,5,6/F9, F12,14/F9 and F4,5,6/F1/F5; endocarp fractions F14 and F20; exocarp fractions including F2.6, F3.8, and F4.9 were subjected to WB by which the preparation and the procedure of WB are described below;

#### **2.6.7.1 The preparation of WB buffers and solutions**

WB buffers were prepared according to the followings;

##### **Transfer buffer**

Glycine, tris base and methanol were measured as illustrated in Table 2.1. Distilled water was then filled up to the mark in 1L volumetric flask.

**Table 2.1:** The measurements for preparing transfer buffer.

<b>Chemicals name</b>	<b>Weight and volume</b>
Glycine	14.4 g
Tris base	3.0 g
Methanol	200 ml

### **TBS (10x) and TBS (1x)**

Tris-buffered saline (TBS 10x) was prepared by measuring 100 ml of 1M tris-cl (pH 7.5) and 375 ml of 4M sodium chloride (NaCl), then were mixed and diluted with distilled water up to 1L volumetric flask (stock solution). 100 ml from the stock solution was pipetted then diluted with distilled water up to 1L of volumetric flask.

### **TBS-tween (1x)**

100 ml of TBS (10x) stock solution was mixed with 2 ml tween 20 (0.2% v/v) and diluted up to 1L with distilled water.

### **Blocking solution**

5 g of skimmed milk powder was weighed and dissolved in 50 ml TBS-tween. However, blocking solution was always freshly prepared just before the moment of using them.

#### **2.6.7.2 The preparation of lysed aliquots for WB analysis**

Pellets in Eppendorf caps were lysed with (1:1) RIPA Lysis Buffer System (RLBS) from Santa-cruz<sup>®</sup> (sc-24948) and (2x) Electrophoresis Sample Buffer (ESB) from Santa-cruz<sup>®</sup> (sc-24945). The aliquots were continuously re-suspended via 1 ml syringe until the blue colour turned to dark violet. The aliquots were then heated into a heat block for 5 minutes.

#### **2.6.7.3 The preparation of antibodies for WB analysis**

400  $\mu$ L of NQO1 rabbit polyclonal antibody (Ab) (PA5-14238, invetrogen, UK) was diluted by blocking solution in a dilution factor of 1:1000. To prevent freeze / thaw cycle, the diluted Ab was split into equal aliquots, then were kept into the -20°C freezer. An aliquot of the diluted NQO1 was thawed at room temperature before the times for them to be used.

#### **2.6.7.4 The preparation of Ab detection by using Enhanced Chemiluminescence Luminol (ECL) solutions**

The following chemicals and solutions were prepared for ECL detection;

##### **250 mM Luminol**

0.07 g of luminol from Fulka<sup>®</sup> (cat no 09253) was weighed and dissolved in 5 ml of DMSO. The solution was then split into equal aliquots of 1 ml and was stored in a dark container at -20°C because they are unstable to light.

##### **90 mM *P*-coumaric acid**

0.07 g of *P*-coumaric acid from Sigma Aldrich<sup>®</sup> (cat no C-9008) was weighed and dissolved in 5 ml DMSO. The solution was then split into equal aliquots of 500 µl and was stored in a dark container at -20°C because they are unstable to light.

##### **ECL<sub>1</sub> solution**

440 µl from *P*-coumaric acid aliquot, 1 ml Luminol aliquot, and 10 ml of 1M tris-base (pH 8.5) were mixed and diluted to 100 ml with distilled water in a dark container to prevent any reaction, then was stored in the fridge.

##### **ECL<sub>2</sub> solution**

64 µl hydrogen peroxide (H<sub>2</sub>O<sub>2</sub>) 30% and 10 ml of 1M tris-base (pH 8.5) were mixed and diluted to 100 ml with distilled water in a dark container to prevent any reaction, then was stored in the fridge.

#### **2.6.7.5 The procedure for preparing WB gels into gel plates.**

##### **2.6.7.5.1 The preparation of resolving gel in the bottom of the plate (10% gel)**

30% acrylamide/bis-acrylamide, resolving buffer (4x), distilled water, ammonium persulphate (APS) (100mg/ml) and N'-N' tetramethylethylene-diamine (TEMED) were measured as illustrated in Table 2.2 and placed into a centrifuge tube then were vortex for 30 seconds.

**Table 2.2:** The measurements for the resolving gel chemicals and buffers.

<b>Chemicals and buffer's name</b>	<b>Volumes</b>
Acrylamide/bisacrylamide (30%)	6.6 ml
Resolving buffer (4X)	5 ml
Distilled water	8.2 ml
APS (100 mg/ml)	100 $\mu$ l
TEMED	10 $\mu$ l

#### **2.6.7.5.2 The preparation of stacking gel at the top of the plate (5% gel)**

30% acrylamide/bis-acrylamide, stacking buffer (4x), distilled water, APS (100mg/ml) and TEMED were measured as illustrated in Table 2.3 and placed into a centrifuge tube then were vortex for 30 seconds.

**Table 2.3:** The measurements for the stacking gel chemicals and buffers.

<b>Chemicals and buffer's name</b>	<b>Volumes</b>
Acrylamide/bisacrylamide (30%)	1.64 ml
Stacking buffer (4X)	2.5 ml
Distilled water	5.86 ml
APS (100 mg/ml)	60 $\mu$ l
TEMED	10 $\mu$ l

Gel plates were thoroughly washed with water and cleaned with 70% ethanol, and were vertically assembled by using the rubber spacers between the edges of the plate's wall and strongly clipped with a proper clipper beside the assembled plates in order to prevent leaking when pouring the buffers into them.

After the resolving solution was prepared and vortex, it was poured directly between the spaces of the assembled plates and was left about 1 to 1.5 cm space at the top of the plates then were overlaid with a very thin layer of isobutanol solution in order to prevent any trapped or further formation of bubbles. After the bottom layer was polymerised, the remaining isopropanol solution was removed by a gently wash with distilled water then was dried up by inserting a strip of a paper towel without affecting or attaching the polymerised bottom layer.

The prepared stock solution was directly poured at the top of the polymerised resolving solution after isopropanolol was completely and gently removed as well as the Teflon comb was immediately inserted into the top of the gel. After the top layer was completely polymerised, the comb, rubber and clips were carefully removed and the gel plates were

directly assembled and adjusted into (ATTO corporation, model AE6450 from Japan) electrophoresis tank, and the tank was filled up with (1x) running buffer. Moreover, 5  $\mu$ l of pre-stained electrophoresis molecular weight marker aliquot was firstly loaded within the starting of the wells and the desired aliquots of the isolated compounds were then loaded with approximately 30  $\mu$ g per lane next to the loaded pre-stained marker by using 10  $\mu$ L micro-syringe. ATTO apparatus was run in order to determine the desired protein at a constant voltage and amplitude of 125V and 200 mA for  $\approx$  1-1.5 hours or until the pre-stained marker dye had almost reached the bottom of the gel.

### 2.6.7.5.3 The procedure for obtaining WB analysis

The gel containing separated protein as revealed in section 2.6.6.5.2 were gently transferred and placed into a cut fitted size nitrocellulose membrane (pore size 0.45 nm), then they were sandwiched between 4 sheets of cut fitted size whatsmen #3 mm and a fitted sheet square of sponge, respectively after they were all soaked in a transfer buffer (1x) solution. The sandwiched layers were then assembled into the plastic holder and the direction of the voltages were organised as can be seen in Figure (2.9).

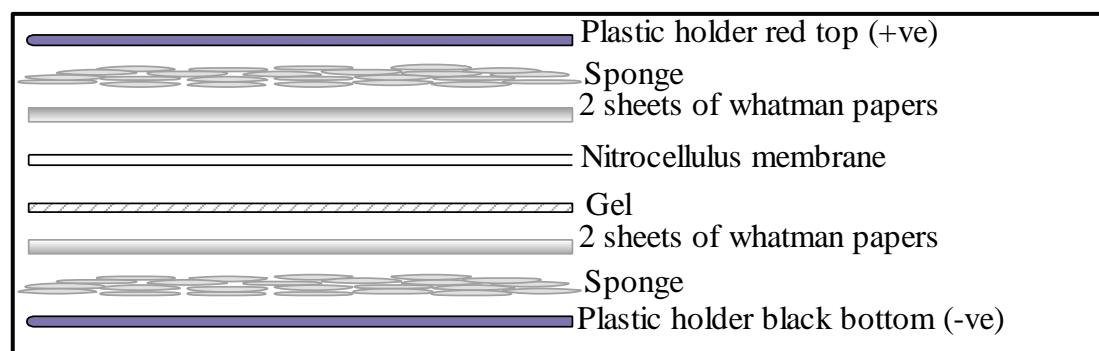


**Figure 2.9:** Shows the sequences for assembling WB sandwich and the directions of (+ve) at the red top and (-ve) at the black top voltages.

The sandwiched plastic holders were assembled into the Bio-Rad mini Trans-Blot™ tank and were filled with transfer buffer (1x). Fitted Ice rack was assembled into the tank, next to the sandwiched plastic holders to prevent the gel from melting. Thereafter, the apparatus was run at a constant current of 300 mA for approximately 2 hours. After the apparatus was stopped, nitrocellulose membrane was gently picked out from the sandwich by using forceps and placed into a clean plastic container which was soaked with a freshly

prepared TBS-tween (1x). The plastic container was held on a shaker apparatus and was incubated over night at 4°C.

The membranes were washed 4 times with TBS-tween each for 10 minutes and one member was added the primary thawed NQO1 Ab and the other membrane was added B-actin Ab, then the membranes were replaced on the shaker and were re-incubated at 4°C over night. Later, each Ab was poured into their specific falcon tubes and were re-stored in the freezer at -20°C. On the other hand, the membranes were re-washed 3 times with TBS-tween each for 7 minutes and once with TBS (1X) solution for 5 minutes. The blots were then developed by using ECL solution. Therefore, equal volumes 1:1 of ECL1 and ECL2 as can be seen in section 2.6.6.4 were added after TBS (1x) solution was removed from the blots. Bands were then detected by using (LAS3000) image from Fujifilm Company. In addition, the intensities of the desired bands were quantified by using Image J analysis software from ([www.imagejdv.org](http://www.imagejdv.org)) and were compared with the control band ( $\beta$ -actin).

#### **2.6.8 Statistical Analysis**

Graphs of *F. carica* fractions were facilitated by Microsoft Excel, and a one-way analysis of variance (ANOVA) was performed using GraphPad Prism 5.0 software (GraphPad Software, San Diego, CA, USA). Significant differences amongst the means were calculated using Prism, with a significance level of  $P = 0.05$  or  $P = 0.01$ . The latest version of the Dictionary of Natural Products (DNP) database was used to identify similar structures.

## **CHAPTER THREE MESOCARP RESULTS**

---

### **3. Isolation and identification of bioactive metabolites from the mesocarp of *Ficus carica* and bioactivity on differentiated SH-SY5Y neuronal cell line**

---

The leaves of the fig tree have been the focus of extensive research, while other parts of the plants have not received the same amount of attention (Singh *et al.*, 2007). For example, the fruits, and in particular the mesocarp part, have been inadequately examined in terms of their phytochemistry, even though they are widely used in traditional medicine in various countries (e.g. India, China and Middle East). Furthermore, the active principles have not been thoroughly investigated in bioassays such as in *in vitro* differentiated SH-SY5Y cell line with the purpose of identifying the compounds. In the present chapter, the investigation undertaken to determine the chemical profile of ethyl acetate crude *F. carica* mesocarp is presented. Mesocarp fractionation was achieved by medium-pressure flash chromatography followed by High-Throughput Screening (HTS). Furthermore, the metabolomic techniques of drug discovery were employed to analyse the mesocarp. Thin layer chromatography (TLC) and nuclear magnetic resonance spectroscopy (NMR) were employed for the analysis of *F. carica* mesocarp fractions and sub fractions. Furthermore, GC-MS was used to analyse the lipophilic fractions. In addition, preliminary cell viability screening, cytotoxicity test and western blotting test were employed for biological investigation.

#### **3.1 First fractionation**

Flash chromatography was employed to fractionate a 1.3 g dried crude *F. carica* mesocarp extract (Figure 3.1). The crude extract was dark brown in colour and had a nutty, sweet smell. Fractionation by flash chromatography afforded 233 fractions. The chromatographic conditions employed for the purification of the crude sample of mesocarp is described in Table 3.1. Figure 3.2 illustrates the elution protocol using hexane, ethyl acetate, dichloromethane, and methanol as solvents in flash chromatography. The total dried weight of the eluted fractions was 1.1288 g resulting to a yield of 86.8%. The failure to collect the peaks below the signal threshold while 2% of volume run going through the ELSD were anticipated to be the likely cause for the loss of 0.1712g.



**Figure 3.1:** Fractionation scheme for crude *F. carica* mesocarp extract (1.3 g) affording 17 fractions shown in green. Further fractionation of the bioactive pooled fractions F4,5,6 and F12,14 yielded an additional 47 sub-fractions. Boxes in red colour were excluded from further bioassay and elucidation work due to their low yield, while fractions in blue boxes were subjected for further work. Purification of F4,5,6 gave six fractions denoted in brown boxes.

**Table 3.1:** Chromatographic conditions employed for the purification of the crude *F. carica* mesocarp via flash chromatography by gradient elution 147.66 min and isocratic elution 68.30 min. EtOAc, MeOH and DCM represent ethyl acetate, methanol and dichloromethane, respectively.

Crude extract	Silica column size	Flow rate mL/min	Duration min	ESLD threshold	UV1
Mesocarp	24 g	10	217 min	20 mV	254 nm
UV2	Sample loading	Solvent A	Solvent B	Solvent C	Solvent D
280 nm	Dry	Hexane	EtOAc	MeOH	DCM

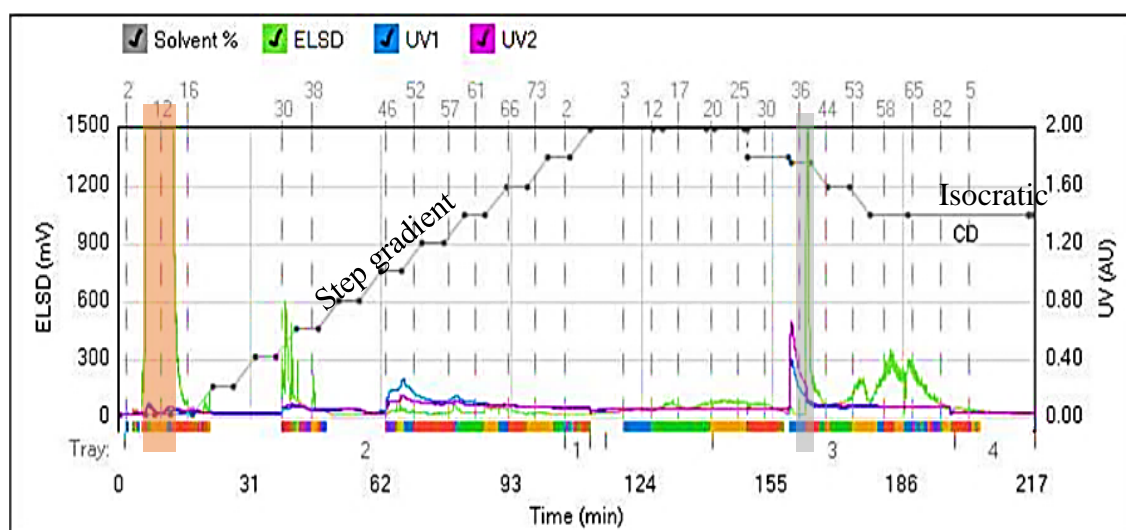


**Figure 3.2:** Normal phase chromatogram for the fractionation of the dry crude *F. carica* mesocarp extract. Solvents used were hexane (A) and ethyl acetate (B) with 0% B at 0-5 min, 10% B at 5-10 min, 20% B at 10-20 min, 30% B at 20-30 min, 40% B at 30-40 min, 50% B at 40-50 min, 60% B at 50-60 min, 70% B at 60-70 min, 80% B at 70-80 min, 90% B at 80-90 min, and 100% B at 90-117 min. Subsequently, solvents were switched to methanol (C) and dichloromethane (D) with gradient elution from 90% to 70% D. The ELSD was denoted by the green line, UV<sup>1</sup> and UV<sup>2</sup> denoted by the blue and violet lines, respectively. Collection volume was set at a maximum of 20 ml and mode of collection was by peak detection as denoted by the coloured bars. The highlighted peaks in orange and grey represented the pooled fractions F4,5,6 and F12,14, respectively. DCM and MeOH respectively stand for dichloromethane and methanol. The % in black colour indicated the solvent ratio.

High intensity green peaks (Figure 3.2) were eluting at higher ratios of non-polar solvents as with 100% hexane and 100% dichloromethane. These high intensity peaks were observed with the evaporative light scattering detector (ELSD). Subsequently, low intensity but sharp peaks were observed at equal ratios of the eluting solvents (Figure

3.2). Weaker broader peaks were observed under UV detection at both 254 and 280 nm. As the ratio of ethyl acetate increased, lesser peaks were being eluted and detected. On the other hand, switching the mobile phase to dichloromethane and methanol increased again the elution of compounds particularly at the isocratic ratio of 70% dichloromethane and 30% methanol.

TLC was used to monitor the eluted fractions (Figure 3.3). A comparison between fractions was subsequently undertaken by running a range of solvent systems for the mobile phase. Beginning with the least polar fractions, fraction codes were allocated; Fractions with similar chromatograms were pooled resulting to 17 fractions for the 1<sup>st</sup> fractionation. F4, F5, and F6 as well as F12 and F14 were pooled together due to similarities in their NMR spectrum (Section 3.4, Figure 3.9). They were subsequently subjected to further chromatographic purification. All 17 fractions were dried and weighed (Figure 3.1). However, F13 was eliminated due to its small yield.

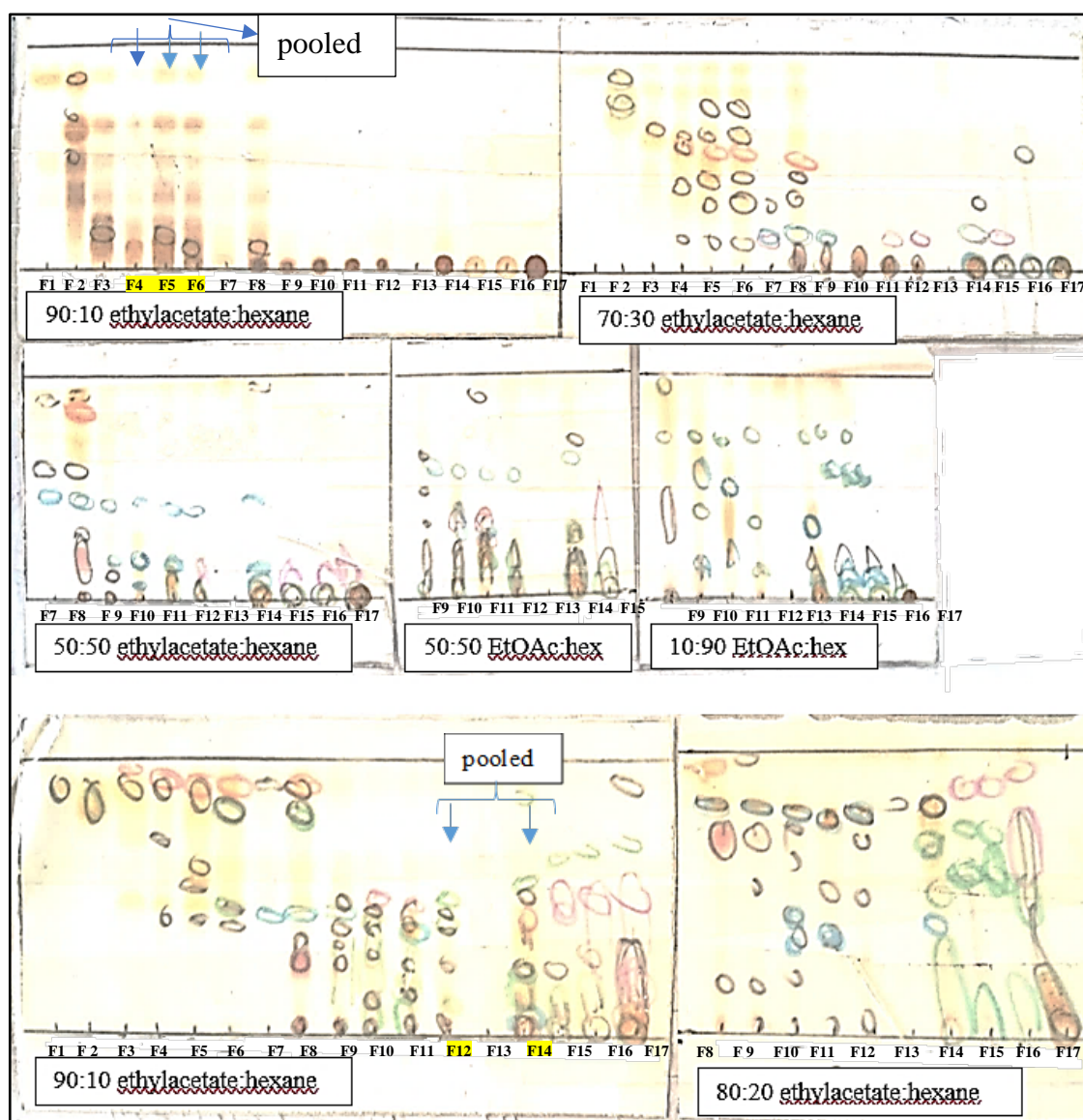


**Figure 3.3:** TLC summary plate of the 1<sup>st</sup> fractionation of mesocarp crude extract on Si60. Hexane (Hex) with ethyl acetate (EtOAc) and dichloromethane with methanol constituted the mobile phase solvents. Hex and EtOAc were employed at ratios of 90:10, 70:30, 50:50, 30,70 and 10:90 and subsequently with dichloromethane and methanol at 90:10 and 80:20. Fractions 4, 5, 6 were pooled, as well as fractions 12 and 14 and were coded F4,5,6 and F12,14, respectively. Eluates observed under long UV were represented by coloured circles and those with pencil markings were detected under short UV, whilst yellow to brown spots of colour were visualised with *P*-anisaldehyde/sulfuric acid spray reagent.

### 3.2 Second fractionation

Fractions were selected for further purification work due to their interesting NMR spectral data (Section 3.4, Figure 3.12) and *in vitro* biological activity on SH-SY5Y cell line as shown in sections 3.5 and 3.6, respectively. Moreover, additional purification was carried out via flash chromatography on the pooled fractions F4,5,6 weighing 372.6 mg and F12,14 at 259.4 mg affording 24 and 17 sub-fractions, respectively (Figure 3.4). The conditions for the fractionation procedure were presented in Table 3.2. Normal phase chromatography was employed to fractionate the metabolites according to their polarity (Figure 3.5). The total weight of the dry sub-fractions obtained from F4,5,6 was 211.4 mg with an elution yield of 56.7%.

**Table 3.2:** REVELERIS<sup>®</sup> flash chromatography system conditions for pooled fractions F4,5,6 and F12,14.

	<b>(F4,5,6/F1) 372.6mg</b>	<b>(F12,14/F1) 259.4mg</b>
Column Reveleris <sup>®</sup>	Silica 12g	Silica 12g
Mobile phase A: B	hexane: ethyl acetate	dichloromethane: methanol
Flow rate	30 mL/min	20 mL/min
Loading method	Dry	Dry
Gradient	10% decrease of hexane with increasing ratio of ethyl acetate to 100%	10% decrease of dichloromethane with increasing ratio of methanol to 30%
Equilibration	4.8 min	3.9 min
ELSD threshold	20 mV	20 mV
UV threshold	0.05 AU	0.05 AU
UV1 wavelengths	254 nm	254 nm
UV2 wavelengths	280 nm	280 nm
Air purge time	0.5 min	0.5 min
Run length	91.0 min	74.6 min

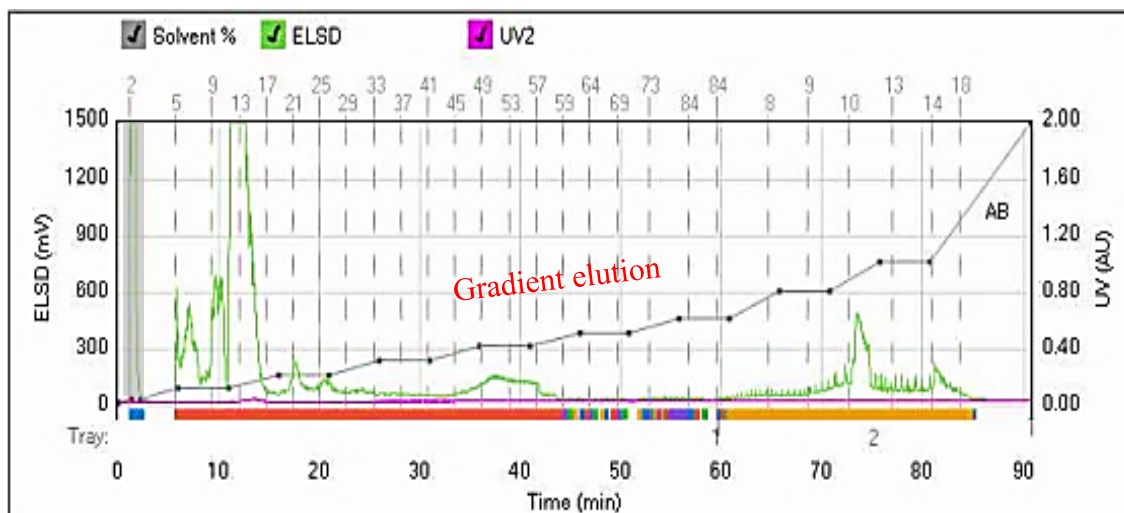


**Figure 3.4:** Normal phase chromatogram for the further fractionation of the pooled fraction F4,5,6. The solvents used were hexane (A) and ethyl acetate (B) with 0% B at 0-5 min, 10% B at 5-10 min, 20% B at 10-20 min, 30% B at 20-30 min, 40% B at 30-40 min, 50% B at 40-50 min, 60% B at 50-60 min, 70% B at 60-70 min, 80% B at 70-80 min, 90% B at 80-90 min, and 100% B at 90-115 min. High, medium and low ELSD peaks were detected. No peaks were detected for both UV<sup>1</sup> and UV<sup>2</sup> wavelengths. Peak highlighted in grey F4,5,6/F1.

The procedure outlined in this section was again applied to achieve the fractionation of metabolites from the pooled fraction F12,14 weighing 259.4 mg. Figure 3.5 presents the collected fractions according to the detected peaks. More specifically, F12,14 afforded 32 fractions weighing a total of 157.3 mg with an elution yield of 60.6%. Fractions with similar TLC traces were pooled resulting to 17 fractions.

As in F4,5,6, the same size of 12g silica REVELERIS<sup>®</sup> Flash Cartridge was used for the chromatographic purification of F12,14. For F4,5,6 a more non-polar solvent system was used, which was hexane and ethyl acetate. However, for F12,14, the mobile phase was more polar consisting of dichloromethane and methanol. The solvent systems used for the respective fractions were optimised by TLC (Figures 3.6 and 3.7). Furthermore, high intensity peaks shown as a green ES LD trace were collected into fractions. Like in F4,5,6, no peaks were detected by UV for F12,14. The collected fractions consisted of UV-inactive compounds, which could be aliphatic in structures. However, the chromatogram also depicted the occurrence of broad and shoulder peaks. The broader peaks at a later retention time could be due to a lower flow rate of 20mL/min for F12,14 when compared to that of the chromatographic condition for F4,5,6.

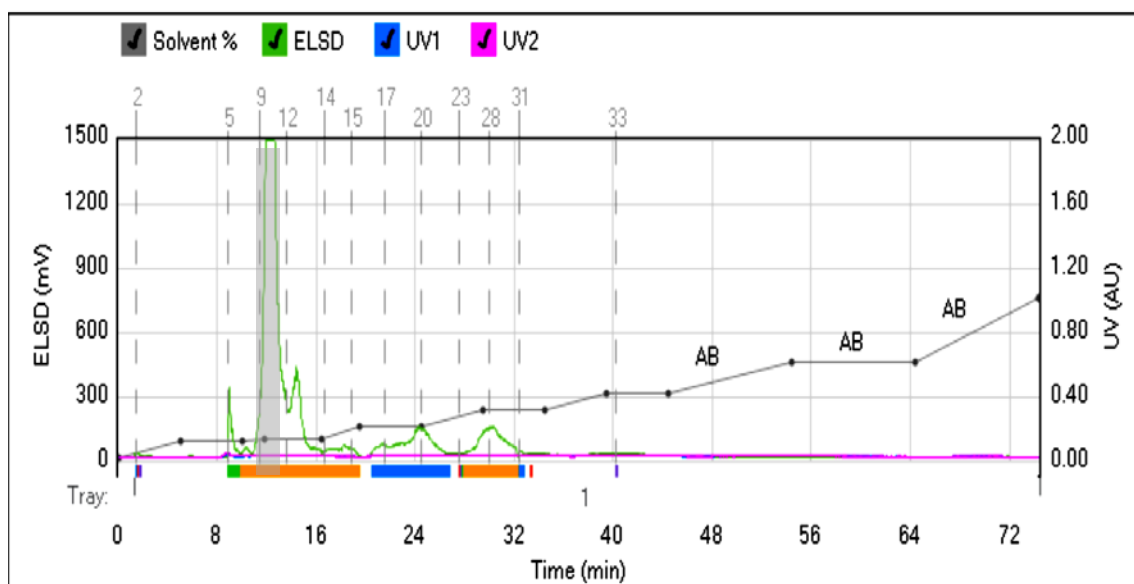


**Figure 3.5:** Normal phase chromatogram for the further fractionation of the pooled fraction F12,14. The solvents used were methanol (C) and dichloromethane (D) commencing with 90% D for 10 min, followed by 85% D for the next 10 min, then with 80% D for another 10 min and increased to 70% D in 30 min. The bioactive sub-fractions F12,14/F8 and F12,14/F9 were highlighted in grey and subjected for further analysis. DCM and MeOH stand for dichloromethane and methanol, respectively.

Fraction were again monitored on TLC using hexane and ethyl acetate as mobile phase for the chromatographic purification of F4,5,6, as shown in Figure 3.6. Dichloromethane and methanol were employed as mobile phase for F12,14 as shown in Figure 3.7. Visualisation of the majority of compounds was enabled by spraying with *P*-anisaldehyde/sulfuric acid reagent. Furthermore, the sub-fractions F8 and F9 eluting from F12,14, which was highlighted in grey (Figure 3.5) were selected for further analysis due to their positive bioactivity result, interesting NMR spectral data and metabolomic profile. The bioactive sub-fractions were coded F12,14/F8 and F12,14/F9.

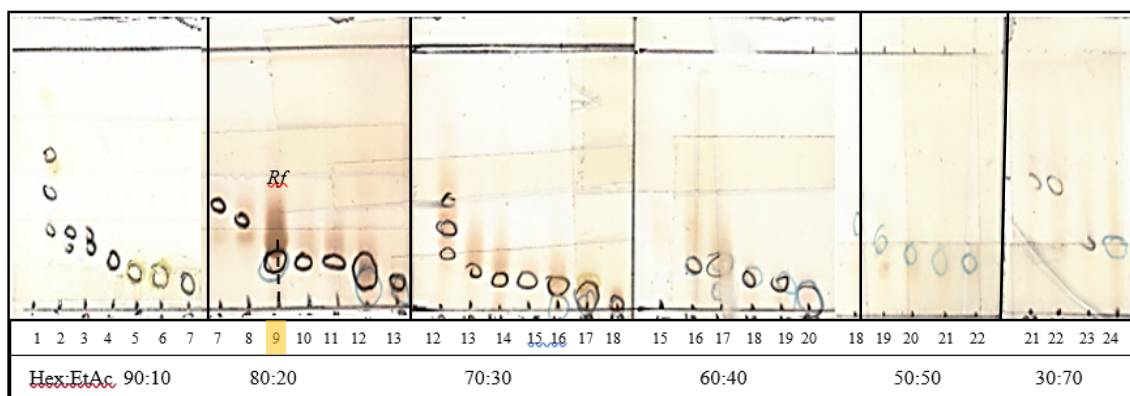


**Figure 3.6:** TLC of fractions obtained from F4,5,6 on silica gel 60A° F254 using hexane and ethyl acetate as mobile phase. The soft black circles denote the spots observed under short UV of 250nm, whereas the circles of varying colours, depending on how the colour was visualised under long UV of 365nm. Spraying with *P*-anisaldehyde/sulfuric acid reagent allowed further differentiation between the observed spots. The  $R_f$  value of the fractions of interest was the same  $F_{4,5,6}/F_9 = 0.4$ , and is indicated in the figure by the black dotted line.

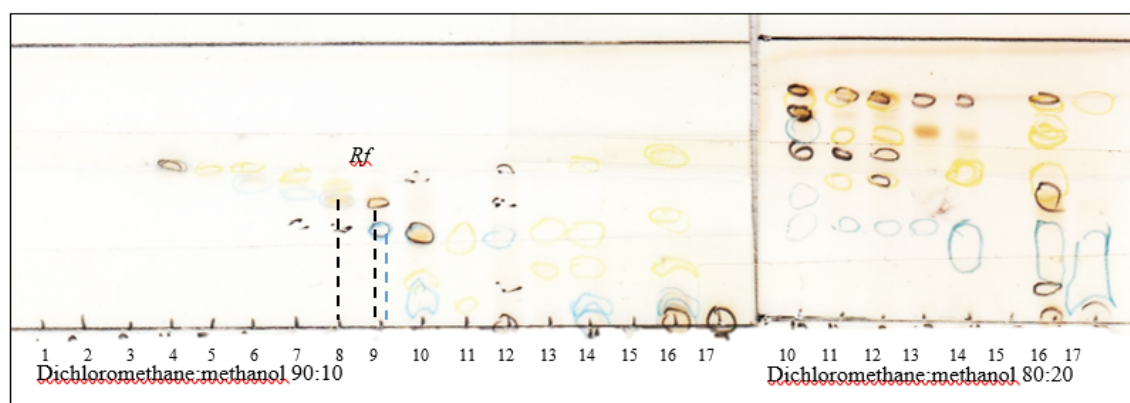


**Figure 3.7:** TLC of fractions obtained from F12,14 on silica gel 60A° F254 using dichloromethane and methanol as mobile phase. The soft black circles denoted the compounds observed under short UV at 250nm, whereas the circles of varying colours, depending on their colour of visualisation under long UV of 280nm. Spraying with *P*-anisaldehyde/sulfuric acid spray reagent allowed differentiation to be made between the observed spots. The  $R_f$  value of the fractions of interest, F8 and F9, was the same at 0.4, and is indicated in the figure by the black dotted line. An additional weak spot with a  $R_f$  value of 0.3 is denoted by the blue dotted line.

### **3.3 Third fractionation**

Further chromatographic purification was employed for the bioactive sub-fraction F1 obtained from the fractionation of F4,5,6. Preparative TLC of F4,5,6/F1 yielded six fractions of F4,5,6/F1/F1 to F4,5,6/F1/F6 (Figures 3.8). Due to the bioactivity of the sub-fraction as shown in section 3.5.3, F4,5,6/F1/F1 at 2 mg was selected for further analysis. F4,5,6/F1/F5 was also selected for further analysis due to its bioactivity, interesting NMR spectral data and metabolomic profile.

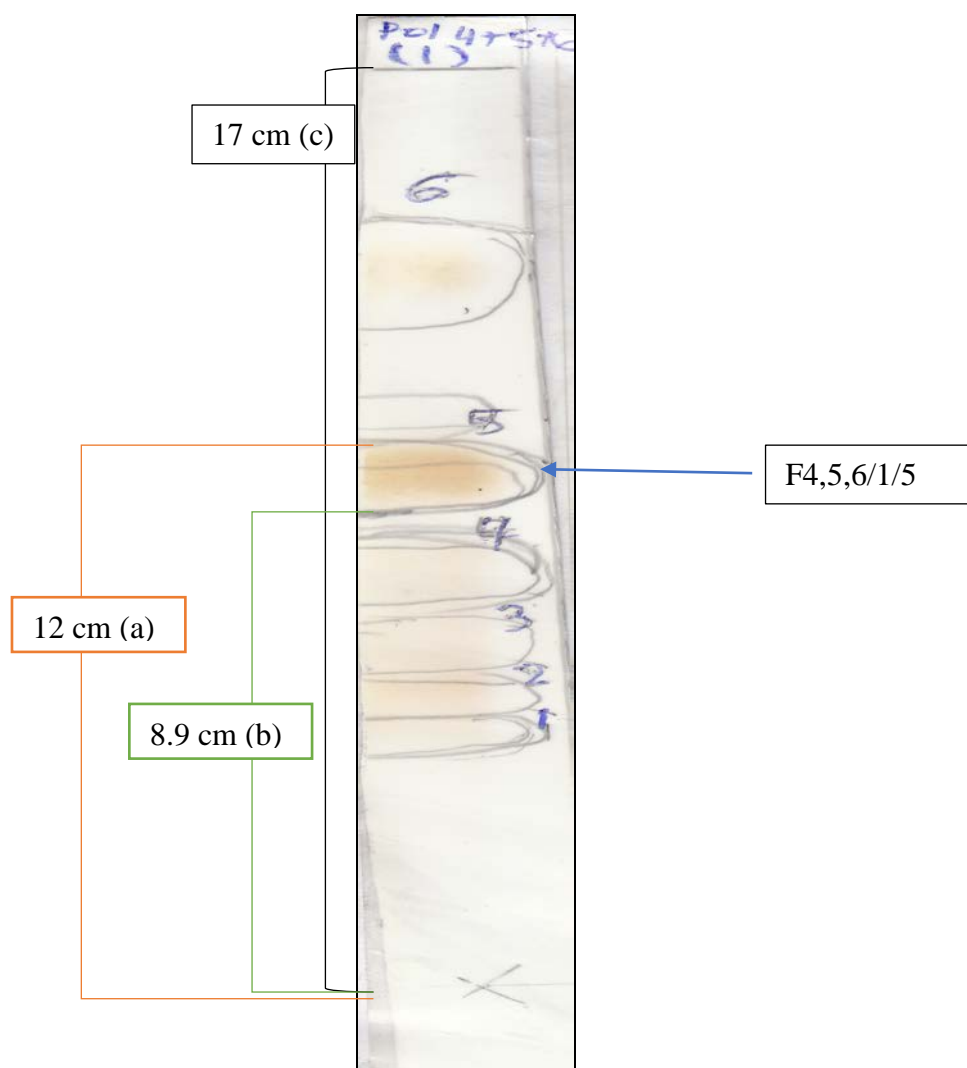


**Figure 3.8:** Preparative TLC of F4,5,6/F1/F5.  $R_f$  value was calculated as  $\{[(a+b)/2]/c = [(12+8.9)/2]/17\} = 0.6$ .

### 3.4 NMR

#### 3.4.1 $^1\text{H-NMR}$ data obtained from 1<sup>st</sup> fractionation of crude organic mesocarp extract

Overall, F1-F17 of the mesocarp exhibited the presence of fatty acid and steroid resonances in the aliphatic (0 - 2.75 ppm) and olefinic (3.5 – 5.5 ppm) regions, but not in the aromatic (6.5-9.75 ppm) regions. Moreover, as presented in Figure 3.9, the aliphatic region contained the overlapping peaks.  $\text{CDCl}_3$  solvent signal was references at 7.25 ppm. Fatty acids and steroids were predicted as the primary metabolites. Despite the similarities apparent between peaks, F4, F5, and F6, as well as between F12 and F14, the fractions were subjected to further fractionation for purification.

F4, F5 and F6 demonstrated identical peaks situated in the aliphatic, olefinic and aromatic regions up to around 8 ppm. Of these three regions, the aliphatic region was associated with peaks of highest intensity. Similarly, the highest intensity peaks for F12 and F14 peaks were also observed in the aliphatic and olefinic regions at 5.5 ppm. By contrast, as shown in Figure 3.9, peaks in the aromatic region were significantly less intense at 6.7-7.5 ppm.

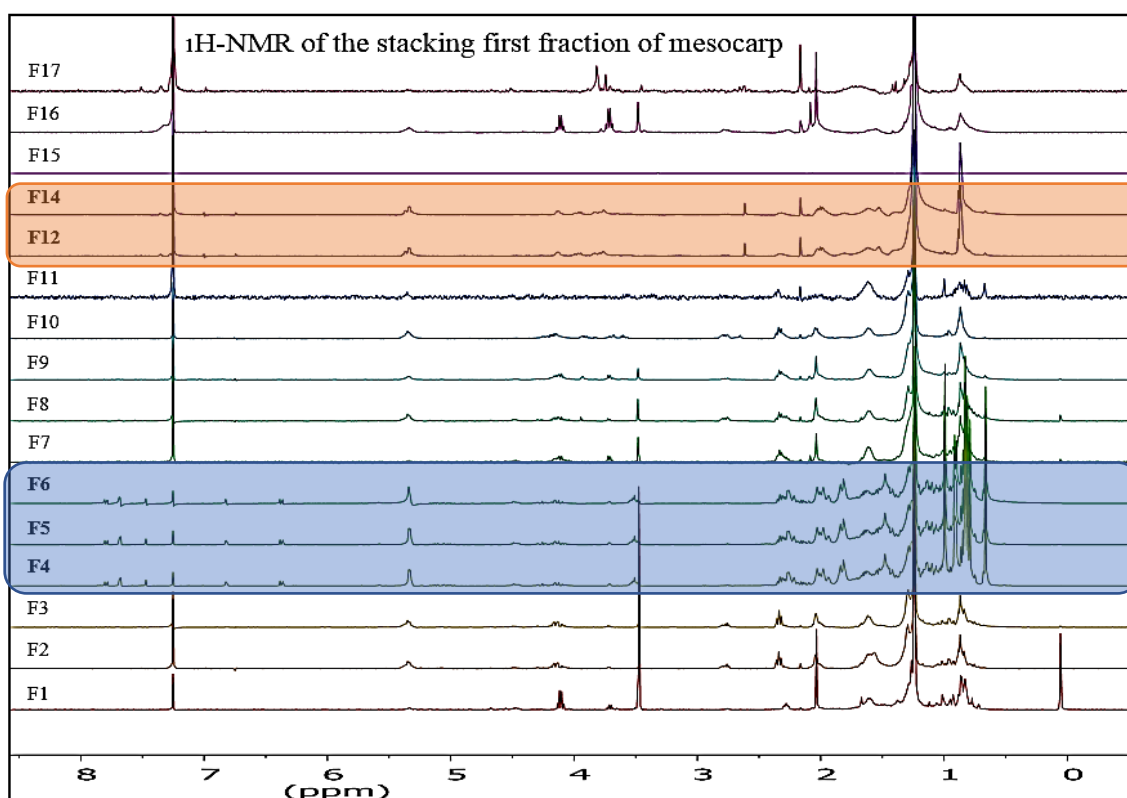


**Figure 3.9:** Stacked <sup>1</sup>H-NMR spectra (400 MHz, CDCl<sub>3</sub>) of fractions obtained from flash chromatography of crude ethyl acetate mesocarp extract. The CDCl<sub>3</sub> solvent peak was referenced at 7.25 ppm.

### 3.4.2 <sup>1</sup>H-NMR data obtained from fractionation of bioactive eluates F4,5,6 and F12,14

<sup>1</sup>H-NMR spectra for fractions F1 to F24 obtained from the chromatographic purification of F4,5,6 were stacked. F6, F10, and F15 were eliminated due to their inadequate amounts (Figure 3.10). Likewise, <sup>1</sup>H-NMR spectra for sub-fractions F1 to F17 of F12,14 were also stacked. Sub-fractions F1 to F3, F5 and F15 from F12,14 were also excluded because of their low yield, which was less than 2 mg. Overall, the stacked NMR spectra were dominated by fatty acid resonances. In the aliphatic region (0-2.75ppm), peaks were

again crowded and overlapping, while in the olefinic region (3.5-5.5ppm), peaks were superimposed, and few or no peaks were found in the aromatic region (6.5-9.75ppm).

Conversely, the least polar (F4,5,6) contained a greater number of resonances in the aliphatic region compared to (F12,14).

<sup>1</sup>H NMR spectra of the fractions were stacked for the purpose of finding resonances unique to the bioactive fractions (Figure 3.10 and Figure 3.11). Among the bioactive fractions from F4,5,6 were F4, F5, F7, F8, F9, F12, F22 while from F12,14; fractions F7, F8, F9, F17 were found to be bioactive. Fractions that were not bioactive in relation to oxidation-related AD were not analysed in detail. <sup>1</sup>H NMR spectra of F8, F9 and F12 from F4,5,6 were relatively similar, but only F9 was analysed further because of its higher purity. In the same fashion, <sup>1</sup>H NMR spectra of F8 and F9 from F12,14 were also relatively comparable but these two fractions were further analysed separately instead of being pooled.

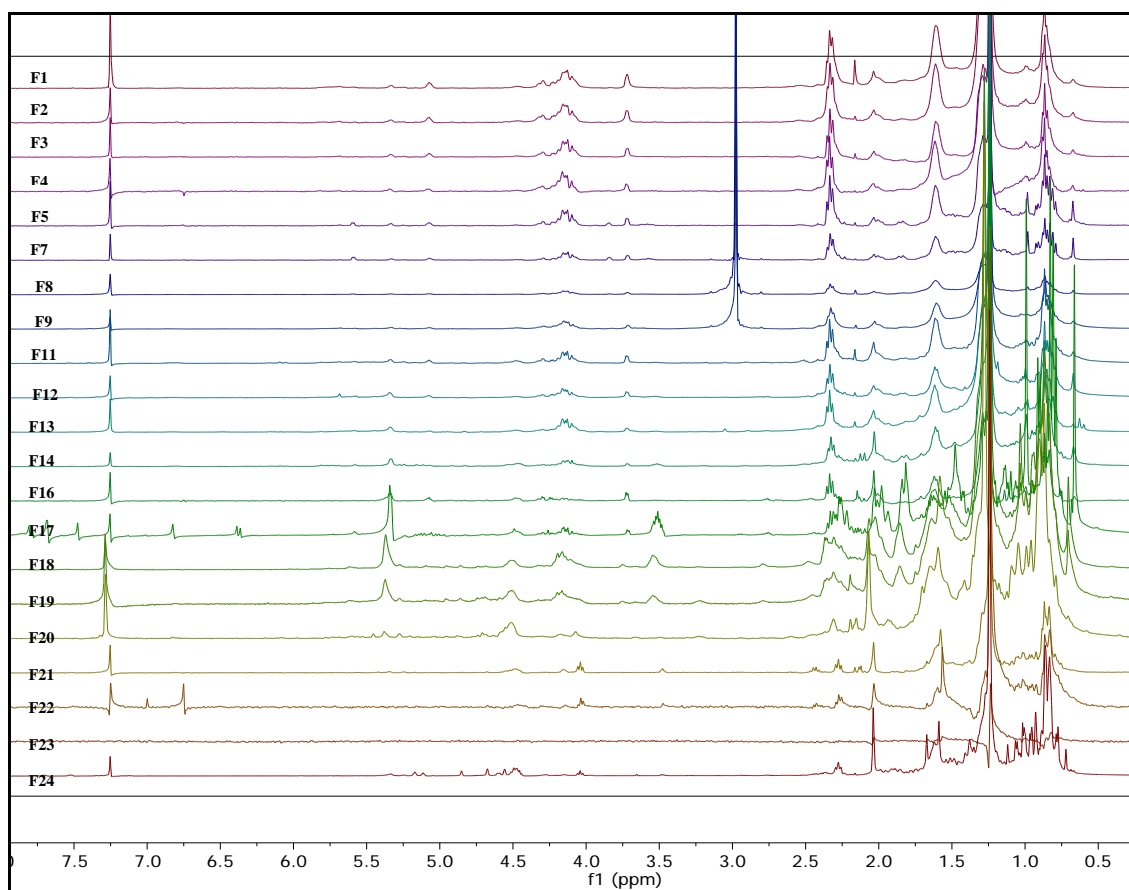


**Figure 3.10:** Stacked  $^1\text{H-NMR}$  spectra (400 and 500 MHz,  $\text{CDCl}_3$ ) of fractions obtained from F4,5,6 by flash chromatography.  $\text{CDCl}_3$  solvent peak referenced at 7.25 ppm.

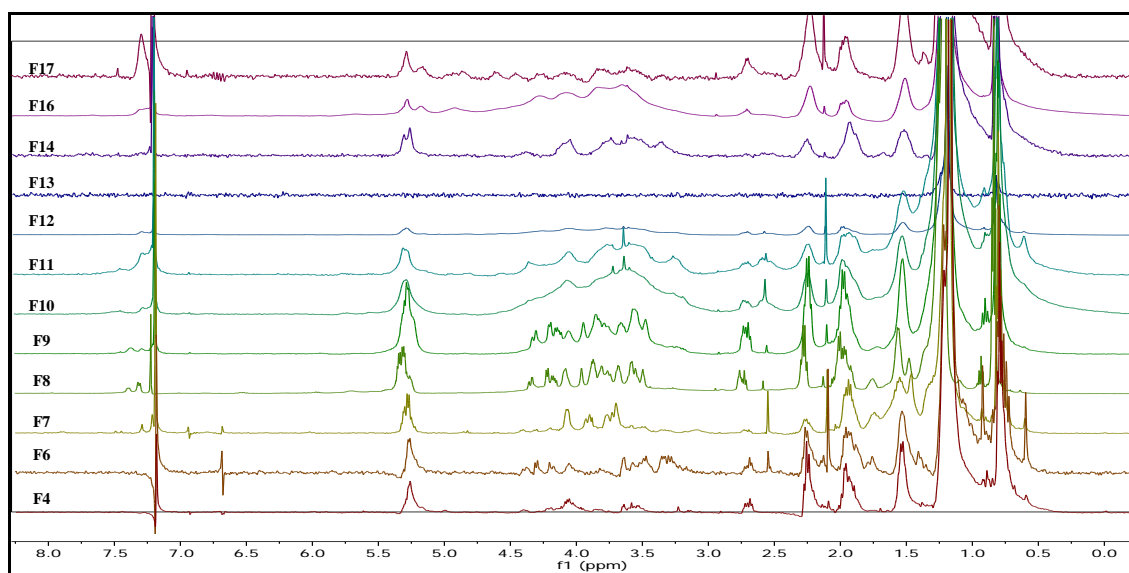


**Figure 3.11:** Stacked  $^1\text{H-NMR}$  spectra (400MHz,  $\text{CDCl}_3$ ) of F12,14 after they were subjected to flash chromatography.  $\text{CDCl}_3$  solvent peaks were resonate at 7.25ppm.

### 3.4.3 $^1\text{H-NMR}$ of fractions obtained from preparative TLC of F4,5,6/F1

$^1\text{H-NMR}$  spectra of fractions F1 to F6 obtained from preparative TLC of F4,5,6/F1 were stacked. F4,5,6/F1/F2 and F4,5,6/F1/F3 were eliminated due to their poor yield (Figure 3.12). It has been demonstrated that crowded peaks were found at 0.5 to 2.5 ppm and 3.5 to 5.5 ppm for aliphatic and olefinic structures, respectively. Meanwhile, in the most downfield region, extremely weak to aromatic peaks were observed. F4,5,6/F1/F1, F4,5,6/F1/F5, and F4,5,6/F1/F6 were found to be bioactive. F4,5,6/F1/F5 and F4,5,6/F1/F6 were particularly similar, but in spite of this, solely F4,5,6/F1/F5 was further analysed due to its higher purity as indicated by TLC as well as its more potent bioactivity result (section 3.5.3).

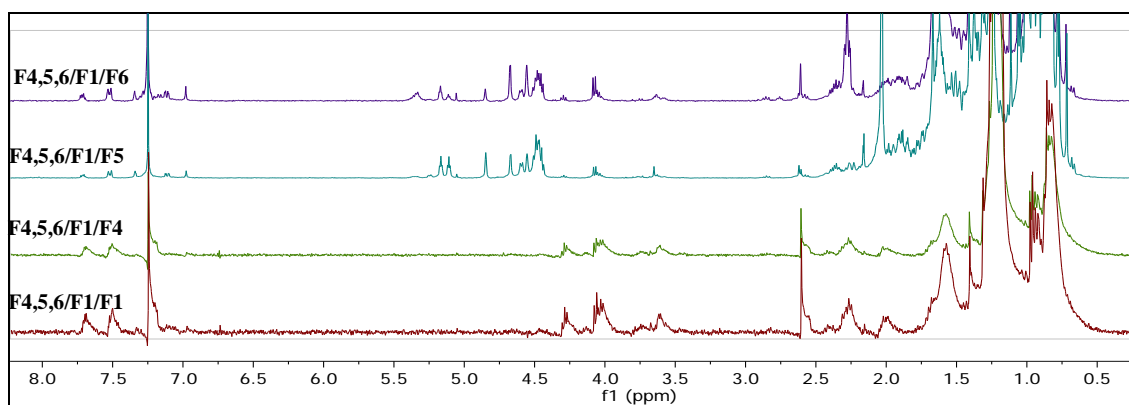


**Figure 3.12:** Stacked  $^1\text{H-NMR}$  spectra (400MHz,  $\text{CDCl}_3$ ) of fractions obtained from preparative TLC of F4,5,6/F1.

## 3.5 Cell viability test

### 3.5.1 Bioscreening of fractions from the crude organic mesocarp extract

The *F. carica* endocarp fractions were subjected to a cell viability assay on differentiated SH-SY5Y cell line. A preliminary cell viability screening was performed using the AlamarBlue<sup>®</sup> assay. For this test, SH-SY5Y cell line were chosen and differentiated with retinoic acid (RA) (Figure 3.13) to mimic human neuron-like cells from the SH-SY5Y neuroblastoma cell line (Encinas *et al.*, 2002). As shown in Figure 3.13B in comparison to that in Figure 3.13A, increase in neurites outgrowth and branches were observed as the

cells were differentiated into dopaminergic neuron-like cells (Lopes *et al.*, 2010), which were indicated by orange arrows.

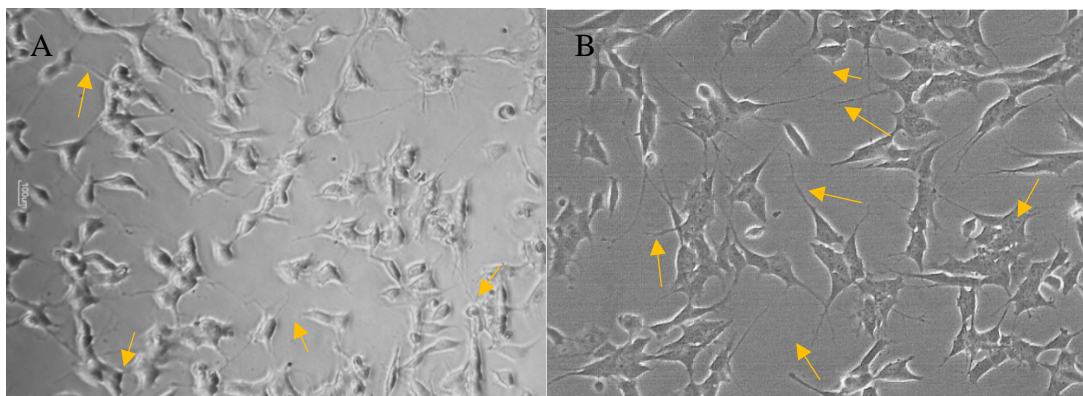


**Figure 3.13:** Photomicrograph of undifferentiated and differentiated SH-SY5Y cell line at 20X Magnification. **A)** Undifferentiated SH-SY5Y cell line shows a loosely supported cell body and a prominent nucleolus, in which neurite length is unchanged without the addition of 10  $\mu\text{M}$  RA for 2 days incubation. **B)** Differentiated SH-SY5Y cell line shows an extensively branching and outgrowth of neurites and ganglions following treatment with 10  $\mu\text{M}$  RA for 2 days; yellow arrows indicated the neurites connection.

Investigations of neurodegenerative disorders like AD typically rely on the *in vitro* differentiated SH-SY5Y cell line. As can be observed in Figure 3.14, at 30  $\mu\text{g/ml}$  concentration, the cells remained viable against neurodegenerative disorder in the case of the fractions F2, F3, F4, F5, F6, F10, F12, F14 and F15. On the other hand, at the same concentration, no activity was exhibited by the remaining fractions F1, F7, F8, F9, F11, F16 and F17. Results obtained following 24-hour incubation markedly exhibited the viable effect of fractions of F2 (106.1%), F3 (105.9%), F4 (112.6%), F5 (111.4%), F6 (110.1%), F10 (103.2%), F12 (116.9%), F14 (114.6%) and F15 (106.7%), all of which exceeded 100% viability. The prism5 software was employed to conduct a statistical analysis for the summary of mean, standard errors and 95% confidence intervals. The pooled fractions F4,5,6 for further purification and isolation was supported by the NMR spectral data, which validated the close similarities of these fractions. Similarly, the NMR spectral data and cell viability test results for F12 and F14 warranted pooling these two fractions coded as F12,14.

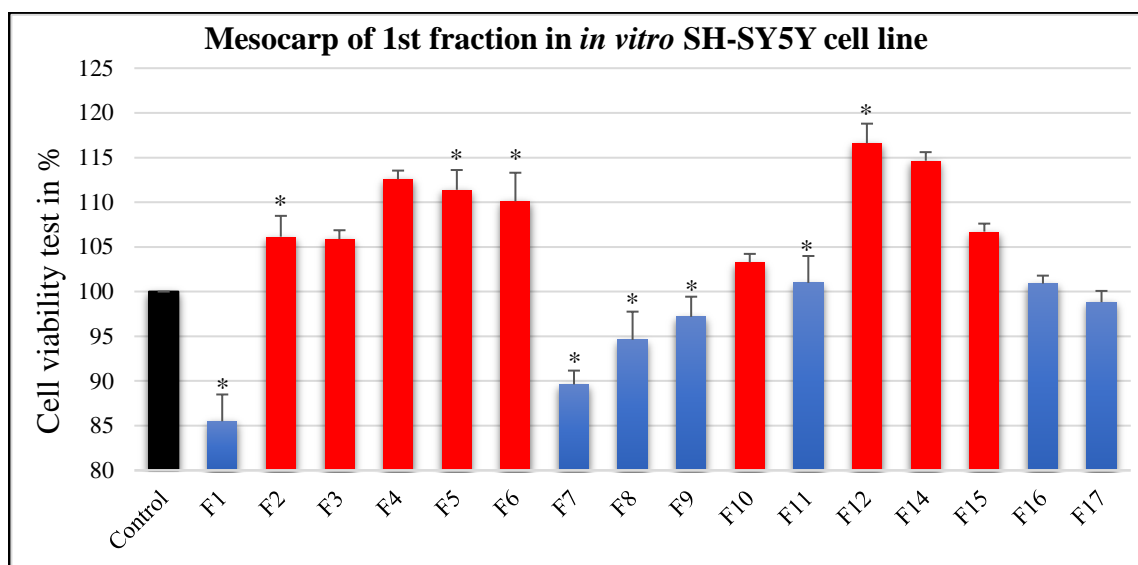


**Figure 3.14:** Preliminary cell viability screening of chromatographic fractions of *F. carica* mesocarp (30 µg/ ml) on differentiated SH-SY5Y cells. Viability was displayed by fractions with values higher than 100% (red), while fractions lacked viability, with values of equally or less than 100% (blue); the control (100%) is shown in black. Every group constituted a mean of three SDs, and ANOVA was significant at  $P < 0.001$  and  $P^* < 0.5$  when compared to the control.

### 3.5.2 Bioscreening of fractions from bioactive eluates F4,5,6 and F12,14

Further cell viability assays on neuro differentiated SH-SY5Y cell line were performed on chromatographic fractions of F4,5,6 and F12,14 (Figure 3.15A and B). Meanwhile, as shown in Figure 3.15B, at 30 µg/ml concentration of F7, F8, F9, and F17 obtained from F12,14 exhibited an increase in *in vitro* differentiated SH-SY5Y cell viability. F9 stood out amongst the four fractions, with a marked up-regulation effect that exceeded 10% compared to the control. Additionally, the sub-fractions of F4,5,6 and F12,14 were further examined for cell cytotoxicity test and metabolomics profile.

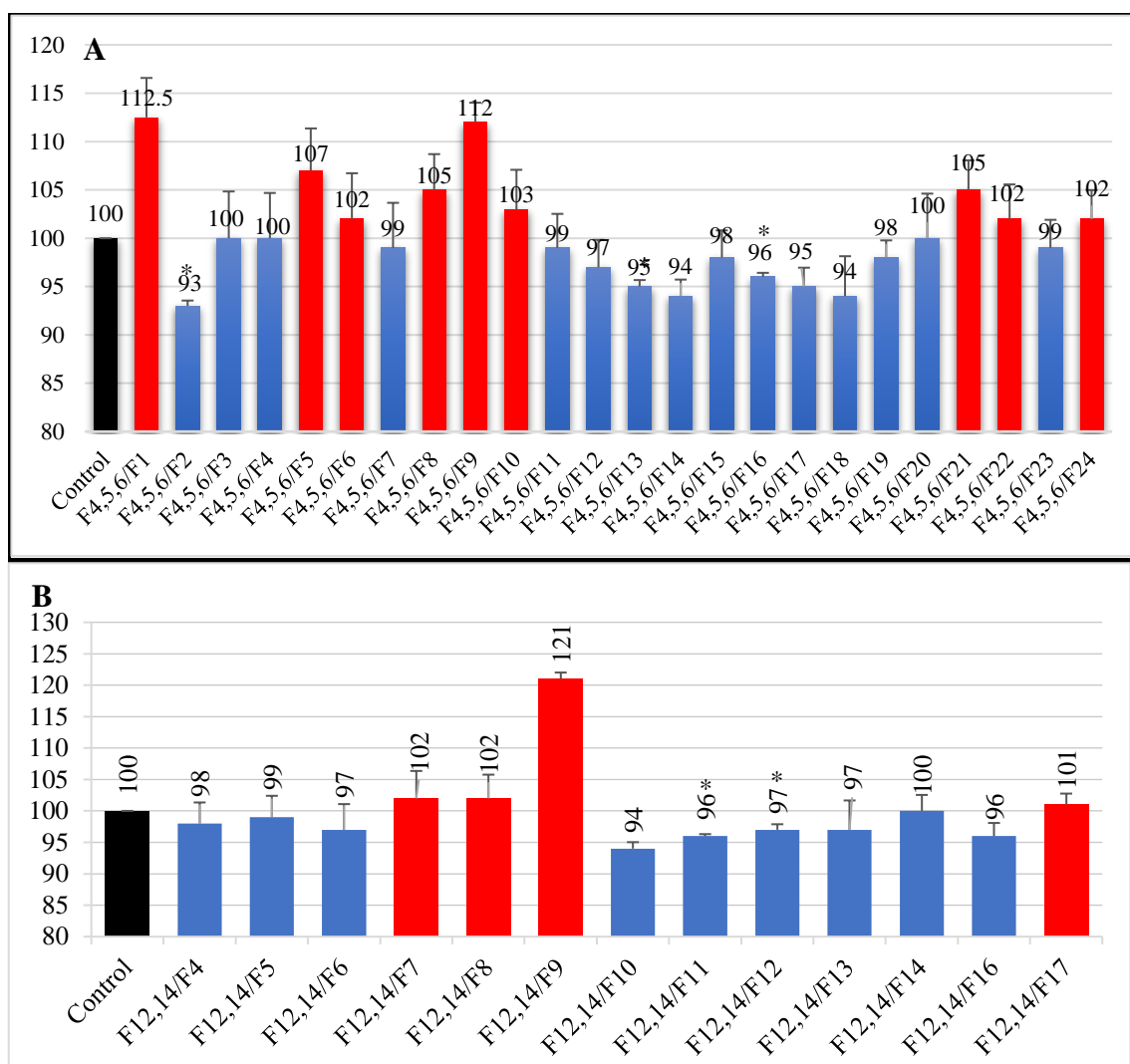


**Figure 3.15:** Preliminary cell viability screening of chromatographic fractions (30 µg/ml) of (A) F4,5,6 and (B) F12,14 on differentiated SH-SY5Y cells. Viability was displayed by fractions with values higher than 100% (red), while fractions lacked viability, with values of equally or less than 100% (blue); the control (100%) is shown in black. Every group constituted a mean of three SDs, and ANOVA was significant at  $P^* < 0.01$  and  $P < 0.5$  when compared to the control.

Moreover, the subfraction F4,5,6/F1 with 112.5% viability was further fractionated and subjected to cell viability test as presented below.

### 3.5.3 Bioscreening of fractions obtained from preparative TLC of F4,5,6/F1

Six TLC band extracts were generated by the fractionation F4,5,6/F1 (Figure 3.16). Preparative TLC bands F4,5,6/F1/F1, F4,5,6/F1/F5, and F4,5,6/F1/F6 exhibited bioactivity on the differentiated SH-SY5Y neuronal cell line. As a result, fractions F4,5,6/F1/F5 exhibited the highest viability of 125% and was further examined for cell cytotoxicity test as well as metabolomics profiling.

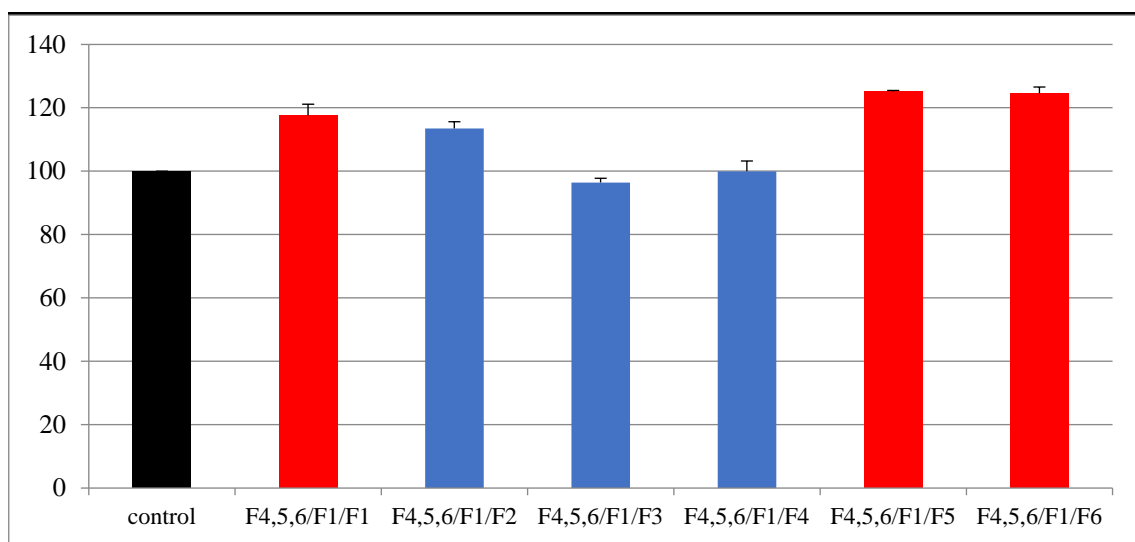


**Figure 3.16:** Preliminary cell viability screening of fractions obtained from preparative TLC of F4,5,6/F1 (30  $\mu\text{g}/\text{ml}$ ) on differentiated SH-SY5Y cells. Viability was displayed by fractions with values higher than 100% (red), while fractions lacked viability, with values of equally or less than 100% (blue); the control (100%) is shown in black. Every group constituted a mean of three SDs, and ANOVA was significant at  $P < 0.001$  when to compare with the control.

### 3.6 Cell cytotoxicity test

In the present study, in order to establish the concentration of acrolein that was most damaging to the cell, varying doses (1-200  $\mu\text{M}$ ) were used on the incubation of SH-SY5Y cells for 24h. An MTT assay was performed to determine cytotoxicity. It was observed that the marked decline in the MTT activity of acrolein was dosage dependent (Figure 3.17).

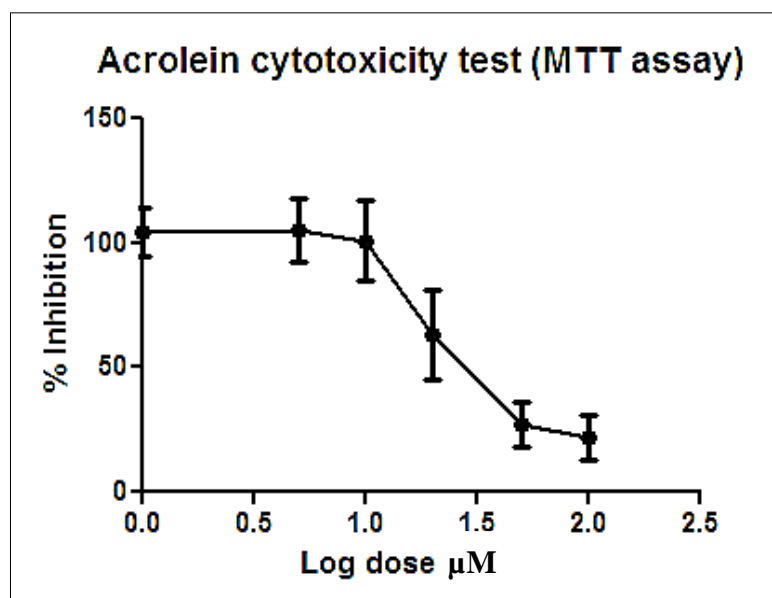


**Figure 3.17:** Cytotoxic effect of acrolein in *in vitro* differentiated SH-SY5Y cell line found at  $\text{IC}_{50}$  value of 20  $\mu\text{M}$ .

Oxidative stress was then triggered for a period of 6 hours through the suppression of acrolein in a concentration of 20  $\mu\text{M}$ . Subsequently, the cells were treated with fractions F12,14/F8 [1], F12,14/F9 [2], F4,5,6/F9 [3] and F4,5,6/F1/F5 [4] over a period of 24 hours at various concentrations of 30, 10, 3, and 1  $\mu\text{g/ml}$ , then at 300, 100, 30, and 10  $\text{ng/ml}$  (Figure 3.18).

In certain conditions, the cells did not become more viable when the concentration was reduced. On the other hand, the concentrations of the fractions that were conducive to enhance cell viability were at 30, 10, and 3  $\mu\text{g/ml}$  of different fractions. Fractions F4,5,6/F9 [3] and F4,5,6/F1/F5 [4] exhibited a greater increase in cell viability in comparison to F12,14/F8 [1] and F12,14/F9 [2]. Furthermore, the generation of oxidative stress was inhibited at concentrations of 10  $\mu\text{g/ml}$  and 30  $\mu\text{g/ml}$ .

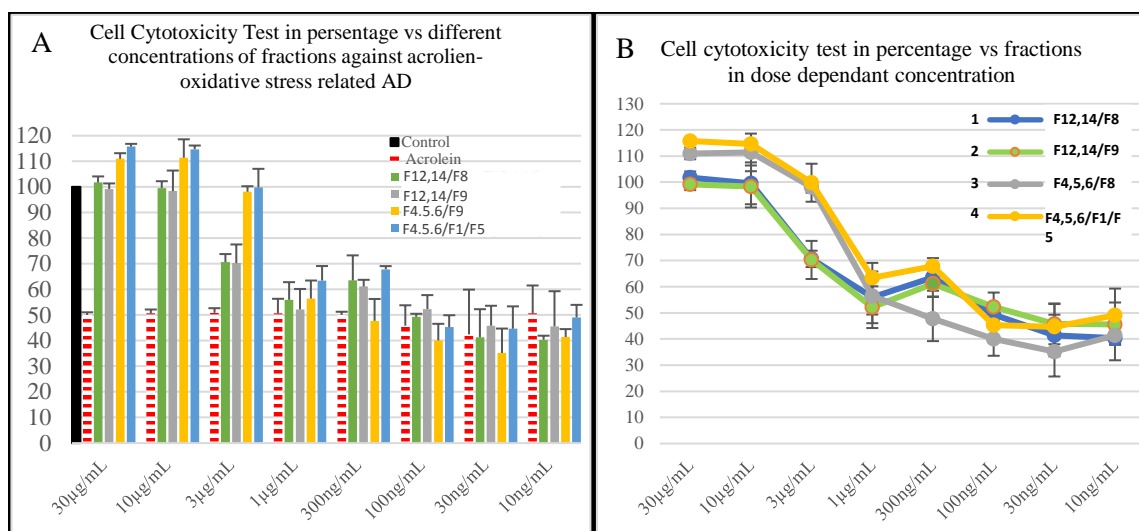


**Figure 3.18:** A) Results of the AlamarBlue® test upon treatment of acrolein-induced oxidative stress associated SH-SY5Y neuroblastoma cells (red) with fractions F12,14/F8 [1] (green), F12,14/F9 [2] (grey), F4,5,6/F9 [3] (orange) and F4,5,6/F1/F5 [4] (blue). (B) The antioxidant effect of the tested fractions against acrolein on differentiated SH-SY5Y cell line. One-way ANOVA indicated significance compared to control at  $p < 0.05$ . Experiments were performed thrice and data expressed in mean  $\pm$  SD.

F4,5,6/F1/F5 [4] and F4,5,6/F9 [3] successfully suppressed oxidative stress on differentiated SH-SY5Y cells at  $0.6395 \pm 2.847 \mu\text{g/ml}$  and  $0.8396 \pm 2.560 \mu\text{g/ml}$ , respectively while both F12,14/F8 [1] and F12,14/F9 [2] suppressed oxidative stress at  $0.9685 \pm 2.626 \mu\text{g/ml}$  and  $0.8694 \pm 1.602 \mu\text{g/ml}$  (Table 3.3). The concentration associated with the highest level of bioactivity and capable of generating an antioxidant effect was at  $10 \mu\text{g/ml}$  (Figure 3.18A). F12,14/F8; F12,14/F9; F4,5,6/F9; and F4,5,6/F1/F5 were later elucidated as oleoyl- $\beta$ -D-arabinoside [1] and [2],  $\gamma$  sitosterol [3], and lupeol acetate [4].

**Table 3.3:** Antioxidant activities vs differentiated SH-SY5Y cell line of the identified fractions of the mesocarp *F. carica*; values were expressed in triplicate.

Compound	[1]	[2]	[3]	[4]
	F12,14/F8	F12,14/F9	F4,5,6/F9	F4,5,6/F1/F5
EC <sub>50</sub> µg/mL	1.6	1.8	1.5	2.8
Acrolein antioxidant test EC <sub>50</sub> µg/mL	0.9685± 2.626	0.8694±1.602	0.8396 ± 2.560	0.6395± 2.847

µM\* was calculated by the equation discovered by Amedeo Avogadro and his number (g = Molar x L x molecular weight) (Kotz *et al.*, 2014).

### 3.7 Western blotting test

To explore whether the protective effect of fractions F12,14/F9, F4,5,6/F9, and F4,5,6/F1/F5 in differentiated SH-SY5Y cells is related with the endogenous antioxidant Nrf2 pathway, the expression of NQO1 (the target gene of Nrf2) were further examined. The results (Figure 3.19) showed that treatment with F12,14/F9, F4,5,6/F9, and F4,5,6/F1/F5 for 24 hours after pre-exposure to 20 µM acrolein for 6 hours significantly upregulated the protein expression of NQO1. The Figure in 3.19 manifest that F12,14/F9, F4,5,6/F9, and F4,5,6/F1/F5 activated the Nrf2-ARE signal pathway by its target gene NQO1 and was able to protect neural cells from oxidative stress. However, F4,5,6/F1/F5 (2.8 µg/mL) have expressed more upregulation, than F4,5,6/F9 (1.5 µg/mL) followed by F12,14/F9 (1.8 µg/mL). The findings demonstrated the potential of the natural products as promising candidates in attenuating Aβ-related cell toxicities.

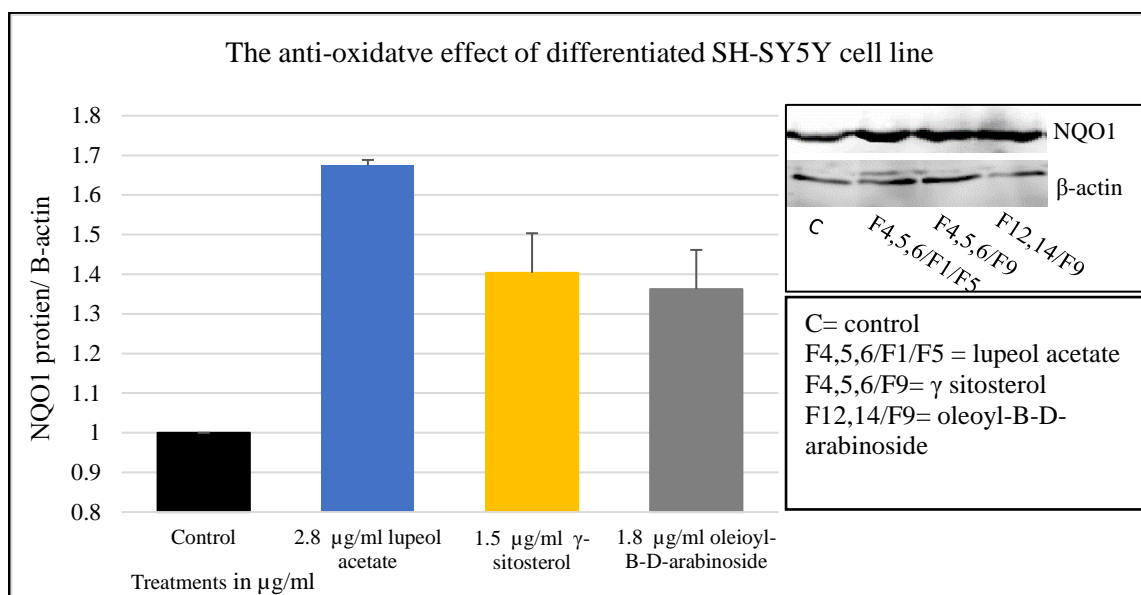


**Figure 3.19:** The effect of F12,14/F9, F4,5,6/F9, and F4,5,6/F1/F5 on the level of protein expressions of NQO1 and β-actin measured by Western blotting using lysates from differentiated SH-SY5Y cell line. All data were significant ( $P < 0.05$ ) and were represented as a mean  $\pm$  SD of three independent experiments.

### 3.8 Metabolomic-guided screening of *F. carica* mesocarp

#### 3.8.1 Metabolomic profiling of fractions from the crude organic mesocarp extract

Fractions were subjected to HCA through a PCA model and heat map with the aim of distinguishing the intrinsic sample clusters. Similarity in secondary metabolite profiles is the basis on which the unsupervised groupings in HCA were achieved. An assumption of similarity between fractions is indicated by the small distance between observations (Figure 3.20).

Seven fractions F1, F2, F3, F11, F12, F14, and F17 were clustered together in the green group while F15 and F16 were obtained in the blue group. On the other hand, F4, F5, F6 and F7 were classified together as the red group, while F8, F9 and F10 were put together as the yellow group.

Programme R (version 3.1.0) enabled the generation of a heat map, which was subsequently compared to the HCA dendrogram. The heat map indicated the chemical diversity in each individual fraction. The presence or increase in concentration of a

metabolite was indicated by a blue bar while absence or decrease in concentration of a metabolite gave a pink bar.

The summary of fitness for the PCA in Figure 3.20 gave R2 and Q2 values of 0.998 and 0.468, respectively. On the basis of these results, the pooling of F12,14 and of F4,5,6 was further validated due to their comparable bioactivity and NMR spectral data. The scores and loadings scatter plots of the PCA model revealed the four groups (Figure 3.21). The blue cluster found on the third quadrant, which were represented by fractions F15 and F16 with weak or no bioactivity with regard to their neuroprotective effect. The fourth and first quadrants were occupied by the red and green clusters dominated by ion peaks at the range of  $m/z$  612.833-818.074 and 151.39-612.833, respectively. Fractions from the red and green clusters were further investigated due to their relatively good bioactivity. The separation of the groupings based on the variation of the X variable was 31.9%, where R2X [1] was at 0.319.

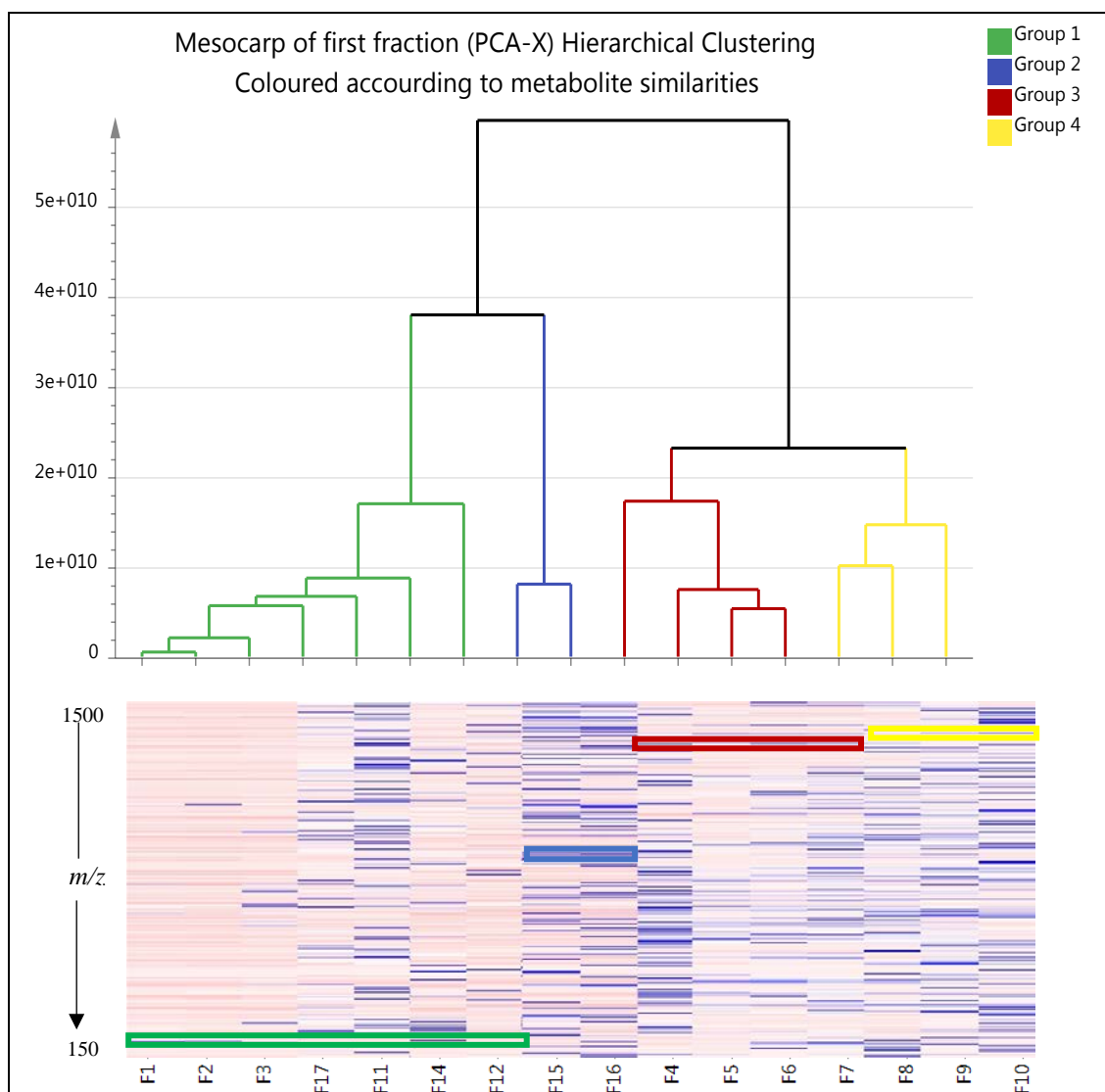


**Figure 3.20:** PCA-HCA dendrogram and heat map of chromatographic fractions of the crude ethyl acetate extract of *F. carica* mesocarp.

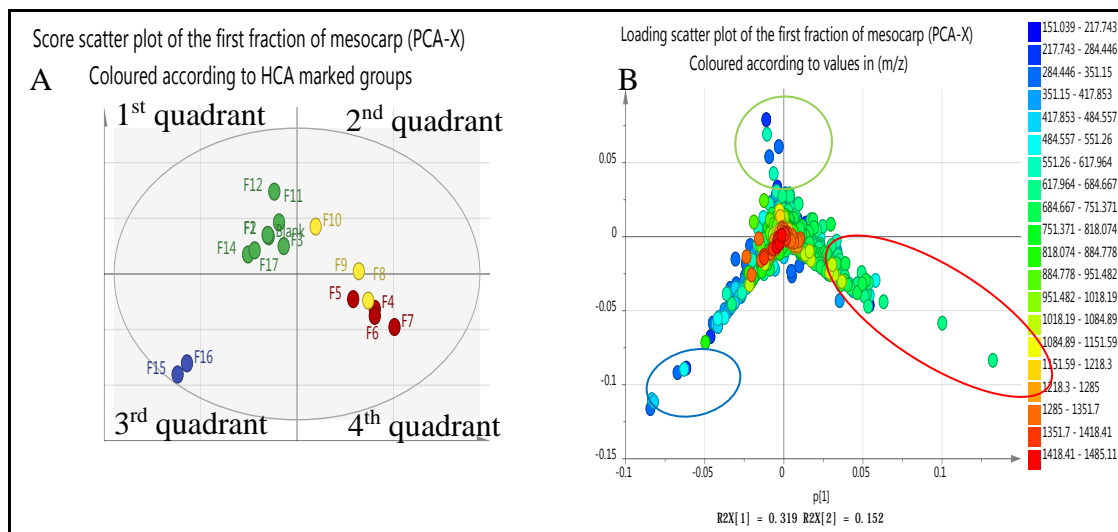


**Figure 3.21:** **A)** PCA scores scatter plot of mass spectral data showed mesocarp fractions groupings based on their similarities in discriminatory metabolites. **B)** PCA loadings scatter plot disclosed the  $m/z$  values of the grouped metabolites.

To detect the metabolites contributing to the bioactivity, a supervised OPLS-DA model was used (Figure 3.22A). Loadings scatter plot of OPLS-DA was generated to pinpoint the discriminatory compounds, which suggested the unique metabolites responsible towards the bioactivity on neuroblastoma differentiated SH-SY5Y cell line (Figure 3.22B). For the OPLS-DA models, the MS-based metabolomics data set was assigned as the X independent variable while the fractions neuroprotective response was the Y dependent variable. Variations between the two groups and within the group were exhibited at 26.4% (R2X[1]) and 25.6% (R2Xo[2]), which is almost similar because of the occurrence of two sub-clusters within the defined classes. Ideally, the variation within the group must be significantly greater than between the group variation. Fitness of the model was at 0.714 (R2Y(cum)) and predictability at 0.531 (Q2(cum)), which were both relatively good. Moreover, to identify the metabolites with the greatest input to the segregation of active versus inactive fractions, an S-plot (Figure 3.22) was generated to target these compounds for isolation work. These target metabolites were considered ideal according to their significant P value at  $< 0.05$ . Moreover, dereplication was accomplished with DNP 2015 (Table 3.4).

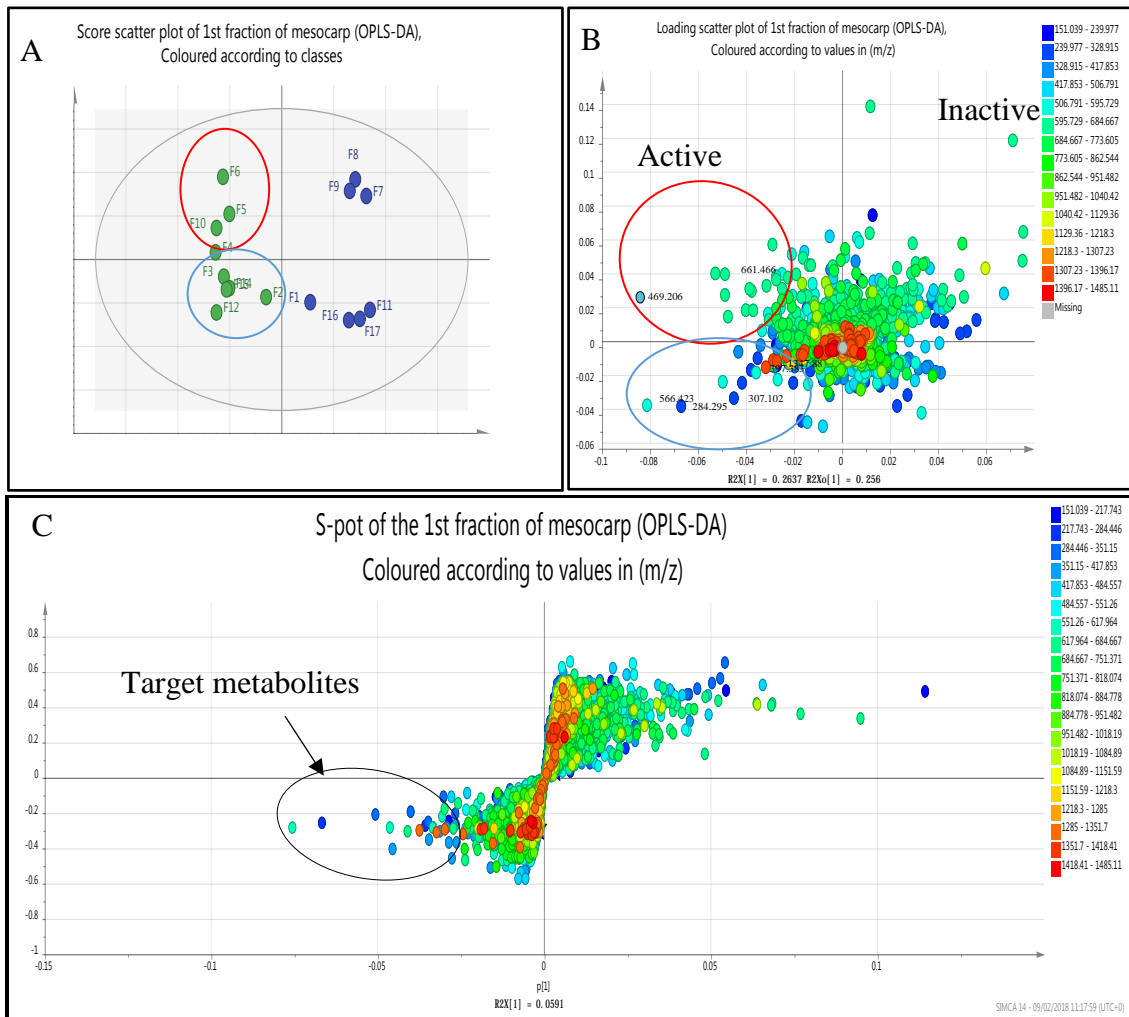


**Figure 3.22:** **A)** Scores scatter plot for the OPLS-DA model of 17 sub-fractions of bioactive eluates from the mesocarp. Green represents the active fractions and blue represent the inactive fractions. **B)** Loadings scatter plot for OPLS-DA model. Target molecules in  $m/z$  encircled in red and blue as distributed in the two active quadrants respectively. Colours represent molecular ion peak ranges in  $m/z$ . **C)** S-plot indicating target molecules in  $m/z$ .

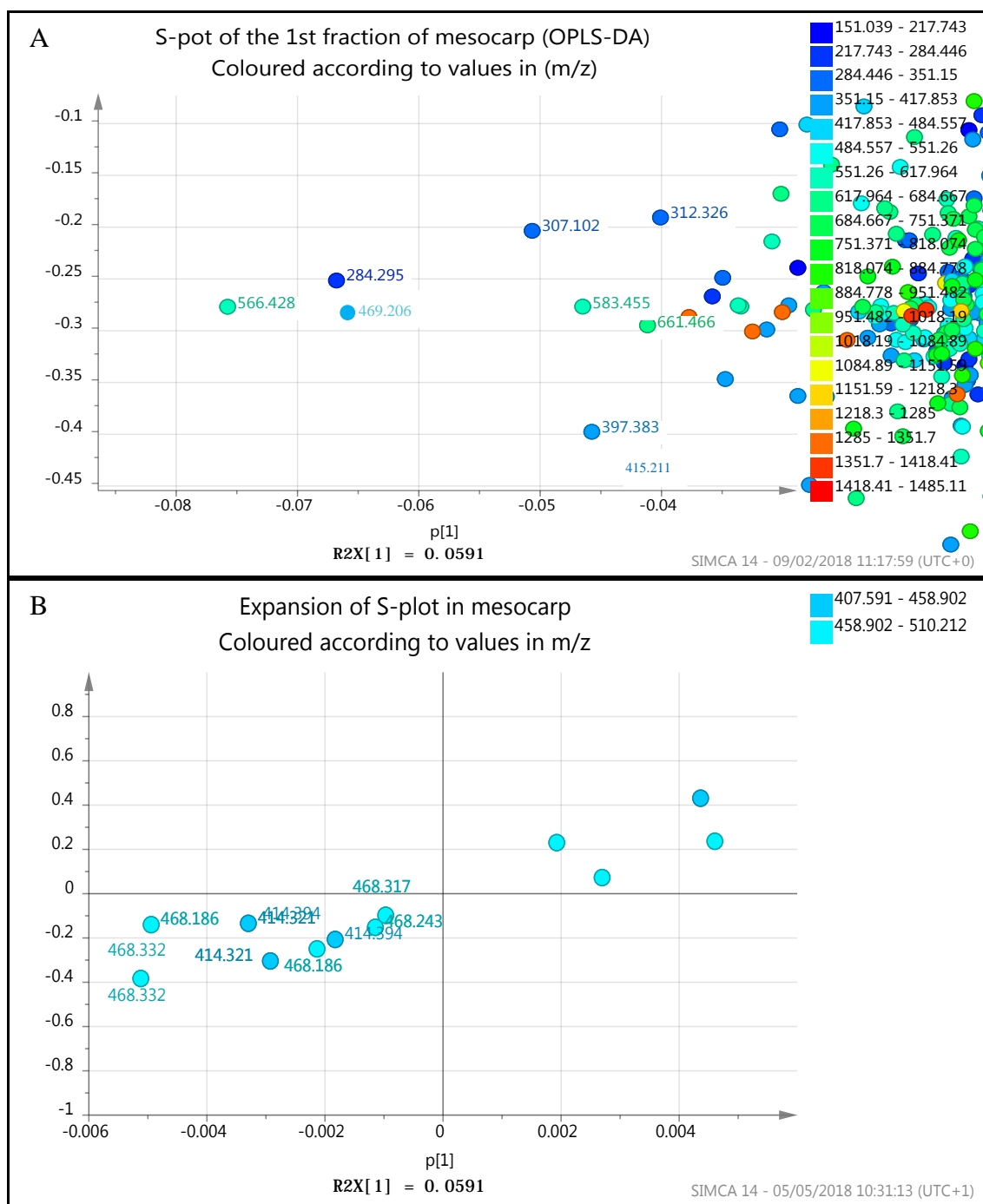
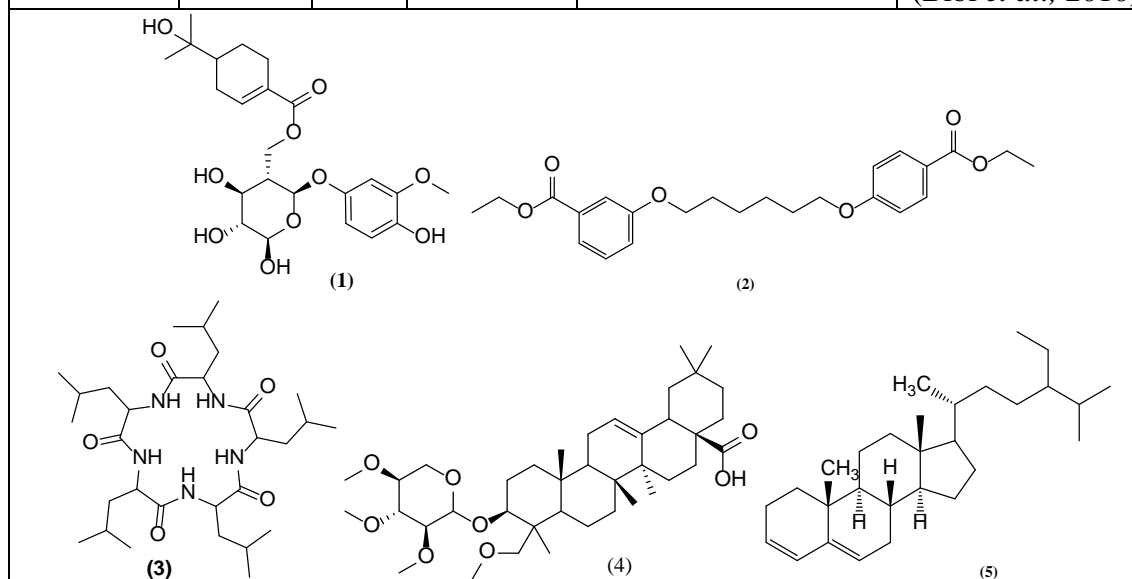


**Figure 3.23:** **A)** Expansion of S-plot indicating the six discriminatory molecules from the mesocarp fractions at  $m/z$  583.455; 566.428, 469.206, 307.102, 415.211, 661.446, 1347.88 and 397.383. **B)** Expansion of S-plot indicating the position of the isolated compounds from the mesocarp fractions at  $m/z$  468.332, 414.321 and 414.394, which are on the bioactive side of the S-plot.

**Table 3.4:** Dereplication of the discriminatory metabolites from DNP 2015 database from the active fractions against oxidative stress related AD prevention obtained from the S-plot in Figure 3.22 and 3.23.

Ionization mode	MS <i>m/z</i>	Rt min	Molecular formula	Name	Source
P	469.199	8.96	C <sub>23</sub> H <sub>32</sub> O <sub>10</sub>	(R)-3-methoxy-4-hydroxyphenol O-(6-O-oleuropeoyl)-β-D-glucopyranoside (1)	<i>Pimenta dioica</i> (Kikuzaki <i>et al.</i> , 2000)
P	415.207	17.42	C <sub>24</sub> H <sub>30</sub> O <sub>6</sub>	1,6-bis(4-carbethoxyphenoxy)hexane (2)	<i>Myrtus communis</i>
P	566.428	20.52	C <sub>30</sub> H <sub>55</sub> N <sub>5</sub> O <sub>5</sub>	viscumamide (3)	<i>Viscum album var. coloratum</i>
P	661.463	33.32	C <sub>39</sub> H <sub>64</sub> O <sub>8</sub>	Leontosid A-methylat (4)	<i>L. eversmannii</i> Bge. (Mzhel'skaya and Abubakirov, 1967)
P	1347.88	35.01	C <sub>89</sub> H <sub>118</sub> O <sub>10</sub>	Unknown	Unknown
P	397.378	38.01	C <sub>29</sub> H <sub>48</sub>	stigmasta-3,5-diene (5)	<i>Haloxylon salicornicum</i> (Bibi <i>et al.</i> , 2010)



### 3.8.2 Metabolomic profiling of fractions from bioactive eluates F4,5,6 and F12,14

Based on their bioactivity against oxidative stress related AD, fractions classified under group 1 (green) on the PCA and HCA were taken into consideration (Figures 3.24A and 3.25A). The fractions triggering metabolic disruptions on neuroblastoma SH-SY5Y cell line could be correlated with each other as demonstrated in the PCA scores scatter plot. The HCA and PCA scores scatter plot reflected the correlation among the different biological/treatment groups. The R<sup>2</sup> and Q<sup>2</sup> values at 1.0 and 0.999 for the clustering of fractions of F4,5,6 confirmed goodness of fit at 100% and goodness of prediction at 99.9%, respectively. For clustering of fractions obtained from F12,14; R<sup>2</sup> and Q<sup>2</sup> values were achieved at 0.845 and 0.202, respectively.

An unsupervised technique was employed to present the data in the PCA scores space. The scores plot could not provide a quantitative representation of the extent of segregation between the data clusters, but solely a qualitative segregation could be achieved (Werth *et al.*, 2010). Consequently, despite the fact that the visualisation afforded a qualitative clustering based on metabolic differences, the PCA score plots failed to answer the fundamental statistical query pertaining to marked discrepancies between clusters. Hence, as recommended by Yamamoto *et al.* (2009), the determinants of clustering variation on a PCA-scores plot were assessed with the help of an OPLS-DA model (Figures 3.24C and 3.25C). Furthermore, the first and third quadrants (Figure 3.24D) contained a notable scatter of fractions within the ion peak range of  $m/z$  400 to 500, as indicated by the OPLS-DA loadings scatter plot. Moreover, the molecular ion peaks  $m/z$  were more discerned in the top active quadrant than the bottom one. Nevertheless, most molecular weights discerned by the OPLS-DA loadings scatter plot regarding the second fraction of (F12,F14) were in the ion peak range at  $m/z$  ~300-500 (Figure 3.25D).

Nevertheless, an S-plot (Figure 3.24E and F) and (Figure 3.25E and F) and dereplication (Table 3.5) were performed to identify the metabolites influential for the bioactivity of the fractions. The S-plot illustrated that M<sup>+</sup> 414.381 and 414.298 were the putative discriminatory compounds for the bioactivities of F4,5,6/F9; F12,14/F8; and F12,14/F9. Therefore, these target metabolites were further subjected to structure elucidation presented in section 3.9.

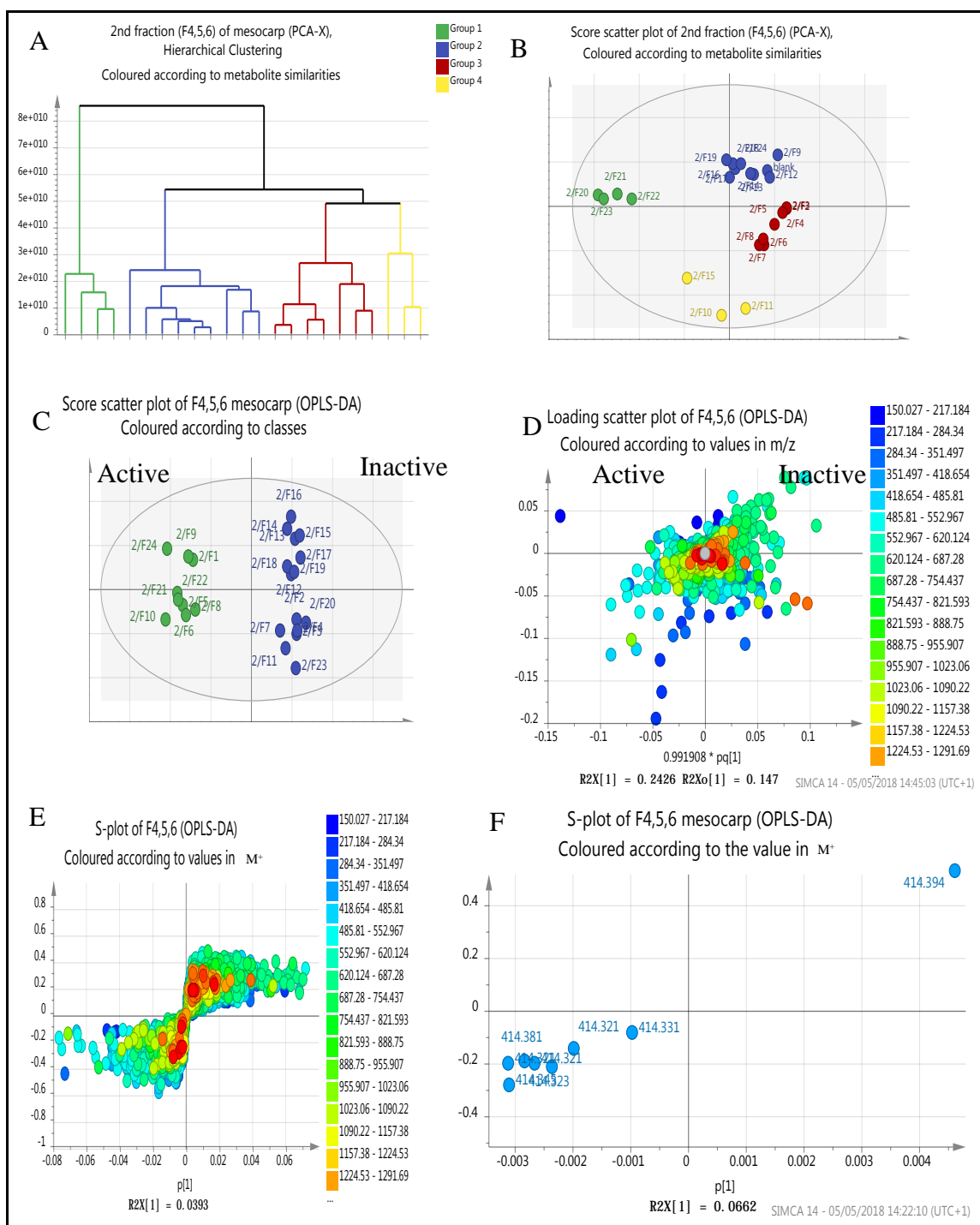


**Figure 3.24:** **A)** PCA-HCA of fractions of bioactive eluate F4,5,6 via ward linkage. **B)** PCA-scores scatter plot of fractions of bioactive eluate F4,5,6. **C)** OPLS-DA scores scatter plot of active and inactive fractions. **D)** OPLS-DA loadings scatter plot showed ion peaks of target metabolites from active fractions. **E)** S-plot generated from the OPLS-DA model to predict the bioactive metabolites. **F)** Expansion of the active end of the S-plot where the interested metabolite ion was detected as  $M^+$  414.381.

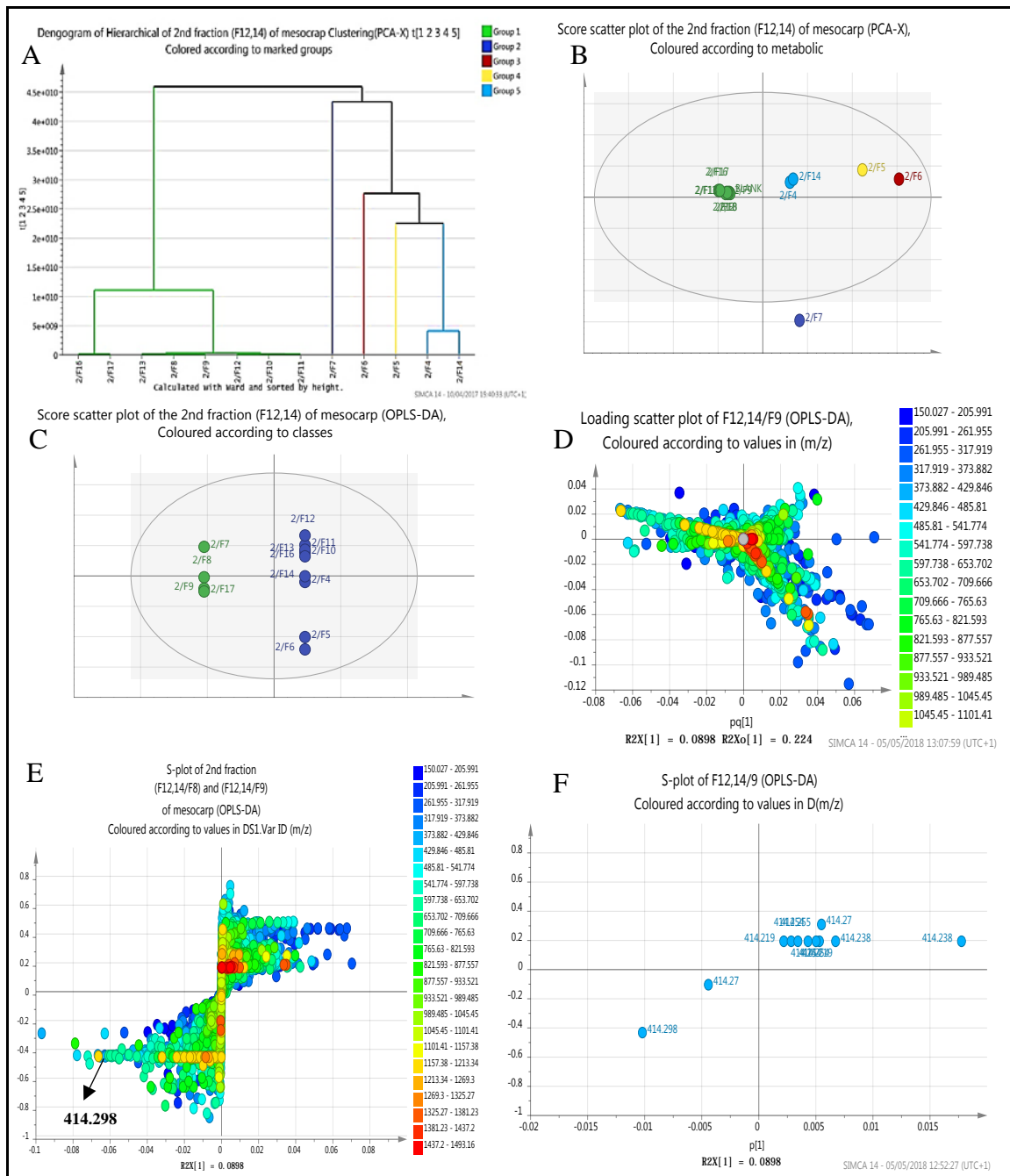


**Figure 3.25:** **A)** PCA-HCA analysis of chromatographic fractions of bioactive eluate F12,14. **B)** PCA scores plot of chromatographic fractions of bioactive eluate F12,14. **C)** OPLS-DA scores plots between active and inactive fractions. **D)** OPLS-DA loadings scatter plot was detected to show metabolites ion peaks of active metabolomes.  $R^2Y(\text{sum}) = 0.984$ ,  $Q^2X = 0.498$ . **E)** and **F)** S-plot analysis was performed and  $M^+$  414.298 was indicated as the target metabolite.

**Table 3.5:** Dereplication of F4,5,6/F9 and F12,14/F9 from DNP 2015 database.

<b>A) F12,14/F9</b>					
<b>Ionization mode</b>	<b>MS M<sup>+</sup></b>	<b>Rt min</b>	<b>Molecular formula</b>	<b>Name</b>	<b>Source</b>
P	414.297	22.96	C <sub>23</sub> H <sub>42</sub> O <sub>6</sub>	Oleoyl-β-D-arabinoside	<i>Maytenus acanthophylla</i> <i>Reissek</i>

<b>B) F4,5,6/F9</b>					
<b>Ionization mode</b>	<b>MS M<sup>+</sup></b>	<b>Rt min</b>	<b>Molecular formula</b>	<b>Name</b>	<b>Source</b>
P	414.381	37.82	C <sub>27</sub> H <sub>42</sub> O <sub>3</sub>	γ-Sitosterol	<i>Polyalthia debilis</i>

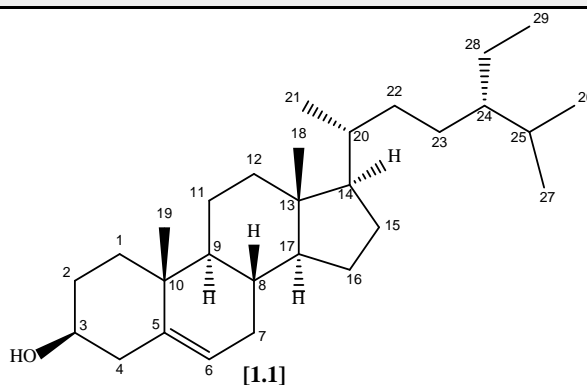
### 3.9 Identification and elucidation of the mesocarp pure fractions

#### 3.9.1 $\gamma$ -Sitosterol 1.1

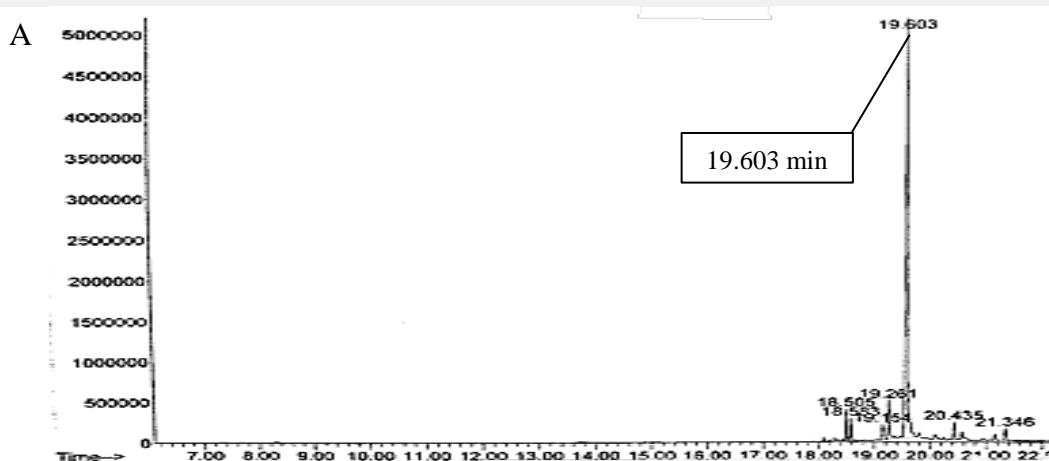
**Table 3.6:** Physical properties of F4,5,6/F9 of *F. carica* mesocarp.

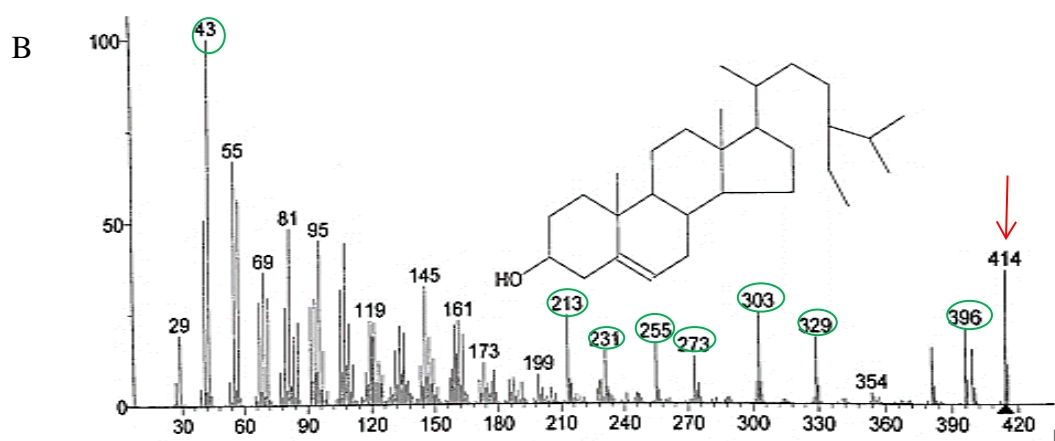
$\gamma$ -Sitosterol
Synonym(s): Fucosterol, $\beta$ -dihydro-campesterol
Source: Mesocarp of <i>F. carica</i>
Metabolite: 2 <sup>nd</sup> fraction (Fraction code: F4,5,6/F9)
Sample amount: 2.9 mg
Physical description: White powder
Molecular formula: C <sub>29</sub> H <sub>50</sub> O
Exact Mass: 414.3862 g/mol

#### Chemical structure



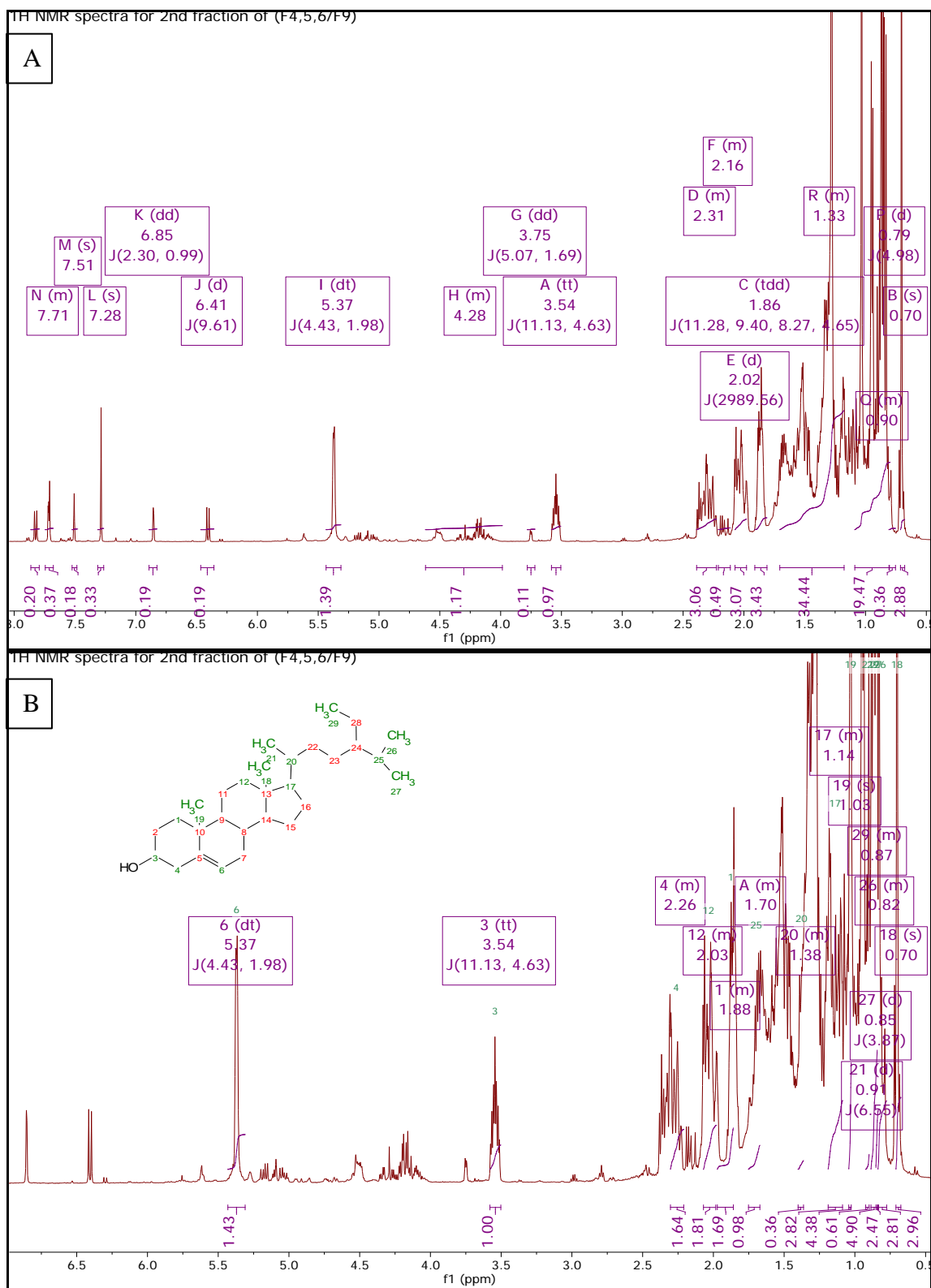
#### Identification via GC-MS (A,B) analysis spectrum





$\gamma$ -Sitosterol **1.1** was isolated as a white coloured powder. Subsequently, a GCMS analysis (Table 3.6A and B) and  $^1\text{H-NMR}$  spectrum were run to gain a better insight of the chemical profile of the fraction (Figure 3.26) indicating the presence of steroids. The results obtained from the GCMS indicated a peak eluting at 19.60 minutes, with a molecular ion peak at  $m/z$  414  $[\text{M}]^+$ . According to the online NIST library linked to the GCMS database, the fraction consisted of various steroidal compounds, but  $\gamma$ -sitosterol was likely the most prevalent compound, as indicated by the GCMS spectrum at  $m/z$  414  $[\text{M}]^+$ .

Detailed assignments of  $^1\text{H-NMR}$  and  $^{13}\text{C-NMR}$  (Figures 3.26 and 3.27) in comparison to the literature (Balamurugan, Stalin and Ignacimuthu, 2012) are presented in Table 3.7 and fully supported the elucidation of F4,5,6/F9 as  $\gamma$ -sitosterol **1.1**.



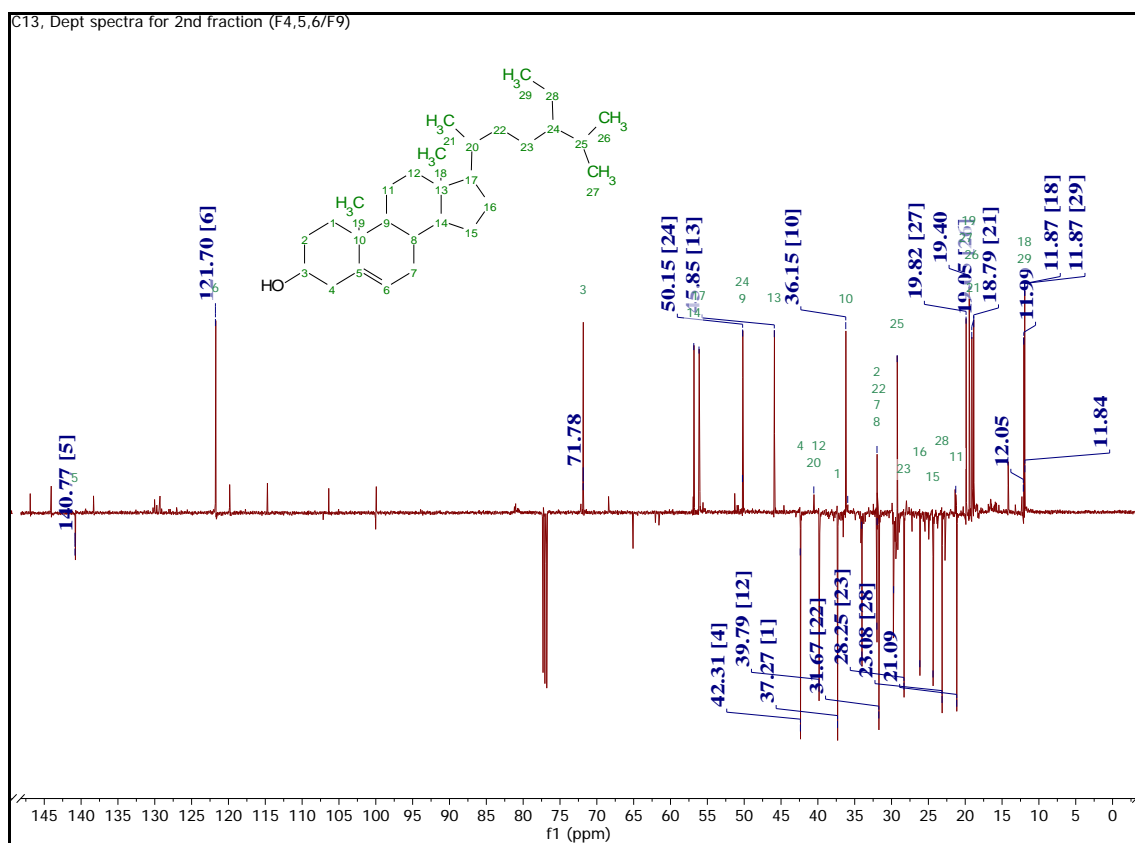


**Figure 3.27:**  $^{13}\text{C}$  & Dept NMR spectrum of  $\gamma$ -sitosterol **1.1** (500 MHz,  $\text{CDCl}_3$ ).

HSQC (Figure 3.28) and HMBC spectra (Figure 3.29) were run to confirm the identity of the major compounds in each of the mixture which was elucidated as  $\gamma$ -sitosterol by observing the specific correlations of signals at positions (C-3), (C-18), (C-19), (C-21), (C-26), (C-27), (C-29). Eleven methylenes, nine methines, and three quaternary carbons were observed in the spectrum. The strong methyl signals of HSQC (Figure 3.28) at  $\delta_{\text{H,C}}$  (0.71, 11.86), (1.03, 19.39), (0.93, 18.70), (0.82, 19.04), (0.86, 19.82), and (0.88, 12.00) were assigned to positions 18, 19, 21, 26, 27, 28, and 29, respectively. Nonetheless, the downfield chemical shifts at  $\delta$  71.80, 121.69 and 140.77 were assigned to the hydroxyl substituent at C-3 and the double bond between C-5 and C-6, respectively.

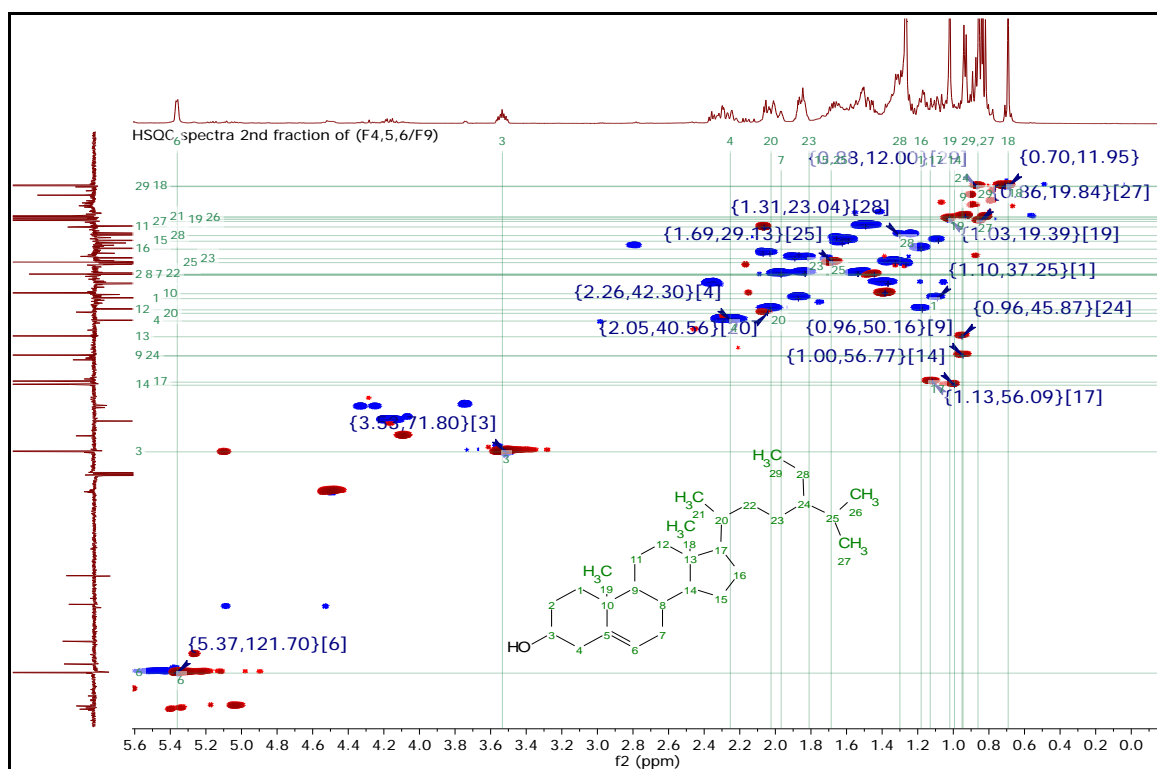


**Figure 3.28:** HSQC spectra of semi-pure  $\gamma$ -sitosterol in  $\text{CDCl}_3$  at 500MHz; X-axis represents H-NMR and Y-axis represents  $\text{C}13$  and Dept; blue colour of signals represents either CH or  $\text{CH}_3$  while the red colour represents  $\text{CH}_2$ ; horizontal lines represents the carbon and vertical lines represent the number of proton.

The HMBC correlations (Figure 3.29 and Figure 3.30) of the side chain confirmed the position of the hydroxyl group on C-3; H-3 at  $\delta 3.53$  correlated to C-1 at  $\delta 42.30$ , C-2 at  $\delta 31.93$  and C-4 at  $\delta 37.63$ . Moreover, long-range correlations were observed between  $\text{CH}_3$ -27 and  $\text{CH}_3$ -29 at  $\delta 0.86$  and  $0.88$ , respectively with the methine carbon at  $\delta 45.87$  (C-24) and methylene carbon at  $\delta 23.04$  (C-28) and vice versa. Long-range correlations were also perceived between H-6 at  $\delta 5.37$  with both methylene carbons at  $\delta 42.30$  (C-4) and  $31.92$  (C-7) as well as with a quaternary carbon at  $\delta 36.15$  (C-10). Cross peaks could be observed from the quaternary carbon at  $\delta 140.77$  (C-5) with H-2 at  $\delta 1.89$ , H-4 at  $\delta 2.26$ , H-7 at  $1.90$  and H-19 at  $\delta 1.03$ . Correlations were also observed from H-4 and H-7 with the methine carbon at  $\delta 5.37$  (C-6). More cross peaks were observed for H-9 at  $\delta 0.96$ , H-11 and H-14 both at  $\delta 1.50$ , and H-15 at  $\delta 1.09$  with the methine carbon at  $31.93$  (C-8). H-1, H-7, H-14 and H-19 correlations with the methine carbon at  $\delta 50.17$  (C-9). Alternatively, H-2, H-9, H-11 and H-14 correlated with the quaternary carbon at  $\delta 36.15$

(C-10). Likewise, *CH*-17 at  $\delta$  1.13 and *CH*<sub>3</sub>-18 at  $\delta$  0.71 gave long-range correlations with the methylene carbon at  $\delta$  39.82 (C-12), quaternary carbon at  $\delta$  42.42 (C-13) and the methine carbon at  $\delta$  56.77 (C-14). Long-range correlations were also observed from  $\delta$  1.13 (H-17), 0.91 (H-21) and 0.96 (H-24) to the methine carbon at  $\delta$  35.89 (C-20) and methylene carbon at  $\delta$  33.96 (C-22). Further cross peaks were observed from  $\delta$  1.13 (H-23) and  $\delta$  1.31 (H-28) to both methine carbons C-24 and C-25 at  $\delta$  45.87 and 29.17, respectively. Moreover, correlations were observed between protons H-25 and H-26 at  $\delta$  1.70 and 0.82, respectively with methyl carbon at  $\delta$  19.82 (C-27), as well as correlations between *CH*<sub>3</sub>-27 and *CH*<sub>3</sub>-29 at  $\delta$  0.86 and 0.88, respectively with the methylene carbon at  $\delta$  23.04 (C-28). Complete assignments of HMBC correlation data are presented in Table 3.7 and Figure 3.30.

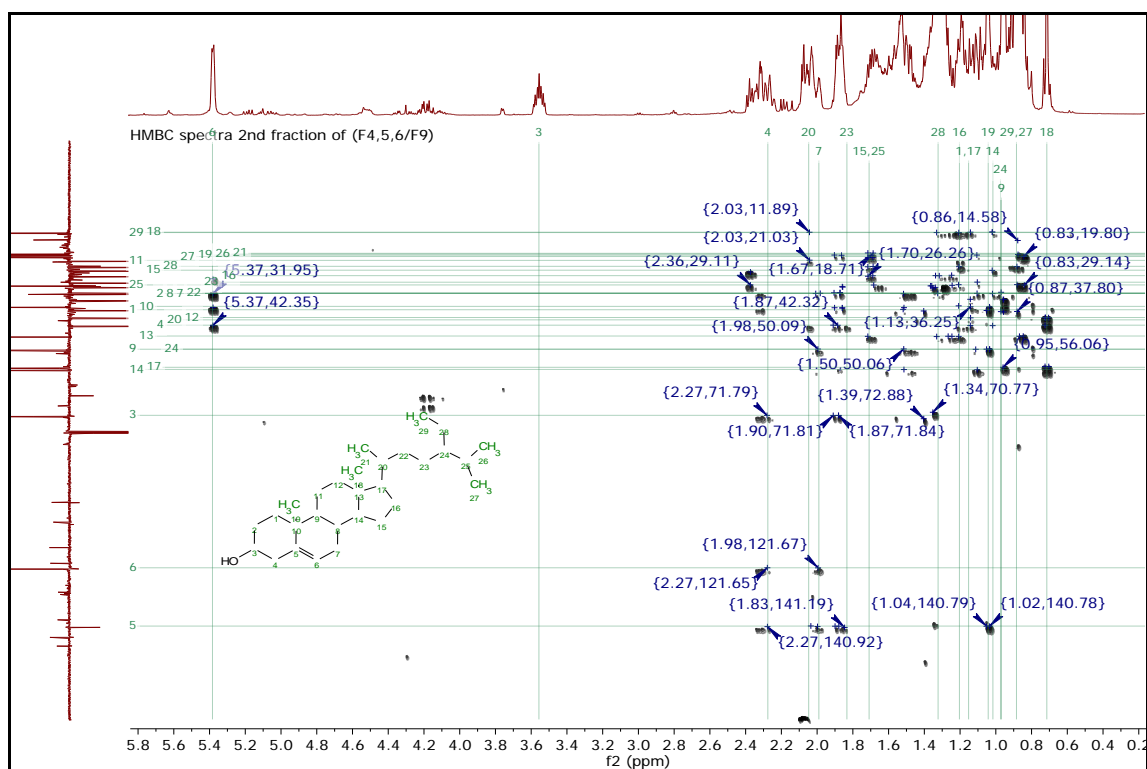


**Figure 3.29:** The overlay of HMBC (500 MHz,  $\text{CDCl}_3$ ) between the correlation of H-NMR vs Dept; horizontal lines are related to the number of carbon, while vertical lines represent the number of proton.

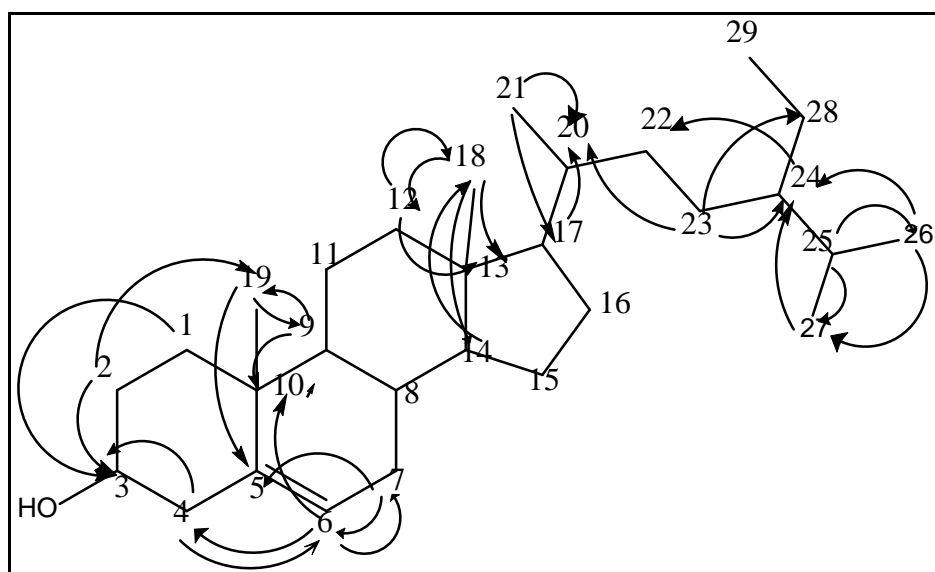


**Figure 3.30:** HMBC correlation of  $\gamma$ -sitosterol structure **1.1**.

**Table 3.7:** Carbon and proton assignments for  $\gamma$ -sitosterol **1.1**  $^{13}\text{C}$ - $^1\text{H}$  cross-signals in the HMBC spectra.  $^{13}\text{C}$ -NMR (100 MHz,  $\text{CDCl}_3$ ) and  $^1\text{H}$ -NMR (400 MHz) are compared with the corresponding articles in  $\text{CDCl}_3$ .

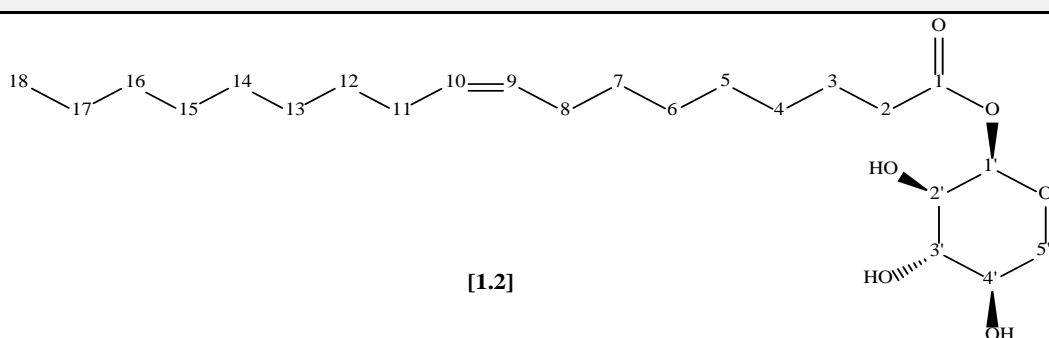
Atom No.	$\gamma$ -Sitosterol <b>1.1</b>			Literature (Balamurugan, Stalin and Ignacimuthu, 2012)	
$\text{CDCl}_3$	Integral, $\delta_{\text{H}}$ , multiplicity, $J$ in Hz	$\delta_{\text{C}}$	HMBC	Integral, $\delta_{\text{H}}$ , multiplicity, $J$ in Hz (400 MHz)	$\delta_{\text{C}}$ (100 MHz)
1	2H, 1.88, m	37.6	9, 3		37.3
2	2H, 1.89	31.9	3, 4, 5, 10, 19		31.9
3	1H, 3.54, tt, $J = 11.13, 4.63$	71.8		1H, 3.50, m	71.8
4	2H, 2.26, m	42.3	3, 5, 6		42.3
5		140.7			140.7
6	1H, 5.37, dt, $J = 4.43, 1.98$	121.7	4, 7, 10	1H, 5.35, m	121.7
7	2H, 1.90, m	31.9	5, 6, 8, 9		31.7
8		31.9			31.7
9	1H, 0.96	50.1	8, 10, 14, 19		50.1
10		36.1			36.1
11	2H, 1.50	21.0	8, 10, 14, 17		21.1
12	2H, 2.04, m	39.8	11, 18		39.8
13		42.4			42.3
14	1H, 1.50	56.7	8, 9, 10, 15, 18		56.7
15	2H, 1.09	24.3	8, 14		26.1
16	1H, 1.14, m	28.2			28.2
17	1H, 1.13	56.1	12, 13, 14, 20, 22		56.1
18	3H, 0.71, s	11.8	12, 13, 14	3H, 0.68, s	11.8
19	3H, 1.03, s	19.3	5, 9	3H, 1.02, s	19.3
20		35.9			36.5
21	3H, 0.91, d, $J = 6.55$	18.7	17, 20, 22	3H, 0.92, d, $J = 6.5$	19.0
22		33.9			33.9
23	2H, 1.13	26.1	20, 24, 25, 28		26.1
24	1H, 0.96	45.8	20, 22		45.8
25	1H, 1.70, m	29.1	23, 24, 26, 27, 28		29.1
26	3H, 0.82, d, $J = 6.5$	19.0	24, 27	3H, 0.82, d, $J = 6.5$	18.7
27	3H, 0.85, d, $J = 6.5$	19.8	24, 28	3H, 0.84, d, $J = 6.5$	19.8
28	2H, 1.31	23.0	24, 25		23.1
29	3H, 0.87, t, $J = 6.5$	12.0	24, 28	3H, 0.85, t, $J = 7$	12.1

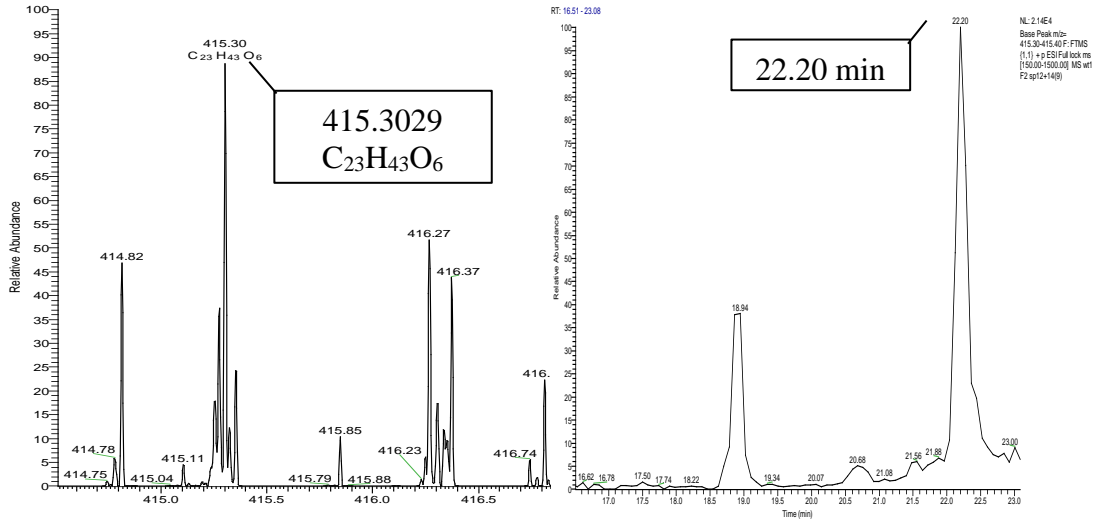
Therefore, the structure of **1.1** was identified and elucidated as  $\gamma$ -sitosterol **1.1**. The analysis of  $^1\text{H}$ ,  $^{13}\text{C}$ , COSY, HSQC, and HMBC NMR data, along with a comparison of

the chemical shift values with relevant published articles (Balamurugan, *et al.*, 2012), determined the structure of **1.1** as  $\gamma$ -sitosterol.

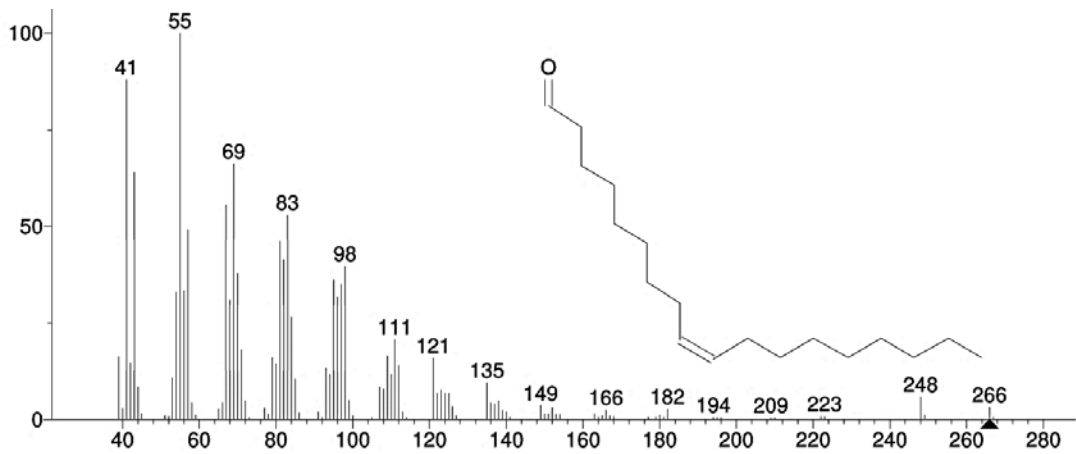
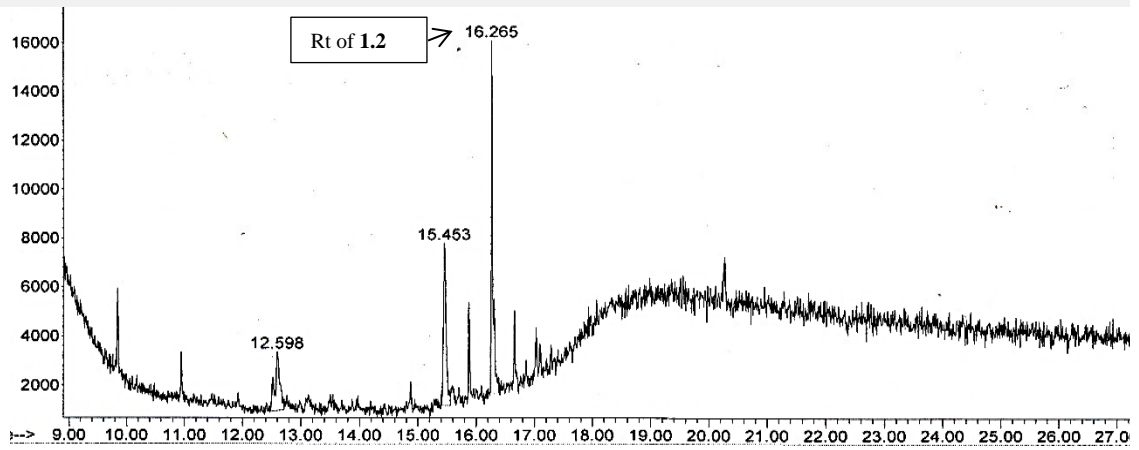
### 3.9.2 Oleoyl- $\beta$ -D-arabinoside **1.2**

**Table 3.8:** Physical properties of F12,14/F8 and F12,14/F9 of *F. carica* mesocarp.

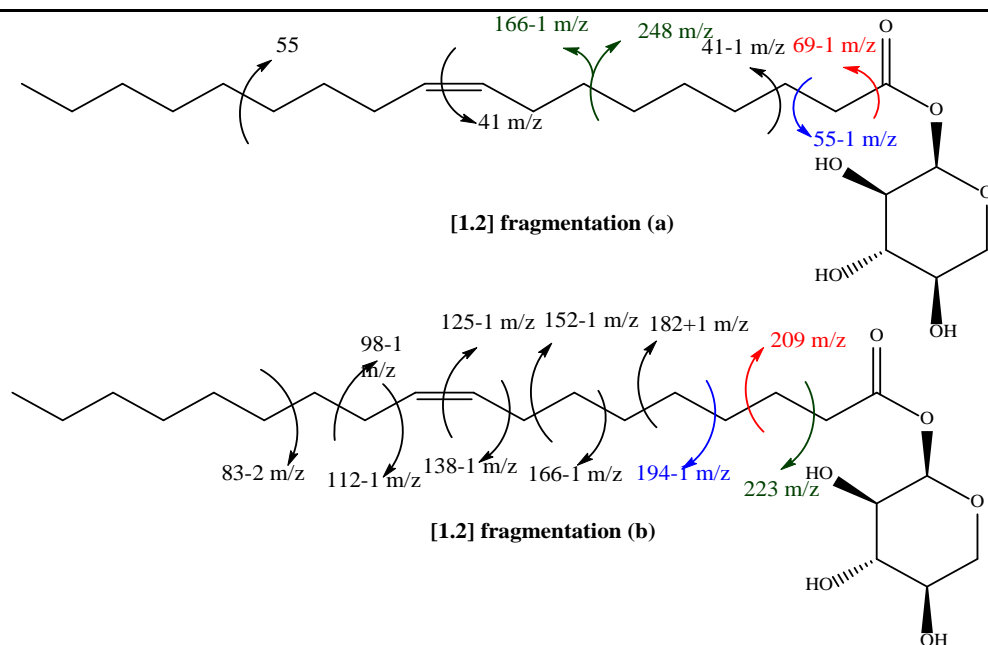
<b>Lupeol acetate</b>
Synonym(s): Oleoyl- $\beta$ -D-arabinoside
Source: Mesocarp of <i>F. carica</i>
Metabolite: 2 <sup>nd</sup> fraction code (F12,14/F8) and (F12,14/F9)
Sample amount: 18 mg and 40 mg
Physical description: light yellow semi-solid
Molecular formula: C <sub>23</sub> H <sub>42</sub> O <sub>6</sub>
Exact Mass: 414.2981 g/mol
<b>Chemical structure</b>
 <p>[1.2]</p>
<b>LC-MS analysis</b>



### Identification via GC-MS analysis



### GC fragmentation analysis



The GC/MS chromatogram of mass spectral fragmentation patterns and NIST library search suggested the identification of a long chain fatty acid between retention time of 15.42 and 15.56 minutes as indicated in Tables 3.8. Fragmentation pathway was generated as shown in Table 3.9, was comparable to those indicated by GCMS. GCMS fragmentation (a) indicated the dehydration at fragment ion  $m/z$  166, which corresponded to the loss of  $C_{12}H_{23}$ . The loss of  $C_{11}H_{19}O_6$  corresponds to  $m/z$  248 that would further yield  $m/z$  69 with loss of  $C_5H_{10}$ . Fragment  $m/z$  55 due to the loss of  $C_4H_8$ , while  $m/z$  41 was due to the fragmentation at the double bond. On the other hand, GCMS fragmentation (b) has been mainly on the loss of  $C_{16}H_{31}$  at  $m/z$  223 then with further fragmentation yielding  $m/z$  209, which corresponds to the loss of  $C_{15}H_{29}$ . Further fragmentations were observed at  $m/z$  194 due to the dehydration of the loss of  $C_{14}H_{27}$  and the loss of  $C_{13}H_{25}$  at  $m/z$  182. Subsequent dehydration afforded fragmentation ion peaks at  $m/z$  166, 152, 138, 125, 112, 98 and 83 due to the loss of  $C_{12}H_{23}$ ,  $C_{11}H_{21}$ ,  $C_{10}H_{19}$ ,  $C_9H_{18}$ ,  $C_8H_{17}$ ,  $C_7H_{15}$  and  $C_6H_{13}$ , respectively. Therefore, this assignment was completely confirmed by NMR, in which the spectral data were compared with the literature for oleoyl-β-D-arabinoside **1.2**.

Oleoyl-β-D-arabinoside **1.2** was obtained as a light yellow semi-solid and its molecular formula,  $C_{23}H_{42}O_6$  was determined on the basis of ESI MS at  $m/z$  415.3029  $[M-H]^+$ . The  $^1H$ -NMR spectrum of oleoyl-β-D-arabinoside **1.2** in (Figure 3.31) displayed two methine

multiplets at  $\delta$  5.37 and  $\delta$  5.39, assigned to vinylic H-9 and H-10 protons, respectively, and a one-proton doublet at  $\delta$  4.28 ( $J = 6.7$  Hz, cis), assigned to H-1'. Three multiplets at  $\delta$  3.56, 3.52, and 3.54 were assigned to H-2' as doublet of doublet ( $J = 5.3$  Hz), H-3' as multiplet, and H-4' as multiplet, as well, and one singlet at  $\delta$  3.96 was assigned to H-5'. Two-proton multiplet at  $\delta$  2.08,  $\delta$  2.15 and  $\delta$  2.33 were assigned to H-3, H-8 and oxygenated methylene at H-2, and other pentet methylene proton signal was observed at  $\delta$  1.61 ( $J = 7.1$  Hz). The remaining multiplet methylene proton were observed between  $\delta$  1.32 and  $\delta$  2.08 and three proton triplet at  $\delta$  0.90 ( $J = 6.6$  Hz) was assigned to primary C-18 methyl protons.

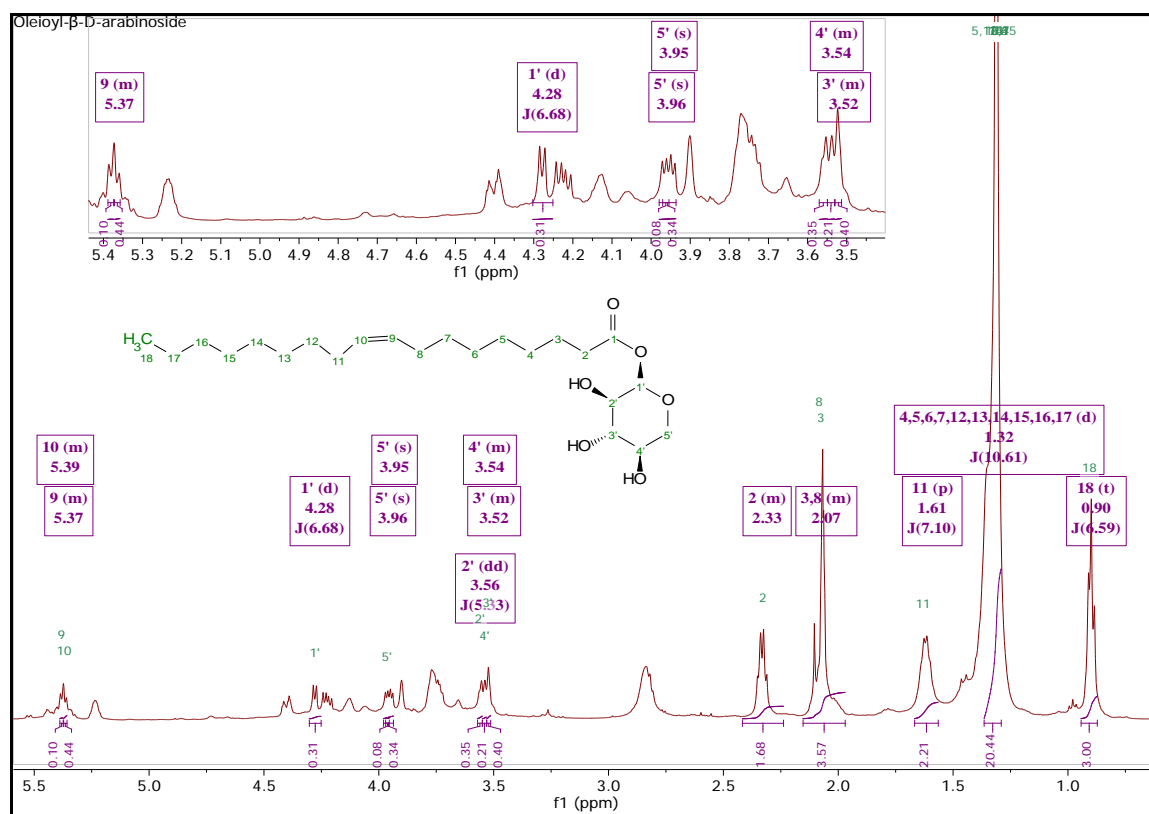
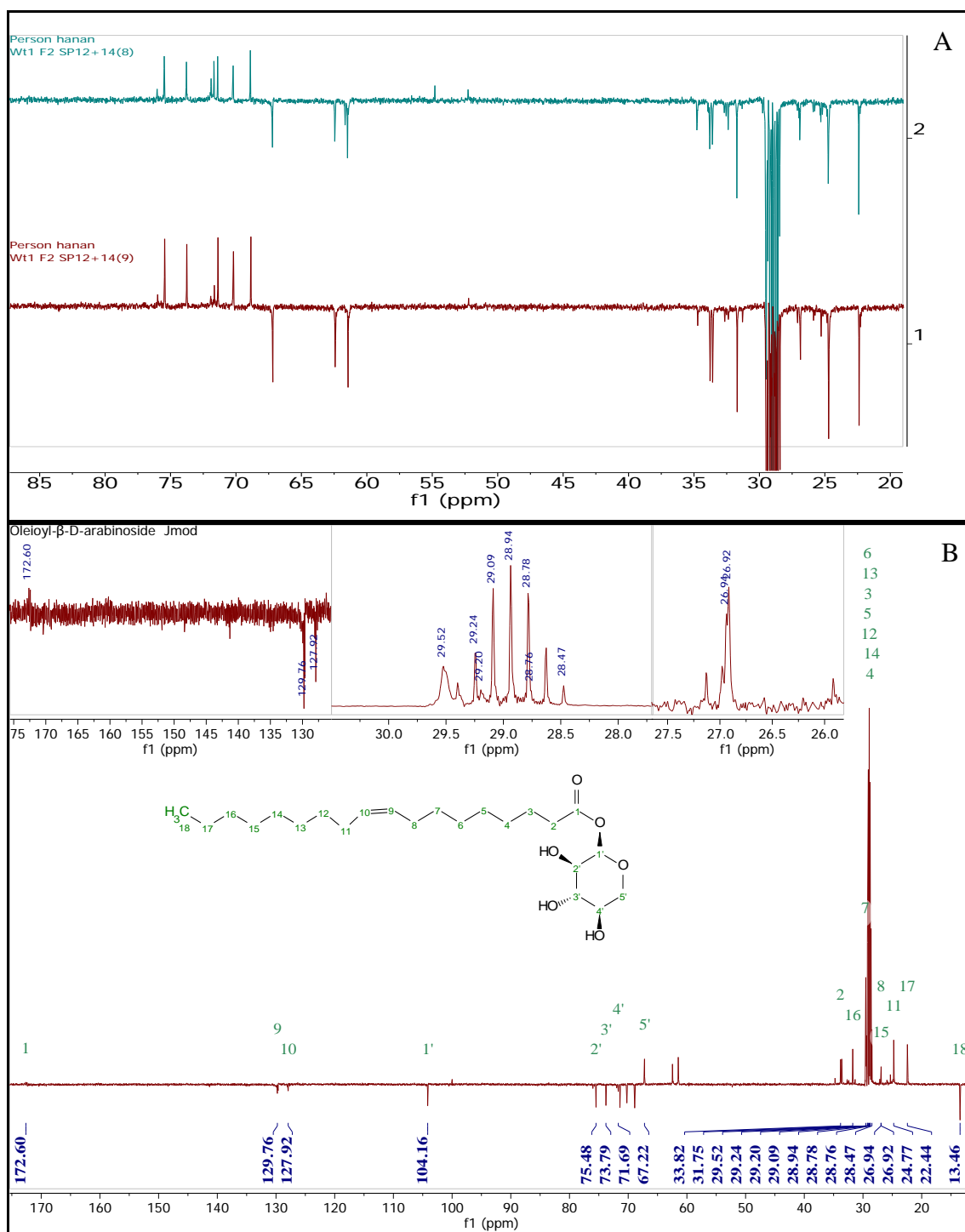


**Figure 3.31:** Over view of  $^1\text{H}$ -NMR spectrum of oleoyl  $\beta$ -D-arabinoside **1.2** dissolved in acetone- $d_6$  and run at 500 MHz; with an expansion of  $^1\text{H}$  NMR spectrum between 3.5 and 5.4 ppm.

The  $^{13}\text{C}$ -NMR spectrum of **1.2** have shown markedly similar carbon signals in both (F12,14/F8) and (F12,14/F9), although (F12,14/F9) has shown less impurity than (F12,14/F8) in Figure 3.32A. As a result, (F12,14/F9) was conducted for further elucidation and have found to display carbon signals for ester carbon at  $\delta$  172 (C-1) in

Figure 3.32B, vinylic carbons at  $\delta$  129.6 (C-9) and 127.2 (C-10), anomeric carbon at  $\delta$  104.2 (C-1'), sugar carbons at  $\delta$  75.4, 75.4, 73.7 and 67.2 for (C-2'), (C-3'), (C-4') and (C-5'), respectively. Oxygenated methylene was also observed at  $\delta$  33.8 (C-2) and the remaining methylene carbons in the range between  $\delta$  31.8 and  $\delta$  22.4 as listed in detail in Table 3.9, and lastly the primary methyl carbon was assigned at  $\delta$  13.5 (C-18).



The  $^1\text{H}$ - $^1\text{H}$  COSY spectrum of **1.2** in Figure 3.33A displayed sugar correlations of H-1 with H-2', H-3' and H-4' and vice versa. In Figure 3.34B displayed the correlations for the fatty acid moiety such as H-18 with H-17; H-17 with H-16; H-16 with H-15; H-15 with H-14; H-14 with H-13; H-13 with H-12 and H-12 with H-11 and vice versa. Further correlation between H-3 and H-8 with vinylic H-9 and H-10 were also observed.

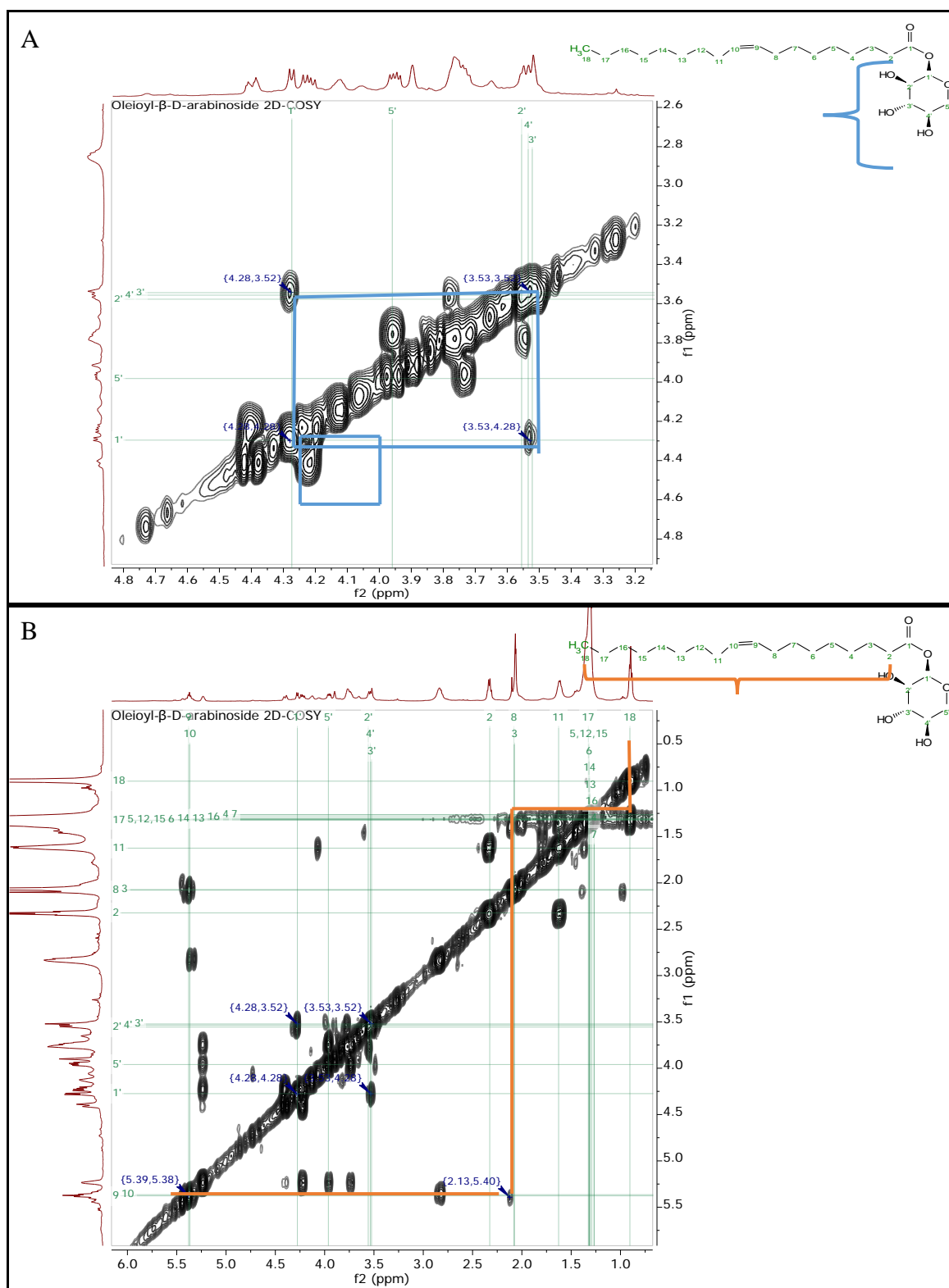


**Figure 3.33:**  $^1\text{H}$ - $^1\text{H}$  COSY correlations of oleoyl  $\beta$ -D-arabinoside 1.2. A) Correlation between protons within arabinoside structure. B) two spin system were detected, as correlations were observed in the oleic side connected in an orange lines while monosaccharide of arabinoside were shown correlation presented in blue lines; other black spots were confirmed as artefacts.

$^1\text{H}$ - $^{13}\text{C}$  HSQC measurements led to full assignments of the  $^1\text{H}$  and  $^{13}\text{C}$  NMR chemical shifts of **1.2** and were measured in acetone- $d_6$  at 500MHz (Figure 3.34). The downfield chemical shifts at  $\delta_{\text{H,C}}$  (3.56,75.5), (3.52,73.7), (3.53,71.6), (3.95,67.2) and (4.28,104) shown in Figure 3.34 were assigned to the mono-saccharide substituent at C-2', C-3', C-4', C-5' and the anomeric C-1' signal, respectively. Nonetheless, the strong methylene signals (Figure 3.34) were observed at  $\delta_{\text{H,C}}$  (2.33,33.8), (2.07,29.1), (1.62,28.8), (1.28,29.2), (1.32,29.2), (1.36,29.5) and (2.08,27) assigned to positions 23, 2, 3, 4, 5, 6, 7, and 8.

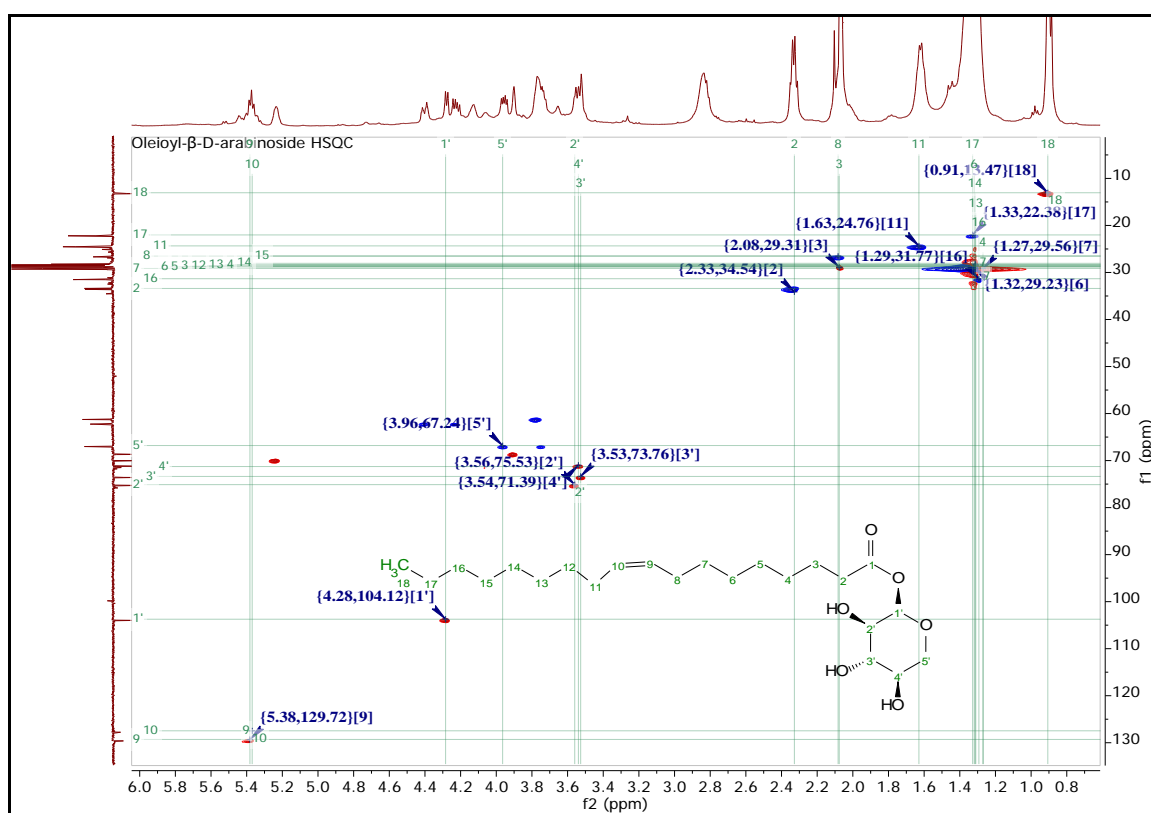


**Figure 3.34:** HSQC spectra of oleoyl  $\beta$ -D-arabinoside **1.2** in acetone- $d_6$  at 500MHz; X-axis represents H-NMR and Y-axis represents J-mod NMR; blue colour of signals represent either CH,  $\text{CH}_3$  while the red colour represents  $\text{CH}_2$ ; Cross link of protons represented as vertical line in green colour with carbon assignments presented horizontally in green colours. Detailed assignments of signals were fully presented in Table 3.9.

The HMBC spectrum is shown in Figure 3.35. The proton of oxygenated methylene at  $\delta$  2.33 ( $CH_2$ -2) correlated with C-1 and C-4 at  $\delta$  172 and 28.8, respectively. The anomeric proton of the sugar moiety (H-1') at  $\delta$  4.28 correlated to the ester carbon (C-1), as well as the sugar carbons (C-4') and (C-5') at  $\delta$  172, 71.6 and 67.2, respectively. The proton at  $\delta$  3.56 of H-2' in arabinoside correlated to C-4', while H-3' at  $\delta$  3.52 correlated with C-1'; H-4' at  $\delta$  3.53 with C-5' and H-5' at  $\delta$  3.95 with C-1' and C-4', as well.

Moreover, the proton attached to the long chain fatty acid of H-3 at  $\delta$  2.07 correlated with the ester carbon of C-1 and methyl carbon of C-5 at  $\delta$  172 and 29.2, respectively. The proton at  $\delta$  1.62 at H-4 correlated with the oxygenated methylene at  $\delta$  33.8 C-2, 29.2 (C-6) and the ester carbon of C-1. The vinylic protons H-9 and H-10 correlated with each other at  $\delta_{H,C}$  (5.37, 129.6) and (5.38, 127.2). The protons of H-12 and H-14 as well as H-13 and H-15 overlapping at  $\delta$  1.31 also correlated with C-13 and C-15 at  $\delta$  29.0 and 28.5 as well as  $\delta$  28.8 and 26.8 of C-12 and C-14. Finally, the primary ( $CH_3$ -18) methyl proton at  $\delta$  0.90 correlated with C-16 at  $\delta$  31.8 and directly correlated to C-17 at  $\delta$  22.4. HMBC correlations with complete assignments are presented below in both Table 3.10 and Figure 3.36. On the basis of spectroscopic data and the comparison with the related article (Ahmad *et al.*, 2013), the structure of **1.2** was established as oleoyl  $\beta$ -D-arabinoside.

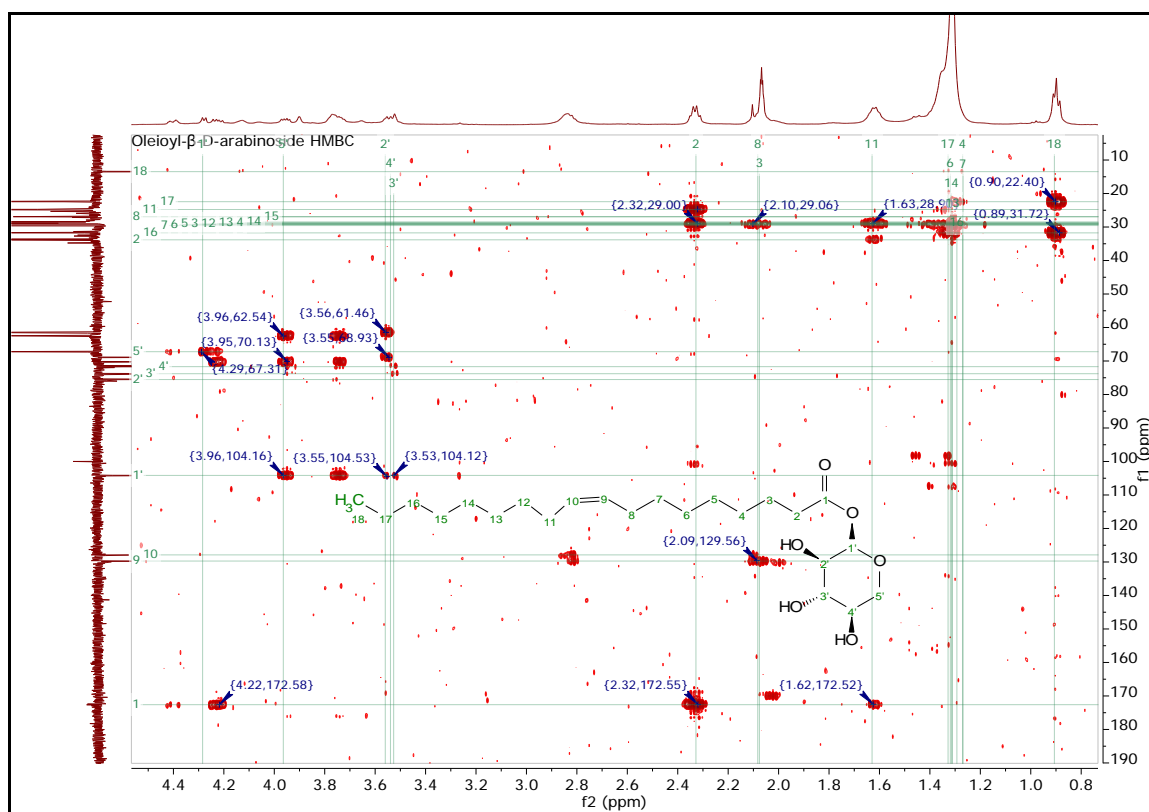


**Figure 3.35:** HMBC of compound **1.2** (500 MHz, acetone- $d_6$ ).

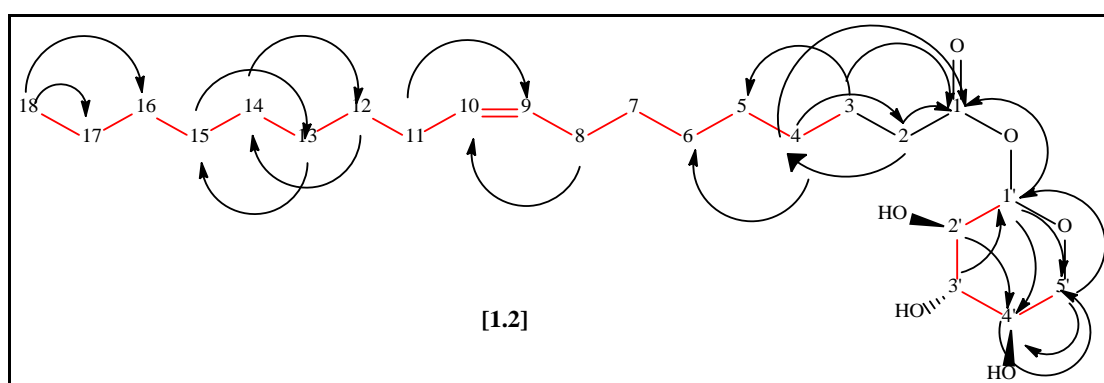


**Figure 3.36:**  $^1\text{H}$ - $^1\text{H}$  COSY correlations of oleoyl  $\beta$ -D-arabinoside compound **1.2** were depicted in red lines and the  $^1\text{H}$ - $^{13}\text{C}$  HMBC correlations are indicated by each carbon with arrows. The carbons were numbered according to IUPAC-IUB. (Detailed assignment of HMBC correlation is described in Table 3.9).

**Table 3.9:** Carbon and proton assignments for oleoyl  $\beta$ -D-arabinoside **1.2**  $^{13}\text{C}$ - $^1\text{H}$  cross-signals in the HMBC spectra.  $^{13}\text{C}$ -NMR (125 MHz, acetone- $d_6$ ) and  $^1\text{H}$ -NMR (400 MHz) are compared with the corresponding articles in CDCl $_3$ .

Atom No.	Oleoyl- $\beta$ -D-arabinoside <b>1.2</b>			Literature (Menezes-de-Oliveira <i>et al.</i> , 2011)	
	Integral, $\delta_{\text{H}}$ , multiplicity, $J$ in Hz	$\delta_{\text{C}}$	HMBC	Integral, $\delta_{\text{H}}$ , multiplicity, $J$ in Hz (400 MHz)	$\delta_{\text{C}}$ (100 MHz)
1		172			175.2
2	2H, 2.33, m	33.8	4, 1	2H, 2.26, m	35.1
3	2H, 2.15, m	31.8	5, 1	2H, 1.27, br s	33.2
4	2H, 1.32, m	29.5	2, 6	2H, 1.27, br s	32.8
5	2H, 1.32, m	29.4		2H, 1.27, br s	30.9
6	2H, 1.32, m	29.2		2H, 1.27, br s	30.9
7	2H, 1.32, m	29.2		2H, 1.27, br s	30.7
8	2H, 2.08, m	29.1	10	2H, 2.08, m	30.7
9	1H, 5.37, m	129.6		1H, 5.37, m	131
10	1H, 5.39, m	127.2		1H, 5.38, m	129.2
11	2H, 1.61, p, $J = 7.1$	28.9	9	2.26 (m, 2H)	30.6
12	2H, 1.32, m	28.8	14	2H, 1.59, m	30.4
13	2H, 1.32, m	28.6	15	2H, 1.31, m	29.3
14	2H, 1.32, m	28.5	12	2H, 1.27, br s	28.3
15	2H, 1.32, m	26.9	13	2H, 1.27, br s	26.7
16	2H, 1.32, m	31.8		2H, 1.27, br s	26.1
17	2H, 1.32, m	22.4		2H, 1.27, br s	23.9
18	3H, 0.90, t, $J = 6.6$	13.5	16, 17	3H, 0.86, t, $J = 6.0$	14.5
1'	1H, 4.28, d, $J = 6.7$	104.2	1, 4', 5'	1H, 4.43, d, $J = 7.5$	105
2'	1H, 3.56, dd, $J = 5.3$	75.4		1H, 4.12, m	71.3
3'	1H, 3.52, m	73.7	1'	1H, 3.89, m	70
4'	1H, 3.54, m	71.4	5'	1H, 3.74, m	66.4
5'	2H, 3.96, s	67.2	1', 4'	2H, 3.63, br s	64.2

### 3.9.3 Lupeol acetate 1.3

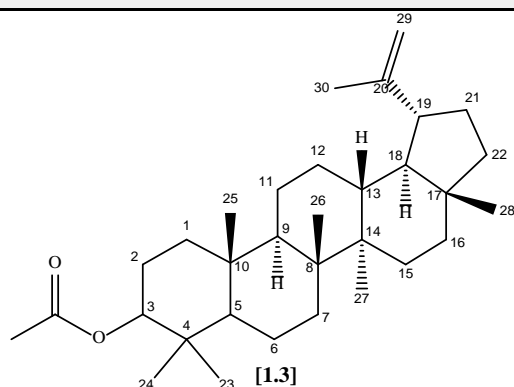
**Table 3.10:** Physical properties of F4,5,6/F1/F5 of *F. carica* mesocarp.

Lupeol acetate
Synonym(s): Lup-20(29)-en-3-ol, acetate, (3 $\beta$ )-
Source: Mesocarp of <i>F. carica</i>
Metabolite: 3 <sup>rd</sup> fraction F4,5,6/F1/F5
Sample amount: 3.5 mg
Physical description: White powder

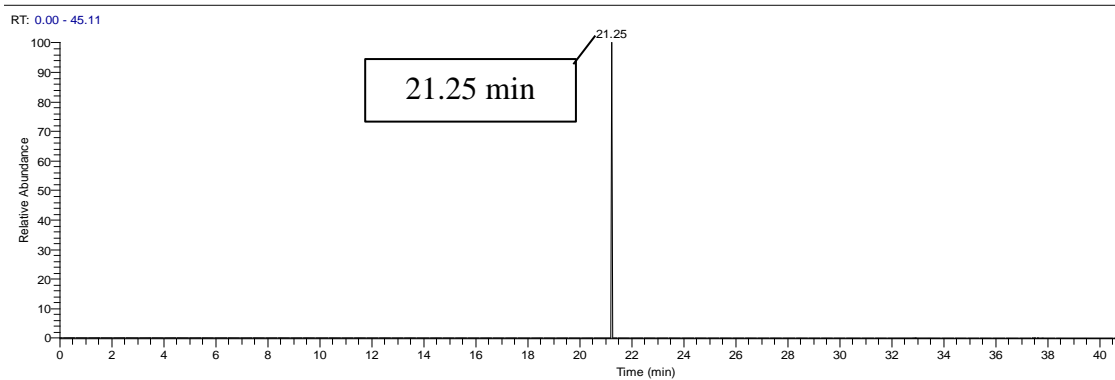
Molecular formula:  $C_{32}H_{52}O_2$

Exact Mass: 468.3967 g/mol

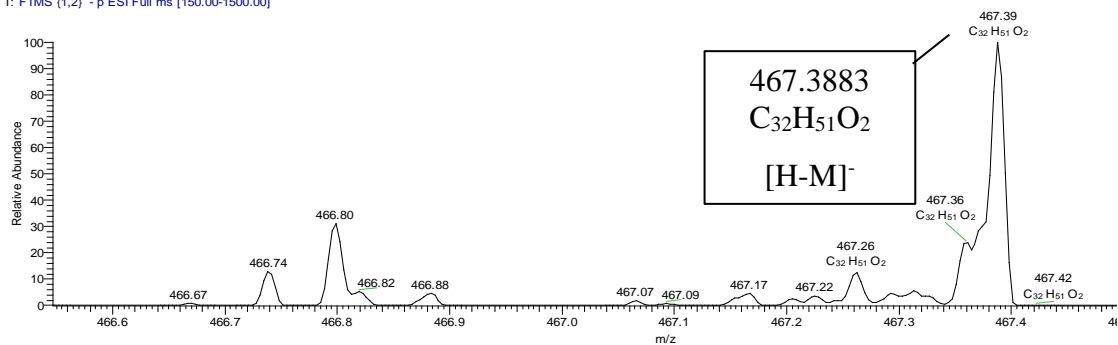
### Chemical structure



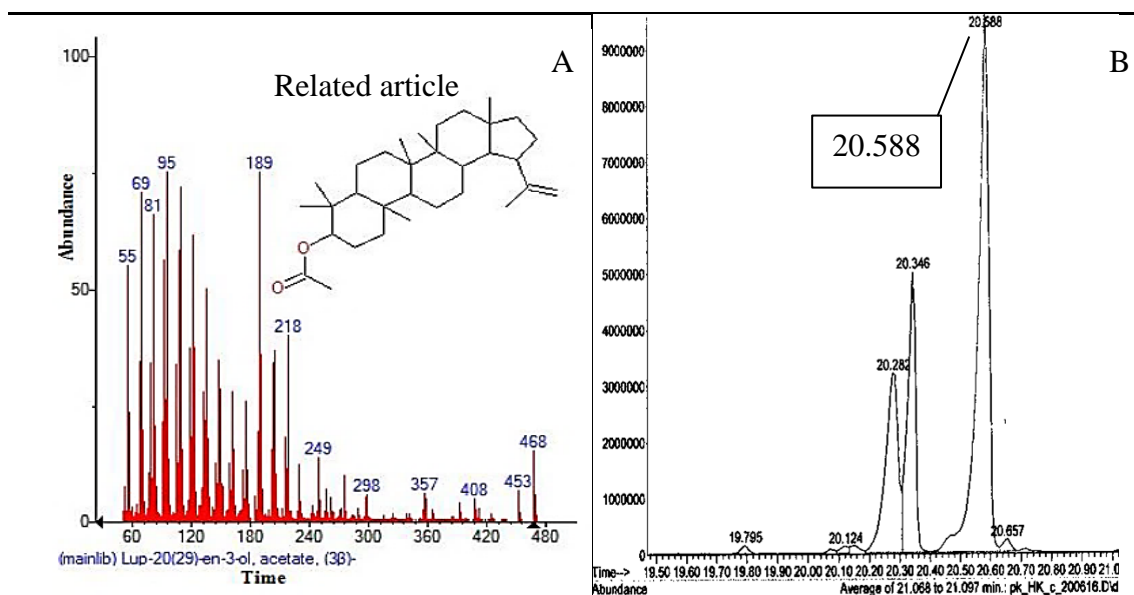
### LC-MS analysis



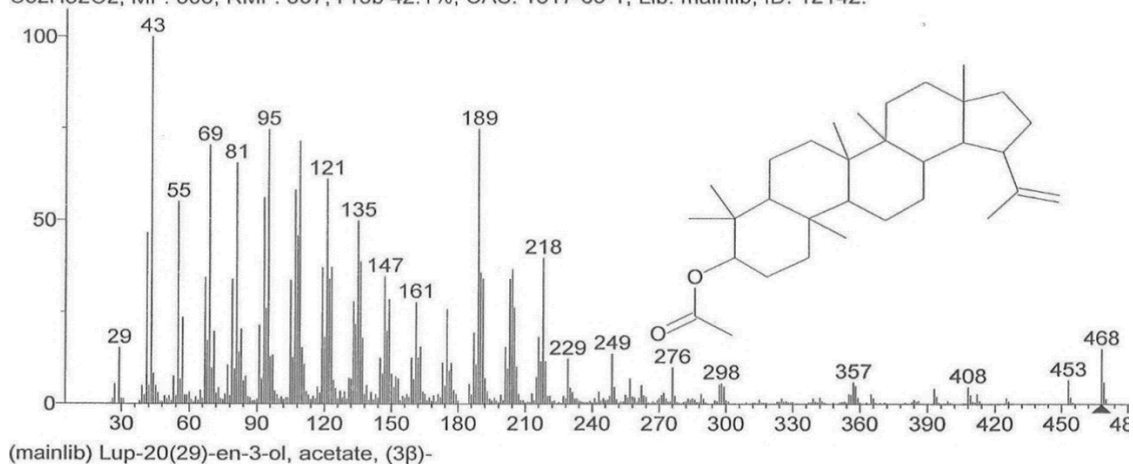
wt1 F3 SP4+5+6(1)BAND5 #506-649 RT: 20.27-25.97 AV: 144 NL: 9.12E2  
T: FTMS (1,2) - p ESI Full ms [150.00-1500.00]



### Identification via GC-MS analysis



Hit 1 : Lup-20(29)-en-3-ol, acetate, (3β)-  
 C32H52O2; MF: 806; RMF: 807; Prob 42.1%; CAS: 1617-68-1; Lib: mainlib; ID: 12142.



The GCMS of Compound **1.3** for lupeol included several ions that shared similarities with fraction F4,5,6/F1/F3 (Mohanad, Azhar and Imad, 2016). Fragment ion peaks at  $m/z$  189 and 408 (Table 3.10A defined the triterpenes fragmentation for a lupine skeleton with a methyl acetate group on position 3 (Misra *et al.*, 1993). Compound **1.3** had a GC retention time (Rt) of 20.59 minutes. The production of the fragment at  $m/z$  249 required C-8/C-14 and C-9/C-11 bonds being cleaved concomitantly, after which a hydrogen was transferred from C-26 to C-11. The stable allylic cation at  $m/z$  218 was the outcome of the concomitant fission of C-8/C-14 and C-9/C-11 bonds with no transfer of hydrogen. Moreover, the compound lupeol acetate **1.3** was obtained as a white powder and its molecular formula  $C_{32}H_{51}O_2$  determined on the basis of ESI MS at  $m/z$  467.3883 [M-H]<sup>-</sup>.

A number of eight methyl singlets were revealed by the  $^1\text{H-NMR}$  spectrum at  $\delta 0.76$  ( $\text{CH}_3$ -28), 0.86 ( $\text{CH}_3$ -25), 0.82 ( $\text{CH}_3$ -24), 0.85 ( $\text{CH}_3$ -23), 0.93 ( $\text{CH}_3$ -27), 1.04 ( $\text{CH}_3$ -26), 1.66 ( $\text{CH}_3$ -30), and 2.06 ( $\text{CH}_3$ -2') for lupeol acetate **1.3** (Figure 3.37). The esterified oxymethine group peak occurred at  $\delta 4.52$  for H-3 alongside with two vinylic protons of the exomethylene group at  $\delta 4.59$  dt ( $J = 2.62, 1.40$  Hz) for  $\text{H}_A$ -29 and  $\delta 4.63$  d ( $J = 2.39$  Hz) for  $\text{H}_B$ -29.

It was observed that similarities existed between the  $J$ mod carbon NMR spectrum of the fraction F4,5,6/F1/F5 and lupeol acetate (Figure 3.38). In addition to ascertaining the occurrence of a carbon bound to an oxygen in C-3 with a signal at  $\delta 80.95$ , the  $J$ mod spectrum also exhibited the anticipated ester carbonyl carbon signals at  $\delta 171.01$  as well as signals for two olefinic carbons of a di-substituted double bond in C-29 at  $\delta 109.36$  and in C-20 at  $\delta 150.95$ . However, it was noted from the GCMS fragment that C-9 had the same methyl group bound to it as in C-8. Hence, the spectral data of the isolated lupeol acetate presented in Table 3.11 is consistent with that reported in the literature.

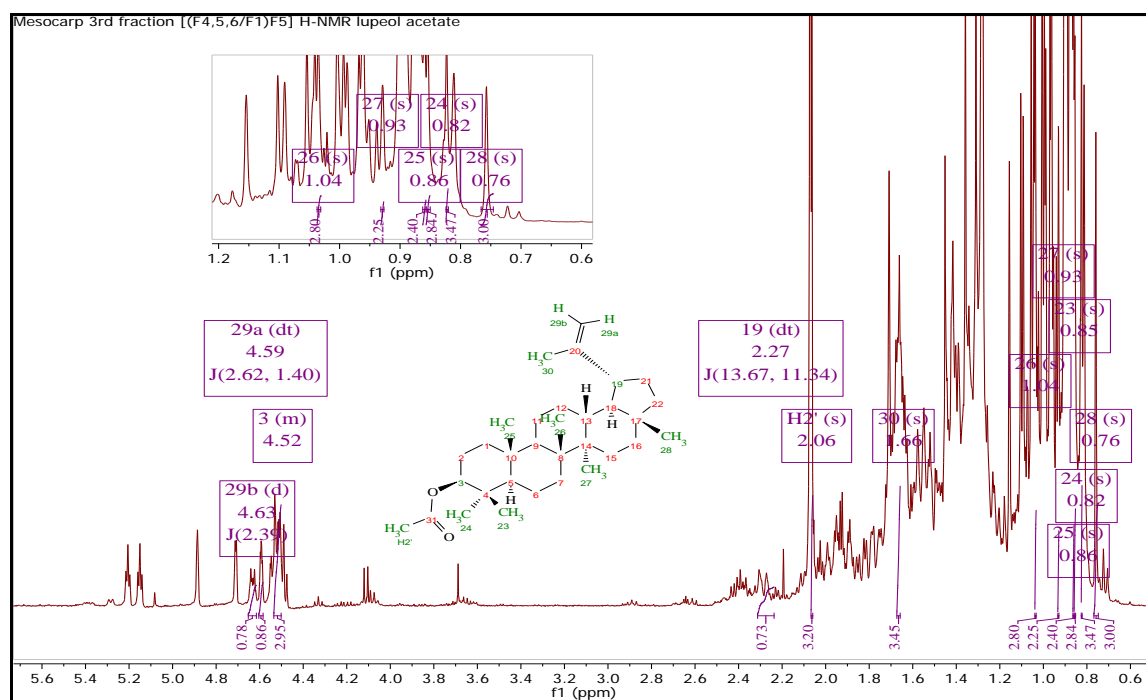


**Figure 3.37:** Overview of a selected  $^1\text{H-NMR}$  spectrum of lupeol acetate **1.3** dissolved in  $\text{CDCl}_3$  and run at 400 MHz.

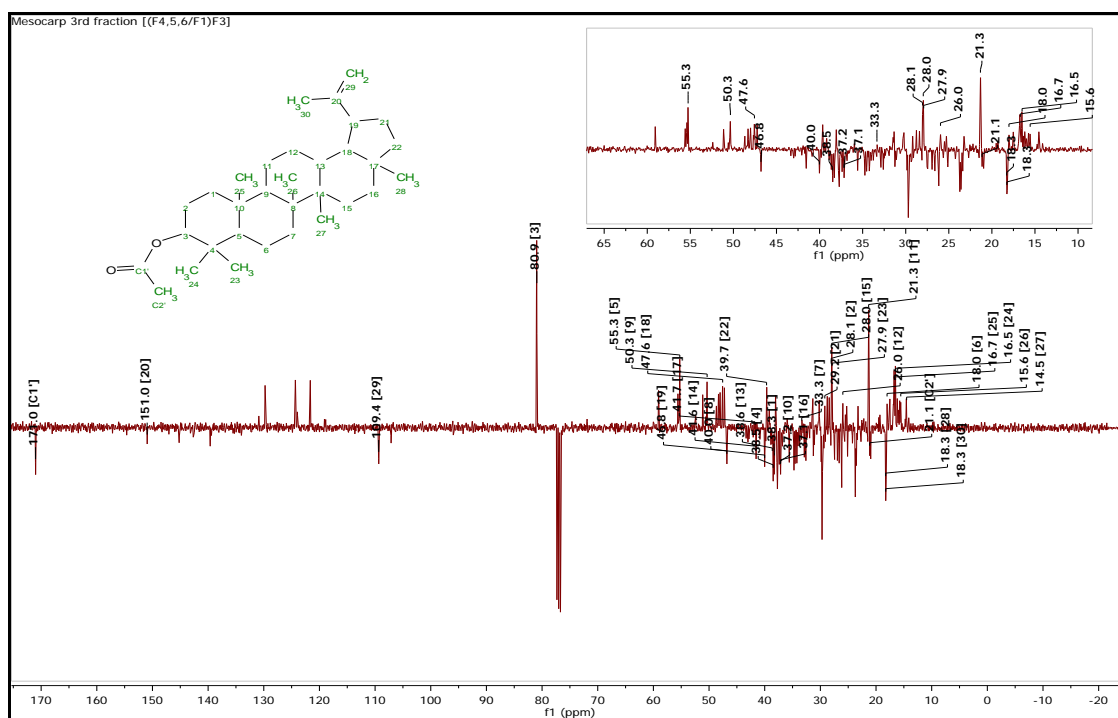


**Figure 3.38:** *J*-mod NMR spectrum of lupeol **1.3** (125 MHz, CDCl<sub>3</sub>) of **3.3**. The signals at  $\delta$  77 were allocated to the CDCl<sub>3</sub> solvent. CH<sub>3</sub> and CH are indicated the positive signals, while quaternary carbon and CH<sub>2</sub> are indicated the negative signals.

**Table 3.11:**  $^1\text{H}$ -NMR (500 MHz),  $J$ -mod-NMR (125 MHz) data of lupeol acetate **1.3** in  $\text{CDCl}_3$  correlated with the literature in  $\text{CDCl}_3$ .

Atom No.	Lupeol acetate <b>1.3</b>		Literature (Menezes-de-Oliveira <i>et al.</i> , 2011)	
	Integral, $\delta_{\text{H}}$ , multiplicity, $J$ in Hz	$\delta_{\text{C}}$	Integral, $\delta_{\text{H}}$ , multiplicity, $J$ in Hz (400 MHz)	$\delta_{\text{C}}$ (100 MHz)
1		38.4		38.4
2		28.1		27.7
3	1H, 4.52, m	80.9	1H, 4.47, m	81.0
4		38.6		37.8
5		55.2		55.4
6		18.2		18.2
7		33.3		34.2
8		40.0		40.8
9		50.3		50.3
10		37.1		37.1
11		21.1		20.9
12		26.0		25.1
13		38.2		38.0
14		41.5		42.8
15		27.9		27.4
16		37.1		35.6
17		41.7		43.0
18		47.5		48.3
19	1H, 2.27, dt, $J = 13.67, 11.34$	46.8	1H, 2.37 dt, $J = 11.0, 5.8$	48.0
20		150.9		150.9
21		29.2		29.8
22		39.6		40.0
23	3H, 0.83, s	27.9	3H, 0.85, s	27.0
24	3H, 0.82, s	15.5	3H, 0.84, s	16.1
25	3H, 0.86, s	16.7	3H, 0.86, s	16.5
26	3H, 1.04, s	16.5	3H, 1.03, s	16.0
27	3H, 0.93, s	14.5	3H, 0.94, s	14.5
28	3H, 0.76, s	18.0	3H, 0.79, s	18.0
29	1H <sub>A</sub> , 4.59, dt, $J = 2.62, 1.40, 1.40$ 1H <sub>B</sub> , 4.63, d, $J = 2.39$	109.3	1H <sub>a</sub> , 4.57, dt, $J = 1.5, 1.5, 0.8$ 1H <sub>b</sub> , 4.69, d, $J = 3.0$	109.3
30	3H, 1.66, s	18.3	3H, 1.68, s	19.3
1'		171.0		171.0
2'	3H, 2.06, s	21.3	3H, 2.04, s	21.3

## **CHAPTER FOUR ENDOCARP RESULTS**

---

#### 4. Isolation and identification of bioactive metabolites from the endocarp of *Ficus carica* and bioactivity on differentiated SH-SY5Y neuronal cell line

##### 4.1. The isolation of *F. carica* endocarp

Normal phase chromatography was conducted under gradient conditions using a 24 g silica column (Table 4.1). The chromatographic condition is presented in Table 4.2.

**Table 4.1:** Step gradient protocol for normal phase chromatography of the *F. carica* endocarp crude extract. Mobile phase A:B=Hexane:Ethyl acetate, C:D=Methanol:Dichloromethane.

Minute	solvent	%2 <sup>nd</sup> solvent	Minute	solvent	%2 <sup>nd</sup> solvent
31.2	AB	0	10	AB	70
27.3	AB	10	10	AB	80
15.8	AB	20	10	AB	90
10	AB	30	10	AB	100
10	AB	40	5	CD	90
10	AB	50	10	CD	80
10	AB	60	25.9	CD	70

**Table 4.2:** The chromatographic conditions for crude ethyl acetate endocarp extract was fractionated via REVELERIS<sup>®</sup> flash chromatography system (Grace Davison Discovery Sciences, USA).

	Endocarp crude fraction 2g
Column REVELERIS <sup>®</sup>	Silica 24g
Mobile phase A: B	Hexane: Ethyl acetate
Mobile phase C: D	Methanol:Dichloromethane
Flow rate	10 mL/min
Injection type	Dry
Step gradient elution	10% decrease of hexane with increasing ethyl acetate to 100%
Equilibration	5 min
ELSD threshold	20 mV
UV threshold	0.05 AU
UV1 wavelengths	254 nm
UV2 wavelengths	280 nm
Air purge time	0.5 min
Collected volume per vial	20 mL
Run length	195.2 min

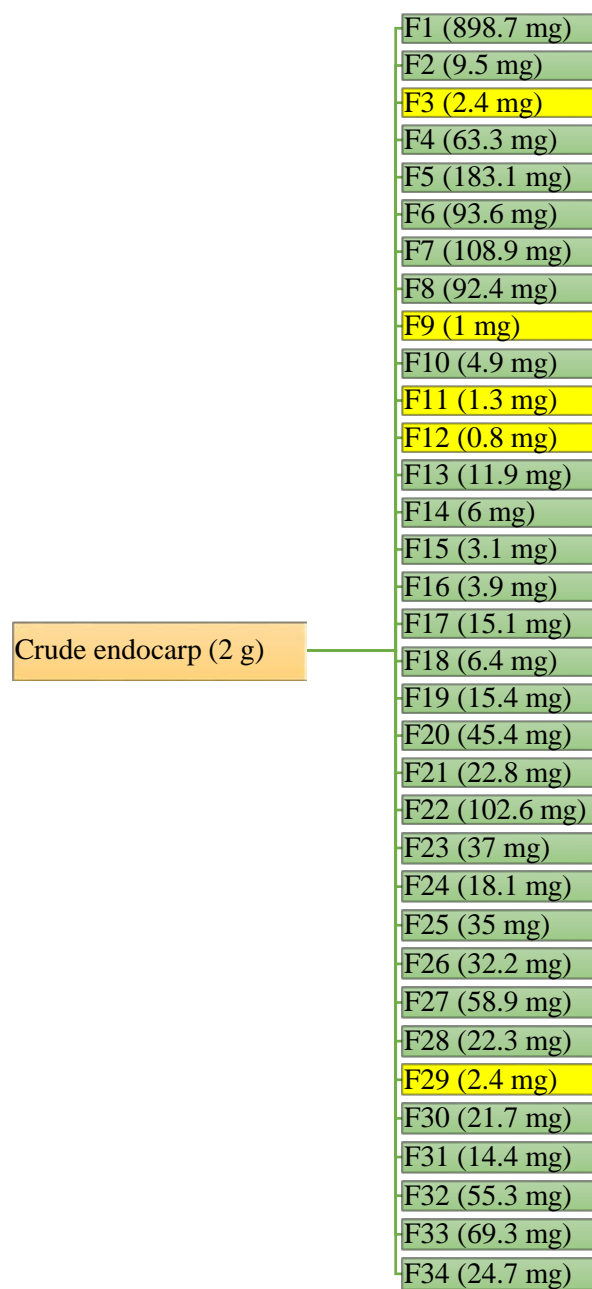


**Figure 4.1:** Fractionation scheme for crude ethyl acetate *F. carica* endocarp extract (2 g). Boxes highlighted in yellow were neglected for further analysis due to their low yield.

#### 4.1.1. Normal phase REVELERIS® flash chromatography from the crude extract

The dried crude *F. carica* endocarp (2 g) (Figure 4.1) was fractionated through a REVELERIS flash chromatography system (Grace, Lancashire, UK). The dried crude extract has a dark brown colour with a nutty sweet taste with a pH value of 4.0 in water at 22° C. Chromatographic separation was accomplished using a normal phase chromatography. Fractions were obtained as shown in Figure 4.2. The total dried weight of the collected fractions obtained from the endocarp was 1.9899 g, resulting to a yield of 99.5%.

Only F14 and F20 were selected for further analysis due to their bioactivity against oxidative stress related AD (section 4.3) and in accordance to their interesting NMR spectral data (section 4.2). In terms of their mobile phase elution, F14 and F20 were eluted with a mixture hexane and ethyl acetate at a ratio of 90:10 highlighted in orange on the chromatogram and a mixture of methanol and dichloromethane at a ratio of approximately 80:20 highlighted in grey, respectively as shown in Figure 4.2. F14 peaks were detected under UV and concomitantly with ELSD indicating the presence of compounds bearing a conjugated double bond system. On the other hand, F20 peaks were only detected with the ELSD, which indicated aliphatic nature of the compounds in F20. The compounds of these fractions were elucidated and presented in section 4.7.

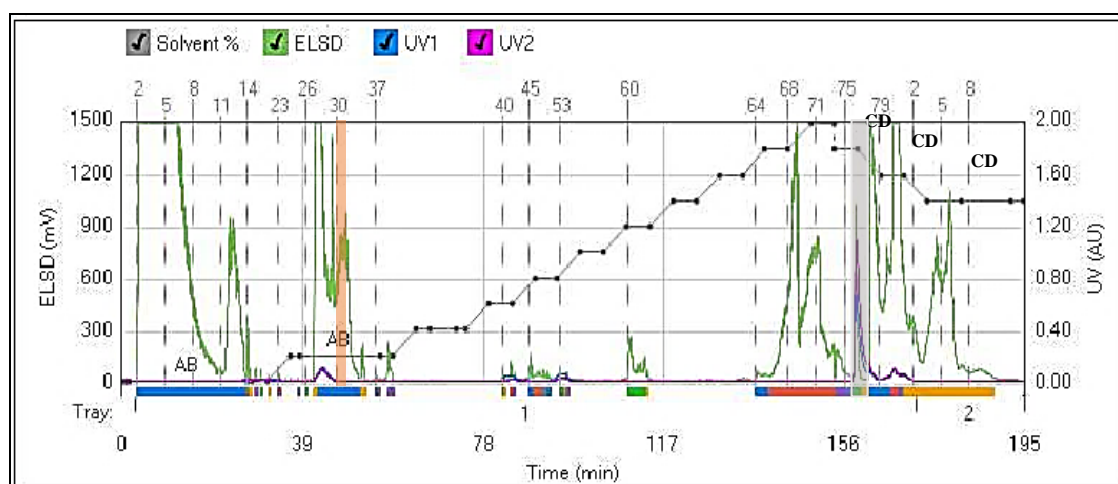


**Figure 4.2:** Chromatogram obtained in the normal phase separation of the dried crude *F. carica* endocarp extract using the REVELERIS® system. Solvent systems: AB = hexane and ethyl acetate, CD = methanol and dichloromethane. UV1 wavelength is at 254 nm represented in blue coloured line, UV2 wavelength is at 280 nm represented in bright

purple coloured line and the green coloured line represented the evaporative light scattering detection (ELSD). The X-axis represents the collected fractions across the area of the respective peaks. The highlighted orange and grey represents F14 and F20, respectively.

#### 4.1.2. Thin-layer chromatography (TLC (Crude extract))

Ninety-two fractions were collected by flash chromatography and were monitored by TLC for their similarity and purity. Similar fractions were pooled together affording 34 fractions as shown in Figure 4.1. TLC enabled localisation of the separated chromatographic spots or bands on the plate surface (Sajewicz *et al.*, 2011). Thereafter, each pooled fraction was dried, weighed and subjected to NMR, LCMS, and biological assays. Due to their low yield, no further work was done on F3, F9, F11, F12 and F29 as shown in Figure 4.1.

Fractions were eluted using the appropriate solvent systems to optimise detection of the various metabolites. The non-polar fractions were eluted with different ratios of hexane and ethyl acetate (90:10, 80:20, 70:30, 50:50, 30:70, and 10:90) while the polar fractions were eluted with dichloromethane and methanol at ratios of 90:10, 80:20 and 70:30. Developed chromatograms are shown in Figure 4.3.

In Figure 4.3, all 34 fractions (F1 to F34) presented a dark zone of spots against the light green fluorescent background of the TLC plate when exposed to short UV (254 nm), except for F3 to F6 and F11 to F12, which showed no dark zones due to their low concentrations. The presence of dark spots indicated fluorescence quenching due to the occurrence of at least one conjugated double bond as those found in anethole, eugenol, safrol, cinnamic acid, phenols and so on (Wagner and Bladt, 2009). Likewise, except for F3, F4, F8–F10, all the fractions exhibited a range of colours including, red, blue, green, and violet under long UV (365 nm). These colours would normally indicate the presence of phenols, terpenes, and steroid (Sherma and Fried, 1996; Wagner and Bladt, 2009). F8 to F10 showed yellow colours under long UV, which may be indicative of sugar constituents (Sherma and Fried, 1996; Wagner and Bladt, 2009).

Moreover, the application of *P*-anisaldehyde-sulfuric acid spray reagent produced an intense brown colour, typical to terpenes and steroid constituents (Wagner and Bladt, 2009). This was visualised in most of the fractions, except F14 and F15, which afforded

pink coloured spots upon spraying, which indicated the presence of a phenolic constituent such as gallic or vanillic acid (Harborne, 1984). The hexane:ethyl acetate fractions showed higher resolution and better separation than the dichloromethane:methanol fractions (Schmid, 2001). Finally, F14 and F20 were chosen for further analysis as they presented some interesting compounds, which gave  $R_f$  values of 0.26 in 50:50 (hexane:ethyl acetate) and 0.5 in 90:10 (dichloromethane:methanol) for F14 and F20, respectively.

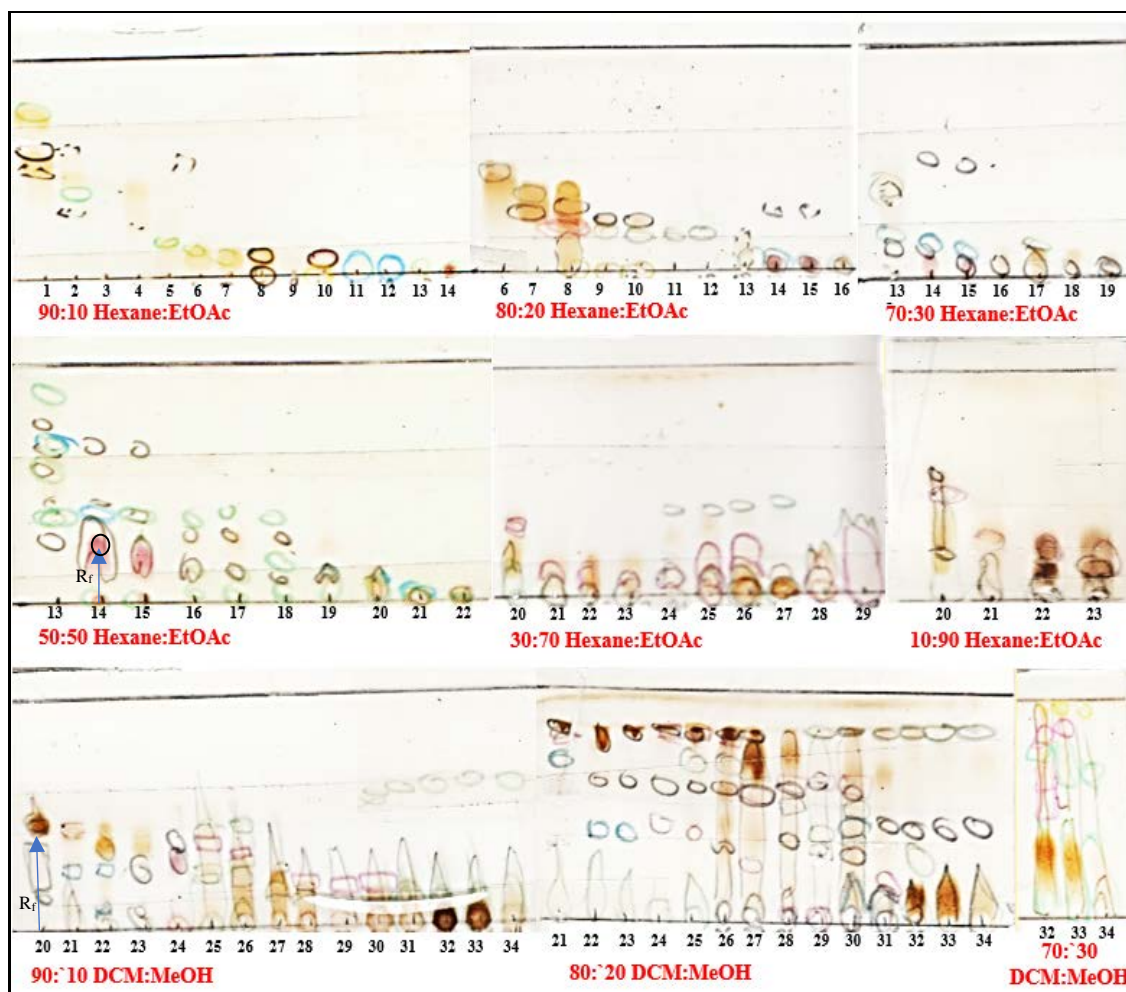


**Figure 4.3:** TLC on silica gel 60 F<sub>254</sub> employing different mixtures of hexane and ethyl acetate or dichloromethane and methanol as mobile phase. Detection was achieved under short UV-250 nm spots drawn in a soft black circle, while under long UV365 nm, spots were drawn in the same colour as the spots were observed. Spots visualised by spraying with *P*-anisaldehyde-sulfuric acid were indicated by charred colours. Blue arrows indicated the two target compounds from the bioactive fractions F14 and F20.

## 4.2. Proton NMR ( $^1\text{H-NMR}$ ) analysis

The chemical profile of the fractions from *F. carica* endocarp were further characterised by  $^1\text{H-NMR}$ . The spectra were processed and stacked together for comparison. Thirty fractions were run; however, only the ten bioactive fractions were displayed and stacked together as shown in Figure 4.4. Based on the  $^1\text{H-NMR}$  spectral data, fractions showed the occurrence of different metabolites such as saponins, glycosides, phenolic compounds, and particularly steroids, which enriched the upfield region with aliphatic signals highlighted in yellow. Olefins were depicted between 3.5 and 5.5 ppm region of the spectra. A few aromatic signals were also observed in the downfield region, highlighted in grey.  $\text{CDCl}_3$  solvent is at 7.25 ppm and is highlighted in green (beneath the grey band).

Although F14 and F15 were quite similar in their  $^1\text{H-NMR}$  resonances while aromatic signals were observed in both, F14 was deemed more interesting than F15. F14 spectrum showed better-resolved signals with less impurity (Figure 4.4).

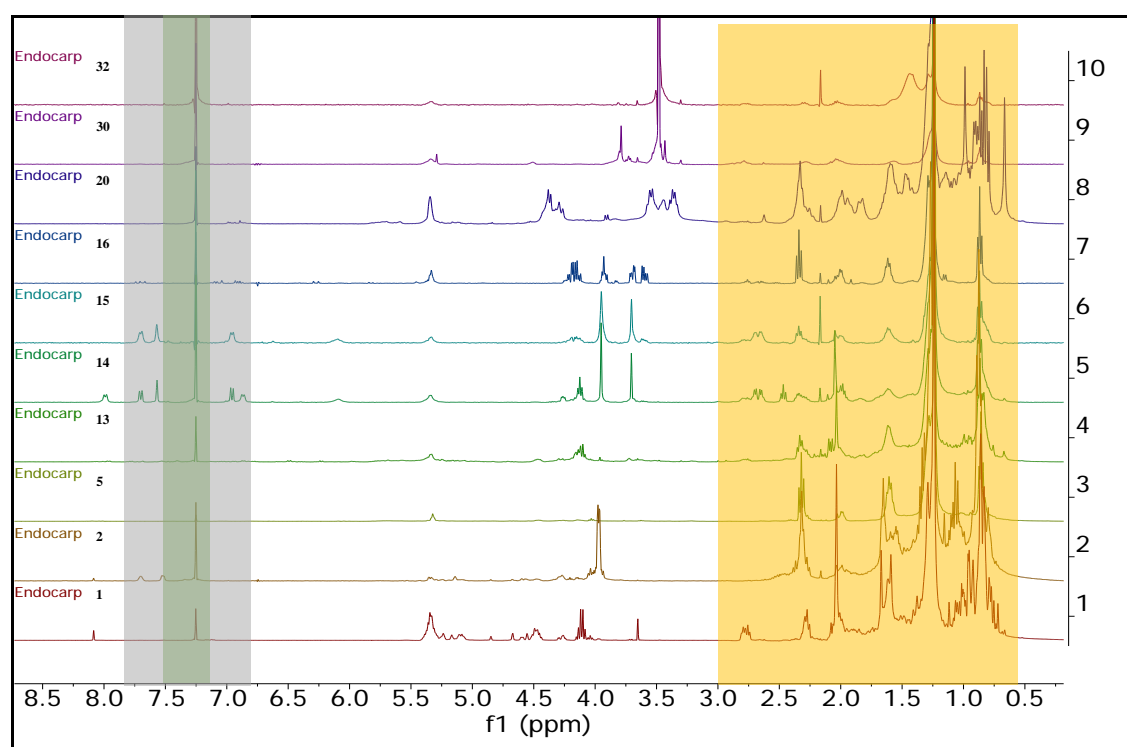


**Figure 4.4:** Stacked  $^1\text{H-NMR}$  spectra of bioactive fractions from *F. carica* endocarp. Shown from the bottom to the top are F1, F2, F5, F13, F14, F15, F16, F20, F30 and F32. Highlighted with the orange grid indicated the resonances for an aliphatic structure found between  $\geq 1.0$  and 2.5 ppm. The aromatic region is highlighted in grey found between

6.75 and 7.75 ppm, while olefinic peaks resonated between 3 and 5.5 ppm.  $\text{CDCl}_3$  appeared at 7.25 ppm, which is highlighted in green.

### 4.3. Cell viability test

Only twelve fractions were found to be bioactive: F1, F2, F5, F10 to F16, F20, F21, F30 and F32 at 105%, 103%, 102%, 106%, 108%, 112%, 104%, 101%, 112%, 105%, 105% and 102%, respectively (Figure 4.5). In contrast, the remaining fractions were not bioactive. At 112% bioactivity, F14 and F20 showed significant highest cell viability. Using acrolein, a cytotoxicity test was conducted to investigate their oxidative stress potential.

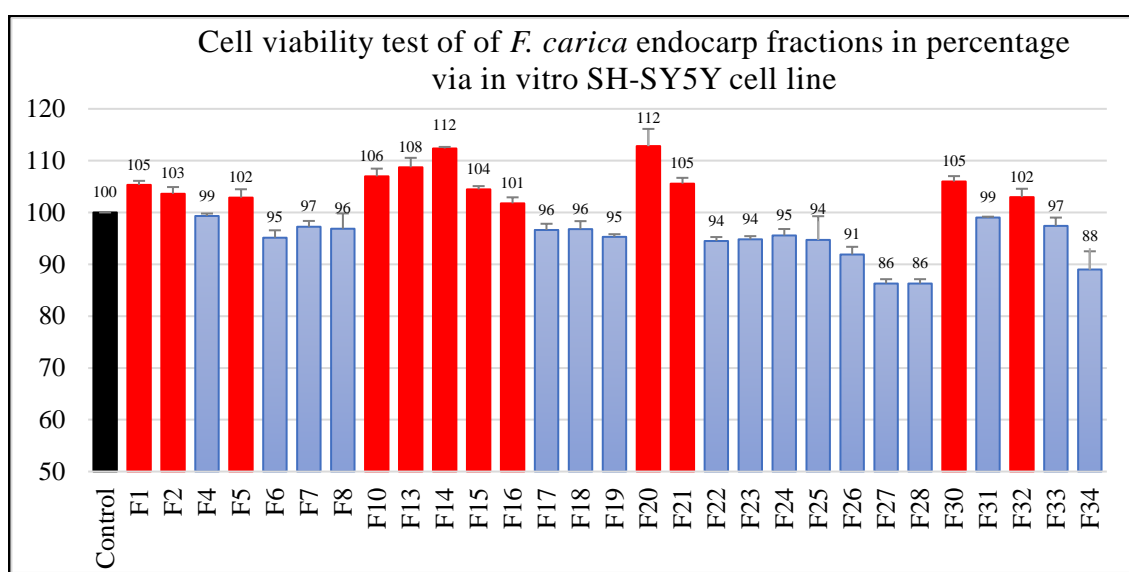


**Figure 4.5:** Cell viability test using differentiated SH-SY5Y cells incubated for 72 hours after 24 hours of RA incubation followed by 24 hours treatment (30  $\mu\text{g}/\text{mL}$ ) with different *F. carica* endocarp fractions at 30  $\mu\text{g}/\text{mL}$ . Y-axis represents percentage cell viability and X-axis represents the respective fraction number. Results are shown as fluorescence counts using a microplate absorbance/fluorometer plate reader with 1420 Multilabel counter. Twelve fractions afforded cell viability at above 100% in red bars. Whereas, seventeen fractions in blue bars have shown viability below 100% of the control that is in black bar. Each group was done in triplicate in a mean 3 SD; ANOVA  $P < 0.05$  compared with control.

#### 4.4. Cell cytotoxicity test

The AlamarBlue<sup>®</sup> assay demonstrated that exposure to acrolein decreased the oxidation-reduction potential in a dose-dependent manner in the differentiated SH-SY5 cell line. The addition of various concentrations of F14 to the culture significantly increased the activities by 1.71%, 54.8%, 59%, 63.9%, and 71.7% at 300 ng/ mL, 1 µg/mL, 3 µg/mL, 30 µg/mL and 10 µg/mL, respectively. Meanwhile, no activity was observed with acrolein doses 100, 30, and 10 ng/mL, (Figure 4.6A). Likewise, adding F20 at concentrations of 30 µg/mL, 10 µg/mL, 1 µg/mL, 3 µg/mL and 300 ng/ mL of to the culture significantly increased activity by 75%, 66%, 52.9%, 52.5% and 0.87%, respectively. EC<sub>50</sub> of F14 and F20 fractions were 3.105 µg/ml and 3.136 µg/ml, respectively. The concentrations inciting optimum bioactivity were at 30 µg/mL for F14 and 10 µg/mL for F20.

The decreased in cell bioactivity in the 24-hour treatment with F14 and F20 was dose-dependent (Figure 4.6B). At fraction concentrations of 30, 10, 3 and 1 µg/mL, cell bioactivity was significantly higher than at 300, 100, 30 and 10 ng/mL. F20 was less sensitive to the cytotoxic effects of acrolein than F14. The compounds in F14 and F20 were identified as, *P*-hydroxybenzoic acid, vanillic acid and lawsaritol, respectively. These compounds were fully elucidated in detail in section 4.7. As a result, compounds in F14 and F20 possess activity at 3.105 µg/ml, 3.136 µg/ml. Each experiment was performed in triplicate and the results represent as the mean ± SE.

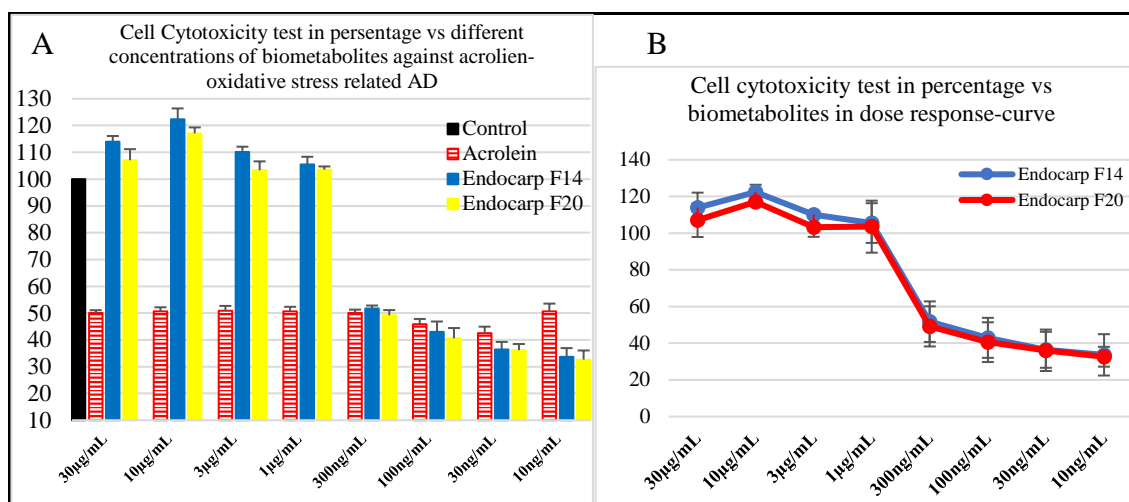


**Figure 4.6:** F14 and F20 protected differentiated SH-SY5Y cells against the toxicity of acrolein. **A)** AlamarBlue<sup>®</sup> assay following exposure to 20 µM acrolein and treatment of differentiated SH-SY5Y cells with F14 and F20. **B)** Dose-response curves for F14 (blue) and F20 (red) suppressing acrolein-induced oxidative stress related AD; which were detected by alamarBlue<sup>®</sup> fluorescence and plotted in percentage viability after 24 hours treatment; (each group represents mean 3 SD; ANOVA P < 0.05 compared with control).

**Table 4.3:** Antioxidant activities of the F14 and F20 from *F. carica* endocarp vs acrolein induced oxidative stress in differentiated SH-SY5Y cell line; values were indicated in triplicate. F20 represents compound and F14 represents a mixture of two compounds.

Compound	F20	F14
	Lawsaritol	<i>P</i> -hydroxybenzoic acid and acid vanillic Acid
The activity of 10 µg/mL in µM	Not applicable	Not applicable
EC <sub>50</sub> µg/ml	3.136	3.105
Acrolein antioxidant test EC <sub>50</sub> µM	Not applicable	Not applicable

#### 4.5. Western blotting test

As the NQO1 transcription factor regulates the expression of numerous ROS and detoxifying agents as well as antioxidants, treatments with lawsaritol from F20 and a

combination of *P*-hydroxybenzoic acid with vanillic acid obtained from F14 were further examined to assess whether these treatments upregulated the expression levels of NQO1. To corroborate these data, Western blot analyses were performed on cell lysates derived from differentiated SH-SY5Y cells stimulated with polyclonal NQO1 antibody and treated with lawsaritol and a combination of *P*-hydroxybenzoic acid and vanillic acid. Western blot analysis (Figure 4.7) showed the protein expression levels of NQO1 (30 kDa) in differentiated SH-SY5Y cells to be significantly upregulated in the *in vitro* model with the exposure to 20  $\mu$ M acrolein compared to the unstimulated control  $\beta$ -actin protein detected at 42 kDa as shown in Figure 4.7. The significant higher level was observed in the mixture of *P*-hydroxybenzoic acid and vanillic acid 3.105  $\mu$ g/ml ( $P < 0.05$ ).

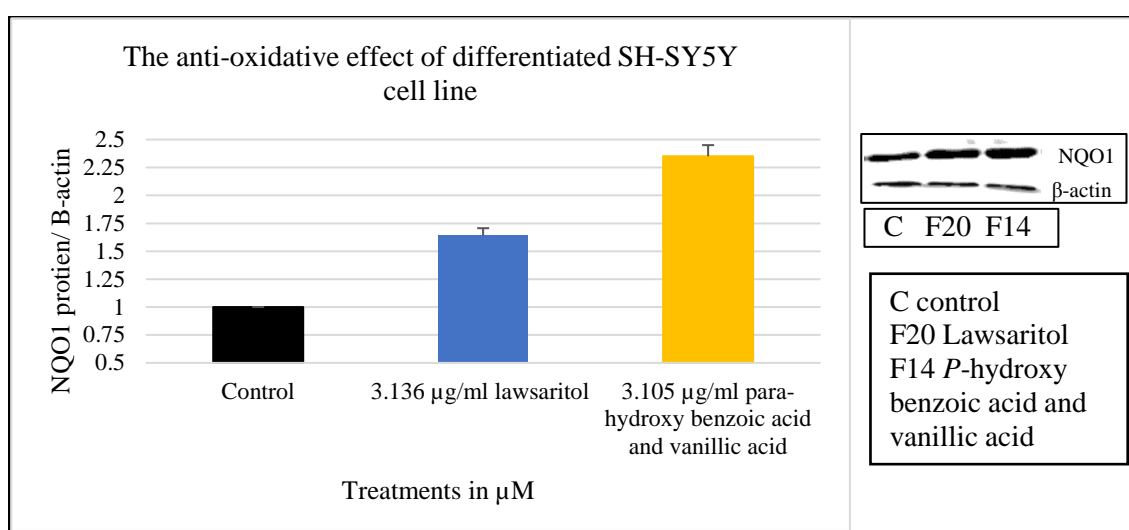


**Figure 4.7:** Quantification of the western blot by densitometry. The bars represent the standard deviation and  $p < 0.05$ . Western blotting image of the total NQO1 protein level (30 kDa) in the presence of acrolein.

#### 4.6. Metabolomic-guided screening of *F. carica* endocarp

The presentation of the PCA-HCA results in the form of a dendrogram made it possible to visualise clustering such that relationships of metabolites can be more readily seen (Figure 4.8). A heat map was generated and compared against the HCA clustering, which to some extent exhibited similarity with HCA tree scheme. The generation of heat map allowed visualising the chemical diversity in each individual fraction. In more detail, the presence of blue bars indicates the increase in concentration of a metabolite while absence or decrease in concentration of a metabolite gives a pink bar as has been described in chapter 3.

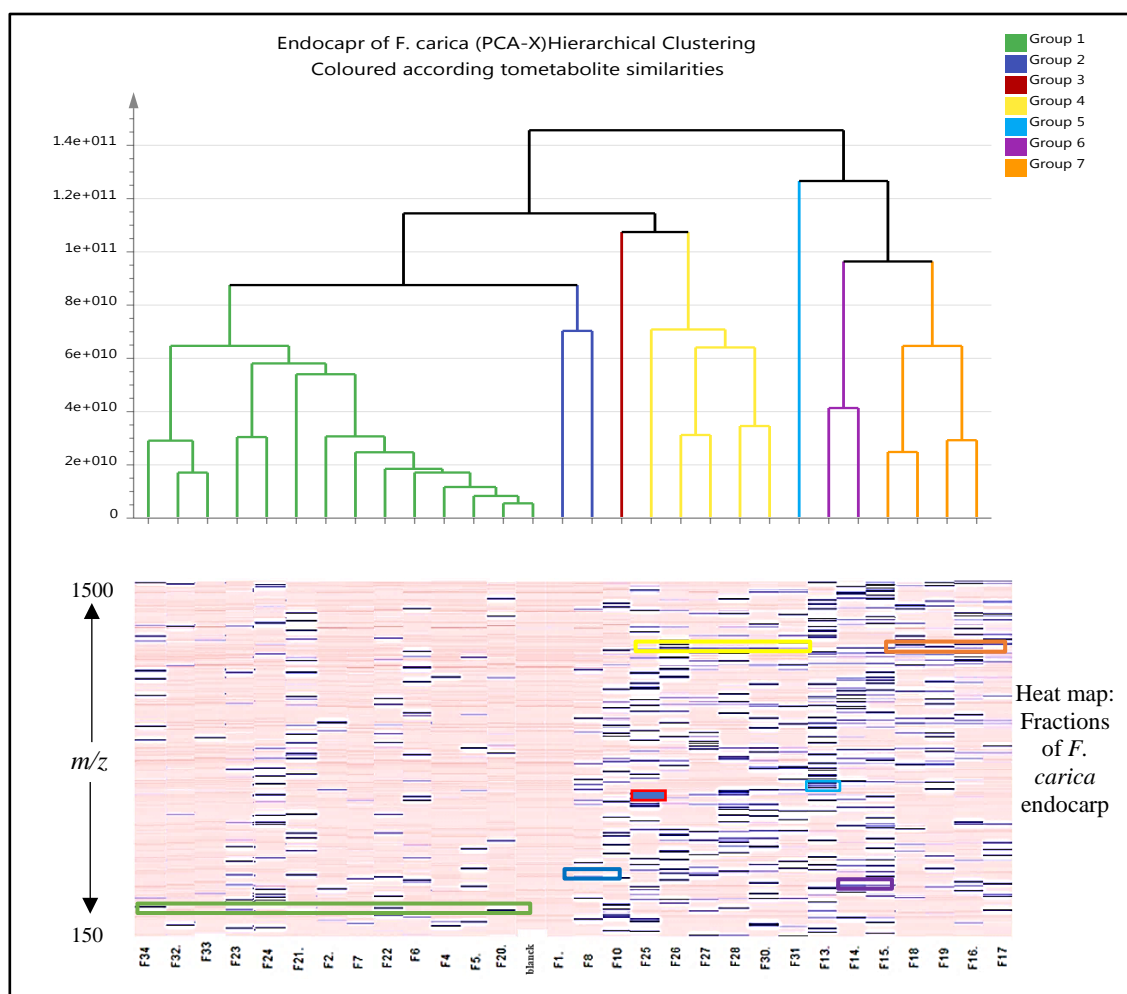


**Figure 4.8:** PCA-HCA dendrogram and heat map of chromatographic fractions of the crude ethyl acetate extract of *F. carica* endocarp.

Secondly, the unsupervised PCA was initially performed concomitantly with pareto scaling to provide the best possible view of the variability in a multivariate data set (Bratchell, 1989). Analysis of the positive and negative ionisation mode data with the SIMCA demonstrated a good separation between fractions on the PCA scores plot (Figure 4.9A). To evaluate the PCA model, the values 0.999 (R2) and 0.0925 (Q2) confirmed goodness of fit at 99.9% and goodness of prediction at 9.25%, respectively. Moreover, the scores of the scatter plot of PCA analysis showed seven groups were observed in four marginal outliers, which are presented in red, violet, navy, green, yellow, orange and blue clusters. They were classified according to their chemical constituent, such as sugars (yellow cluster), fatty acids and sterols (green clusters) and phenols (violet colour). These classifications also agreed with the preliminary NMR spectral data described in section 4.2. Additionally, the scatter plot was generated to demonstrate the distance of each

variable from the origin (scores scatter plot of PCA), while in the loadings scatter plot of PCA as ion peak  $m/z$  (Bakeev, 2010). From correlating the score and loading scatter plot in Figures 4.9A and B, the violet circles depict the ion peaks  $m/z$  between 100 and 300, while yellow and green circles show the entire molecular ion peak in  $m/z$  except where it diminishes by  $\geq 1000$   $m/z$  in the yellow circles.

To highlight the discriminatory metabolites between the active and inactive fractions, feature selections were performed using OPLS-DA. The finding presented by Figure 4.9C shows clearer separation when supervised OPLS-DA analysis was applied, demonstrating the variable differences between the active, represented by green spots, and inactive, represented by blue spots. To evaluate the OPLS-DA model,  $R^2Y(\text{cum})$ , and  $Q^2(\text{cum})$ , the fraction of the variation of Y that can be predicted by the model according to cross-validation, were used. The  $R^2Y(\text{cum})$  and  $Q^2(\text{cum})$  are 0.887 and 0.109, respectively. These results suggest that the model explains 88.7% of the variations of Y, with a predictive ability ( $Q^2$ ) of 10.9%; the closeness of these values indicates the goodness of the model. Suspected fatty acids and phenols derivatives were observed in the same upper quadrant, while the sterols with sugar derivatives were likely to be observed in the same lower quadrant and were confirmed by their NMR spectral data. The value between group discrimination were thereafter evaluated and exhibited in the X-axis in  $R^2X[1]$  yield 14.97% which is significantly greater than the variation within group exhibited in the y-axis in  $R^2Xo[1]$  yield 10.60%. Nevertheless, the outlier was not considered for further analysis because the fraction was biologically inactive. Notably, the most bioactive fractions F14 and F20 were marked as two black spots on the scores scatter plot. Additionally, OPLD-SA loadings scatter plot pinpointed the discriminatory target metabolites while the isolated bioactive metabolites were shown at  $m/z$  168.030 at the upper left margin and  $m/z$  414.381 at the lower left margin (Figure 4.9D).

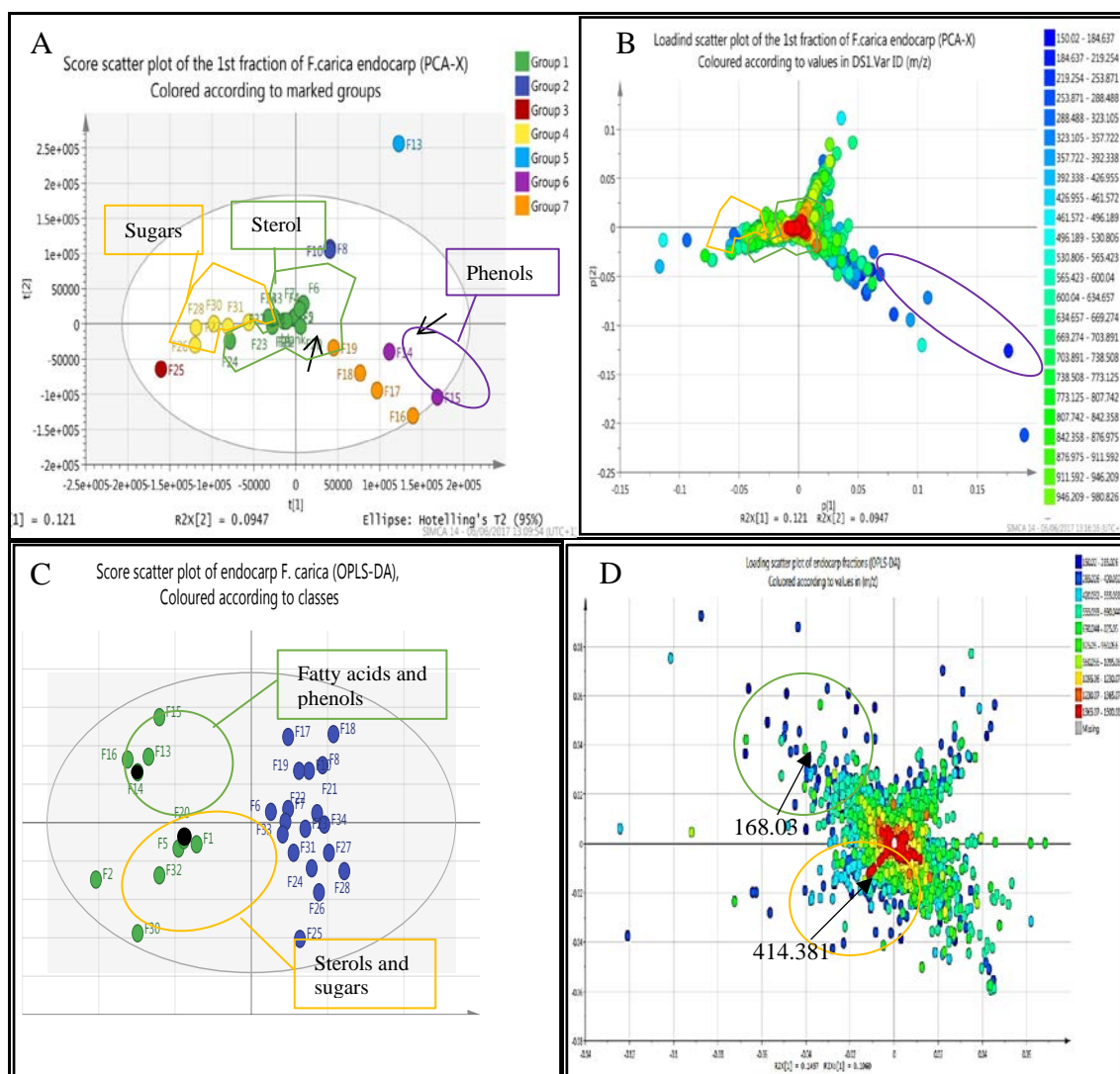


**Figure 4.9:** (A) Unsupervised PCA scores scatter plot for *F. carica* endocarp with 29 fractions; orange irregular circle indicates sugar metabolites, irregular green circles indicate sterol derivatives, violet circle indicates phenol and flavonoid metabolites and black arrows indicate the metabolite of interest. (B) PCA loadings scatter plot indicated the corresponding *m/z* features related to the regular and irregular circles. (C) OPLS-DA scores scatter plot resulting from the preliminary bioassay screening with active metabolites labelled in green spots and inactive in blue; green circle is most likely to represent fatty acids and phenols; orange circle is most likely to represent sterols and sugars, while, black spots represent the fractions of interest. (D) OPLS-DA loadings scatter plot indicated the corresponding *m/z* features with the isolated metabolites at *m/z* 168.03 and 414.381.

An S-plot was generated to visualise the variables that had significant contribution to the discrimination between experimental groups (Kang *et al.*, 2012). Amongst this two metabolites were shown at the active profile, meaning that 168.03 *m/z* (Figure 4.10B) and 414.381 *m/z* (Figure 4.10C) biomarkers featured closely to the outlier margin. These

target metabolites considered difficult due to their low magnitude -0.006 and high reliability  $p(\text{corr})_1$  equal to 0.45 ( $p > 0.05$ ), due to these metabolites were semi-pure fractions. The other metabolites were indicated as listed in Table 4.4 by the exploration of DNP dereplication.

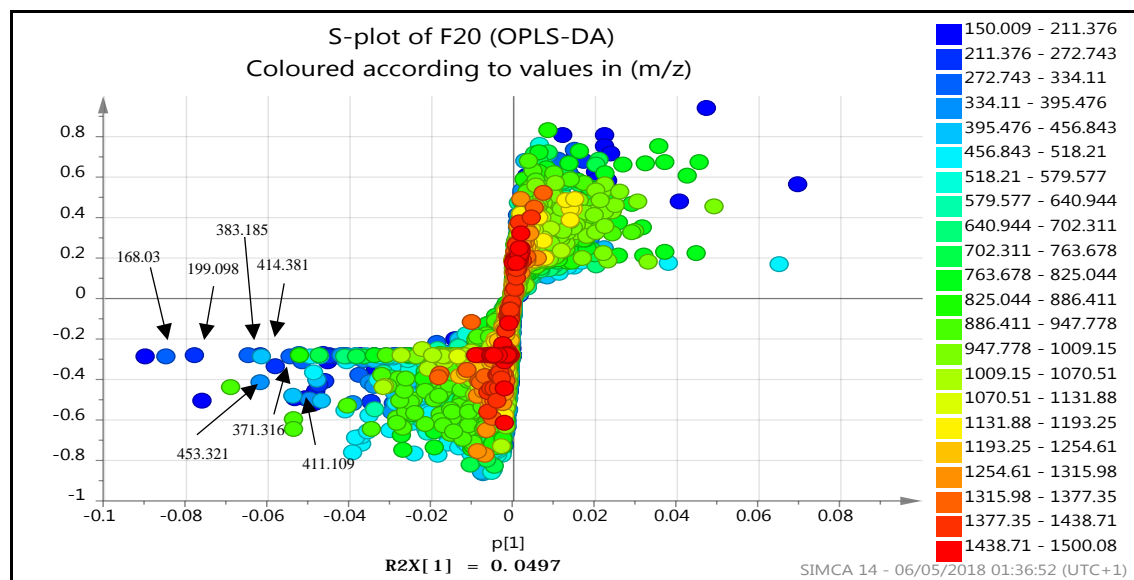
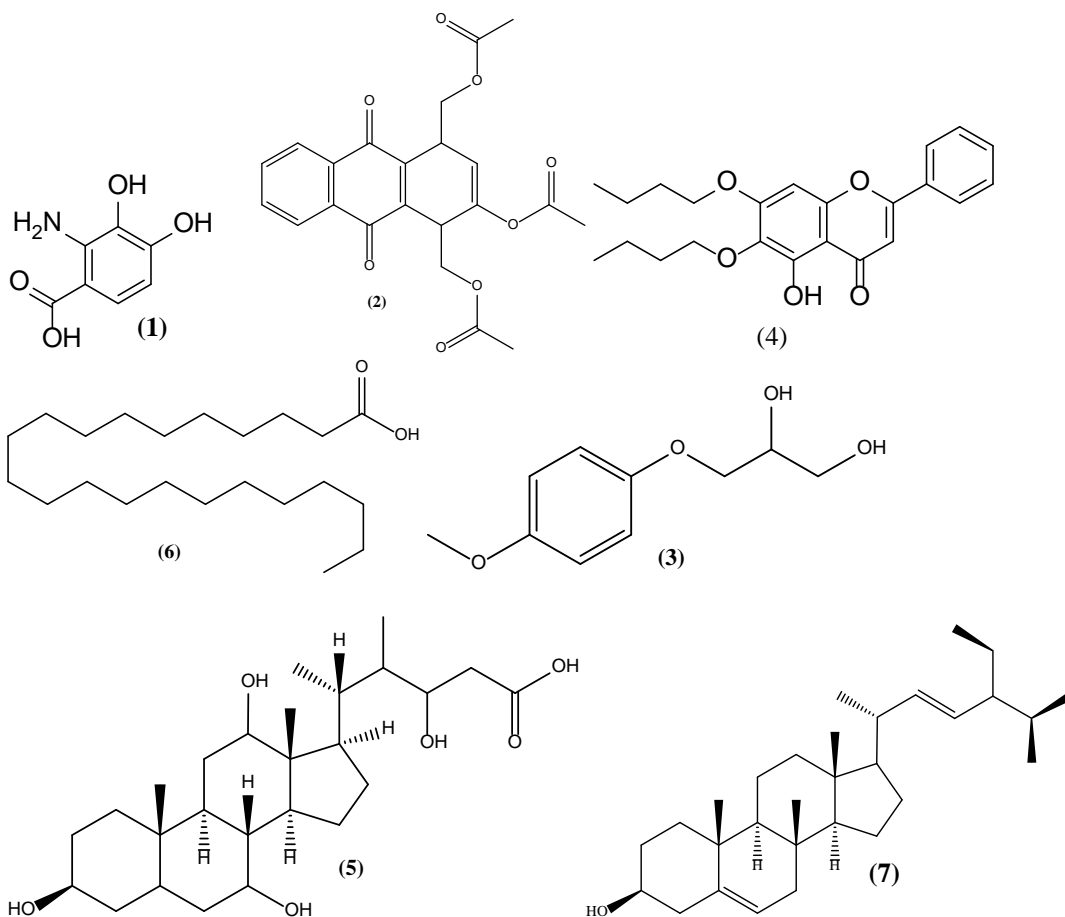


**Figure 4.10:** Putative discriminatory metabolites were selected using an S-plot.

**Table 4.4:** Discriminatory metabolites deduced from the active fractions obtained from the S-plot “end point” data shown in Figure 4.12. Dereplication was accomplished from the DNP 2015 database. (P indicated positive mode, N indicated negative mode).

Ionization Mode	MS <i>m/z</i>	Rt min	Chemical Formula	Name	Source
N	168.030	5.43	C <sub>7</sub> H <sub>7</sub> NO <sub>4</sub>	2-amino-3,4-dihydroxybenzoic acid (1)	<i>Berberis koreana</i> leaves
N	411.109	13.19	C <sub>22</sub> H <sub>20</sub> O <sub>8</sub>	<i>cis</i> -2-acetoxy-1,4-diacetoxymethyl-1,4-dihydroanthraquinone (2)	<i>Millettia brandisiana</i>
N	199.098	17.39	C <sub>10</sub> H <sub>14</sub> O <sub>4</sub>	3-(4-methoxyphenoxy)-1,2-propanediol (3)	<i>Patrinia villosa</i>
P	383.185	22.35	C <sub>23</sub> H <sub>26</sub> O <sub>5</sub>	6,7-dibutoxy-5-hydroxyflavone (4)	<i>Athanasia calva</i>
P	453.321	30.62	C <sub>26</sub> H <sub>44</sub> O <sub>6</sub>	Ethylene glycol monocholate (5)	<i>Cinnamomum laubatii</i>
N	371.316	33.30	C <sub>22</sub> H <sub>44</sub> O <sub>4</sub>	Docosanoic acid (6)	<i>Cardamine impatiens</i>
P	414.381	38.47	C <sub>29</sub> H <sub>50</sub> O	β-stigmasterol (7)	<i>Berberis lycium</i> fruit



## 4.7. Identification and elucidation of bioactive compounds from *F. carica* endocarp

### 4.7.1. Lawsaritol 2.1

**Table 4.5:** F20 of *F. carica* endocarp. Description of lawsaritol **2.1**; chemical structure; LC-MS analysis, and the identification of GCMS.

<b>lawsaritol 2.1</b>
Synonym(s): Stigmasta-3,5-dien-7-one, stigmast-4-en-3-ol; 24-ethylcholest-4-en-3-ol
Source: Endocarp of <i>F. carica</i>
Metabolite: 1 <sup>st</sup> fraction F20
Sample amount: 45.4 mg
Physical description: White powder
Molecular formula: C <sub>29</sub> H <sub>50</sub> O
Exact Mass: 414.3862 g/mol
<b>Chemical structure</b>

NIST library linked to GCMS analysis has identified various compounds in F20, which included 7-dehydrogiosgenin **2.2**, cholesta-4,6-dien-3-ol **2.3**, stigmasta-3,5-dien-7-one **2.4**, 3a, 10, 10, 12b-tetramethyl-3-(6 methylheptan-2-yl) 1,2,3a,4,6,8,9,10,10a,11,12,12a,12b-tetradecahydrobenzo(4,5) cyclohepta (1,2-e)indene **2.5** as shown in Figure 4.11A.

The mass spectral fragmentation pattern afforded the fragment ion peaks at  $m/z$  174, 187 and 269 characteristic of a cholesta-3,5-dien-7-one skeleton. The ion peaks at  $m/z$  174 and 187 can be rationalised by cleavage of the C-ring, while the ion peak at  $m/z$  269 is

due to loss of the side chain at C-17 (Figure 4.11B), as described earlier in the literature (Sarwar Alam *et al.*, 1992).

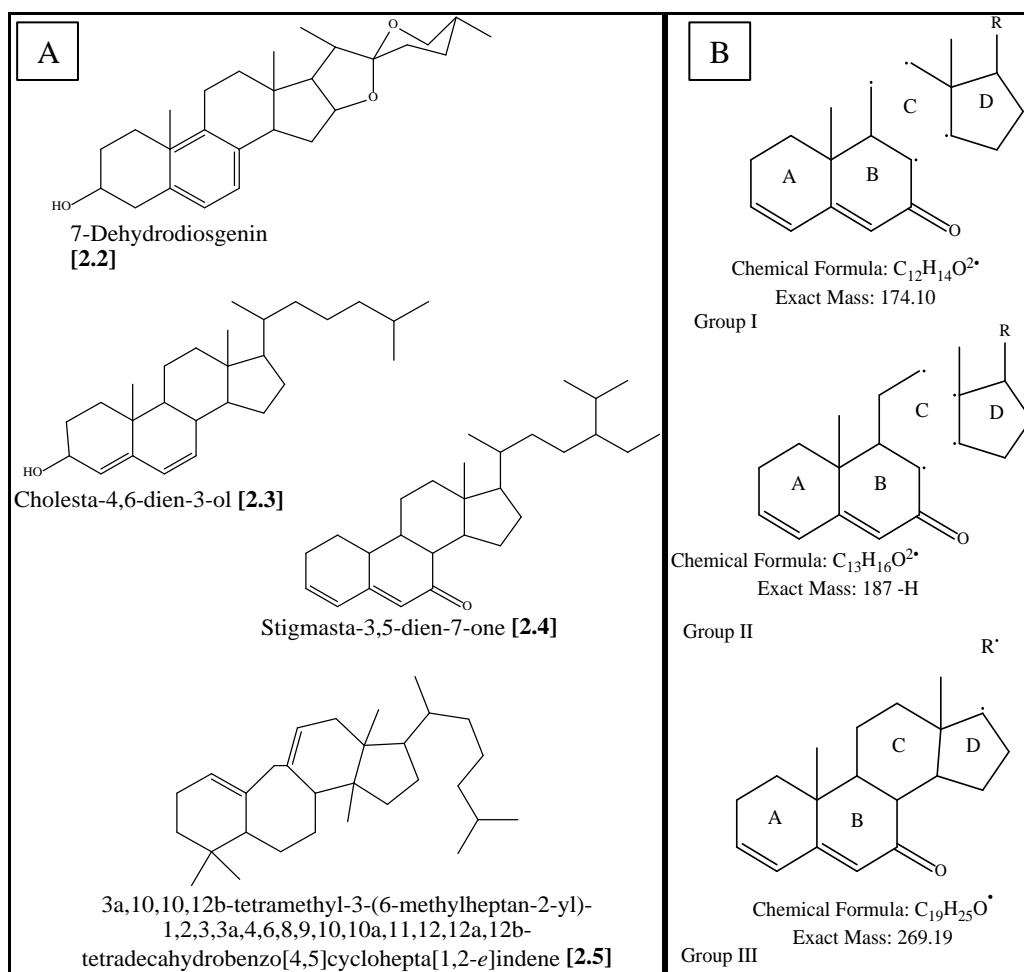


**Figure 4.11:** **A)** Structures of non-polar constituents identified from *F. carica* endocarp by GC-MS analysis. **B)** Characteristic fragmentation of a cholesta-3,5-dien-7-one skeleton. Groups I and II was fragmented through ring C to observe  $C_{12}H_{14}O_2^+$  at  $m/z$  174.10, and  $C_{13}H_{16}O_2^+$  at  $m/z$  187. Group III was fragmented at aliphatic chain to yield  $C_{19}H_{25}O^+$  at  $m/z$  269.19. The fragmentation pattern is similar to that earlier described in the literature (Sarwar Alam *et al.*, 1992).

The NIST library hit gave similarity scores of 27.7% for cholesta-4,6-dien-3-ol for the peak at 18.11 min and 84.5% for stigmasta-3,5-dien-7-one for the peak at 19.42 min in F20 (Figure 4.12). The mass spectral fragmentation pattern supported the characteristic fragmentation for cholesta-3,5-dien-7-one skeleton as mentioned above. Further structural elucidation confirmed the structure to be a derivative of stigmasterol.

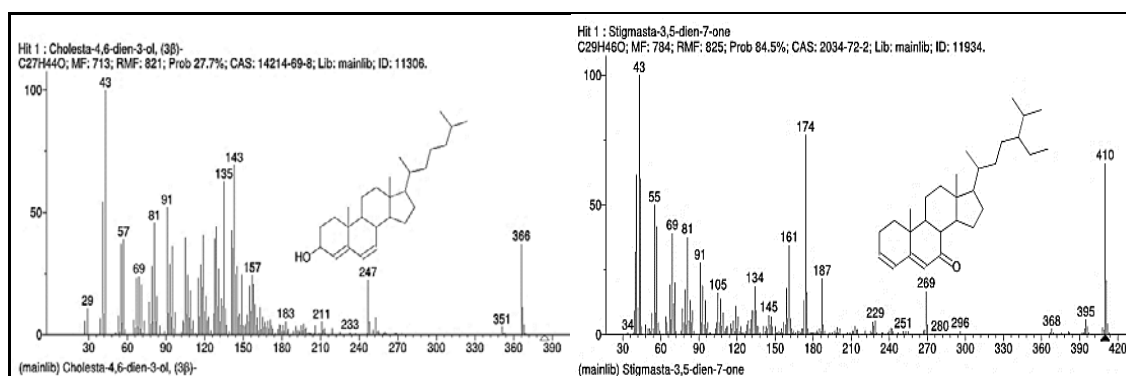


**Figure 4.12:** Dereplication of major GCMS. peaks from the NIST library with similarity scores of 27.7% for cholesta-4,6-dien-3-ol **2.3** and 84.5% for stigmasta-3,5-dien-7-one.

Based on the mass and NMR spectral data for F20, the structure of its metabolite could be identified as stigmast-4-en-3-ol **2.1**, also known as 24-ethylcholest-4-en-3-ol. This sterol, also named as lawsaritol **2.1** is a  $\beta$ -sitosterol isomer, first reported from the roots of *Lawsonia inermis* (Alam *et al.*, 1992), while its characterisation in *F. carica* endocarp has not yet been reported.

The fragment ions at  $m/z$  55 and 69 indicated that a hydroxyl group is present at C-3 in ring A. The structural skeleton and the presence of their functionalities in lawsaritol were supported by the appearance of additional resonances in the  $^{13}\text{C}$ -NMR spectrum that recorded carbon signals for twenty-nine different carbons. The  $^{13}\text{C}$ -chemical shift values and their respective DEPT-135 clearly indicated a steroid skeleton for F20 (Figure 4.13). It has one primary methyl (C-29 at  $\delta$  12.0), three secondary methyls (C-21 at  $\delta$  18.8, C-26 at  $\delta$  19 and C-27 at  $\delta$  19.8), two tertiary methyls (C-18 at  $\delta$  11.9 and C-19 at  $\delta$  19.3), eleven methylenes, nine methines and three quaternary carbons.  $^{13}\text{C}$ -NMR assignments are presented below in Table 4.6. The functionalities present in **2.1** were also supported by  $^{13}\text{C}$ -NMR spectral data with the resonances at  $\delta$  70.2 for a CHOH at C-3 attached with a  $\beta$ -oriented OH,  $\delta$  122.1 and 140 for a tri-substituted C=C bond at C4 and C5.

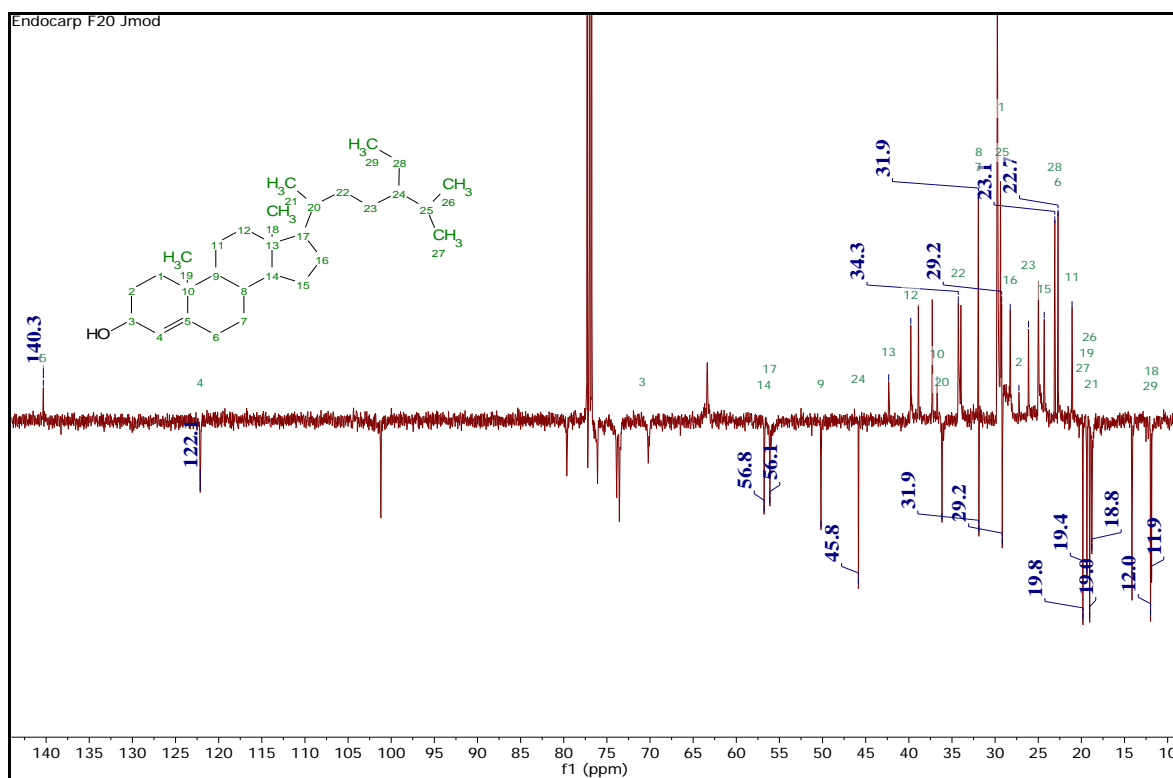


**Figure 4.13:** *J*-mod-NMR spectrum (125 MHz,  $\text{CDCl}_3$ ) of compound **2.1**. Positive signals correspond to  $\text{CH}_2$ s, while negative signals correspond to either  $\text{CH}_3$ s,  $\text{CH}$ s or quaternary-Cs.

$^1\text{H}$ -NMR spectrum of F20 supported the existence of a mono-substituted double bond in H-4 at  $\delta$  5.35, a doublet,  $J = 5.33$  MHz as well as a terminal isopropyl group in the side chain at  $\delta$  0.83 (3H, a doublet,  $J = 1.89$  MHz, H-26-Me) and at  $\delta$  0.86 (3H, multiplet, H-27-Me). Two singlets at  $\delta$  0.67 and at  $\delta$  1.12 were present, corresponding to H-18 and H-19 methyl protons, respectively. Two multiplets each integrating for 3H appeared at  $\delta$  0.91 and  $\delta$  0.99 due to H-29 and H-21 methyl protons, respectively. Signals due to protons attached to carbon-bearing hydroxyl group were observed at  $\delta$  3.54 as a multiplet.

However, in H-22 at  $\delta$  2.32, multiplet (Figure 4.14) was integrated as 4H, due to overlapping of signals. Another integration of 46H at  $\delta$  1.26, multiplet were observed due to proton overlaps and signals resonated in the same upfield region including H-6 for 2H integral, H-12 for 2H integral, H-17 for 1H integral, H-23 for 2H integral and H-25 for 1H integral. Likewise, an integration of six protons were also resonate at the upfield region at  $\delta$  0.91, hence, were assigned for (H-29, integral of 3H), (H-28, integral of 2H)

and (H-24, integral of 1H).  $^1\text{H-NMR}$  spectral data (Figure 4.16 and Table 4.6) was comparable to that reported in the literature (Manjari *et al.*, 2009).

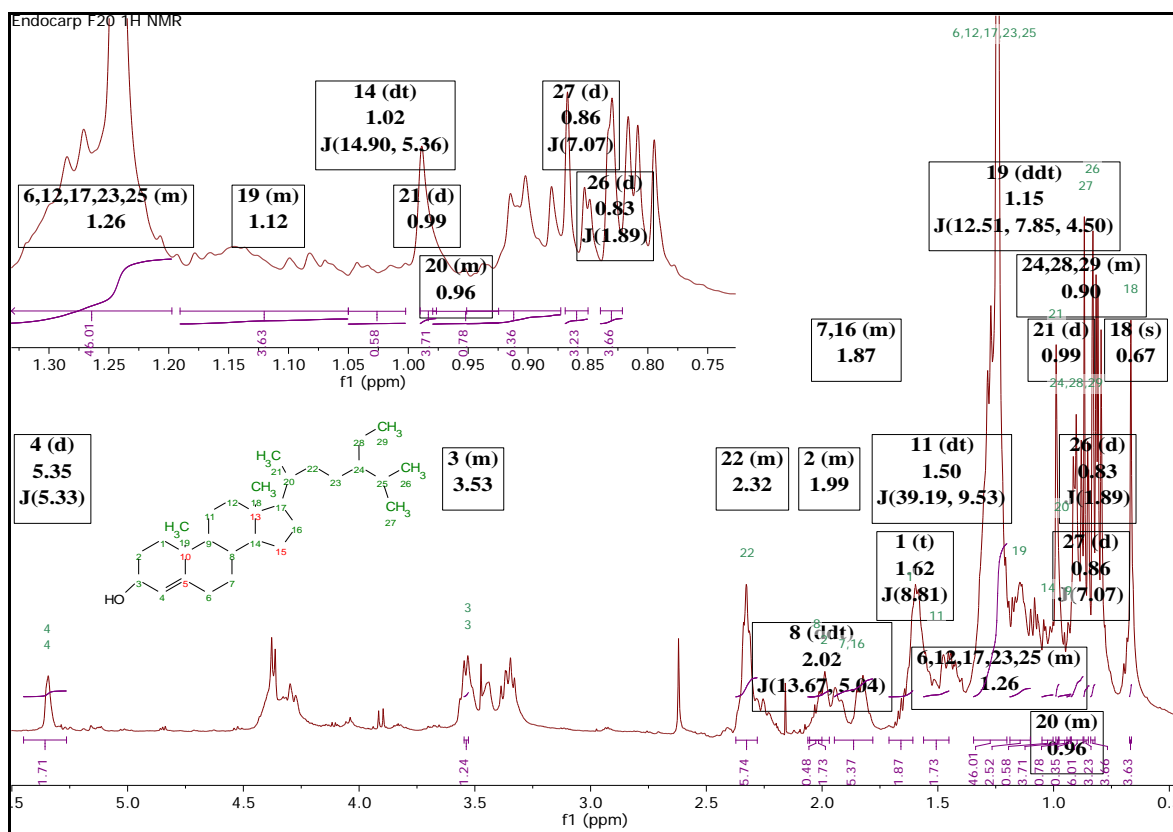


**Figure 4.14:**  $^1\text{H-NMR}$  spectrum of F20 elucidated as lawsaritol **2.1** in  $\text{CDCl}_3$  and run at 400 MHz.

Stereochemistry was assigned  $\beta$  and equatorial based on larger coupling constant of hydroxyl group attached to proton at C-3,  $J = 5.33$  Hz. The most downfield proton at  $\delta$  5.35 that showed connectivity to two neighbouring protons in the  $^1\text{H-}^1\text{H}$  COSY spectrum and hence could be assigned to C-3. The two protons H-1 at  $\delta$  1.62 and H-2 at  $\delta$  1.99 showed further connectivity to H-6 and H-7 as illustrated in a blue connection line in Figure 4.15. The isopropyl group and the ethane group at the most upfield region have showed connectivity (yellow lines) to the aliphatic side chain up to H-22 which was further connected to H-11, H-12, H-17 and H-20. Methyl group in H-21 has showed connectivity to H-20 and further to H-19 as illustrated in green line. Two methyl groups on the A-D aliphatic ring and side chains were assigned by employing an HMBC correlation (Figure 4.19). The positions of double bond and hydroxyl groups were further confirmed by HMBC correlations, as well.

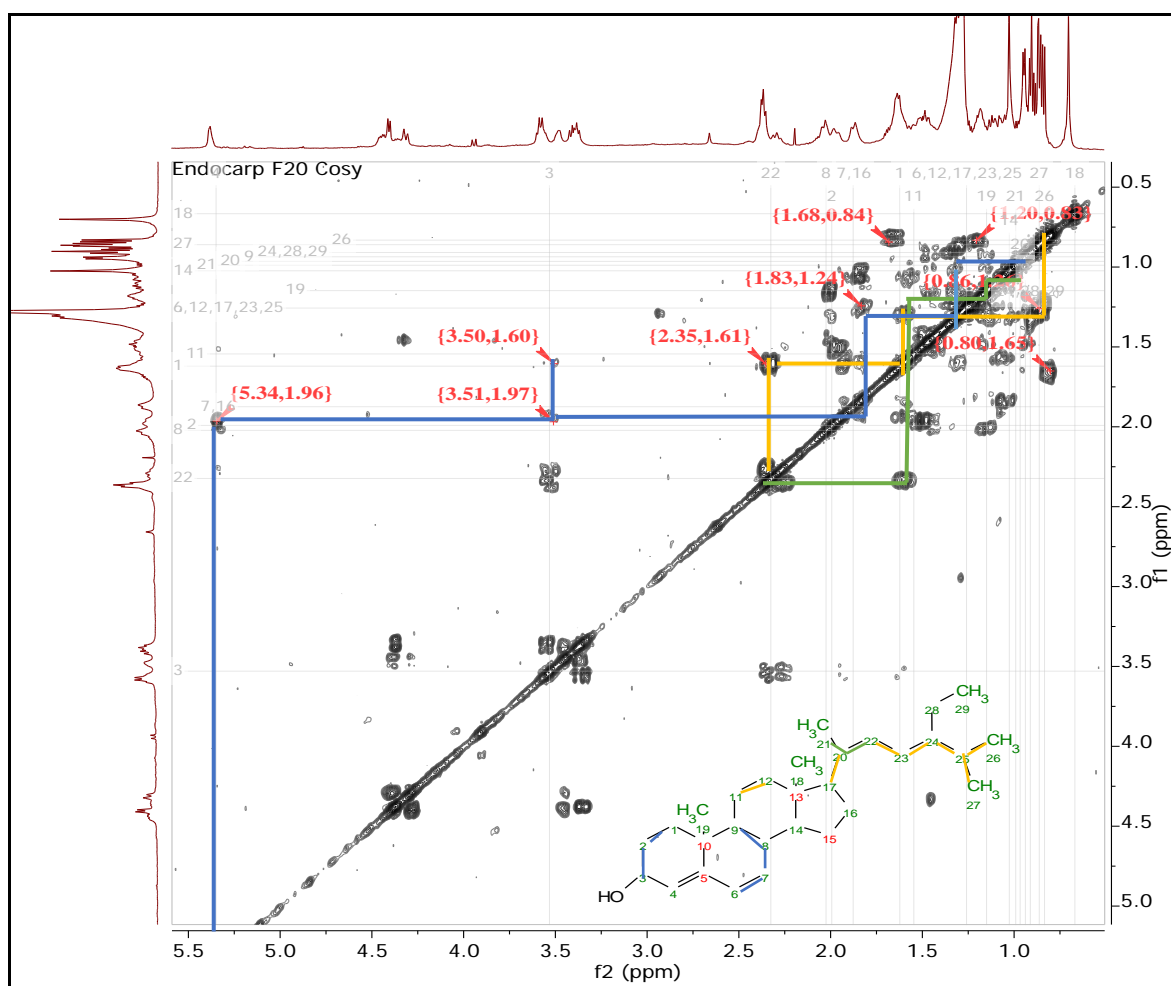


**Figure 4.15:** 2D  $^1\text{H}$ - $^1\text{H}$  COSY correlations of F20 elucidate as lawsaritol **2.1**.

Furthermore, HSQC (Figure 4.18) correlations of F20 confirmed the carbon and proton assignments such as hydroxyl bearing carbon on position-3 at  $\delta_{\text{H,C}}$  3.41, 70.2 and the double bond substitution on position-4 at  $\delta_{\text{H,C}}$  5.38, 122.1. In the upfield region, secondary methyl group attached on position-25 at  $\delta_{\text{H,C}}$  1.28, 29.7; as well as positions 26 and 27 at  $\delta_{\text{H,C}}$  0.83, 19.0 and 0.86, 19.8, respectively. In addition, four methyl groups were observed for positions 18, 19, 21 and 29 at  $\delta_{\text{H,C}}$  (0.70, 11.9); (1.02, 19.4); (0.94, 18.8); and (0.87, 12), respectively.

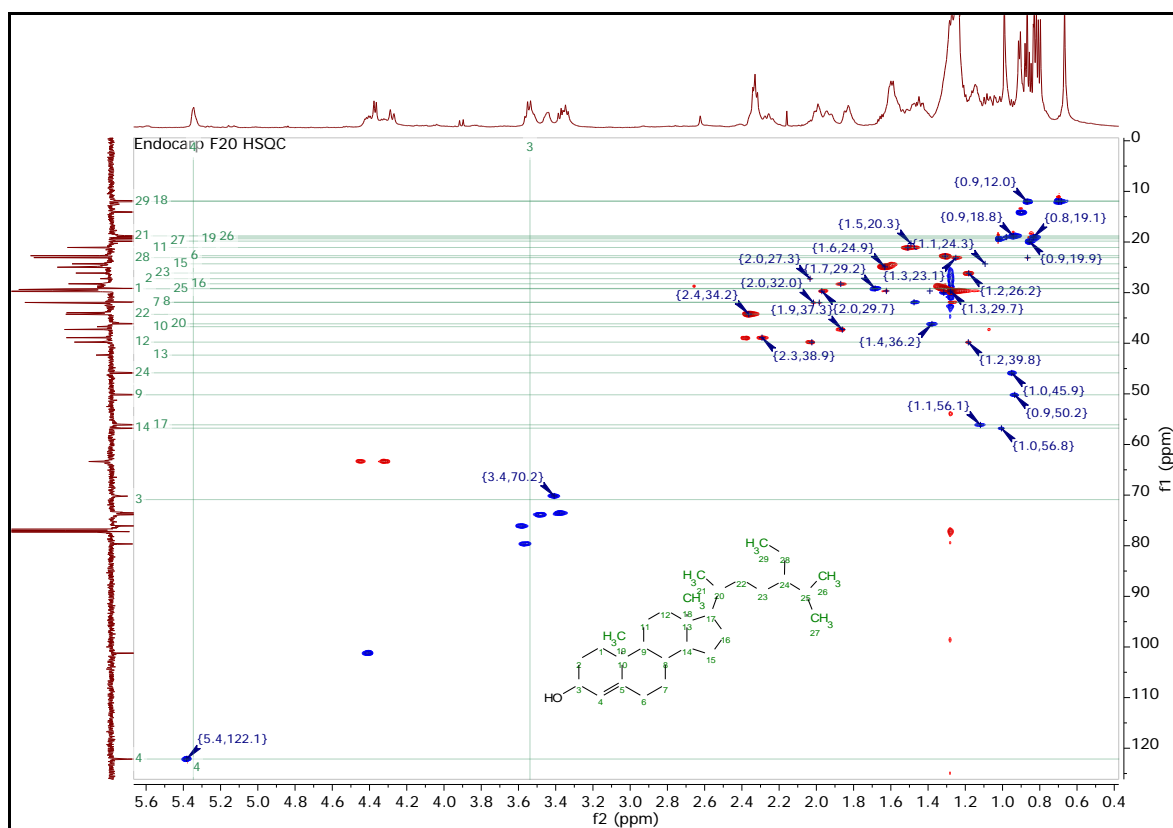


**Figure 4.16:** HSQC spectrum of F20 elucidated as lawsaritol 2.1 in  $\text{CDCl}_3$  at 500MHz. Blue colour of signals represent either CH,  $\text{CH}_3$  or quaternary-C while the red colour represents  $\text{CH}_2$ .

The HMBC correlations (Figure 4.17A and Figure 4.17B) of the side chain also confirmed the long-range correlation of the hydroxyl group on H-3 at  $\delta$  3.41 to the methylene carbon C-2 at  $\delta$  27.25, to C-1 at  $\delta$  29.2 and C-10 at  $\delta$  38.9. The methyl proton on H-1 at  $\delta$  1.28 correlated back to the hydroxyl group on C-3 at  $\delta$  70.2 and further to the methyl carbon on C-19 at  $\delta$  19.39, as well as to C-6 at  $\delta$  22.7. H-2 at  $\delta$  2.03 also directly correlated to C-1. The methyl group on H-19 correlated to C-1 and to both the double bond resonances on C-5 at  $\delta$  140 and C-9 at  $\delta$  50.2.

The HMBC in the B-ring (Figure 4.17) also showed correlation to each other, as the methylene group in H-7 at  $\delta$  1.98 and H-8 at  $\delta$  2.02 both correlated to C-6 and to C-9 at  $\delta$  22.7 and 50.2, respectively, in addition to the long-range correlation of H-8 at  $\delta$  2.02 to C-1. In the C-ring of the structure (Figure 4.18), H-12 at  $\delta$  1.18 correlated to methylene C-11 at  $\delta$  21.1 and further to C-8 at  $\delta$  31.9. Likewise, H-14 at  $\delta$  1.01 correlated to the methyl group on C-18 at  $\delta$  11.9 and to C-9. H-9 also correlated to C-14 at  $\delta$  56.8, as well

as to C-12 at  $\delta$  39.8. Moreover, H-17 attached to D-ring at  $\delta$  1.12 directly correlated to C-16 at  $\delta$  28.2 and to C-12. Likewise, H-15 at  $\delta$  1.09 gave a long-range correlation with C-17 at  $\delta$  56.2.

The side chain of the steroid structure was attached to position-17. The methyl group on H-21 at  $\delta$  0.94, correlated to the methine group on C-17 and to both methylene groups on C-22 at  $\delta$  34.4 and C-23 at  $\delta$  26.1. While H-22 at  $\delta$  2.36 gave a long correlation to C-28 at  $\delta$  23.1 and to the isopropyl group in C-25 at  $\delta$  29.6. An HMBC correlation was also observed from H-23 at  $\delta$  1.18 to methine C-24 at  $\delta$  45.8. Likewise, correlations were obtained on H-24 at  $\delta$  0.95 to C-25 at  $\delta$  29.7 and the methyl group C-29 at  $\delta$  12, respectively. In return, methyl group in H-29 at  $\delta$  0.87 was correlated back to C-24 and was directly correlated to C-28 at  $\delta$  23.1. The methyl group on H-26 at  $\delta$  0.83 correlated to methine C-25 and the methyl group on C-27 at  $\delta$  19.8. In return, H-27 at  $\delta$  0.86 correlated to C-26 at  $\delta$  19 and to C-28 at  $\delta$  23.1.

Therefore, the NMR spectral data for F20 was found to be in full agreement with those reported in literature (Manjari Mishra and Sree, 2009) for lawsaritol **2.1**, which was isolated from the *F. carica* endocarp as a white powder.

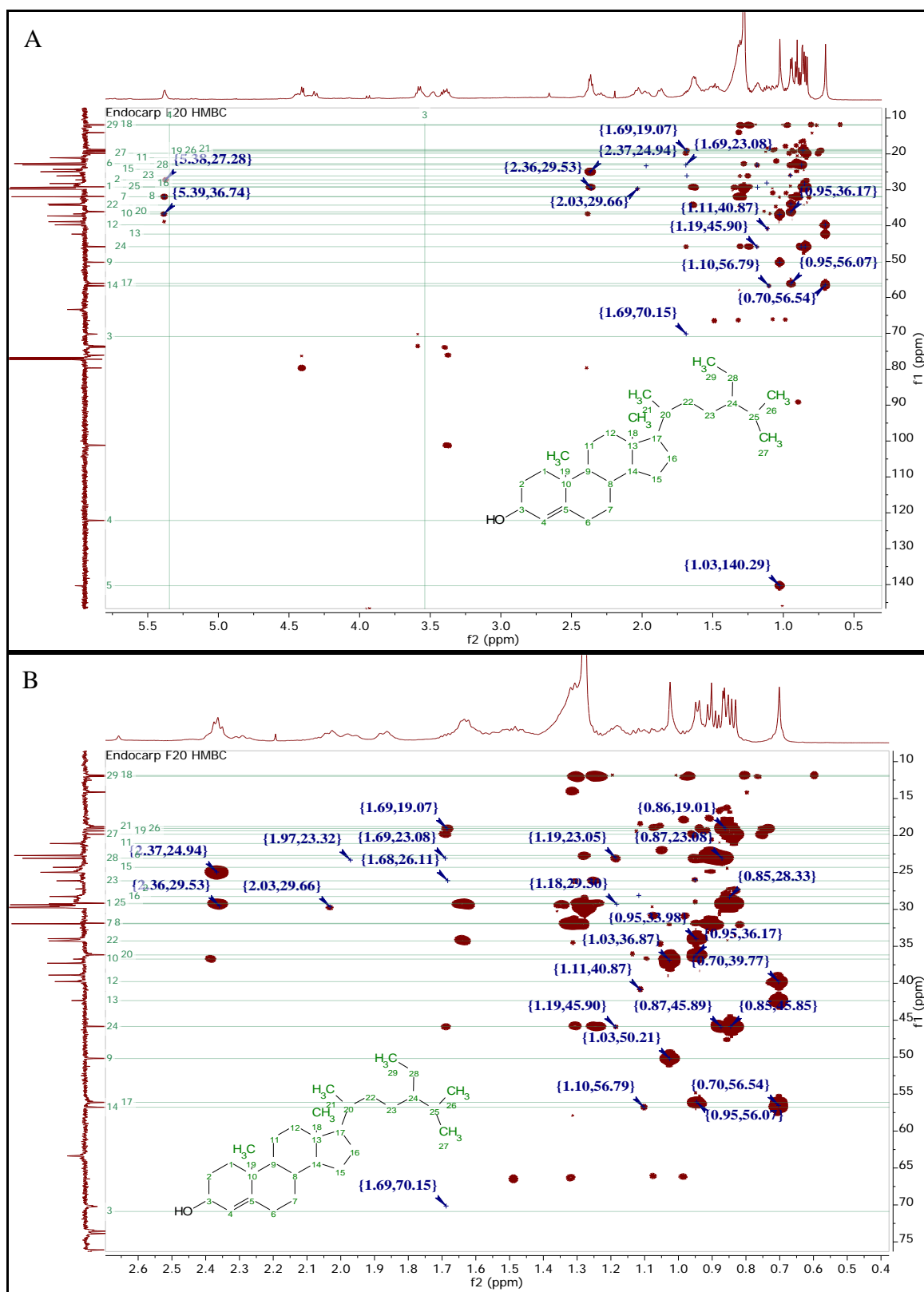


**Figure 4.17:** A)  $^1\text{H}$ - $^{13}\text{C}$ -HMBC spectrum of F20 elucidated as lawsaritol **2.1** in  $\text{CDCl}_3$  at 500MHz; X-axis represents H-NMR and Y-axis represents J-mod-NMR; horizontal lines

correspond to the carbon number in the structural drawing. **B)** Expansion of  $^1\text{H}$ - $^{13}\text{C}$ -HMBC spectrum of F20 in the upfield region.

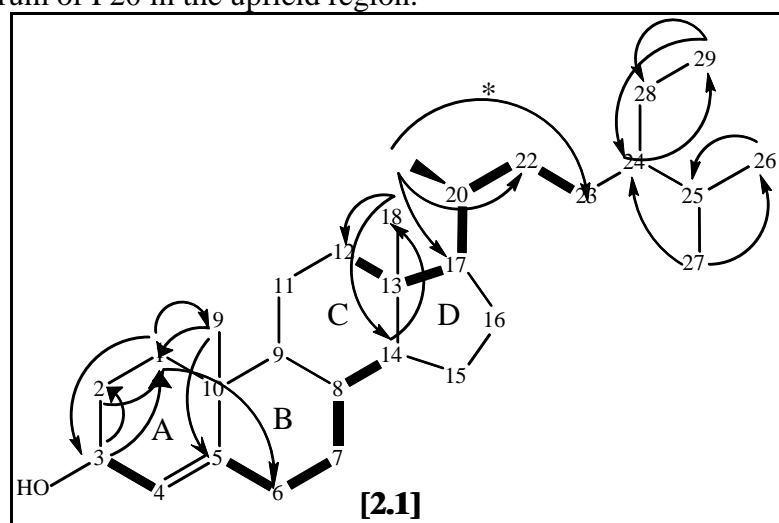


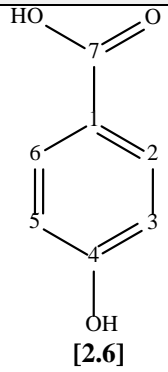
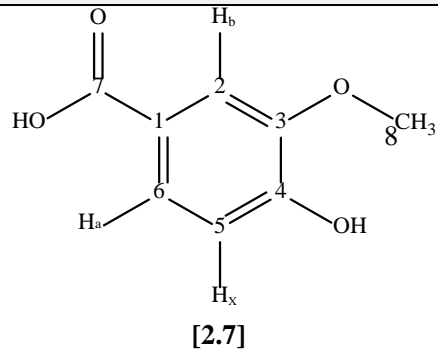
**Figure 4.18:** The  $^1\text{H}$ - $^1\text{H}$  COSY correlations of F20 elucidated as lawsaritol **2.1** were depicted in bold lines and the  $^1\text{H}$ - $^{13}\text{C}$  HMBC correlations are indicated by each carbon with arrows. The carbons were numbered according to IUPAC-IUB. (Detailed assignment of HMBC correlation is presented in Table 4.6). \* indicated  $4J$  coupling “W coupling”.

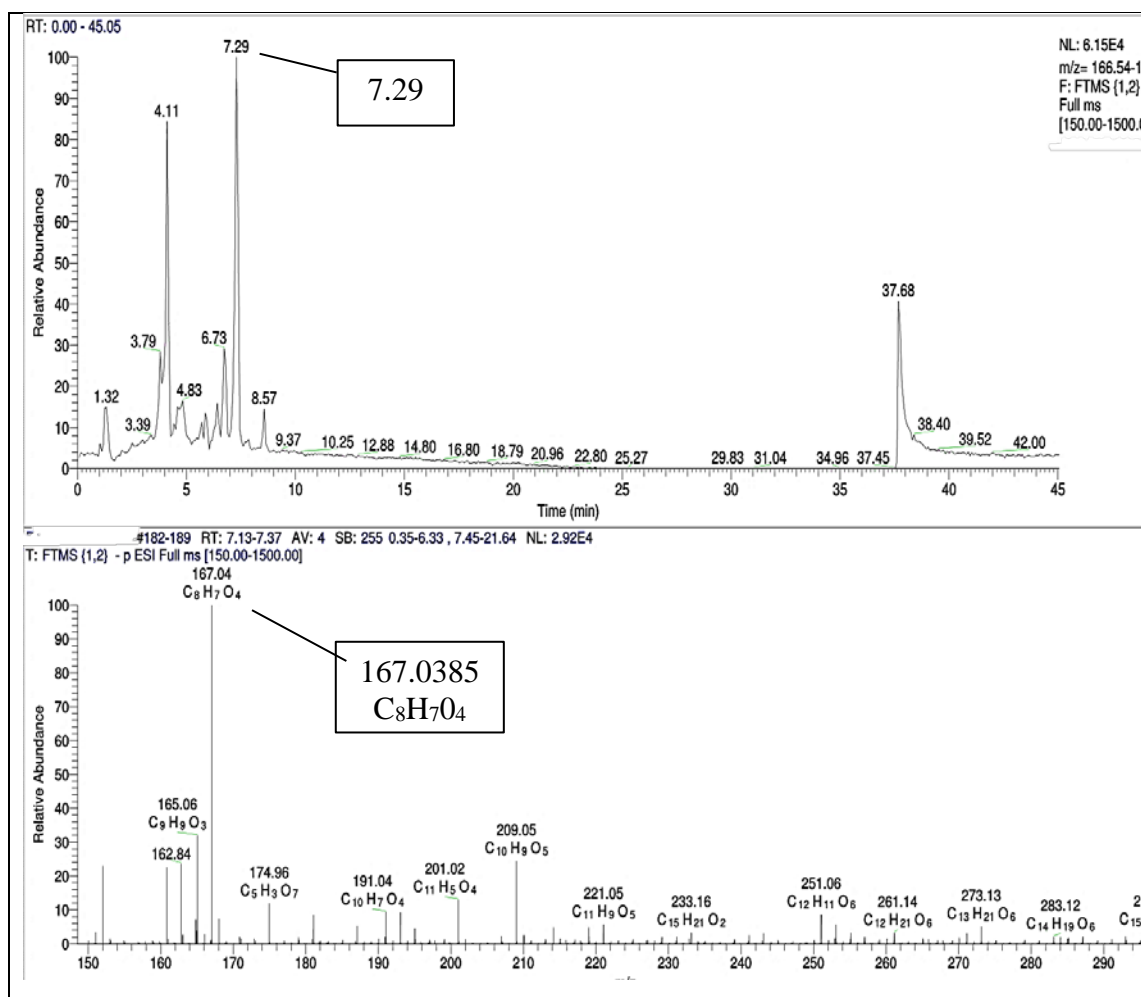
**Table 4.6:** Compound **2.1**;  $^1\text{H-NMR}$  (500 MHz) including integral, coupling constant and multiplicity,  $J$ -mod-NMR (125 MHz), HSQC data and HMBC correlation of lawsaritol and correlated literature at  $^1\text{H-NMR}$ , 400MHz in  $\text{CDCl}_3$  and  $^{13}\text{C-NMR}$  (100 MHz).

Atom No.	(F20) lawsaritol <b>2.1</b>			Literature (Manjari Mishra and Sree, 2009)	
	Integral, $\delta_{\text{H}}$ , multiplicity, $J$ in Hz	$\delta_{\text{C}}$	HMBC	Integral, $\delta_{\text{H}}$ , multiplicity, $J$ in Hz (400 MHz)	$\delta_{\text{C}}$ (100 MHz)
1	2H, 1.62, t, $J = 8.81$	29.2	3, 6, 19	2H, 1.25, ddd, $J = 16.11, 9.77, 5.37$	37.2
2	2H, 1.99, m	27.3	1	2H, 1.87, m	31.6
3	1H, 5.35, d, $J = 5.33$	70.2	1, 2, 10	1H, 5.35, d	71.8
4	1H, 3.53, m	122.1		1H, 3.5, m	121.7
5		140			140.7
6	2H, 1.26, m	22.7	9	2H, 1.33, m	25.4
7	2H, 1.87, m	31.9	6, 9	2H, 1.66, m	31.8
8	1H, 2.02, ddt, $J = 13.67, 5.04$	31.9	1, 6, 9	1H, 1.16, m	30.9
9		80.2			50.1
10		38.9			36.4
11	2H, 1.50, dt, $J = 39.19, 9.53$	21.1		2H, 2.03, m	21.1
12	2H, 1.26, m	39.8	8, 11	2H, 1.07, m	39.7
13		42.3			42.2
14	2H, 1.02, dt, $J = 14.90, 5.36$	56.8	9, 18	1H, 1.15, m	56.7
15		24.3	17	2H, 1.09, m	24.2
16	2H, 1.87, m	28.2		2H, 1.62, m	28.2
17	1H, 1.26, m	56.2	12, 16	2H, 1.42, m	56.0
18	3H, 0.67, s	11.9	12, 14	3H, 0.61, s	11.9
19	3H, 1.12, s	19.4	1, 5, 9	3H, 1.23, s	19.3
20	1H, 0.96, m	36.2			36.1
21	3H, 0.99, m	18.8	17, 22, 23	3H, 1.15, d	18.7
22	2H, 2.32, m	34.2	25, 28	2H, 1.54, m	33.9
23	2H, 1.26, m	26.2	24	2H, 1.26, m	26.0
24	1H, 0.91, m	45.9	25, 29	1H, 1.19, m	45.9
25	1H, 1.26, m	29.7		1H, 1.54, m	29.1
26	3H, 0.83, d, $J = 1.89$	19	25	3H, 0.83, d, $J = 6.8$	19.0
27	3H, 0.86, m	19.8	24, 26, 28	3H, 0.85, d, $J = 6.8$	19.8
28	2H, 0.91, m	23.1		2H, 1.15, m	23.0
29	3H, 0.91, m	12	24, 28	3H, 1.02, t, $J = 7.32$	11.8

#### 4.7.2. *P*-hydroxybenzoic acid 2.6 and vanillic acid 2.7

**Table 4.7:** Semi-pure F14 fraction of *F. carica* endocarp; *P*-hydroxybenzoic acid 2.6 and vanillic acid 2.7; chemical configurations; LCMS detection of 2.7 at Rt run 7.29 min.

<b><i>P</i>-hydroxybenzoic acid 2.6</b>	<b>Vanillic acid 2.7</b>
Synonym(s): 4-hydroxy-benzoic acid Source: Endocarp of <i>F. carica</i> Metabolite: Fraction F14 Sample amount: 6 mg Physical description: White amorphous powder with yellow gum Molecular formula: C <sub>7</sub> H <sub>6</sub> O <sub>3</sub> Exact Mass: 138.0317 g/mol	Synonym(s): 3-methoxy-4-hydroxybenzoic acid Source: Endocarp of <i>F. carica</i> Metabolite: Fraction F14 Sample amount: 6 mg Physical description: White amorphous powder with yellow gum Molecular formula: C <sub>8</sub> H <sub>8</sub> O <sub>4</sub> Exact Mass: 168.0423 g/mol
<b>Chemical structure</b>	<b>Chemical structure</b>
 <p>[2.6]</p>	 <p>[2.7]</p>
<b>LC-MS analysis 2.7</b>	



*P*-hydroxy benzoic acid **2.6** was obtained as white amorphous powder with yellow gum. TLC spot (see section 4.3) was visualised as blue spot.

The  $^1\text{H}$ - and  $^{13}\text{C}$ -NMR data of **2.6** (Table 4.8) were similar to those of a *P*-hydroxy benzoic acid described by Lu *et al.*, (2016).  $^1\text{H}$ -NMR spectrum (Figure 4.19) have shown one 1,4 tri-substituted aromatic ring with AA'BB' spin system due to structure symmetry which consists of two equivalent pairs of proton for both H-2/H-6 and H-3/H-5. H-2/H-6 at  $\delta$ 7.98 (2H, dd,  $J = 8.3$  MHz) was more de-shielded due to its ortho position to an electron withdrawing carboxylic group while H-3/H-5 at  $\delta$ 6.96 (2H, d,  $J = 8.25$  MHz) was shielded due to its ortho position to the electron donating hydroxyl group.

$^1\text{H}$ - $^1\text{H}$  COSY (Figure 4.20) confirmed that H-6 is adjacent to H-5 due to the direct correlation of their respective resonances at  $\delta$  7.98 and 6.96. Additionally, correlating signals between  $\delta$  7.98 and 6.96 revealed that H-3 is adjacent to H-2.

$^{13}\text{C}$ -NMR spectra of **2.6** were distinguished by HSQC (Figure 4.21), which revealed seven carbons, of which; six signals were assigned to the aromatic moiety. Two sets of symmetrical carbons were observed at  $\delta$  132.1 and 132.1 for C-2/ C-6 and C-3/ C-5, respectively. One hydroxyl bearing carbon for C-4 was observed at  $\delta$  160.7. One quaternary carbon for C-1 resonated at  $\delta$  121.5 while a carbonyl unit for C-7 was found at  $\delta$  173.8.

C-1 was confirmed by HMBC (Figure 4.22) cross peaks from both H-5 at  $\delta$  6.96 and H-3 at  $\delta$  6.96 to both C-1 at  $\delta$  121.8 and C-7 at  $\delta$  173.8. On the other hand, both H-6 at  $\delta$  7.98 and H-2 at  $\delta$  7.98 correlated with C-4 at  $\delta$  160.7 confirming that a hydroxyl group is attached on C-4 *para* to the carboxylic group on C-1. Consequently, the structure of **2.6** was determined as *P*-hydroxy benzoic acid.

Vanillic acid compound **2.7** was obtained as a white amorphous powder and its molecular formula,  $\text{C}_8\text{H}_8\text{O}_4$  was determined on the basis of ESI MS at  $m/z$  167.0385  $[\text{M}-\text{H}]^-$ . TLC spot (section 4.1.2) was distinguished as pink spot. The  $^1\text{H}$ -NMR spectrum of **2.7** in  $\text{CDCl}_3$  is presented on Table 4.8. The proton spectrum showed one methoxy singlet at  $\delta$  3.95, assigned to H-22 of the vanillic acid; and one 1,3,4-trisubstituted aromatic ring with ABX coupling patterns due to three different protons coupling to another at  $[\delta\text{H}_a$  7.70 (integral of 1H, dd,  $J = 8.3, 1.3$  MHz) as ortho to  $\delta\text{H}_x$  and meta to  $\delta\text{H}_b$ ;  $\delta\text{H}_b$  7.57 (integral of 1H, d,  $J = 1.9$  MHz) as meta to  $\delta\text{H}_a$ ; and  $\delta\text{H}_x$  6.87 (integral of 1H, d,  $J = 8.3$ ) which has a strong upfield chemical shielding effect due to ortho position to hydroxyl group acting as an electron donating as well as ortho coupling constant to  $\delta\text{H}_a$ ].

In addition to  $^1\text{H}$ - $^1\text{H}$  COSY (Figure 4.20) which confirmed a direct proton correlation of H-6 at  $\delta$  7.70 adjacent to H-5 at  $\delta$  6.87. The degree of unsaturated double bond was calculated  $[\frac{(2 \times \text{C} + 2) - \text{H}}{2}] = [\frac{(2 \times 8 + 2) - 8}{2}]$ , resulting in 5 DOU, which revealed four unsaturated double bonds to the benzene moiety and one double bond to the carbonyl moiety.

The  $^{13}\text{C}$ -NMR spectra of compound **2.7** was also distinguished by HSQC (Figure 4.22) and HMBC spectrum (Figure 4.23) and was showed in HSQC typical signals of vanillic acid of carbon signals including a conjugated carbonyl group at  $\delta$  170.3 in C-7, methoxy

group in C-8 at  $\delta$  56.2. In addition to the presence of ABX pattern system in the aromatic moiety distinguished to C<sub>a</sub>-2 at  $\delta$  125.1, C<sub>b</sub>-6 at  $\delta$  112.1 and C<sub>x</sub>-3 at  $\delta$  115.3.

In the HMBC spectrum (Figure 4.22 and Figure 4.23), a conjugated carbonyl group in OH at  $\delta$  7.60 gave a correlation to the carboxylic acid group on C-1 at  $\delta$  121.3 and the methoxy group in C-8 at  $\delta$  56.1. Likewise, proton H-8 at  $\delta$  3.95 afforded a long-range correlation with C-5 at  $\delta$  146.2 and the hydroxyl group at  $\delta$  150.7 in C-4. Moreover, a doublet of a doublet proton signal at  $\delta$  7.70 on H-2 correlated with carbons C-4 at  $\delta$  150.7, C-6 at  $\delta$  112.1, and C-7 at  $\delta$  170.3. The *meta* proton doublet at  $\delta$  7.57 on H-6 revealed a long-range correlation with C-2 at  $\delta$  125.1, C-4 at  $\delta$  150.7, C-5 at  $\delta$  146.2 and C-7 at  $\delta$  170.3. The *ortho* proton doublet at  $\delta$  6.87 on H-3 yielded long-range correlation with C-1 at  $\delta$  121.3, C-4 at  $\delta$  150.7, and C-15 at  $\delta$  146.2. HMBC correlations confirmed the attachment of one oxygenated methylene, one hydroxyl group and a carboxylic acid at C-3, C-4 and C-1, respectively, resulting to the elucidation of **2.7** as vanillic acid.

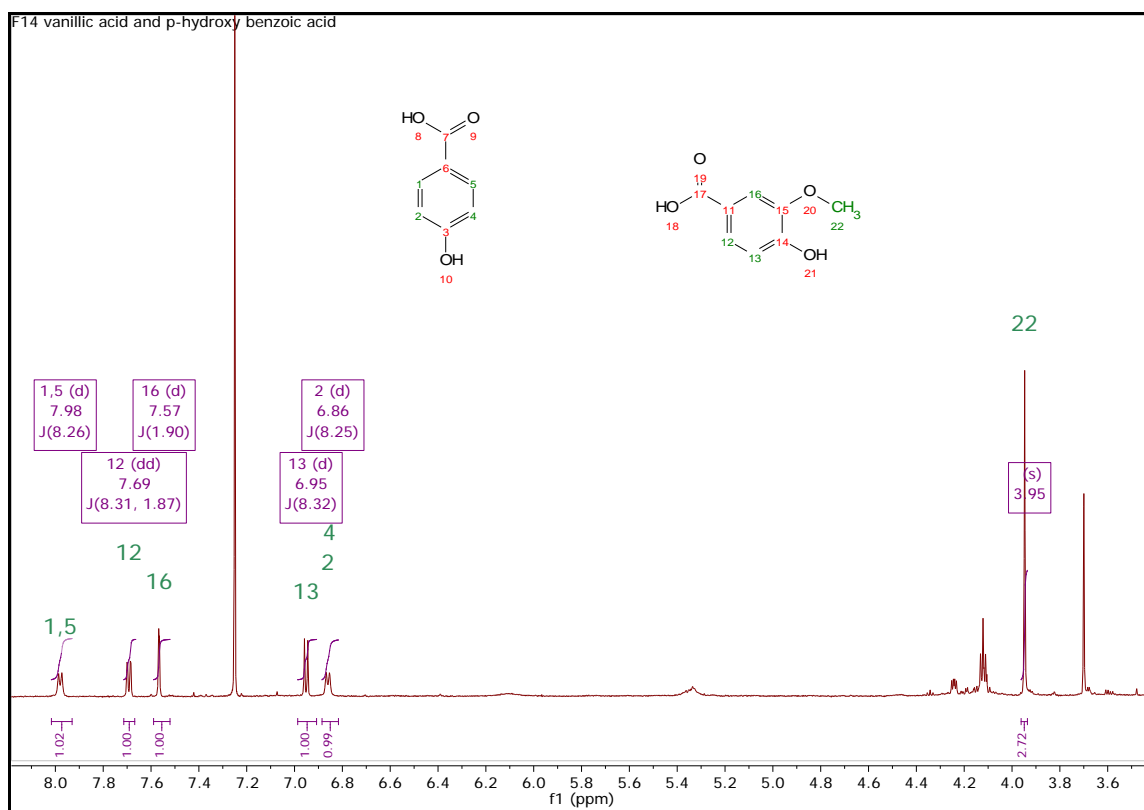


**Figure 4.19:**  $^1\text{H-NMR}$  spectrum of F14 consisting of both *P*-hydroxy benzoic acid **2.6** and vanillic acid **2.7** dissolved in  $\text{CDCl}_3$  and run at 500 MHz.

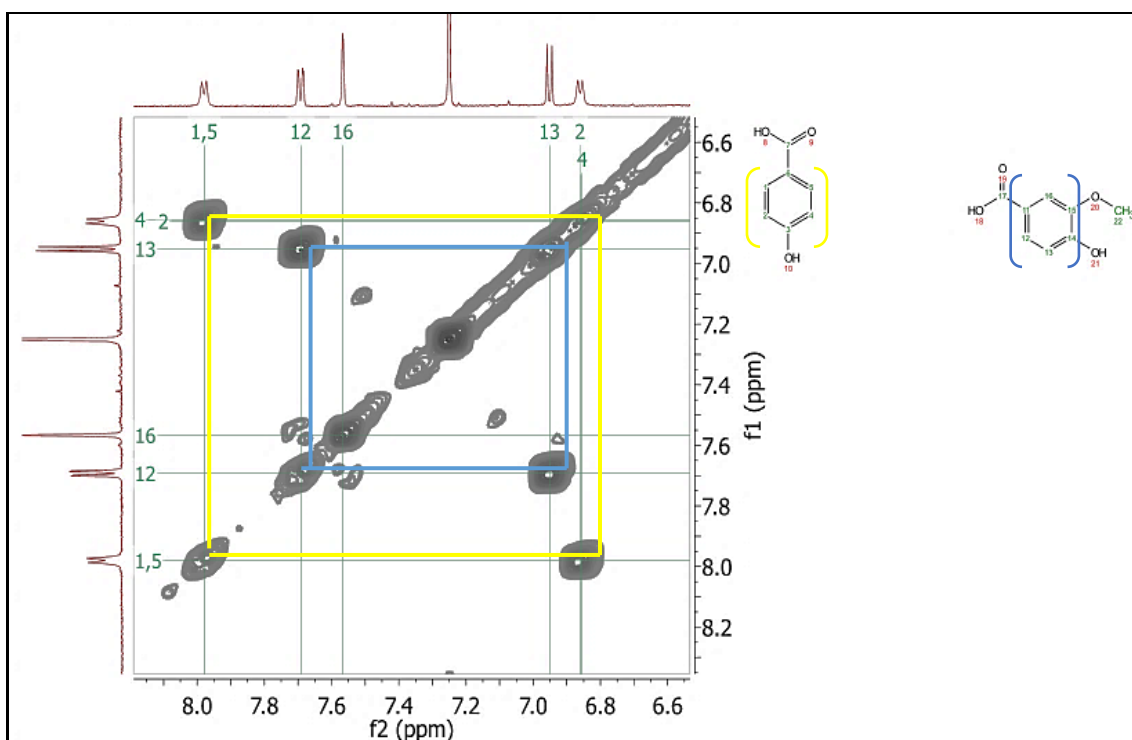


**Figure 4.20:** Cosy spectrum for F14 revealing two spin systems; blue line for vanillic acid; and yellow line for *P*-hydroxybenzoic acid.

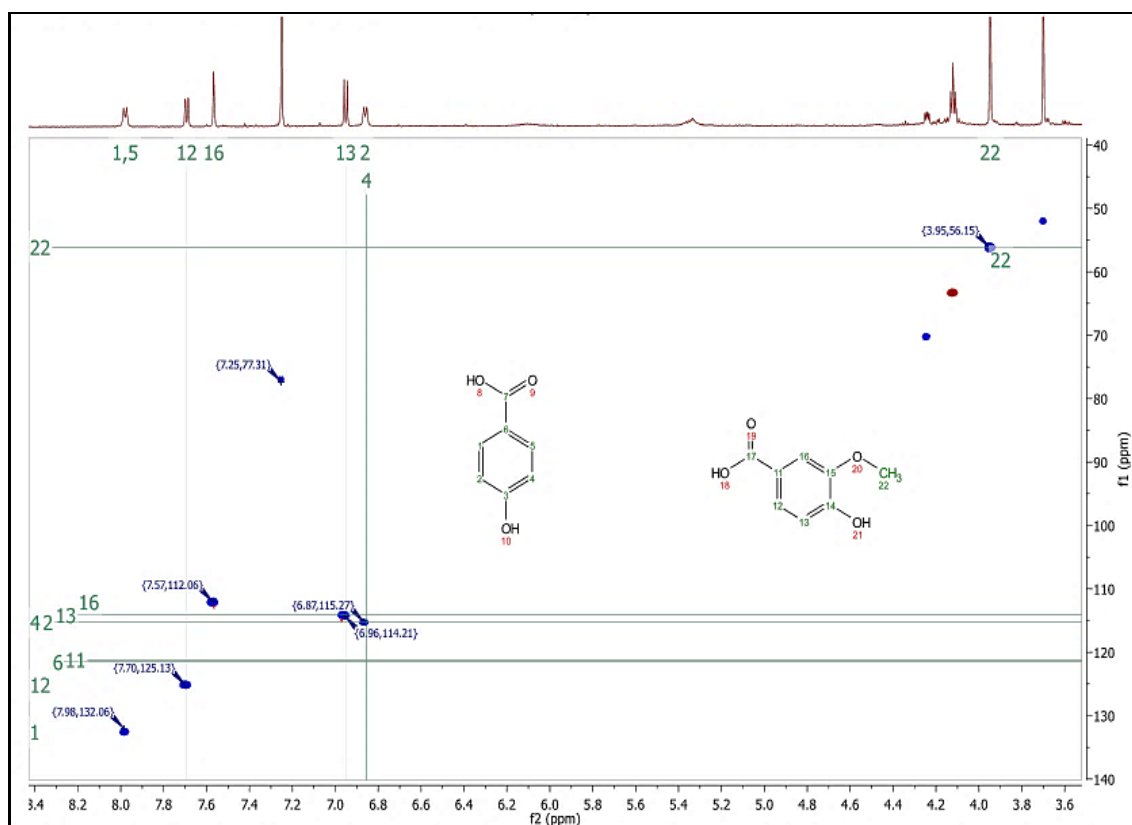


**Figure 4.21:** HSQC spectrum of F14 for *P*-hydroxybenzoic acid **2.6** and vanillic acid compound **2.7** in  $\text{CDCl}_3$  at 500MHz.

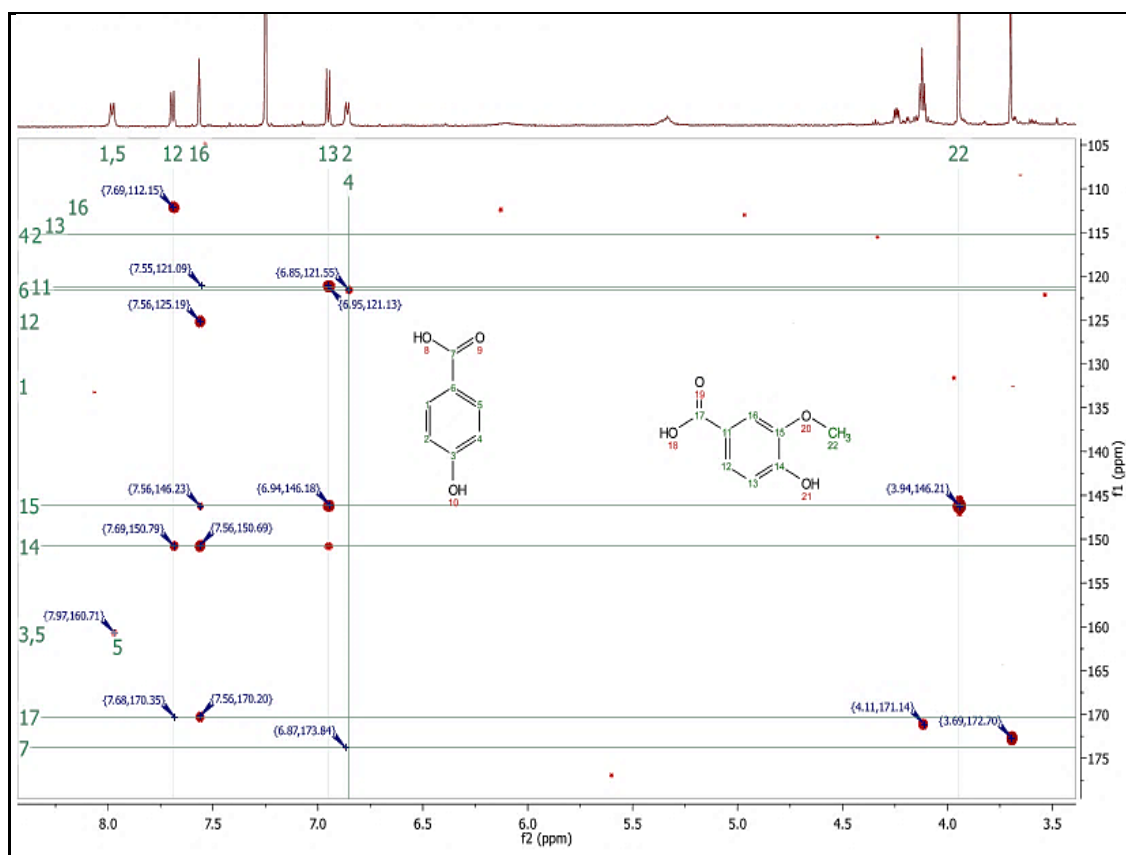


**Figure 4.22:** -HMBC spectrum of F14 for *P*-hydroxybenzoic acid **2.6** and vanillic acid compound **2.7** in  $\text{CDCl}_3$  at 500MHz

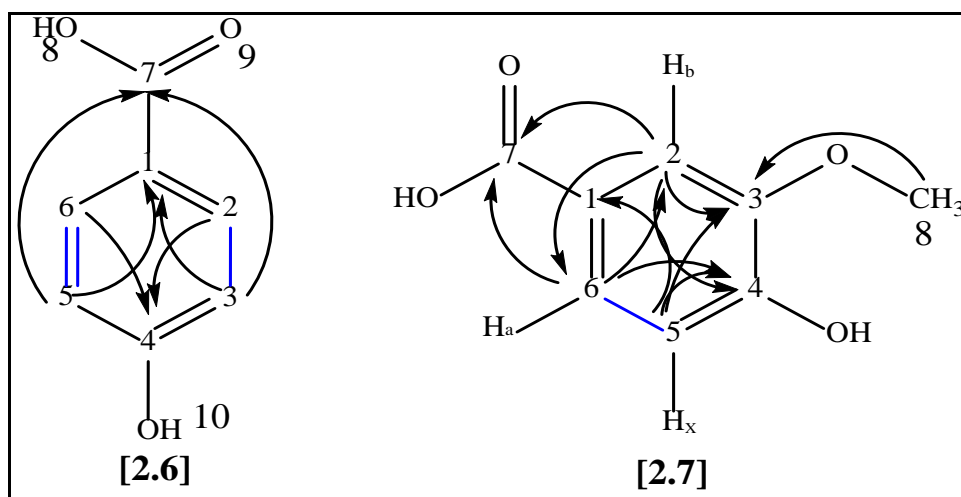


**Figure 4.23:** The  $^1\text{H}$ - $^1\text{H}$  COSY correlations of *P*-hydroxybenzoic acid **2.6** and vanillic acid compound **2.7** depicted in vibrant blue lines and the  $^1\text{H}$ - $^{13}\text{C}$  HMBC correlations are indicated to their correlation of carbon as each in arrows.

**Table 4.8:** Compounds **2.6**;  $^1\text{H-NMR}$  (500 MHz), including integral, coupling constant and multiplicity, HSQC and HMBC correlation of **2.6** and **2.7** exhibited consistency with previous studies.  $^1\text{H-NMR}$  was recorded at 400MHz in  $\text{CDCl}_3$  and HSQC and HMBC at 500 MHz.

Atom No.	<i>P</i> -hydroxybenzoic Acid <b>2.6</b>			Literature (Alqasoumi <i>et al.</i> , 2014; Lu <i>et al.</i> , 2016)	
	Integral, $\delta\text{H}$ , multiplicity, $J$ in Hz	$\delta\text{C}$ (125 MHz)	HMBC	Integral, $\delta\text{H}$ , multiplicity, $J$ in Hz (500 MHz)	$\delta\text{C}$ (125 MHz)
1		121.3			121.9
2	1H, 7.98, d, $J = 8.26$	132.1	4	1H, 7.79, d, $J = 7.95$	132.0
3	1H, 6.86, d, $J = 8.25$	114.2	1, 7	1H, 6.81, d, $J = 7.95$	115.5
4				1H, 10.25, br s	162.0
5	1H, 6.86, d, $J = 8.25$	114.2	1, 7	1H, 6.81, d, $J = 7.95$	115.5
6	1H, 7.98, d, $J = 8.26$	132.1	4	1H, 7.79, d, $J = 7.95$	132.0
7		172.7			178.4

**Table 4.9:** Compounds **2.7**;  $^1\text{H-NMR}$  (500 MHz), including integral, coupling constant and multiplicity, HSQC and HMBC correlation of **2.7** exhibited consistency with previous studies.

Atom No.	Vanillic acid <b>2.7</b>			Literature (Alqasoumi <i>et al.</i> , 2014; Lu <i>et al.</i> , 2016)	
	Integral, $\delta\text{H}$ , multiplicity, $J$ in Hz	$\delta\text{C}$ (125 MHz)	HMBC	Integral, $\delta\text{H}$ , multiplicity, $J$ in Hz (500 MHz)	$\delta\text{C}$ (125 MHz)
1		121.3			121.7
2	1H, 7.69, dd, $J = 8.31$ , 1.87	125.3	4, 6, 7	1H, 7.52, dd, $J = 8, 2$	123.5
3	1H, 6.95, d, $J = 8.32$	114.2	1, 4, 3	1H, 6.85, d, $J = 8$	114.9
4		150.7			150.9
5		146.2			147.1
6	1H, 7.57, d, $J = 1.90$	112.1	6, 4, 3, 7	1H, 7.47, d, $J = 2$	112.6
7		170.3	1, 8		167.4
8	3H, 3.95, s	56.2	3, 4	3H, 3.81, s	55.42

## **CHAPTER FIVE EXOCARP RESULTS**

---

## **5 Isolation and identification of bioactive metabolites from the exocarp of *Ficus carica* and their bioactivity on differentiated SH-SY5Y neuronal cell line**

---

The focus of this chapter is to characterise the phytochemical composition of the exocarp obtained from *F. carica* fruit. By using REVELERIS<sup>®</sup> flash and thin layer chromatography, the required purification process was accomplished. In addition, high resolution LC-MS was employed for metabolomics profiling. Isolated compounds were identified using NMR and GC-MS for steroidal compounds. Finally, an evaluation of its biological potential was conducted to establish the impact of oxidative stress triggered by acrolein on a differentiated SH-SY5Y cell line, with which no previous study has been described earlier

### **5.1 The isolation of *F. carica* exocarp**

The normal phase flash chromatography separation of the crude extract was performed on a 40g 40 µm silica column with REVELERIS<sup>®</sup> solid sample loader by gradient elution as summarised in Table 5.1. A total of 21 fractions was obtained from this process (Figure 5.1); from which F2, F3, F4, F15, F18, and F19 were subjected to additional flash chromatographic sub-fractionation due to their bio-activity effect, interesting NMR spectral data and metabolomics profile, affording a total of 51 sub-fractions (Figure 5.1). The sub-fractions were then further purified on REVELERIS<sup>®</sup> silica by gradient elution as summarised in Table 5.1.

**Table 5.1:** Chromatographic conditions employed for the purification of the crude and sub-fractions of the exocarp, via the REVELERIS<sup>®</sup> flash chromatography system (Grace Davison Discovery Sciences, USA). EtOAc, MeOH and DCM represent ethyl acetate, methanol and dichloromethane, respectively.

Description	Crude	Sub-fraction					
		F2	F3	F4	F15	F18	F19
Silica column size (gram)	40	4	12	12	4	4	4
Flow rate mL/min	40	12	10	10	10	10	10
Duration min	112.6	37.9	86.7	67	10.8	41.1	15
ESLD threshold (mV)	20	20	20	20	20	20	20
UV1 wavelength (nm)	254	254	254	254	254	254	254
UV2 wavelength (nm)	280	280	280	280	280	280	280
Sample loading	Dry	Dry	Dry	Dry	Dry	Dry	Dry
Solvent A	Hexane	Hexane	Hexane	Hexane	Hexane	Hexane	Hexane
Solvent B	EtoAc	EtoAc	EtoAc	EtoAc	EtoAc	EtoAc	EotAc
Solvent C	MeOH	-	-	-	MeOH	-	MeOH
Solvent D	DCM	-	-	-	DCM	-	DCM

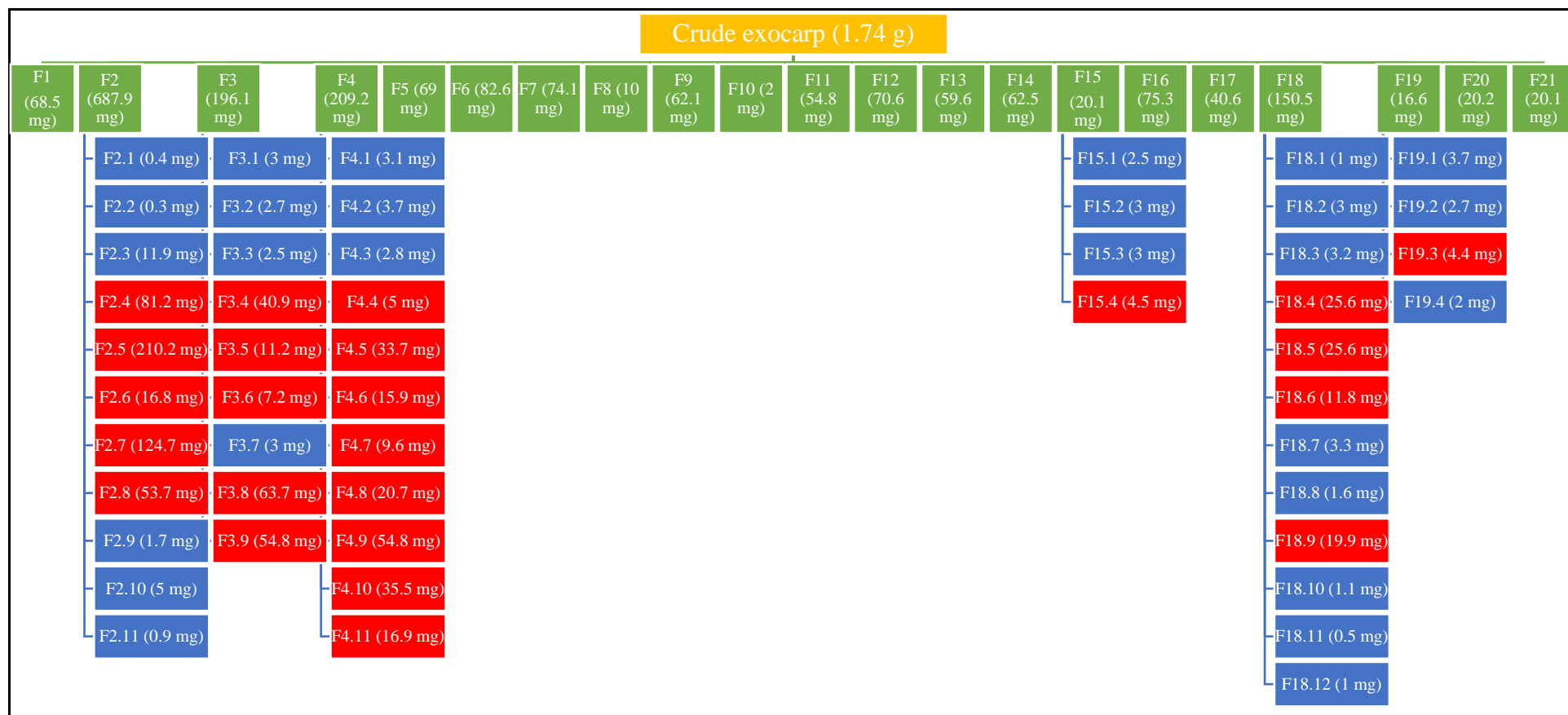


**Figure 5.1:** The fractionation scheme for the crude *F. carica* exocarp (1.74 g) extract affording 21 fractions (green box). Further fractionation of the bioactive fractions F2, F3, F4, F15, F18 and F19 yielded an additional of 51 sub-fractions. Fractions in blue coloured boxes were excluded from further work due to their low yield, while the rest of the fractions in red boxes were subjected for further bioassays and elucidation work.

### 5.1.1 Normal phase REVELERIS® flash chromatography from crude extract

Normal phase REVELERIS® flash chromatography was employed in order to attain an adequate separation of polar compounds, such as polyphenols with which chlorophyll and tannins were largely associated along with short-chained fatty acids (Lawton *et al.*, 1999; Yu *et al.*, 2013; Yvon *et al.*, 2013). The chromatographic separation of *F. carica* exocarp crude extract afforded 21 fractions (Figure 5.1) by gradient elution commencing with 100% hexane to 100% ethyl acetate in 97.1 minutes followed by 100% dichloromethane to 70% dichloromethane and 30% methanol in 15.5 minutes. The combination of ELSD and UV detectors at 254nm and 280nm revealed the richness of chromatographic responses exhibited by the crude extract. This indicated that the presence of compounds reactive to ELSD, such as terpenes and unsaturated fatty acids (Kirke *et al.*, 2017). F1 to F18 were eluted by the mobile phase of hexane and ethyl acetate, while F19 to F21 were eluted by dichloromethane and methanol. Even though fractions of F19 to F21 were UV active, they were not considered for further analysis due to their weak bioactivity (see section 5.2.1) as well as their uninteresting <sup>1</sup>H-NMR spectral data (see section 5.1.4). Bioactive fractions F2, F3, F4 and F18 were further subjected to sub fractionation as shown below in section 5.1.2.

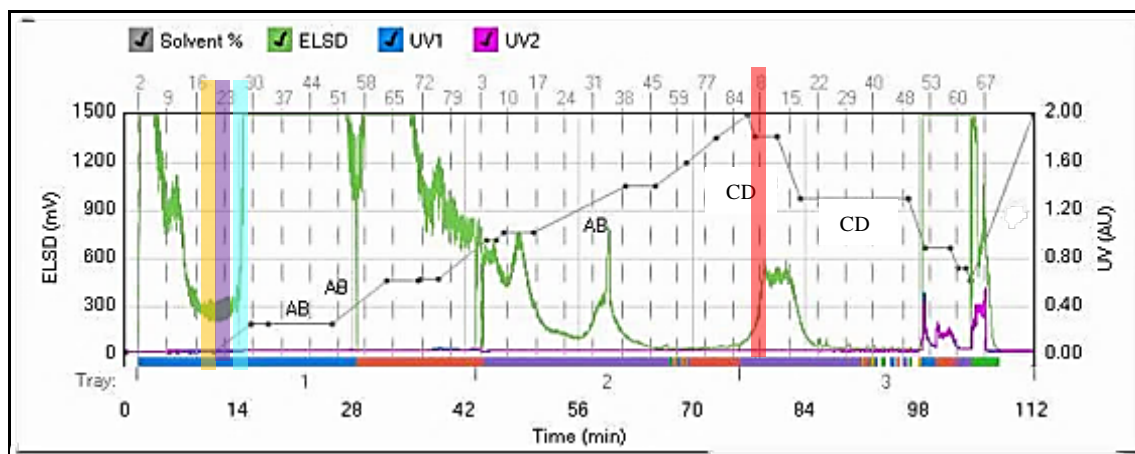


**Figure 5.2:** Normal phase REVELERIS<sup>®</sup> flash chromatogram of the crude exocarp extract. The pink, blue, and green lines represented the chromatogram detected by UV1 at 254nm, UV2 at 280nm, and ELSD, respectively. AB indicated the hexane and ethyl acetate mobile phase solvent ratio and CD indicated the dichloromethane and methanol used for gradient elution. The fractions of interest, F2, F3, F4, and F18, which were subjected for further purification work, were highlighted in orange, purple, light blue and red bars, respectively.

### 5.1.2 Normal phase REVELERIS<sup>®</sup> flash chromatography for purification

According to their bioactivity (see section 5.2) and high yield, F2 (687.9 mg), F3 (196.1 mg), F4 (196.1 mg) and F18 (150.5 mg) were selected from the 21 fractions, for further purification work by normal phase flash chromatography to eliminate simple sugars, chlorophyll and tannins (Kirke *et al.*, 2017). In the case of F3 (Figure 5.3B), F4 (Figure 5.3C), F15, F18 and F19 (Figure 5.4A, 5.4B and 5.4C), a flow rate of 10 mL/min was used, while for of F2 as shown in Figure 5.3A, it was slightly higher at 12 mL/min. The flow rate was optimised to prevent peak broadening resulting to sharp symmetrical peaks.

UV (254 nm and 280 nm) and ELSD permitted the detection of the elution of the fractions yielding well-resolved sharp peaks between 2-12 min as illustrated in Figures 5.3 and 5.4, while peaks were more crowded between 18 and 34 minutes. F2, F3, F4, and F15 were chromatographed by gradient elution using, while F18 and F19 were eluted with dichloromethane and methanol. Optimisation of the solvent system used for MPLC and flash chromatography was optimised by TLC.

A total of 51 sub-fractions was obtained during chromatographic purification of the selected fractions. Based on their TLC traces, (section 5.1.3), <sup>1</sup>H-NMR (section 5.1.4) and mass spectral data (section 5.3.1), as well as bioactivity (section 5.2), particularly notable were

F2.6 (4.9 mg) derived from F2, F3.8 (63.7 mg) from F3, F4.9 (44 mg) from F4, F15.4 (4.5 mg) from F15, F18.6 (11.8 mg) from F18 and F19.3 ( 4.4 mg) from F19, which were highlighted in light blue, purple, orange, red, yellow and brown bars, respectively. However, F15.4 and F19.3 were discontinued for elucidation work (section 5.4) as well as cytotoxicity (section 5.2.2) and western blotting tests (see section 5.2.3) due to their low yields.

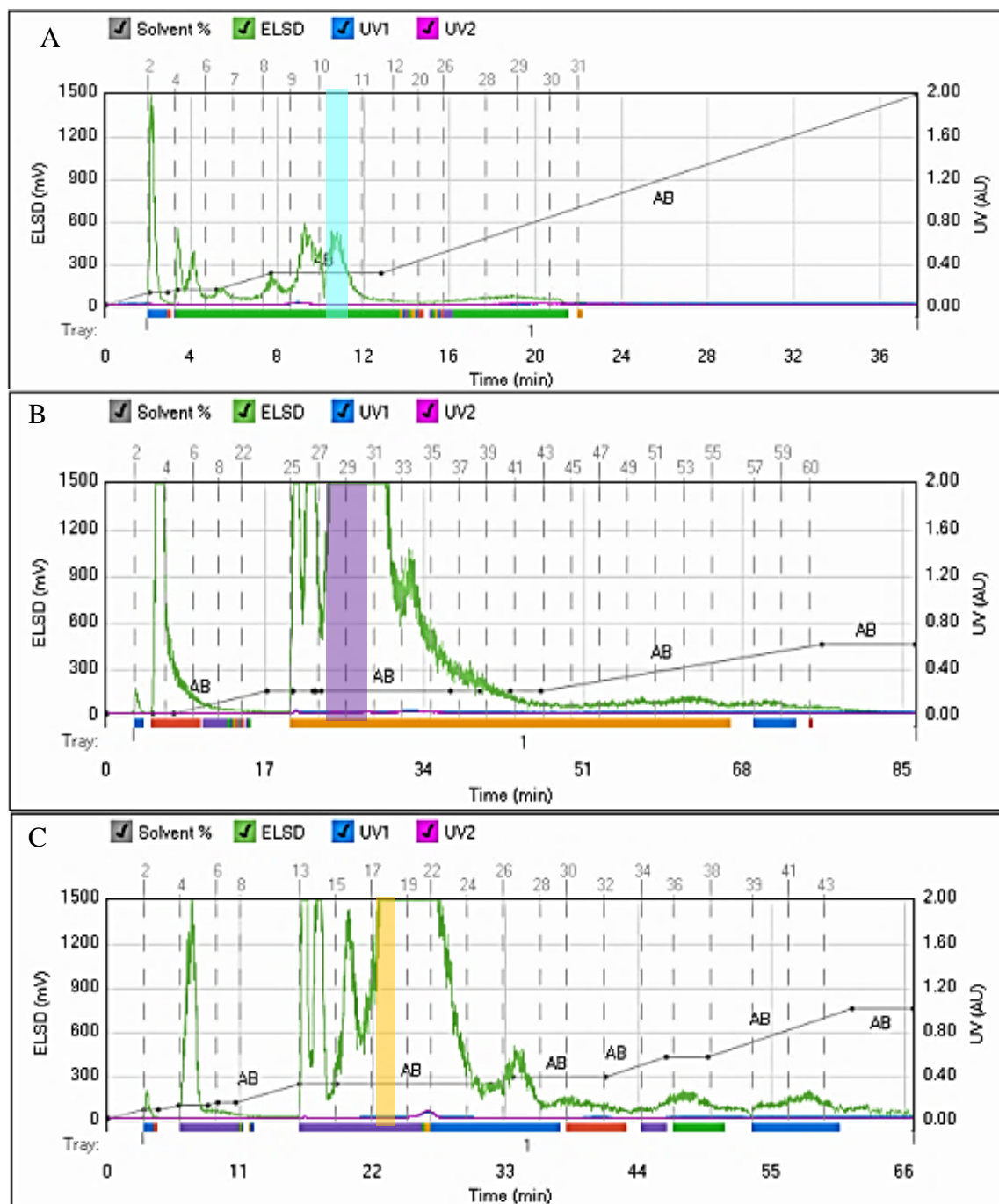


**Figure 5.3:** Normal phase REVELERIS® flash chromatograms of fractions F2 (A) F3 (B) and F4 (C) employing the ELSD detector as shown by the green peaks. AB indicated gradient elution with hexane and ethyl acetate ratio. The semi-purified sub-fractions of interest, F2.6, F3.8 and F4.9 were highlighted with light blue, purple and orange bars, respectively.

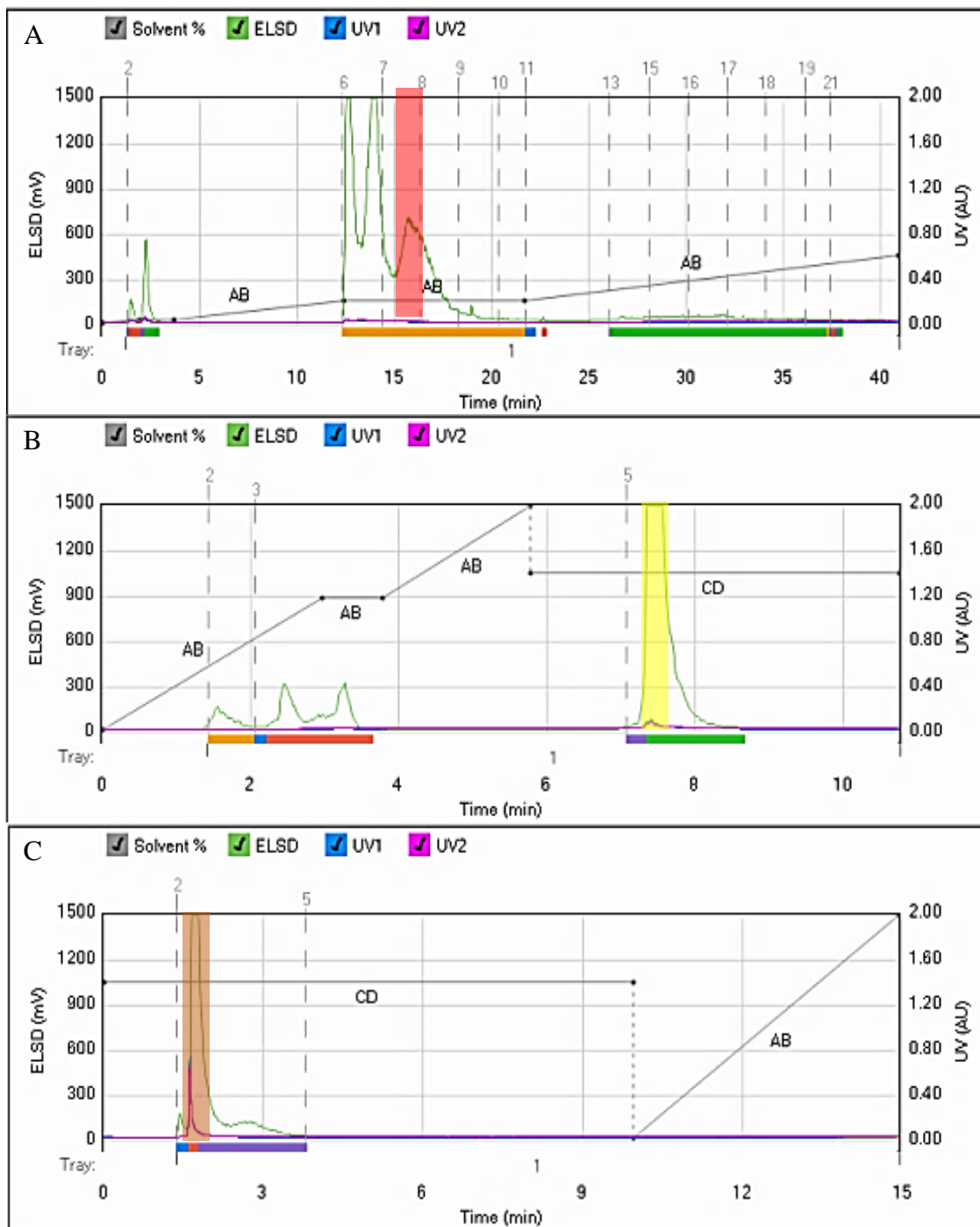


**Figure 5.4:** Normal phase REVELERIS<sup>®</sup> flash chromatograms of fractions F15 (A) F18 (B) and F19 (C) employing the ELSD detector as shown by the green peaks. AB indicated the step gradient elution with hexane and ethyl acetate and CD indicated isocratic elution by dichloromethane and methanol. The semi-purified sub-fractions of interest, F15.4, F18.6 and F19.3 were highlighted with red, yellow and brown bars, respectively.

### 5.1.3 TLC screening

The same TLC technique described in the methodology section was adopted in order to ensure the optimisation of the conditions for chromatographic conditions. Additional analysis was conducted on sub-fractions from F2, F3, F4, F15, F18 and F19 due to their positive preliminary biological screening results (see section 5.2.1).

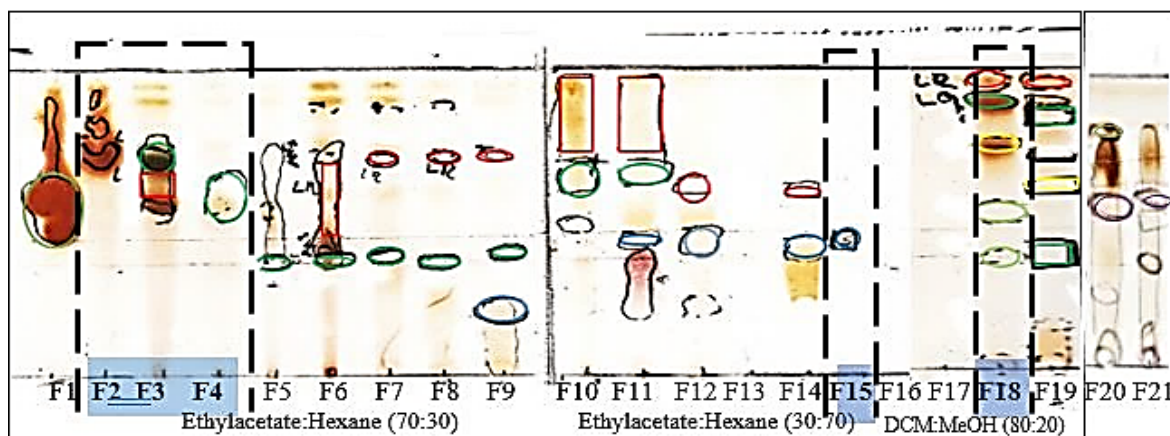


**Figure 5.5:** TLC screening of 21 fractions obtained from the crude exocarp extract. Coloured circles, squares and rectangles were allocated to those spots visualised under UV at 365nm. Colours used represent the same colour visualised by 365 nm. Spots detected under 254nm were drawn with a black contour line. *P*-anisaldehyde/sulfuric acid spray reagent was also used to visualise other secondary metabolites.

As shown in Figure 5.6  $R_f$  values were determined for F2.6, F3.8, F4.9, F15.4, F18.6, and F19.3, as 0.8 (F2.6 and F19.3), 0.4 (F3.8, F4.9 and F15.4) and 0.6 (F18.6) for the purified and semi-purified fractions of interest. These selected bioactive fractions were subjected to further isolation work.

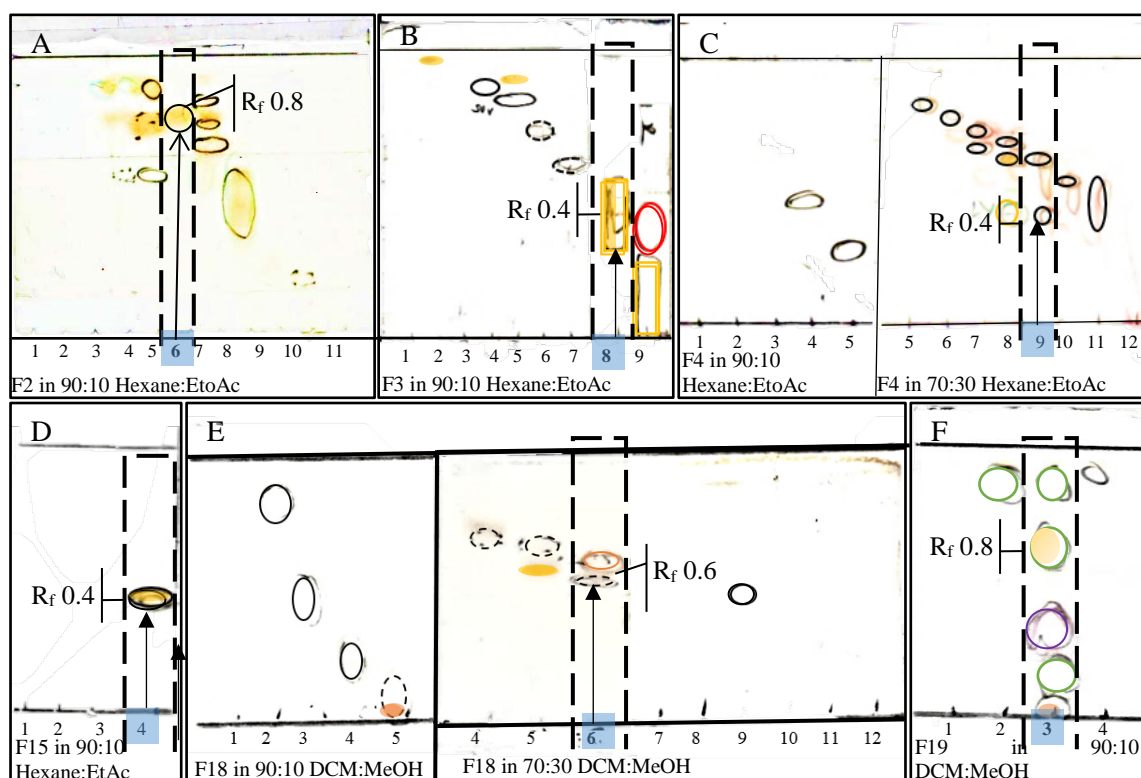


**Figure 5.6:** TLC plates showing the elution of **A)** F2.6, **B)** F3.8, and **D)** F15.4 in 90:10 v/v of ethyl acetate and hexane, represented as semi-brown to brown spots, with the elution of **C)** F4.9 in a 70:20 v/v ratio of hexane and ethyl acetate, represented as reddish-brown spot, together with **E)** F18.6 and **F)** F19.3 in a 70:20 v/v ratio and in a 90:10 v/v ratio of dichloromethane and methanol, respectively after spraying with *P*-anisaldehyde- $H_2SO_4$  reagent, respectively.

#### 5.1.4 $^1H$ -NMR spectra of exocarp fractions

During components visualisation on TLC, spots may overlap because their  $R_f$  values of phytosterols are not significantly different (Azadmard-Damirchi, 2010). A preliminary  $^1H$ -NMR experiment was accomplished on the bioactive fractions and sub-fractions of the *F. carica* exocarp (section 5.2) to monitor their purity. The stacked spectra of the bioactive sub-fractions of *F. carica* exocarp extract are shown in Figure 5.7. The presence of aliphatic structures resonating as complex signals in the region between  $\delta$  0.5 and 2.5 ppm was observed. Deshielded aliphatic groups were caused by the presence of olefinic signals occurring at  $\delta$  3.0 to 5.5, as electronegative atoms such as O, N, C=C, and C=O could be directly attached to the alkyl group (CH). As a result, the electron density surrounding the protons decreased concurrently with the diminishing shielding effect (Watson, Edrada-Ebel and Patel, 2017). It could be thus be deduced that *F. carica* was rich in phytosterols compounds and their esters as indicated by the peaks in the *F. carica* exocarp spectrum.

F2.6, F3.8 and F4.9 were predicted to contain phytosterols, whilst F18.6 exemplified the presence of a long-chain fatty acid that was also detected in the mesocarp fraction **1.2**.

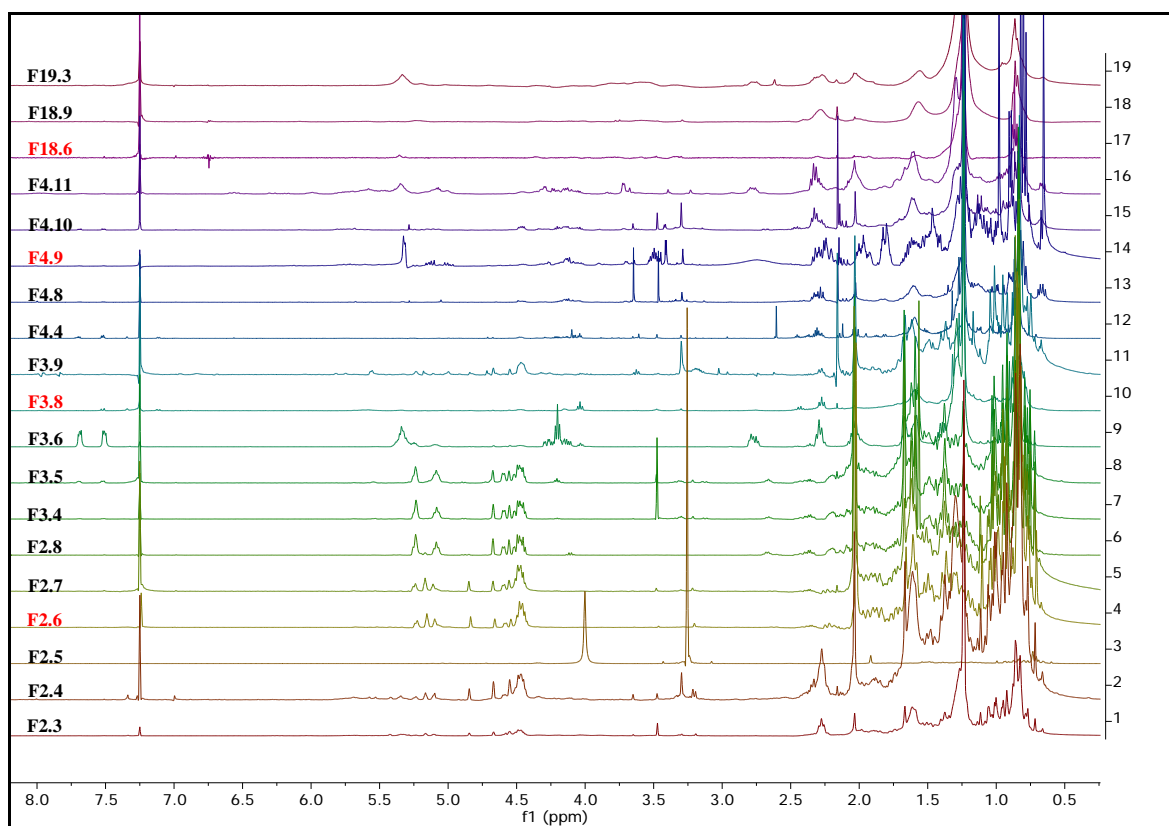


**Figure 5.7:** Stacked <sup>1</sup>H-NMR (400 MHz, CDCl<sub>3</sub>) spectra of bioactive sub-fractions. F2.6, F3.8 and F4.9 presented features of phytosterol derivatives whereas F18.6 displayed features of fatty acid derivatives-extracted from *F. carica* exocarp.

## 5.2 Biological assay

### 5.2.1 Cell viability test

*F. carica* exocarp fractions were subjected to preliminary cell viability screening. The AlamarBlue® assay was employed in order to assess the fractions in relation to an *in vitro* differentiated SH-SY5Y cell line (Figure 5.8). The extracts were classified as being active when cell viability exceeded 100%. Ten fractions, namely F1 (108%), F2 (114%), F3 (111%), F4 (114%), F6 (104%), F7 (105%), F8 (110%), F15 (105%), F18 (113%) and F19 (111%) (Figure 5.8) were found active. Among the bioactive fractions, those with the highest viability were F2, F3, F4, F8, F18 and F19. Therefore, these fractions were subjected for further fractionations as mentioned above in section 5.1.2 and cell viability screening as shown below in Figure 5.9 except for F8 due to its small yield (10 mg). The bioassay was conducted thrice and they exhibited significance at  $p < 0.05$ .

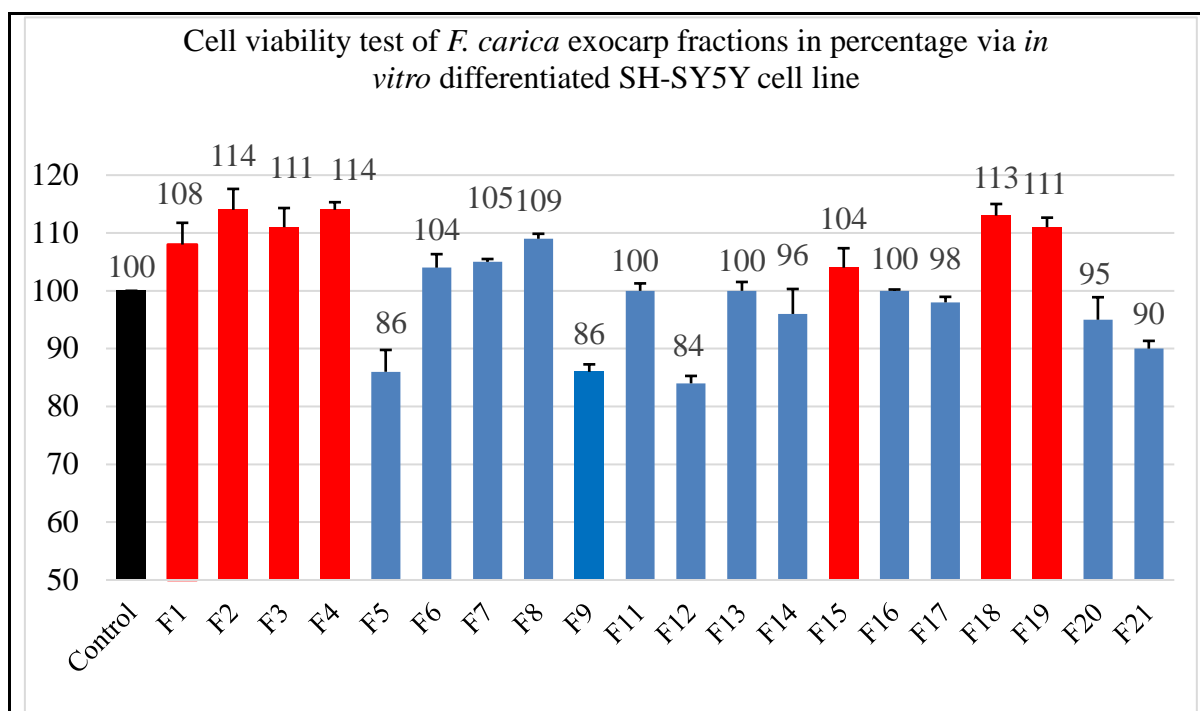


**Figure 5.8:** Preliminary cell viability screening of the fractions of *F. carica* exocarp in differentiated SH-SY5Y cells. Viability was displayed by 10 fractions with values higher than 100% (red), while 10 fractions lacked viability, with values of equally or less than 100% (blue); the control (100%) is shown in black. Every group constituted a mean of 3 SDs, and ANOVA was significant ( $P < 0.05$ ) by comparison to the control.

Significant cell viability was exhibited by 19 sub-fractions, namely F2.4 to F2.8, F3.4 to F3.6, F3.8, F3.9, F4.4, F4.6 F4.8 to F4.11, F18.6, F18.9, and F19.3 (Figure 5.9). Among the bioactive fractions, those with the highest viability were F2.6 (158%), F4.9 (134%), F3.8 (133%) and F18.6 (131%) were subjected to further examination for their cytotoxicity (Figure 5.10). In general, cell viability screening was obtained in order to predict the potential for their bioactivity effect against oxidative-related AD.

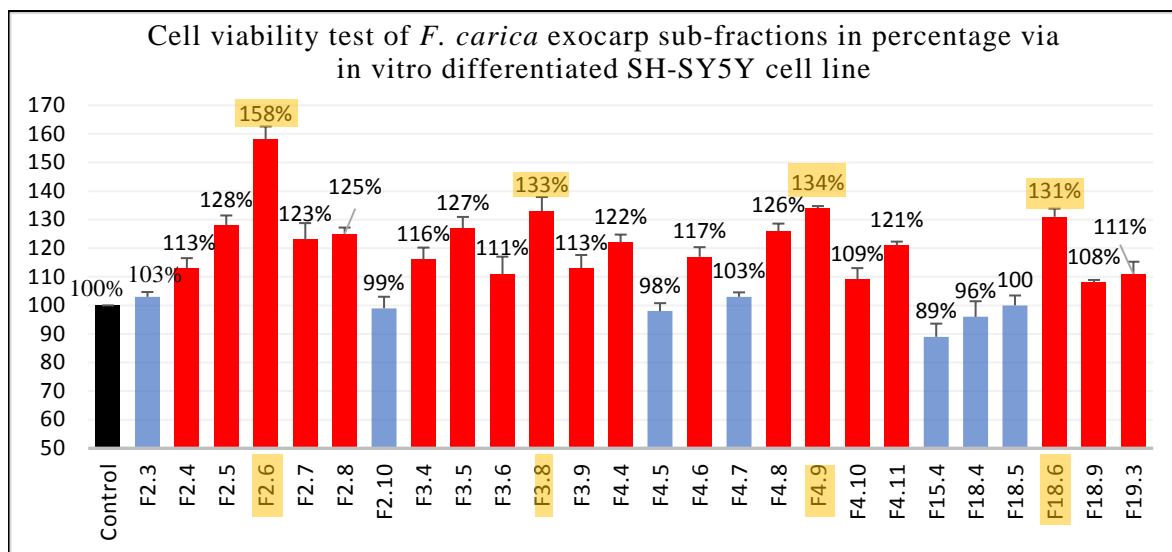


**Figure 5.9:** Preliminary cell viability screening of the sub-fractions of *F. carica* exocarp in differentiated SH-SY5Y cells. Viability was displayed by 19 fractions with values greater than 100% (red), while seven fractions lacked viability, with values of less than 100% (blue); the control (100%) is shown in black. Every group constituted a mean of 3 SDs, and ANOVA was significant at  $P < 0.05$  by comparison to the control. Highlighted in yellow are the most bioactive fractions.

## 5.2.2 Cell cytotoxicity test

The oxidation-reduction potential of the isolated compounds was evaluated by means of an AlamarBlue® *in vitro* differentiated SH-SY5Y cell line. This reduction test is helpful in investigating proliferation and cytotoxicity in a culture of actively growing cells (Imamura *et al.*, 2006). Cytotoxicity test was performed, by inducing oxidative stress using acrolein on a differentiated SH-SY5Y cell line (Figure 5.10). A compound decreasing cell viability to less than 50% was considered cytotoxic. For compounds that displayed 50% of the maximum response.

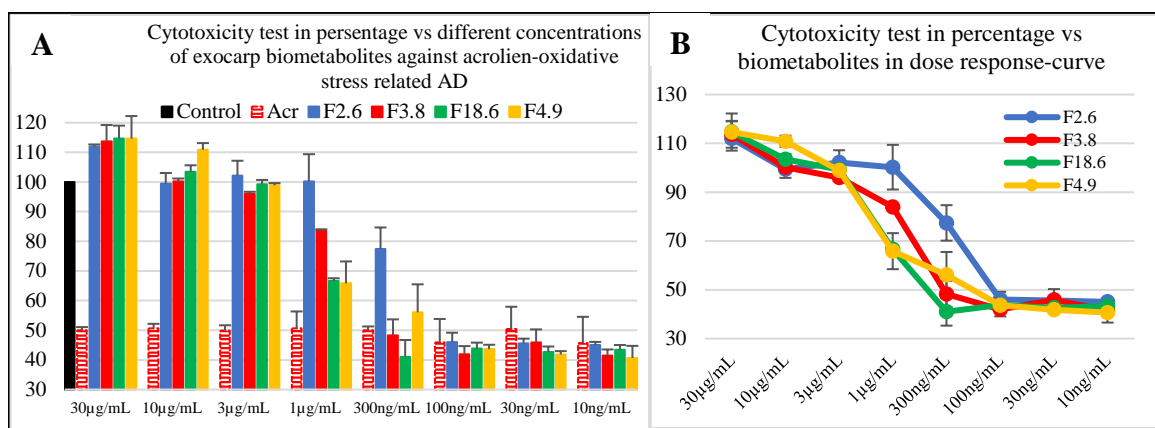


**Figure 5.10:** The cytotoxicity of bioactive fractions. **(A)** Acrolein cytotoxicity on cell viability; **(B)** EC<sub>50</sub> calculation for F2.6, F3.8, F4.9 and F18.6, based on the dose-response curve. The AlamarBlue<sup>®</sup> assay was used to analyse the cell viability, with the significance of confidence intervals at 95%, and values representing the means of  $n = 3 \pm \text{SEM}$ .

The test results revealed that the bioactive fractions isolated from *F. carica* exocarp displayed a protective effect against the cytotoxicity associated with oxidative stress triggered by acrolein. By comparison to the bioactive metabolites described in Table 5.2, F18.6 had an EC<sub>50</sub> of  $10.84 \pm 15.35 \mu\text{g/ml}$ , and was protected against the cytotoxicity caused by acrolein-related oxidative stress in a differentiated SH-SY5Y cell line.

Protective effects against the cytotoxicity caused by oxidative stress triggered by acrolein were exhibited by F3.8, F4.9 and F18.6. As discussed in detail in section 5.4.1, F2.6 contained both  $\beta$ -amyrin acetate and lupeol acetate at a ratio of 3:1, while F3.8 and F4.9 were identified to constitute higher purities of lupeol acetate and campesterol, respectively. F4.9 displayed the strongest effect against cytotoxicity in a differentiated SH-SY5Y cell line (EC<sub>50</sub> =  $1.46 \pm 4.58 \mu\text{g/ml}$ ), followed by F3.8 (EC<sub>50</sub> =  $1.3 \pm 3.15 \mu\text{g/ml}$ ), and F2.6 (EC<sub>50</sub> =  $1.42 \pm 1.78 \mu\text{g/ml}$ ). Western blotting test was carried out to expand the findings of the effects of the bioactive fractions against the cytotoxicity associated with acrolein-triggered oxidative stress on a differentiated SH-SY5Y cell line, and to investigate the mechanisms underpinning these effects.

**Table 5.2:** The capability of *F. carica* exocarp metabolites to protect against oxidative stress caused by acrolein in a differentiated SH-SY5Y cell line. The values were verified thrice.

Fraction sample	F2.6	F3.8	F4.9	F18.6
Compound	$\beta$ -amyirin acetate and lupeol acetate	lupeol acetate	campesterol	Long chain Fatty acid
EC <sub>50</sub> $\mu$ g/mL	1.951	1.478	2.493	6.578
Acrolein antioxidant test EC <sub>50</sub> $\mu$ g/mL	1.42 $\pm$ 1.78	1.3 $\pm$ 3.15	1.46 $\pm$ 4.58	6.54 $\pm$ 15.35

### 5.2.3 Western blotting test

Oxidative stress related AD prevention is mediated by the Nrf2 proteins such as the uP-regulation of NQO1. To investigate the effects of F2.6, F3.8, and F4.9 on the antioxidant proteins NQO1 after exposure to acrolein, *in-vitro* differentiated SH-SY5Y cells were subjected to 20  $\mu$ M of acrolein for 6 hours then incubated with the test fractions at concentrations of 1.59  $\mu$ M, 3.15  $\mu$ M and 6.22  $\mu$ M, respectively for 24 hours (Figure 5.11). After incubation, levels of NQO1 were examined by western blotting as described in the methodology section.

At a concentration of 1.951  $\mu$ g/ml of F2.6 ( $\beta$ -amyirin acetate and lupeol acetate), there was a significant increase in NQO1 protein level about 0.36 of the control level. Moreover, lupeol acetate in 1.478  $\mu$ g/ml showed higher activity than campesterol in 2.493  $\mu$ g/ml for 24 hours, whereas the mixture of  $\beta$ -amyirin acetate and lupeol acetate fraction was the most effective. B-actin protein level was detected as total protein. The effect of 24 hours treatments with F2.6 ( $\beta$ -amyirin acetate and lupeol acetate), F3.8 (lupeol acetate) and F4.9 (campesterol) after exposure to acrolein on the level of NQO1 protein at concentrations of 1.951  $\mu$ g/ml, 1.478  $\mu$ g/ml and 2.493  $\mu$ g/ml, respectively are shown in Figure 5.11.

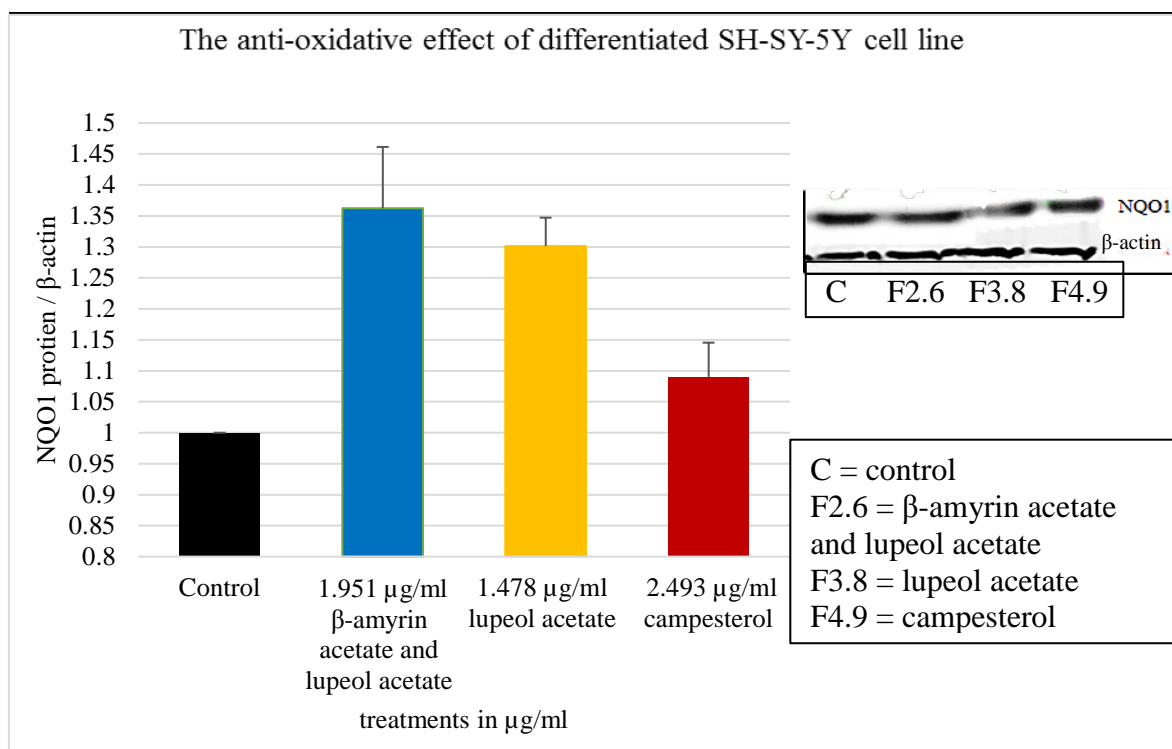


**Figure 5.11:** Effect of F2.6, F3.8, and F4.9 on differentiated SH-SY5Y cell line in the level of NQO1 protein in the presence of acrolein after 24 hours prior to 6 hours incubation with 20 µM acrolein. The control was an untreated differentiated SH-SY5Y cell. Cell lysates were then carried out to western blot analysis with antibody against NQO1. Protein levels were normalised to total protein level of B-actin and expressed relative to the corresponding value of the control. Results were plotted as mean±SD from three experiments and P value showed significance as  $P < 0.05$  vs control in one-way ANOVA test.

### 5.3 Metabolomic-guided screening of *F. carica* exocarp

#### 5.3.1 First fractionation of *F. carica* exocarp

In this study, the HCA plot revealed four groups of linkage represented in green (F19 to F21) as group 1, blue (F7) as group 2, red (F12 to F15) as group 3 and the remaining fractions in yellow as group 4. The statistical heatmap data indicated the respective metabolite compositions in terms of their molecular weight (Figure 5.12). More specifically, the clusters exhibiting a greater number of blue lines in the heatmap exhibited the larger density of diverse metabolites, whereas the clusters exhibiting a greater number of pink lines exhibited lesser density of metabolites. However, due to the low yield of F10 (2 mg), F10 was discarded for further analysis and metabolomics screening.

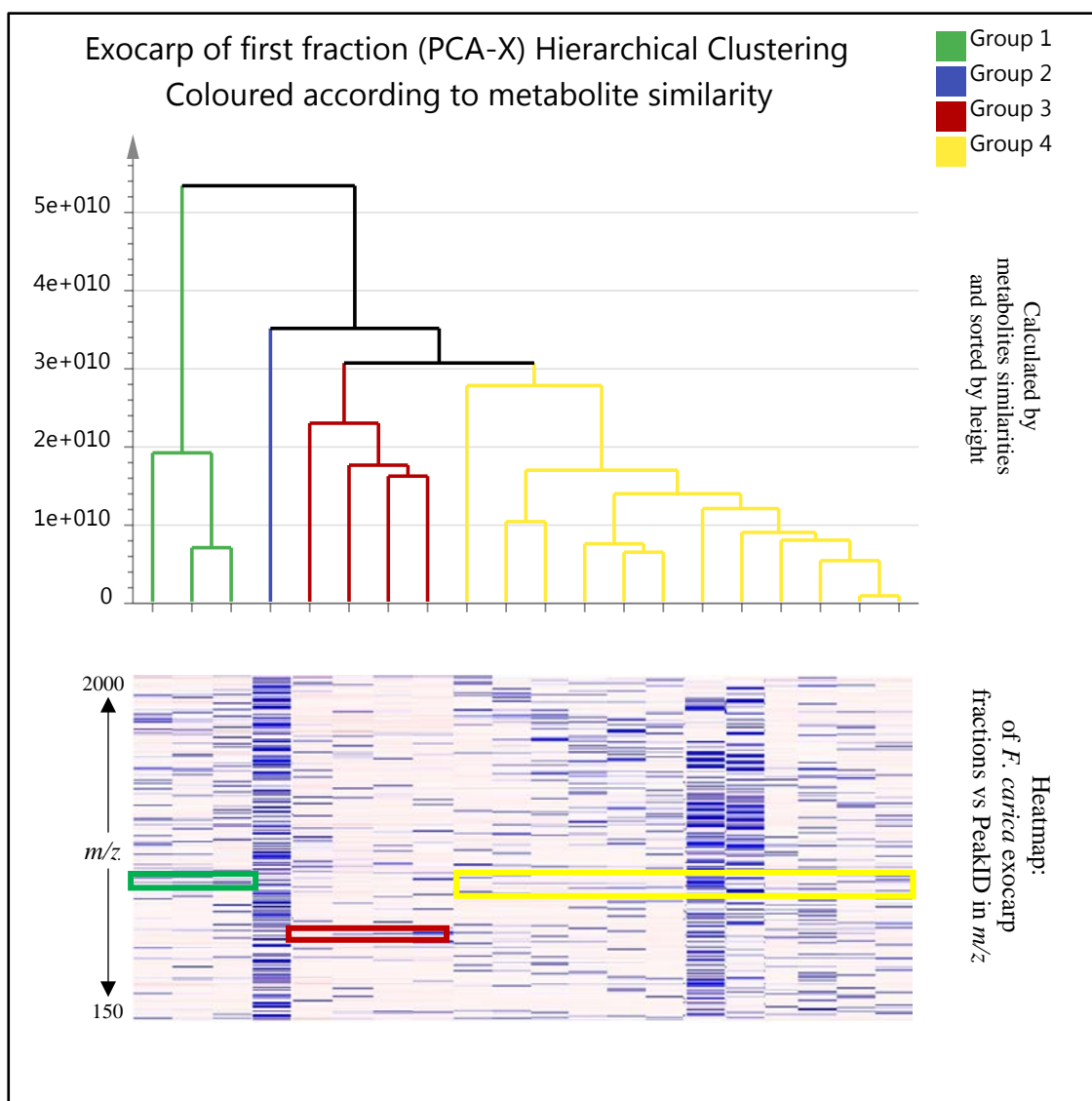


**Figure 5.12:** HCA dendrogram determined by Ward's linkage technique, showing the suggested four group of clusters, based on their metabolite similarities. HCA dendrogram were correlated through the linkage of a statistical heatmap.

Moreover, a PCA scores scatter plot was initiated. As shown in Figure 5.13A, PCA afforded four clusters, encircled in red, yellow, blue, and green indicating a shared set of metabolites. The PCA scores plot showed the positioning of the observations in four groups for the 20 fractions (Figure 5.13A). F7 was observed as an outlier, which indicated that F7 is fundamentally different from the other groups in terms of its chemical diversity as also shown on the heat map (Figure 5.12). A PCA loadings scatter plot was also generated (Figure 5.13B), in order to extract information on the discriminatory metabolites responsible for the clustering, which were displayed in *m/z*. As can be seen in Figure 5.13B the loadings scatter

plot followed the same positioning of the observations from the scores plot. F7 yielded an intense molecular ion peak at  $m/z$  812.617 not found in the other clusters.

An OPLS-DA scores scatter plot was generated to differentiate the type of metabolites between active and inactive fractions of *F. carica* exocarp on oxidative stress related AD. The active fractions versus the inactive fractions were grouped together in the score scatter plot of the OPLS-DA (Figure 5.13C). The results of the analysis led to the prediction of compounds that contribute towards the AD prevention activity of the fractions. As shown in Figure 5.13C in the OPLS-DA models, the mass spectral data set was assigned as the X independent variable while the AD prevention response was the Y dependent variable. To validate the model of OPLS-DA, a validation test was performed. The model's R<sup>2</sup> (goodness of fit) was 0.803 and Q<sup>2</sup> (prediction ability of the model) was 0.553. This indicated a well-fitted model exhibiting good prediction. Under the active group, fractions F19 (group 1), F15 (group 3), and F2 to F4 and F18 (group 4) clustered together in the upper left quadrant indicating a shared set of metabolites. These fractions were subjected to further isolation work because of their more potent bioactivity on the cell viability test (see section 5.2.1). F7 (group2) and F8 (group4) found in the bottom left of the active quadrant were neglected due to their weaker bioactivity on the cell viability test as well as their lower yields. An OPLS-DA loadings scatter plot (Figure 5.13D) was also generated to correlate of the distribution of the type of metabolites between the active and inactive group.

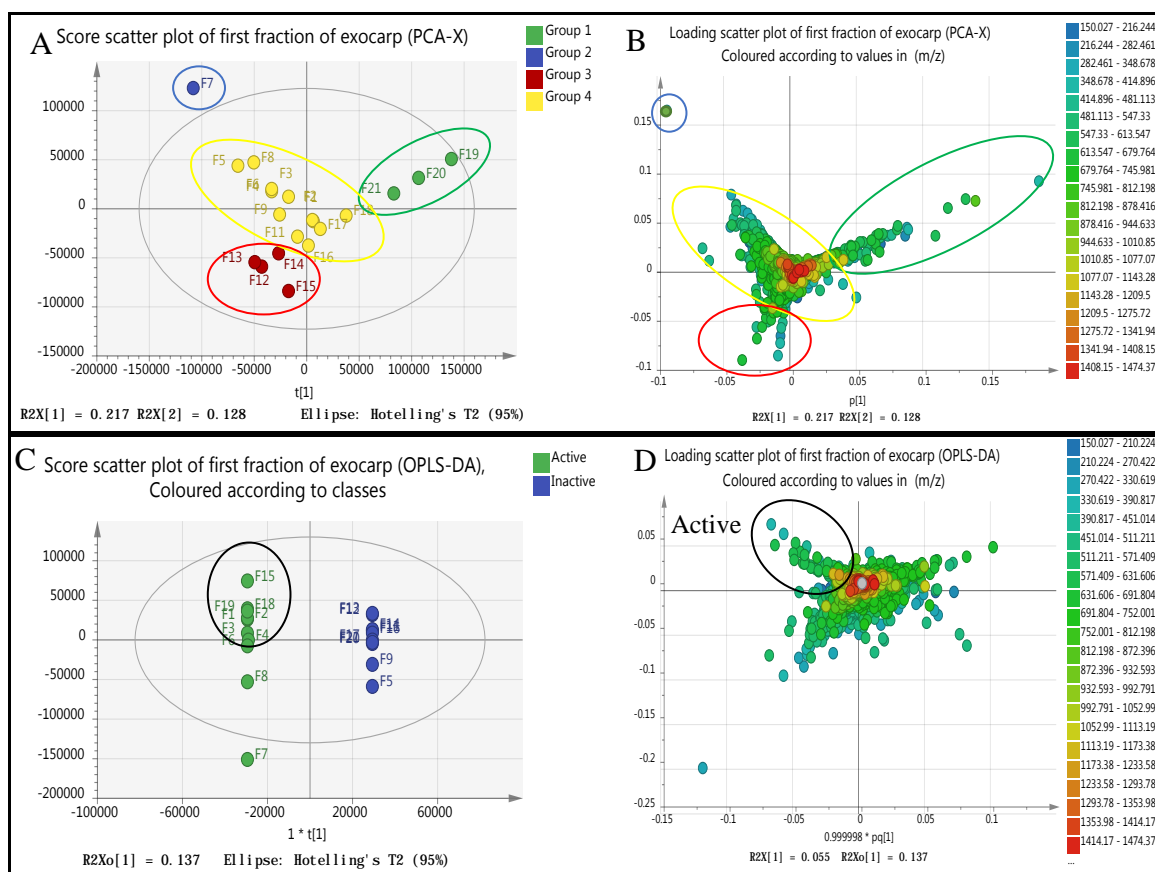


**Figure 5.13:** **A)** PCA scores scatter plot of mass spectral data shows the exocarp fractions grouped based on similarity of their metabolites. **B)** PCA loadings scatter plot shows the  $m/z$  values of the grouped metabolites encircled in blue, red, yellow, and green. **C)** OPLS-DA scores scatter plot shows the active fractions denoted in green versus inactive fractions denoted in blue against oxidative stress related AD prevention. **D)** OPLS-DA loadings scatter plot shows the distribution of metabolites in  $m/z$  between active versus inactive groups.

The generated S-plot (Figure 5.14) determined the “end point” compounds, indicating the unique metabolites that are potentially responsible for the bioactivity against oxidative stress related AD prevention and discriminate the active from the inactive fractions of *F. carica* exocarp. Seven metabolites were identified by dereplication from the database DNP-2015 as shown in Table 5.2. The end point compounds have been targeted for further isolation work and metabolomic-guided screening as described below with 1 active compound found to be highly concentrated in Group 3 (F15) and the remaining four active compounds determined in Group 4 (F2 to F4, F18 and F19).

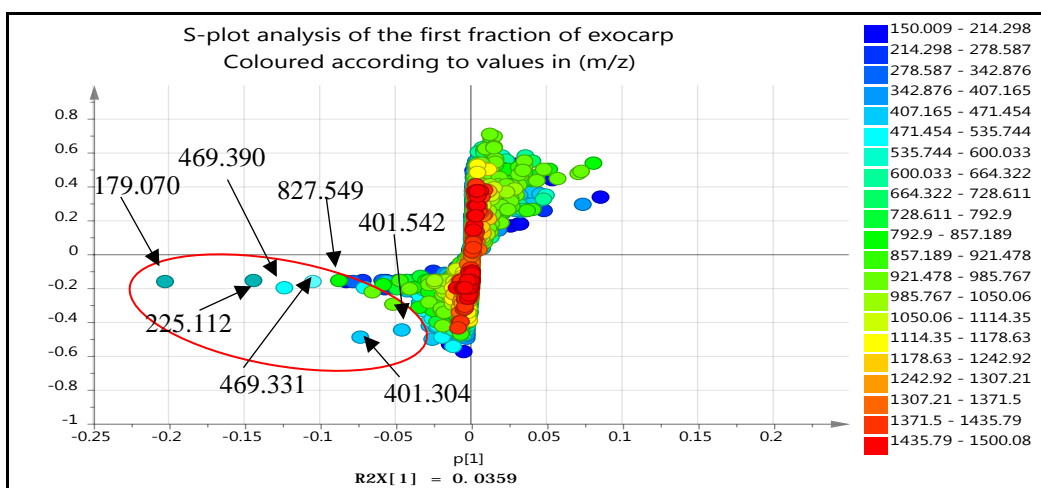
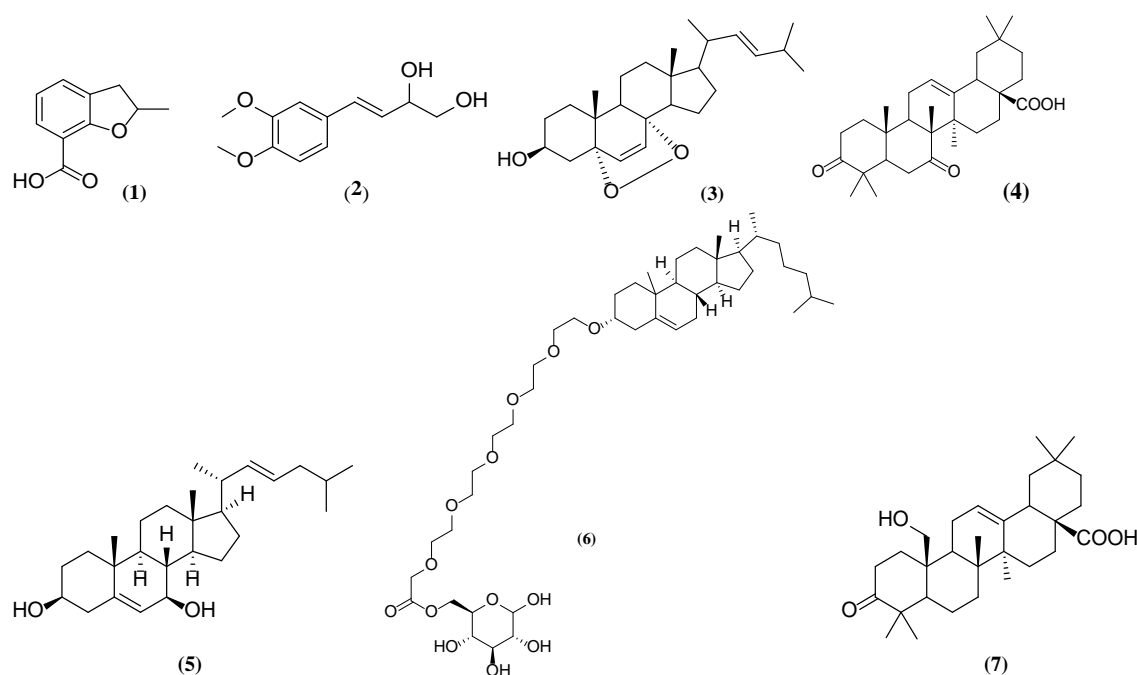


**Figure 1.14:** S-plot generated from the OPLS-DA model shows the end point compounds of *F. carica* exocarp fractions that are the predicted metabolites responsible for the bioactivity encircled in red. Identity of the metabolites listed in Table 5.2.

**Table 5.2:** Dereplication list of unique metabolites from the active fractions of *F. carica* exocarp against oxidative stress related AD prevention identified from the DNP 2015 database. (P indicated positive mode and N indicated negative mode).

Ionization Mode	MS <i>m/z</i>	Rt min	Chemical Formula	Name	Source
P	179.070	10.38	C <sub>10</sub> H <sub>10</sub> O <sub>3</sub>	2-methyl-2,3-dihydro-1-benzofuran-7-carboxylic acid (1)	<i>Amomum tsao-ko</i>
P	225.112	11.64	C <sub>12</sub> H <sub>16</sub> O <sub>4</sub>	4-(3,4-dimethoxyphenyl)dimethoxyphenyl-3-butene-1,2-diol (2)	<i>Zingiber cassumunar</i>
P	401.304	20.62	C <sub>26</sub> H <sub>40</sub> O <sub>3</sub>	5,8-epidioxyepidioxy-24-norcholesta-6,22-dien-3-ol (3)	<i>Xylocarpus moluccensis</i>
P	469.331	22.54	C <sub>30</sub> H <sub>44</sub> O <sub>4</sub>	rubonic acid (4)	<i>Rubus moluccanus</i>
P	401.542	22.56	C <sub>27</sub> H <sub>44</sub> O <sub>2</sub>	cholestacholesta-5,22-diene-3,7-diol (5)	<i>Cliona copiosa</i>
P	827.549	29.19	C <sub>45</sub> H <sub>78</sub> O <sub>13</sub>	3,4,5,6-tetrahydroxytetrahydropyran-17-methyl-10,13-dimethyl-6-methylheptyl-tetradecahydro-cyclopentaphenanthrenyloxy-3,6,9,12,15-pentaoxaheptadecanoate (6)	spinach
N	469.390	37.17	C <sub>30</sub> H <sub>46</sub> O <sub>4</sub>	25-hydroxy-3-oxoolean-12-en-28-oic acid (7)	<i>Kokoona ochracea</i>



### 5.3.2 Sub-fractions of *F. carica* exocarp

Metabolomic-guided screening was also used to analyse the similarity of the data sets between exocarp sub-fractions obtained from the purification work on fractions procured from the first chromatographic separation step. The HCA plot revealed five clusters while the statistical heatmap data indicated the respective metabolites in terms of their molecular weight (Figure 5.15). More specifically, the clusters exhibiting a greater number of blue lines in the heatmap exhibited a decrease of the presence of the respective metabolites, whereas the clusters exhibiting a greater number of pink lines exhibited an increase of the presence of the respective metabolites.

The respective fractions F4.10 and F18.6 found in group 1 (green colour) and group 2 (navy blue colour) likely exhibited the most diverse composition of metabolites. F19.3, F18.5 and F18.9 in group 5 (light blue colour) consisted of a higher density of low molecular weight compounds.

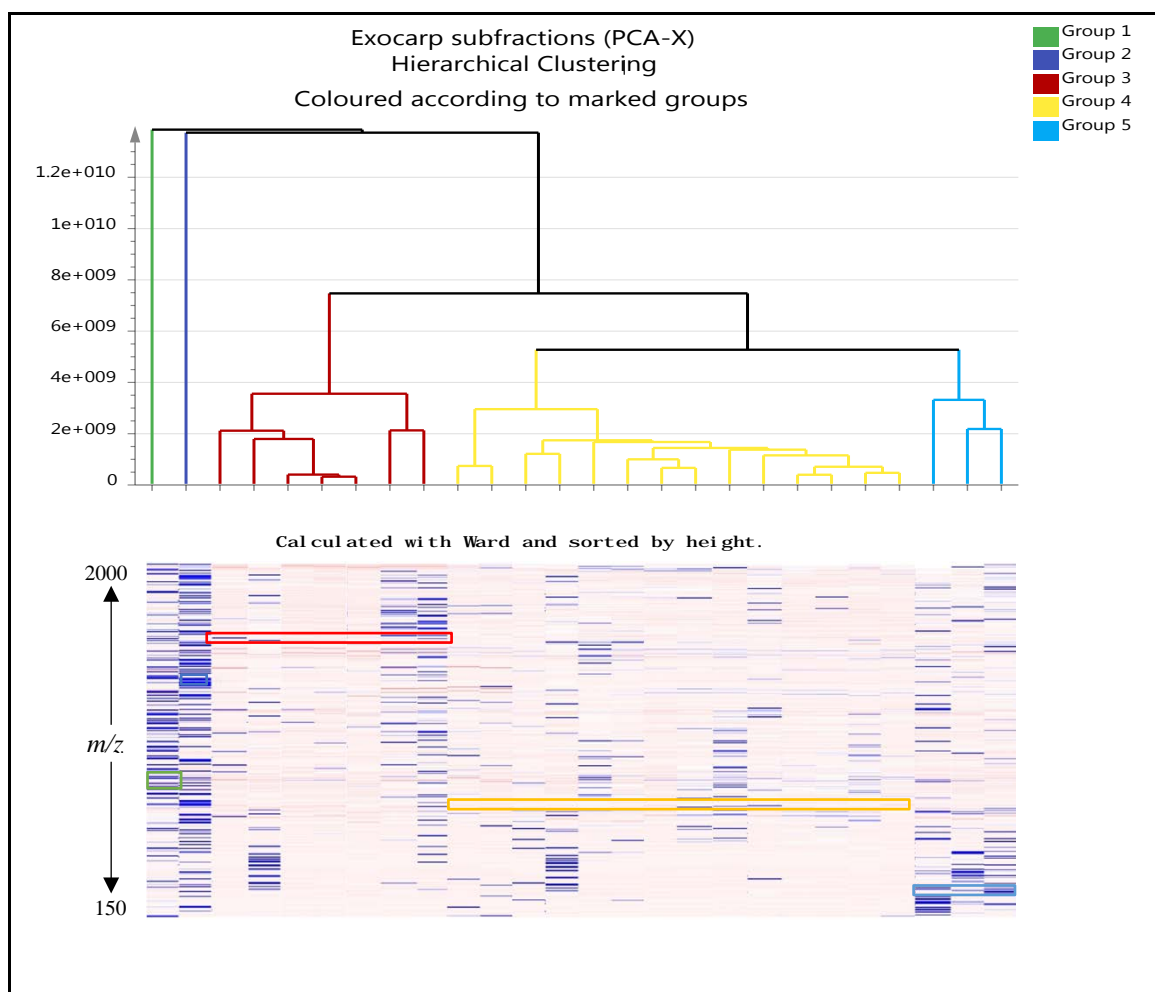


**Figure 5.15:** HCA dendrogram determined by Ward’s linkage, showing the suggested five clusters, based on metabolite similarities.

PCA was employed to extract compound signals from background noise and to provide an orthogonal linear transformation of possibly correlated variables into a smaller number of uncorrelated variables (Hou *et al.*, 2012; Madala *et al.*, 2014). As shown in Figure 5.16A, the same clusters were identified when the score plots of PCA were applied to the HCA profiles. As indicated by Madala *et al.* (2014) clustered samples indicated a particular “metabolic phenotype”. The same analysis was performed using SIMCA 14 software on the equivalent loadings plots (Figure 5.16B). In addition, the differentiation between the active and inactive metabolites against AD was achieved based on the OPLS-DA loadings plot (Figure 5.16C). The seven inactive fractions were assigned the colour blue, while the remaining active fractions were shown in green in the scores plot. The compounds

highlighted in the  $m/z$  loadings plot (Figure 5.16D) was dynamically linked to the scores plot (Figure 5.16C), with the dispersal of molecular ions at  $m/z$  401.341 and  $m/z$  469.331.

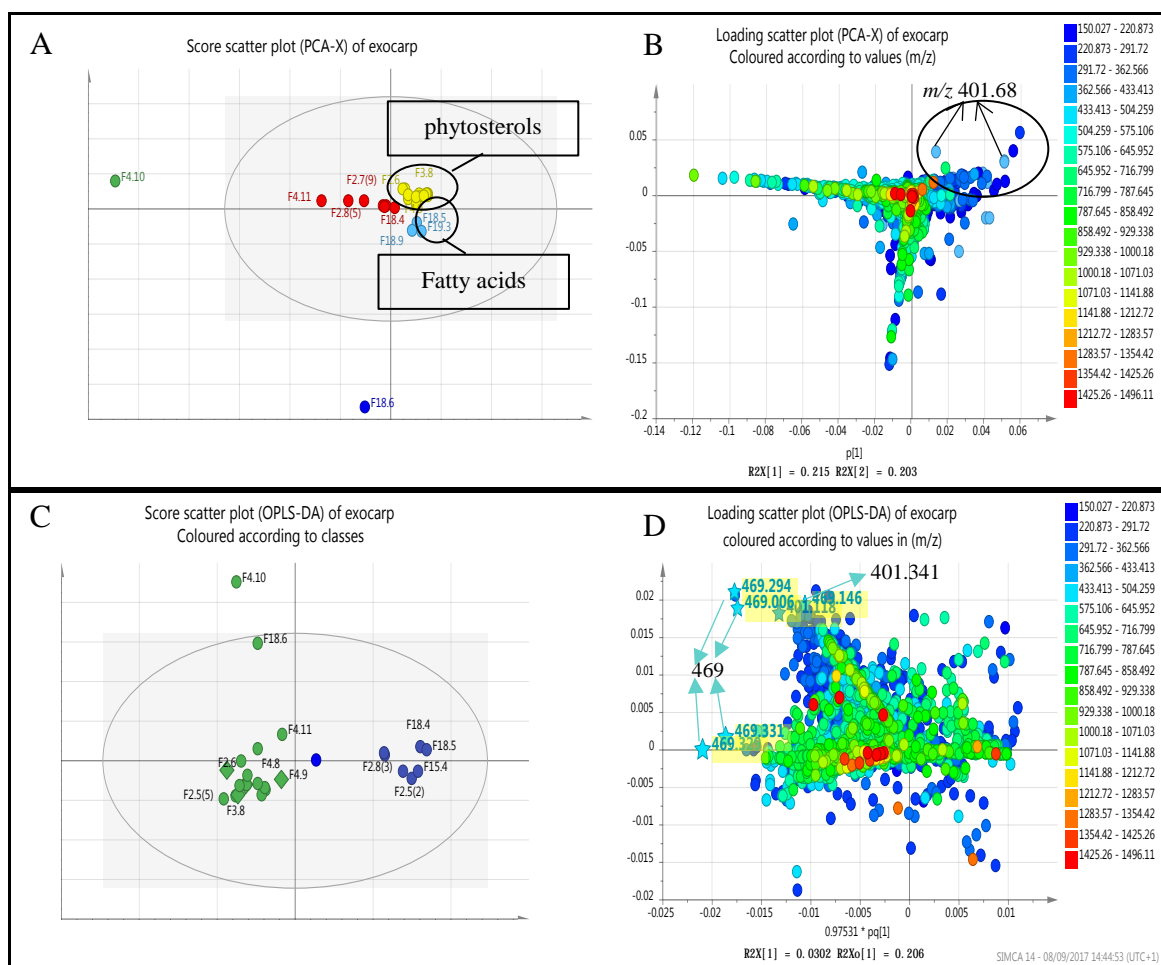


**Figure 5.16:** **A)** PCA scores plot of mass spectral data indicating three chemical groups; **B)** PCA loadings plot via  $m/z$  values; **C)** OPLS-DA scores plot to discriminate the active versus the inactive metabolites against oxidative stress in AD prevention; **D)** OPLS-DA loadings plot via  $m/z$  values determining the bioactive target metabolites at  $m/z$  401[M+H] and 469[M+H].

Data variability was illustrated by the scores plot, with differences between the secondary metabolites being greater, the wider was the separation between the clusters. From a geometrical perspective, a correlation existed between the loadings plot and the scores plot, and the variability distinguished in the scores plot was expressed with the molecular ion peak  $m/z$  values. Nonetheless, the ability to target the putative secondary metabolites interactively was greatly assisted by an OPLSD-DA S-plot, which emphasised the putative biometabolites against oxidative stress prevention in AD. The results shown in Figure 5.17 suggested that

the potential bioactive metabolites were represented by the values  $m/z$  469.331, 469.404 and  $m/z$  401.341. These predicted metabolites were identified with the dereplication database (Table 5.3), which were coupled to MZmine by in-house algorithms.

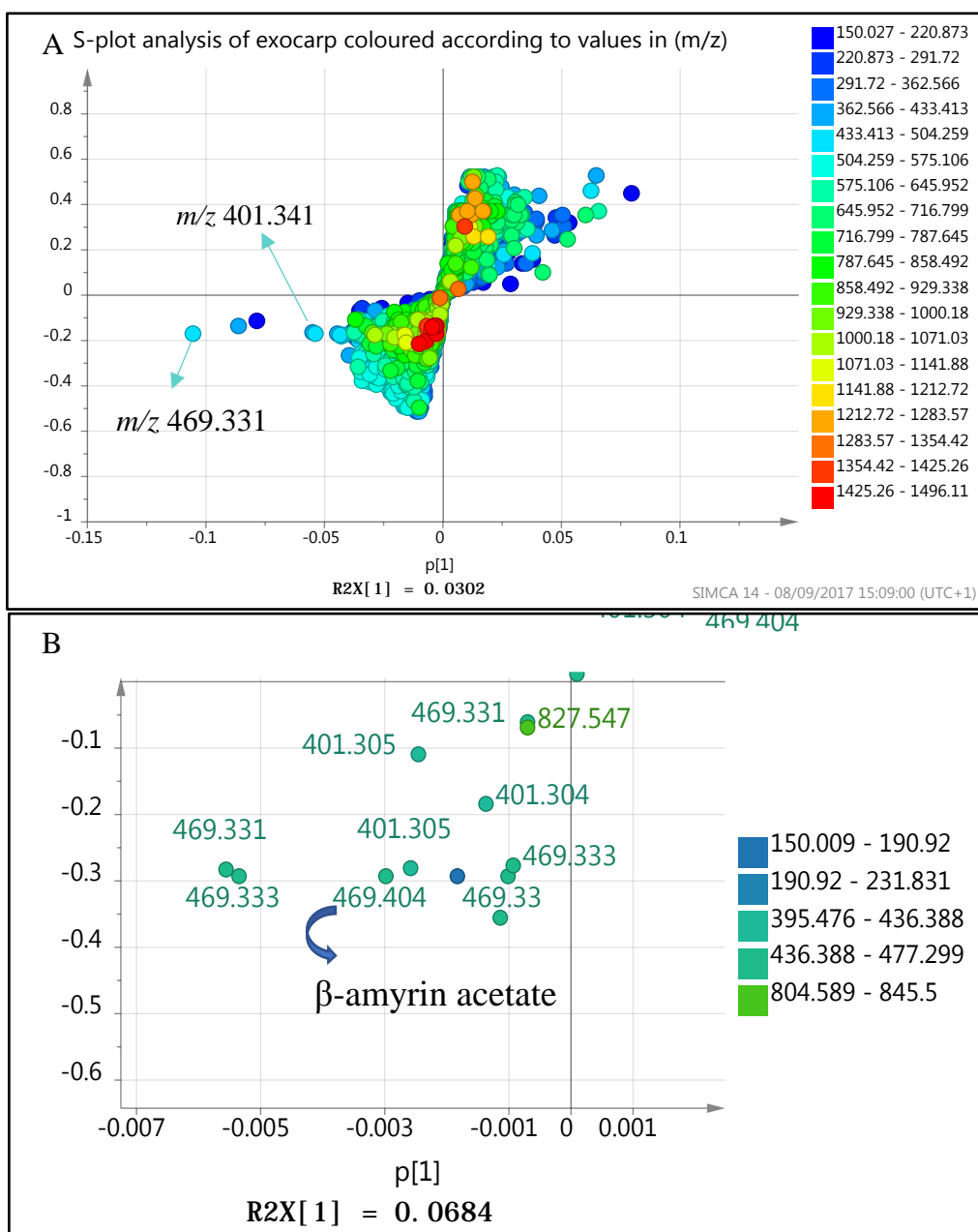


**Figure 5.17:** **A)** OPLS-DA S-plot analysis of the putative bioactive metabolites in *F. carica* exocarp fractions corresponding to the analysis of, values of  $m/z$  401.341 and  $m/z$  469.331 were determined as the putative molecular biomarkers against oxidative stress related AD prevention. **B)** Expansion of S-Plot quadrant showing the predicted bioactive metabolites in *F. carica* exocarp fractions, values of  $m/z$  469.404.

**Table 5.3:** The dereplication list of unique metabolites using macro DNP 2015 database from the active fractions against oxidative stress related AD prevention obtained from the S-plot “end point” data shown in Figure 5.17. (P indicated positive mode). Highlighted rows represented the isolated compounds.

<b>Ionization Mode</b>	<b>MS <i>m/z</i></b>	<b>Rt min</b>	<b>Chemical Formula</b>	<b>Name</b>	<b>Source</b>
P	401.253	16.37	C <sub>28</sub> H <sub>48</sub> O	campesterol	<i>Taiwania flousiana</i>
P	469.331	22.54	C <sub>30</sub> H <sub>44</sub> O <sub>4</sub>	rubonic acid	<i>Rubus moluccanus</i>
P	401.542	22.56	C <sub>29</sub> H <sub>44</sub> O <sub>2</sub>	cholestacholesta-5,22-diene-3,7-diol	<i>Cliona copiosa</i>
P	469.404	30.63	C <sub>32</sub> H <sub>53</sub> O <sub>2</sub>	β-amyrin acetate	<i>Euphorbia pulcherrima</i>

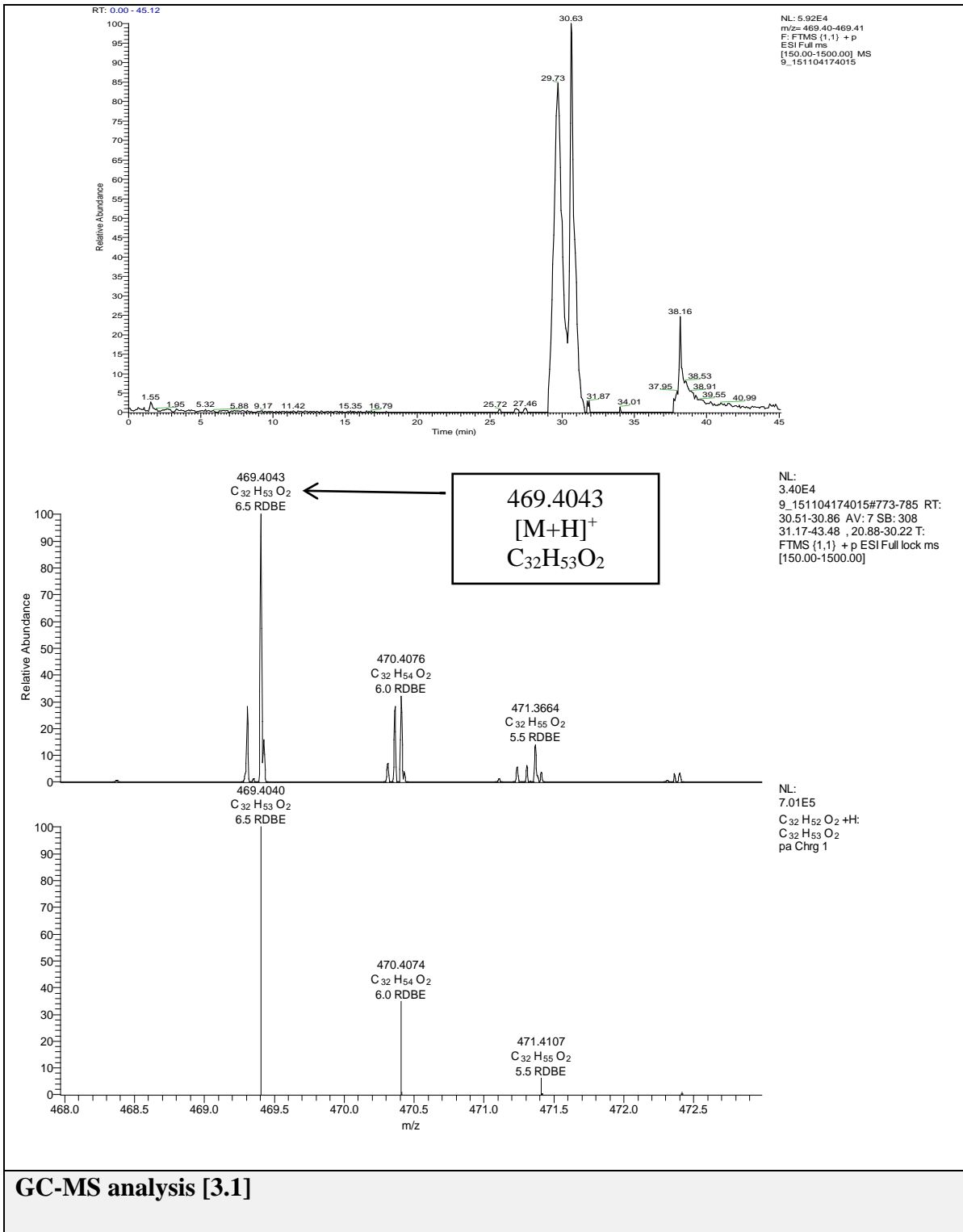
Therefore, as F18.6 was predicted to exemplify a long-chain fatty acid and was predicted similar to those found from the mesocarp compound **1.2**, F2.6, F3.8, and F4.9 were selected for further identification and elucidation as described below, while F15.4 and F19.3 were neglected due to small fractions yields, which were less than 5 mg.

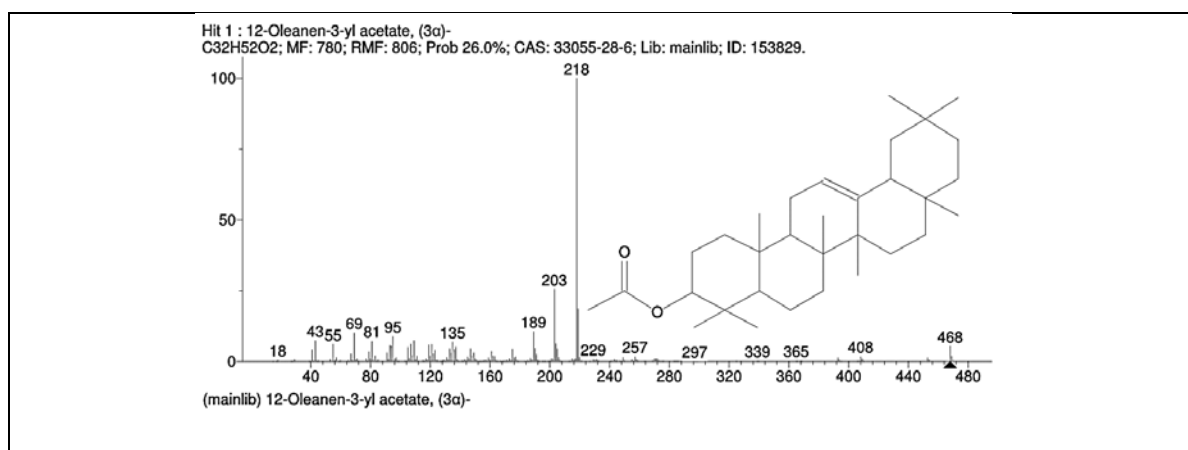
## 5.4 Identification and elucidation and of *F. carica* exocarp

### 5.4.1 $\beta$ -amyrin acetate 3.1 and lupeol acetate 3.2

**Table: 5.4:** Semi-pure F2.6 fraction of *F. carica* exocarp; characterisation of  $\beta$ -amyrin acetate 3.1 and lupeol acetate 3.2; chemical configurations; LCMS detection of 3.1; and GCMS of 3.1 at Rt run 20.55 min.

<b><math>\beta</math>-amyrin acetate 3.1</b>	<b>lupeol acetate 3.2</b>
Synonym(s): 3-O-acetyl- $\beta$ -amyrin, 12-oleanen-3-yl acetate	Synonym(s): luP-20(29)-en-3-ol, acetate, lupeyl acetate
Source: Exocarp of <i>F. carica</i>	Source: Exocarp of <i>F. carica</i>
Metabolite: Fraction F2.6	Metabolite: Fraction F2.6 and F3.8
Sample amount: 4.9 mg	Sample amount: 4.9 and 10 mg
Physical description: White needle crystals	Physical description: White amorphous
Molecular formula: C <sub>32</sub> H <sub>52</sub> O <sub>2</sub>	Molecular formula: C <sub>30</sub> H <sub>50</sub> O
Exact Mass: 468.3967 g/mol	Exact Mass: 468.3967 g/mol
<b>Chemical structure</b>	<b>Chemical structure</b>
<p style="text-align: center;">[3.1]</p>	<p style="text-align: center;">[3.2]</p>
<b>LC-MS analysis 3.1</b>	





The structure was entirely elucidated by 1D and 2D NMR as well as HRMS that established the molecular formula C<sub>32</sub>H<sub>52</sub>O<sub>2</sub>, ESI-MS:  $m/z$  469.3917 [M+H]<sup>+</sup>. The findings of the GCMS fragmentation pattern of **3.1** in Table 5.4 was characterised by ion peaks at  $m/z$  (intensity): 218 (100), 468 (10), 95 (11), 81 (9), 408 (5), 69 (15), 135, 257 (5), 203 (25) and 189 (36) typical of a pentacyclic triterpene alcohol. Through comparison with the data available in the literature, this was identified as  $\beta$ -amyrin acetate (Charalambous, 1983; Fingolo *et al.*, 2013; Schmidt, Kuhnt and Adam, 1994; Tulloch and Hoffman, 1982).

$\beta$ -amyrin acetate **3.1** and lupeol acetate **3.2** were obtained in the form of white to colourless needle-like crystals. TLC exhibited the occurrence of triterpene, which appeared as two overlapping yellow brown spots (section 5.1.3), as earlier described by Geevananda *et al.*, (1980). In general,  $\beta$ -amyrin acetate **3.1** and lupeol acetate **3.2** were likely to be eluted together in TLC (Hoffman, 1982), due to their similarities in molecular weight at 468.77 g/mol and basic structure.

The stacked spectrum of <sup>13</sup>C NMR and *J*mod data (Figure 5.18) for both fractions (F3.8 and F2.6) of the exocarp closely matched those of **1.3** in F4,5,6/F1/F5 mesocarp supporting the fact that both fractions indicated the presence of lupeol acetate. This was further established by the presence of a quaternary signal at  $\delta_c$  151.05, assigned to C-20, and the exomethylene signal at  $\delta_c$  109.21, assigned for C-29.

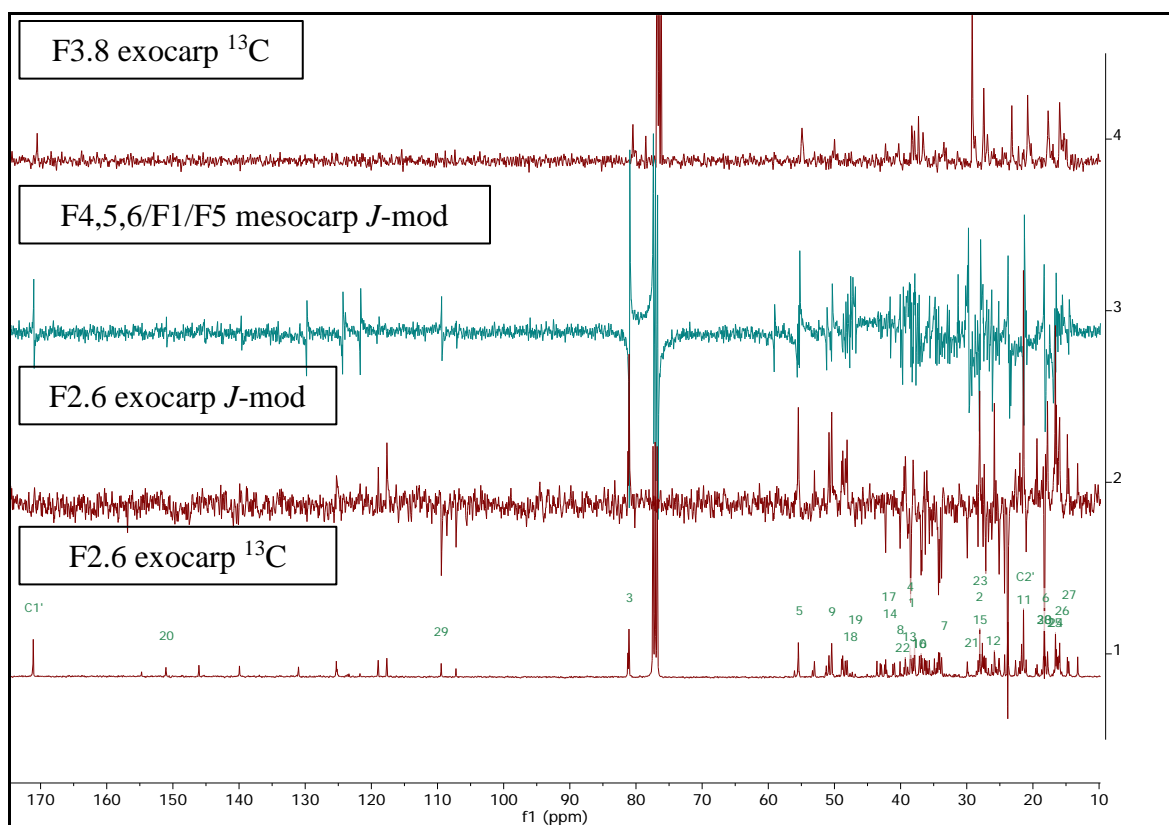


**Figure 5.18:** Stacked  $^{13}\text{C}$ -Dept and  $J$ -mod NMR spectra (125 MHz,  $\text{CDCl}_3$ ) illustrated the similarities between fractions of F2.6 exocarp and F4,5,6/F1/F5 mesocarp. F3.8 exocarp presented similar signals to F4,5,6/F1/F5 mesocarp as well, indicating the presence of lupeol acetate. The numbers in green correspond to the carbon signals of the lupeol acetate.

The  $^1\text{H}$ -NMR spectrum of **3.1** (Figure 5.19 and Figure 5.20) demonstrated the characteristic eight methyl singlet (s) signals in the aliphatic ring at  $\delta_{\text{H}}$  0.86 (Me-23), 0.84 (Me-24), 0.82 (Me-25), 0.94 (Me-26), 1.67 (Me-27), 0.95 (Me-28), 0.99 (Me-29), and 0.86, (Me-30). The acetyl group occurred as a singlet signal at  $\delta_{\text{H}}$  2.04 ( $\text{CH}_3\text{CO}$ ). The  $^1\text{H}$ -NMR spectrum also demonstrated the presence of an oxymethine resonance at  $\delta_{\text{H}}$  4.45 (t,  $J = 10$  Hz, H-3). In addition, the olefinic signal at  $\delta_{\text{H}}$  5.25 (t,  $J = 5.09$  Hz, H-12) was assigned to the presence of a mono-substituted double bond, which was unambiguously confirmed by the  $^1\text{H}$ - $^1\text{H}$  COSY spectrum, which coupled vicinally with the methylene group for H-11 at 1.61 ppm (Figure 5.21).

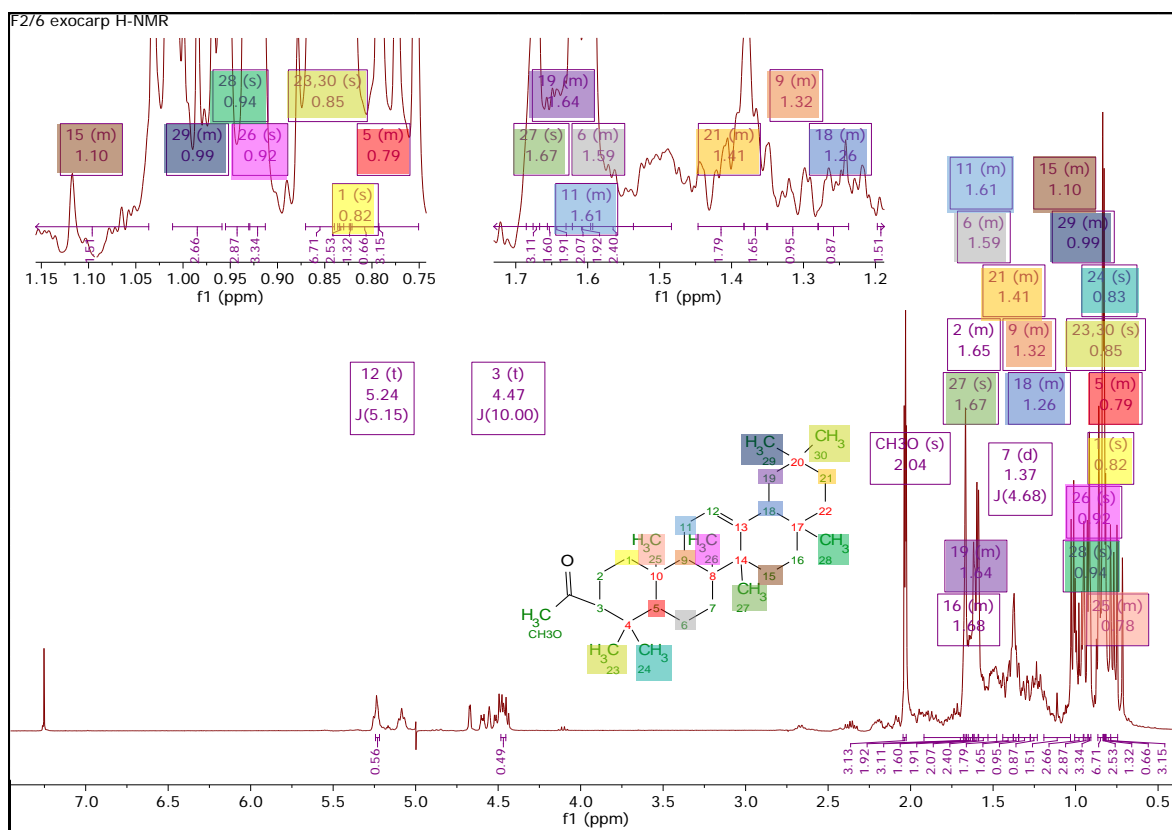


**Figure 5.19:**  $^1\text{H-NMR}$  spectrum of  $\beta$ -amyirin acetate **3.1** in  $\text{CDCl}_3$  at 400 MHz.

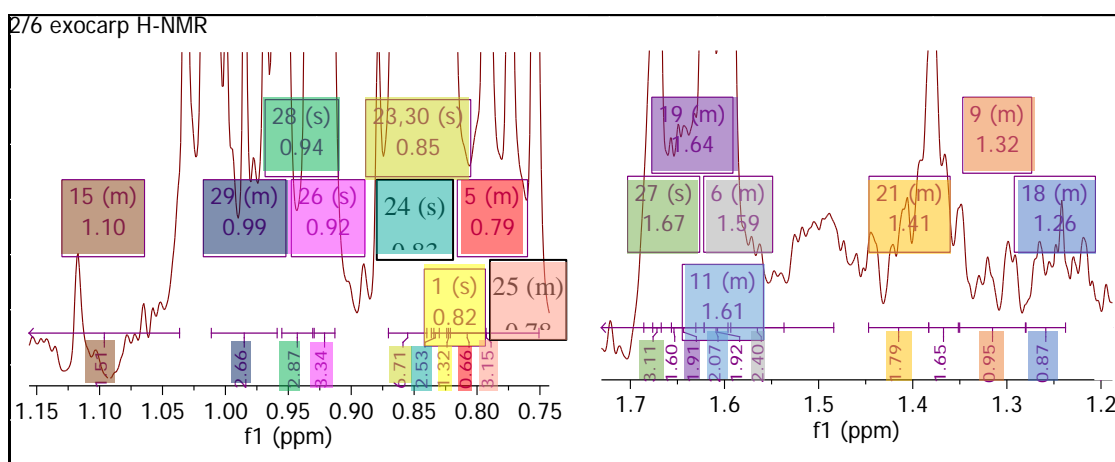


**Figure 5.20:** Expansion of the upfield region  $^1\text{H-NMR}$  spectrum of  $\beta$ -amyirin acetate **3.1** in  $\text{CDCl}_3$  at 400 MHz.

In addition, Figure 5.21 showed 2D-COSY correlations between the protons resonating at  $\delta$  1.31 (H-9), 1.47 (H-11), and 2.03 (H-12); which were connected through an orange line. A further strong 2D-COSY correlation was between the proton H-3 and H-2, resonating at  $\delta$  3.56 and 2.24, and protons at  $\delta$  0.69 and 1.02, assigned to H18 and H-19.

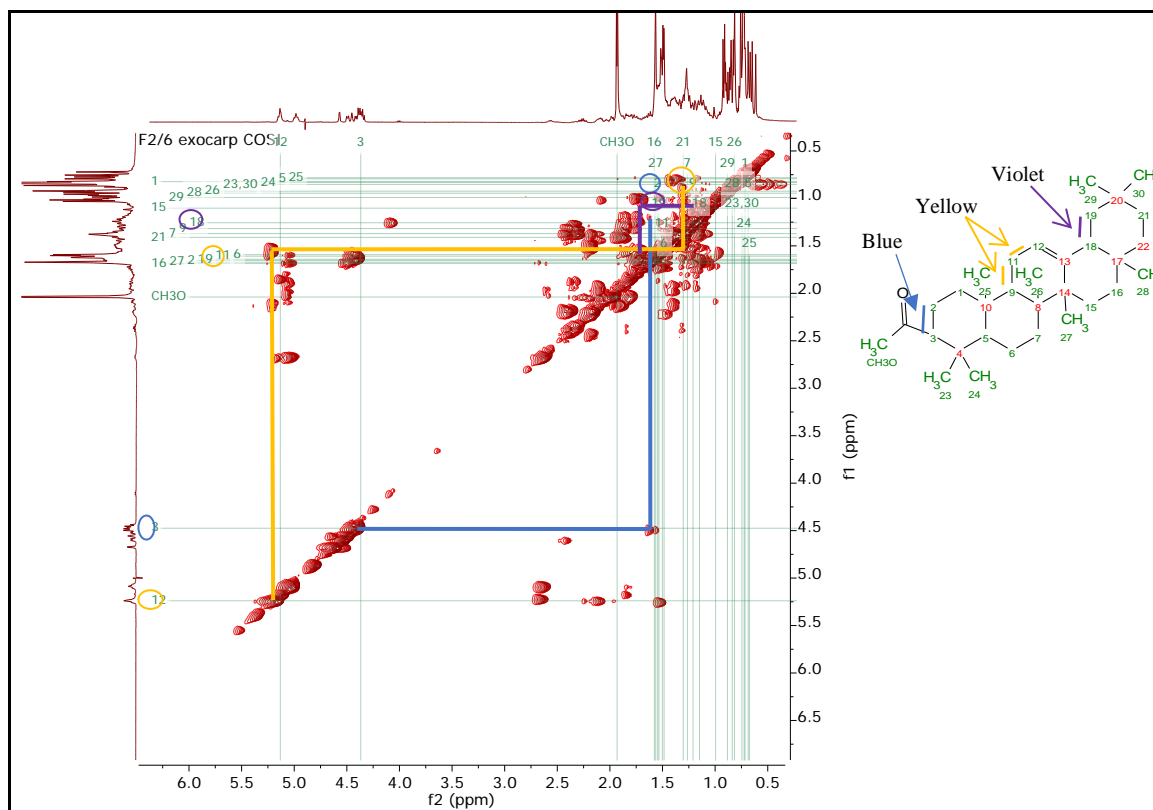


**Figure 5.21:** 2D-COSY of compound **3.1** exhibited proton correlations between H-3 and H-2 (blue line); between H-9, H-11, and H-12 (orange line); and between H-18 and H-19 (violet line). Cross peak lines shown in green were allocated to their corresponding proton signals.

The *J*mod carbon NMR spectrum of **3.1** suggested a close structural homology with that of  $\beta$ -amyrin acetate (Figure 5.22). The upfield shifts of the eight carbon signals of the methyl groups at  $\delta$  37.2 (C-23), 16.6, (C-24), 16 (C-25), 17.8 (C-26), 27.4 (C-27), 17.8 (C-28), 23.8 (C-29), and 22.6 (C-30), in addition to the occurrence of downfield shifts of a oxygen-bound carbon for C-3 at 81.06 ppm, an ester carbonyl carbon signals at 171 ppm, and a mono-substituted double bond for C-12 at 125.5 ppm and C-13 at 146 ppm were comparative to that found in the literature (Table 5.5) for  $\beta$ -amyrin acetate.

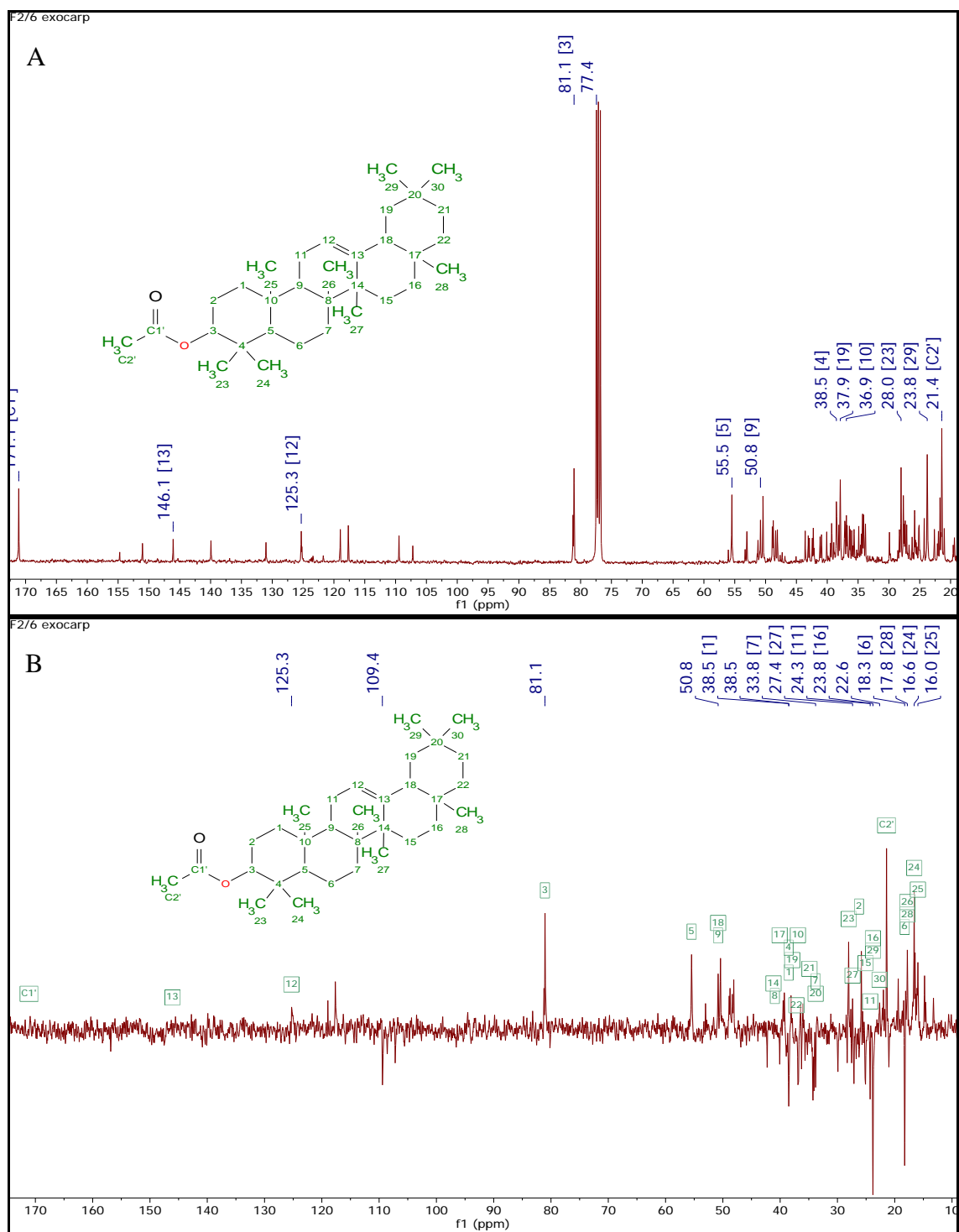


**Figure 5.22: A)**  $^{13}\text{C}$ -NMR of **3.1** and **B)**  $J_{\text{mod}}$ -NMR spectrum (125 MHz,  $\text{CDCl}_3$ ) of **3.1**.

The HSQC NMR spectrum of the  $\beta$ -amyirin acetate **3.1** were measured in  $\text{CDCl}_3$  (Figure 5.23). The downfield chemical shifts at  $\delta_{\text{H,C}}$  4.45, 81.1 and 5.25, 125.5 shown in Figure 5.23A were assigned to the acetate substituent at C-3 and the double bond at C-12,

respectively. Nonetheless, the strong methyl signals (Figure 5.23B) were observed at  $\delta_{H,C}$  (0.88, 28.4), (0.84, 16.6), (0.82, 16), (0.92, 17.8), (1.67, 27.4), (0.95, 17.8), (1.62, 23.8), (0.92, 22.6), and (2.04, 21.2) assigned to positions 23, 24, 25, 26, 27, 28, 29, 30, and  $CH_3CO$ .

The HMBC spectrum (Figure 5.24) exhibited the long-range correlations of protons at  $\delta$  0.86 (H-23) with a carbon at  $\delta$  4.45 (C-3) and 55.5 (C-5) indicating that the methyl unit was bound to C-3. The long-range correlations of protons at  $\delta$  81.1 (H-3) with two methyl moieties at  $\delta$  28.4 (C-23), and 16.6 (C-24), as well as the acetate unit at  $\delta$  171 (C1') established that both methyl units C-23 and C-24 were bonded to the quaternary carbon (C-4) at  $\delta$  38.52. Long-range correlations of the double bond proton at  $\delta$  5.25 (H-12) with both quaternary carbon at  $\delta$  41.2 (C-14), and at 36.9 (C-10, 'w' coupling), and methine carbon at  $\delta$  50.9 (C-18) confirmed that the quaternary double bond carbon (C-13) at  $\delta$  146 was vicinal to C-18.

In addition, long-range correlations between protons at  $\delta$  1.67 ( $CH_3$ -29) with methyl carbon at  $\delta$  22.6 (C-30), and methylene carbon at  $\delta$  37.9 (C-19); between the methyl proton at  $\delta$  0.92 ( $CH_3$ -30) with methine carbon at  $\delta$  50.8 (C-18), and both methylene carbon at  $\delta$  37.9 (C-19), and 37.2 (C-22) supported the fact that both methyl carbons C-29 and C-30 were bound to the quaternary carbon (C-20) at  $\delta$  33.8. Correlation between protons at  $\delta$  0.95 (H-28) with methylene carbons at  $\delta$  1.12 (C-15), 1.64 (C-19), and 1.21 (C-22) as well as between protons at  $\delta$  0.95 (H-27) with methyl carbon at  $\delta$  17.8 (C-26), and methine carbons  $\delta$  50.8 (C-18), 50.4 (C-9), and 37.2 (C-12), between the methyl proton at  $\delta$  0.92 (H-26) with methyl carbon at  $\delta$  27.4 (C-27), methine carbons  $\delta$  50.4 (C-9), and quaternary carbon at  $\delta$  36.9 (C-10) afforded that the methyl carbons at C-28, C-27 and C-26 were bound to the quaternary carbons of C-17, C-14, and C-8, respectively. Further details of 2D-COSY and 2D-HMBC spectrum correlation can be found in Figure 5.25.

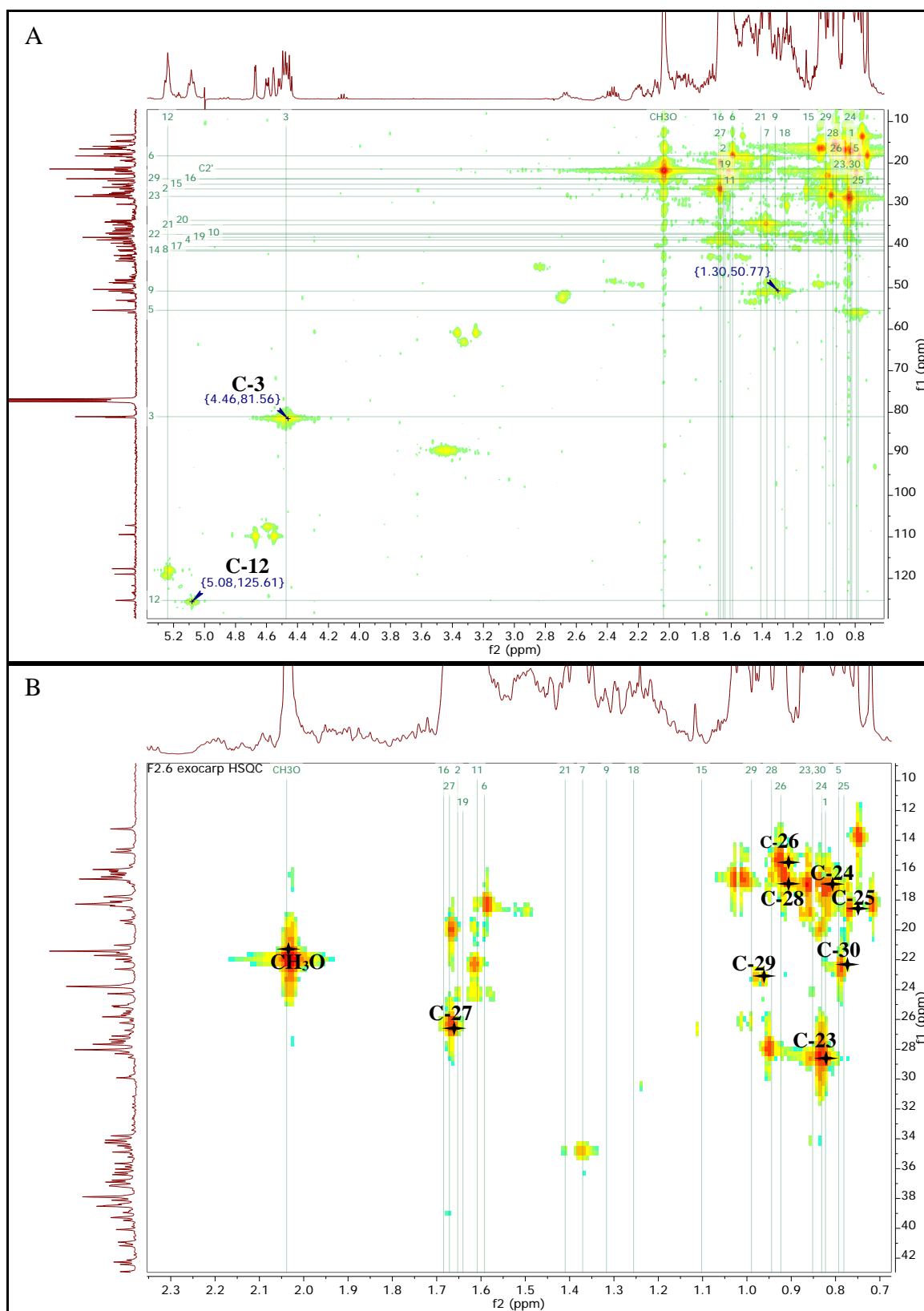


**Figure 5.23:** A)  $^1\text{H}$ - $^{13}\text{C}$  HSQC NMR spectrum of [3.1] highlighting the cross peaks positions 3 and C-12. B) The expansion of the  $^1\text{H}$ - $^{13}\text{C}$  HSQC NMR spectrum showing the allocation of methyl group signals.

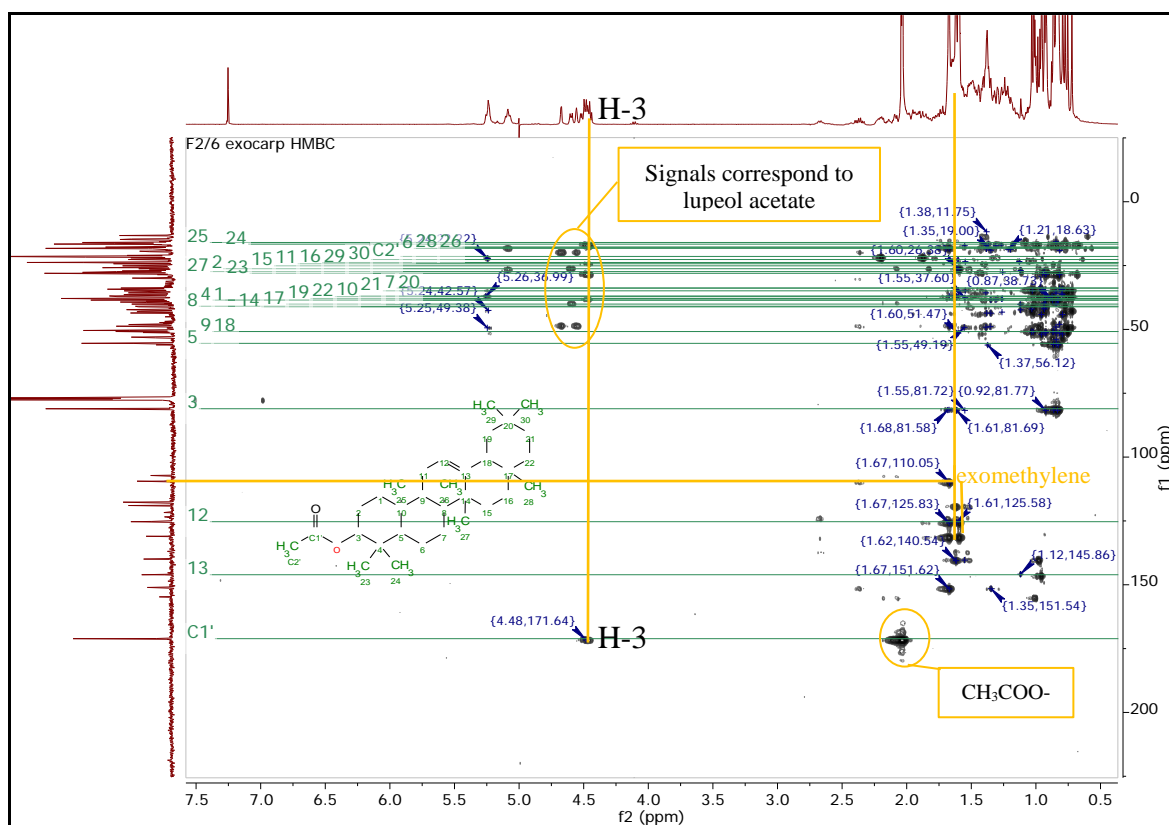


**Figure 5.24:** The  $^1\text{H}$ - $^{13}\text{C}$ -HMBC spectrum in  $\text{CDCl}_3$  at 500MHz of  $\beta$ -amyrin acetate **3.1** are indicated by the horizontal green lines; The presence of lupeol acetate **3.2** are indicated by the yellow lines.

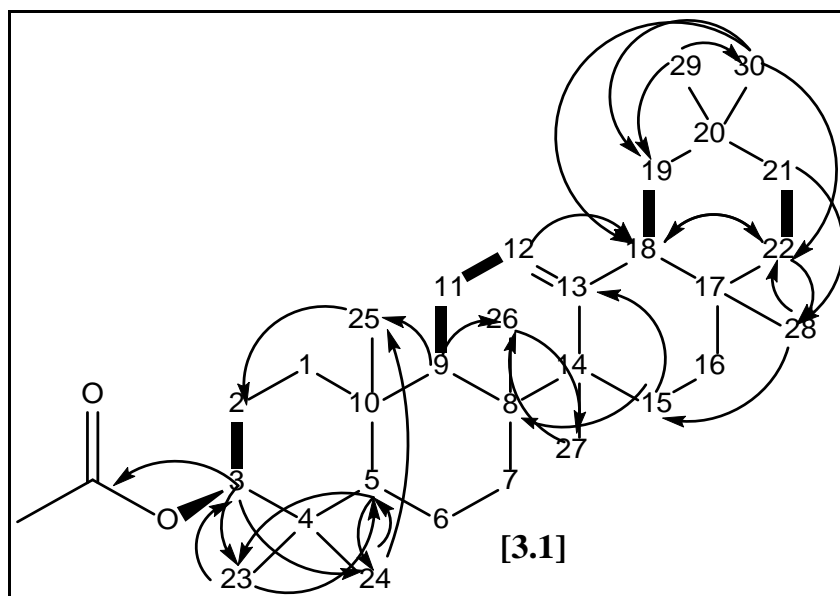


**Figure 5.25:** Representative  $^1\text{H}$ - $^1\text{H}$ -COSY and  $^1\text{H}$ - $^{13}\text{C}$ -HMBC correlations of **3.1**; the  $^1\text{H}$ - $^1\text{H}$ -COSY correlation and the  $^1\text{H}$ - $^{13}\text{C}$ -HMBC correlation are respectively indicated by the bold lines, and arrows.  $4 J$ -coupling is anonymous of  $W J$ -coupling.

**Table 5.5:** Full carbon and proton assignments for  $\beta$ -amyrin acetate **3.1**  $^{13}\text{C}$ - $^1\text{H}$  cross-signals in the HSQC and HMBC spectra.  $^{13}\text{C}$ -NMR (125 MHz,  $\text{CDCl}_3$ ) and  $^1\text{H}$ -NMR (400 MHz,  $\text{CDCl}_3$ ) are compared with the corresponding articles in  $\text{CDCl}_3$ .

Atom No.	$\beta$ -amyrin acetate <b>3.1</b>			Literature (Nasution <i>et al.</i> , 2017; Shi <i>et al.</i> , 2014)	
$\text{CDCl}_3$	Integral, $\delta_{\text{H}}$ , multiplicity, $J$ in Hz	$\delta_{\text{C}}$	HMBC	Integral, $\delta_{\text{H}}$ , multiplicity, $J$ in Hz (400 MHz)	$\delta_{\text{C}}$ (100 MHz)
1	2H, 0.82, m	38.5	6, 5, 9	2H, 0.93, m	38.7
2	2H, 1.65, m	26.2	10	2H, 1.67, m	27.0
3	1H, 4.45, t, $J = 10$	81.1	1', 23, 24	1H, 4.50, t, $J = 8.0$	81.0
4		38.5			38.1
5	1H, 0.79, m	55.5	23, 24	1H, 0.84, m	55.4
6	2H, 1.59, m	18.3	1, 26, 10, 3	2H, 1.54, m	18.4
7	2H, 1.37, d, $J = 4.7$	33.8	9, 5	2H, 1.38, m	32.7
8		40.9			39.9
9	1H, 1.32, m	50.4	25, 26, 6	1H, 1.32, m	47.7
10		36.9			36.9
11	2H, 1.61, m	24.3	10, 18, 12	2H, 1.62, m	23.6
12	1H, 5.25, t, $J = 5.1$	125.5	14, 10, 18	1H, 5.18, t, $J = 3.5$	121.7
13		146.0			145.2
14		41.2			41.8
15	2H, 1.10, m	25.1	13, 8	2H, 1.15, m	25.0
16	2H, 1.68, m	23.8	28, 19, 22	2H, 1.75, m	23.3
17		40.1			32.4
18	1H, 1.26, m	50.9	22, 28, 14	1H, 1.33, m	47.4
19	2H, 1.64, m	37.9	28, 22, 21, 20, 12	2H, 1.67, m	37.3
20		33.8			31.4
21	2H, 1.41, m	34.9		2H, 1.30, m	33.4
22		37.2	28, 18		37.2
23	3H, 0.86, s	28.4	3, 5	3H, 0.88, s	28.0
24	3H, 0.84, s	16.6	25, 5	3H, 0.83, s	16.7
25	3H, 0.82, s	16.0	5, 2, 9	3H, 0.84, s	15.6
26	3H, 0.94, s	17.8	27, 10, 9	3H, 0.97, s	16.7
27	3H, 1.67, s	27.4	26, 18, 9, 12	3H, 1.13, s	26.0
28	3H, 0.95, s	17.8	15, 22, 19	3H, 0.84, s	27.0
29	3H, 0.99, s	23.8	19, 30	3H, 0.95, s	23.6
30	3H, 0.86, s	22.6	19, 22, 18	3H, 0.87, s	23.5
$\text{CH}_3\text{O}$	3H, 2.04, s	171.0		3H, 2.03, s	171.0

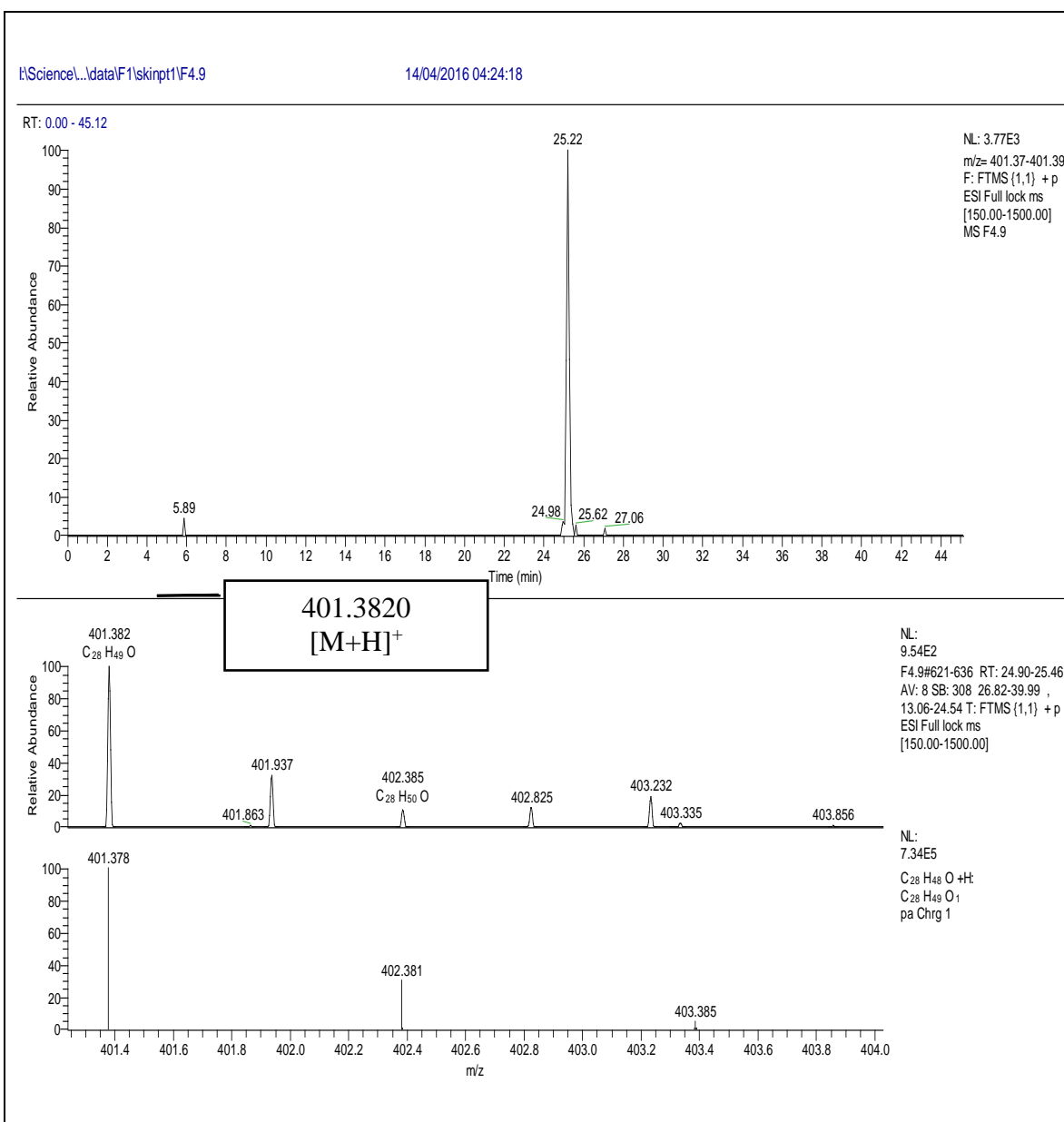
The structure of **3.1** was identified and elucidated as  $\beta$ -amyrin acetate **3.1**. The analysis of  $^1\text{H}$ ,  $^{13}\text{C}$ , COSY, HSQC, and HMBC NMR data, along with a comparison of the chemical

shift values with relevant published articles (Nasution *et al.*, 2017; Shi *et al.*, 2014), established the structure of **3.1** as  $\beta$ -amyirin acetate.

#### 5.4.2 Campesterol 3.3

**Table 5.6:** F4.9 of *F. carica* exocarp. Description of campesterol **3.3**; chemical structure; LC-MS analysis, and the identification of GCMS.

<b>Campesterol [3.3]</b>
Synonym(s): Campest-5-en-3 $\beta$ -ol
Source: Exocarp of <i>F. carica</i>
Metabolite: F4.9
Sample amount: 44 mg
Physical description: semi-colourless solid
Molecular formula: C <sub>28</sub> H <sub>48</sub> O
Exact Mass: 400.3705 g/mol
<b>Chemical structure</b>
<p>The chemical structure of Campesterol (3.3) is a steroid with a hydroxyl group at C-3 and a branched alkyl side chain at C-17. The side chain consists of carbons 18 through 28. The structure is labeled [3.3].</p>
<b>LC-MS analysis</b>



The positive-ion high-resolution ESIMS of **3.3** showed an accurate mass ion peak at  $m/z$  401.2533 [M+ H]<sup>+</sup>, in accordance with a molecular formula of C<sub>28</sub>H<sub>49</sub>O.

Evidence of the chirality of the C-24 epimer of campesterol, instead of brassicasterol, was established with 1D and 2D NMR spectroscopic techniques and was assigned based on comparison with the literature (Prakasa Rao *et al.*, 2010; Rahelivao *et al.*, 2017; Sica, Piccialli and Masullo, 1984). Moreover, Uomori *et al.*, (1992) reported fingerprint peaks, where H-27 was observed at double the height of H-21 in campesterol, as opposed to brassicasterol, as shown in [Figure 1S](#).

Campesterol **3.3** was isolated from organic solvent in the form of semi-colourless solid needles. Campesterol **3.3**, the C-24 epimer of brassicasterol, was first described in rapeseed oil *Brassica campestris* L. (Fernholz and MacPhillamy, 1941; Garg and Nes, 1986; Sica, Piccialli and Masullo, 1984), and later isolated from diverse natural sources, including from soft corals and fungi. The first synthesis of **3.3** was described in 2012 by O'Connell and co-workers, and was the first to be specifically identified in *F. carica* fruit in 2010 by Pande and Akoh. In this study, campesterol **3.3** was isolated from the exocarp of *F. carica*.

The <sup>1</sup>H-NMR of campesterol **3.3** was run at 600 MHz in CDCl<sub>3</sub> (Figure 5.26), and the spectrum confirmed the presence of six methyl groups at δ 0.69 (s, H-18), 1.02 (s, H-19), 0.93 (d, *J* = 6.58 Hz, H-21), 0.86 (d, *J* = 7.68 Hz, H-26), 0.84 (d, *J* = 6.58 Hz, H-27), and 0.83 (d, *J* = 6.92 Hz, H-28). A hydroxyl substituent and an olefinic double bond were indicated at δ 3.52 (m, H-3) and 5.35 (t, *J* = 1.88 Hz, H-6), respectively. Full details of the <sup>1</sup>H-NMR spectrum of **3.3** are presented in Table 5.7.

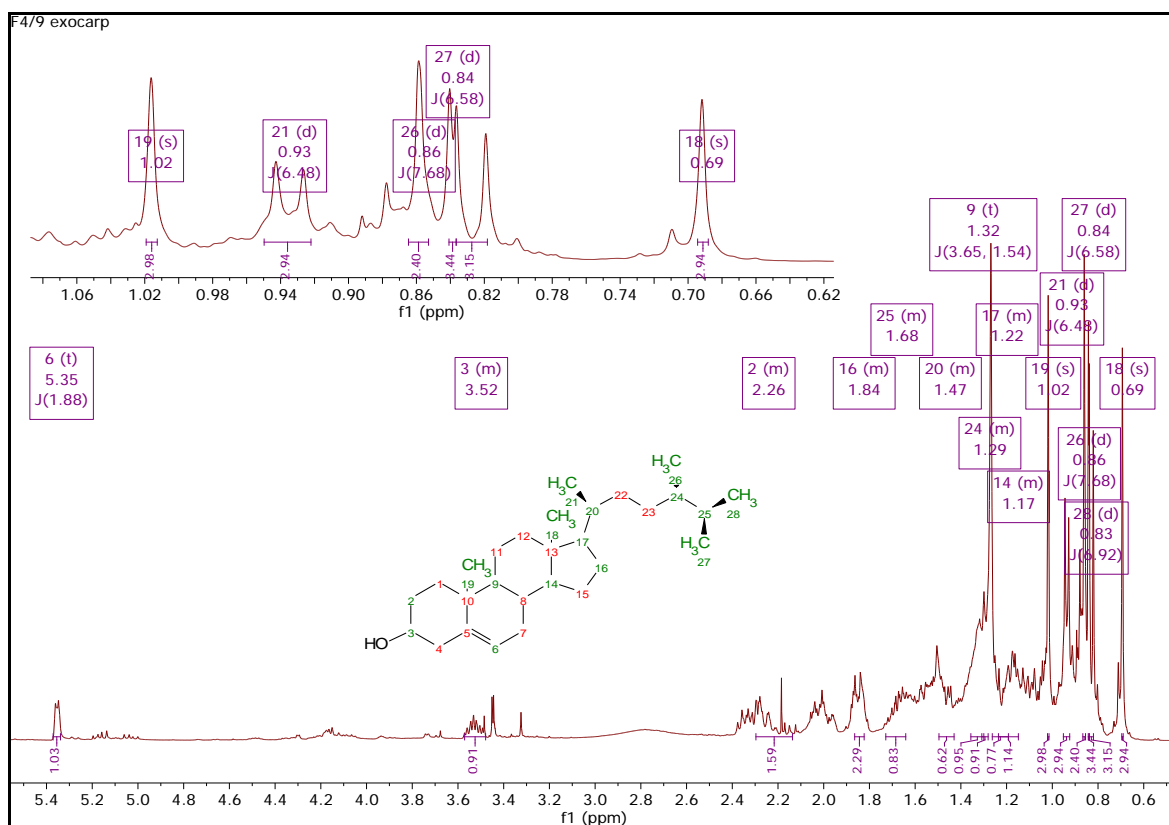


**Figure 5.26:**  $^1\text{H-NMR}$  spectrum of campesterol **3.3** (500 MHz,  $\text{CDCl}_3$ ), with an expansion of the  $^1\text{H-NMR}$  spectrum between 0.66 to 1.06 ppm.

The  $J_{\text{mod}}$  at 125MHz in  $\text{CDCl}_3$  of **3.3** in Figure 5.27 revealed the presence of the hydroxyl group at  $\delta$  71.8 (C-3) as well as a double bond at  $\delta$  140.7 (C-5) and 121.7 (C-6). Six methyl carbons were also present at  $\delta$  11.9 (C-18),  $\delta$  19.8 (C-19),  $\delta$  18.8 (C-21),  $\delta$  18.7 (C-26),  $\delta$  21.1 (C-27), and  $\delta$  14.1 (C-28). In addition to the quaternary C-5, two quaternary carbons occurred at  $\delta$  36.1 (C-10), and 45.8 (C-13). Full details of the  $J_{\text{mod}}$  and  $^{13}\text{C-NMR}$  are presented in Table 5.7.

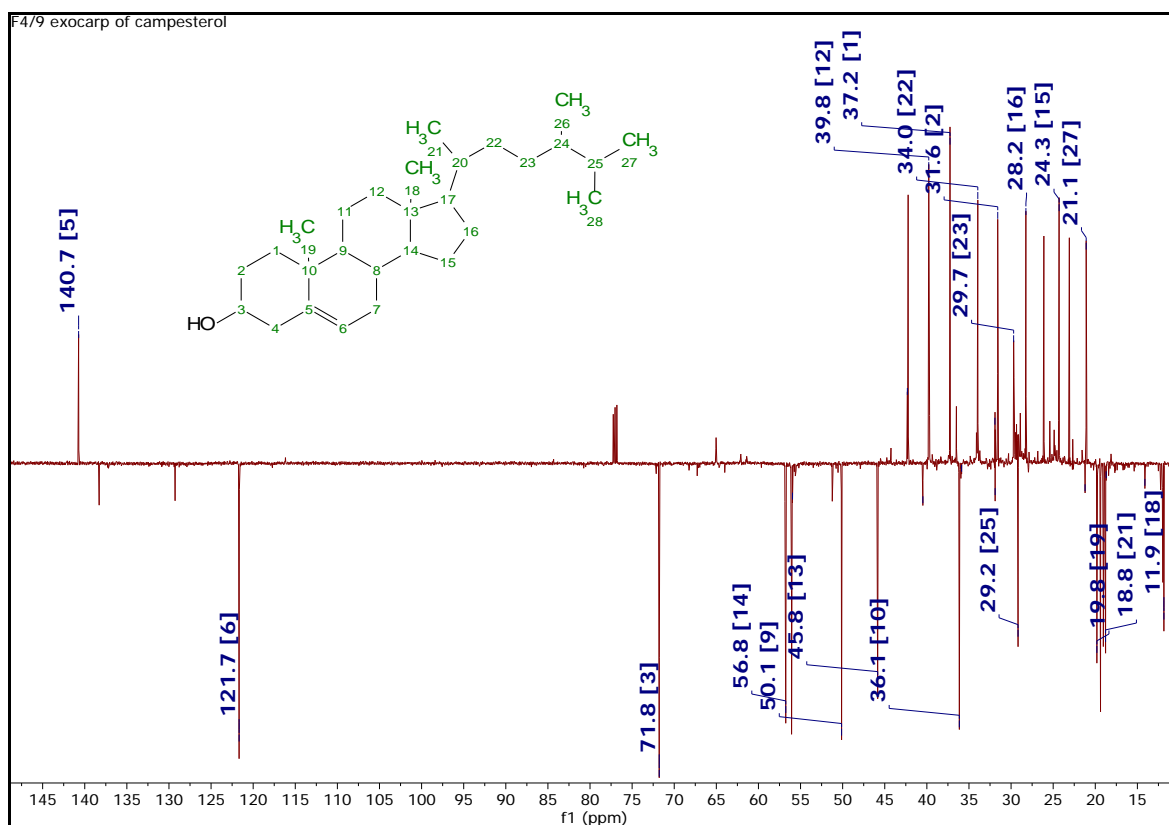


**Figure 5.27:** *J*-mod-NMR spectrum (125 MHz,  $\text{CDCl}_3$ ) of **3.3**. The signals at 77 ppm were allocated to the  $\text{CDCl}_3$  solvent.  $\text{CH}_3$  and  $\text{CH}$  constituted the negative signals, whereas quaternary carbon and  $\text{CH}_2$  are indicated by the positive signals.

The COSY spectrum of **3.3** (Figure 5.28) identified the correlation between  $\delta$  2.24 and 3.56, corresponding to the hydroxyl group linked with H-3 to H-2, while the cross peak of  $\delta$  5.38 with 1.95 corresponded to the double bond between H-6 to H-7. A three-bond correlation of H-27 at  $\delta$  0.84 and H-28 at  $\delta$  0.83, with H-25 at  $\delta$  1.68, which was linked to H-24 at  $\delta$  1.33, and that of H-20 at  $\delta$  1.47 correlated with H-21 at  $\delta$  0.94, confirmed the attachment of the methyl moieties  $\text{CH}_3$ -28,  $\text{CH}_3$ -27, and  $\text{CH}_3$ -21 on the side chain of **3.3**.

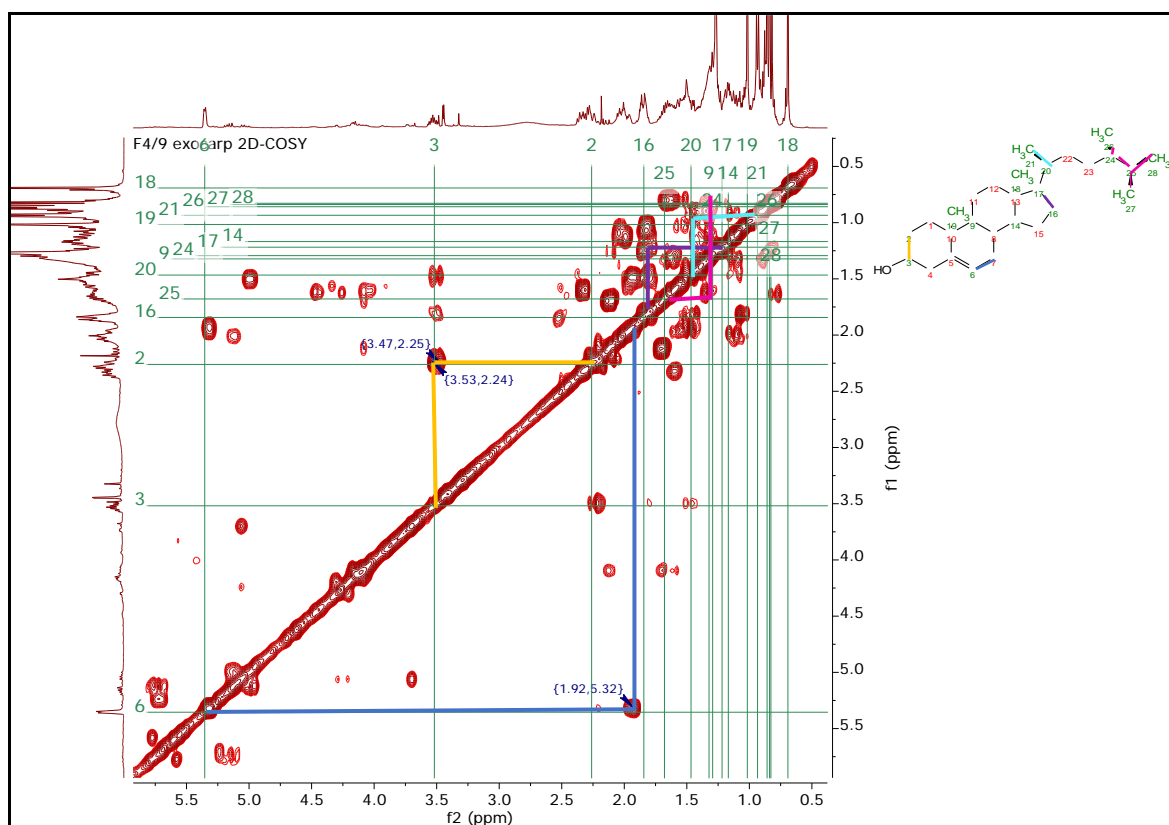


**Figure 5.28:**  $^1\text{H}$ - $^1\text{H}$ -COSY spectrum of **3.3**. Their chemical shift within the campesterol structure is denoted by the green lines.

Final confirmation of the structure was achieved using HMBC (Figure 5.29). The HMBC spectrum demonstrated a correlation of H-2 at  $\delta$  2.24 with C-3 at  $\delta$  71.8, and C-5 at  $\delta$  140.7. The olefinic signals at  $\delta$  5.38 (H-6) correlating with C-1 at  $\delta$  37.2, C-8 at  $\delta$  31.9, and C-10 at  $\delta$  36.1 revealed the position of the monosubstituted double bond (C-5/C-6). The correlation of H-28 at  $\delta$  0.83 with C-23 at  $\delta$  29.7, and C-24 at  $\delta$  40.5, H-27 at  $\delta$  0.84 with C-23 at  $\delta$  29.7, C-24 at  $\delta$  40.5, and C-28 at  $\delta$  14.1 in addition to the correlation of H-26 at  $\delta$  0.86 with C-23 at  $\delta$  21.1, C-27 at  $\delta$  21.1, and C-28 at  $\delta$  14.1 established that methyl carbons C-28 and C-27 were bound to C-25 at  $\delta$  29.2 while C-26 was linked C-24 at  $\delta$  40.5. Furthermore, the correlation of H-21 at  $\delta$  0.94 with C-22 at  $\delta$  34, and C-23 at  $\delta$  29.7, correlation of H-19 at  $\delta$  1.02 with C-1 at  $\delta$  37.2, C-2 at  $\delta$  31.6, C-5 at  $\delta$  140.7, C-6 at  $\delta$  121.7, and C-9 at  $\delta$  50.1, correlation of H-18 at  $\delta$  0.96 with C-12 at  $\delta$  39.8, C-14 at  $\delta$  56.8, and C-20 at  $\delta$  35.9 confirmed that the methyl carbons C-21, C-19 and C-18 were bound to C-20 at  $\delta$  35.9, C-10 at  $\delta$  36.1, and C-13 at  $\delta$  45.8, respectively.

The combined information gathered from the COSY and HMBC spectra allowed a complete assignment of **3.3**, as shown in Figure 5.30. These spectroscopic features suggested that compound **3.3** possesses a skeleton similar to that of cholesterol. Comparison of the spectral data with the literature (Rahelivao *et al.*, 2017) confirmed that **3.3** is campesterol.

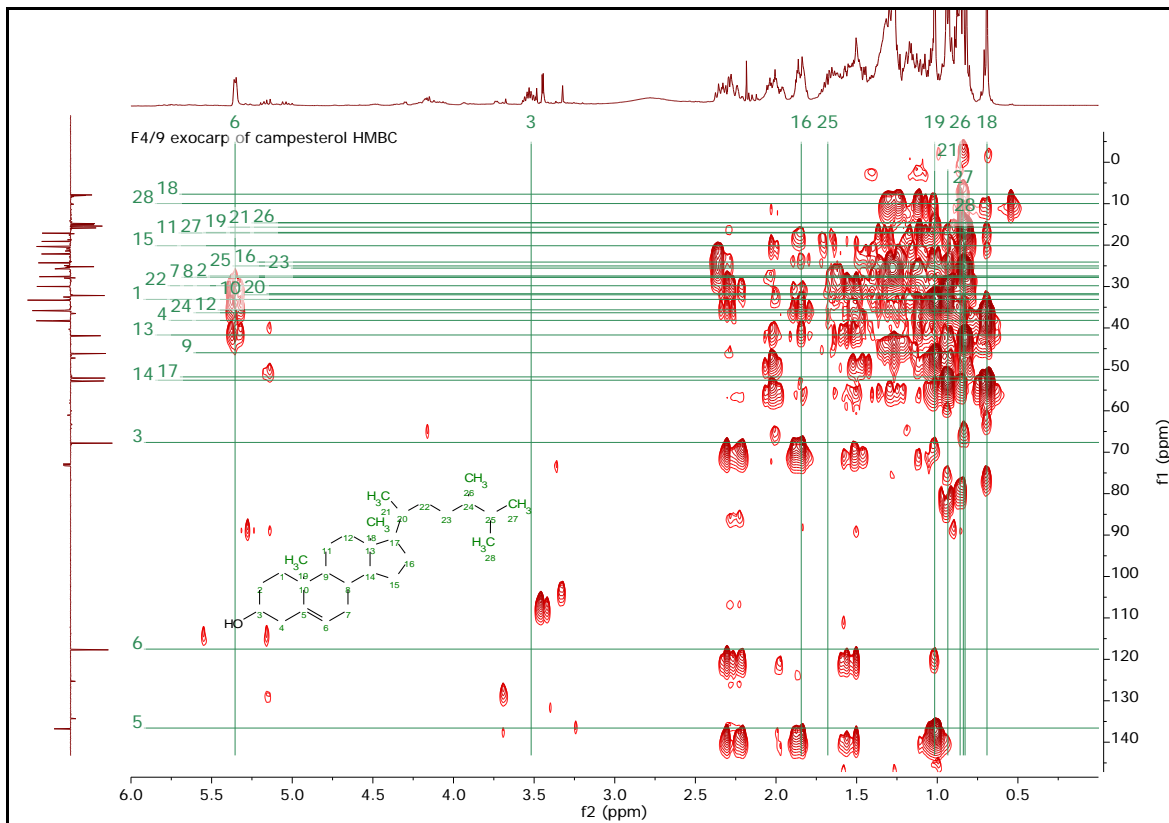


**Figure 5.29:**  $^1\text{H}$ - $^{13}\text{C}$ -HMBC spectrum of **3.3** in  $\text{CDCl}_3$  at 500MHz.

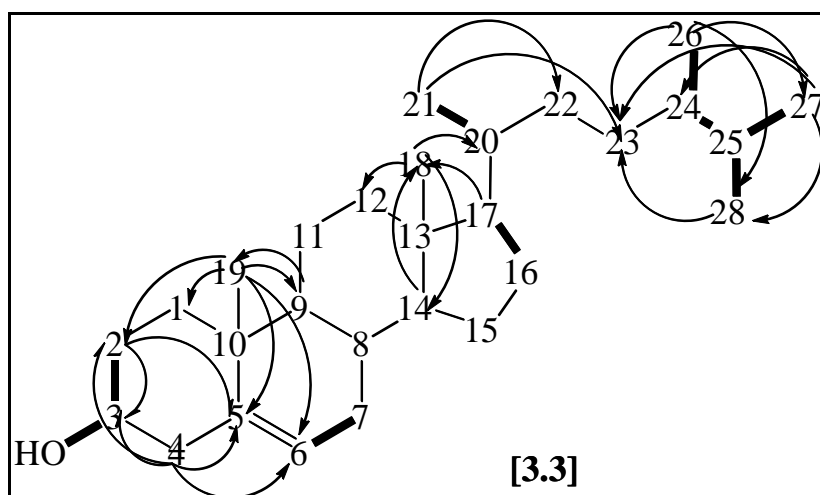


**Figure 5.30:** Characteristic  $^1\text{H}$ - $^1\text{H}$ -COSY and  $^1\text{H}$ - $^{13}\text{C}$ -HMBC correlations of compound **3.3**.  $4 J$ -coupling is anomalous of  $W J$ -coupling.

**Table 5.7:** Compound **3.3**;  $^1\text{H-NMR}$  (500 MHz), including integral, coupling constant and multiplicity,  $J$ mod-NMR (125 MHz) and HMBC correlation of **3.3** exhibited consistency with previous studies.  $^1\text{H-NMR}$  was recorded at 600MHz in  $\text{CDCl}_3$  and  $^{13}\text{C-NMR}$  at 150 MHz).

No	Campesterol <b>3.3</b>			(Rahelivao <i>et al.</i> , 2017)	
	$\delta_{\text{H}}$ , multiplicity, $J$ in Hz	$\delta_{\text{C}}$	HMBC	$\delta_{\text{H}}$ , multiplicity, $J$ in Hz	$\delta_{\text{C}}$
1		37.2	3, 5, 10		37.25
2		31.6	3, 5		31.67
3	1H, 3.52, m	71.8			71.81
4		42.3	2, 3, 5, 6		42.31
5		140.7			140.7
6	1H, 5.35, t, $J = 1.9$	121.7	1, 8, 10	1H, 5.33, m	121.7
7		31.9	4, 14		31.90
8		31.9	1, 11, 13, 16, 18		31.90
9	1H, 1.32, dd, $J = 3.6, 1.5$	50.1	1, 2, 7, 13, 15, 19		50.12
10		36.1			36.50
11		21.2	7, 8, 14, 17		21.08
12		39.8	9, 14, 16		39.76
13		45.8			42.31
14	1H, 1.17, m	56.8	11, 18		56.75
15		24.3	7, 8		24.29
16	2H, 1.84, m	28.2	12, 14, 20		28.19
17	1H, 1.22, m	56.0	11, 14, 15, 18		55.98
18	3H, 0.69, s	11.9	12, 14, 20	3H, 0.66, s	11.85
19	3H, 1.02, s	19.8	1, 2, 5, 6, 9	3H, 1.00, s	19.40
20	1H, 1.47, m	35.9	12, 15, 16, 17		36.18
21	3H, 0.93, d, $J = 6.6$	18.8	22, 23	3H, 0.91, d, $J = 6.8$	18.88
22		34	23, 25		33.71
23		29.7	25		30.56
24	1H, 1.29, m	40.5	20, 22, 27, 28		39.06
25	1H, 1.68, m	29.2	23		31.90
26	3H, 0.86, d, $J = 6.7$	18.7	23, 27, 28	3H, 0.77, d, $J = 6.8$	17.88
27	3H, 0.84, d, $J = 6.6$	21.1	23, 24, 28	3H, 0.84, d, $J = 6.8$	20.52
28	3H, 0.83, d, $J = 6.9$	14.1	23, 24, 28	3H, 0.76, d, $J = 6.8$	15.44

**CHAPTER SIX DISCUSSION AND CONCLUSION OF *F. CARICA***

---

## 6. General discussion and conclusion

---

### 6.1. The discovery and the chemistry study

Traditional drugs have been used since ancient times while in modern times native medicines continue to be considered of great importance from both economic and professional points of view (Tapsell *et al.*, 2006). The search for functional foods that reduce the risk for neurodegenerative diseases brought nuts and fruits into a focus of research. *F. carica* is one of the most common fruit that has been used for nutritional as well as medicinal purposes for centuries and has been identified as providing protection against AD (Kristbergsson and Ötleş, 2016). This current study conducted empirical work utilising the antioxidative stress effects of *F. carica* endocarp, exocarp, and mesocarp. However, to date, the efficacy of non-polar ethyl acetate extracts of *F. carica* endocarp, exocarp and mesocarp as an acrolein attenuator of oxidative stress-related of AD has never been described in the literature. No other study has also been reported on the cytotoxicity and the expression of NQO1 protein caused by triterpenoids, fatty acid, and phenols that were currently isolated from *F. carica*. In this study, for the first time, a metabolomic profile of *F. carica* has been presented, highlighting the isolation of bioactive compounds that included  $\gamma$ -sitosterol **1.1**, oleoyl- $\beta$ -D-arabinoside **1.2**, lupeol acetate **1.3**, lawsaritol **2.1**, parahydroxybenzoic acid **2.6**, vanillic acid **2.7**,  $\beta$ -amyrin acetate **3.1**, and campesterol **3.3**. Specifically, the study focused on the cytotoxicity caused by oxidative stress triggered by acrolein, and the protective antioxidant protein expression of NQO1, in the context of AD.

In this study, as described in the methodology section, methanol, acetone, ethyl acetate and water were used to fractionate the different phytochemical constituents from the *F. carica* endocarp, exocarp and mesocarp. Within the process of obtaining and purifying the respective bioactive plant constituents, the first and crucial step is extraction (Bachir bey *et al.*, 2014). Accordingly, non-polar metabolites were isolated from the crude aqueous extracts with low polarity solvent by using ethyl acetate. An increase occurrence of protein content in the aqueous phase suggested that fractionation was a tool for concentrating polar components as well. Nonetheless, overall, the polar layer was later excluded from the analysis because the aqueous extracts contained polysaccharides and

sugar in greater quantities. As a result, the non-polar EtOAc-soluble fraction was found to exhibit antioxidative stress activity in *in vitro* differentiated SH-SY5Y cell line. Further fractionation of the non-polar extract with hexane and ethyl acetate increased the antioxidant activity. However, further purification decreased the bioactivity in some fractions. It was also implied that the antioxidant effect might be the outcome of the symbiotic activity of bioactive compounds in crude extracts. Furthermore, certain compounds (e.g. phenols and flavonoids) might likely have also been eliminated through fractionation. The observation regarding the symbiotic behaviour of multiple plant antioxidants corroborates the findings reported by Misbah *et al.* (2013).

However, the major bottleneck that continues to affect NP drug discovery, is the isolation and purification of the active metabolites from some exceptionally complex elements. Non-polar extracts were fractionated by normal phase flash chromatography through gradient elution of a mixture of hexane and ethyl acetate mixture through silica gel and monitored by TLC for their similarity and purity. This afforded 71 fractions, which was distributed to 16 fractions from the mesocarp, 29 fractions from the endocarp, and 26 fractions from the exocarp. The use of high-throughput fractionation method was valuable in terms of simplifying the chemical profile of crude mixtures and enhancing the impact of natural chemical diversity on the drug discovery process.

The application of TLC was an indispensable preliminary screening step in each of the fractionation and purification steps used in this current study. A range of various solvent systems was employed for the qualitative TLC assay. The application of TLC assay could configure some of the compounds in which can be preliminarily detected by the colour of the fractions as in the purification of vanillic acid **2.7** (Báthori *et al.*, 2003; Harborne, 1984). For example, the pink colour of F14 (section 4.3) was attributed to the pigment of vanillic acid **2.7**, which was consistent with Harborne's (1984) description of distinguishing vanillic acid that attains the pink colour from the blue colour of isovanillic acid isomer, which may have rather similar  $R_f$  values. Free radical scavenging attributes were also revealed by other fractions of certain bioactive mesocarp and exocarp metabolites manifested by moderate yellow spot on the TLC plate (section 3.5 and 5.1.3).

Identification and elucidation of the bioactive compounds were fully investigated by GCMS and predominantly with NMR spectroscopy. The structures of these compounds were confirmed by comparing their spectroscopic data to those in the literature. Oleoyl- $\beta$ -D-arabinoside **1.2** was described in *F. carica* mesocarp for the first time, whereas  $\gamma$ -sitosterol **1.1** and lupeol acetate **1.3** were earlier reported in several *Ficus* species (Jeong and Lachance, 2001; Mawa, Husain and Jantan, 2017). Meanwhile,  $\gamma$ -sitosterol **1.1**, the major bioactive phytosterol in *F. carica*, exhibited the suppression of acrolein amongst the other compounds. In this context, one study found that a symbiotic cooperation frequently arises between many natural antioxidative compounds, generating various antioxidative effects targeting the action of free radicals (Belguith-Hadriche *et al.*, 2017).

According to the literature review conducted, no study had addressed the chemical composition of the constituents of *F. carica* fruit, especially that of oleoyl- $\beta$ -D-arabinoside **1.2**. oleoyl- $\beta$ -D-arabinoside was first isolated from rice straw (*Oryza sativa* Straw) (Ahmad *et al.*, 2013). Meanwhile, Seshadri and Vydeeswaran (1971) were the first to extract lupeol acetate **1.3** from the root *Pergularia daemia*, a member of the *Asclepiadoideae* family. However, as far as the current researcher is aware, this was the first *in vitro* study to examine oleoyl- $\beta$ -D-arabinoside **1.2** in the context of acrolein-triggered oxidative stress. Meanwhile, lupeol acetate **1.3** was first reported from the root *Pergularia daemia*, a member of the *Asclepiadoideae* family (Seshadri and Vydeeswaran, 1971). On the other hand, lawsaritol **2.1** was already earlier identified from *F. carica*. lawsaritol **2.1** was first isolated from the root of *Lawsonia inermis*<sup>16</sup> (Sarwar Alam *et al.*, 1992). It was later described from two green algae species, *Cedrus deodara* (Srivastava and Kulshreshtha, 2010) and *Chaetomorpha basiretorsa* Setchell (Shi *et al.*, 2008) as well as the aerial parts of *Stachys byzanthina* C. Koch<sup>17</sup> (Khanavi *et al.*, 2005). Vanillic acid **2.7** has been identified and isolated from the endocarp of *F. carica* that is consistent with previous studies (Russo *et al.*, 2014) indicating that the pulp of the fig contains low concentrations of vanillic acid **2.7**. Parahydroxybenzoic acid **2.6** has been isolated from almond skin (*Prunus amygdalus* Batsch) and reported to form a strong antioxidant DPPH

---

<sup>16</sup> *Lawsonia inermis* is known as henna plant and it is commonly used as cosmetically, medicinally and traditionally in India and middle east for over 9,000 years (Chaudhary, Goyal and Poonia, 2010).

<sup>17</sup> *Stachys byzanthina* C. Koch belongs to the family Lamiaceae and the genus of *Stachys*. It is widespread in the flora of Turkey and has been used in Turkish folk medicine as a stomachic (Erdemoglu *et al.*, 2006).

radical scavenging activity (Sang *et al.*, 2002). Both **2.6** and **2.7** have been earlier identified and isolated from *F. erecta* (Park *et al.*, 2011).

In order to gain a basic understanding of the isolated bioactive component, it is important to take into consideration their chemistry before its biology can be understood. Plant sterols such as  $\beta$ -amyrin acetate **3.1** and campesterol **3.3** are structurally comparable to cholesterol with substituents on the side chain at the C<sub>24</sub> position. They are not synthesised in animals, and in this manner, studies have shown sitosterol and other mixtures of plant sterols to effectively reduce serum cholesterol levels by about 10% in humans at doses of approximately 1 g/day (Kris-Etherton *et al.*, 2002). Previous study has also reported that vanillic acid **2.7** has an inhibitory effect on the methylglyoxal-mediated oxidative-sensitive pathway activated in apoptotic neuro-2A cells (Huang *et al.*, 2008). Despite the fact that leaf parts are traditionally used, this current study has also demonstrated that the exocarp of *F. carica* showed effective antioxidant properties via either electron or hydrogen atom transfer (Choo *et al.*, 2012).

In  $\beta$ -amyrin acetate **3.1**, chirality plays an important role on its bioactivity. Chiral compounds can behave very differently in biological systems due to their diverging orientations in a three-dimensional space (McConathy and Owens, 2003). It has been earlier described that both  $\alpha$  and  $\beta$  amyrin epimers are produced in different parts of plant, which raises questions concerning their specific physiological roles such as in cell proliferation, elongation, and expansion (Crumley *et al.*, 1990).

Meanwhile, another study promoted the *in vitro* accumulation of A $\beta$  peptide and tau protein (Fraser *et al.*, 2009). Conversely, *in vivo* studies showed that increased dose levels of oleic acid protected TgCRND8 mice brains against AD-type neuropathology (Amtul *et al.*, 2010). It is interesting to note that oleic acid represented the aglycone part of oleioyl- $\beta$ -D-arabinoside **1.2** that was isolated from the mesocarp of *F. carica*.

There has been evidence that significant changes in clinical and biological activities were demonstrated by different respective isomers. For example, D(+) amphetamine exceeds the potency of L(-) amphetamine by tenfold in suppressing noradrenaline aggregation in nerve terminals (Parkes and Fenton, 1973), while analgesia in male CD-1 mice was only observed to be effective with D-morphine but not with L-morphine (Wu, 2005).

In the case of oleoyl aglycone (18:1n-9 *cis*), the *cis-trans* configuration was of great significance as well. *Cis* oleoyl- $\beta$ -D-arabinoside has been reported to reduce oxidative stress *in vitro* (Cordain, 2012). On the other hand, the *trans* configuration of elaidic fatty acid was set apart from the adverse side effect of its *trans* isomer on the increase levels of blood cholesterol.

Alternatively, the antioxidant activity of the  $\gamma$ - isomer of tocopherol was half of the effect of its  $\alpha$  isomer, which constituted the second defence line against oxidative stress in LDL (Vessby and Sundlof, 1996). From these observations, the biological activity of *F. carica* on *in vitro* differentiated SH-SY5Y cell line could be inferred on the isolated  $\gamma$ -sitosterol **1.1**. However, no research has so far been conducted on the mechanism through which these isomers support molecular biological binding.

## **6.2. Metabolomics**

Earlier research indicated that the greatest antioxidant effect was exhibited by fruit and vegetables widely included in diets, particularly those of a dark blue or red colour, such as berries and figs (Liu *et al.*, 2002; Wu *et al.*, 2006; Solomon *et al.*, 2006; Elik *et al.*, 2008). This study therefore confirmed that validity existed in the use of fig fruit and peel in traditional medicine employed to combat oxidative stress (Misbah *et al.*, 2013; Solomon *et al.*, 2006). Ideally, a combination of biological assays incorporated with HTS is a useful technique to obtain information on the antioxidant capacity of a *F. carica* fruit. Thus, the additional aim of this study was to explore the analytical tools of metabolomics by employing high resolution LC-MS.

The respective fruit parts of *F. carica* was separately extracted, concentrated, fractionated, and purified to afford the biologically active metabolites. Unsupervised PCA analysis facilitated the separation of *F. carica* fractions to clusters in a scores scatter plot while the discriminatory metabolites were putatively identified by utilising the loadings scatter plot. HCA dendrograms was used to visualise the similarity of fractions according to their chemical profiles, which was achieved with ward's tree linkage. Small distances between metabolites implied that greater similarity, while dissimilar metabolites were separated by relatively longer distances (Lozano *et al.*, 2014). Alternatively, supervised OPLS-DA and S-plot analysis were employed to explore in targeting the bioactive

metabolites, which were the ion peaks at  $m/z$  469.404, 414.381, 414.297, 401.253, 168.030, and 168.031.

HTS process has been limited and suffered most often in the rapid identification of known compounds as the major hurdle (Smyth *et al.*, 2012). Multivariate analysis including dereplication MACROS were used in this study to overcome the aforementioned limitation and to achieve the final objectives of this work. The study conducted the dereplication of phytochemicals in the three fruit parts of *F. carica* using the HPLC-ESI mass spectral data, which were pre-processed using MZmine that also partially achieved the dereplication process through a molecular formula prediction algorithm. The molecular formulas  $C_{29}H_{50}O$ ,  $C_{23}H_{12}O_6$ ,  $C_{32}H_{52}O_2$ ,  $C_{29}H_{50}O$ ,  $C_7H_6O_3$ ,  $C_8H_8O_4$ ,  $C_{30}H_{50}O$ , and  $C_{32}H_{52}O_2$  were further characterised by both the fragmentation pattern generated from GCMS data and the structural elucidation achieved through NMR, which afforded the identification of  $\gamma$ -sitosterol **1.1**, oleoyl  $\beta$ -D-arabinoside **1.2**, lupeol acetate **1.3**, lawsaritol **2.1**, parahydroxybenzoic acid **2.6**, vanillic acid **2.7**,  $\beta$ -amyrin acetate **3.1**, and campesterol **3.3**, respectively.

### **6.3. The biological study**

Multiple studies have demonstrated that oxidative stress and related damage are correlated with chronic diseases such as AD (Habtemariam, 2018a; Yang *et al.*, 2009). For example, abnormal deposits of A $\beta$  peptide in the CNS of AD patients are known to increase intracellular oxidative damage and contribute to inflammatory responses (Yan *et al.*, 2013). In addition to such direct oxidative damage, by-products of lipid peroxidation, such as acrolein, are also known to play a role in the aetiology of AD (Bonamigo *et al.*, 2017). A study has been published, in which acrolein was described to cause the inactivation of astrocytes in upregulating beta-secretase enzyme BACE-1 and degrading ApoE4 cofactor enzyme (a lipoprotein receptor) resulting in AD both *in vitro* and *in vivo* (Harbison *et al.*, 2015; Novak, 1999). Another study also found elevated plasma concentrations of acrolein in patients with chronic renal failure. Furthermore, the abundance of protein-acrolein adducts was also observed to increase in tissues from patients with AD, Parkinson's disease (PD), atherosclerosis and chronic obstructive lung disease (Pizzimenti *et al.*, 2013). Chaudhary and Ali, (2011) established the neuroprotective effect of methanolic leaf extract of *Ficus hispida* on A $\beta$  and oxidative

stress suppression by upregulation of glutathione peroxidase, glutathione reductase and superoxide dismutase *in vivo* mice model.

Additionally, acrolein-triggered AD and the effects of triterpenes, non-saturated fatty acid (FA) and phenols on the *in vitro* differentiated SH-SY5Y cell line have not been extensively investigated. This study sought to make up for this gap by employing an acrolein-induced antioxidant model to examine the antioxidant potential of non-polar *F. carica* extract in the context of AD. The amount of acrolein used to trigger oxidative stress was 20  $\mu$ M. Preliminary results suggested that AD development might be hindered by antioxidants (section 3.5, 4.5 and 5.2). This is consistent with the findings of earlier studies. It has been earlier reported that AD could be prevented by phytosterol (Kim *et al.*, 2015), while it was also revealed that AD levels were markedly reduced by stigmasterol, sitosterol and cholesterol (Kim *et al.*, 2015).

The isolated compounds were also investigated for their cytotoxicity during acrolein-induced oxidative stress against AD through an AlamarBlue<sup>®</sup> assay. Overall, the test demonstrated outstanding oxidative stress prevention of acrolein related AD. Furthermore, while the AD-prevention potential of *F. carica* ethyl-acetate extracts was investigated, a significant protection against acrolein-induced oxidative stress was shown. Parahydroxybenzoic acid **2.6** demonstrated the most significant EC<sub>50</sub> ( $13.7562 \pm 36.7434$   $\mu$ g/ml) activity against 20  $\mu$ M of acrolein-induced oxidative stress amongst all the isolated fractions.

Comparison of the *in vitro* suppressive effect of the bioactive fractions, parahydroxybenzoic acid [F14], vanillic acid [F14], lawsaritol [F20] and campesterol [F4.9] showed the significant greater efficacy against acrolein at (IC<sub>50</sub>  $13.76 \pm 36.74$   $\mu$ g/ml), (IC<sub>50</sub>  $11.30 \pm 30.18$   $\mu$ g/ml), (IC<sub>50</sub>  $3.92 \pm 14.63$   $\mu$ g/ml) and (IC<sub>50</sub>  $1.46 \pm 26.58$   $\mu$ g/ml), respectively. By contrast, the suppressive effect of the combination of  $\beta$ -amyrin acetate and lupeol acetate [F2.6], oleoyl- $\beta$ -D-arabinoside [F12,14/F9],  $\gamma$ -sitosterol [F4,5,6/F9] and lupeol acetate [F4,5,6/F1/F5] against acrolein was the least potent (IC<sub>50</sub>  $1.42 \pm 1.78$   $\mu$ g/ml), (IC<sub>50</sub>  $0.87 \pm 1.60$   $\mu$ g/ml), (IC<sub>50</sub>  $0.84 \pm 2.56$   $\mu$ g/ml) and (IC<sub>50</sub>  $0.64 \pm 2.85$   $\mu$ g/ml), respectively.

Nevertheless, a potent neuroprotective effect against acrolein-related AD was achievable with parahydroxybenzoic acid [F14]. Nonetheless, research is yet to be conducted regarding the sufficiency of these concentrations for diminishing A $\beta$  peptide production in humans.

Likewise, the endogenous antioxidant NQO1 enzyme is one of the most consistently and robustly inducible genes among the members of the family of cytoprotective proteins against oxidative stress (Shen *et al.*, 2016; Simoni *et al.*, 2017). In the brain of AD patients, NQO1 immunostaining closely correlated with the extent of local AD pathology across the various brain regions examined, suggesting that increased NQO1 activity may be neuroprotective (Masoudi *et al.*, 2014; Simoni *et al.*, 2017; Torres-Lista *et al.*, 2014). In APP/PS1 mice, NQO1 in cortex was slightly higher than controls at three months of age, but declined at 6 months. The over-expression of Nrf2 was neuroprotective against A $\beta$  peptide, and this effect was only associated to high-level expression of NQO1 among all Nrf2-ARE dependent genes (Torres-Lista *et al.*, 2014). Proelectrophiles from natural sources have attracted interest from a broad range of researchers in the drug discovery community (Simoni *et al.*, 2017). In particular, proelectrophile compounds, which include hydroquinone cores of terpenoids and flavonoids, are only converted to their active electrophilic forms in response to pathological oxidation, offering prospects of minimal potential side effects (Simoni *et al.*, 2017).

In the pursuit of finding more effective antioxidant properties, the antioxidant profile of the isolated compounds were also investigated for their ability to trigger the Nrf2 pathway in terms of up-regulation of the Nrf2-dependent defensive gene NQO1. Interestingly, in *in vitro* differentiated SH-SY5Y neuroblastoma cells, all compounds tested exhibited remarkable free radical scavenging properties and offered protection against oxidative stress by means of electrophilic activation of Nrf2-mediated response. As different biological features were exploited to regulate NQO1 activity, these findings pointed to the of the effectivity of the isolated compounds **2.6 > 2.7 > 1.3 > 2.1 > 1.1 > 1.2 > 3.2 > 3.3** arranged with the most to the least therapeutic potential on the NQO1 cellular network. This paved the way for the generation of new compound leads to confront AD prevention. However, the exact protective mechanisms underlying the effect of these isolated compounds on differentiated SH-SY5Y cell line remains to be fully examined.

### 6.3.1. The study of prevention of oxidative stress

As known antioxidants, phenolic compounds have been recognised for their importance in minimising pathological and toxic effects in accordance with oxidative stress (Kanski *et al.*, 2002). Antioxidants retard or prevent the oxidation of substrates and are highly beneficial to health as they protect cells and macromolecules from oxidising agents, in which are capable in neutralising free radicals by aromatic hydroxylation mechanisms and/or through the chelation of transition-metal ions and donating a hydrogen atom (Bonamigo *et al.*, 2017; Jung *et al.*, 2016; Shahidi and Zhong, 2010). The antioxidant radical is stabilised by delocalisation of the unpaired electron around the phenolic ring to the phenoxy free radical to form stable resonance hybrids (Shahidi and Zhong, 2010; Sumi *et al.* 2016). Moreover, the antioxidant radicals further scavenge free radicals by participating in the termination of oxidation (Shahidi and Zhong, 2010). This mechanism contradicts the published article by Shaikh *et al.* (2016), in which it is argued that compound **2.6** was found to be inactive to free radical scavenging. The current findings are in agreement with a published article that plant or animal extracts containing a mixture of antioxidant substances are also used directly to inhibit *in vitro* and *in vivo* oxidation (Shahidi and Zhong, 2010).

Nevertheless, concerning vanillic acid **2.7**, a literature search reported that the administration of vanillic acid **2.7** (30 mg/kg, Intraperitoneal injection, 3 times per weeks) in the murine A $\beta$ <sub>1-42</sub> model attenuates A $\beta$ <sub>1-42</sub>-induced ROS, memory impairment, synaptic deficits, neuroinflammation and neurodegeneration. However, the mechanisms that underlie many features of AD remains to be determined (Amin *et al.*, 2017). Other literature revealed that the presence of electron donating groups on the benzene ring the 3-methoxy 4-hydroxyl in **2.7** and its derivatives, such as ferulic acid, cinnamic acid, and cumaric acid; contribute to the stability of the intermediate. Phenoxy radicals may even break free radical chain reactions that are the same as their planar structure, the number and position of their OH groups, as well as the presence of the C2-C3 double bond are essential for antioxidant and free radical scavenging activities (Kanski *et al.*, 2002; Sumi *et al.*, 2016). Both **2.6** and **2.7** possess three distinctive structural motifs that possibly play a role to their free-radical scavenging capability (Figure 6.1). As such, both **2.6** and **2.7**

have the carboxylic acid substituents, and 4-OH, as well as the additional 3-methoxy group in vanillic acid **2.7**.

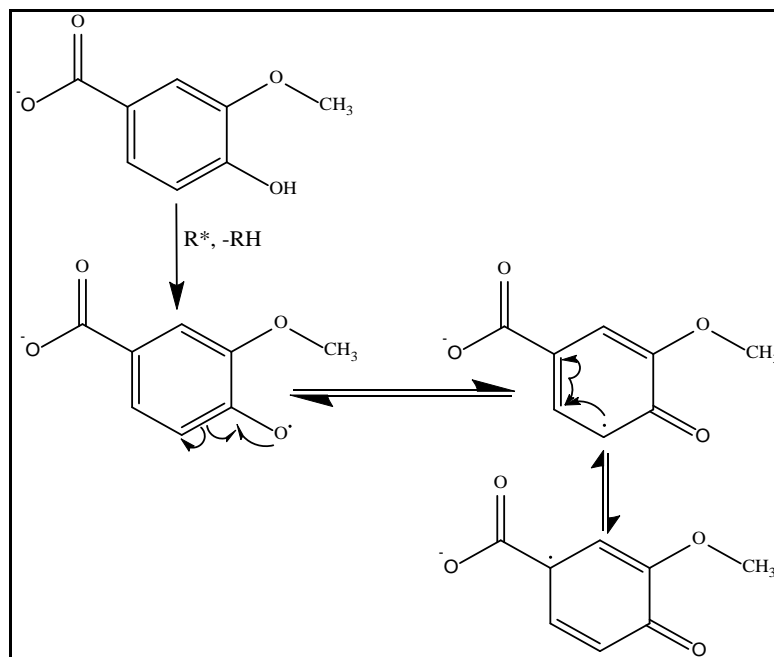


**Figure 6.1:** Possible resonance structures of **2.7** phenoxyl radical. Free radical initiation occurs at the 4-hydroxyl group by abstraction of hydroxyl H-atom; possible free radical initiation at carboxylic group is conceivable.

Moreover, the carboxylic acid group in parahydroxybenzoic acid **2.6** and vanillic acid **2.7** can further contribute to the stability of the radical by resonance or by providing additional sites for free radicals (Kanski *et al.*, 2002). It has been reported that this third functional group could facilitate anchoring of ferulic acid into the lipid bilayer, providing some protection against lipid-peroxidation (Sumi *et al.*, 2016). Compound **2.7** may also have this ability, even though it lacks the additional two carbon atoms adjacent to carboxylic acid as in ferulic acid (Figure 6.2). Given these and other characteristics, phenolic compounds are well recognised as potent antioxidants.

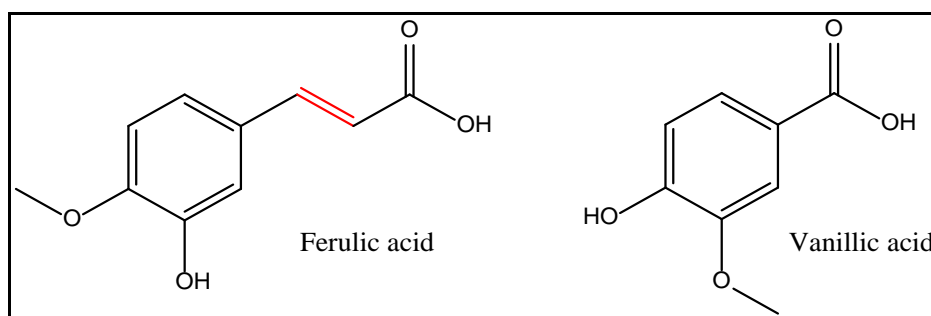


**Figure 6.2:** Chemical structure of ferulic acid and vanillic acid; both possess the same functionality with the additional of double bond in the aliphatic chain of ferulic acid (red colour).

Phenolic compounds are known for their antioxidant activity and for preventing radical scavenging due to their ability to act as hydrogen donors (i.e. parahydroxybenzoic acid **2.6** and vanillic acid **2.7**). Fatty acids (FA) such as the isolated oleoyl- $\beta$ -D-arabinoside **1.2** were also effective antioxidant compounds in ROS scavenging, which prevent potential damage to cellular proteins and lipids components (Abu Bakar *et al.*, 2017; Çalışkan and Aytakin Polat, 2011). Unfortunately, the levels of oleic acid isomers and omega-6 FA were demonstrated to be unusual in AD compared to that of omega-3 FA which may be linked to cognitive deterioration (Cunnanea *et al.*, 2012). The perturbation levels of plasma FA might be partly responsible for the AD-related fluctuations of brain FA (Cunnanea *et al.*, 2012). The levels of A $\beta$  species were suppressed by increasing concentration of supplemental oleic acid (Amtul *et al.*, 2010). This can be explained in terms of the fact that the membrane bilayer became more rigid or that the A $\beta$ <sub>24</sub> transport was disrupted by oleic acid enrichment, causing cellular pH to become more acidic.

Meanwhile, with the limited content of polyunsaturated species, the FA with the second greatest abundance after arachidonic acid in phosphatidylcholine from para-hippocampal cortex of AD was monounsaturated oleic acid (Corrigan *et al.*, 1998). These FA are of interest due to monounsaturated long-chain fatty acids can act as precursors for the biosynthesis of very-long chain monounsaturated acids such as nervonic acid (C<sub>26:1n-9</sub>) which are known to be important in neural function (Corrigan *et al.*, 1998). Likewise, a recent study has demonstrated that almost 20% of the body's consumption of glucose occurs in the brain, suggesting that the metabolic deficits present in AD patients may significantly contribute to pathogenesis (Williams *et al.*, 2011). It has been reported by that the positions of the methyl groups at carbons 18, 19, 21, 26 and 27 in phytosterols

such as sitosterol played a significant role in suppressing  $\beta$ -secretase 1 (BACE1) enzyme activity related to AD *in vitro* model (Jung *et al.*, 2016). This evidence suggested that suppression of AD-related acrolein cytotoxicity is also achieved by these active sites in a structure of the aforementioned compound. Furthermore, active sites in numerous antioxidant structures (e.g. fucosterol, fucoxanthin, quercetin) have been described to consist of methyl groups, double bonds and cyclic ring systems (Jung *et al.*, 2016). It could thus be inferred that acrolein suppression is accomplished by methyl groups present in FA structures as in oleoyl - $\beta$ -D-arabinoside **1.2** in reducing the oxidative stress of acrolein-related AD through a dual action, in terms of the glycol moiety (arabinoside) attachment to the oleoyl fatty acid.

In addition, the patent US 8609726 B2 registered by Bryhn (2013) relates to the use of FA composition, including oleic acid congeners, for the treatment of AD by targeting the A $\beta$  peptide. Bazinet and Layé (2014) have also explained the mechanism by which FA are accumulated in the myelin sheath of the brain. The brain accelerates its accumulation of polyunsaturated fatty acids PUFAs as well as oleic acid (monounsaturated fatty acid) through the diet, which act as the foundations of arachidonic acid (ARA) and docosahexaenoic acid (DHA) fatty acids. These FA are then metabolised in the brain by PUFAs, activated by the acyl-CoA synthetase (ACSL) and then esterified to the phospholipid membranes. Other PUFAs, such as linoleic acid (LNA),  $\alpha$ -linolenic acid (ALA), and eicosapentaenoic acid (EPA) are  $\beta$ -oxidised. Some fatty acid transporters also have ACSL activity and therefore probably facilitate the partitioning of FA to either esterification or metabolism in combination with fatty-acid-binding proteins (FABPs) in the brain.

Fat-soluble plant antioxidants, other than phenols and FA such as triterpenes and phytosterols have been also shown to possess *in vitro* neuronal bioactivity (Saratha *et al.*, 2011). It is noteworthy to mention that triterpenes have been reported to possess antioxidant effects (Saratha *et al.*, 2011). Clinical studies on more than 2,400 subjects, who were given various kinds of triterpenes in doses of 25 g or more daily, did not report any harmful effects (Saratha *et al.*, 2011). After sitosterol **1.1** (70%),  $\beta$ -amyrin **3.1** is the second most prevalent compound (60%) in the fig fruit, and was also identified as being present in the exocarp (Jeong and Lachance, 2001). Furthermore, antioxidant effects have

been attributed to the triterpene oleanolic acid-based  $\beta$ -amyrin derivative, diminishing oxidative stress, and improving mitochondrial function in PC12 cells treated with H<sub>2</sub>O<sub>2</sub> (Gonzalez-Burgos and Gomez-Serranillos, 2012). In addition, the defining feature of compound **1.3** in its lupine-type skeleton, which demonstrated its bioactivity due to the numerous natural estrogenic centres at positions C-3 and C-20 (Gupta *et al.*, 2016). Likewise, the isolated lawsaritol **2.1** may have also contributed to antioxidant protection against acrolein-related AD that has been observed to scavenge ROS and to be responsible for the increased antioxidant activity as lipophilic antioxidant systems in AD (Burg *et al.*, 2013; Bonamigo *et al.*, 2017; Guardiola, 2002). Hydroxyl groups and olefinic bonds seem to play a key role in the inhibitory potential of phytosterol compounds through hydrogen bonding and  $\pi$ - $\pi$  stacking interactions with the amino acid residues of the active centre of AChE enzymes in AD as reported for lawsaritol isolated from *Haloxylon recurvum*<sup>18</sup> (Ahmed *et al.*, 2006). These findings suggested that of the OH group and olefinic bonds in lawsaritol **2.1** could attenuate the acrolein-oxidation stress related AD

The presence of an ethyl group at C24 in stigmasterol that is structurally similar to lawsaritol, , which cholesterol does not have, has been shown to decrease BACE1 activity, by reducing 10% of the cholesterol content in the lipid bilayer and the expression of all c-secretase components (Burg *et al.*, 2013; Rao *et al.*, 2006; Uddin *et al.*, 2014). In parallel, c-secretase activity was dose-dependently significantly decreased in the CNS of mice fed with 0.39% stigmasterol-enriched diet (Amtul *et al.*, 2010; Cheng *et al.*, 2014). The presence of campesterol increased the expression of BACE1, with minor expression of secretase in SH-SY5Y cells where APP expression was uP-regulated (Burg *et al.*, 2013). Meanwhile, it has also been described that campesterol occurring in the temporal and parietal cortex, at concentrations of 5–10 ng/mg wet tissue could cross the endothelial barrier without difficulty (Vanmierlo *et al.*, 2015). Despite this, it has also been found that half or more of the  $\beta$ -sitosterol concentration was required for *in vivo* prevention of AD in combination with campesterol and stigmasterol, combined (Novak, 1999).

Stigmasterol, sitosterol, and campesterol and combinations thereof have already been patented in the United States (patent number: EP2405773 A1) for the treatment of AD by

---

<sup>18</sup> *Haloxylon recurvum* belongs to the family Chenopodiaceae. It is a perennial shrub with glabrous leaves and is widely distributed in Turkey, Syria, Iraq, Iran, Afghanistan, Kashmir, India and Central Asia (Ahmed *et al.*, 2006).

targeting the A $\beta$  peptide (Grimm *et al.*, 2012). Furthermore, stigmasterol significantly decreased A $\beta$  levels in comparison to  $\beta$ -sitosterol and cholesterol (Burg *et al.*, 2013). A further study, described lupeol to protect mouse hippocampal cell lines HT-22 against glutamate toxicity in AD sufferers (Szakiel *et al.*, 2012).

The extent of membrane fluidity of sterol molecules depends on their stereochemistry (i.e.  $\alpha/\beta$  isomers) and structural features of their side chains. Sterols with 3 $\beta$ -monohydroxyl group manifest more membrane fluidity than those with the  $\alpha$ -OH substituent (Hartmann, 1998). Less branched side chain exhibited higher membrane fluidity as in the order of campesterol > sitosterol > stigmasterol (Vanmierlo *et al.* 2012). Unlike plant stanols, plant sterols were more absorbed to cell membrane due to the presence of unsaturation than in their saturated form as in stanols (Weingartner, Bohm and Laufs, 2008). In the present study,  $\gamma$ -sitosterol [1.1], lupeol acetate [1.3], lawsaritol [2.1],  $\beta$ -amyrin acetate [3.1], and campesterol [3.3] significantly attenuated acrolein-induced oxidative stress at concentrations ranging from 30  $\mu$ g/mL to 10 ng/mL. These findings revealed decreasing levels of anti-cytotoxic activity against acrolein for the isolated series of phytosterols in the following order: campesterol > sitosterol > stigmasterol. The differences in these structural moieties along with their corresponding bioactivity were in alignment with those described in the literature (Vanmierlo *et al.*, 2012).

Although campesterol caused the most significant reduction of acrolein-induced oxidative stress amongst the isolated phytosterols, it remains unclear whether concentrations of campesterol in this range can be reached via nutritional supplementation. Thus, more research is required to determine if phytosterols mediate their neuroprotective effects exclusively via the reduction of acrolein-induced oxidative stress. In addition to the impact of phytosterols on the pathophysiology of AD, phytosterols can act as biomarkers for AD. In another study, brassicasterol (an isomer of campesterol) and sitosterol were identified as clinically relevant cerebrospinal fluid (CSF) biomarkers for early AD, although only sitosterol reached significance levels of reducing oxidative stress (Vanmierlo *et al.*, 2015).

### 6.3.2. Passing the blood brain barrier

A key feature of compounds targeting neuronal protection is that they must be able to cross the blood brain barrier (BBB) readily. The ability of flavonoids to cross the BBB is believed to be reliant on their lipophilicity. Small phenolics have been reported to traverse the BBB via amino acid transporters, such as 4-ethylcatechol (Vauzour *et al.*, 2010). The presence of parahydroxybenzoic acid in Tg2576 mice blood has been described to reduce A $\beta$  neuropathology and improve cognitive performance (Dal-Pan *et al.*, 2016). Likewise, clinical findings indicated that certain levels of vanillic acid that has been detected in all areas of the brain including the hippocampus gradually decreased with age (Adolfsson *et al.*, 1979). The diminishing concentrations of vanillic acid may involve many neurobehavioral and neurotransmitter abnormalities such as AD (Wolfe *et al.*, 2017). Based on the structural similarity of vanillic acid to salicylic acid, which does also cross the BBB, it has been considered that vanillic acid is able to enter the central nervous system (Wolfe *et al.*, 2017).

Phytosterols such as those isolated and elucidated in this study that included compounds **1.1**, **1.2**, **1.3**, **2.1**, **3.1** and **3.3** have been earlier described to cross BBB through high-density lipoprotein-SR-B1 (HDL-SR-B1) receptor, which are mainly located at the apical side of cerebral endothelial cells (Vanmierlo *et al.*, 2011). With regard to which phytosterols are capable of crossing endothelial cells more easily,

It has been found that phytosterols with a less complex side-chain, such as those found in cholesterol and campesterol, would cross the endothelial cells more easily than phytosterols with more complex hydrophobic side-chains, like in sitosterol **1.1** and stigmasterol or its derivative as in **2.1** (Vanmierlo *et al.*, 2015). Apart from that, the higher lipophilic solubility of these compounds produced greater antioxidant activity due to their lower solubility, higher penetration through the BBB and higher protein binding when their partition coefficient ( $\log P_{ow} > 4$ ) (Bonamigo *et al.*, 2017; Janjušević *et al.*, 2017; Pyka and Babuska, 2006; Taylor and Triggler, 2007). Likewise, the mechanism by which these lipophilic compounds produces more antioxidant effectiveness in the cellular environment was determined due to the attachment of the hydroxyl groups by cytochrome P450 enzyme, as reported by Shakunthala, (2009).

Moreover, the more methyl group within the structure will often lead to the higher lipophilic solubility resulting in higher BBB penetration, such as, addition of one methyl group to morphine produces codeine (Figure 6.3), which has a 10-fold higher BBB permeation, and the addition of two acetyl groups to produce heroin further increases BBB permeation (Di and Kerns, 2016). Nevertheless, the molecular size of the target metabolites was small. In this context, it has been reported by Di and Kerns, (2016) that the more molecular size are reduced the good passive diffusion through lipid bilayer membranes are improved.

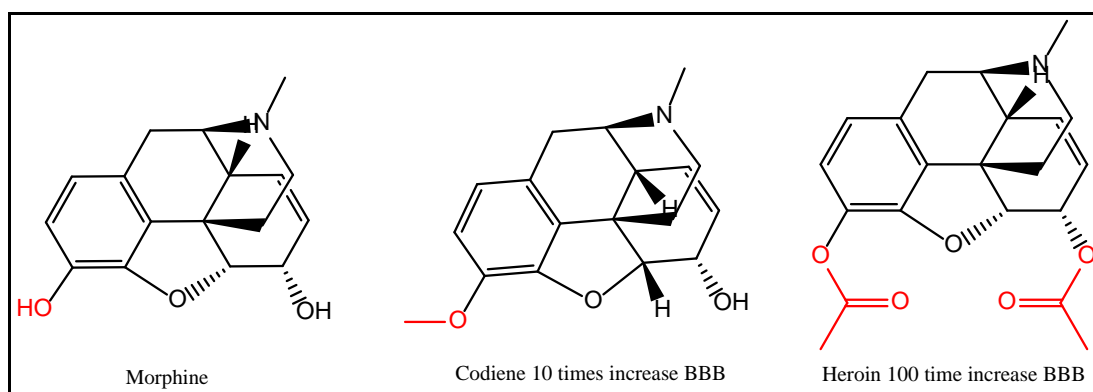


**Figure 6.3:** The effect of lipophilicity on penetrating BBB (Di and Kerns, 2016).

#### 6.4. Biosynthesis of the secondary metabolites

Most aromatic compounds, including phenols and flavonoids, are derived from shikimic acid pathway in plants (Seigler, 1998). Vanillic acid and parahydroxybenzoic acid were isolated in this study. Converti *et al.* (2017) reported that the biotransformation (Figure 6.4) of these compounds enabled vanillin synthesis from caffeic acid to ferulic acid, and a subsequent oxidation of vanillin into a vanillic acid structure. In the case of parahydroxybenzoic acid, the formation of ferulic acid from caffeic acid followed another schematic pathway, which was catalysed by the enzymatic oxidation of the bifunctional peroxisomal enzyme (PhCHD) (Ni *et al.*, 2015).

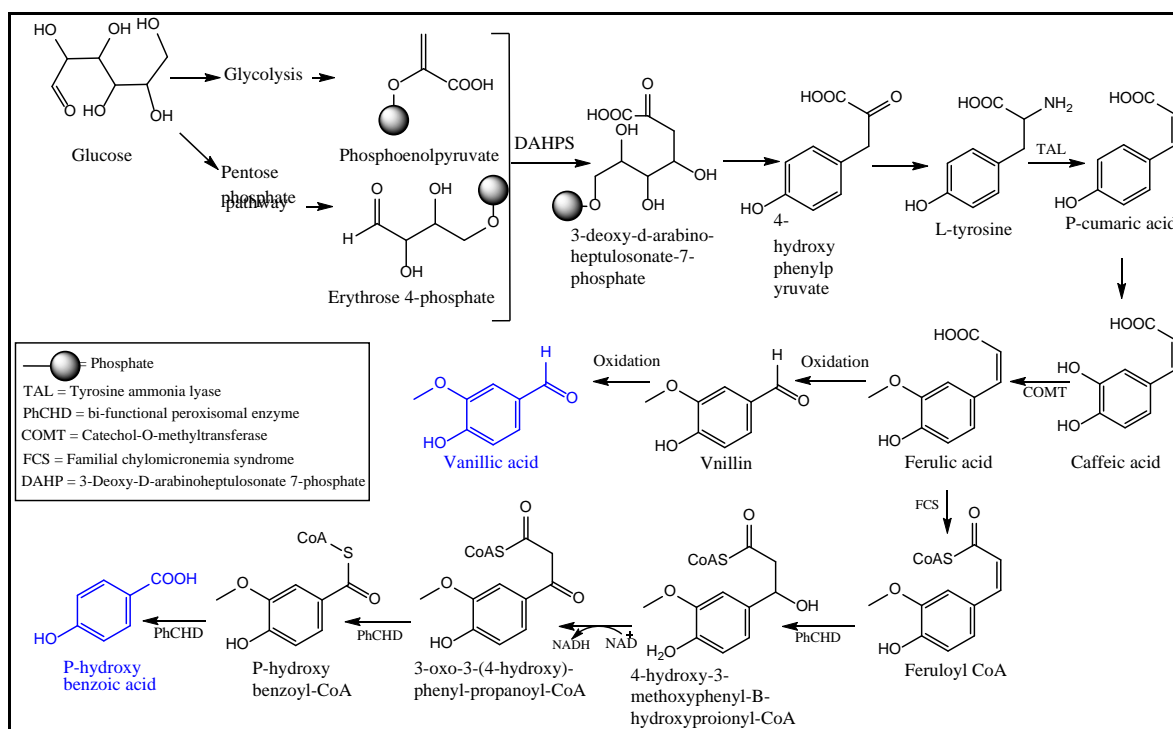


**Figure 6.4:** Biosynthesis pathway of vanillic acid and parahydroxybenzoic acid via the shikimate pathway (Ni *et al.*, 2015).

Phytosterols were isolated from the three parts of the fruit of *F. carica*. Phytosterols are compounds derived from the linear hydrocarbon squalene and are notable for their significant structural diversity and numerous biological activities. Phytosterols are known to be biosynthesised via the mevalonic acid (MVA) pathway (Figure 6.5). The cyclisation of the metabolite 2,3-oxidosqualene followed by rearrangements of the methyl units, yielded various structures, mostly tetra- or penta-cyclic. 2,3-Oxidosqualene is an earlier intermediate in the synthesis of plant steroids. In this case, 2,3-oxidosqualene is further cyclised to the triterpene cycloartenol, which is then converted to the C-27 compound cholesterol with the loss of three methyl groups (Springob and Kutchan, 2009). The oxygen of 2,3-oxidosqualene is usually retained as a hydroxyl group on C-3 in both triterpenes and steroids (Springob and Kutchan, 2009). In contrast to animals, where cholesterol is the major sterol, many plant sterols are methylated or ethylated at C-24 of

the side chain like in campesterol, sitosterol, and stigmasterol or even depolarised and expanded by the oleanyl cationic structure to form as in lupeol and  $\beta$ -amyrin.

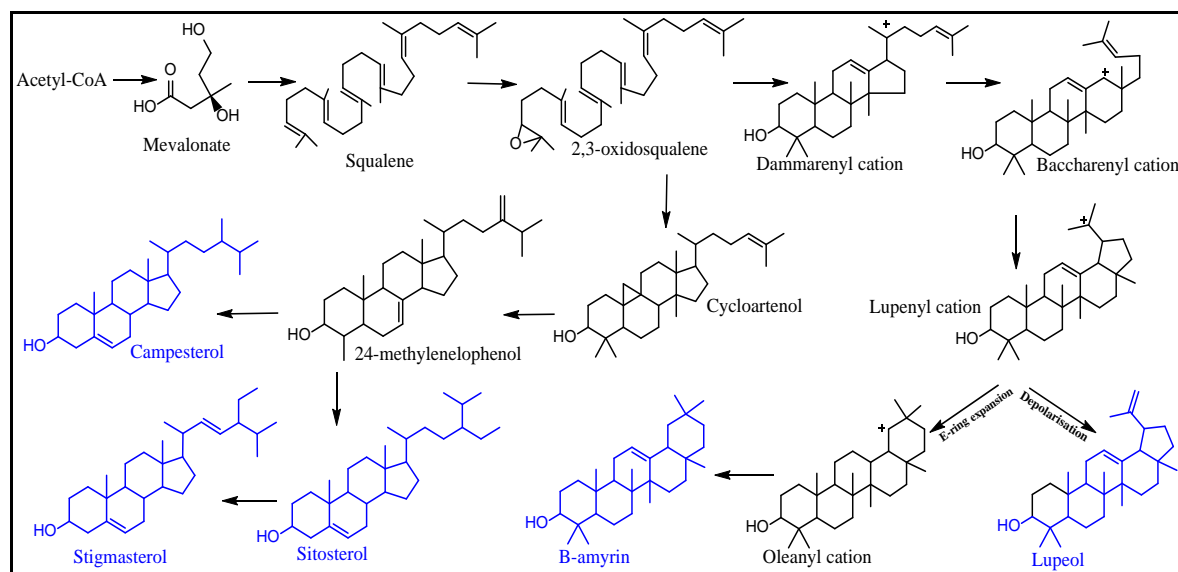


**Figure 6.5:** Biosynthesis of phytosterols via the MVA pathway (Hartmann, 1998; Springob and Kutchan, 2009).

Nevertheless, the fatty acid of oleoyl- $\beta$ -D-arabinoside **1.2** was isolated from the *F. carica* mesocarp, and is known to be biosynthesised via the fatty acid synthesis pathway (Chow, 2008). As shown in Figure 6.6, the acetyl-CoA structure is formed into malonyl-CoA by the acetyl-CoA carboxylase enzyme, at which point malonyl-CoA goes into the fatty acid synthesis pathway to the synthesis of oleic acid (Chow, 2008) which is the aglycone structure in oleoyl- $\beta$ -D-arabinoside.

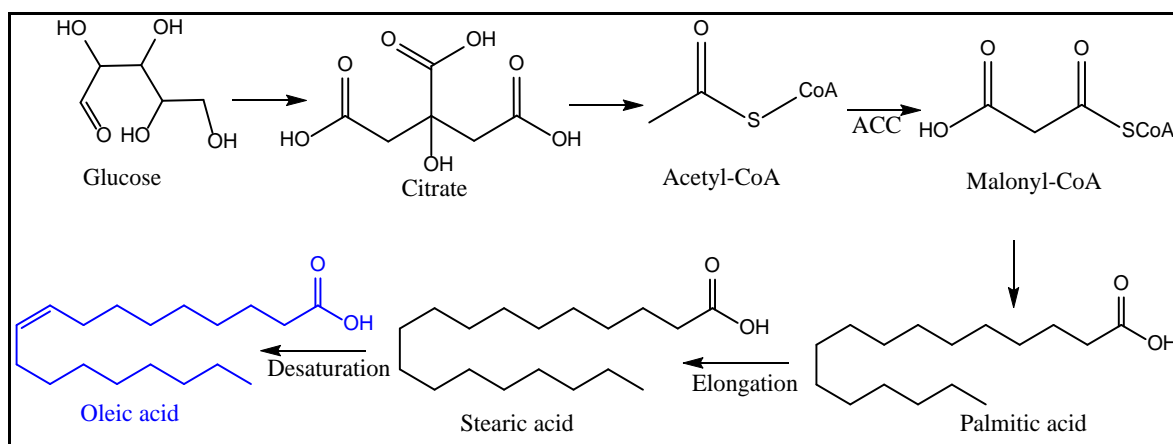


**Figure 6.6:** Fatty acid biosynthesis. ACC: Acetyl-CoA carboxylase (Chow, 2008).

### 6.5. Significances and limitations

This study has several scientific strengths and limitations. This was the first research activity on *F. carica* focusing on the relationship between the isolated active metabolites and their anti-oxidant activities against the acrolein assay. The bioactive metabolites were targeted from a chemometric data set, which revealed hidden relationships amongst variables in an unbiased manner to classify metabolites to their antioxidative capacity. Metabolomics has the great advantage to pinpoint target metabolites regardless of their concentration in an extract or fraction, but with the limitation that low-yielding compounds would be difficult to isolate (Tawfike *et al*, 2017; Kamal *et al.*, 2016). In conventional natural products isolation work, it is usually the case that unknowingly, major components were prioritised for isolation while their bioactivity is being misjudged; the potent component is actually present at very small concentrations. In this study, some metabolites in the *F. carica* samples, apart from those elucidated, may have been overlooked, and could have been in part responsible for the observed antioxidant capacity. The problem of ion suppression or enhancement is often observed in different types of ion sources employed in mass spectrometry. Depending on the ion source, some compounds may or may not be detected, which affects the dereplication or metabolomic profiling results. In this study, metabolomics tools were used to target the bioactive metabolites on the basis of HRESI-MS (high resolution electrospray ionisation-mass spectrometry). However, not all compounds will have the same capability to ionise in all the different types of ion sources available. In ESI, the amount of charged ion in the gas phase that ultimately reaches the detector is affected negatively or positively due to the presence of less or more volatile compounds that can change or improve the efficiency

of droplet formation (Morelato *et al.*, 2013). In this case, it is impossible to detect all metabolites from a single ion source, which pose a problem in untargeted metabolomics. The isolated compounds posted in chapters 3 and 4 were not detected during the dereplication step while other structurally related compounds were identified instead. The structures of the isolated bioactive compounds were elucidated then confirmed by their GCMS fragmentation profile and 2D NMR.

On the other hand, the findings supported the traditional use of this edible fruit as an antioxidant, which is worth undergoing further, large-scale investigation. The use of an *in vitro* cell line to investigate the cytotoxic effect demonstrated a dose-dependent antioxidant effect. Thus, it would be relevant to use additional *in vivo* animal models to provide a more comprehensive insight in the future.

## **6.6. Future work and recommendation**

A drug discovery and development protocol approach was undertaken to develop lead drugs with the active compounds isolated and identified from *F. carica*, as the global scenario is now changing towards the use of non-toxic NP having traditional medicinal use (Subash *et al.*, 2017). Further evaluation and work needs to be carried out on *F. carica* in order to explore their fully characterised active compounds, which can be used for the well-being of the humankind as thoroughly illustrated in Figure 6.7. In addition, the richness of lipids and phytosterols in *F. carica* extracts make this fruit as a future source of natural triterpenoid-rich source that help and support the pharmaceutical industry in the pharmaceutical production and marketing.

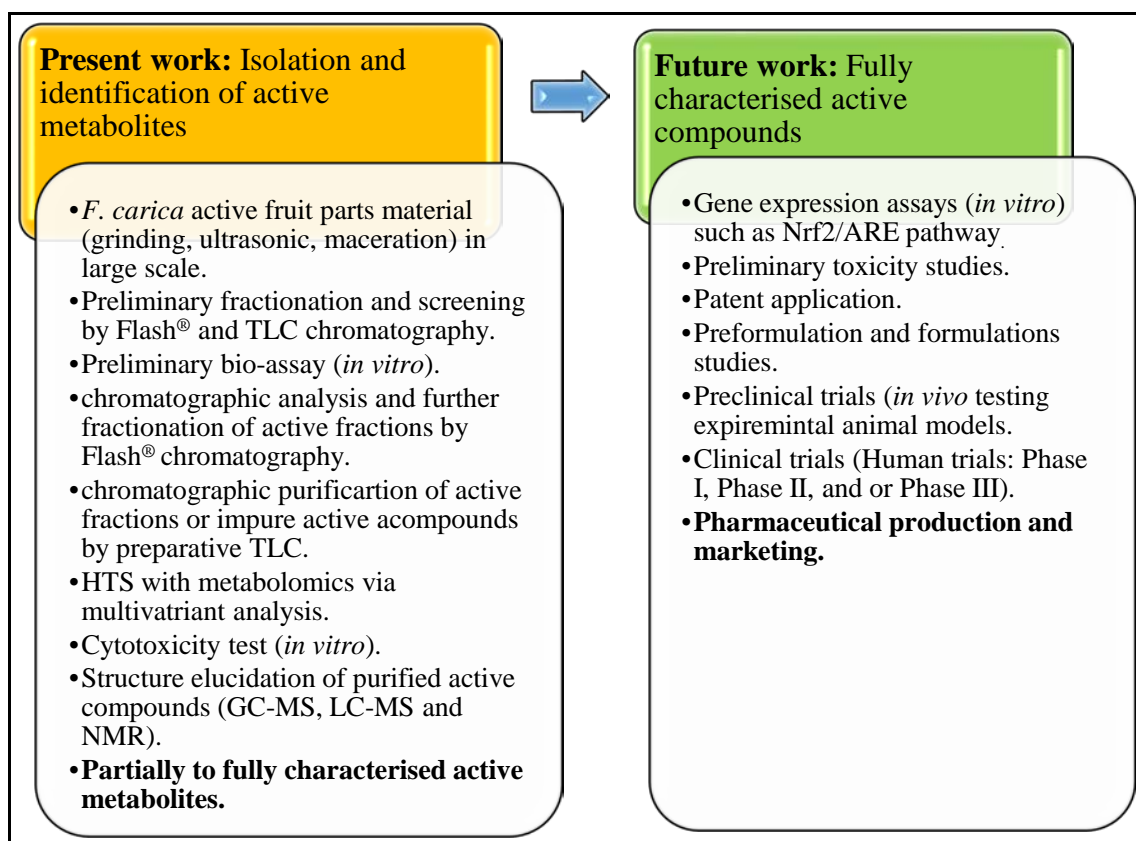


**Figure 6.7:** A general scheme protocol for drug discovery and development from NP (*F. carica*) using HTS.

## 6.7. Conclusion

In conclusion, phenolic, fatty acids and five major phytosterols compounds were isolated in this study through Flash<sup>®</sup> chromatography and TLC. These identified secondary metabolites demonstrated promising antioxidative activity against acrolein-induced oxidative stress related to AD. These results were then subjected to HTS via metabolomics, including dereplication, HCA, heat map, PCA, and OPLS-DA. In addition, through the comparison of PCA and OPLS-DA, it was possible to identify groups of chemical compositions with similar properties, and identify their associations via HPLC-ESI-MS, GCMS, and NMR. Therefore, a combination of chromatographic analysis, metabolomics, and spectroscopic analysis could be a useful method for identifying the common (or distinctive) sample characteristics responsible for the biological outcomes from a complex mixture. The combination of additional phytosterol components contained in the extract may explain the noted biological activity including cytotoxicity and antioxidative NQO1 gene expression, contributing to the augmentation

of the antioxidant effects. The findings of WB test have revealed compounds **2.6**, **2.7**, **1.3** and **2.1** to upregulate NQO1 antioxidant protein expression with a marked ability of preventing cytotoxicity, being significantly more effective than the prototypes **1.1**, **1.2**, **3.2** and **3.3**. However, further research is required in order to elucidate the correlation between the chemical composition of the *F. carica* parts, and the manifested biological activities, in terms of their molecular biology. Finally, the research filled many gaps identified at the beginning of the project, and improved the general understanding of using metabolomics to isolate and identify the chemical compositions which are most effective for treating oxidative stress-related AD.

## References

---

- Abbasi, A., Shah, M. and Khan, M. (2015). *Wild edible vegetables of Lesser Himalayas*. 1st ed. Cham: Springer.
- Abu Bakar, A., Manaharan, T., Merican, A. and Mohamad, S. (2017). Experimental and computational approaches to reveal the potential of *Ficus deltoidea* leaves extract as  $\alpha$ -amylase inhibitor. *Natural Product Research*, pp.1-4.
- Adejare, A. (2016). *Drug discovery approAChEs for the treatment of neurodegenerative disorders*. London: Academic Press, p.117.
- Adler, J. (1983). Configuration at C-24 of sterols from the liverwort *Palavicinnia lyellii*. *Phytochemistry*, 22(2), pp.607-608.

- Adolfsson, R., Gottfries, C., Roos, B. and Winblad, B. (1979). Post-mortem distribution of dopamine and homo-vanillic acid in human brain, variations related to age, and a review of the literature. *Journal of Neural Transmission*, 45(2), pp.81-105.
- Aghel, N., Kalantari, H. and Rezazadeh, S. (2011). Hepatoprotective Effect of Ficus carica Leaf Extract on Mice Intoxicated with Carbon Tetrachloride. *Iran J Pharm Res*, 10(1), pp.63–68.
- Ahmad, A., Kim, S., Ali, M., Park, I., Kim, J., Kim, E., Lim, J., Kim, S. and Chung, I. (2013). New Chemical Constituents from Oryza sativa Straw and Their Algicidal Activities against Blue-Green Algae. *Journal of Agricultural and Food Chemistry*, 61(34), pp.8039-8048.
- Ahmed, E., Nawaz, S., Malik, A. and Choudhary, M. (2006). Isolation and cholinesterase-inhibition studies of sterols from Haloxylon recurvum. *Bioorganic & Medicinal Chemistry Letters*, 16(3), pp.573-580.
- Ahmed, M., Laing, M. and Nsahlai, I. (2012). *In vitro* anthelmintic activity of crude extracts of selected medicinal plants against Haemonchus contortus from sheep. *Journal of Helminthology*, 87(02), pp.174-179.
- Akhtar, N., Syed, D., Khan, M., Adhami, V., Mirza, B. and Mukhtar, H. (2016). The pentacyclic triterpenoid, plectranthoic acid, a novel activator of AMPK induces apoptotic death in prostate cancer cells. *Oncotarget*.
- Alam, P., Basudan, O., Siddiqui, N., Al-Rehaily, A., Alqasoumi, S., Abdel-Kader, M., Donia, A. and Alam, P. (2015). Development of a densitometric high-performance thin-layer chromatographic method for the quantitative analysis of biomarker lupeol in the leaves of different species of genus Ficus. *Journal of Planar Chromatography – Modern TLC*, 28(1), pp.30-35.
- Alam, P., Siddiqui, N., Basudan, O., Al-Rehaily, A., Alqasoumi, S., Alam, P., Abdel-Kader, M., Donia, A. and Shakeel, F. (2015). Comparative profiling of biomarker psoralen in antioxidant active extracts of different species of genus Ficus by validated HPTLC method. *African Journal of Traditional, Complementary and Alternative Medicines*, 12(1), pp.57-67.
- Alamgeer, Iman, S., Asif, H. and Saleem, M. (2017). Evaluation of antihypertensive potential of Ficus carica fruit. *Pharmaceutical Biology*, 55(1), pp.1047-1053.
- Ali, B., Mujeeb, M., Shams, S. and Ali, B. (2015). Pharmacognostic standardization of leaf of Ficus carica leaves. *Toxicology Letters*, 238(2), pp.S64-S65.
- Ali, N., Faizi, S. and Kazmi, S. (2011). Antibacterial activity in spices and local medicinal plants against clinical isolates of Karachi, Pakistan. *Pharmaceutical Biology*, 49(8), pp.833-839.
- Allahyari, S., Delazar, A. and Najafi, M. (2014). Evaluation of General Toxicity, Anti-Oxidant Activity and Effects of Ficus Carica Leaves Extract on Ischemia/Reperfusion Injuries in Isolated Heart of Rat. *Adv Pharm Bull*, 4(2), pp.577–582.

- Allai, L., Druart, X., Öztürk, M., BenMoula, A., Nasser, B. and El Amiri, B. (2016). Protective effects of *Opuntia ficus-indica* extract on ram sperm quality, lipid peroxidation and DNA fragmentation during liquid storage. *Animal Reproduction Science*.
- Alqasoumi, S., Basudan, O., Al-Rehaily, A. and Abdel-Kader, M. (2014). Phytochemical and pharmacological study of *Ficus palmata* growing in Saudi Arabia. *Saudi Pharmaceutical Journal*, 22(5), pp.460-471.
- Amin, F., Shah, S. and Kim, M. (2017). Vanillic acid attenuates A $\beta$ 1-42-induced oxidative stress and cognitive impairment in mice. *Scientific Reports*, 7, p.40753.
- Ammar, S., del Mar Contreras, M., Belguith-Hadrich, O., Segura-Carretero, A. and Bouaziz, M. (2015). Assessment of the distribution of phenolic compounds and contribution to the antioxidant activity in Tunisian fig leaves, fruits, skins and pulps using mass spectrometry-based analysis. *Food Funct.*, 6(12), pp.3663-3677.
- Amtul, Z., Westaway, D., Cechetto, D. and Rozmahel, R. (2010). Oleic Acid Ameliorates Amyloidosis in Cellular and Mouse Models of Alzheimer's Disease. *Brain Pathology*, 21(3), pp.321-329.
- Ango, P., Kapche, D., Fotso, G., Fozing, C., Yeboah, E., Mapitse, R., Demirtas, I., Ngadjui, B. and Yeboah, S. (2016). Thonningiiflavanonol A and thonningiiflavanonol B, two novel flavonoids, and other constituents of *Ficus thonningii* Blume (Moraceae). *Zeitschrift für Naturforschung C*, 71(3-4).
- Ansari, M., Keller, J. and Scheff, S. (2008). Protective effect of Pycnogenol in human neuroblastoma SH-SY5Y cells following acrolein-induced cytotoxicity. *Free Radical Biology and Medicine*, 45(11), pp.1510-1519.
- Ansari, N. and Khodagholi, F. (2013). Natural Products as Promising Drug Candidates for the Treatment of Alzheimer's Disease: Molecular Mechanism Aspect. *Current Neuropharmacology*, 11(4), pp.414-429.
- Ariffin, N. and Hasham, R. (2016). Potential dermatological application on Asian plants. *Biotechnology and Bioprocess Engineering*, 21(3), pp.337-354.
- Athari Nik Azm, S., Vafa, M., Sharifzadeh, M., Safa, M., Barati, A. and Mirshafiey, A. (2017). Effects of M2000 (D-Mannuronic Acid) on Learning, Memory Retrieval, and Associated Determinants in a Rat Model of Alzheimer's Disease. *American Journal of Alzheimer's Disease & Other Dementias*®, 32(1), pp.12-21.
- Avagyan, R., Åberg, M. and Westerholm, R. (2016). Suspect screening of OH-PAHs and non-target screening of other organic compounds in wood smoke particles using HR-Orbitrap-MS. *Chemosphere*, 163, pp.313-321.
- Awan, A., Shaw, W. and Ellis, T. (2016). Biosynthesis of therapeutic natural products using synthetic biology. *Advanced Drug Delivery Reviews*, 105, pp.96-106.
- Azadmard-Damirchi, S. (2010). Review of the use of phytosterols as a detection tool for adulteration of olive oil with hazelnut oil. *Food Additives & Contaminants: Part A*, 27(1), pp.1-10.

- Azam, F., QADIR, M., UZAIR, M. and AHMAD, B. (2013). Evaluation of Antibacterial and Antifungal Activity of *Ficus carica* and *Cassia fistula*. *Latin American Journal of Pharmacy*, 32(9), pp.1412-1414.
- B. Pocernich, C., L.B. Lange, M., Sultana, R. and A. Butterfield, D. (2011). Nutritional Approaches to Modulate Oxidative Stress in Alzheimers Disease. *Current Alzheimer Research*, 8(5), pp.452-469.
- Bachir bey, M., Meziat, L., Benchikh, Y. and Louaileche, H. (2014). Deployment of response surface methodology to optimize recovery of dark fresh fig (*Ficus carica* L., var. Azenjar) total phenolic compounds and antioxidant activity. *Food Chemistry*, 162, pp.277-282.
- Badgujar, S., Patel, V., Bandivdekar, A. and Mahajan, R. (2014). Traditional uses, phytochemistry and pharmacology of *Ficus carica*: A review. *Pharmaceutical Biology*, 52(11), pp.1487-1503.
- Baek, H., Ha, K., Kim, H., Choi, E., Park, E., Park, B., Yang, H., Kim, M., Kang, H. and Chae, S. (2016). Randomized, double-blind, placebo-controlled trial of *Ficus carica* paste for the management of functional constipation. *Asia Pac J Clin Nutr*, 25(3), pp.487-496.
- Baerheim Svendsen, A. and Verpoorte, R. (1983). *Chromatography of alkaloids*.
- Bahadori, S., Kamalinejad, M., Ahmadzadeh, A., Ardekani, M., Salamzadeh, J. and Keshavarz, M. (2016). Does Regular Use of a Complementary Medicine of *Olea Europe* and *Ficus carica* Have Adverse Effects on Lipid Profile and Fasting Blood Glucose of Rheumatoid Arthritis (RA) Patients Under Treatment with DMARD Regimens Containing Methotrexate?. *Iran J Pharm Res*, 15(4), pp.933-940.
- Bakeev, K. (2010). *Process Analytical Technology: Spectroscopic Tools and Implementation Strategies for the Chemical and Pharmaceutical Industries*. 2nd ed. UK: John Wiley & Sons, p.300.
- Balamurugan, R., Stalin, A. and Ignacimuthu, S. (2012). Molecular docking of  $\gamma$ -sitosterol with some targets related to diabetes. *European Journal of Medicinal Chemistry*, 47, pp.38-43.
- Baldé, A., Apers, S., De Bruyne, T., Van Den Heuvel, H., Claeys, M., Vlietinck, A. and Pieters, L. (2000). Steroids from *Harrisonia abyssinica*. *Planta Medica*, 66(1), pp.67-69.
- Ballatore, C., Smith, A., Lee, V., Trojanowski, J. and Brunden, K. (2016). Microtubule Stabilization. *Developing Therapeutics for Alzheimer's Disease*, pp.305-326.
- Barh, D., Khan, M. and Davies, E. (2015). *PlantOmics: The Omics of Plant Science*. 1st ed. India: Springer.
- Barolo, M., MostaceroSilvia, N. and López, N. (2014). *Ficus carica* L. (Moraceae): An ancient source of food and health. *Food Chemistry*, 164, pp.119-127.

- Barone, E., Head, E., Butterfield, D. and Perluigi, M. (2016). HNE-modified proteins in Down syndrome: Involvement in development of Alzheimer disease neuropathology. *Free Radical Biology and Medicine*.
- Báthori, M., Kalász, H., Janicsák, G., Pongrácz, Z. and Vámos, J. (2003). Thin-Layer Chromatography of Phytoecdysteroids. *Journal of Liquid Chromatography & Related Technologies*, 26(16), pp.2629-2649.
- Bazinet, R. and Layé, S. (2014). Polyunsaturated fatty acids and their metabolites in brain function and disease. *Nature Reviews Neuroscience*, 15(12), pp.771-785.
- Belguith-Hadriche, O., Ammar, S., Contreras, M., Fetoui, H., Segura-Carretero, A., El Feki, A. and Bouaziz, M. (2017). HPLC-DAD-QTOF-MS profiling of phenolics from leaf extracts of two Tunisian fig cultivars: Potential as a functional food. *Biomedicine & Pharmacotherapy*, 89, pp.185-193.
- Belguith-Hadriche, O., Ammar, S., Contreras, M., Turki, M., Segura-Carretero, A., El Feki, A., Makni-Ayedi, F. and Bouaziz, M. (2016). Antihyperlipidemic and Antioxidant Activities of Edible Tunisian *Ficus carica* L. Fruits in High Fat Diet-Induced Hyperlipidemic Rats. *Plant Foods for Human Nutrition*, 71(2), pp.183-189.
- Belkacemi, A. and Ramassamy, C. (2016). Anthocyanins Protect SK-N-SH Cells Against Acrolein-Induced Toxicity by Preserving the Cellular Redox State. *Journal of Alzheimer's Disease*, 50(4), pp.981-998.
- Benjamin, B. and Burns, A. (2007). Donepezil for Alzheimer's disease. *Expert Review of Neurotherapeutics*, 7(10), pp.1243-1249.
- Benzie, I. and Wachtel-Galor, S. (2011). *Herbal medicine*. 1st ed. Boca Raton: CRC Press.
- Berezkin, V. and Chausov, A. (2012). THE SIMPLE CHROMATOGRAPHIC CHAMBER AND ITS APPLICATION IN CIRCULAR AND LINEAR TLC. *Journal of Liquid Chromatography & Related Technologies*, 35(2), pp.294-307.
- Bernhardi, R. and Inestrosa, N. (2008). *Neurodegenerative diseases*. 1st ed. New York: Nova Biomedical Books.
- Bhangale, J. and Acharya, S. (2016). Anti-Parkinson Activity of Petroleum Ether Extract of *Ficus religiosa*(L.) Leaves. *Advances in Pharmacological Sciences*, 2016, pp.1-9.
- Bhanushali, M., Joshi, Y. and Makhija, D. (2014). Central nervous system activity of an aqueous acetonc extract of *Ficus carica* L. in mice. *Journal of Ayurveda and Integrative Medicine*, 5(2), p.89.
- Bhatt, I., Rawat, S., Badhani, A. and Rawal, R. (2016). Nutraceutical potential of selected wild edible fruits of the Indian Himalayan region. *Food Chemistry*, 215, pp.84-91.
- Bonamigo, T., Campos, J., Alfredo, T., Balestieri, J., Cardoso, C., Paredes-Gamero, E., de Picoli Souza, K. and dos Santos, E. (2017). Antioxidant, Cytotoxic, and Toxic Activities of Propolis from Two Native Bees in Brazil: *Scaptotrigona depilis* and

- Melipona quadrifasciata anthidioides. *Oxidative Medicine and Cellular Longevity*, 2017, pp.1-12.
- Bounihi, A., Bitam, A., Bouazza, A., Yargui, L. and Koceir, E. (2016). Fruit vinegars attenuate cardiac injury via anti-inflammatory and anti-adiposity actions in high-fat diet-induced obese rats. *Pharmaceutical Biology*, pp.1-10.
- Bouyahya, A., Bakri, Y., Khay, E., Edaoudi, F., Talbaoui, A., Et-Touys, A., Abrini, J. and Dakka, N. (2016). Antibacterial, antioxidant and antitumor properties of Moroccan medicinal plants: A review. *Asian Pacific Journal of Tropical Disease*, 7(1), pp.57-64.
- Bradshaw, R. and Dennis, E. (2010). *Handbook of cell signaling*. 1st ed. Amsterdam: Elsevier/Academic Press.
- Brahmachari, G., Mondal, A., Nayek, N., Kumar, A., Srivastava, A. and Misra, N. (2017). Experimental and quantum chemical studies on poriferasterol – A natural phytosterol isolated from *Cassia sophera* Linn. (Caesalpinaceae). *Journal of Molecular Structure*, 1143, pp.184-191.
- Brantley, M., Osborn, M., Sanders, B., Rezaei, K., Lu, P., Li, C., Milne, G., Cai, J. and Sternberg, P. (2012). The Short-term Effects of Antioxidant and Zinc Supplements on Oxidative Stress Biomarker Levels in Plasma: A Pilot Investigation. *American Journal of Ophthalmology*, 153(6), pp.1104-1109.e2.
- Bratchell, N. (1989). Chemometrics and intelligent laboratory systems. *Chemometrics and Intelligent Laboratory Systems*, 6(2), pp.105-125.
- Bryhn, M. (2013). *Fatty acid composition for treatment of Alzheimer's disease and cognitive dysfunction*. US 8609726 B2.
- Burg, V., Grimm, H., Rothhaar, T., Grosgen, S., Hundsdorfer, B., Hauptenthal, V., Zimmer, V., Mett, J., Weingartner, O., Laufs, U., Broersen, L., Tanila, H., Vanmierlo, T., Lutjohann, D., Hartmann, T. and Grimm, M. (2013). Plant Sterols the Better Cholesterol in Alzheimer's Disease? A Mechanistical Study. *Journal of Neuroscience*, 33(41), pp.16072-16087.
- Burlando, B., Clericuzio, M. and Cornara, L. (2016). Moraceae plants with tyrosinase inhibitory activity: a review. *MRMC*, 16(999), pp.1-1.
- Burns, A., Rossor, M., Hecker, J., Gauthier, S., Petit, H., Möller, H., Rogers, S. and Friedhoff, L. (1999). The Effects of Donepezil in Alzheimer's Disease – Results from a Multinational Trial. *Dementia and Geriatric Cognitive Disorders*, 10(3), pp.237-244.
- Butler, M. (2004). The Role of Natural Product Chemistry in Drug Discovery †. *J. Nat. Prod.*, 67(12), pp.2141-2153.
- Butterfield, D., Bader Lange, M. and Sultana, R. (2010). Involvements of the lipid peroxidation product, HNE, in the pathogenesis and progression of Alzheimer's disease☆. *Biochimica et Biophysica Acta (BBA) - Molecular and Cell Biology of Lipids*, 1801(8), pp.924-929.

- BVL-Reporte (2014). *List of Substances of the Competent Federal Government and Federal State Authorities*. Plants and plant parts. [online] Cham: Springer International Publishing. Available at: [http://dx.doi.org/10.1007/978-3-319-10732-5\\_3](http://dx.doi.org/10.1007/978-3-319-10732-5_3) %P 9-141 [Accessed 16 Nov. 2016].
- Bylesjö, M., Rantalainen, M., Cloarec, O., Nicholson, J., Holmes, E. and Trygg, J. (2006). OPLS discriminant analysis: combining the strengths of PLS-DA and SIMCA classification. *Journal of Chemometrics*, 20(8-10), pp.341-351.
- Cagno, V., Civra, A., Kumar, R., Pradhan, S., Donalisio, M., Sinha, B., Ghosh, M. and Lembo, D. (2015). *Ficus religiosa* L. bark extracts inhibit human rhinovirus and respiratory syncytial virus infection *in vitro*. *Journal of Ethnopharmacology*, 176, pp.252-257.
- Çalışkan, O. and Aytakin Polat, A. (2011). Phytochemical and antioxidant properties of selected fig (*Ficus carica* L.) accessions from the eastern Mediterranean region of Turkey. *Scientia Horticulturae*, 128(4), pp.473-478.
- Camero, M., Marinaro, M., Losurdo, M., Larocca, V., Bodnar, L., Patruno, G., Buonavoglia, C. and Tempesta, M. (2015). Caprine herpesvirus 1 (CpHV-1) vaginal infection of goats: clinical efficacy of fig latex. *Natural Product Research*, 30(5), pp.605-607.
- Camero, M., Marinaro, M., Lovero, A., Elia, G., Losurdo, M., Buonavoglia, C. and Tempesta, M. (2014). *In vitro* antiviral activity of *Ficus carica* latex against caprine herpesvirus-1. *Natural Product Research*, 28(22), pp.2031-2035.
- Canal, J., Torres, M., Romero, A. and Pérez, C. (2000). A chloroform extract obtained from a decoction of *Ficus carica* leaves improves the cholesterolaemic status of rats with streptozotocin-included diabetes. *Acta Physiologica Hungarica*, 87(1), pp.71-76.
- Canning, P. and Bullock, A. (2014). New strategies to inhibit KEAP1 and the Cul3-based E3 ubiquitin ligases. *Biochemical Society Transactions*, 42(1), pp.103-107.
- Cao, H., Wang, L., Chen, B., Zheng, P., He, Y., Ding, Y., Deng, Y., Lu, X., Guo, X., Zhang, Y., Li, Y. and Yu, G. (2016). DNA Demethylation Upregulated Nrf2 Expression in Alzheimer's Disease Cellular Model. *Frontiers in Aging Neuroscience*, 7.
- Cao, L., Xu, X., Chen, S. and Ma, H. (2016). Cloning and expression analysis of *Ficus carica* anthocyanidin synthase 1 gene. *Scientia Horticulturae*, 211, pp.369-375.
- Carini, M., Aldini, G., Beretta, G., Arlandini, E. and Facino, R. (2003). Acrolein-sequestering ability of endogenous dipeptides: characterization of carnosine and homocarnosine/acrolein adducts by electrospray ionization tandem mass spectrometry. *Journal of Mass Spectrometry*, 38(9), pp.996-1006.

- Cavero, R., Akerreta, S. and Calvo, M. (2013). Medicinal plants used for dermatological affections in Navarra and their pharmacological validation. *Journal of Ethnopharmacology*, 149(2), pp.533-542.
- Chackalamannil, S., Rotella, D. and Ward, S. (2017). *Comprehensive Medicinal Chemistry III*. 3rd ed. Cambridge, UK: Elsevier Academic Press, pp.327-384.
- Charalambous, G. (1983). *Instrumental analysis of food VI*. Oxford: Elsevier Science, p.204.
- Chaudhary, G., Goyal, S. and Poonia, P. (2010). *Lawsonia inermis* Linnaeus: a phytopharmacological review. *Int J Pharm Sci Drug Res*, 2(2), pp.91-8.
- Chaudhary, N. and Ali, M. (2011). *Ficus hispida* Linn.: A review of its pharmacognostic and ethnomedicinal properties. *Pharmacognosy Reviews*, 5(9), p.96.
- Chawla, A., Kaur, R. and Sharma, A. (2012). *Ficus carica* Linn.: A Review on its Pharmacognostic, Phytochemical and Pharmacological Aspects. *Int.J.Pharm.Phytopharmacol.Res*, 1(4), pp.215-232.
- Chen, C., Wan, C., Peng, X., Chen, Y., Chen, M. and Chen, J. (2015). Optimization of Antifungal Extracts from *Ficus hirta* Fruits Using Response Surface Methodology and Antifungal Activity Tests. *Molecules*, 20(11), pp.19647-19659.
- Chen, G., Xu, T., Yan, Y., Zhou, Y., Jiang, Y., Melcher, K. and Xu, H. (2017). Amyloid beta: structure, biology and structure-based therapeutic development. *Acta Pharmacologica Sinica*.
- Chen, H., Peng, Y., Zhang, Y. and Corlett, R. (2015). Winter cropping in *Ficus tinctoria*: an alternative strategy. *Sci. Rep.*, 5, p.16496.
- Chen, T., Chou, M., Lai, C., Wu, S., Hsu, C. and Yang, Y. (2017). Factors affecting therapeutic response to Rivastigmine in Alzheimer's disease patients in Taiwan.
- Chen, Y., Huang, M., Wu, W., Wang, A., BAO, T., Zheng, C., Chou, L., Tzeng, H. and Tu, S. (2016). The floral scent of *Ficus pumila* var. *pumila* and its effect on the choosing behavior of pollinating wasps of *Wiebesia pumilae*. *Acta Ecologica Sinica*, 36(5), pp.321-326.
- Cheng, D., Spiro, A., Jenner, A., Garner, B. and Karl, T. (2014). Long-term cannabidiol treatment prevents the development of social recognition memory deficits in Alzheimer's disease transgenic mice. *Journal of Alzheimer's Disease*, 42(4), pp.383-1396.
- Cheng, S., Huang, M. and Shiea, J. (2011). Thin layer chromatography/mass spectrometry. *Journal of Chromatography A*, 1218(19), pp.2700-2711.

- Chindo, B., Kahl, E., Trzeciak, D., Dehmel, P., Becker, A. and Fendt, M. (2015). Standardized extract of *Ficus platyphylla* reverses apomorphine-induced changes in prepulse inhibition and locomotor activity in rats. *Behavioural Brain Research*, 293, pp.74-80.
- Chindo, B., Schröder, H. and Becker, A. (2015). Methanol extract of *Ficus platyphylla* ameliorates seizure severity, cognitive deficit and neuronal cell loss in pentylenetetrazole-kindled mice. *Phytomedicine*, 22(1), pp.86-93.
- Chindo, B., Schröder, H., Koeberle, A., Werz, O. and Becker, A. (2016). Analgesic potential of standardized methanol stem bark extract of *Ficus platyphylla* in mice: Mechanisms of action. *Journal of Ethnopharmacology*, 184, pp.101-106.
- Chinsembu, K. (2016). *Ethnobotanical Study of Plants Used in the Management of HIV/AIDS-Related Diseases in Livingstone, Southern Province, Zambia. Evidence-Based Complementary and Alternative Medicine*, 2016, pp.1-14.
- Choo, Y., Yung, C. and Ma, A. (2012). Oil Palm. *Handbook of Bioenergy Crop Plants*, pp.433-451.
- Chou, W., Chen, C., Hsieh, H., Lo, T., Juan, P. and Mai, F. (2015). G2/M arrest and apoptosis of human colorectal cancer cells induced by water extract from residues of jelly fig AChEne. *Technology and Health Care*, 24(s1), pp.S147-S153.
- Chow, C. (2008). *Fatty acids in foods and their health implications*. Boca Raton [Fla.]: CRC Press, Taylor & Francis Group.
- Conforti, F., Menichini, G., Zanfini, L., Tundis, R., Statti, G., Provenzano, E., Menichini, F., Somma, F. and Alfano, C. (2012). Evaluation of phototoxic potential of aerial components of the fig tree against human melanoma. *Cell Proliferation*, 45(3), pp.279-285.
- Converti, A., Aliakbarian, B., Domínguez, J., Vázquez, G. and Perego, P. (2017). *Microbial production of biovanillin*.
- Cordain, L. (2012). *AARP The Paleo Diet Revised*. Hoboken: John Wiley & Sons.
- Coronado-Aceves, E., Sánchez-Escalante, J., López-Cervantes, J., Robles-Zepeda, R., Velázquez, C., Sánchez-Machado, D. and Garibay-Escobar, A. (2016). Antimycobacterial activity of medicinal plants used by the Mayo people of Sonora, Mexico. *Journal of Ethnopharmacology*, 190, pp.106-115.
- Corrigan, F., Horrobin, D., Skinner, E., Besson, J. and Cooper, M. (1998). Abnormal content of n-6 and n-3 long-chain unsaturated fatty acids in the phosphoglycerides and cholesterol esters of parahippocampal cortex from Alzheimer's disease patients and its relationship to acetyl CoA content. *The International Journal of Biochemistry & Cell Biology*, 30(2), pp.197-207.

- Coyle, E. (1995). Substrate utilization during exercise in active people. *American Journal of Clinical Nutrition*. *American Journal of Clinical Nutrition*, 61(4 Suppl.), pp.968S–979S.
- Crivellaro, A. and Schweingruber, F. (2013). *Atlas of wood, bark and pith anatomy of Eastern Mediterranean trees and shrubs*. 1st ed. Berlin: Springer.
- Cromwell, B. (1933). Experiments on the origin and function of berberine in *Berberis Darwinii*. *Biochemical Journal*, 27(3), pp.860-872.
- Crumley, F., Nest, W., Kalinowska, M. and Nes, W. (1990). Stereochemical differences in the anatomical distribution of C-24 alkylated sterols in *Kalanchoe daigremontiana*. *Phytochemistry*, 29(11), pp.3427-3434.
- Cseke, L. (2006). *Natural products from plants*. 1st ed. Boca Raton, FL: CRC/Taylor & Francis.
- Cummings, J., Lee, G., Mortsdorf, T., Ritter, A. and Zhong, K. (2017). Alzheimer's disease drug development pipeline: 2017. *Alzheimer's & Dementia: Translational Research & Clinical Interventions*, 3(3), pp.367-384.
- Cunnanea, S., Schneiderb, J., Tangneye, C., Tremblay-Merciera, J., Fortier, M., Bennettb, D. and Morris, M. (2012). Plasma and Brain Fatty Acid Profiles in Mild Cognitive Impairment and Alzheimer's Disease. *Journal of Alzheimer's Disease*, 29(3), pp.691–697.
- Desai, A. and Grossberg, G. (2005). Rivastigmine for Alzheimer's disease. *Expert Review of Neurotherapeutics*, 5(5), pp.563-580.
- Deyrup, S., Eckman, L., McCarthy, P., Smedley, S., Meinwald, J. and Schroeder, F. (2011). 2D NMR-spectroscopic screening reveals polyketides in ladybugs. *Proceedings of the National Academy of Sciences*, 108(24), pp.9753-9758.
- Di, L. and Kerns, E. (2016). Blood-Brain Barrier. *Drug-Like Properties*, pp.141-159.
- Dias, D., Urban, S. and Roessner, U. (2012). A Historical Overview of Natural Products in Drug Discovery. *Metabolites*, 2(4), pp.303-336.
- Diaz, G. (2015). Toxicosis by Plant Alkaloids in Humans and Animals in Colombia. *Toxins*, 7(12), pp.5408-5416.
- Ding, Y., Ding, C., Ye, N., Liu, Z., Wold, E., Chen, H., Wild, C., Shen, Q. and Zhou, J. (2016). ChemInform Abstract: Discovery and Development of Natural Product Oridonin-Inspired Anticancer Agents. *ChemInform*, 47(43).
- Dominy, N., Yeakel, J., Bhat, U., Ramsden, L., Wrangham, R. and Lucas, P. (2016). How chimpanzees integrate sensory information to select figs. *Interface Focus*, 6(3), p.20160001.

- Drayer, D. (1986). Pharmacodynamic and pharmacokinetic differences between drug enantiomers in humans: An overview. *Clinical Pharmacology and Therapeutics*, 40(2), pp.125-133.
- Eagger, S., Levy, R. and Sahakian, B. (1991). Tacrine in Alzheimer's disease. *The Lancet*, 337(8748), pp.989-992.
- Ekwall, B. (1983). Correlation between cytotoxicity *in vitro* and LD50-values. *Acta Pharmacologica et Toxicologica*, 52, pp.80-99.
- El-Sakhawy, F., Kassem, H., Abou-Hussein, D., El-Gayed, S., Mostafa, M. and Ahmed, R. (2016). Phytochemical investigation of the bioactive extracts of the leaves of *Ficus cyathistipula* Warb. *Zeitschrift für Naturforschung C*, 71(5-6).
- Encinas, M., Iglesias, M., Liu, Y., Wang, H., Muhaisen, A., Ceña, V., Gallego, C. and Comella, J. (2002). Sequential Treatment of SH-SY5Y Cells with Retinoic Acid and Brain-Derived Neurotrophic Factor Gives Rise to Fully Differentiated, Neurotrophic Factor-Dependent, Human Neuron-Like Cells. *Journal of Neurochemistry*, 75(3), pp.991-1003.
- Erdemoglu, N., Turan, N., Caköcö, I., Sener, B. and Aydön, A. (2006). Antioxidant activities of some Lamiaceae plant extracts. *Phytotherapy Research*, 20(1), pp.9-13.
- Eriksson, L. (2013). *Multi- and megavariable data analysis*. 1st ed. Malmö: MKS Umetrics.
- Eriksson, L., Antti, H., Gottfries, J., Holmes, E., Johansson, E., Lindgren, F., Long, I., Lundstedt, T., Trygg, J. and Wold, S. (2004). Using chemometrics for navigating in the large data sets of genomics, proteomics, and metabonomics (gpm). *Analytical and Bioanalytical Chemistry*, 380(3), pp.419-429.
- Erlanson, D., Jahnke, W., Mannhold, R., Kubinyi, H. and Folkers, G. (2016). *Fragment-based Drug Discovery - Lessons and Outlook*. Weinheim: John Wiley & Sons, p.345.
- Essa, M., Akbar, M. and Guillemin, G. (2016). *The Benefits of Natural Products for Neurodegenerative Diseases*. 1st ed. Switzerland: Springer, pp.96-99.
- Essa, M., Subash, S., Akbar, M., Al-Adawi, S. and Guillemin, G. (2015). Long-Term Dietary Supplementation of Pomegranates, Figs and Dates Alleviate Neuroinflammation in a Transgenic Mouse Model of Alzheimer's Disease. *PLOS ONE*, 10(3), p.e0120964.
- Eteraf-Oskouei, T., Allahyari, S., Akbarzadeh-Atashkhosrow, A., Delazar, A., Pashaii, M., Gan, S. and Najafi, M. (2015). Methanolic Extract of *Ficus carica* Linn. Leaves Exerts Antiangiogenesis Effects Based on the Rat Air Pouch Model of Inflammation. *Evidence-Based Complementary and Alternative Medicine*, 2015, pp.1-9.
- Eugster, P., Boccard, J., Debrus, B., Bréant, L., Wolfender, J., Martel, S. and Carrupt, P. (2014). Retention time prediction for dereplication of natural products (C<sub>x</sub>H<sub>y</sub>O<sub>z</sub>) in LC-MS metabolite profiling. *Phytochemistry*, 108, pp.196-207.

- Farlow, M. (1992). A Controlled Trial of Tacrine in Alzheimer's Disease. *JAMA: The Journal of the American Medical Association*, 268(18), p.2523.
- Fingolo, C., Santos, T., Filho, M. and Kaplan, M. (2013). Triterpene Esters: Natural Products from *Dorstenia arifolia* (Moraceae). *Molecules*, 18(4), pp.4247-4256.
- Flis, V. and Daum, G. (2013). Lipid Transport between the Endoplasmic Reticulum and Mitochondria. *Cold Spring Harbor Perspectives in Biology*, 5(6), pp.a013235-a013235.
- Francis, P., Palmer, A., Snape, M. and Wilcock, G. (1999). The cholinergic hypothesis of Alzheimer's disease: a review of progress. *Journal of Neurology, Neurosurgery & Psychiatry*, 66(2), pp.137-147.
- Fraser, T., Tayler, H. and Love, S. (2009). Fatty Acid Composition of Frontal, Temporal and Parietal Neocortex in the Normal Human Brain and in Alzheimer's Disease. *Neurochemical Research*, 35(3), pp.503-513.
- Frisardi, V., Panza, F., Seripa, D., Farooqui, T. and Farooqui, A. (2011). Glycerophospholipids and glycerophospholipid-derived lipid mediators: A complex meshwork in Alzheimer's disease pathology. *Progress in Lipid Research*, 50(4), pp.313-330.
- Gad, H., El-Ahmady, S., Abou-Shoer, M. and Al-Azizi, M. (2012). Application of Chemometrics in Authentication of Herbal Medicines: A Review. *Phytochemical Analysis*, 24(1), pp.1-24.
- Gajalakshmi, S., Vijayalakshmi, S. and Deni-Rajeswari, V. (2012). pharmacological activities of *Aerva Lanata*: a respective review. *International research journal of Pharmacy*, 3(1), pp.28-30.
- Galanakis, C. (2015). Separation of functional macromolecules and micromolecules: From ultrafiltration to the border of nanofiltration. *Trends in Food Science & Technology*, 42(1), pp.44-63.
- Galil, J. and Meiri, L. (2006). Number and Structure of Anthers in Fig *Syconia* in Relation to Behavior of the Pollen Vectors. *New Phytologist*, 88(1), pp.83-87.
- Gao, J., Inagaki, Y., Li, X., Kokudo, N. and Tang, W. (2013). Research progress on natural products from traditional Chinese medicine in treatment of Alzheimer's disease. *Drug Discoveries & Therapeutics*, 7(2), pp.46-57.
- Gao, Z., Huang, K. and Xu, H. (2001). Protective effects of flavonoids in the roots of *scutellaria baicalensis georgi* against hydrogen peroxide-induced oxidative stress in hs-sy5y cells. *Pharmacological Research*, 43(2), pp.173-178.
- Garg, V. and Nes, W. (1986). Occurrence of  $\Delta^5$ -sterols in plants producing predominantly  $\Delta^7$ -sterols: Studies on the sterol compositions of six cucurbitaceae seeds. *Phytochemistry*, 25(11), pp.2591-2597.
- Geevananda, Y., Gunawardana, P., S. Sultanbawa, M. and Balasubramaniam, S. (1980). Distribution of some triterpenes and phenolic compounds in the extractives of

- endemic dipterocarpaceae species of Sri Lanka. *Phytochemistry*, 19(6), pp.1099-1102.
- Ghafari, S., Naghibi, F., Esmaeili, S., Sahranavard, S. and Mosaddegh, M. (2015). Investigating the cytotoxic effect of some medicinal plants from northern parts of Iran. *Research Journal of Pharmacognosy*, 2(2), pp.47-51.
- Ghambarali, Z., Bidmeshkipouri, A., Akrami, H., Azadbakht, M. and Rabzia, A. (2014). Ethanolic extract of *Ficus carica* leaf Suppresses Angiogenesis by Regulating VEGF-A and Integrin  $\beta 3$  mRNA Expression in Human umbilical vein endothelial cells. *Indian J Physiol Pharmacol*, 58(4), pp.407–415.
- Ghias Uddin, A. (2013). Bioassay-guided Isolation of New Antitumor Agent from *Ficus faveolata* (Wall. ex Miq.). *Journal of Cancer Science & Therapy*, 05(11).
- Ghimeray, A., Jung, U., Lee, H., Kim, Y., Ryu, E. and Chang, M. (2015). *In vitro* antioxidant, collagenase inhibition, and *in vivo* anti-wrinkle effects of combined formulation containing *Punica granatum*, *Ginkgo biloba*, *Ficus carica*, and *Morus alba* fruits extract. *Clinical, Cosmetic and Investigational Dermatology*, p.389.
- Gholamhose, A., Shahouzehi, B. and Sharifi-fa, F. (2010). Inhibitory Effect of Some Plant Extracts on Pancreatic Lipase. *International Journal of Pharmacology*, 6(1), pp.18-24.
- Ghosh, M., Civra, A., Rittà, M., Cagno, V., Mavuduru, S., Awasthi, P., Lembo, D. and Donalisio, M. (2016). *Ficus religiosa* L. bark extracts inhibit infection by herpes simplex virus type 2 *in vitro*. *Archives of Virology*, 161(12), pp.3509-3514.
- Giblin-Davis, R., Center, B., Nadel, H., Howard, J. and Ramírez, W. (1995). Nematodes Associated with Fig Wasps, *Pegoscopus* spp. (Agaonidae), and *Syconia* of Native Floridian Figs (*Ficus* spp.). *The Journal of Nematology*, [online] 27(1), pp.1–14. Available at: <http://journals.fcla.edu/jon/article/view/66701> [Accessed 24 Nov. 2016].
- Gilani, A., Mehmood, M., Janbaz, K., Khan, A. and Saeed, S. (2008). Ethnopharmacological studies on antispasmodic and antiplatelet activities of *Ficus carica*. *Journal of Ethnopharmacology*, 119(1), pp.1-5.
- Gilgun-Sherki, Y., Melamed, E. and Offen, D. (2003). Antioxidant Treatment in Alzheimer's Disease: Current State. *Journal of Molecular Neuroscience*, 21(1), pp.1-12.
- Girish, S., Kumar, S. and Aminudin, N. (2015). Tongkat Ali (*Eurycoma longifolia*): a possible therapeutic candidate against *Blastocystis* sp. *Parasites & Vectors*, 8(1), p.332.
- Godyń, J., Jończyk, J., Panek, D. and Malawska, B. (2016). Therapeutic strategies for Alzheimer's disease in clinical trials. *Pharmacological Reports*, 68(1), pp.127-138.
- Goedert, M. (2004). Tau protein and neurodegeneration. *Seminars in Cell & Developmental Biology*, 15(1), pp.45-49.

- Gond, N. and Khadabadi, S. (2008). Hepatoprotective activity of *Ficus carica* leaf extract on rifampicin-induced hepatic damage in rats. *Indian Journal of Pharmaceutical Sciences*, 70(3), p.364.
- Gonzalez-Burgos, E. and Gomez-Serranillos, M. (2012). Terpene Compounds in Nature: A Review of Their Potential Antioxidant Activity. *Current Medicinal Chemistry*, 19(31), pp.5319-5341.
- Goossens, E., Wijnants, M., Packet, D. and Lemière, F. (2016). Enhanced separation and analysis procedure reveals production of tri-acylated mannosylerythritol lipids by *Pseudozyma aphidis*. *Journal of Industrial Microbiology & Biotechnology*, 43(11), pp.1537-1550.
- Gosslau, A., Li, S., Ho, C., Chen, K. and Rawson, N. (2010). The importance of natural product characterization in studies of their anti-inflammatory activity. *Molecular Nutrition & Food Research*, 55(1), pp.74-82.
- Gray, A. (1880). *Structural Botany*. 6th ed. UK: Harvard university press.
- Grimm, M., Hartmann, T., FRIEß-JAVORKOVÁ, P., Laufs, U. and WEINGÄRTNER, O. (2012). *Stigmasterol for the treatment of Alzheimer's disease*. WO2010104394A1.
- Guardiola, F. (2002). *Cholesterol and phytosterol oxidation products*. 1st ed. Champaign (Illinois): AOCS press.
- Guo, Q., Du, G., He, H., Xu, H., Guo, D. and Li, R. (2015). Two nematocidal furocoumarins from *Ficus carica* L. leaves and their physiological effects on pine wood nematode (*Bursaphelenchus xylophilus*). *Natural Product Research*, 30(17), pp.1969-1973.
- Gupta, S., Prasad, S. and Aggarwal, B. (2016). *Drug discovery from mother nature*. 1st ed. Switzerland.
- Habtemariam, S. (2018a). Iridoids and Other Monoterpenes in the Alzheimer's Brain: Recent Development and Future Prospects. *Molecules*, 23(1), p.117.
- Habtemariam, S. (2018b). Molecular Pharmacology of Rosmarinic and Salvianolic Acids: Potential Seeds for Alzheimer's and Vascular Dementia Drugs. *International Journal of Molecular Sciences*, 19(2), p.458.
- Han, L., Stanley, P., Wood, P., Sharma, P., Kuruppu, A., Bradshaw, T. and Moses, J. (2016). Horner–Wadsworth–Emmons approach to piperlongumine analogues with potent anti-cancer activity. *Org. Biomol. Chem.*, 14(31), pp.7585-7593.
- Hanessian, S. (2014). *Natural products in medicinal chemistry*. 1st ed. Wiley-VCH Verlag GmbH & Co. KGaA, pp.43-74.
- Hansen, R., Gartlehner, G., Webb, A., Morgan, L., Moore, C. and Jonas, D. (2008). Efficacy and safety of donepezil, galantamine, and rivastigmine for the treatment of Alzheimer's disease: A systematic review and meta-analysis. *Clin Interv Aging*, 3(2), pp.211–225.

- Harbison, R., Bourgeois, M. and Johnson, G. (2015). *Hamilton & Hardy's industrial toxicology*. 6th ed. Canada: John Wiley & Sons, Inc, p.458.
- Harborne, J. (1967). Comparative biochemistry of flavonoids—V. : Luteolin 5-glucoside and its occurrence in the umbelliferae. *Phytochemistry*, 6(11), pp.1569-1573.
- Harborne, J. (1984). *Phytochemical Methods*. Dordrecht: Springer Netherlands, p.42.
- Harisha, S. (2006). *Introduction to practical biotechnology*. Bangalore: Laxmi Publication, pp.390-394.
- Hartmann, M. (1998). Plant sterols and the membrane environment. *Trends in Plant Science*, 3(5), pp.170-175.
- Harvey, A., Edrada-Ebel, R. and Quinn, R. (2015). The re-emergence of natural products for drug discovery in the genomics era. *Nature Reviews Drug Discovery*, 14(2), pp.111-129.
- Hasani-Ranjbar, S., Larijani, B. and Abdollahi, M. (2009). A Systematic Review of the Potential Herbal Sources of Future Drugs Effective in Oxidant-Related Diseases. *Inflammation & Allergy-Drug Targets*, 8(1), pp.2-10.
- Hashemi, S. and Abediankenari, S. (2013). Suppressive Effect of Fig (*Ficus Carica*) Latex on Esophageal Cancer Cell Proliferation. *Acta Facultatis Medicae Naissensis*, 30(2).
- Hashemi, S., Dehpour, A., Yousefzadeh, Y., Azadbakht, M., Ghasemi, M. and Abediankenari, S. (2011). The Effect of Fig Tree Latex (*Ficus carica*) on Stomach Cancer Line. *Iran Red Crescent Med J*, 13(4), pp.272-5.
- Heinrich, M. (2004). *Fundamentals of pharmacognosy and phytotherapy*. Churchill Livingstone: Elsevier, p.309.
- Holenz, J., Mannhold, R., Kubinyi, H. and Folkers, G. (2016). *Lead generation, Volume 68: Methods and Strategies, Volume 2*. Weinheim, Germany: John Wiley & Sons, p.142.
- Holmquist, L., Stuchbury, G., Berbaum, K., Muscat, S., Young, S., Hager, K., Engel, J. and Münch, G. (2007). Lipoic acid as a novel treatment for Alzheimer's disease and related dementias. *Pharmacology & Therapeutics*, 113(1), pp.154-164.
- Hou, Y., Braun, D., Michel, C., Klassen, J., Adnani, N., Wyche, T. and Bugni, T. (2012). Microbial Strain Prioritization Using Metabolomics Tools for the Discovery of Natural Products. *Analytical Chemistry*, 84(10), pp.4277-4283.
- Huang, S., Hsu, C., Chuang, H., Shih, P., Wu, C. and Yen, G. (2008). Inhibitory effect of vanillic acid on methylglyoxal-mediated glycation in apoptotic Neuro-2A cells. *NeuroToxicology*, 29(6), pp.1016-1022.
- Huang, W., Niu, H., Xinsheng, X., Junxiang, L. and Chenwei, L. (2010). Robinetinidol-(4 $\beta$ →8)-epigallocatechin 3-O-gallate, A Galloyl Dimer Prorobinetinidin From *Acacia Mearnsii* De Wild, Effectively Protects Human Neuroblastoma SH-SY5Y Cells Against Acrolein-Induced Oxidative Damage. *Journal of Alzheimer's Disease*, 21(2), pp.493-506.

- Huang, Y., Jin, M., Pi, R., Zhang, J., Chen, M., Ouyang, Y., Liu, A., Chao, X., Liu, P., Liu, J., Ramassamy, C. and Qin, J. (2013). Protective effects of caffeic acid and caffeic acid phenethyl ester against acrolein-induced neurotoxicity in HT22 mouse hippocampal cells. *Neuroscience Letters*, 535, pp.146-151.
- Huang, Y., Jin, M., Pi, R., Zhang, J., Ouyang, Y., Chao, X., Chen, M., Liu, P., Yu, J., Ramassamy, C., Dou, J., Chen, X., Jiang, Y. and Qin, J. (2013). Acrolein induces Alzheimer's disease-like pathologies *in vitro* and *in vivo*. *Toxicology Letters*, 217(3), pp.184-191.
- Huang, Y., Qin, J., Chen, M., Chao, X., Chen, Z., Ramassamy, C., Pi, R. and Jin, M. (2014). Lithium Prevents Acrolein-Induced Neurotoxicity in HT22 Mouse Hippocampal Cells. *Neurochemical Research*, 39(4), pp.677-684.
- Hung, S. and Fu, W. (2017). Drug candidates in clinical trials for Alzheimer's disease. *Journal of Biomedical Science*, 24(1).
- Imamura, K., Takeshima, T., Kashiwaya, Y., Nakaso, K. and Nakashima, K. (2006). D- $\beta$ -hydroxybutyrate protects dopaminergic SH-SY5Y cells in a rotenone model of Parkinson's disease. *Journal of Neuroscience Research*, 84(6), pp.1376-1384.
- Imbimbo, B., Ottonello, S., Frisardi, V., Solfrizzi, V., Greco, A., Seripa, D., Pilotto, A. and Panza, F. (2012). Solanezumab for the treatment of mild-to-moderate Alzheimer's disease. *Expert Review of Clinical Immunology*, 8(2), pp.135-149.
- Iqbal, D., Khan, M., Khan, M., Ahmad, S., Hussain, M. and Ali, M. (2015). Bioactivity guided fractionation and hypolipidemic property of a novel HMG-CoA reductase inhibitor from *Ficus virens* Ait. *Lipids Health Dis*, 14(1).
- Irudayaraj, S., Stalin, A., Sunil, C., Duraipandiyan, V., Al-Dhabi, N. and Ignacimuthu, S. (2016). Antioxidant, antilipidemic and antidiabetic effects of ficusin with their effects on GLUT4 translocation and PPAR $\gamma$  expression in type 2 diabetic rats. *Chemico-Biological Interactions*, 256, pp.85-93.
- Ishimaru, K., Nonaka, G. and Nishioka, I. (1987). Gallic acid esters of proto-quercitol, quinic acid and (-)-shikimic acid from *quercus mongolica* and *q. myrsin aefolia*. *Phytochemistry*, 26(5), pp.1501-1504.
- Islam, A., Khandker, S., Alam, F., Khalil, I., Kamal, M. and Gan, S. (2017). Alzheimer's Disease and Natural Products: Future Regimens Emerging from Nature. *Current Topics in Medicinal Chemistry*, 17(12), pp.1408-1428.
- Ito, T. and Masubuchi, M. (2014). Dereplication of microbial extracts and related analytical technologies. *The Journal of Antibiotics*, 67(5), pp.353-360.
- Jain, P. and Bari, S. (2010). Isolation of Lupeol, Stigmasterol and Campesterol from Petroleum Ether Extract of Woody Stem of *Wrightia tinctoria*. *Asian Journal of Plant Sciences*, 9(3), pp.163-167.
- Janjušević, L., Karaman, M., Šibul, F., Tommonaro, G., Iodice, C., Jakovljević, D. and Pejin, B. (2017). *The lignicolous fungus Trametes versicolor (L.) Lloyd (1920): a promising natural source of antiradical and AChE inhibitory agents.*

- Jann, M. (2000). Rivastigmine, a New-Generation Cholinesterase Inhibitor for the Treatment of Alzheimer's Disease. *Pharmacotherapy*, 20(1), pp.1-12.
- Jasinghe, V. and Perera, C. (2005). Distribution of ergosterol in different tissues of mushrooms and its effect on the conversion of ergosterol to vitamin D<sub>2</sub> by UV irradiation. *Food Chemistry*, 92(3), pp.541-546.
- Jeong, W. and Lachance, P. (2001). Phytosterols and Fatty Acids in Fig (*Ficus carica*, var. Mission) Fruit and Tree Components. *Journal of Food Science*, 66(2), pp.278-281.
- Ji, H., Li, X. and Zhang, H. (2009). Natural products and drug discovery. Can thousands of years of ancient medical knowledge lead us to new and powerful drug combinations in the fight against cancer and dementia?. *EMBO reports*, 10(3), pp.194-200.
- Jing, L., Zhang, Y., Luo, J. and Kong, L. (2015). Tirucallane-Type Triterpenoids from the Fruit of *Ficus carica* and Their Cytotoxic Activity. *Chemical and Pharmaceutical Bulletin*, 63(3), pp.237-243.
- Joerin, L., Kauschka, M., Bonnländer, B., Pischel, I., Benedek, B. and Butterweck, V. (2013). *Ficus carica* Leaf Extract Modulates the Lipid Profile of Rats Fed with a High-Fat Diet through an Increase of HDL-C. *Phytotherapy Research*, 28(2), pp.261-267.
- Jomova, K., Vondrakova, D., Lawson, M. and Valko, M. (2010). Metals, oxidative stress and neurodegenerative disorders. *Molecular and Cellular Biochemistry*, 345(1-2), pp.91-104.
- Jones, D. (2006). Extracellular Redox State: Refining the Definition of Oxidative Stress in Aging. *Rejuvenation Research*, 9(2), pp.169-181.
- Joshi, G. and A. Johnson, J. (2012). The Nrf2-ARE Pathway: A Valuable Therapeutic Target for the Treatment of Neurodegenerative Diseases. *Recent Patents on CNS Drug Discovery*, 7(3), pp.218-229.
- Joshi, G. and A. Johnson, J. (2012). The Nrf2-ARE Pathway: A Valuable Therapeutic Target for the Treatment of Neurodegenerative Diseases. *Recent Patents on CNS Drug Discovery*, 7(3), pp.218-229.
- Joshi, H., Vaishnav, D., Sanghvi, G., Rabadia, S., Airao, V., Sharma, T., Parmar, S. and Sheth, N. (2016). *Ficus recemosa* bark extract attenuates diabetic complications and oxidative stress in STZ-induced diabetic rats. *Pharmaceutical Biology*, 54(9), pp.1586-1595.
- Jung, H., Ali, M., Choi, R., Jeong, H., Chung, H. and Choi, J. (2016). Kinetics and molecular docking studies of fucosterol and fucoxanthin, BACE1 inhibitors from brown algae *Undaria pinnatifida* and *Ecklonia stolonifera*. *Food and Chemical Toxicology*, 89, pp.104-111.

- Kamal, N., Viegelmann, C., Clements, C. and Edrada-Ebel, R. (2016). Metabolomics-Guided Isolation of Anti-trypanosomal Metabolites from the Endophytic Fungus *Lasiodiopodia theobromae*. *Planta Medica*, 83(06), pp.565-573.
- Kang, Y., Park, Y., Park, Y., Yoon, S., JongAhn, H., Kim, G. and Kwon, S. (2012). UPLC/Q-TOF MS based metabolomics approach to post-mortem-interval discrimination: mass spectrometry based metabolomics approach. *Journal of Pharmaceutical Investigation*, 42(1), pp.41-46.
- Kannur, D. and Khandelwal, K. (2012). Phytochemical Investigation and Evaluation of Antihyperlipidemic Activity of *Ficus Carica* Linn Fruit Extracts. *Global Journal For Research Analysis*, 3(6), pp.184-187.
- Kanski, J., Aksenova, M., Stoyanova, A. and Butterfield, D. (2002). Ferulic acid antioxidant protection against hydroxyl and peroxy radical oxidation in synaptosomal and neuronal cell culture systems *in vitro*: structure-activity studies. *The Journal of Nutritional Biochemistry*, 13(5), pp.273-281.
- Karasek, F. and Clement, R. (2012). *Basic Gas Chromatography-Mass Spectrometry: Principles and Techniques*. 4th ed. Netherland: Elsevier Science, pp.1-3.
- Katz, L. and Baltz, R. (2016). Natural product discovery: past, present, and future. *Journal of Industrial Microbiology & Biotechnology*, 43(2-3), pp.155-176.
- Kawaguchi-Niida, M., Shibata, N., Morikawa, S., Uchida, K., Yamamoto, T., Sawada, T. and Kobayashi, M. (2006). Crotonaldehyde accumulates in glial cells of Alzheimer's disease brain. *Acta Neuropathologica*, 111(5), pp.422-429.
- Keshari, A., Kumar, G., Kushwaha, P., Bhardwaj, M., Kumar, P., Rawat, A., Kumar, D., Prakash, A., Ghosh, B. and Saha, S. (2016). Isolated flavonoids from *Ficus racemosa* stem bark possess antidiabetic, hypolipidemic and protective effects in albino Wistar rats. *Journal of Ethnopharmacology*, 181, pp.252-262.
- Khan, H., Akhtar, N. and Ali, A. (2014). Effects of Cream Containing *Ficus carica* L. Fruit Extract on Skin Parameters: *In vivo* Evaluation. *Indian J Pharm Sci*, 76(6), pp.560-564.
- Khan, H., Akhtar, N., Khan, H. and Khan, B. (2014). Fabrication and *In vitro* Characterization of *Ficus carica* L. Fruit Extract W/O Emulsion. *Latin American Journal of Pharmacy*, 33(7), pp.1193-1197.
- Khanavi, M., Sharifzadeh, M., Hadjiakhoondi, A. and Shafiee, A. (2005). Phytochemical investigation and anti-inflammatory activity of aerial parts of *Stachys byzanthina* C. Koch. *Journal of Ethnopharmacology*, 97(3), pp.463-468.
- Khedr, A., Ibrahim, S., Mohamed, G., Ahmed, H., Ahmad, A., Ramadan, M., El-Baky, A., Yamada, K. and Ross, S. (2016). New ursane triterpenoids from *Ficus pandurata* and their binding affinity for human cannabinoid and opioid receptors. *Arch. Pharm. Res.*, 39(7), pp.897-911.

- Khodarahmi, G., Ghasemi, N., Hassanzadeh, F. and Safaie, M. (2011). Cytotoxic Effects of Different Extracts and Latex of *Ficus carica* L. on HeLa cell Line. *Iran J Pharm Res.* 2011 Spring;10(2):273-7, 10(2), pp.273-277.
- Khorassani, F. and Hilas, O. (2013). Bapineuzumab, an Investigational Agent For Alzheimer's Disease. *Pharmacy and Therapeutics*, 38(2), pp.89-91.
- Kikuzaki, H., Sato, A., Mayahara, Y. and Nakatani, N. (2000). Galloylglucosides from Berries of *Pimenta dioica*. *Journal of Natural Products*, 63(6), pp.749-752.
- Kim, H., Choi, Y. and Verpoorte, R. (2010). NMR-based metabolomic analysis of plants. *Nature Protocols*, 5(3), pp.536-549.
- Kim, J., Lim, H., Shin, D., Kim, C., Kim, M., Chun, J. and Shin, E. (2015). Compositions of fatty acids and phytosterols of plant-based oils and their associations with anti-oxidative capacity: Application of principal component analysis. *Horticulture, Environment, and Biotechnology*, 56(4), pp.561-567.
- Kinghorn, A., Falk, H. and Kobayashi, J. (2015). *Progress in the Chemistry of Organic Natural Products 100*. 1st ed. Cham: Springer.
- Kinghorn, A., Falk, H., Gibbons, S. and Kobayashi, J. (2016). *Progress in the Chemistry of Organic Natural Products 102*. 1st ed. Cham: Springer International Publishing.
- Kirke, D., Smyth, T., Rai, D., Kenny, O. and Stengel, D. (2017). The chemical and antioxidant stability of isolated low molecular weight phlorotannins. *Food Chemistry*, 221, pp.1104-1112.
- Klayman, D. (1985). Qinghaosu (artemisinin): an antimalarial drug from China. *Science*, 228(4703), pp.1049-1055.
- Knopman, D. (1995). Tacrine for Alzheimer's Disease. *Pharmacoeconomics*, 7(4), pp.275-279.
- Koehn, F. and Carter, G. (2005). The evolving role of natural products in drug discovery. *Nature Reviews Drug Discovery*, 4(3), pp.206-220.
- Kogan, E., Korczyn, A., Virchovsky, R., Klimovizky, S., Treves, T. and Neufeld, M. (2001). EEG changes during long-term treatment with donepezil in Alzheimer's disease patients. *Journal of Neural Transmission*, 108(10), pp.1167-1173.
- Konstantinova, S., Tell, G., Vollset, S., Ulvik, A., Drevon, C. and Ueland, P. (2008). Dietary patterns, food groups, and nutrients as predictors of plasma choline and betaine in middle-aged and elderly men and women. *American Journal of Clinical Nutrition*, 88(6), pp.1663-1669.
- Kotz, J., Treichel, P., Townsend, J. and Treichel, D. (2014). *Chemistry & chemical reactivity*. 9th ed. Stamford: Cengage learning.
- Krause, J. and Tobi, G. (2013). Discovery, Development, and Regulation of Natural Products. *Using Old Solutions to New Problems - Natural Drug Discovery in the 21st Century*.

- Kris-Etherton, P., Hecker, K., Bonanome, A., Coval, S., Binkoski, A., Hilpert, K., Griel, A. and Etherton, T. (2002). Bioactive compounds in foods: their role in the prevention of cardiovascular disease and cancer. *The American Journal of Medicine*, 113(9), pp.71-88.
- Kristbergsson, K. and Ötles, S. (2016). *Functional properties of traditional foods*. 1st ed. New York: Springer Nature.
- Kubo, M., Yatsuzuka, W., Matsushima, S., Harada, K., Inoue, Y., Miyamoto, H., Matsumoto, M. and Fukuyama, Y. (2016). Antimalarial Phenanthroindolizine Alkaloids from *Ficus septica*. *Chemical and Pharmaceutical Bulletin*, [online] 64(7), pp.957-960. Available at: <http://doi.org/10.1248/cpb.c16-00181> [Accessed 10 Nov. 2016].
- Ky, C., Louarn, J., Dussert, S., Guyot, B., Hamon, S. and Noirot, M. (2001). Caffeine, trigonelline, chlorogenic acids and sucrose diversity in wild *Coffea arabica* L. and *C. canephora* P. accessions. *Food Chemistry*, 75(2), pp.223-230.
- Lahlou, M. (2013). The Success of Natural Products in Drug Discovery. *Pharmacology & Pharmacy*, 04(03), pp.17-31.
- Lansky, E., Paavilainen, H., Pawlus, A. and Newman, R. (2008). *Ficus* spp. (fig): Ethnobotany and potential as anticancer and anti-inflammatory agents. *Journal of Ethnopharmacology*, 119(2), pp.195-213.
- Lawton, L., McElhiney, J. and Edwards, C. (1999). Purification of closely eluting hydrophobic microcystins (peptide cyanotoxins) by normal-phase and reversed-phase flash chromatography. *Journal of Chromatography A*, 848(1-2), pp.515-522.
- Lazreg-Aref, H., Mars, M., Fekih, A., Aouni, M. and Said, K. (2011). Chemical composition and antibacterial activity of a hexane extract of Tunisian caprifig latex from the unripe fruit of *Ficus carica*. *Pharmaceutical Biology*, 50(4), pp.407-412.
- Lee, H., Kim, J., Jeung, H., Lee, C., Kim, D., Li, B., Lee, G., Sung, M., Ha, K., Back, H., Kim, S., Park, S., Oh, M., Kim, M., Jeon, J., Im, Y., Hwang, M., So, B., Shin, S., Yoo, W., Kim, H., Chae, H. and Chae, S. (2012). Effects of *Ficus carica* paste on loperamide-induced constipation in rats. *Food and Chemical Toxicology*, 50(3-4), pp.895-902.
- Li, S., Liu, H., Jin, Y., Lin, S., Cai, Z. and Jiang, Y. (2011). Metabolomics study of alcohol-induced liver injury and hepatocellular carcinoma xenografts in mice. *Journal of Chromatography B*, 879(24), pp.2369-2375.
- Liang, X., Ma, Y., Zhang, H. and Liu, R. (2016). A new helvolic acid derivative from an endophytic *Fusarium* sp. of *Ficus carica*. *Natural Product Research*, 30(21), pp.2407-2412.
- Lim, T. (2012). *Edible medicinal and non-medicinal plants*. 1st ed. Dordrecht: Springer.
- Liu, Y., Garzon, J., Friesen, J., Zhang, Y., McAlpine, J., Lankin, D., Chen, S. and Pauli, G. (2016). Countercurrent assisted quantitative recovery of metabolites from plant-associated natural deep eutectic solvents. *Fitoterapia*, 112, pp.30-37.

- Loizzo, M., Bonesi, M., Pugliese, A., Menichini, F. and Tundis, R. (2014). Chemical composition and bioactivity of dried fruits and honey of *Ficus carica* cultivars Dottato, San Francesco and Citrullara. *Journal of the Science of Food and Agriculture*, 94(11), pp.2179-2186.
- LoPachin, R., Geohagen, B. and Gavin, T. (2008). Synaptosomal Toxicity and Nucleophilic Targets of 4-Hydroxy-2-Nonenal. *Toxicological Sciences*, 107(1), pp.171-181.
- Lopes, F., Schröder, R., Júnior, M., Zanotto-Filho, A., Müller, C., Pires, A., Meurer, R., Colpo, G., Gelain, D., Kapczinski, F., Moreira, J., Fernandes, M. and Klamt, F. (2010). Comparison between proliferative and neuron-like SH-SY5Y cells as an *in vitro* model for Parkinson disease studies. *Brain Research*, 1337, pp.85-94.
- Lozano, N., Oliveira, R., Weber, K., Honorio, K., Guido, R., Andricopulo, A., de Sousa, A. and da Silva, A. (2014). Pattern Recognition Techniques Applied to the Study of Leishmanial Glyceraldehyde-3-Phosphate Dehydrogenase Inhibition. *International Journal of Molecular Sciences*, 15(2), pp.3186-3203.
- Lu, Q., Sun, Y., Shu, Y., Tan, S., Yin, L., Guo, Y. and Tang, L. (2016). HSCCC Separation of the Two Iridoid Glycosides and Three Phenolic Compounds from *Veronica ciliata* and Their *in vitro* Antioxidant and Anti-Hepatocarcinoma Activities. *Molecules*, 21(9), p.1234.
- Luo, J., Li, S., Qin, X., Peng, Q., Liu, Y., Yang, S., Qin, X., Xiong, Y. and Zeng, Z. (2015). Association of the NQO1 C609T polymorphism with Alzheimer's disease in Chinese populations: a meta-analysis. *International Journal of Neuroscience*, 126(3), pp.199-204.
- M.D. Dias, SYNGENTA PARTICIPATIONS AG (2013). *Method of extraction of an enzyme from plant or animal tissue*. U.S. Patent Application 13/768,164.
- Ma, Y., Liang, X., Zhang, H. and Liu, R. (2016). Cytotoxic and Antibiotic Cyclic Pentapeptide from an Endophytic *Aspergillus tamarii* of *Ficus carica*. *Journal of Agricultural and Food Chemistry*, 64(19), pp.3789-3793.
- Maczurek, A., Hager, K., Kenklies, M., Sharman, M., Martins, R., Engel, J., Carlson, D. and Münch, G. (2008). Lipoic acid as an anti-inflammatory and neuroprotective treatment for Alzheimer's disease☆. *Advanced Drug Delivery Reviews*, 60(13-14), pp.1463-1470.
- Madala, N., Piater, L., Steenkamp, P. and Dubery, I. (2014). Multivariate statistical models of metabolomic data reveals different metabolite distribution patterns in isonitrosoacetophenone-elicited *Nicotiana tabacum* and *Sorghum bicolor* cells. *SpringerPlus*, 3(1), p.254.
- Mahmoudi, S., Khali, M., Benkhaled, A., Benamirouche, K. and Baiti, I. (2016). Phenolic and flavonoid contents, antioxidant and antimicrobial activities of leaf extracts from ten Algerian *Ficus carica* L. varieties. *Asian Pacific Journal of Tropical Biomedicine*, 6(3), pp.239-245.

- Manjari Mishra, P. and Sree, A. (2009). Chemical investigation and antibacterial study of hexane extract of leaves of *Finlaysonia obovata*. *Chemistry of Natural Compounds*, 45(1), pp.129-131.
- Marrelli, M., Menichini, F., Statti, G., Bonesi, M., Duez, P., Menichini, F. and Conforti, F. (2012). Changes in the phenolic and lipophilic composition, in the enzyme inhibition and antiproliferative activity of *Ficus carica* L. cultivar Dottato fruits during maturation. *Food and Chemical Toxicology*, 50(3-4), pp.726-733.
- Marum, R. (2009). Update on the use of memantine in Alzheimer's disease. *Neuropsychiatric Disease and Treatment*, 5, p.237.
- Masoudi, S., Ploen, D., Kunz, K. and Hildt, E. (2014). The adjuvant component  $\alpha$ -tocopherol triggers via modulation of Nrf2 the expression and turnover of hypocretin *in vitro* and its implication to the development of narcolepsy. *Vaccine*, 32(25), pp.2980-2988.
- Mata, A., Ferreira, J., Semedo, C., Serra, T., Duarte, C. and Bronze, M. (2016). Contribution to the characterization of *Opuntia* spp. juices by LC–DAD–ESI–MS/MS. *Food Chemistry*, 210, pp.558-565.
- Máthé, A. (2015). *Medicinal and aromatic plants of the world*. 1st ed. Dordrecht: Springer.
- Mawa, S., Husain, K. and Jantan, I. (2013). *Ficus carica* L. (Moraceae): Phytochemistry, Traditional Uses and Biological Activities. *Evidence-Based Complementary and Alternative Medicine*, 2013, pp.1-8.
- Mawa, S., Husain, K. and Jantan, I. (2017). *Ficus carica* L. (Moraceae): Phytochemistry, Traditional Uses and Biological Activities.
- Mawa, S., Jantan, I. and Husain, K. (2016). Isolation of Terpenoids from the Stem of *Ficus aurantiaca* Griff and their Effects on Reactive Oxygen Species Production and Chemotactic Activity of Neutrophils. *Molecules*, 21(1), p.9.
- Mbosso Teinkela, J., Assob Nguedia, J., Meyer, F., Vouffo Donfack, E., Lenta Ndjakou, B., Ngouela, S., Tsamo, E., Adiogo, D., Guy Blaise Azebaze, A. and Wintjens, R. (2016). *In vitro* antimicrobial and anti-proliferative activities of plant extracts from *Spathodea campanulata*, *Ficus bubu*, and *Carica papaya*. *Pharmaceutical Biology*, 54(6), pp.1086-1095.
- Mbosso Teinkela, J., Siwe Noundou, X., Nguemfo, E., Meyer, F., Djoukoue, A., Van Antwerpen, P., Ngouela, S., Tsamo, E., Mpondo Mpondo, E., Vardamides, J., Azebaze, G. and Wintjens, R. (2016). Identification of compounds with anti-proliferative activity from the wood of *Ficus elastica* Roxb. ex Hornem. aerial roots. *Fitoterapia*, 112, pp.65-73.
- McConathy, J. and Owens, M. (2003). Stereochemistry in Drug Action. *The Primary Care Companion to The Journal of Clinical Psychiatry*, 05(02), pp.70-73.
- Megoulas, N. and Koupparis, M. (2005). Twenty Years of Evaporative Light Scattering Detection. *Critical Reviews in Analytical Chemistry*, 35(4), pp.301-316.

- Mehta, D., Jackson, R., Paul, G., Shi, J. and Sabbagh, M. (2017). Why do trials for Alzheimer's disease drugs keep failing? A discontinued drug perspective for 2010-2015. *Expert Opinion on Investigational Drugs*, 26(6), pp.735-739.
- Menezes-de-Oliveira, D., Aguilar, M., King-Díaz, B., Vieira-Filho, S., Pains-Duarte, L., Silva, G. and Lotina-Hennsen, B. (2011). The Triterpenes 3 $\beta$ -LuP-20(29)-en-3-ol and 3 $\beta$ -LuP-20(29)-en-3-yl Acetate and the Carbohydrate 1,2,3,4,5,6-Hexa-O-acetyl-dulcitol as Photosynthesis Light Reactions Inhibitors. *Molecules*, 16(12), pp.9939-9956.
- Menichini, G., Alfano, C., Provenzano, E., Marrelli, M., A. Statti, G., Somma, F., Menichini, F. and Conforti, F. (2012). Fig Latex (*Ficus carica* L. cultivar Dottato) in Combination with UV Irradiation Decreases the Viability of A375 Melanoma Cells *In vitro*. *Anti-Cancer Agents in Medicinal Chemistry*, 12(8), pp.959-965.
- Misbah, H., Aziz, A. and Aminudin, N. (2013). Antidiabetic and antioxidant properties of *Ficus deltoidea* fruit extracts and fractions. *BMC Complementary and Alternative Medicine*, 13(1).
- Misra, T., Singh, R., Srivastava, R., Pandey, H., Prasad, C. and Singh, S. (1993). A New Triterpenoidal from *Vernonia cinerea*. *Planta Medica*, 59(05), pp.458-460.
- Mitra, A., De, B., Bhandari, K., Singla, R., Katakam, P., Samanta, T., Kushwaha, D. and Gundamaraju, R. (2015). Chemometrics optimized extraction procedures, phytosynergistic blending and *in vitro* screening of natural enzyme inhibitors amongst leaves of Tulsi, Banyan and Jamun. *Pharmacognosy Magazine*, 11(44), p.522.
- Moghadasian, M. (2000). Pharmacological properties of plant sterols. *Life Sciences*, 67(6), pp.605-615.
- Moghe, A., Ghare, S., Lamoreau, B., Mohammad, M., Barve, S., McClain, C. and Joshi-Barve, S. (2015). Molecular Mechanisms of Acrolein Toxicity: Relevance to Human Disease. *Toxicological Sciences*, 143(2), pp.242-255.
- Mohan, C. and Gupta, S. (2016). QSAR Models towards Cholinesterase Inhibitors for the Treatment of Alzheimer's Disease. *Oncology*, 2, pp.591-636.
- Mohanad, J., Azhar, A. and Imad, H. (2016). Evaluation of anti-bacterial activity and bioactive chemical analysis of *Ocimum basilicum* using Fourier transform infrared (FT-IR) and gas chromatography-mass spectrometry (GC-MS) techniques. *Journal of Pharmacognosy and Phytotherapy*, 8(6), pp.127-146.
- Mohimani, H. and Pevzner, P. (2016). Dereplication, sequencing and identification of peptidic natural products: from genome mining to peptidogenomics to spectral networks. *Nat. Prod. Rep.*, 33(1), pp.73-86.
- Morelato, M., Beavis, A., Kirkbride, P. and Roux, C. (2013). Forensic applications of desorption electrospray ionisation mass spectrometry (DESI-MS). *Forensic Science International*, 226(1-3), pp.10-21.

- Mount, C. and Downton, C. (2006). Alzheimer disease: progress or profit?. *Nature Medicine*, 12(7), pp.780-784.
- Mujeeb, M., Alam, K., Aeri, V. and Ali, B. (2011). Hepatoprotective Activity of the Ethanolic Extract of *Ficus carica* Linn. Leaves in Carbon Tetrachloride-Induced Hepatotoxicity in Rats. *Iran J Pharm Res. 2011 Spring;10(2):301-6*, 10(2), pp.301-306.
- Mzhel'skaya, L. and Abubakirov, N. (1967). Triterpene glycosides of *Leontice eversmannii*. *Chemistry of Natural Compounds*, 3(2), pp.84-87.
- Naghdi, M., Maghbool, M., Seifalah-Zade, M., Mahaldashtian, M., Makoolati, Z., Kouhpayeh, S., Ghasemi, A. and Fereydouni, N. (2016). Effects of Common Fig (*Ficus carica*) Leaf Extracts on Sperm Parameters and Testis of Mice Intoxicated with Formaldehyde. *Evidence-Based Complementary and Alternative Medicine*, 2016, pp.1-9.
- Naidu, K. (2003). Vitamin C in human health and disease is still a mystery? An overview. *Nutrition Journal*, 2(1).
- Najjari, A., Rajabi, Z., Vasfi Marandi, M. and Dehghan, G. (2015). The effect of the hexanic extracts of fig (*Ficus carica*) and olive (*Olea europaea*) fruit and nanoparticles of selenium on the immunogenicity of the inactivated avian influenza virus subtype H9N2. *Veterinary Research Forum*, 6(3), pp.227-231.
- Nama, D., Arseneault, M., Zarkovic, N., Waeg, G. and Ramassamy, C. (2010). Molecular Regulations Induced by Acrolein in Neuroblastoma SK-N-SH Cells: Relevance to Alzheimer's Disease. *Journal of Alzheimer's Disease*, 21, pp.1197-1216.
- Nasution, R., Marianne, M. and Marzuki, I. (2017). Isolation Compound Anti-Obesity from the Bark Ara (*Ficus Racemosa*) of Aceh. *Oriental Journal of Chemistry*, 32(5).
- Naumoska, K. and Vovk, I. (2015). Analysis of triterpenoids and phytosterols in vegetables by thin-layer chromatography coupled to tandem mass spectrometry. *Journal of Chromatography A*, 1381, pp.229-238.
- Nautiyal, S., Bhaskar, K. and Khan, Y. (2015). *Biodiversity of semiarid landscape*. 1st ed. Cham: Springer.
- Nayak, D., Ashe, S., Rauta, P., Kumari, M. and Nayak, B. (2016). Bark extract mediated green synthesis of silver nanoparticles: Evaluation of antimicrobial activity and antiproliferative response against osteosarcoma. *Materials Science and Engineering: C*, 58, pp.44-52.
- Nciri, R., Desmoulin, F., Allagui, M., Murat, J., Feki, A., Vincent, C. and Croute, F. (2012). Neuroprotective effects of chronic exposure of SH-SY5Y to low lithium concentration involve glycolysis stimulation, extracellular pyruvate accumulation and resistance to oxidative stress. *The International Journal of Neuropsychopharmacology*, 16(02), pp.365-376.
- Neidle, S. (2014). *Cancer drug design and discovery*. London: Elsevier, p.97.

- Newman, D. and Cragg, G. (2016). Natural Products as Sources of New Drugs from 1981 to 2014. *J. Nat. Prod.*, 79(3), pp.629-661.
- Ngadjui, E., Nkeng-Efouet, P., Nguenefack, T., Kamanyi, A. and Watcho, P. (2015). High fat diet-induced estrus cycle disruption: effects of *Ficus asperifolia*. *Journal of Complementary and Integrative Medicine*, 12(3).
- Ni, J., Tao, F., Du, H. and Xu, P. (2015). Mimicking a natural pathway for de novo biosynthesis: natural vanillin production from accessible carbon sources. *Scientific Reports*, 5(1).
- Nordberg, A. and Svensson, A. (1998). Cholinesterase Inhibitors in the Treatment of Alzheimer's Disease. *Drug Safety*, 19(6), pp.465-480.
- Nostro, A., Guerrini, A., Marino, A., Tacchini, M., Di Giulio, M., Grandini, A., Akin, M., Cellini, L., Bisignano, G. and Saraçoğlu, H. (2016). *In vitro* activity of plant extracts against biofilm-producing food-related bacteria. *International Journal of Food Microbiology*, 238, pp.33-39.
- Novak, E. (1999). *Method of preventing and delaying onset of Alzheimer's disease and composition therefor*. US 5985936 A.
- Ntchapda, F., Djedouboum, A., Talla, E., Sokeng Dongmo, S., Nana, P., Adjia, H., Nguimbou, R., Bonabe, C., Gaimatakon, S., Njintang Yanou, N. and Dimo, T. (2015). Hypolipidemic and anti-atherogenic effect of aqueous extract leaves of *Ficus glumosa* (Moraceae) in rats. *Experimental Gerontology*, 62, pp.53-62.
- Nugroho, A., Akbar, F., Wiyani, A. and Sudarsono, S. (2015). Cytotoxic Effect and Constituent Profile of Alkaloid Fractions from Ethanolic Extract of *Ficus septica* Burm. f. Leaves on T47D Breast Cancer Cells. *Asian Pacific Journal of Cancer Prevention*, 16(16), pp.7337-7342.
- Nutmakul, T., Pattanapanyasat, K., Soonthornchareonnon, N., Shiomi, K., Mori, M. and Prathanturarug, S. (2016). Antiplasmodial activities of a Thai traditional antipyretic formulation, Bencha-Loga-Wichian: A comparative study between the roots and their substitutes, the stems. *Journal of Ethnopharmacology*, 193, pp.125-132.
- O'Connell, N., O'Callaghan, Y., O'Brien, N., Maguire, A. and McCarthy, F. (2012). Synthetic routes to campesterol and dihydrobrassicasterol: a first reported synthesis of the key phytosterol dihydrobrassicasterol. *Tetrahedron*, 68(25), pp.4995-5004.
- Oh, H., Lee, H., Seo, M., Kang, Y., Kim, J., Park, J., Kim, O., Back, H., Kim, S., Oh, M., Park, S., Kim, M., Jeon, J., Hwang, M., Shin, S. and Chae, S. (2011). Effects of *Ficus caricapaste* on constipation induced by a high-protein feed and movement restriction in beagles. *Laboratory Animal Research*, 27(4), p.275.
- Ohta, Y., Darwish, M., Hishikawa, N., Yamashita, T., Sato, K., Takemoto, M. and Abe, K. (2017). Therapeutic effects of drug switching between acetylcholinesterase inhibitors in patients with Alzheimer's disease. *Geriatrics & Gerontology International*.

- Okmen, G., Turkcan, O., Erdal, P. and Isik, D. (2014). THE NON-ENZYMATIC ANTIOXIDANT ACTIVITIES OF FICUS CARICA L. SUBSP. CARICA LEAVES AND ITS ANTIMICROBIAL ACTIVITIES AGAINST FOOD PATHOGENS. *International Journal of Pharmaceutical sciences and research*, 5(12), pp.5145-5150.
- Olaokun, O., McGaw, L., Janse van Rensburg, I., Eloff, J. and Naidoo, V. (2016). Antidiabetic activity of the ethyl acetate fraction of *Ficus lutea* (Moraceae) leaf extract: comparison of an *in vitro* assay with an *in vivo* obese mouse model. *BMC Complementary and Alternative Medicine*, 16(1).
- Oliveira, A., Pereira, J., Andrade, P., Valentão, P., Seabra, R. and Silva, B. (2008). Organic acids composition of *Cydonia oblonga* Miller leaf. *Food Chemistry*, 111(2), pp.393-399.
- Oliveira, A., Silva, L., Ferreres, F., Guedes de Pinho, P., Valentão, P., Silva, B., Pereira, J. and Andrade, P. (2010). Chemical Assessment and *in vitro* Antioxidant Capacity of *Ficus carica* Latex. *Journal of Agricultural and Food Chemistry*, 58(6), pp.3393-3398.
- Oliveira, A., Valentão, P., Pereira, J., Silva, B., Tavares, F. and Andrade, P. (2009). *Ficus carica* L.: Metabolic and biological screening. *Food and Chemical Toxicology*, 47(11), pp.2841-2846.
- Palaniyappan, V., Bommireddy, E., Gudipudi, H., Chitturi, R. and Yandamala, N. (2013). *IN VIVO* FERTILITY ENHANCING ACTIVITY (APHRODISIAC) OF FICUS CARICA FRUIT ON MALE WISTAR RATS. *International Journal of Pharmacy and Pharmaceutical Sciences*, 5(2).
- Panday, D. and Rauniar, G. (2016). Effect of root-extracts of *Ficus benghalensis* (Banyan) in memory, anxiety, muscle co-ordination and seizure in animal models. *BMC Complementary and Alternative Medicine*, 16(1).
- Pande, G. and Akoh, C. (2010). Organic acids, antioxidant capacity, phenolic content and lipid characterisation of Georgia-grown underutilized fruit crops. *Food Chemistry*, 120(4), pp.1067-1075.
- Park, S., Oh, T., Kim, S., Kim, J., Lee, S. and Lee, N. (2011). Constituents with tyrosinase inhibitory activities from branches of *Ficus erecta* var. *sieboldii* King. *Journal of Enzyme Inhibition and Medicinal Chemistry*, 27(3), pp.390-394.
- Parkes, J. and Fenton, G. (1973). Levo(-) amphetamine and dextro(+) amphetamine in the treatment of narcolepsy. *Journal of Neurology, Neurosurgery & Psychiatry*, 36(6), pp.1076-1081.
- Patridge, E., Gareiss, P., Kinch, M. and Hoyer, D. (2016). An analysis of FDA-approved drugs: natural products and their derivatives. *Drug Discovery Today*, 21(2), pp.204-207.
- Pérez, C., Canal, J. and Torres, M. (2003). Experimental diabetes treated with *Ficus carica* extract: effect on oxidative stress parameters. *Acta Diabetologica*, 40(1), pp.3-8.

- Pérez, C., Canal, J., Campillo, J., Romero, A. and Torres, M. (1999). Hypotriglyceridaemic activity of *Ficus carica* leaves in experimental hypertriglyceridaemic rats. *Phytotherapy Research*, 13(3), pp.188-191.
- Pérez, C., Domínguez, E., Canal, J., Campillo, J. and Torres, M. (2000). Hypoglycaemic Activity of an Aqueous Extract from *Ficus Carica* (Fig Tree) Leaves in Streptozotocin Diabetic Rats. *Pharmaceutical Biology*, 38(3), pp.181-186.
- Pizzimenti, S., Ciamporcero, E., Daga, M., Pettazzoni, P., Arcaro, A., Cetrangolo, G., Minelli, R., Dianzani, C., Lepore, A., Gentile, F. and Barrera, G. (2013). Interaction of aldehydes derived from lipid peroxidation and membrane proteins. *Frontiers in Physiology*, 4.
- Pluskal, T., Castillo, S., Villar-Briones, A. and Orešič, M. (2010). MZmine 2: Modular framework for processing, visualizing, and analyzing mass spectrometry-based molecular profile data. *BMC Bioinformatics*, 11(1), p.395.
- Polinsky, R. (1998). Clinical pharmacology of rivastigmine: a new-generation acetylcholinesterase inhibitor for the treatment of alzheimer's disease. *Clinical Therapeutics*, 20(4), pp.634-647.
- Powell, K. (2016). *Synthetic and Biophysical Studies on the Tridachiahydropyrone Family of Natural Products*. 1st ed. Cham: Springer International Publishing.
- Prakasa Rao, T., Sarma, N., Murthy, Y., Kantamreddi, V., Wright, C. and Parameswaran, P. (2010). New polyhydroxy sterols from the marine sponge *Callyspongia fibrosa* (Ridley & Dendly). *Tetrahedron Letters*, 51(27), pp.3583-3586.
- Pyka, A. and Babuska, M. (2006). Lipophilicity of Selected Steroid Compounds. I. Investigations on RP18W Stationary Phase by RP-HPTLC. *Journal of Liquid Chromatography & Related Technologies*, 29(13), pp.1891-1903.
- Rabel, F. and Sherma, J. (2016). A review of advances in two-dimensional thin-layer chromatography. *Journal of Liquid Chromatography & Related Technologies*, 39(14), pp.627-639.
- Rabel, F. and Sherma, J. (2016). New TLC/HPTLC commercially prepared and laboratory prepared plates: A review. *Journal of Liquid Chromatography & Related Technologies*, 39(8), pp.385-393.
- Rahelivao, M., Lübken, T., Gruner, M., Kataeva, O., Ralambondrahety, R., Andriamanantoanina, H., Checinski, M., Bauer, I. and Knölker, H. (2017). Isolation and structure elucidation of natural products of three soft corals and a sponge from the coast of Madagascar. *Org. Biomol. Chem.*, 15(12), pp.2593-2608.
- Rahman, A. (2014). *Studies in natural products chemistry*. 1st ed. Amsterdam: Elsevier.
- Rahman, A. (2016). *Studies in natural products chemistry*. 1st ed. [Place of publication not identified]: Elsevier.

- Rahman, I., Ijaz, F., Afzal, A., Iqbal, Z., Ali, N. and Khan, S. (2016). Contributions to the phytotherapies of digestive disorders: Traditional knowledge and cultural drivers of Manoor Valley, Northern Pakistan. *Journal of Ethnopharmacology*, 192, pp.30-52.
- Raina, A., Templeton, D., deak, J., Perry, G. and Smith, M. (1999). Quinone reductase (NQO1), a sensitive redox indicator, is increased in Alzheimer's disease. *Redox Report*, 4(1-2), pp.23-27.
- Ramawat, K., Mérillon, J. and Shivanna, K. (2014). *Reproductive biology of plants*. 1st ed. Boca Raton: CRC Press, Taylor & Francis Group.
- Rampersad, S. (2012). Multiple Applications of Alamar Blue as an Indicator of Metabolic Function and Cellular Health in Cell Viability Bioassays. *Sensors*, 12(12), pp.12347-12360.
- Rao, K., Donia, M., Peng, J., Garcia-Palomero, E., Alonso, D., Martinez, A., Medina, M., Franzblau, S., Tekwani, B., Khan, S., Wahyuono, S., Willett, K. and Hamann, M. (2006). Manzamine B and E and Ircinal A Related Alkaloids from an Indonesian Acanthostrongylophora Sponge and Their Activity against Infectious, Tropical Parasitic, and Alzheimer's Diseases. *Journal of Natural Products*, 69(7), pp.1034-1040.
- Raskind, M., Carta, A. and Bravi, D. (1995). Is Early-Onset Alzheimer Disease a Distinct Subgroup Within the Alzheimer Disease Population?. *Alzheimer Disease & Associated Disorders*, 9(Supplement), p.S7.
- Raskovic, B., Lazic, J. and Polovic, N. (2015). Characterisation of general proteolytic, milk clotting and antifungal activity of *Ficus carica* latex during fruit ripening. *Journal of the Science of Food and Agriculture*, 96(2), pp.576-582.
- Reddy, J., Reddy, S., Hopkins, D. and Gabriel, D. (2007). ToIC is Required for Pathogenicity of *Xylella fastidiosa* in *Vitis vinifera* Grapevines. *Molecular Plant-Microbe Interactions*, 20(4), pp.403-410.
- Research progress on natural products from traditional Chinese medicine in treatment of Alzheimer's disease. (2013). *Drug Discoveries & Therapeutics*.
- Ribechini, E., Pérez-Arantegui, J. and Colombini, M. (2011). Gas chromatography/mass spectrometry and pyrolysis-gas chromatography/mass spectrometry for the chemical characterisation of modern and archaeological figs (*Ficus carica*). *Journal of Chromatography A*, 1218(25), pp.3915-3922.
- Robinette, S., Brüsweiler, R., Schroeder, F. and Edison, A. (2012). NMR in Metabolomics and Natural Products Research: Two Sides of the Same Coin. *Accounts of Chemical Research*, 45(2), pp.288-297.
- Rodriguez-Estrada, M., Cilla Tatay, A., Cardenia, V. and Garcia-Llatas, G. (2014). *Reference Module in Biomedical Sciences*. 1st ed. Elsevier, pp.351-364.
- Rogers, S. and Friedhoff, L. (1996). The Efficacy and Safety of Donepezil in Patients with Alzheimer's Disease: Results of a US Multicentre, Randomized, Double-Blind,

- Placebo-Controlled Trial. *Dementia and Geriatric Cognitive Disorders*, 7(6), pp.293-303.
- Ruamrungsri, N., Siengdee, P., Sringarm, K., Chomdej, S., Ongchai, S. and Nganvongpanit, K. (2016). *In vitro* cytotoxic screening of 31 crude extracts of Thai herbs on a chondrosarcoma cell line and primary chondrocytes and apoptotic effects of selected extracts. *In vitro Cellular & Developmental Biology - Animal*, 52(4), pp.434-444.
- Rubnov, S., Rabinowitz, R., Schlesinger, M., Mechoulam, R. and Kashman, Y. (2001). Suppressors of cancer cell proliferation from fig (*Ficus carica*) resin: isolation and structure elucidation. *J Nat Prod*, 64(7), pp.993-996.
- Rui, X., Wenfang, L., Jing, C., Meng, C., Chengcheng, D., Jiqu, X. and Shuang, R. (2017). Neuroprotective effects of phytosterol esters against high cholesterol-induced cognitive deficits in aged rat. *Food Funct.*, 8(3), pp.1323-1332.
- Russo, F., Caporaso, N., Paduano, A. and Sacchi, R. (2014). Phenolic Compounds in Fresh and Dried Figs from Cilento (Italy), by Considering Breba Crop and Full Crop, in Comparison to Turkish and Greek Dried Figs. *Journal of Food Science*, 79(7), pp.C1278-C1284.
- Sá e Melo, M., Cruz Silva, M., Iuliano, L. and Lizard, G. (2015). Oxysterols and related sterols: Chemical, biochemical and biological aspects. *Steroids*, 99, pp.117-118.
- Sabiu, S., Garuba, T., Sunmonu, T., Sulyman, A. and Ismail, N. (2015). Indomethacin-induced gastric ulceration in rats: Ameliorative roles of *Spondias mombin* and *Ficus exasperata*. *Pharmaceutical Biology*, 54(1), pp.180-186.
- Sabnis, R. (2010). *Handbook of biological dyes and stains*. Hoboken, NJ: Wiley-Blackwell, p.293.
- Sadeghi, M., Ganji, F., Taghizadeh, M. and Daraei, B. (2016). Preparation and Characterization of Rivastigmine Transdermal Patch Based on Chitosan Microparticles. *Iran J Pharm Res*, 15(3), pp.283-294.
- Saitō, K., Dixon, R. and Willmitzer, L. (2006). *Plant metabolomics*. 1st ed. Berlin: Springer.
- Sajewicz, M., Staszek, D., Natić, M., Wojtal, Ł., Waksmundzka-Hajnos, M. and Kowalska, T. (2011). TLC-MS versus TLC-LC-MS fingerprints of herbal extracts. Part II. phenolic acids and flavonoids. *Journal of Liquid Chromatography & Related Technologies*, 34(10-11), pp.864-887.
- Saleem, M. (2009). Lupeol, a novel anti-inflammatory and anti-cancer dietary triterpene. *Cancer Letters*, 285(2), pp.109-115.
- Sánchez, E., Rivas Morales, C., Castillo, S., Leos-Rivas, C., García-Becerra, L. and Ortiz Martínez, D. (2016). Antibacterial and Antibiofilm Activity of Methanolic Plant Extracts against Nosocomial Microorganisms. *Evidence-Based Complementary and Alternative Medicine*, 2016, pp.1-8.

- Sang, S., Lapsley, K., Jeong, W., Lachance, P., Ho, C. and Rosen, R. (2002). Antioxidative Phenolic Compounds Isolated from Almond Skins (*Prunus amygdalus*Batsch). *Journal of Agricultural and Food Chemistry*, 50(8), pp.2459-2463.
- SantaCruz, K., Yazlovitskaya, E., Collins, J., Johnson, J. and DeCarli, C. (2004). Regional NAD(P)H:quinone oxidoreductase activity in Alzheimer's disease. *Neurobiology of Aging*, 25(1), pp.63-69.
- Saoudi, M. and El Feki, A. (2017). *Protective Role of Ficus carica Stem Extract against Hepatic Oxidative Damage Induced by Methanol in Male Wistar Rats*.
- Saratha, V., Pillai, S. and Subramanian, S. (2011). Isolation and Characterization of Lupeol, a Triterpenoid from *Calotropis Gigantea* Latex. *International Journal of Pharmaceutical Sciences Review and Research*, 10(2), pp.54-57.
- Sardari, M., Rezaeizadeh, H., Minaei, B. and Heydari, M. (2015). *Ficus carica* (fig) paste supplementation in patients with multiple sclerosis associated constipation; a double blind randomized clinical trial. *Planta Medica*, 81(16).
- Sarwar Alam, M., Niwa, M., Sakai, T., Gupta, S. and Ali, M. (1992). 24 $\beta$ -Ethylcholest-4-en-3 $\beta$ -ol from the roots of *Lawsonia inermis*. *Phytochemistry*, 31(7), pp.2558-2560.
- Sato, S., Arita, M., Soga, T., Nishioka, T. and Tomita, M. (2008). Time-resolved metabolomics reveals metabolic modulation in rice foliage. *BMC Systems Biology*, 2(1), p.51.
- Saxena, V., Gupta, D. and Saraf, S. (2012). *Ficus carica* leaf extract in regulation of thyroidism using elisa technique. *Asian Journal of Pharmaceutical and Clinical Research*, 5(2), pp.44-48.
- Schmid, R. (2001). Recent Advances in the Description of the Structure of Water, the Hydrophobic Effect, and the Like-Dissolves-Like Rule. *Monatshefte fuer Chemie/Chemical Monthly*, 132(11), pp.1295-1326.
- Schmidt, J., Kuhnt, C. and Adam, G. (1994). Brassinosteroids and sterols from seeds of *Beta vulgaris*. *Phytochemistry*, 36(1), pp.175-177.
- Schofield, P., Mbugua, D. and Pell, A. (2001). Analysis of condensed tannins: a review. *Animal Feed Science and Technology*, 91(1-2), pp.21-40.
- Schripsema, J. (2010). Application of NMR in plant metabolomics: techniques, problems and prospects. *Phytochemical Analysis*, 21(1), pp.14-21.
- Seigler, D. (1998). Shikimic Acid Pathway. *Plant Secondary Metabolism*, pp.94-105.
- Seneci, P. (2015). *Chemical modulators of protein misfolding and neurodegenerative disease*. San Diego: Academic Press, p.176.
- Seo, D. and Choi, C. (2016). Inhibition of Murine Norovirus and Feline Calicivirus by Edible Herbal Extracts. *Food and Environmental Virology*.

- Serraclara, A., Hawkins, F., Pérez, C., Domínguez, E., Campillo, J. and Torres, M. (2017). Hypoglycemic action of an oral fig-leaf decoction in type-I diabetic patients.
- Serraclara, A., Hawkins, F., Pérez, C., Domínguez, E., Campillo, J. and Torres, M. (1998). Hypoglycemic action of an oral fig-leaf decoction in type-I diabetic patients. *Diabetes Res Clin Pract.*, 39(1), pp.19-22.
- Seshadri, T. and Vydeeswaran, S. (1971). Chemical constituents of *Demia extensa*. *current science*, 40(22), pp.594-595.
- Seyedan, A., Alshawsh, M., Alshagga, M., Koosha, S. and Mohamed, Z. (2015). Medicinal Plants and Their Inhibitory Activities against Pancreatic Lipase: A Review. *Evidence-Based Complementary and Alternative Medicine*, 2015, pp.1-13.
- Shad, A., Ahmad, S., Ullah, R., AbdEl-Salam, N., Fouad, H., Rehman, N., Hussain, H. and Saeed, W. (2014). Phytochemical and Biological Activities of Four Wild Medicinal Plants. *The Scientific World Journal*, 2014, pp.1-7.
- Shahidi, F. and Zhong, Y. (2010). Lipid oxidation and improving the oxidative stability. *Chemical Society Reviews*, 39(11), p.4067.
- Shaikh, Q., Yang, M., Memon, K., Lateef, M., Na, D., Wan, S., Eric, D., Zhang, L. and Jiang, T. (2016). 1,2,3,4,6-Pentakis[*-O*-(3,4,5-trihydroxybenzoyl)]- $\alpha,\beta$ -D-glucopyranose (PGG) analogs: design, synthesis, anti-tumor and anti-oxidant activities. *Carbohydrate Research*, 430, pp.72-81.
- Shakunthala, N. (2009). New cytochrome P450 mechanisms: implications for understanding molecular basis for drug toxicity at the level of the cytochrome. *Expert Opinion on Drug Metabolism & Toxicology*, 6(1), pp.1-15.
- Shara, M. and Stohs, S. (2015). Efficacy and Safety of White Willow Bark (*Salix alba*) Extracts. *Phytotherapy Research*, 29(8), pp.1112-1116.
- Sharma, U., Jandaik, S., Mehta, J. and Mohan, M. (2016). Synergistic And Efflux Pump Inhibitory Activity Of Plant Extracts And Antibiotics On *Staphylococcus Aureus* Strains. *Asian Journal of Pharmaceutical and Clinical Research*, p.277.
- Sheeja Malar, D., Beema Shafreen, R., Karutha Pandian, S. and Pandima Devi, K. (2016). Cholinesterase inhibitory, anti-amyloidogenic and neuroprotective effect of the medicinal plant *Grewia tiliaefolia* – An *in vitro* and *in silico* study. *Pharmaceutical Biology*, 55(1), pp.381-393.
- Shen, C., Cheng, W., Yu, P., Wang, L., Zhou, L., Zeng, L. and Yang, Q. (2016). Resveratrol pretreatment attenuates injury and promotes proliferation of neural stem cells following oxygen-glucose deprivation/reoxygenation by upregulating the expression of Nrf2, HO-1 and NQO1 *in vitro*. *Molecular Medicine Reports*, 14(4), pp.3646-3654.
- Sherma, J. and Fried, B. (1996). *Practical thin-layer chromatography*. New York: Boca Raton.

- Shi, D., Fan, X., Sun, J., Han, L. and Shi, J. (2008). Steroids from green alga *Chaetomorpha basiretorsa* Setchell. *Chinese Journal of Oceanology and Limnology*, 26(4), pp.415-418.
- Shi, L., Wu, C., Yang, T., Yao, C., Lin, H. and Chang, W. (2014). Cytotoxic effect of triterpenoids from the root bark of *Hibiscus syriacus*. *Fitoterapia*, 97, pp.184-191.
- Shi, Z., Lei, C., Yu, B., Wang, H. and Hou, A. (2016). New Alkaloids and  $\alpha$ -Glucosidase Inhibitory Flavonoids from *Ficus hispida*. *Chem. Biodiversity*, 13(4), pp.445-450.
- Shipley, M., Mangold, C. and Szpara, M. (2016). Differentiation of the SH-SY5Y Human Neuroblastoma Cell Line. *Journal of Visualized Experiments*, (108).
- Sica, D., Piccialli, V. and Masullo, A. (1984). Configuration at C-24 of sterols from the marine phanerogames *Posidonia oceanica* and *Cymodocea nodosa*. *Phytochemistry*, 23(11), pp.2609-2611.
- Siddiqui, M., AlOthman, Z. and Rahman, N. (2017). Analytical techniques in pharmaceutical analysis: A review. *Arabian Journal of Chemistry*, 10, pp.S1409-S1421.
- Silva, B., Andrade, P., Valentão, P., Ferreres, F., Seabra, R. and Ferreira, M. (2004). Quince (*Cydonia oblonga* Miller) Fruit (Pulp, Peel, and Seed) and Jam: Antioxidant Activity. *Journal of Agricultural and Food Chemistry*, 52(15), pp.4705-4712.
- Simoni, E., Serafini, M., Caporaso, R., Marchetti, C., Racchi, M., Minarini, A., Bartolini, M., Lanni, C. and Rosini, M. (2017). Targeting the Nrf2/Amyloid-Beta Liaison in Alzheimer's Disease: A Rational Approach. *ACS Chemical Neuroscience*, 8(7), pp.1618-1627.
- Singab, A., Ayoub, N., Ali, E. and Mostafa, N. (2010). Antioxidant and hepatoprotective activities of Egyptian moraceous plants against carbon tetrachloride-induced oxidative stress and liver damage in rats. *Pharmaceutical Biology*, 48(11), pp.1255-1264.
- Singh, A., Singh, D., Srivastava, S., Govindarajan, R. and Rawat, A. (2007). A validated quantitative HPTLC method for analysis of biomarkers in *Ficus carica* L. *Journal of Planar Chromatography – Modern TLC*, 20(6), pp.437-441.
- Singh, P., Singh, D. and Goel, R. (2014). *Ficus religiosa* L. figs — A potential herbal adjuvant to phenytoin for improved management of epilepsy and associated behavioral comorbidities. *Epilepsy & Behavior*, 41, pp.171-178.
- Smeaton, W. (1986). Carl Wilhelm Scheele (1742–1786). *Endeavour*, 10(1), pp.28-30.
- Smyth, W., McClean, S., Massaro, C., Smyth, T., Brooks, P. and Robledo, V. (2017). *Characterization of Synthetic and Natural Product Pharmaceuticals by Functional Group Analysis using Electrospray Ionization-Ion Trap Mass Spectrometry: A Mini-Review*.

- Smyth, W., Smyth, T., Ramachandran, V., O'Donnell, F. and Brooks, P. (2012). Dereplication of phytochemicals in plants by LC-ESI-MS and ESI-MSn. *TrAC Trends in Analytical Chemistry*, 33, pp.46-54.
- Solomon, A., Golubowicz, S., Yablowicz, Z., Bergman, M., Grossman, S., Altman, A., Kerem, Z. and Flaishman, M. (2010). Protection of Fibroblasts (NIH-3T3) against Oxidative Damage by Cyanidin-3-rhamnoglucoside Isolated from Fig Fruits (*Ficus carica*L.). *Journal of Agricultural and Food Chemistry*, 58(11), pp.6660-6665.
- Solomon, A., Golubowicz, S., Yablowicz, Z., Bergman, M., Grossman, S., Altman, A., Kerem, Z. and Flaishman, M. (2010). EPR Studies of O<sub>2</sub><sup>•-</sup>, OH, and <sup>1</sup>O<sub>2</sub> Scavenging and Prevention of Glutathione Depletion in Fibroblast Cells by Cyanidin-3-rhamnoglucoside Isolated from Fig (*Ficus carica* L.) Fruits. *Journal of Agricultural and Food Chemistry*, 58(12), pp.7158-7165.
- Solomon, A., Golubowicz, S., Yablowicz, Z., Grossman, S., Bergman, M., Gottlieb, H., Altman, A., Kerem, Z. and Flaishman, M. (2006). Antioxidant Activities and Anthocyanin Content of Fresh Fruits of Common Fig (*Ficus carica*L.). *Journal of Agricultural and Food Chemistry*, 54(20), pp.7717-7723.
- Soltana, H., Tekaya, M., Amri, Z., El-Gharbi, S., Nakbi, A., Harzallah, A., Mechri, B. and Hammami, M. (2016). Characterization of fig AChEnes' oil of *Ficus carica* grown in Tunisia. *Food Chemistry*, 196, pp.1125-1130.
- Sousa, C., Pereira, D., Taveira, M., Dopico-García, S., Valentão, P., Pereira, J., Bento, A. and Andrade, P. (2009). Brassica oleraceavar.costata: comparative study on organic acids and biomass production with other cabbage varieties. *Journal of the Science of Food and Agriculture*, 89(6), pp.1083-1089.
- Springob, K. and Kutchan, T. (2009). Introduction to the Different Classes of Natural Products. *Plant-derived Natural Products*, pp.3-50.
- Srivastava, S. and Kulshreshtha, D. (2010). Centdaroic Acid, a New Diterpene Acid from *Cedrus deodara*. *ChemInform*, 32(31).
- Stalin, C., Dineshkumar, P. and Nithiyanthan, K. (2012). Evaluation of antidiabetic activity of methanolic leaf extract of *Ficus carica* in alloxan - induced diabetic rats. *Asian Journal of Pharmaceutical and Clinical Research*, 5(3), pp.85-87.
- Stephen Irudayaraj, S., Christudas, S., Antony, S., Duraipandiyar, V., Naif Abdullah, A. and Ignacimuthu, S. (2017). Protective effects of *Ficus carica* leaves on glucose and lipids levels, carbohydrate metabolism enzymes and  $\beta$ -cells in type 2 diabetic rats. *Pharmaceutical Biology*, 55(1), pp.1074-1081.
- Subash, S., Essa, M., Al-Asmi, A., Al-Adawi, S. and Vaishnav, R. (2014). Chronic Dietary Supplementation of 4% Figs on the Modification of Oxidative Stress in Alzheimer's Disease Transgenic Mouse Model. *BioMed Research International*, 2014, pp.1-8.
- Subash, S., Essa, M., Al-Asmi, A., Al-Adawi, S. and Vaishnav, R. (2017). *Chronic Dietary Supplementation of 4% Figs on the Modification of Oxidative Stress in Alzheimer's Disease Transgenic Mouse Model*.

- Subash, S., Essa, M., Braidy, N., Al-Jabri, A., Vaishnav, R., Al-Adawi, S., Al-Asmi, A. and Guillemain, G. (2017). *Consumption of fig fruits grown in Oman can improve memory, anxiety, and learning skills in a transgenic mice model of Alzheimer's disease.*
- Sultana, R., Perluigi, M. and Allan Butterfield, D. (2013). Lipid peroxidation triggers neurodegeneration: A redox proteomics view into the Alzheimer disease brain. *Free Radical Biology and Medicine*, 62, pp.157-169.
- Sumi, S., Siraj, M., Hossain, A., Mia, M., Afrin, S. and Rahman, M. (2016). Investigation of the Key Pharmacological Activities of *Ficus racemosa* and Analysis of Its Major Bioactive Polyphenols by HPLC-DAD. *Evidence-Based Complementary and Alternative Medicine*, 2016, pp.1-9.
- Sun, S., Li, H., Zhou, W., Liu, A. and Zhu, H. (2015). Bacterial Quorum Sensing Inhibition Activity of the Traditional Chinese Herbs, *Ficus carica* L. and *Perilla frutescens*. *Chemotherapy*, 60(5-6), pp.379-383.
- Szakiel, A., Paćzkowski, C., Koivuniemi, H. and Huttunen, S. (2012). Comparison of the Triterpenoid Content of Berries and Leaves of Lingonberry *Vaccinium vitis-idaea* from Finland and Poland. *Journal of Agricultural and Food Chemistry*, 60(19), pp.4994-5002.
- Takahashi, T., Okiura, A., Saito, K. and Kohno, M. (2014). Identification of Phenylpropanoids in Fig (*Ficus carica*L.) Leaves. *Journal of Agricultural and Food Chemistry*, 62(41), pp.10076-10083.
- Takano, H., Osakabe, N., Sanbongi, C., Yanagisawa, R., Inoue, K., Yasuda, A., Natsume, M., Baba, S., Ichiishi, E. and Yoshikawa, T. (2004). Extract of *Perilla frutescens* Enriched for Rosmarinic Acid, a Polyphenolic Phytochemical, Inhibits Seasonal Allergic Rhinoconjunctivitis in Humans. *Experimental Biology and Medicine*, 229(3), pp.247-254.
- Talapatra, S. and Talapatra, B. (2015). *Chemistry of plant natural products*. 1st ed. Berlin: Springer.
- Tan, C., Yu, J., Wang, H., Tan, M., Meng, X., Wang, C., Jiang, T., Zhu, X. and Tan, L. (2014). Efficacy and Safety of Donepezil, Galantamine, Rivastigmine, and Memantine for the Treatment of Alzheimer's Disease: A Systematic Review and Meta-Analysis. *Journal of Alzheimer's Disease*, 41(2), pp.615-631.
- Tapsell, L., Hemphill, I., Cobiac, L., Sullivan, D., Fenech, M., Patch, C., Roodenrys, S., Keogh, J., Clifton, P., Williams, P., Fazio, V. and Inge, K. (2006). Health benefits of herbs and spices: the past, the present, the future. *The Medical Journal of Australia*, 185(4), pp.1-24.
- Tashiro, R. and Pater, R. (1996). *Compositions and method of treating cardio-, cerebrovascular and alzheimer's diseases and depression*. US5589182 A.
- Tawfike, A., Tate, R., Abbott, G., Young, L., Viegelmann, C., Schumacher, M., Diederich, M. and Edrada-Ebel, R. (2017). Metabolomic Tools to Assess the

- Chemistry and Bioactivity of Endophytic *Aspergillus* Strain. *Chemistry & Biodiversity*, 14(10), p.e1700040.
- Taylor, J. and Triggle, D. (2007). *Comprehensive medicinal chemistry II*. Amsterdam: Elsevier.
- Tezcan, G., Tunca, B., Bekar, A., Yalcin, M., Sahin, S., Budak, F., Cecener, G., Egeli, U., Demir, C., Guvenc, G., Yilmaz, G., Erkan, L., Malyer, H., Taskapilioglu, M., Evrensel, T. and Bilir, A. (2014). Ficus carica Latex Prevents Invasion Through Induction of Let-7d Expression in GBM Cell Lines. *Cellular and Molecular Neurobiology*, 35(2), pp.175-187.
- Tian, J., Zhang, Y., Yang, X., Rui, K., Tang, X., Ma, J., Chen, J., Xu, H., Lu, L. and Wang, S. (2014). Ficus carica Polysaccharides Promote the Maturation and Function of Dendritic Cells. *International Journal of Molecular Sciences*, 15(7), pp.12469-12479.
- Tong, G., Wang, J., Sverdllov, O., Huang, S., Slemmon, R., Croop, R., Castaneda, L., Gu, H., Wong, O., Li, H., Berman, R., Smith, C., Albright, C. and Dockens, R. (2012). Multicenter, Randomized, Double-Blind, Placebo-Controlled, Single-Ascending Dose Study of the Oral  $\gamma$ -Secretase Inhibitor BMS-708163 (Avagacestat): Tolerability Profile, Pharmacokinetic Parameters, and Pharmacodynamic Markers. *Clinical Therapeutics*, 34(3), pp.654-667.
- Tönnies, E. and Trushina, E. (2017). Oxidative Stress, Synaptic Dysfunction, and Alzheimer's Disease. *Journal of Alzheimer's Disease*, pp.1-17.
- Torres-Lista, V., Parrado-Fernández, C., Alvarez-Montón, I., Frontiñán-Rubio, J., Durán-Prado, M., Peinado, J., Johansson, B., Alcaín, F. and Giménez-Llort, L. (2014). Neophobia, NQO1 and SIRT1 as premorbid and prodromal indicators of AD in 3xTg-AD mice. *Behavioural Brain Research*, 271, pp.140-146.
- Touchstone, J. (2001). Thin Layer Chromatography. *Handbook of Analytical Techniques*, pp.327-344.
- Trinh, B., Staerk, D. and Jäger, A. (2016). Screening for potential  $\alpha$ -glucosidase and  $\alpha$ -amylase inhibitory constituents from selected Vietnamese plants used to treat type 2 diabetes. *Journal of Ethnopharmacology*, 186, pp.189-195.
- Tsai, P., De Castro-Cruz, K., Shen, C., Chiou, C. and Ragasa, C. (2012). Chemical constituents of Ficus odorata. *Pharm Chem J*, 46(4), pp.225-227.
- Tseng, M., Lin, K., Huang, Y., Chang, Y., Huang, S., Kuo, L. and Huang, Y. (2017). Detection of chlorophylls in spores of seven ferns. *Journal of Plant Research*, 130(2), pp.407-416.
- Tsou, H., Hu, C. and Liu, T. (2016). The presence of protein-conjugated acrolein and 3-Hydroxypropyl Mercapturic Acid (3-HPMA) in patients with Alzheimer's disease. *Toxicology Letters*, 259, pp.S144-S145.
- Tsuchiya, H., Sato, M., Miyazaki, T., Fujiwara, S., Tanigaki, S., Ohyama, M., Tanaka, T. and Inuma, M. (1996). Comparative study on the antibacterial activity of

- phytochemical flavanones against methicillin-resistant *Staphylococcus aureus*. *Journal of Ethnopharmacology*, 50(1), pp.27-34.
- Tugizimana, F., Steenkamp, P., Piater, L. and Dubery, I. (2016). A Conversation on Data Mining Strategies in LC-MS Untargeted Metabolomics: Pre-Processing and Pre-Treatment Steps. *Metabolites*, 6(4), p.40.
- Tulloch, A. and Hoffman, L. (1982). Epicuticular Wax of *Cirsium Arvense*. *Phytochemistry (Elsevier)*, 21(7), pp.1639-1642.
- Turan, A. and Celik, I. (2016). Antioxidant and hepatoprotective properties of dried fig against oxidative stress and hepatotoxicity in rats. *International Journal of Biological Macromolecules*, 91, pp.554-559.
- Uchida, K., Kanematsu, M., Sakai, K., Matsuda, T., Hattori, N., Mizuno, Y., Suzuki, D., Miyata, T., Noguchi, N., Niki, E. and Osawa, T. (1998). Protein-bound acrolein: Potential markers for oxidative stress. *Proceedings of the National Academy of Sciences*, 95(9), pp.4882-4887.
- Uddin, M., Sarker, M., Ferdosh, S., Akanda, M., Easmin, M., Bt Shamsudin, S. and Yunus, K. (2014). Phytosterols and their extraction from various plant matrices using supercritical carbon dioxide: a review. *Journal of the Science of Food and Agriculture*, 95(7), pp.1385-1394.
- Ullman, S., Clark, G. and Roan, K. (1952). The effects of the fraction R3 of the latex of *ficus carica* L. on the tissues of mice bearing spontaneous mammary tumors. *Exp Med Surg*, 10(4), pp.287-305.
- Ullman, S., Halberstaedter, L. and Leibowitz, J. (1945). Some pharmacological and biological effects of the latex of *Ficus carica*. *Exp. Med. Surg.*, 3, pp.11-23.
- Umerie, S. (2004). Stabilization of palm oils by using *Ficus exasperata* leaves in local processing methods. *Bioresource Technology*, 94(3), pp.307-310.
- Uomori, A., Nakagawa, Y., Yoshimatsu, S., Seo, S., Sankawa, U. and Takeda, K. (1992). Biosynthesis of campesterol and dihydrobrassicasterol in cultured cells of *Amsonia elliptica*. *Phytochemistry*, 31(5), pp.1569-1572.
- Uttara, B., Singh, A., Zamboni, P. and Mahajan, R. (2009). Oxidative Stress and Neurodegenerative Diseases: A Review of Upstream and Downstream Antioxidant Therapeutic Options. *Current Neuropharmacology*, 7(1), pp.65-74.
- Valentão, P., Lopes, G., Valente, M., Barbosa, P., Andrade, P., Silva, B., Baptista, P. and Seabra, R. (2005). Quantitation of Nine Organic Acids in Wild Mushrooms. *Journal of Agricultural and Food Chemistry*, 53(9), pp.3626-3630.
- Vanmierlo, T., Bogie, J., Mailleux, J., Vanmol, J., Lütjohann, D., Mulder, M. and Hendriks, J. (2015). Plant sterols: Friend or foe in CNS disorders?. *Progress in Lipid Research*, 58, pp.26-39.
- Vanmierlo, T., Popp, J., Kölsch, H., Friedrichs, S., Jessen, F., Stoffel-Wagner, B., Bertsch, T., Hartmann, T., Maier, W., von Bergmann, K., Steinbusch, H., Mulder,

- M. and Lütjohann, D. (2011). The plant sterol brassicasterol as additional CSF biomarker in Alzheimer's disease. *Acta Psychiatrica Scandinavica*, 124(3), pp.184-192.
- Vanmierlo, T., Weingärtner, O., van der Pol, S., Husche, C., Kerksiek, A., Friedrichs, S., Sijbrands, E., Steinbusch, H., Grimm, M., Hartmann, T., Laufs, U., Böhm, M., de Vries, H., Mulder, M. and Lütjohann, D. (2012). Dietary intake of plant sterols stably increases plant sterol levels in the murine brain. *Journal of Lipid Research*, 53(4), pp.726-735.
- Vauzour, D., Corona, G. and Spencer, J. (2010). Caffeic acid, tyrosol and *P*-coumaric acid are potent inhibitors of 5-S-cysteinyl-dopamine induced neurotoxicity. *Archives of Biochemistry and Biophysics*, 501(1), pp.106-111.
- Veberic, R., Colaric, M. and Stampar, F. (2008). Phenolic acids and flavonoids of fig fruit (*Ficus carica* L.) in the northern Mediterranean region. *Food Chemistry*, 106(1), pp.153-157.
- Veer, V. and Gopalakrishnan, R. (2016). *Herbal insecticides, repellents and biomedicines*. 1st ed. New Delhi: Springer.
- Villareal, M., Sasaki, K., Margout, D., Savry, C., Almaksour, Z., Larroque, M. and Isoda, H. (2016). Neuroprotective effect of Picholine virgin olive oil and its hydroxycinnamic acids component against  $\beta$ -amyloid-induced toxicity in SH-SY5Y neurotypic cells. *Cytotechnology*, 68(6), pp.2567-2578.
- Wagner, H. and Bladt, S. (2009). *Plant drug analysis : a thin layer chromatography atlas*. 1st ed. Berlin [etc.]: Springer.
- Waksmundzka-Hajnos, M., Sherma, J. and Kowalska, T. (2008). *Thin layer chromatography in phytochemistry*. Boca Raton: CRC Press, p.888.
- Wan, C., Han, J., Chen, C., Yao, L., Chen, J. and Yuan, T. (2016). Monosubstituted Benzene Derivatives from Fruits of *Ficus hirta* and Their Antifungal Activity against Phytopathogen *Penicillium italicum*. *J. Agric. Food Chem.*, 64(28), pp.5621-5624.
- Wang, L., Wang, M., Hu, J., Shen, W., Hu, J., Yao, Y., Wang, X., Afzal, C., Ma, R. and Li, G. (2017). Protective effect of 3H-1, 2-dithiole-3-thione on cellular model of Alzheimer's disease involves Nrf2/ARE signaling pathway. *European Journal of Pharmacology*, 795, pp.115-123.
- Wang, Y., Lin, H., Zhao, W., Huang, H., Lo, Y., Wang, H. and Maan-Yuh Lin, A. (2017). Acrolein acts as a neurotoxin in the nigrostriatal dopaminergic system of rat: involvement of  $\alpha$ -synuclein aggregation and programmed cell death. *Scientific Reports*, 7, p.45741.
- Waragai, M., Yoshida, M., Mizoi, M., Saiki, R., Kashiwagi, K., Takagi, K., Akatsu, H., Arai, H., Tashiro, J., Yamamoto, T., Uemura, K., Iwai, N. and Igarashi, K. (2012). Increased protein-conjugated acrolein and beta-amyloid 40/42 ratio in the plasma in patients with mild cognitive impairment and Alzheimer's disease. *Alzheimer's & Dementia*, 8(4), pp.P289-P290.

- Ward, J. (1963). Hierarchical Grouping to Optimize an Objective Function. *Journal of the American Statistical Association*, 58(301), pp.236-244.
- Ward, L. and Pasinetti, G. (2016). Recommendations for Development of Botanical Polyphenols as “Natural Drugs” for Promotion of Resilience Against Stress-Induced Depression and Cognitive Impairment. *Neuromol Med*, 18(3), pp.487-495.
- Watkins, P. (1994). Hepatotoxic Effects of Tacrine Administration in Patients With Alzheimer's Disease. *JAMA: The Journal of the American Medical Association*, 271(13), p.992.
- Watson, D., Edrada-Ebel, R. and Patel, B. (2017). *Pharmaceutical analysis*. 4th ed. Edinburgh: Elsevier.
- Watson, R., Gerald, J. and Preedy, V. (2011). *Nutrients, dietary supplements, and nutraceuticals*. 1st ed. Totowa, N.J.: Humana.
- Weingartner, O., Bohm, M. and Laufs, U. (2008). Controversial role of plant sterol esters in the management of hypercholesterolaemia. *European Heart Journal*, 30(4), pp.404-409.
- Weli, A., Al-Blushi, A. and Hossain, M. (2015). Evaluation of antioxidant and antimicrobial potential of different leaves crude extracts of Omani *Ficus carica* against food borne pathogenic bacteria. *Asian Pacific Journal of Tropical Disease*, 5(1), pp.13-16.
- Werth, M., Halouska, S., Shortridge, M., Zhang, B. and Powers, R. (2010). Analysis of metabolomic PCA data using tree diagrams. *Analytical Biochemistry*, 399(1), pp.58-63.
- Wightman, E. (2017). Potential benefits of phytochemicals against Alzheimer's disease. *Proceedings of the Nutrition Society*, 76(02), pp.106-112.
- Williams, P., Sorribas, A. and Howes, M. (2011). Natural products as a source of Alzheimer's drug leads. *Nat. Prod. Rep.*, 28(1), pp.48-77.
- Wishart, D., Tzur, D., Knox, C., Eisner, R., Guo, A., Young, N., Cheng, D., Jewell, K., Arndt, D., Sawhney, S., Fung, C., Nikolai, L., Lewis, M., Coutouly, M., Forsythe, I., Tang, P., Shrivastava, S., Jeroncic, K., Stothard, P., Amegbey, G., Block, D., Hau, D., Wagner, J., Miniaci, J., Clements, M., Gebremedhin, M., Guo, N., Zhang, Y., Duggan, G., MacInnis, G., Weljie, A., Dowlatabadi, R., Bamforth, F., Clive, D., Greiner, R., Li, L., Marrie, T., Sykes, B., Vogel, H. and Querengesser, L. (2007). HMDB: the Human Metabolome Database. *Nucleic Acids Research*, 35(Database), pp.D521-D526.
- Wolfe, N., Katz, D., Albert, M., Almozlino, A., Durso, R., Smith, M. and Volicer, L. (2017). *Neuropsychological profile linked to low dopamine: in Alzheimer's disease, major depression, and Parkinson's disease.*
- World Scientific (Firm) and Brahmachari, G. (2012). *Bioactive Natural Products: Opportunities And Challenges In Medicinal Chemistry*. 1st ed. World Scientific.

- Wu, H. (2005). Antianalgesia: Stereoselective Action of dextro-Morphine over levo-Morphine on Glia in the Mouse Spinal Cord. *Journal of Pharmacology and Experimental Therapeutics*, 314(3), pp.1101-1108.
- Yamamoto, H., Yamaji, H., Abe, Y., Harada, K., Waluyo, D., Fukusaki, E., Kondo, A., Ohno, H. and Fukuda, H. (2009). Dimensionality reduction for metabolome data using PCA, PLS, OPLS, and RFDA with differential penalties to latent variables. *Chemometrics and Intelligent Laboratory Systems*, 98(2), pp.136-142.
- Yamashita, M. and Fenn, J. (1984). Negative ion production with the electrospray ion source. *Journal of Physical Chemistry*, 88(20), pp.4671-4675.
- Yang, P. and Mahmood, T. (2012). Western blot: Technique, theory, and trouble shooting. *North American Journal of Medical Sciences*, 4(9), p.429.
- Yang, X., Guo, J., Ye, J., Zhang, Y. and Wang, W. (2015). The effects of Ficus carica polysaccharide on immune response and expression of some immune-related genes in grass carp, *Ctenopharyngodon idella*. *Fish & Shellfish Immunology*, 42(1), pp.132-137.
- Yang, X., Yu, W., Ou, Z., Ma, H., Liu, W. and Ji, X. (2009). Antioxidant and Immunity Activity of Water Extract and Crude Polysaccharide from Ficus carica L. Fruit. *Plant Foods for Human Nutrition*, 64(2), pp.167-173.
- Yim, O. and Ramdeen, K. (2015). Hierarchical Cluster Analysis: Comparison of Three Linkage Measures and Application to Psychological Data. *The Quantitative Methods for Psychology*, 11(1), pp.8-21.
- Yu, X., Wang, Q., Xu, X., Lv, W., Zhao, M. and Liang, Z. (2013). Preparative isolation of Heteroclitin D from *Kadsurae Caulis* using normal-phase flash chromatography. *Journal of Pharmaceutical Analysis*, 3(6), pp.456-459.
- Yuan, H., Ma, Q., Ye, L. and Piao, G. (2016). The Traditional Medicine and Modern Medicine from Natural Products. *Molecules*, 21(5), p.559.
- Yuliana, N., Jahangir, M., Verpoorte, R. and Choi, Y. (2013). Metabolomics for the rapid dereplication of bioactive compounds from natural sources. *Phytochemistry Reviews*, 12(2), pp.293-304.
- Yvon, C., Macdonell, A., Buchwald, S., Surman, A., Follet, N., Alex, J., Long, D. and Cronin, L. (2013). A collection of robust methodologies for the preparation of asymmetric hybrid Mn-Anderson polyoxometalates for multifunctional materials. *Chem. Sci.*, 4(10), pp.3810-3817.
- Zadina, J., Chang, S., Ge, L. and Kastin, A. (1993). Mu opiate receptor down-regulation by morphine and uP-regulation by naloxone in SH-SY5Y human neuroblastoma cells. *Journal of Pharmacology and Experimental Therapeutics*, 265(1), pp.254-262.
- Zheng, W., Thorne, N. and McKew, J. (2013). Phenotypic screens as a renewed approach for drug discovery. *Drug Discovery Today*, 18(21-22), pp.1067-1073.

- Zhou, J., Xie, G. and Yan, X. (2011). *Encyclopedia of traditional Chinese medicines*. 1st ed. Berlin: Springer.
- Zilka, N., Zilkova, M., Kazmerova, Z., Sarisky, M., Cigankova, V. and Novak, M. (2011). Mesenchymal stem cells rescue the Alzheimer's disease cell model from cell death induced by misfolded truncated tau. *Neuroscience*, 193, pp.330-337.
- Zingue, S., Michel, T., Tchatchou, J., Chantal Beatrice Magne, N., Winter, E., Monchot, A., Awounfack, C., Djiogue, S., Clyne, C., Fernandez, X., Creczynski-Pasa, T. and Njamen, D. (2016). Estrogenic effects of *Ficus umbellata* Vahl. (Moraceae) extracts and their ability to alleviate some menopausal symptoms induced by ovariectomy in Wistar rats. *Journal of Ethnopharmacology*, 179, pp.332-344.

## **Supplementary information**

---

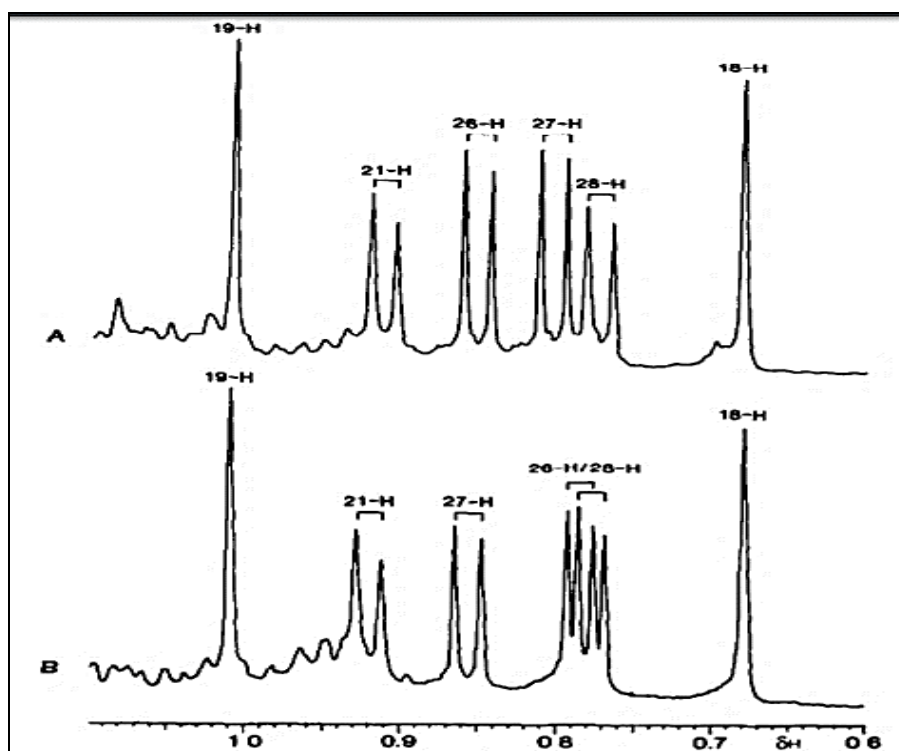


**Figure 1S:** A comparison of <sup>1</sup>H-MNR srpectrum (400 MHz, CDCl<sub>3</sub>) of **A)** campesterol fraction and **B)** brassicasterol fraction (Uomori *et al.*, 1992).

